Technical Report CHL-99-11
June 1999

US Army Corps of Engineers
Waterways Experiment Station

Florida Bay Field Data Report

by Thad C. Pratt, WES
Ned P. Smith, Harbor Branch Oceanographic Institution, Inc.

19990726 090

Approved For Public Release; Distribution Is Unlimited

DTIC QUALITY INSPECTED 4

Prepared for U.S. Army Engineer District, Jacksonville

The contents of this report are not to be used for advertising, publication, or promotional purposes. Citation of trade names does not constitute an official endorsement or approval of the use of such commercial products.

The findings of this report are not to be construed as an official Department of the Army position, unless so designated by other authorized documents.

PRINTED ON RECYCLED PAPER

Technical Report CHL-99-11
June 1999

Florida Bay Field Data Report

by Thad C. Pratt

U.S. Army Corps of Engineers
Waterways Experiment Station
3909 Halls Ferry Road
Vicksburg, MS 39180-6199

Ned P. Smith

Harbor Branch Oceanographic Institution, Inc.
5600 U.S. 1 North
Fort Pierce, FL 34946

Final report

Approved for public release; distribution is unlimited

Prepared for U.S. Army Engineer District, Jacksonville
Jacksonville, FL 32232-0019

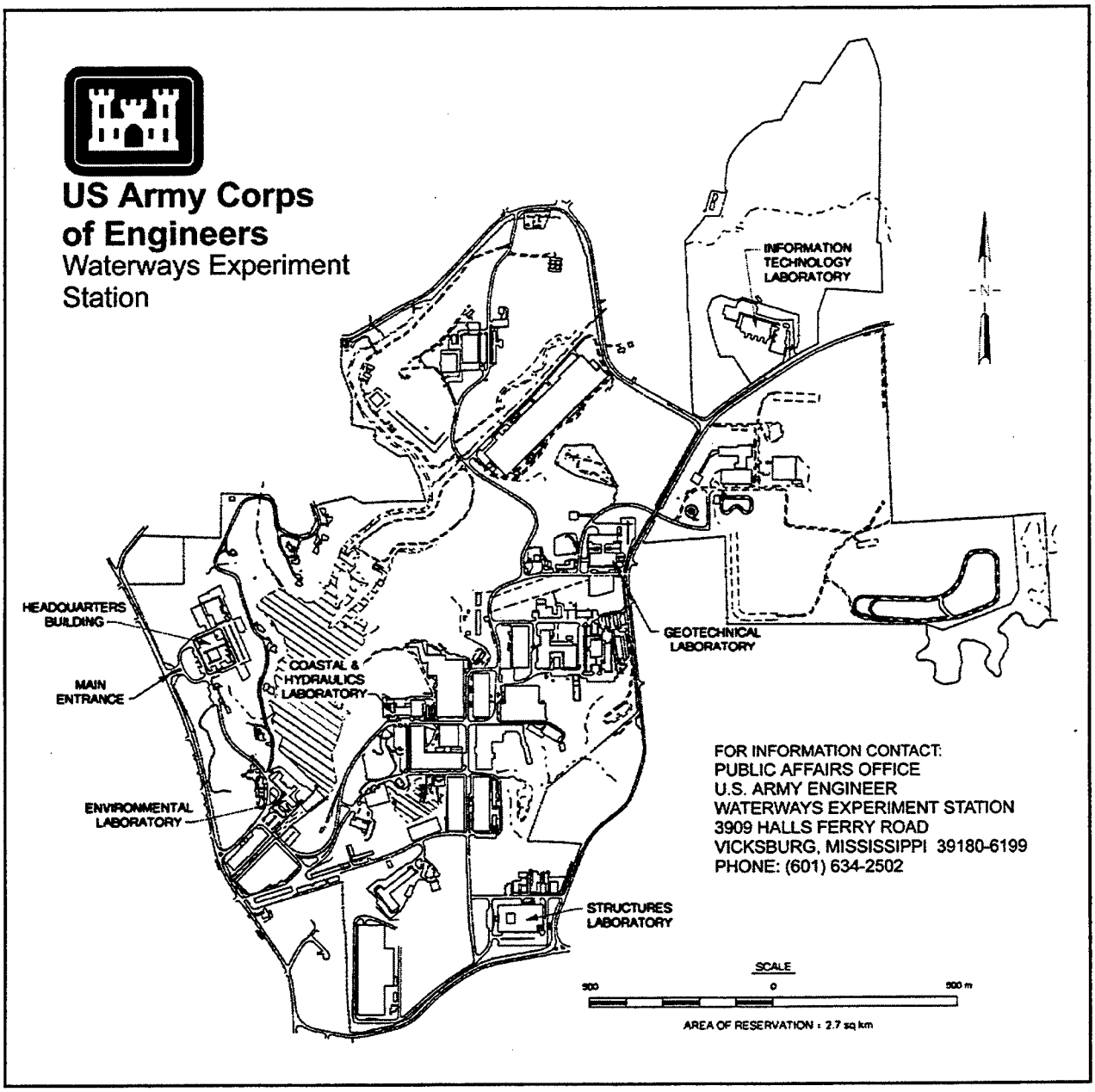

Waterways Experiment Station Cataloging-in-Publication Data

Pratt, Thad C.

Florida Bay field data report / by Thad C. Pratt, Ned P. Smith ; prepared for U.S. Army Engineer District, Jacksonville.

348 p. : ill. ; 28 cm. — (Technical report ; CHL-99-11)

Includes bibliographic references.

1. Florida Bay (Fla.) 2. Tidal currents — Florida — Florida Bay. 3. Weather — Florida — Florida Bay. 4. Hydrodynamics — Florida — Florida Bay. I. Smith, Ned P. II. United States. Army. Corps of Engineers. Jacksonville District. III. U.S. Army Engineer Waterways Experiment Station. IV. Coastal and Hydraulics Laboratory (U.S. Army Engineer Waterways Experiment Station) V. Title. VI. Series: Technical report (U.S. Army Engineer Waterways Experiment Station) ; CHL-99-11.

TA7 W34 no.CHL-99-11

Contents

Preface v

Conversion Factors, Non-SI to SI Units of Measurement vi

1 - Introduction 1

Background 1
Purpose 1
Approach 2

2 - Data Collection Program and Equipment 3

Long-term Monitoring 3
Short-term Intensive Surveys 3
Data Collection Procedures 4
Equipment 4

3 - Data Presentation 5

Weather Data 5
ADP Velocity Data 6
ADCP Velocity Data 8
Tide Data 8

4 - Summary 9

Weather Data 9
ADP Velocity Data 9
ADCP Data 10

Tables 1-13

Figures 1-27

Plates 1-89

Appendix A: Hydraulic Analysis Group Data Collection Equipment and Laboratory Analysis Procedures A1

Appendix B: An Analysis of Weather Data from Northern Florida Bay B1

Appendix C: An Analysis of Acoustic Doppler Profiler Data From Western Florida Bay ... C1

Appendix D: An Analysis of Acoustic Doppler Current Profiler Data from Tidal Channels in Eastern Florida Bay D1

SF 298

Preface

The field investigation reported herein was conducted by the Coastal and Hydraulics Laboratory (CHL) of the U.S. Army Engineer Waterways Experiment Station (WES) under the sponsorship of the U.S. Army Engineer District, Jacksonville, to provide the necessary data for support of the Florida Bay hydrodynamic modeling study. The field data collection was conducted from March 1996 through April 1997 and was funded by the Jacksonville District under the management of Mr. M. Choate. WES liaison was Mr. T. C. Pratt of the Hydraulic Analysis Group (HAG). WES is a complex of five laboratories of the Engineer Research and Development Center (ERDC).

The work was performed under the general supervision of Dr. J. R. Houston, Director, CHL, and Messrs. R. A. Sager, Assistant Director, CHL, and T. L. Fagerburg, Group Leader, HAG. The data collection program was designed by Messrs. Pratt and Fagerburg. Data reduction was performed by Mrs. C. J. Coleman and Messrs. Pratt, M. T. Hebler, and H. A. Benson. This report was prepared by Mr. Pratt and Mrs. Coleman of WES and Dr. Ned Smith, Senior Scientist, Harbor Branch Oceanographic Institution, Inc., Division of Marine Science, Fort Pierce, FL.

At the time of publication of this report, COL Robin R. Cababa, EN, was Commander of ERDC. This report was prepared and published at the WES complex of ERDC.

The contents of this report are not to be used for advertising, publications, or promotional purposes. Citation of trade names does not constitute an official endorsement or approval for the use of such commercial products.

Conversion Factors, Non-SI to SI Units of Measurement

Non-SI units of measurement used in this report can be converted to SI units as follows:

Multiply	By	To Obtain
cubic feet	0.02831685	cubic meters
feet	0.3048	meters
inches	2.54	centimeters
miles (U.S. statute)	1.609347	kilometers

1 Introduction

Background

Florida Bay is located south of the Everglades National Park, Florida, and is part of the Florida Keys from Biscayne Bay to Marathon, FL. Figure 1 is a project map of the study area. Florida Bay is economically important as a tourist, commercial fishing, and recreational area. Florida Bay has been deteriorating for many years, as evidenced by marked increases in the size and persistence of algal blooms, die-offs in seagrass beds, storm-event damage, and general water-quality decline throughout the bay. Water-quality problems are further complicated by the lack of freshwater inflow and poor circulation patterns.

The study of circulation patterns in a system such as Florida Bay is a complex issue. Physical processes that impact on the water quality within the system can vary both spatially and temporally. Bathymetry and geometry of the navigation channels, interconnecting canals and inlets, astronomical tide-induced currents, wind-induced currents, and freshwater inflow are major factors that determine circulation patterns. At the present time, only a small amount of historical information is available. An investigation of this estuarine system was conducted to determine the existing hydrodynamics and to develop recommendations for improving Corps management of this system. To determine these effects in a technically rigorous manner, a sophisticated approach was taken that utilizes state-of-the-art numerical models supplemented with field investigations.

Purpose

The purpose of the field data collection program was to provide hydrodynamic results including current velocities, flow distributions, circulation patterns, water levels, and meteorological measurements during long-term monitoring and short-term intensive surveys. These data were used in the development and verification of a two-dimensional numerical hydrodynamic model of the study area. The purpose of the numerical model was to develop an understanding of the circulation patterns in Florida Bay and determine the importance of winds, tides, and freshwater inflow on circulation patterns.

Approach

The study was structured to incorporate existing information from previous studies wherever possible to provide better coverage and results in a timely manner. To obtain the necessary data in the Florida Bay estuary, a long-term monitoring program was conducted over a 13-month period which included two short-term intensive data collection periods. The long-term monitoring data consisted of three bottom-mounted Acoustic Doppler Profilers (ADP) velocity meters , vessel-mounted Acoustic Doppler Current Profilers (ADCP), five tide gages, and three meteorological stations within the study area. Data collected at continuous monitoring stations by the Florida Marine Research Institute and Everglades National Park were also used in the model verification. These data were used by Dr. Ned Smith in developing the tidal constituents for long-term monitoring locations that were not necessarily collected during the exact period of this study. The short-term intensive surveys included collection of cross-sectional current speed and direction measurements for 12-hr periods at approximately 20 channel openings or inlets from Key Largo to Marathon Key. Water-level recorders were deployed at or near the channel openings during the short-term data collections periods.

2 Data Collection Program and Equipment

The field effort, as stated previously, included the long-term monitoring of velocity profiles and meteorological data and the short-term intensive data collection of current speed and direction, water-level fluctuations, and temperature at several openings into Florida Bay. The data were collected by the Hydraulic Analysis Group (HAG) of the Coastal and Hydraulics Laboratory (CHL) at WES. A reconnaissance trip was performed in August 1995 to determine locations for the long-term monitoring equipment deployment and to examine the channel openings for the short-term intensive surveys.

Long-term Monitoring

Bottom-mounted ADP's were deployed at three locations along the west boundary of Florida Bay in the Gulf of Mexico (Figure 1). The ADP's provided long-term velocity and direction profiles for determination of circulation patterns and flow distributions. Three meteorological stations were deployed for monitoring wind and weather patterns. Five water-level recorders were deployed at strategic locations for continuous water-level (tide) data recording. Figure 1 shows the approximate locations of instruments, and Table 1 gives the exact location during the survey period. The parameters to be monitored included wind speed and direction, precipitation, temperature, relative humidity, solar radiation, evaporation, and barometric pressure. The locations for the ADP's and meteorological stations were based on the modelers' needs. Monthly service trips were performed to download the data and service the equipment .

Short-term Intensive Surveys

Two intensive surveys monitoring seasonal variations were conducted at two different hydrodynamic conditions. During each survey, boat-mounted ADCP's were used to obtain current speed and direction data (flow measurements) at 20 channel openings/inlets over a 12-hr period (Figure 2). Each survey was combined with one of the monthly service trips. Prior to the

first intensive survey, five recording water-level sensors were deployed in or around channel openings and were left in position until the end of the second intensive survey. These instruments were useful in providing local water-level elevations and water temperatures at the channel openings for both the short-term and long-term data collection efforts.

Data Collection Procedures

The long-term data collection equipment was deployed at the start of the data collection program at the locations shown in Figure 1 and remained in place for a period of 13 months. The instruments collected data at sample intervals from 15 minutes to 1 hour depending on the equipment and the modelers' needs.

During the short-term data collection effort, the water-level recorders collected data every 15 minutes during the deployment period. The current speed and direction data were obtained by traversing each cross-channel transect approximately once each hour, over a 12-hr period, using boat-mounted ADCP's. The transect starting and ending positions were located with global positioning system (GPS) equipment to ensure line accuracy throughout the survey. Two boats were required for monitoring all the channel openings. The data were collected over several days for each survey. The number of openings that could be monitored daily in order to obtain hourly measurements were limited by the width of the openings and distances between them.

Equipment

The current speed and direction measurements were performed using boat-mounted 1200-kHz Broadband ADCP's. The water-level sensors deployed were ENDECO 1152SSM differential pressure gage water-level, temperature, and conductivity sensors. This equipment was available from HAG equipment inventory and was ready for use in Florida Bay. For the long-term collection of current speed and direction, bottom-mounted ADP's that were deployed were 1.5 MHZ SonTek Acoustic Doppler Profilers. Special mounting platforms were designed to rest on the bottom while the units collected data. The mounting platforms were designed to protect the current meters from nets and fishermen during deployment. Meteorological stations were W2000 WEATHER PAK's. The field equipment was designed for extreme exposure and harsh marine environments. A more detailed description of the above equipment is provided in Appendix A.

3 Data Presentation

The data collected in the field were brought back to WES for processing and analysis. All necessary data compilation from the field effort was conducted, and the data were prepared in formats suitable for numerical model verification and District needs. Further analysis and interpretation of portions of the data were provided by the Harbor Branch Oceanographic Institution (HBOI). This work was performed as part of a cooperative effort between the Jacksonville District, WES, and HBOI in support of the numerical model study.

Weather Data

Weather data are available from three locations along an east-west latitude (25° 05') across northern Florida Bay (Figure 1). The weather data were plotted on 15-min intervals for an entire month for visual inspection and analysis. Plates 1-14 are representative plots that were produced for each station during the period of record. These types of plots enabled us to identify trends and changes in data during the period of record. They also were useful in identifying any problems with sensors so they could be properly serviced. The data for each station are compiled into one file for the entire 13-month period. This file contains the 15-min, 1-hr, and 24-hr average data for each station. Processing codes were developed to interrogate these files and retrieve the required information for plotting and visualization. Weather parameters include resultant (vector average) wind speed, resultant wind direction, average air temperature, relative humidity, 15-min accumulated rainfall, barometric pressure, average solar radiation rate, and accumulated solar radiation flux.

Wind speed is expressed in meters/second with wind direction expressed in degrees clockwise from true north. A calculation of the standard deviation of the wind direction is plotted to show the spread in the data. Air temperature is plotted in degrees Celsius. Relative humidity is expressed as a percentage of water in air where 100 percent is the point at which saturation occurs. Rainfall is plotted for the hourly and daily values to show total values on both time scales. Barometric pressure is expressed in millimeters of mercury and plotted in 15-min increments to show fluctuations throughout the day. Solar radiation rate, expressed in watts/square meter, and solar radiation time-integrated flux through a 60-sec period, expressed in kiloJoules/square meter, are plotted in 15-min increments. The evaporation data are plotted on several graphs. The New Evaporation Pan Level, expressed in millimeters and plotted in 15-min

increments, shows how the pan level decreases in time while the New Evaporation plot, in millimeters, shows the inverse of the pan-level change. Cumulative Evaporation is plotted in millimeters hourly and daily to show the cumulative evaporation on two different time scales. Tables 2-4 are a summary of the weather data.

Wind data obtained during the March 1996 to April 1997 period generally support the annual cycle that has been observed in previous weather records. The cycle consists of winds being predominantly easterly during the spring and summer months, followed by a shift to northeasterly winds during the fall and winter months.

Solar radiation flux maximum values generally follow the seasonally varying zenith angle of the sun at local noon time. Maximum values occur during the months of June - August when the sun is more nearly directly overhead at the latitude of Florida Bay. The minimum values occur during the winter months (September - January) when clouds are more prevalent due to passing storm fronts.

Annual evaporation totals indicate large evaporative losses from the bay. The lowest evaporation rates in evaporation pan calculations were observed to occur during the winter months (December - February). This reduction is possibly due to the lower water temperatures and solar radiation flux present during this period. The cumulative water loss measured at the three stations during the 298-day collection period was 61.4 cm.

In addition to analysis of the weather data by WES, the HBOI performed further analyses. The results of these analyses were useful in quantifying the spatial correlation of wind stress and precipitation-evaporation balances across the northern part of the bay. A detailed summary of the HBOI analyses of the weather data is provided in Appendix B.

ADP Velocity Data

The ADP velocity data were collected on the same time interval as the weather data, 15 minutes between points. The difference between the velocity and the weather data sets are that the individual weather data points are an average value for an entire 15-min period, whereas, the individual ADP velocity data points are an average value for only a 2-min interval within each 15-min period. This data collection procedure for the ADP data was necessary to conserve battery life and storage space during the deployment period. The meters were deployed at three locations in the bay in water depths of 2 to 3 m. The ADP units were bottom-mounted with the sensing head oriented to look upward in the water column while making a measurement. A current speed and direction measurement was recorded at every 30 cm through the water column. The data were plotted for one-month periods at the surface, middepth, and bottom measurement points.

In addition to current speed and direction, the units are capable of measuring water-level and temperature. These parameters are measured by a pressure and temperature sensor incorporated into the ADP head. From the pressure sensor data, the range and phase of the water-level fluctuations above the instrument were obtained. The readings of pressure are for total pressure including local barometric pressure changes. Lack of available barometric pressure readings for the deployment areas made it difficult remove this component from the depth readings so an absolute water surface elevation could be obtained. The temperature sensor, mounted in the head of the ADP, provides a temperature measurement only at the head of the ADP. The elevation of this measurement is constant at 45 cm above the bottom. Plates 15-39 are representative plots generated from one month of ADP data at Station 1. By plotting the data at three elevations in the water column, differences in flow patterns throughout the water column and across the bay could be observed. Tables 5-7 summarize the ADP data for the three stations throughout the collection period. The velocity directions displayed in the tables represent the direction toward which the current is flowing.

All three ADP's experienced periods when data were not recorded. The missing data occurred randomly and could not be associated with external problems, such as acts of nature or commercial fishing interference. Table 8 summarizes the data collected during the long-term survey and identifies missing data at each station during the period of record. The majority of the missing data were single time interval readings, and only a small percentage (9%) of the missing data were multiple time interval readings. The available database is sufficient for the purposes of numerical model verification.

The ADP data for all three instrument locations illustrated that the magnitude of the flood tidal velocities over the depth of flow were generally higher than the ebb tidal velocities, however, not by an appreciable amount. Seasonal changes (wet months vs dry months) were not clearly evident at Stations 1 and 2. However, Station 3 displayed a marked increase in velocity magnitudes occurring during December and January, which is a typically wet season . During this period, the maximum velocity magnitudes at the surface during the ebb tide were considerably higher than was observed for any other period or station.

Additional analysis of the ADP data was provided by the HBOI in support of the hydrodynamic numerical modeling effort. The result of this analysis is to provide various harmonic constituents (amplitude and phase) of the vertically averaged currents, cumulative net transport (inflow or outflow), and wind-drift speeds and directions. The HBOI analysis of the ADP data is described in more detail in Appendix C.

The ADP data presented herein is the most comprehensive information available for interpreting the tidal and non-tidal exchange across the western boundary of the bay. Net inflow is found to occur in the central and northern part of the bay, whereas, net outflow is found to occur in the southern area of the western boundary. The current speed of ebb and flood tides indicates only slight variations with depth at all three stations. The amplitudes of the currents in the near-bottom layer were generally 80-85% of the near-surface layer.

ADCP Velocity Data

Figures 3-27 are representative depth-averaged plan-view velocity vector plots of the ADCP velocity and direction data obtained during the data collection periods. Maximum discharges within the openings ranged from 200 - 210,000 cfs. It should be noted that these magnitudes are for the extreme ebb and flood tide conditions. Data were collected in September 1996 during the typically wet season and again in February 1997 during the typically dry season. Table 9 is the station summary of the ADCP transects for the September 1996 and February 1997 surveys. Tables 10 and 11 lists the transect coordinates used for the September 1996 and February 1997 surveys, respectively. Tables 12 and 13 summarize the discharge information for the measured cross-sections for the two data collection periods. Seasonal variations in discharges were observable from the data collected.

Additional analysis of the ADCP data was provided by the HBOI in support of the hydrodynamic numerical modeling effort. The result of this analysis is to provide maximum discharge values and cumulative half-tidal-cycle discharge values for each of the principal tidal constituents. In addition, analysis results will provide the time series discharge through each of the tidal channels monitored and a determination of the relative importance of transient wind events. The HBOI analysis of the ADP data is described in more detail in Appendix D.

Tide Data

Plates 40-79 are the plots of the continuous time-history plots of tide data from the five water-level sensors deployed in Florida Bay for the entire data collection period. Data were recorded on the same time interval as the ADP and weather data at 15-min intervals. Tide ranges varied from 20 - 60 cm during the deployment period.

The continuous recordings of tide level overlapped with the periods of the short-term intensive surveys. The discharge data from the various transects were obtained near or adjacent to the deployment locations of the water-level sensors. A phase relationship between the tidal discharge and tide level was expected to exist which would lend confidence to the accuracy of the ADCP tidal discharge values. Plates 80-89 are the time-history plots of discharge versus tide for the ADCP transect nearest or adjacent to the five water-level sensor deployment locations during the two short-term intensive surveys. These plots corroborate the expected phase relationship between the tidal discharge and the water level.

4 Summary

Weather Data

Wind data obtained during the March 1996 to April 1997 period generally support the annual cycle that has been observed in previous weather records. The cycle consists of winds being predominantly easterly during the spring and summer months, followed by a shift to northeasterly winds during the fall and winter months.

The wind directions for Station 1 start in March 1996 with a direction of approximately 120°. As the season progressed through the summer of 1996, the direction changed to the low 80° range. The late fall and early winter directions tend to fall even further to the low 40° range with a return to the 120° range for the spring. The same results are seen in the data for Stations 2 and 3 within Florida Bay.

Temperatures range from 15°C to 28°C throughout the year on all three stations. The highest rainfall seemed to occur in September and October 1996. All three stations exhibited very similar results annually.

Solar radiation maximum values generally follow the seasonally varying zenith angle of the sun at local noon time. Maximum values occur during the months of June - August and minimum values occur during the winter months (September - January).

Annual evaporation totals indicate large evaporative losses from the bay. The lowest evaporation rates were observed to occur during the winter months (December - February). The cumulative water loss measured at the three stations during the 298-day collection period was 61.4 cm.

ADP Velocity Data

The ADP data presented herein is the most comprehensive information available for interpreting the tidal and non-tidal exchange across the western boundary of the bay. Net inflow is found to occur in the central and northern part of the bay; whereas, net outflow is found to

occur in the southern area of the western boundary. The magnitudes of ebb and flood tidal velocities indicate only slight variations with depth at all three stations.

The ADP data provides the best information to date for describing tidal and long-term non-tidal exchanges across the open western boundary of Florida Bay. The central and northern part of the 81° 05' W meridian, from East Cape to Marathon, has the characteristics as a region of net inflow, while the southern part of the western boundary appears to be a region of net outflow. Tide-induced transport is apparently eastward across the boundary. Wind effects are more pronounced in the southern area of the bay where tidal amplitudes are reduced, as indicated in the current and water-level data.

The need to consider the water column in multiple layers seems to depend upon the questions being asked. The instantaneous current (dominated by the ebb and flood of the tide) is similar in speed and direction from top to bottom. Only when one considers cumulative effects over longer time scales do the top-to-bottom differences become apparent and significant--and then only at two of the three stations investigated here. At Station 3, except for stronger currents in the top layer, both the top and bottom parts of the water column appear to be moving as a single unit.

The ADP data illustrated that the flood tidal velocity magnitudes over the depth of flow were generally higher than the ebb tidal velocities. Seasonal changes (wet months vs dry months) were not clearly evident at most locations; however, Station 3 displayed a marked increase in velocity magnitudes occurring during December and January, which is a typically wet season .

ADCP Data

The intensive surveys constitute a valuable addition to an understanding of the circulation of Florida Bay. While the data are restricted to the eastern and southern fringes of the bay (Figure 2), these short time series provide a first look at 20 channels that play important roles in moving water within the bay. The two surveys were conducted to investigate seasonal differences.

The primary advantage of the boat-mounted ADCP technique of measuring channel discharge is the excellent spatial resolution that it provides in the lateral (across-channel) and vertical dimensions.

The ADCP database consists of 9-11 channel crossings. These surveys provide discharge and velocity values for the channels throughout a single tidal cycle. An important function of defining and collecting these type data is bounding the cross-section to capture as much flow as possible. When the channel is bounded on both sides, the only practical problem is water depth and how close to the shore a boat with an ADCP can go. When the channel is unbounded, then

exchanges that occur outside the last measurement on either side of the channel can influence the volume transport calculations. Similarly, when the channel is bounded by mangroves, "leakage" into or out of the channel can result in over- or underestimates of discharge through the cross section defined for the measurements. Therefore, location of lines was critical to capture as much of the flow as possible. Transect lines chosen for the ADCP data collection effort were bounded by distinct "hard" boundaries where possible in order to minimize the underestimate of flow. Maximum discharges observed within the openings ranged from 200 - 210,000 cfs for the extreme ebb and flood tide conditions. Seasonal variations in discharges were observable from the data collected.

Table 1
Location of Equipment

Type of Equipment	Location	Coordinates[1]	
		x	y
Acoustic Doppler Profiler	Station 1	628929	272514
	Station 2	628587	211875
	Station 3	628418	163482
Water Level Recorder	TG01 - Estes Fish Camp/MM84.0	785114	220640
	TG02 - Hungry Tarpon/MM77.5	758838	199879
	TG03 - Sea Bird Marina/MM69.5	722673	183761
	TG04 - Nichols Seafood/MM62.9	692750	166263
	TG05 - Pigeon Key/MM44.9	604527	134986
Weather Station	Station 1 - Johnson Key	687238	261378
	Station 2 - Buttonwood Key	749555	270546
	Station 3 - Butternut Key	815007	274105

[1]Positions are NAD 83 State Plane Zone 0901, U. S. foot.

Table 2
Florida Bay, Station 1, Weather Data Summary

Time Period	Data Range	Wind Speed m/sec	Resultant Wind Direction deg	Air Temperature °C	Relative Humidity %	Cumulative Rainfall mm	Barometric Pressure mm of Hg	Solar Radiation Flux* W/m²	Solar Radiation* kJ/m²
1996									
3/14-3/31	Maximum	12.51	124.863	27.28	97	22.61	767	1048	943
	Minimum	0.181		13.28	50.34		756	946	844
	Average of Maximum and Minimum	6.345		20.28	73.67		761.5	997	893.5
4/1-4/30	Maximum	14.01	96.084	28.95	96.7	54.86	767	1070	963
	Minimum	0.081		16.15	37.68		757	208.5	187.6
	Average of Maximum and Minimum	7.046		22.55	67.19		762	639.25	575.3
5/1-5/31	Maximum	11.55	115.102	30.6	98.2	170.70	767	1158	1042
	Minimum	0.014		23.34	61.5		755	491.1	442
	Average of Maximum and Minimum	5.782		26.97	79.85		761	824.55	742
6/1-6/13	Maximum	13.29	94.701	30.22	94.6	17.78	765	1084	976
	Minimum	0.183		22.98	51.44		761	148.4	133.5
	Average of Maximum and Minimum	6.736		26.6	73.02		763	616.2	554.75
7/23-7/31	Maximum	10.46	95.167	31.36	91.8	9.14	766	1104	994
	Minimum	0.258		26.06	60.25		763	848	764
	Average of Maximum and Minimum	5.359		28.71	76.025		764.5	976	879
8/1-8/31	Maximum	11.68	86.183	31.58	97.6	115.06	766	1101	991

(Continued)

Table 2 (Continued)

Time Period	Data Range	Wind Speed m/sec	Resultant Wind Direction deg	Air Temperature °C	Relative Humidity %	Cumulative Rainfall mm	Barometric Pressure mm of Hg	Solar Radiation Flux* W/m²	Solar Radiation* kJ/m²
8/1-8/31 (Cont)	Minimum	0.04		22.91	57.79		758	756	680.7
	Average of Maximum and Minimum	5.86		27.245	77.695		762	928.5	835.85
9/1-9/30	Maximum	9.31	81.873	33.57	95.5	148.60	764	1086	978
	Minimum	0.063		24.13	57.26		755	419.5	377.5
	Average of Maximum and Minimum	4.687		28.85	76.38		759.5	752.75	677.75
10/1-10/31	Maximum	13.61	65.149	30.17	98.6	122.68	767	1050	945
	Minimum	0.18		21.4	55.09		752	295.7	266.1
	Average of Maximum and Minimum	6.895		25.785	76.845		759.5	672.85	605.55
11/1-11/30	Maximum	14.45	47.718	29.29	97.8	10.69	770	847	762
	Minimum	0.05		15.2	40.16		759	391.8	352.6
	Average of Maximum and Minimum	7.25		22.245	68.98		764.5	619.4	557.3
12/1-12/31	Maximum	12.44	41.913	26.93	100	2.03	769	751	676.2
	Minimum	0.122		8.25	34.46		759	438.6	394.7
	Average of Maximum and Minimum	6.281		17.59	67.23		764	594.8	535.45
1997									
1/1-1/31	Maximum	13.68	45.732	26.71	100	109.48	771	894	805
	Minimum	0.083		6.065	28.64		757	398.9	359

(Continued)

Table 2 (Concluded)

Time Period	Data Range	Wind Speed m/sec	Resultant Wind Direction deg	Air Temperature °C	Relative Humidity %	Cumulative Rainfall mm	Barometric Pressure mm of Hg	Solar Radiation Flux* W/m²	Solar Radiation* kJ/m²
1/1-1/31 (Cont)	Average of Maximum and Minimum	6.882		16.387	64.32		764	646.45	
2/1-2/28	Maximum	12.84	81.873	27.14	100	8.89	770	910	819
	Minimum	0.132		15.52	54.59		762	493.4	444.1
	Average of Maximum and Minimum	6.486		21.33	77.295		766	701.7	631.55
3/1-3/31	Maximum	12.55	89.118	27.95	100	74.93	768	1079	971
	Minimum	0.16		20.77	62.59		756	418.1	376.3
	Average of Maximum and Minimum	6.355		24.36	81.295		762	748.55	673.65
4/1-4/23	Maximum	11.02	86.858	27.54	98.7	18.55	766	1069	962
	Minimum	0.152		15.15	26.3		754	768	691.6
	Average of Maximum and Minimum	5.586		21.345	62.5		760	918.5	826.8

* Minimum values are the minimum of the maximum values.

Table 3
Florida Bay, Station 2, Weather Data Summary

Time Period	Data Range	Wind Speed m/sec	Resultant Wind Direction deg	Air Temperature °C	Relative Humidity %	Cumulative Rainfall mm	Barometric Pressure mm of Hg	Solar Radiation Flux* W/m²	Solar Radiation* kJ/m²
1996									
3/15-3/31	Maximum	13.03	135.722	27.42	97.1	25.65	766	1085	976
	Minimum	0.157		12.47	45.46		755	948	853
	Average of Maximum and Minimum	6.593		19.945	71.28		760.5	1016.5	914.5
4/1-4/20	Maximum	13.54	96.682	28.07	96.6	27.94	766	1218	1096
	Minimum	0.219		16.03	32.71		757	209.3	188.3
	Average of Maximum and Minimum	6.879		22.05	64.655		761.5	713.65	642.15
6/1-6/12	Maximum	11.96	101.89	29.87	99.1	92.71	764	1091	982
	Minimum	0.208		23.39	52.78		760	777	699
	Average of Maximum and Minimum	6.084		26.63	75.94		762	934	840.5
7/22-7/31	Maximum	10.48	103.104	31.33	95.7	6.86	766	1104	993
	Minimum	0.053		26.53	56.16		762	860	774
	Average of Maximum and Minimum	5.266		28.93	75.93		764	982	883.5
8/1-8/31	Maximum	12.14	98.054	31.63	100	125.99	766	1145	1031
	Minimum	0.166		23.45	0.398		757	584.3	525.9
	Average of Maximum and Minimum	6.153		27.54	50.199		761.5	864.65	778.45

(Continued)

Table 3 (Continued)

Time Period	Data Range	Wind Speed m/sec	Resultant Wind Direction deg	Air Temperature °C	Relative Humidity %	Cumulative Rainfall mm	Barometric Pressure mm of Hg	Solar Radiation Flux* W/m²	Solar Radiation* kJ/m²
9/1-9/30	Maximum	11.79	108.796	32.13	99.6	138.68	765	1047	943
	Minimum	0.178		23.8	0.464		754	389.7	350.8
	Average of Maximum and Minimum	5.984		27.965	50.032		759.5	718.35	646.9
10/1-10/31	Maximum	13.55	73.402	29.74	100	185.67	768	989	890
	Minimum	0.2		20.84	0		752	221.1	199
	Average of Maximum and Minimum	6.875		25.29	50		760	605.05	544.5
11/1-11/30	Maximum	14.02	55.449	29.2	98.5	14.48	770	930	837
	Minimum	0.179		15.31	44.15		759	343	308.7
	Average of Maximum and Minimum	7.1		22.255	71.325		764.5	636.5	572.85
12/1-12/31	Maximum	12.93	44.122	26.29	100	4.57	769	761	685.2
	Minimum	0.142		8.46	28.61		760	264.9	238.4
	Average of Maximum and Minimum	6.536		17.375	64.305		764.5	512.95	461.8
1997									
1/1-1/31	Maximum	13.71	48.734	26.64	100	55.88	771	921	829
	Minimum	0.146		5.31	26.97		757	314	282.6
	Average of Maximum and Minimum	6.928		15.975	63.485		764	617.5	555.8
2/1-2/28	Maximum	12.41	96.158	26.59	100	12.95	771	1062	956

(Continued)

Table 3 (Concluded)

Time Period	Data Range	Wind Speed m/sec	Resultant Wind Direction deg	Air Temperature °C	Relative Humidity %	Cumulative Rainfall mm	Barometric Pressure mm of Hg	Solar Radiation Flux* W/m²	Solar Radiation* kJ/m²
2/1-2/28 (Cont)	Minimum	0.048		14.83	49.78		762	0	0
	Average of Maximum and Minimum	6.229		20.71	74.89		766.5	531	478
3/1-3/31	Maximum	11.73	105.986	28.3	100	48.00	769	1049	944
	Minimum	0.091		19.98	57.99		757	702	631.6
	Average of Maximum and Minimum	5.91		24.14	78.995		763	875.5	787.8
4/1-4/26	Maximum	12.06	105.162	--	100	1.52	767	1036	932
	Minimum	0.178		--	17.65		753	561.4	505.2
	Average of Maximum and Minimum	6.119		--	58.825		760	798.7	718.6

* Minimum values are the minimum of the maximum values.
-- Equipment malfunction; data unavailable

Table 4
Florida Bay, Station 3, Weather Data Summary

Time Period	Data Range	Wind Speed m/sec	Resultant Wind Direction deg	Air Temperature °C	Relative Humidity %	Cumulative Rainfall mm	Barometric Pressure mm of Hg	Solar Radiation Flux* W/m²	Solar Radiation* kJ/m²
1996									
3/16-3/31	Maximum	12.56	156.148	26.42	97.9	0.0	766	1040	936
	Minimum	0.128		12.86	52		755	917	825
	Average of Maximum and Minimum	6.344		19.64	74.95		760.5	978.5	880.5
4/1-4/20	Maximum	14.41	92.43	28.56	97.4	1.52	766	1049	944
	Minimum	0.196		16.24	47.78		756	204.7	184.2
	Average of Maximum and Minimum	7.303		22.4	72.59		761	626.85	564.1
6/1-6/13	Maximum	11.12	95.462	29.88	96.8	3.30	765	1061	955
	Minimum	0.123		23.39	52.82		760	336.5	302.9
	Average of Maximum and Minimum	5.622		26.635	74.81		762.5	698.75	628.95
7/22-7/31	Maximum	9.87	99.593	30.96	93.8	0.0	767	1056	950
	Minimum	0.196		25.65	63.79		763	514.4	463
	Average of Maximum and Minimum	5.033		28.305	78.795		765	785.2	706.5
8/1-8/31	Maximum	10.45	103.669	31.27	93.8	2.03	765	1110	999
	Minimum	0.063		25.43	60.6		760	748	673.3
	Average of Maximum and Minimum	5.256		28.35	77.2		762.5	929	836.15
9/1-9/30	Maximum	9.93	116.959	32.56	98.3	.76	765	1170	1053

(Continued)

Table 4 (Continued)

Time Period	Data Range	Wind Speed m/sec	Resultant Wind Direction deg	Air Temperature °C	Relative Humidity %	Cumulative Rainfall mm	Barometric Pressure mm of Hg	Solar Radiation Flux* W/m²	Solar Radiation* kJ/m²
9/1-9/30 (Cont)	Minimum	0.028		23.74	60.86		754	420.9	378.8
	Average of Maximum and Minimum	4.979		28.15	79.58		759.5	795.45	715.9
10/1-10/31	Maximum	13.98	72.008	29.73	100	2.03	768	940	846
	Minimum	0.212		21.4	57.22		752	115.6	104
	Average of Maximum and Minimum	7.096		25.565	78.61		760	527.8	475
11/1-11/30	Maximum	10.67	63.172	28.64	96.7	.25	766	849	765
	Minimum	0.103		23.26	72.3		760	773	695.8
	Average of Maximum and Minimum	5.386		25.95	84.5		763	811	730.4
12/1-12/31	Maximum	13.47	45.642	26.5	100	.51	769	897	808
	Minimum	0.154		9.18	31.87		760	281.4	253.3
	Average of Maximum and Minimum	6.812		17.84	65.935		764.5	589.2	530.65
1997									
1/1-1/31	Maximum	14.47	51.221	26.69	100	97.79	770	825	743
	Minimum	0.101		7.01	30.96		757	246.4	221.7
	Average of Maximum and Minimum	7.286		16.85	65.48		763.5	535.7	482.35
2/1-2/28	Maximum	12.35	90.637	26.91	100	9.91	770	982	884
	Minimum	0.037		15.54	52.27		762	498.8	448.9

(Continued)

Table 4 (Concluded)

Time Period	Data Range	Wind Speed m/sec	Resultant Wind Direction deg	Air Temperature °C	Relative Humidity %	Cumulative Rainfall mm	Barometric Pressure mm of Hg	Solar Radiation Flux* W/m²	Solar Radiation* kJ/m²
2/1-2/28 (Cont)	Average of Maximum and Minimum	6.194		21.225	76.135		766	740.4	666.45
3/1-3/31	Maximum	11.42	103.305	28.35	99.2	30.48	769	1023	920
	Minimum	0.025		20.29	58.89		757	697.9	628.1
	Average of Maximum and Minimum	5.722		24.32	79.045		763	860.45	774.05
4/1-4/24	Maximum	12.7	102.889	29.08	99.4	18.54	767	1106	996
	Minimum	0.122		15.82	24.32		753	267.5	240.8
	Average of Maximum and Minimum	6.411		22.45	61.86		760	686.75	618.4

* Minimum values are the minimum of the maximum values.

Table 5
Florida Bay, Station 1, Acoustic Doppler Profiler Data Summary

Time Period	Depth	Flow Direction	Velocity				Head of Water Above Instrument		Temperature	
			Direction		Magnitude					
			Minimum deg	Maximum deg	Minimum cm/sec	Maximum cm/sec	Minimum m	Maximum m	Minimum °C	Maximum °C
1996										
3/14-3/31	Surface	Ebb	90.0	281.8	3.3	76.6	2.0	3.6	16.1	27.4
		Flood	108.4	111.3	.9	106.4				
	Middepth	Ebb	299.5	283.5	2.6	54.4				
		Flood	21.3	101.5	4.4	86.7				
	Bottom	Ebb	0	279.3	2.0	52.1				
		Flood	337.6	99.3	5.0	83.8				
4/23-4/30	Surface	Ebb	342.5	286.3	2.0	72.0	2.2	3.5	24.4	29.2
		Flood	63.4	112.5	.9	62.8				
	Middepth	Ebb	189.5	277.2	2.4	50.5				
		Flood	135.0	105.9	3.8	53.3				
	Bottom	Ebb	210.6	287.2	2.6	44.3				
		Flood	35.1	110.6	3.3	45.8				
5/1-5/31	Surface	Ebb	302.5	267.2	1.3	79.3	1.9	3.6	25.4	31.2
		Flood	135.0	105.7	.3	72.5				
	Middepth	Ebb	180.0	275.8	1.0	52.5				
		Flood	346.0	103.8	1.2	54.3				
	Bottom	Ebb	198.4	273.3	1.3	51.5				

(Continued)

Table 5 (Continued)

Time Period	Depth	Flow Direction	Velocity				Head of Water Above Instrument		Temperature	
			Direction		Magnitude					
			Minimum deg	Maximum deg	Minimum cm/sec	Maximum cm/sec	Minimum m	Maximum m	Minimum °C	Maximum °C
5/1-5/31 (Cont)	Bottom (Cont)	Flood	94.4	102.2	1.3	48.0				
6/1-6/30	Surface	Ebb	284.0	251.3	.4	79.7	1.9	3.7	26.2	30.8
		Flood	346.0	94.0	0.8	68.4				
	Middepth	Ebb	241.7	274.9	1.5	50.8				
		Flood	0	103.5	.6	53.1				
	Bottom	Ebb	66.0	301.9	1.0	69.3				
		Flood	0	120.1	.4	65.6				
7/1-7/31	Surface	Ebb	200.6	260.1	1.7	77.5	2.1	3.9	27.7	31.8
		Flood	270.0	96.1	.1	80.4				
	Middepth	Ebb	274.4	268.5	1.3	53.3				
		Flood	288.4	93.4	.9	64.1				
	Bottom	Ebb	168.7	269.4	.5	55.7				
		Flood	0	91.0	.2	56.3				
8/1-8/31	Surface	Ebb	143.1	268.8	1.5	73.6	2.2	3.9	27.4	31.8
		Flood	333.4	91.1	.2	76.0				
	Middepth	Ebb	90.0	271.2	.6	50.7				
		Flood	355.6	93.4	1.3	62.0				
	Bottom	Ebb	180.0	268.0	1.1	49.9				

(Continued)

Table 5 (Continued)

Time Period	Depth	Flow Direction	Velocity				Head of Water Above Instrument		Temperature	
			Direction		Magnitude					
			Minimum deg	Maximum deg	Minimum cm/sec	Maximum cm/sec	Minimum m	Maximum m	Minimum °C	Maximum °C
8/1-8/31 (Cont)	Bottom (Cont)	Flood	108.4	94.6	.9	56.5				
9/1-9/30	Surface	Ebb	320.7	261.8	1.4	83.4	2.3	3.8	27.7	32.1
		Flood	270.0	97.7	.9	90.0				
	Middepth	Ebb	139.1	262.8	2.0	53.6				
		Flood	344.5	94.0	1.9	69.8				
	Bottom	Ebb	278.1	270.9	.7	53.6				
		Flood	123.7	99.9	.4	59.2				
10/1-10/31	Surface	Ebb	190.6	286.0	1.6	83.6	2.3	4.0	23.6	28.5
		Flood	225.0	124.6	.1	70.5				
	Middepth	Ebb	348.7	283.1	2.0	55.9				
		Flood	38.7	109.9	2.6	65.4				
	Bottom	Ebb	66.4	291.6	1.7	57.5				
		Flood	45.0	103.6	1.0	58.4				
11/1-11/30	Surface	Ebb	222.7	270.8	1.9	80.4	2.0	3.8	19.0	27.8
		Flood	350.5	140.6	.6	88.3				
	Middepth	Ebb	317.3	294.4	1.8	57.8				
		Flood	265.4	123.3	2.5	64.3				
	Bottom	Ebb	122.5	286.9	1.3	55.2				

(Continued)

Table 5 (Continued)

Time Period	Depth	Flow Direction	Velocity				Head of Water Above Instrument		Temperature	
			Direction		Magnitude					
			Minimum deg	Maximum deg	Minimum cm/sec	Maximum cm/sec	Minimum m	Maximum m	Minimum °C	Maximum °C
11/1-11/30 (Cont)	Bottom (Cont)	Flood	63.4	121.2	1.3	61.5				
12/1-12/31	Surface	Ebb	132.3	281.9	1.5	69.4	1.8	3.5	14.8	24.2
		Flood	180.0	112.5	.1	70.1				
	Middepth	Ebb	260.5	284.7	3.0	60.9				
		Flood	153.4	109.3	1.1	64.2				
	Bottom	Ebb	0	278.5	.1	57.6				
		Flood	31.0	111.2	.6	59.3				
1997										
1/1-1/31	Surface	Ebb	286.9	300.8	2.4	78.7	1.2	3.7	12.8	24.8
		Flood	153.4	126.9	.7	96.8				
	Middepth	Ebb	157.8	287.9	2.4	57.5				
		Flood	270.0	116.3	.6	79.1				
	Bottom	Ebb	213.7	281.7	.7	61.2				
		Flood	119.1	116.5	1.0	72.9				
2/1-2/28	Surface	Ebb	189.5	283.4	.6	79.2	1.9	3.7	19.7	25.7
		Flood	217.6	134.4	1.6	71.4				
	Middepth	Ebb	133.0	292.8	2.1	55.0				
		Flood	225.0	125.4	.4	65.3				

(Continued)

Table 5 (Concluded)

Time Period	Depth	Flow Direction	Velocity				Head of Water Above Instrument		Temperature	
			Direction		Magnitude					
			Minimum deg	Maximum deg	Minimum cm/sec	Maximum cm/sec	Minimum m	Maximum m	Minimum °C	Maximum °C
2/1-2/28 (Cont)	Bottom (Cont)	Ebb	303.7	285.7	.4	64.5				
		Flood	63.4	127.0	1.3	67.7				
3/1-3/31	Surface	Ebb	270.0	289.0	1.1	78.8	1.9	3.7	22.8	28.4
		Flood	80.5	131.5	.6	79.2				
	Middepth	Ebb	0	290.5	.7	52.0				
		Flood	220.6	128.2	.9	54.1				
	Bottom	Ebb	15.9	297.8	.7	51.3				
		Flood	158.2	126.7	.5	54.2				
4/1-4/22	Surface	Ebb	0	313.8	1.5	76.2	1.9	3.6	22.1	27.0
		Flood	100.6	132.0	1.6	60.0				
	Middepth	Ebb	260.5	294.1	.6	49.0				
		Flood	70.0	125.4	1.2	58.3				
	Bottom	Ebb	0	302.0	1.9	49.8				
		Flood	265.6	123.1	1.3	51.3				

Table 6
Florida Bay, Station 2, Acoustic Doppler Profiler Data Summary

Time Period	Depth	Flow Direction	Velocity				Head of Water Above Instrument		Temperature	
			Direction		Magnitude					
			Minimum deg	Maximum deg	Minimum cm/sec	Maximum cm/sec	Minimum m	Maximum m	Minimum °C	Maximum °C
1996										
3/14-3/31	Surface	Ebb	285.9	308.1	1.5	44.4	2.0	3.5	17.4	25.4
		Flood	338.2	136.4	2.7	53.7				
	Middepth	Ebb	180.0	316.7	2.4	42.4				
		Flood	125.0	135.2	1.2	52.4				
	Bottom	Ebb	230.7	314.8	1.4	37.3				
		Flood	319.9	138.0	2.5	50.3				
4/1-4/30	Surface	Ebb	156.8	313.5	2.3	44.9	1.9	3.4	22.0	28.0
		Flood	16.5	132.0	2.8	49.3				
	Middepth	Ebb	246.8	311.3	.8	41.8				
		Flood	9.5	135.2	1.8	45.3				
	Bottom	Ebb	296.6	311.5	.2	40.7				
		Flood	0	136.6	.3	40.3				
5/1-5/31	Surface	Ebb	258.7	312.7	.5	46.6	1.8	3.3	25.9	30.7
		Flood	40.6	133.2	.9	43.8				
	Middepth	Ebb	270.0	304.2	1.7	45.2				
		Flood	110.2	133.5	2.0	41.1				
	Bottom	Ebb	254.1	310.1	.7	45.5				

(Continued)

Table 6 (Continued)

Time Period	Depth	Flow Direction	Velocity				Head of Water Above Instrument		Temperature	
			Direction		Magnitude					
			Minimum deg	Maximum deg	Minimum cm/sec	Maximum cm/sec	Minimum m	Maximum m	Minimum °C	Maximum °C
5/1-5/31 (Cont)	Bottom (Cont)	Flood	58.0	133.9	1.9	34.4				
6/1-6/30	Surface	Ebb	249.0	269.6	1.4	51.6	1.7	3.4	27.2	31.2
		Flood	336.0	208.3	2.0	53.4				
	Middepth	Ebb	18.4	63.9	.3	117.0				
		Flood	71.6	84.8	1.6	105.4				
	Bottom	Ebb	180.0	63.2	.5	171.8				
		Flood	0	73.1	.5	153.0				
7/1-7/31	Surface	Ebb	209.1	307.8	2.1	44.5	1.7	3.4	28.2	31.8
		Flood	94.4	39.1	1.3	46.9				
	Middepth	Ebb	293.2	247.4	.8	99.1				
		Flood	49.4	270.1	2.8	62.1				
	Bottom	Ebb	346.0	71.3	.8	105.3				
		Flood	352.9	81.6	.8	118.4				
8/1-8/31	Surface	Ebb	213.7	311.6	.4	43.7	1.9	3.3	28.1	31.7
		Flood	55.8	131.7	3.0	46.0				
	Middepth	Ebb	62.1	313.0	1.9	39.8				
		Flood	338.2	134.0	.5	42.5				
	Bottom	Ebb	253.3	189.1	1.0	44.8				

(Continued)

Table 6 (Continued)

Time Period	Depth	Flow Direction	Velocity				Head of Water Above Instrument		Temperature	
			Direction		Magnitude					
			Minimum deg	Maximum deg	Minimum cm/sec	Maximum cm/sec	Minimum m	Maximum m	Minimum °C	Maximum °C
8/1-8/31 (Cont)	Bottom (Cont)	Flood	122.5	122.4	1.3	34.1				
9/1-9/30	Surface	Ebb	225.0	314.9	1.3	40.8	1.9	3.3	28.0	31.8
		Flood	279.0	129.9	1.9	42.9				
	Middepth	Ebb	63.4	317.1	.2	40.1				
		Flood	135.0	141.1	1.1	41.7				
	Bottom	Ebb	108.4	333.3	.3	42.4				
		Flood	28.3	120.4	1.5	31.2				
10/1-10/31	Surface	Ebb	276.3	326.0	.9	43.8	1.9	3.4	24.4	28.7
		Flood	111.8	141.7	1.1	42.8				
	Middepth	Ebb	315.0	325.6	1.7	40.4				
		Flood	37.6	150.3	1.6	37.1				
	Bottom	Ebb	302.7	315.4	1.7	37.9				
		Flood	113.2	149.7	1.5	32.5				
11/1-11/30	Surface	Ebb	180.0	295.6	.8	41.6	1.9	3.4	20.0	27.4
		Flood	213.7	111.5	1.1	42.6				
	Middepth	Ebb	180.0	289.5	1.2	40.7				
		Flood	262.9	126.0	.8	43.9				
	Bottom	Ebb	123.7	298.5	.7	42.1				

(Continued)

Table 6 (Continued)

Time Period	Depth	Flow Direction	Velocity				Head of Water Above Instrument		Temperature	
			Direction		Magnitude					
			Minimum deg	Maximum deg	Minimum cm/sec	Maximum cm/sec	Minimum m	Maximum m	Minimum °C	Maximum °C
11/1-11/30 (Cont)	Bottom (Cont)	Flood	45.0	119.1	1.3	39.0				
12/1-12/31	Surface	Ebb	180.0	292.8	2.0	44.1	1.8	3.3	16.7	23.9
		Flood	90.0	108.5	.4	44.1				
	Middepth	Ebb	123.7	291.5	1.8	41.3				
		Flood	251.6	107.8	.3	43.6				
	Bottom	Ebb	26.6	289.2	.7	37.9				
		Flood	3.8	118.7	1.5	37.1				
1997										
1/1-1/31	Surface	Ebb	143.1	294.0	1.5	46.5	1.8	3.5	15.1	24.3
		Flood	189.5	117.8	1.2	57.9				
	Middepth	Ebb	146.3	294.7	.4	47.7				
		Flood	66.4	126.8	1.7	55.9				
	Bottom	Ebb	49.4	297.4	.9	38.7				
		Flood	53.1	129.5	2.0	52.8				
2/1-2/8	Surface	Ebb	186.7	299.4	3.4	46.3	1.8	3.5	20.3	23.4
		Flood	29.9	121.4	3.8	47.0				
	Middepth	Ebb	159.0	300.2	2.8	44.9				
		Flood	32.5	118.2	3.9	43.1				

(Continued)

Table 6 (Concluded)

Time Period	Depth	Flow Direction	Velocity				Head of Water Above Instrument		Temperature	
			Direction		Magnitude					
			Minimum deg	Maximum deg	Minimum cm/sec	Maximum cm/sec	Minimum m	Maximum m	Minimum °C	Maximum °C
2/1-2/8 (Cont)	Bottom (Cont)	Ebb	0	294.6	0	38.4				
		Flood	15.4	121.0	3.0	38.0				
3/20-3/21	Surface	Ebb	166.0	318.1	7.0	32.6	2.2	3.3	24.7	25.2
		Flood	37.0	146.9	6.6	37.1				
	Middepth	Ebb	266.1	322.9	2.9	33.0				
		Flood	22.7	127.8	6.0	34.6				
	Bottom	Ebb	250.3	322.5	3.0	29.1				
		Flood	347.2	121.5	5.8	29.9				

Table 7
Florida Bay, Station 3, Acoustic Doppler Profiler Data Summary

Time Period	Depth	Flow Direction	Velocity				Head of Water Above Instrument		Temperature	
			Direction		Magnitude					
			Minimum deg	Maximum deg	Minimum cm/sec	Maximum cm/sec	Minimum m	Maximum m	Minimum °C	Maximum °C
1996										
3/14-3/31	Surface	Ebb	330.3	168.7	3.2	29.5	1.4	2.3	17.7	26.5
		Flood	176.6	164.8	5.0	37.1				
	Middepth	Ebb	119.7	170.8	.8	25.7				
		Flood	103.8	166.6	5.5	33.7				
	Bottom	Ebb	28.6	162.0	1.3	28.5				
		Flood	226.5	168.0	2.8	35.7				
4/23-4/30	Surface	Ebb	317.2	17.1	3.7	29.9	1.4	2.1	24.4	28.6
		Flood	16.9	176.4	2.4	28.9				
	Middepth	Ebb	86.6	350.7	1.7	26.6				
		Flood	74.1	181.8	2.9	28.0				
	Bottom	Ebb	4.4	11.5	2.6	26.1				
		Flood	68.2	10.8	1.6	24.6				
5/1-5/31	Surface	Ebb	310.6	216.9	3.7	29.6	1.4	2.2	25.8	31.5
		Flood	290.2	184.7	2.0	29.5				
	Middepth	Ebb	8.6	354.8	3.3	28.7				
		Flood	219.0	184.7	2.7	28.3				
	Bottom	Ebb	71.6	34.2	3.2	30.5				

(Continued)

Table 7 (Continued)

Time Period	Depth	Flow Direction	Velocity				Head of Water Above Instrument		Temperature	
			Direction		Magnitude					
			Minimum deg	Maximum deg	Minimum cm/sec	Maximum cm/sec	Minimum m	Maximum m	Minimum °C	Maximum °C
5/1-5/31 (Cont)	Bottom (Cont)	Flood	288.4	34.8	.9	33.8				
6/1-6/30	Surface	Ebb	44.1	70.6	4.3	30.8	1.4	2.3	26.9	31.7
		Flood	87.7	177.9	2.5	29.6				
	Middepth	Ebb	225.0	359.0	2.4	27.4				
		Flood	79.2	176.2	2.1	30.4				
	Bottom	Ebb	219.8	358.5	1.6	26.5				
		Flood	126.5	168.9	3.4	26.6				
7/1-7/31	Surface	Ebb	342.5	213.3	4.0	30.3	1.4	2.5	27.7	32.1
		Flood	270.0	155.5	1.5	31.8				
	Middepth	Ebb	325.8	241.0	3.4	27.9				
		Flood	46.6	153.5	2.5	28.5				
	Bottom	Ebb	346.0	243.9	1.6	26.8				
		Flood	301.0	177.9	.6	30.5				
8/1-8/31	Surface	Ebb	314.0	340.0	4.0	26.9	1.6	2.3	28.1	32.5
		Flood	90.0	144.2	1.9	33.0				
	Middepth	Ebb	210.3	225.8	2.8	25.2				
		Flood	36.9	149.7	1.0	31.5				
	Bottom	Ebb	69.4	256.1	1.7	27.4				

(Continued)

Table 7 (Continued)

Time Period	Depth	Flow Direction	Velocity				Head of Water Above Instrument		Temperature	
			Direction		Magnitude					
			Minimum deg	Maximum deg	Minimum cm/sec	Maximum cm/sec	Minimum m	Maximum m	Minimum °C	Maximum °C
8/1-8/31 (Cont)	Bottom (Cont)	Flood	108.4	147.9	1.3	28.6				
9/1-9/30	Surface	Ebb	171.3	171.4	1.3	26.6	1.6	2.3	27.7	32.7
		Flood	152.2	143.7	2.1	30.9				
	Middepth	Ebb	302.7	162.4	1.7	27.4				
		Flood	87.3	159.8	2.1	31.2				
	Bottom	Ebb	250.3	254.2	1.5	26.1				
		Flood	318.8	146.4	1.1	29.8				
10/1-10/31	Surface	Ebb	0	25.6	.8	30.3	1.6	2.3	24.4	28.7
		Flood	58.4	183.6	3.1	31.7				
	Middepth	Ebb	348.7	10.1	3.1	30.8				
		Flood	91.7	172.5	3.3	28.4				
	Bottom	Ebb	119.1	19.9	1.0	29.7				
		Flood	161.6	99.2	1.6	30.6				
11/1-11/30	Surface	Ebb	264.0	176.4	3.8	30.2	1.7	2.6	19.7	27.8
		Flood	90.0	189.8	.3	34.2				
	Middepth	Ebb	304.4	249.8	4.6	33.3				
		Flood	243.4	187.2	.9	30.3				
	Bottom	Ebb	254.3	245.9	3.3	32.6				

(Continued)

Table 7 (Continued)

Time Period	Depth	Flow Direction	Velocity				Head of Water Above Instrument		Temperature	
			Direction		Magnitude					
			Minimum deg	Maximum deg	Minimum cm/sec	Maximum cm/sec	Minimum m	Maximum m	Minimum °C	Maximum °C
11/1-11/30 (Cont)	Bottom (Cont)	Flood	78.7	147.2	2.0	41.0				
12/1-12/31	Surface	Ebb	199.2	110.7	4.6	267.3	1.7	2.9	16.7	24.4
		Flood	162.6	115.8	3.4	276.4				
	Middepth	Ebb	171.9	102.1	.7	188.8				
		Flood	100.6	69.8	1.6	192.4				
	Bottom	Ebb	265.0	320.2	2.3	201.2				
		Flood	34.7	83.5	1.6	249.8				
1997										
1/1-1/31	Surface	Ebb	84.9	44.4	4.5	94.8	1.7	2.8	14.5	25.0
		Flood	9.5	31.9	1.8	106.9				
	Middepth	Ebb	341.6	219.2	2.2	121.2				
		Flood	131.2	225.0	1.1	136.7				
	Bottom	Ebb	90.0	39.7	.2	197.6				
		Flood	180.0	185.6	.1	203.9				
2/1-2/28	Surface	Ebb	297.9	26.3	3.8	29.1	1.5	2.5	20.7	25.6
		Flood	277.4	193.8	2.3	36.1				
	Middepth	Ebb	231.8	332.7	1.8	56.6				
		Flood	296.6	184.9	1.1	32.6				

(Continued)

Table 7 (Concluded)

Time Period	Depth	Flow Direction	Velocity				Head of Water Above Instrument		Temperature	
			Direction		Magnitude					
			Minimum deg	Maximum deg	Minimum cm/sec	Maximum cm/sec	Minimum m	Maximum m	Minimum °C	Maximum °C
2/1-2/28 (Cont)	Bottom (Cont)	Ebb	304.5	29.3	1.9	26.7				
		Flood	244.4	185.5	2.8	31.0				
3/1-3/31	Surface	Ebb	303.0	19.3	2.4	30.0	1.5	2.5	23.3	28.8
		Flood	354.3	195.7	1.0	32.9				
	Middepth	Ebb	16.9	15.3	3.4	28.5				
		Flood	42.7	174.3	1.8	32.4				
	Bottom	Ebb	53.1	34.7	.5	27.6				
		Flood	105.9	159.3	.7	29.7				
4/1-4/22	Surface	Ebb	300.3	28.1	1.4	28.9	1.6	2.3	23.2	27.6
		Flood	321.3	212.1	1.3	32.2				
	Middepth	Ebb	5.7	302.4	2.0	28.9				
		Flood	333.4	234.0	2.2	29.3				
	Bottom	Ebb	312.0	37.0	1.3	28.9				
		Flood	252.5	201.4	2.0	27.4				

Table 8
Florida Bay, Stations 1-3, ADP Collection Summary

Station	Start Date	End Date	Quarter Hours[1]	Number Missing[2]	Percent Missing
ADP1	3/14/96	4/22/97	38,820	3,013	7.76
ADP2[3]	3/14/96	2/8/97	31,814	2,651	8.33
ADP3[4]	3/14/96	4/22/97	38,844	3,668	9.44

[1]Maximum possible number of observations between start and end dates.
[2]Number of quarter-hour observations randomly dropped during study period.
[3]Data recorded 6/26/96-7/1/96 contain spurious values; this part of record not used to characterize general flow patterns, including tidal currents, nor to quantify the response to wind forcing.
[4]Data recorded 12/5/96-2/8/97 contain spurious values; this part of record not used to characterize general flow patterns, including tidal currents, nor to quantify the response to wind forcing.

Table 9
Station Summary for ADCP Transects

Range	Channel Name	Survey 1			Survey 2			Latitude deg	Longitude deg
		Date	No. of Crossings	Hours est	Date	No. of Crossings	Hours est		
1	Jewfish Creek	9/26/96	11	0725-1657	2/11/97	9	0841-1605	25.18	80.39
2	Adams Cut	9/26/96	11	0746-1708	2/11/97	9	0857-1620	25.14	80.41
3	Dusenbury Creek	9/26/96	10	0830-1718	2/11/97	9	0821-1548	25.14	80.43
4	Grouper Creek	9/26/96	10	0712-1602	2/11/97	9	0752-1600	25.12	80.45
5	Baker Cut	9/26/96	10	0722-1614	2/11/97	9	0805-1608	25.09	80.47
6	Tavernier Creek	9/27/96	10	0646-1557	2/10/97	10	0730-1600	25.01	80.55
7	Cowpens Cut	9/27/96	10	0654-1602	2/10/97	10	0733-1605	25.00	80.56
8	Snake Creek	9/27/96	9	0850-1623	2/10/97	10	0709-1555	24.96	80.59
9	Whale Harbor Channel	9/27/96	9	0812-1607	2/10/97	10	0725-1607	24.94	80.61
10	Tea Table Relief	9/28/96	10	0637-1600	2/9/97	10	0653-1606	24.90	80.66
11	Tea Table Channel	9/28/96	10	0645-1609	2/9/97	10	0658-1612	24.90	80.67
12	Indian Key Channel	9/28/96	10	0701-1621	2/9/97	10	0710-1622	24.89	80.68
13	Lignumvitae Channel	9/28/96	10	0708-1630	2/10/97	10	0722-1631	24.89	80.69
14	Channel Two	9/28/96	10	0710-1604	2/9/97	10	0735-1555	24.84	80.75
15	Channel Five	9/28/96	10	0724-1619	2/9/97	10	0748-1609	24.84	80.77
16	Long Key Channel	9/29/96	10	0720-1606	2/8/97	10	0743-1555	24.80	80.87

(Continued)

Table 9 (Concluded)

Range	Channel Name	Survey 1			Survey 2			Latitude deg	Longitude deg
		Date	No. of Crossings	Hours est	Date	No. of Crossings	Hours est		
17	Tom's Harbor Cut	9/29/96	10	0621-1543	2/8/97	10	0735-1558	24.78	80.91
18	Tom's Harbor Channel	9/29/96	10	0633-1608	2/8/97	10	0744-1612	24.78	80.92
19	Seven Mile Bridge, east	9/30/96	8	0720-1530	2/7/97	9	0830-1558	24.71	81.14
20	Seven Mile Bridge, west	9/30/96	8	0730-1439	2/7/97	10	0728-1610	24.70	81.18

Note: Latitudes and longitudes are for the approximate midpoints of each range.

Table 10
Transect Line Coordinates, Intensive Survey 1

Line No.	Coordinates[1]			
	Start		End	
	x	y	x	y
1	858375	309764	858548	309583
2	853089	293102	853279	293120
3	846716	294563	846475	294608
4	839226	286906	839585	286935
5	832631	275810	832274	275859
6	806689	247767	806844	247809
7	802414	244452	802506	244353
8	790871	227996	791309	228199
9	784286	220612	785117	220867
10	768751	205273	768972	205394
11	767060	204490	766183	204026
12	762592	202034	760710	201063
13	759637	200577	758864	200094
14	739846	186164	738038	184982
15	733881	183023	728818	184263
16	694212	166371	706155	171098
17	687352	163655	685804	163169
18	683151	162017	681437	161410
19	614948	136166	604434	134118
20	604477	134189	580148	127040

[1]Positions are NAD 83 State Plane Zone 0901, U. S. foot.

Table 11
Transect Line Coordinates, Intensive Survey 2

Line No.	Coordinates[1]			
	Start		End	
	x	y	x	y
1	858375	309764	858548	309583
2	853089	293102	853279	293120
3	846716	294563	846475	294608
4	839226	286906	839585	286935
5	832631	275810	832274	275859
6	806689	247767	806844	247809
7	802414	244452	802506	244353
8	790871	227996	791309	228199
9	784286	220612	785117	220867
10	768751	205273	768972	205394
11	767060	204490	766183	204026
12	762592	202034	760710	201063
13	759637	200577	758864	200094
14	740018	186303	737744	184796
15	734110	183061	728601	184322
16	693648	166174	706098	171058
17	687352	163655	685804	163169
18	683151	162017	681437	161410
19	614948	136166	599960	133502
20	599960	133502	580482	126715

[1]Positions are NAD 83 State Plane Zone 0901, U. S. foot.

Table 12
Florida Bay Discharges, Intensive Survey 1

Date	Range No.	Time est	Discharge cfs
9/26/96	1[1]	725	-298
		806	-669
		902	-1,566
		956	-2,176
		1100	-2,756
		1157	-2,930
		1258	-3,265
		1359	-2,968
		1503	-2,871
		1558	-2,755
		1657	-2,263
	2[2]	746	-1,997
		819	-2,227
		915	-2,630
		1015	-2,720
		1120	-2,120
		1214	-1,643
		1320	+653
		1415	+1,038
		1520	+1,375
		1611	+1,345
		1708	+1,312
	3[1]	830	-1,085
		925	-774
		1024	-1,173
		1129	-1,196
		1226	-1,489
		1329	-1,222
		1425	-1,529

(Continued)

[1]Flow is to the north or to the south. Positive values are to the north; negative values are to the south.
[2]Flow is to the east or to the west. Positive values are to the east; negative values are to the west.

Table 12 (Continued)

Date	Range No.	Time est	Discharge cfs
9/26/96	3[1]	1530	-1,505
		1618	-1,220
		1718	-1,459
	4[1]	712	-724
		807	-795
		903	-1,012
		1004	-1,067
		1108	-847
		1214	-984
		1322	-1,239
		1402	-996
		1506	-1,016
		1602	-1,039
	5[1]	722	+889
		819	-169
		915	+169
		1015	+1,007
		1117	+929
		1222	+976
		1332	+439
		1414	+557
		1516	+455
		1614	+296
9/27/96	6[1]	646	+1,363
		751	+1,704
		848	+1,907
		950	+1,695
		1049	+1,692
		1156	+454
		1256	+689
		1358	-1,070

(Continued)

Table 12 (Continued)

Date	Range No.	Time est	Discharge cfs
9/27/96	6[1]	1506	-1,100
		1557	-971
	7[1]	654	-1,223
		756	-1,165
		851	-525
		956	+565
		1054	+800
		1201	+947
		1304	+571
		1404	-213
		1511	-686
		1602	-1,001
	8[1]	850	+7,666
		927	+7,192
		1015	+5,402
		1117	+1,030
		1218	-3,241
		1322	-4,226
		1411	-4,491
		1511	-3,851
		1623	-3,100
	9[1]	812	+15,050
		908	+14,250
		957	+10,850
		1056	+5,299
		1159	-4,921
		1258	-7,766
		1354	-8,291
		1454	-8,533
		1607	-6,860

(Continued)

Table 12 (Continued)

Date	Range No.	Time est	Discharge cfs
9/28/96	10[3]	637	+1,676
		737	+3,500
		846	+4,203
		1003	+4,341
		1105	+1,938
		1204	-862
		1303	-1,404
		1407	-1,471
		1528	-820
		1600	-909
	11[3]	645	+9,568
		743	+15,316
		854	+17,661
		1009	+16,207
		1110	+7,677
		1210	-1,601
		1309	-10,405
		1415	-12,974
		1533	-12,139
		1609	-9,758
	12[3]	701	+18,026
		755	+26,811
		907	+24,900
		1022	+21,412
		1122	+10,914
		1220	-4,219
		1319	-17,983
		1428	-20,443
		1544	-16,265
		1621	-15,231

(Continued)

[3]Flow is to the northwest or to the southeast. Positive values are to the northwest; negative values are to the southeast.

Table 12 (Continued)

Date	Range No.	Time est	Discharge cfs
9/28/96	13[3]	708	+7,443
		805	+9,198
		915	+9,608
		1031	+7,289
		1133	+2,994
		1232	-3,569
		1329	-5,851
		1435	-6,031
		1551	-5,430
		1630	-5,775
	14[3]	710	+32,267
		759	+48,050
		853	+53,650
		959	+49,200
		1105	+30,200
		1200	+7,120
		1256	-15,280
		1356	-38,970
		1505	-46,950
		1604	-42,550
	15[1]	724	+61,630
		825	+79,860
		910	+85,800
		1013	+77,260
		1118	+47,500
		1217	-210
		1310	-44,530
		1411	-66,600
		1519	-74,530
		1619	-69,850
9/29/96	16[3]	720	-19,330

(Continued)

Table 12 (Continued)

Date	Range No.	Time est	Discharge cfs
9/29/96	16[3]	802	-135,920
		856	-202,900
		958	-203,700
		1104	-174,700
		1202	-132,057
		1258	-59,400
		1401	+99,130
		1456	+189,900
		1606	+210,800
	17[1]	621	-11,291
		731	+5,164
		835	+16,100
		938	+22,250
		1032	+21,420
		1136	+16,269
		1230	+12,132
		1420	-12,016
		1503	-15,900
		1543	-21,610
	18[1]	633	-5,586
		742	+8,790
		844	+13,851
		948	+18,693
		1041	+18,652
		1145	+14,710
		1240	+10,615
		1440	-11,081
		1515	-15,886
		1608	-16,189
9/30/96	19[1]	720	-36,360
		820	+70,463

(Continued)

Table 12 (Concluded)

Date	Range No.	Time est	Discharge cfs
9/30/96	19[1]	935	+144,800
		1030	+144,655
		1230	+128,594
		1330	+76,935
		1430	-41,297
		1530	-34,600
	20[3]	730	+32,900
		839	+159,600
		942	+218,400
		1047	+244,000
		1147	+204,500
		1247	+139,540
		1341	+46,800
		1439	-173,500

Table 13
Florida Bay Discharges, Intensive Survey 2

Date	Range No.	Time est	Discharge cfs
2/7/97	19[1]	830	+203,261
		924	+61,000
		1009	+157,684
		1100	+100,290
		1159	-30,097
		1304	-186,795
		1358	-221,250
		1500	-220,481
		1558	-187,480
	20[2]	728	+205,928
		830	+217,006
		927	+190,040
		1028	+127,530
		1129	-24,340
		1229	-180,720
		1328	-226,480
		1428	-245,750
		1520	-229,200
		1610	-155,700
2/8/97	16[2]	743	+178,517
		838	+206,200
		943	+196,274
		1035	+150,600
		1123	+93,500
		1215	-5,880
		1311	-141,220
		1402	-204,250
		1454	-218,740
		1555	-220,300

(Continued)

[1]Flow is to the north or to the south. Positive values are to the north; negative values are to the south.
[2]Flow is to the northwest or to the southeast. Positive values are to the northwest; negative values are to the southeast.

Table 13 (Continued)

Date	Range No.	Time est	Discharge cfs
2/8/97	17[1]	735	+10,885
		804	+16,272
		900	+20,773
		1002	+17,693
		1112	+11,460
		1204	+6,772
		1303	-8,510
		1404	-13,852
		1504	-14,590
		1558	-17,459
	18[1]	744	+9,463
		814	+13,206
		912	+15,735
		1012	+15,001
		1121	+10,423
		1212	+5,757
		1315	-7,238
		1416	-13,082
		1517	-14,496
		1612	-15,078
2/9/97	10[2]	653	+625
		800	+2,576
		900	+3,442
		1004	+4,483
		1104	+3,079
		1205	-192
		1305	-2,138
		1402	-1,757
		1502	-1,403
		1606	-1,216
	11[2]	658	-568

(Continued)

Table 13 (Continued)

Date	Range No.	Time est	Discharge cfs
2/9/97	11[2]	806	+12,645
		904	+15,301
		1012	+14,842
		1108	+11,506
		1213	-1,651
		1312	-12,486
		1407	-15,105
		1507	-16,227
		1612	-14,101
	12[2]	710	-1,464
		820	+21,778
		915	+25,171
		1023	+20,813
		1120	+15,362
		1228	-5,000
		1322	-18,797
		1418	-20,890
		1516	-23,212
		1622	-20,165
	13[2]	722	+1,754
		829	+7,500
		922	+8,970
		1030	+8,453
		1128	+5,240
		1236	-3,400
		1330	-7,193
		1425	-7,991
		1526	-7,626
		1631	-6,647
	14[2]	735	+8,617
		818	+37,800

(Continued)

Table 13 (Continued)

Date	Range No.	Time est	Discharge cfs
2/9/97	14[2]	904	+49,360
		957	+52,150
		1109	+39,350
		1204	+14,600
		1257	-23,870
		1402	-39,660
		1500	-48,000
		1555	-49,500
	15[1]	748	+18,239
		830	+65,000
		919	+81,640
		1015	+87,186
		1123	+63,600
		1218	+23,246
		1311	-36,720
		1417	-63,000
		1519	-79,350
		1609	-83,500
2/10/97	6[1]	730	-939
		803	-450
		858	+892
		1003	+1,419
		1100	+1,641
		1155	+1,351
		1312	+315
		1402	-685
		1458	-1,018
		1600	-1,427
	7[1]	733	-1,525
		812	-1,350
		903	-969

(Continued)

Table 13 (Continued)

Date	Range No.	Time est	Discharge cfs
2/10/97	7[1]	1009	-241
		1105	+971
		1200	+1,196
		1317	+1,697
		1408	+1,121
		1504	-569
		1605	-265
	8[1]	709	-2,958
		759	+910
		857	+4,750
		957	+6,180
		1100	+6,122
		1157	+4,600
		1258	-879
		1358	-4,317
		1457	-5,200
		1555	-5,331
	9[1]	725	-3,930
		816	+5,211
		912	+9,790
		1011	+11,970
		1117	+10,600
		1211	+6,300
		1312	-4,976
		1412	-8,792
		1511	-10,089
		1607	-10,118
2/11/97	1[1]	841	-420
		937	+1,040
		1034	+1,413
		1123	+1,190

(Continued)

Table 13 (Continued)

Date	Range No.	Time est	Discharge cfs
2/11/97	1[1]	1232	+141
		1326	-1,069
		1417	-1,747
		1509	-2,302
		1605	-2,700
	2[3]	857	+950
		1001	+369
		1052	-1,039
		1139	-1,501
		1245	-1,935
		1340	-1,739
		1429	-1,537
		1523	-760
		1620	+697
	3[1]	821	-530
		920	-323
		1010	+440
		1108	-436
		1215	+695
		1304	-404
		1403	-741
		1453	-695
		1548	-728
	4[1]	752	+285
		903	+105
		1000	-260
		1102	-182
		1203	-297
		1318	-532
		1402	-245

(Continued)

[3]Flow is to the east or to the west. Positive values are to the east; negative values are to the west.

Table 13 (Concluded)

Date	Range No.	Time est	Discharge cfs
2/11/97	4[1]	1500	-193
		1600	-503
	5[1]	805	+222
		912	-758
		1013	+560
		1112	-481
		1212	+256
		1300	+1,175
		1410	+634
		1508	+977
		1608	-55

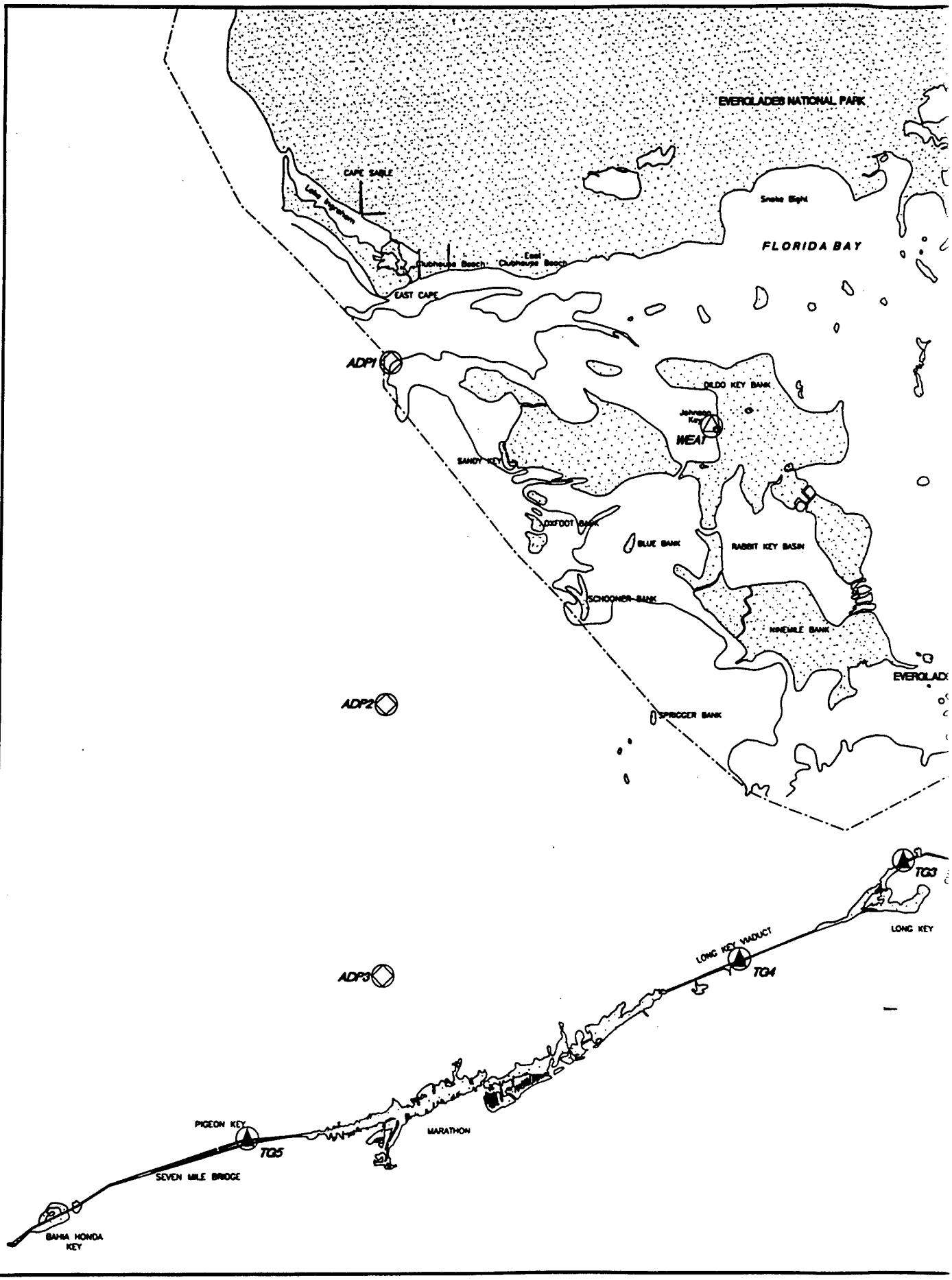
EVERGLADES NATIONAL PARK
CAPE SABLE
Lake Ingraham
Snake Bight
FLORIDA BAY
Clubhouse Beach
East Clubhouse Beach
EAST CAPE
ADP1
DILDO KEY BANK
Johnson Key
WEA1
SANDY KEY
OXFOOT BANK
BLUE BANK
RABBIT KEY BASIN
SCHOONER BANK
NINEMILE BANK
EVERGLADE
ADP2
SPRIGGER BANK
TG3
LONG KEY
LONG KEY VIADUCT
TG4
ADP3
PIGEON KEY
TG5
MARATHON
SEVEN MILE BRIDGE
BAHIA HONDA KEY

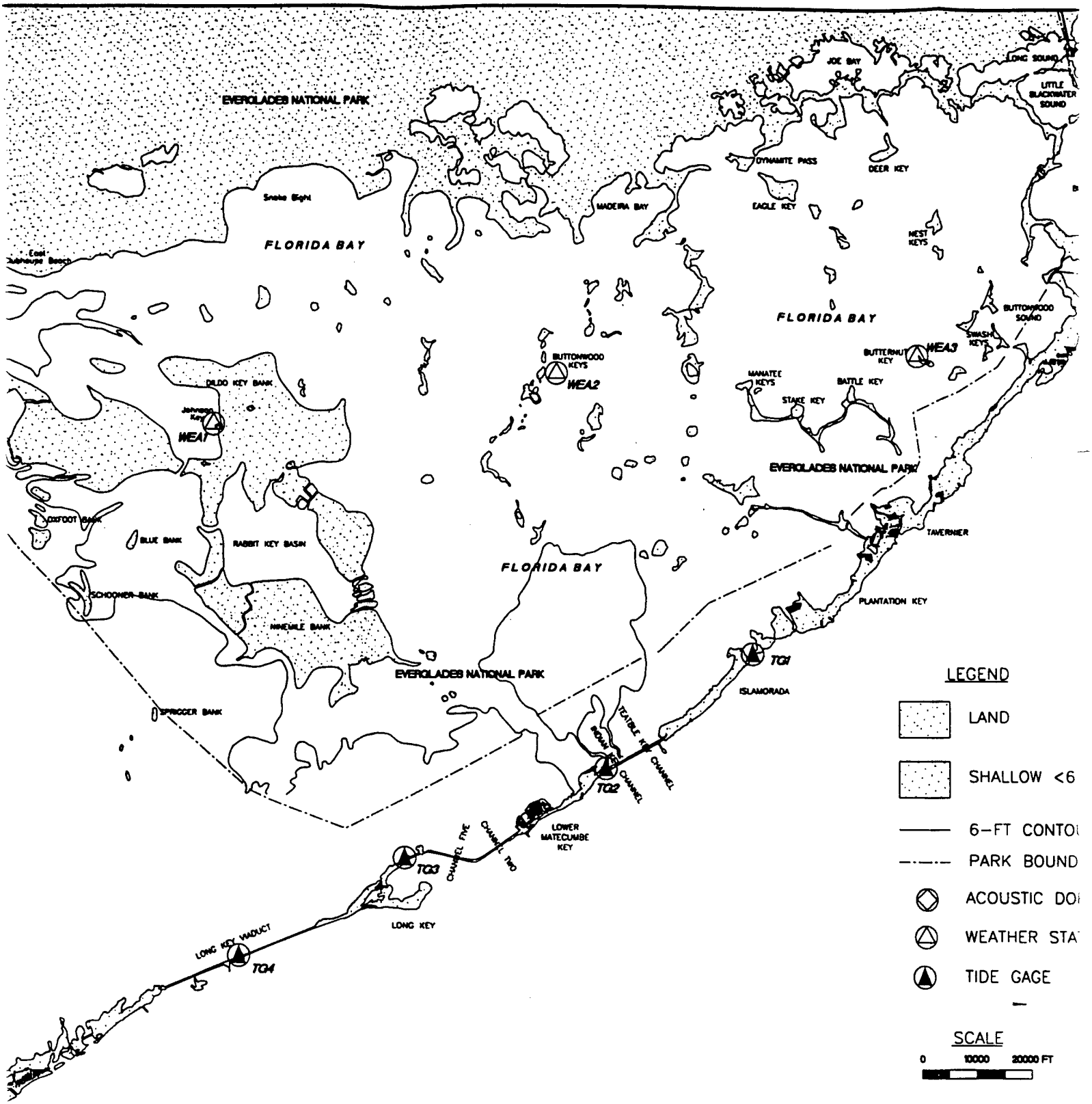
EVERGLADES NATIONAL PARK
FLORIDA BAY
JOE BAY
LONG SOUND
LITTLE BLACKWATER SOUND
DYNAMITE PASS
DEER KEY
EAGLE KEY
MADEIRA BAY
WEST KEYS
BUTTONWOOD SOUND
SWASH KEYS
BUTTERNUT KEY
WEA3
BUTTONWOOD KEYS
WEA2
MANATEE KEYS
BATTLE KEY
STAKE KEY
DILDO KEY BANK
WEA1
COFFOOT BANK
BLUE BANK
RABBIT KEY BASIN
SCHOONER BANK
NINEMILE BANK
SPRIGGER BANK
TAVERNIER
PLANTATION KEY
TG1
ISLAMORADA
TG2
TG3
LOWER MATECUMBE KEY
CHANNEL FIVE
CHANNEL TWO
LONG KEY
LONG KEY VIADUCT
TG4
LEGEND
LAND
SHALLOW <6
6-FT CONTOU
PARK BOUND
ACOUSTIC DO
WEATHER STA
TIDE GAGE
SCALE
0 10000 20000 FT

EQUIPMENT

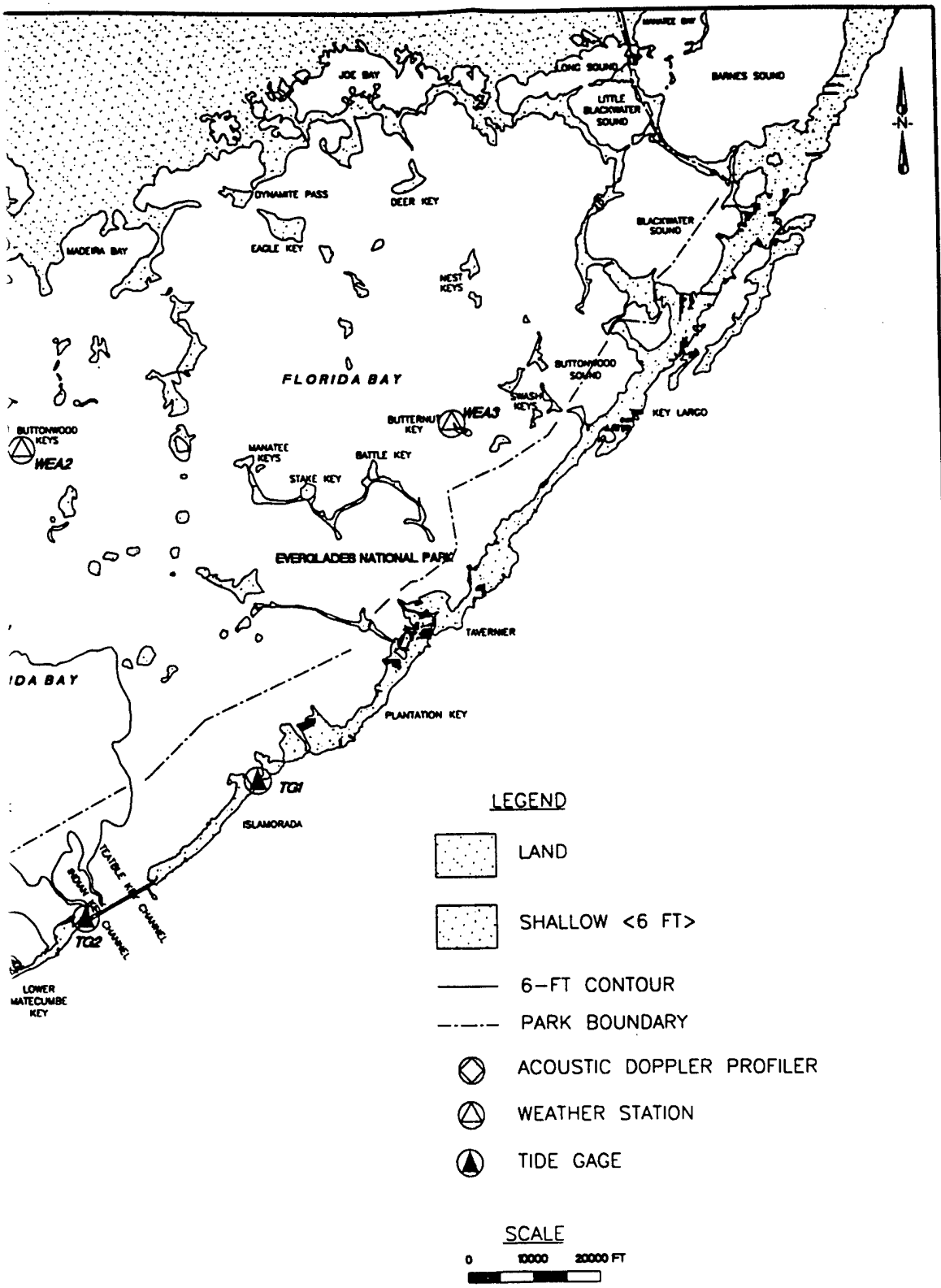

EQUIPMENT LOCATION MAP

Figure 1

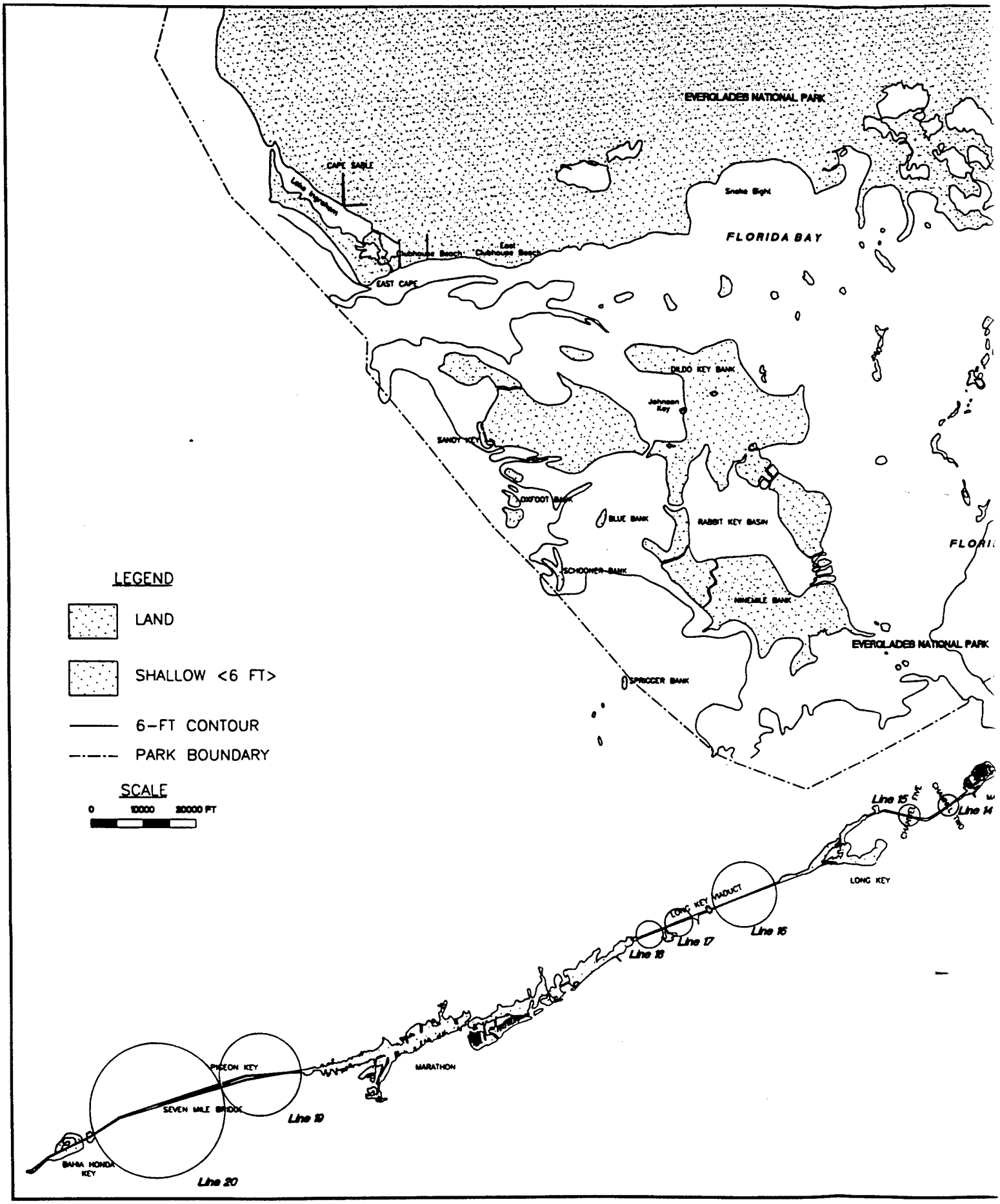
EVERGLADES NATIONAL PARK
CAPE SABLE
Little Rabbit Key
Snake Bight
FLORIDA BAY
Clubhouse Beach
East Clubhouse Beach
EAST CAPE
DILDO KEY BANK
Johnson Key
SANDY KEY
OXFOOT BANK
BLUE BANK
RABBIT KEY BASIN
SCHOONER BANK
NINEMILE BANK
SPRIGGER BANK
EVERGLADES NATIONAL PARK
LEGEND
LAND
SHALLOW <6 FT>
6-FT CONTOUR
PARK BOUNDARY
SCALE
0 10000 20000 FT
Line 15
Line 14
LONG KEY
LONG KEY VIADUCT
Line 16
Line 17
Line 18
MARATHON
PIGEON KEY
SEVEN MILE BRIDGE
Line 19
BAHIA HONDA KEY
Line 20

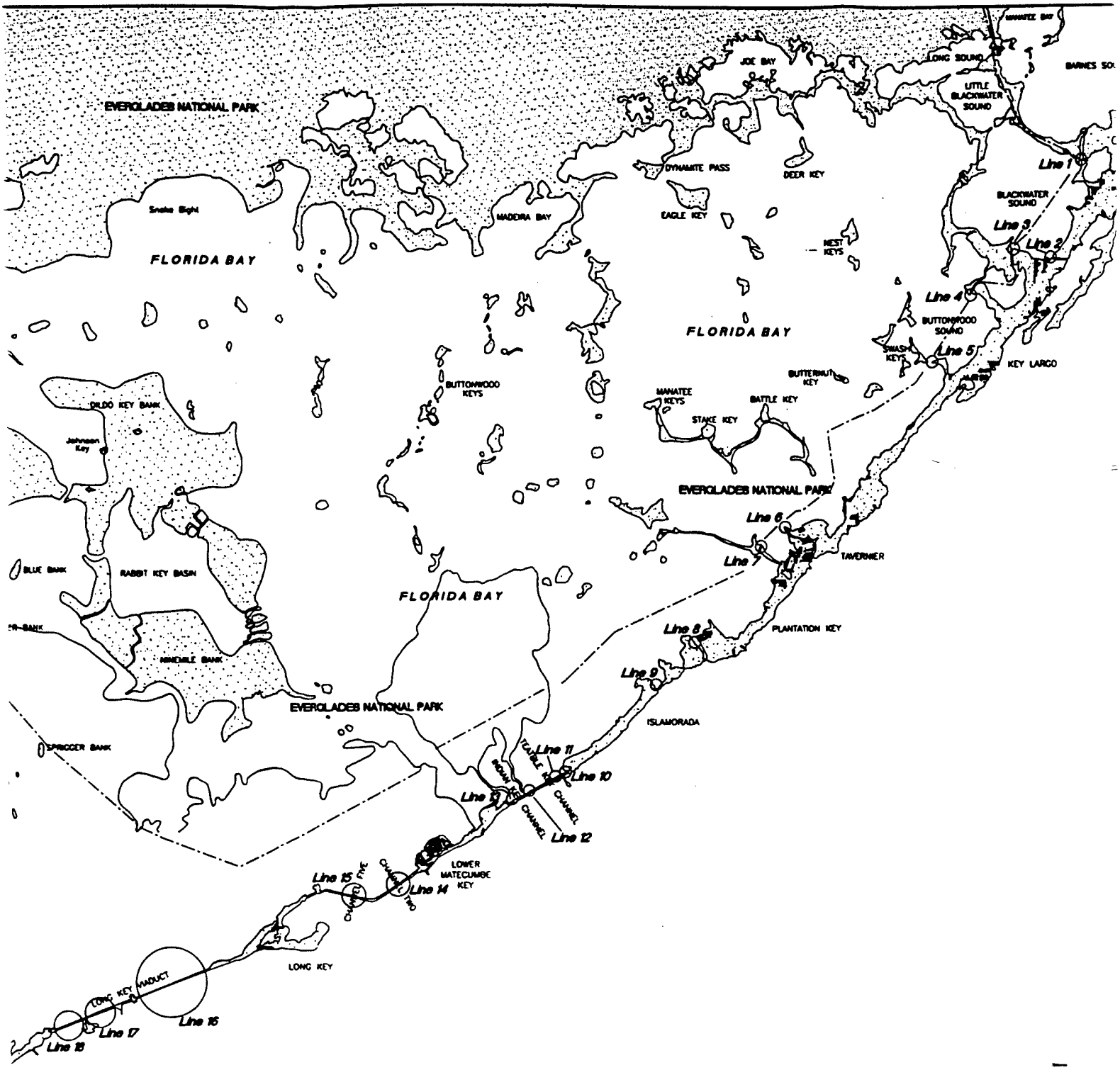

INTENSIVE SURVEY TRA
LOCATION MAP

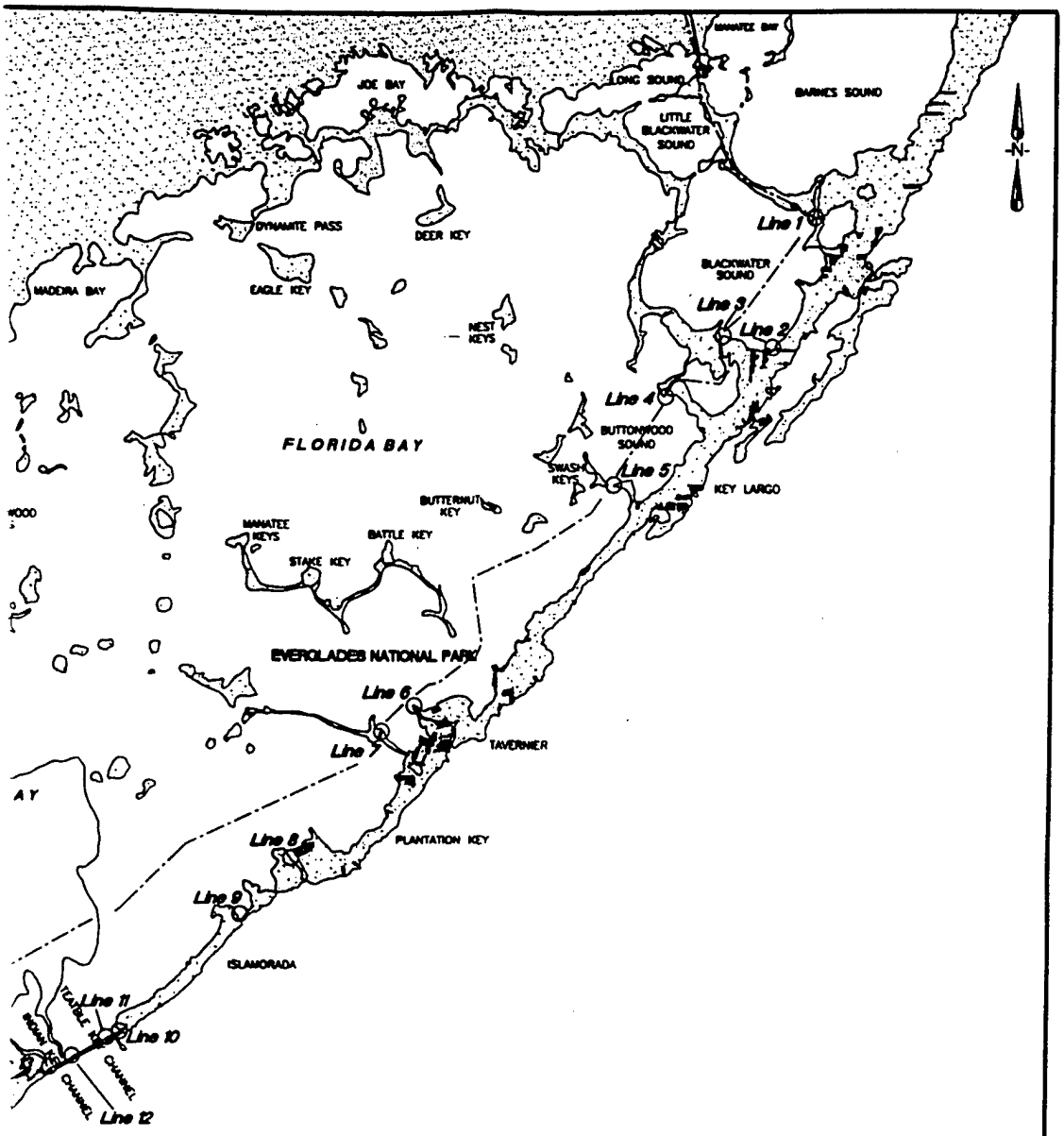

INTENSIVE SURVEY TRANSECT
LOCATION MAP

Figure 2

(3)

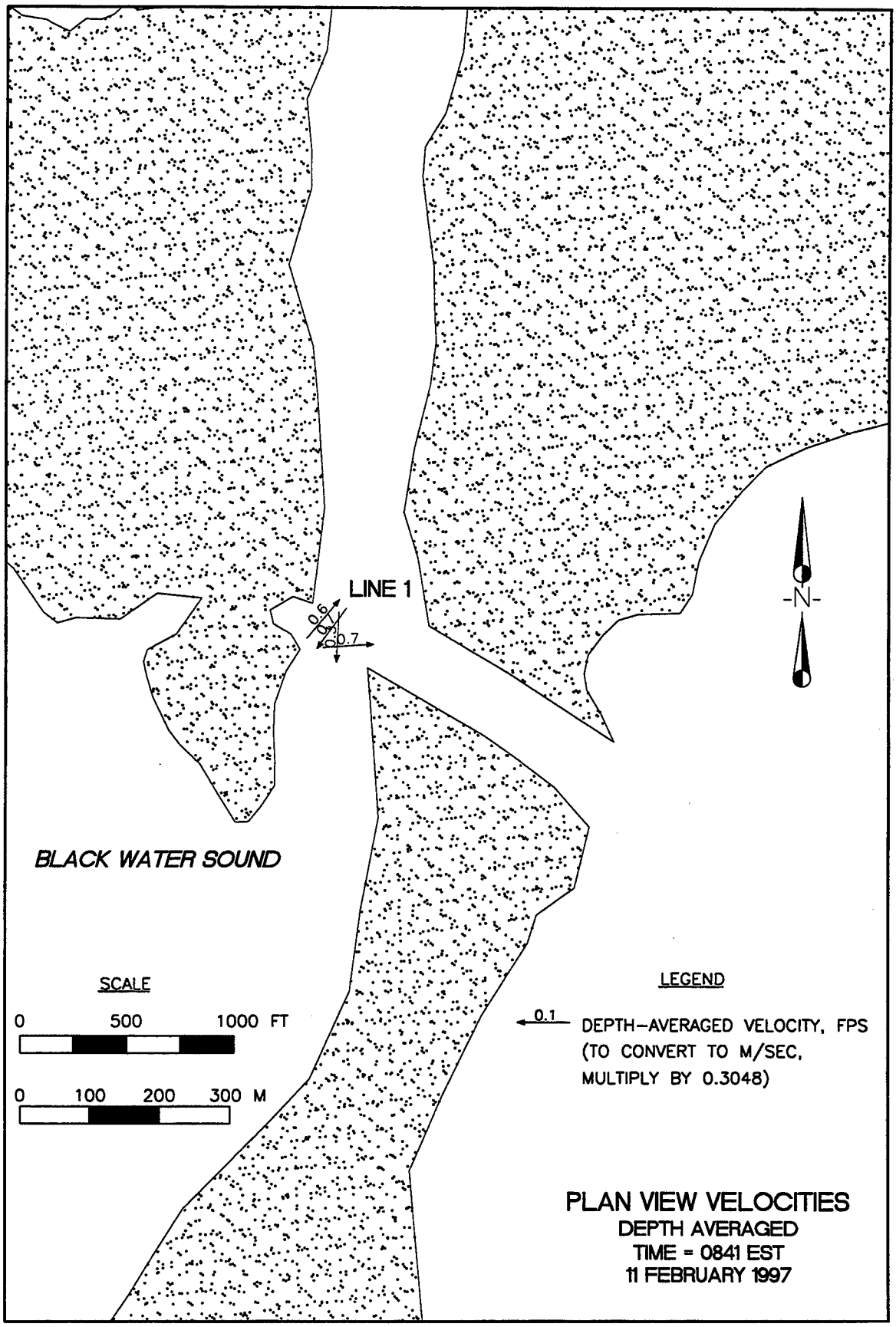
LINE 1
0.6
0.7
0.7
-N-
BLACK WATER SOUND
SCALE
0 500 1000 FT
0 100 200 300 M
LEGEND
0.1
DEPTH-AVERAGED VELOCITY, FPS
(TO CONVERT TO M/SEC,
MULTIPLY BY 0.3048)
PLAN VIEW VELOCITIES
DEPTH AVERAGED
TIME = 0841 EST
11 FEBRUARY 1997

Figure 3

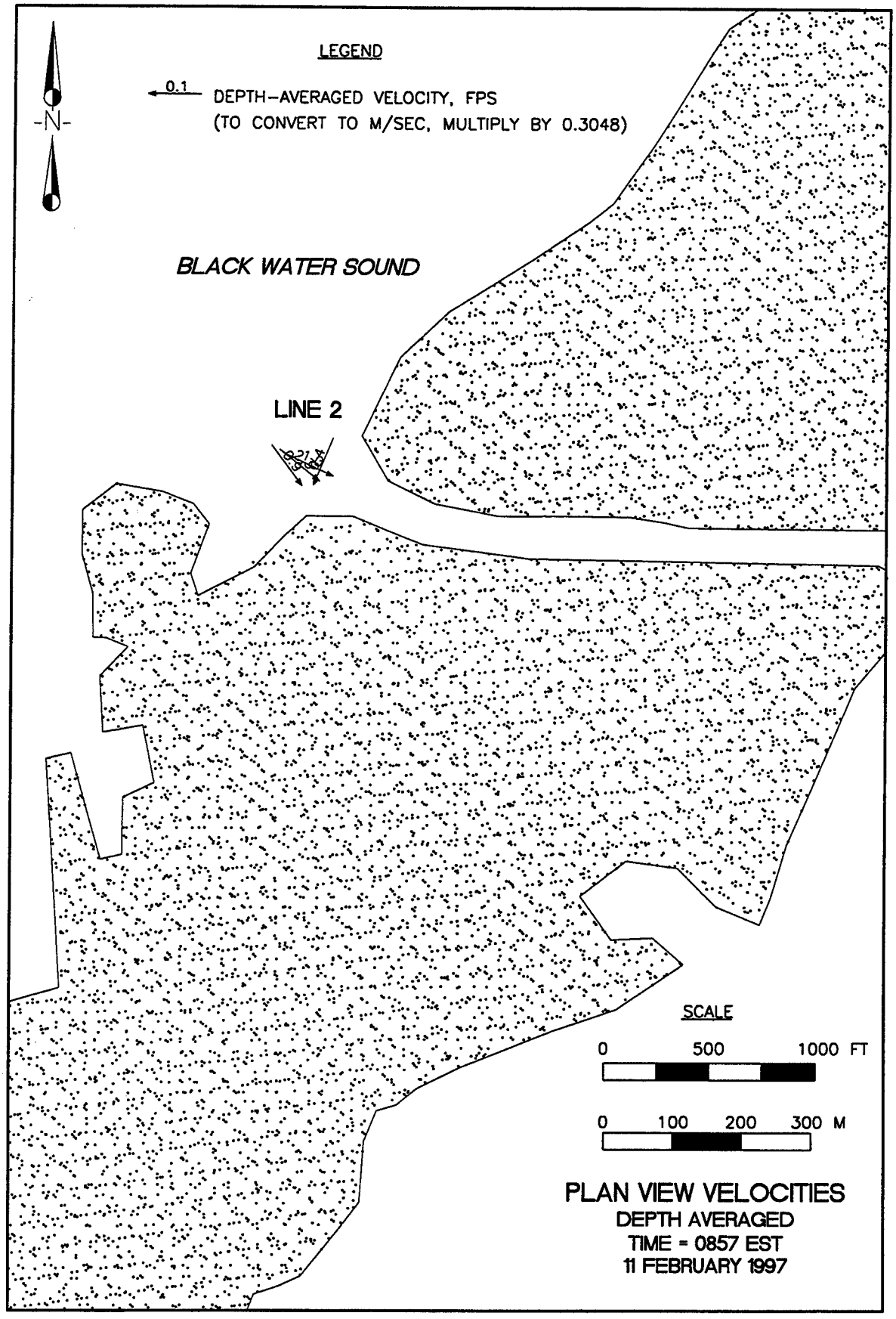
LEGEND
0.1
DEPTH-AVERAGED VELOCITY, FPS
(TO CONVERT TO M/SEC, MULTIPLY BY 0.3048)
-N-
BLACK WATER SOUND
LINE 2
SCALE
0 500 1000 FT
0 100 200 300 M
PLAN VIEW VELOCITIES
DEPTH AVERAGED
TIME = 0857 EST
11 FEBRUARY 1997

Figure 4

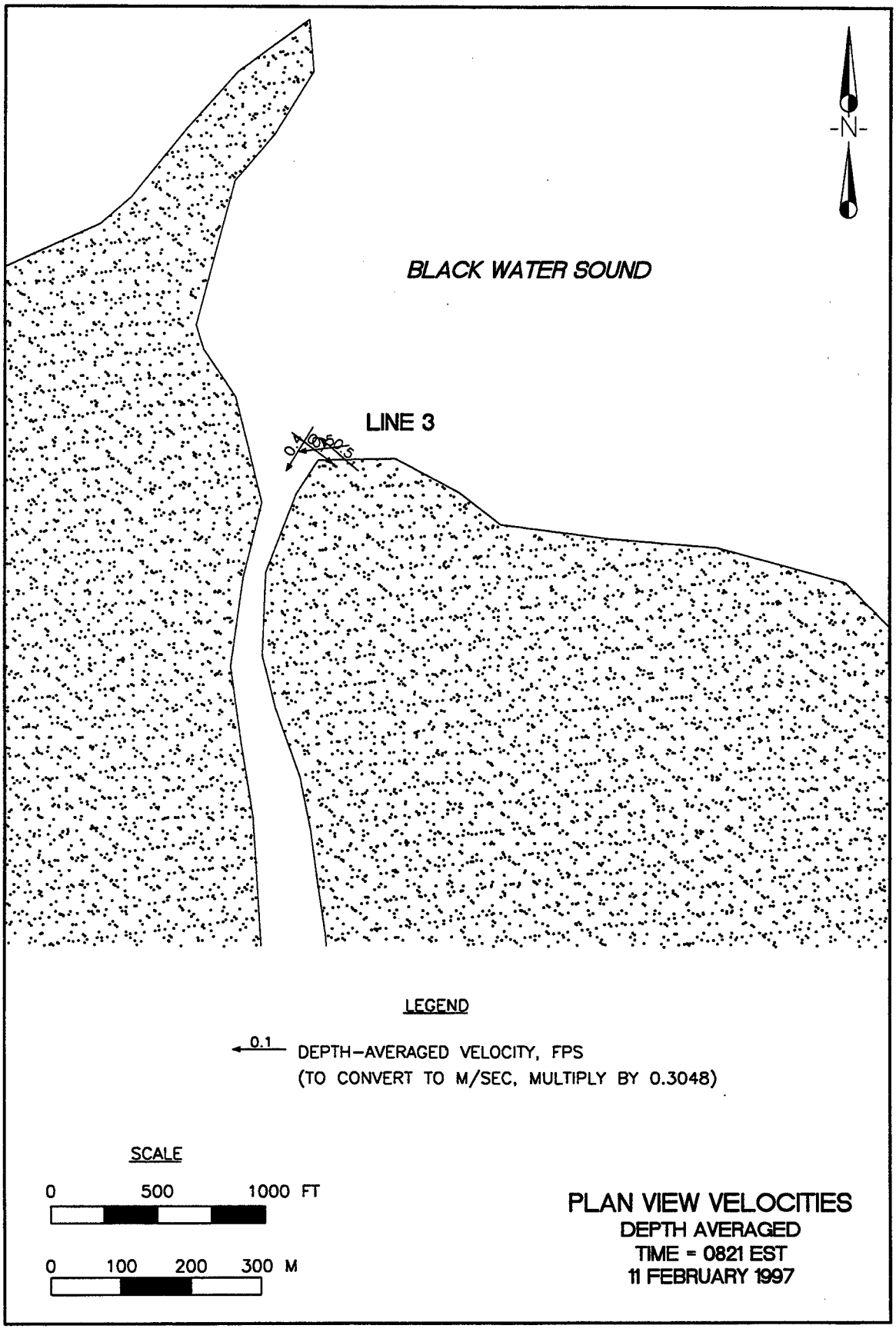
-N-
BLACK WATER SOUND
LINE 3
0.4
0.5
0.5
LEGEND
0.1
DEPTH-AVERAGED VELOCITY, FPS
(TO CONVERT TO M/SEC, MULTIPLY BY 0.3048)
SCALE
0
500
1000 FT
0
100
200
300 M
PLAN VIEW VELOCITIES
DEPTH AVERAGED
TIME = 0821 EST
11 FEBRUARY 1997

Figure 5

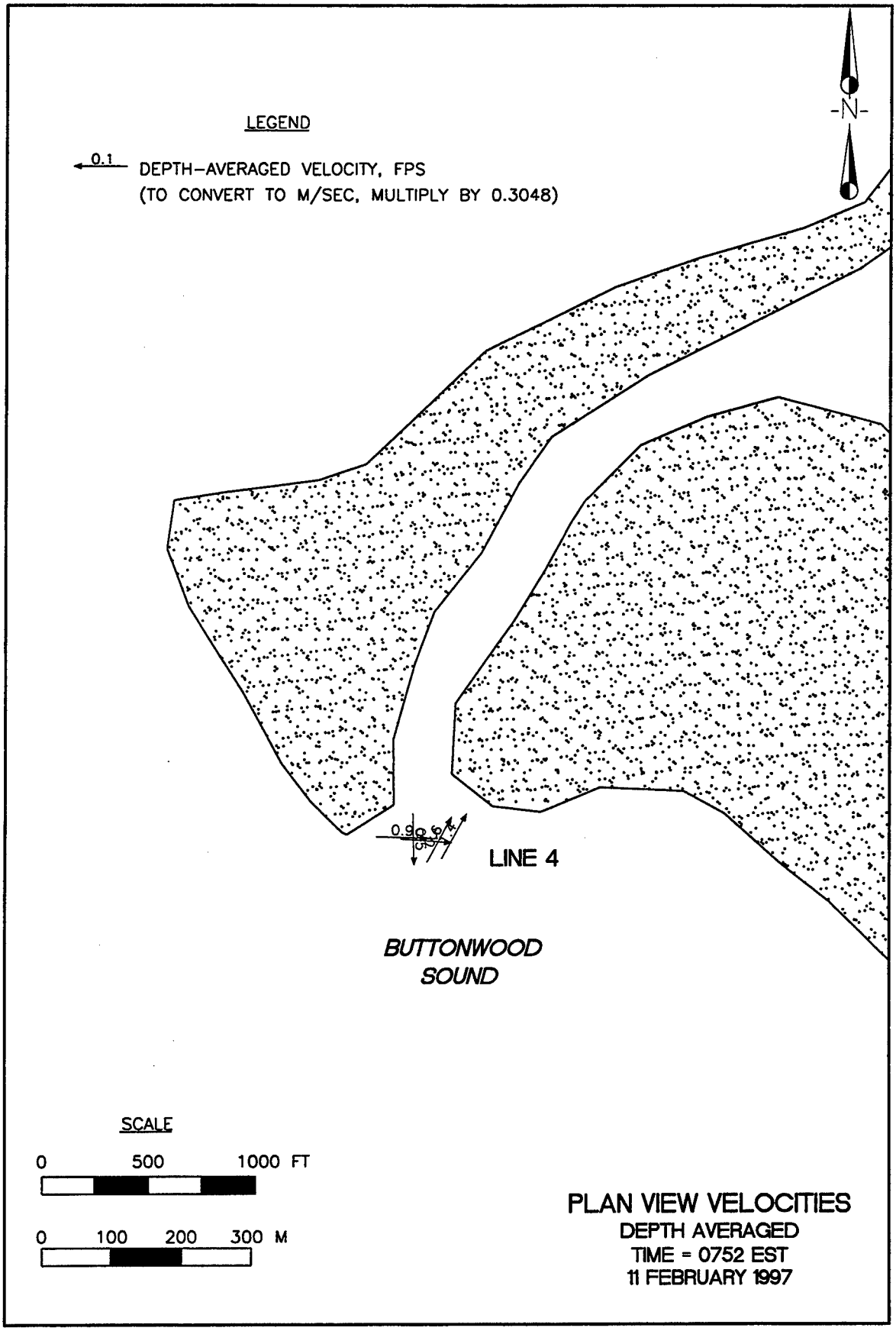
LEGEND
0.1
DEPTH-AVERAGED VELOCITY, FPS
(TO CONVERT TO M/SEC, MULTIPLY BY 0.3048)
-N-
0.9
LINE 4
BUTTONWOOD
SOUND
SCALE
0 500 1000 FT
0 100 200 300 M
PLAN VIEW VELOCITIES
DEPTH AVERAGED
TIME = 0752 EST
11 FEBRUARY 1997

Figure 6

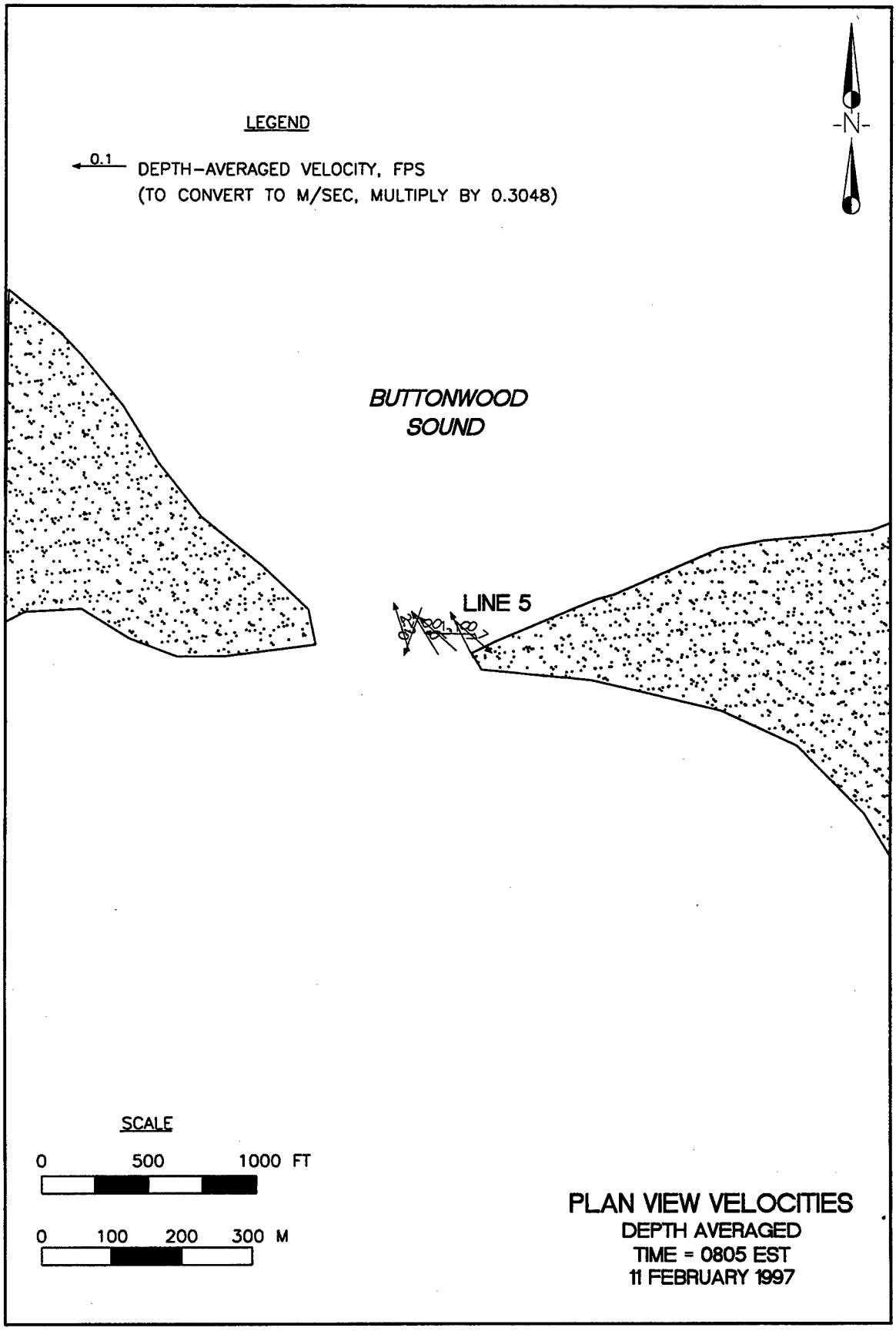
LEGEND
0.1
DEPTH-AVERAGED VELOCITY, FPS
(TO CONVERT TO M/SEC, MULTIPLY BY 0.3048)
-N-
BUTTONWOOD
SOUND
LINE 5
SCALE
0 500 1000 FT
0 100 200 300 M
PLAN VIEW VELOCITIES
DEPTH AVERAGED
TIME = 0805 EST
11 FEBRUARY 1997

Figure 7

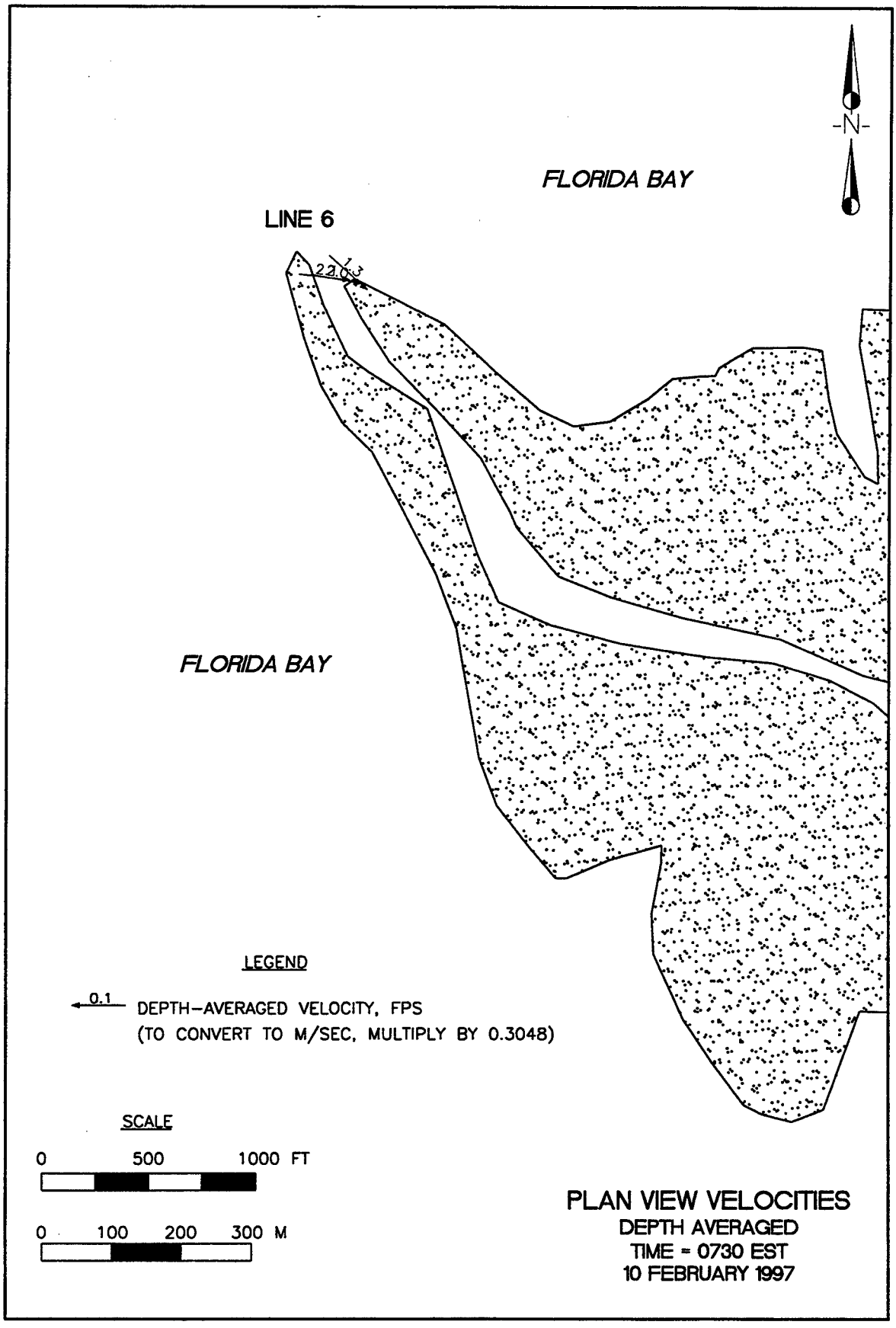
-N-
FLORIDA BAY
LINE 6
FLORIDA BAY
LEGEND
0.1
DEPTH-AVERAGED VELOCITY, FPS
(TO CONVERT TO M/SEC, MULTIPLY BY 0.3048)
SCALE
0 500 1000 FT
0 100 200 300 M
PLAN VIEW VELOCITIES
DEPTH AVERAGED
TIME = 0730 EST
10 FEBRUARY 1997

Figure 8

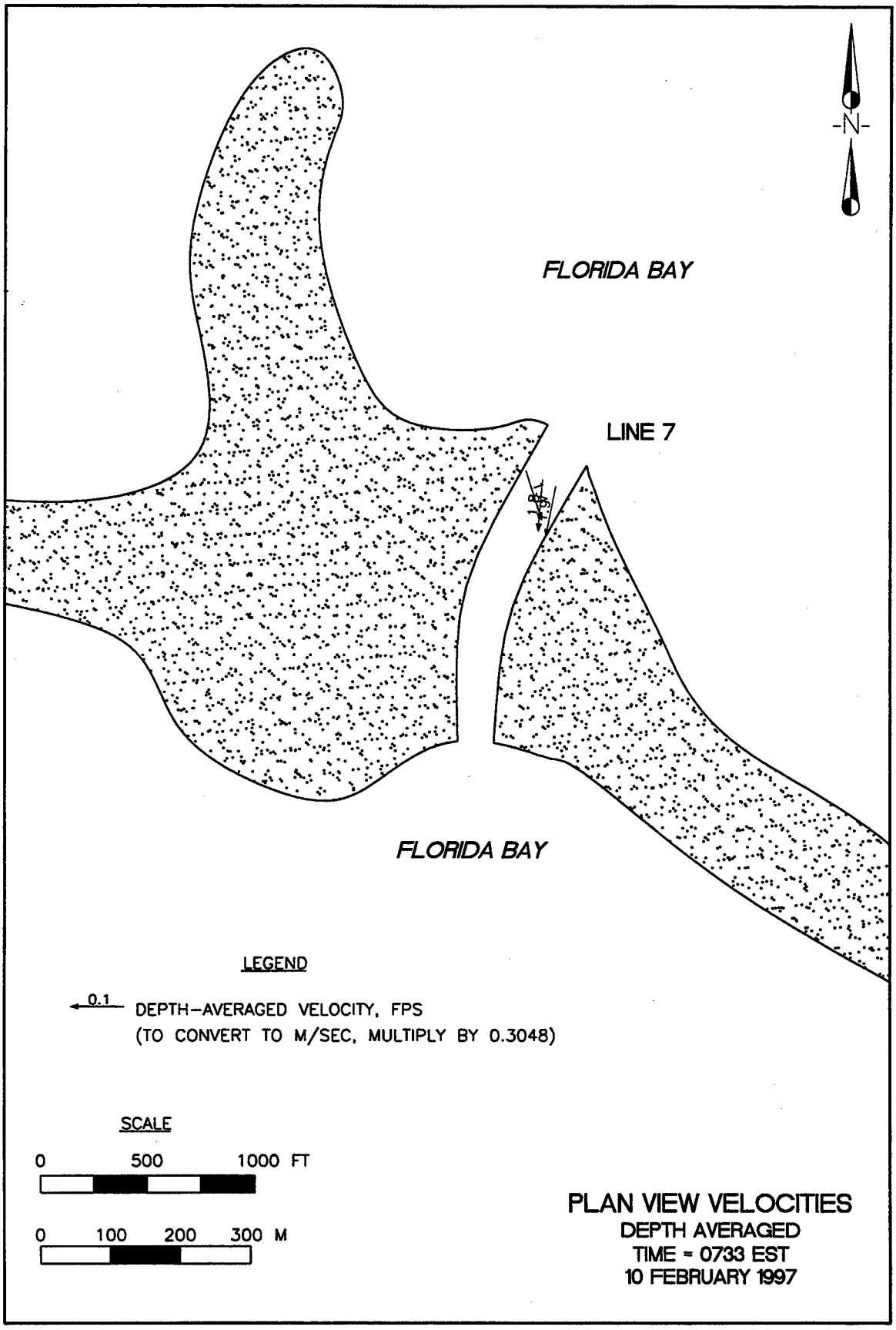
-N-
FLORIDA BAY
LINE 7
FLORIDA BAY
LEGEND
0.1
DEPTH-AVERAGED VELOCITY, FPS
(TO CONVERT TO M/SEC, MULTIPLY BY 0.3048)
SCALE
0 500 1000 FT
0 100 200 300 M
PLAN VIEW VELOCITIES
DEPTH AVERAGED
TIME = 0733 EST
10 FEBRUARY 1997

Figure 9

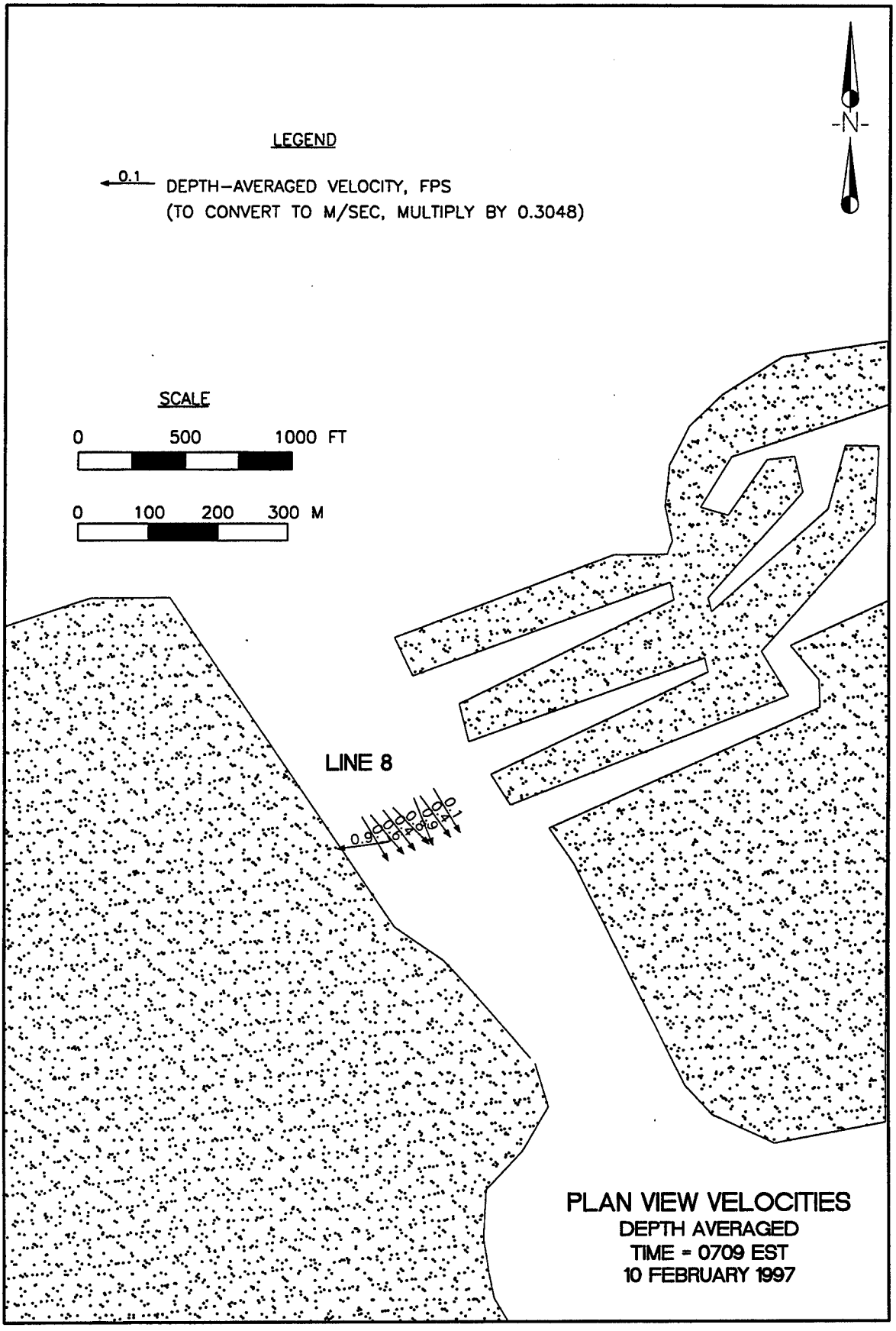
LEGEND
0.1
DEPTH-AVERAGED VELOCITY, FPS
(TO CONVERT TO M/SEC, MULTIPLY BY 0.3048)
-N-
SCALE
0 500 1000 FT
0 100 200 300 M
LINE 8
0.9
1.0
PLAN VIEW VELOCITIES
DEPTH AVERAGED
TIME = 0709 EST
10 FEBRUARY 1997

Figure 10

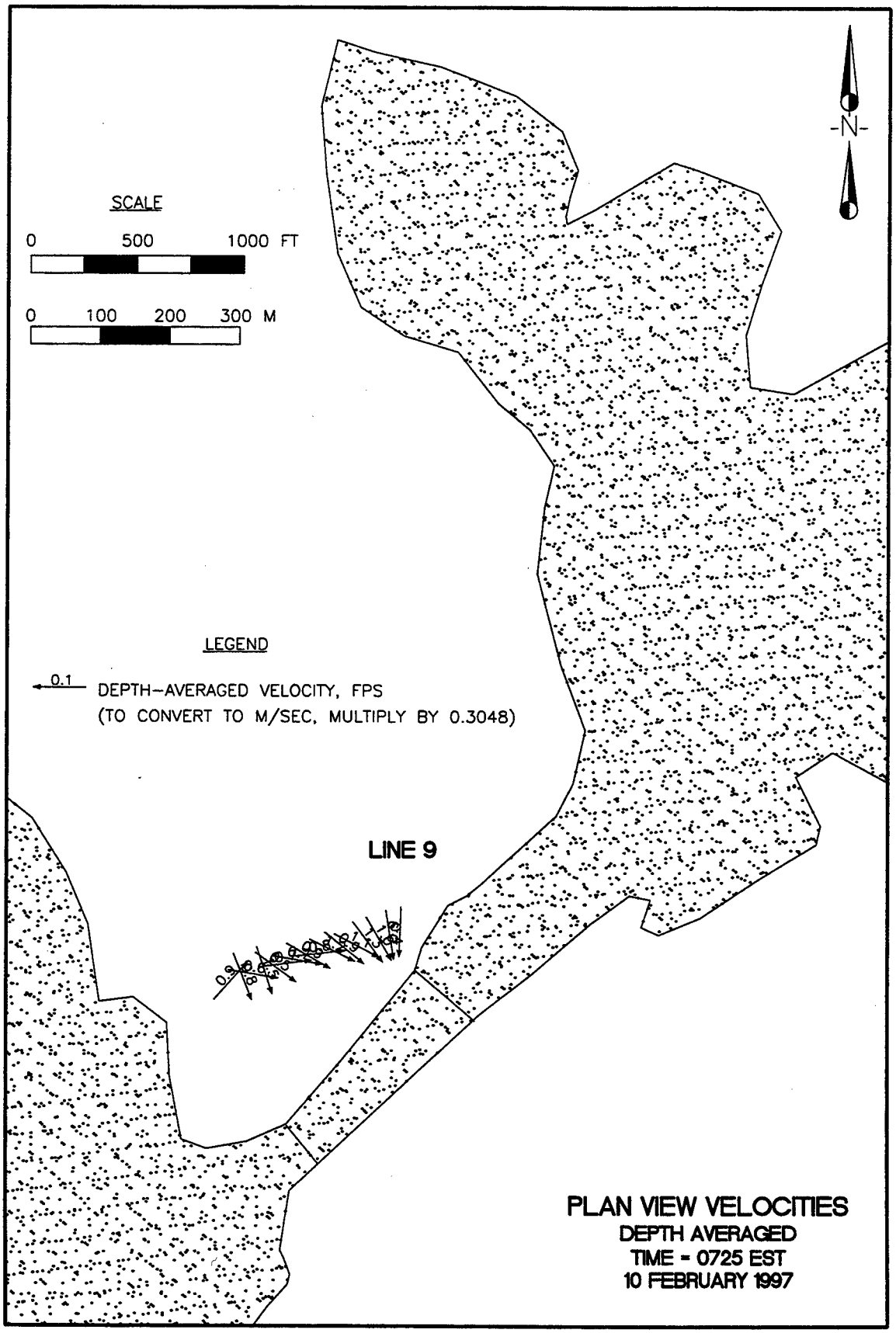
SCALE
0 500 1000 FT
0 100 200 300 M
-N-
LEGEND
0.1 DEPTH-AVERAGED VELOCITY, FPS
(TO CONVERT TO M/SEC, MULTIPLY BY 0.3048)
LINE 9
PLAN VIEW VELOCITIES
DEPTH AVERAGED
TIME = 0725 EST
10 FEBRUARY 1997

Figure 11

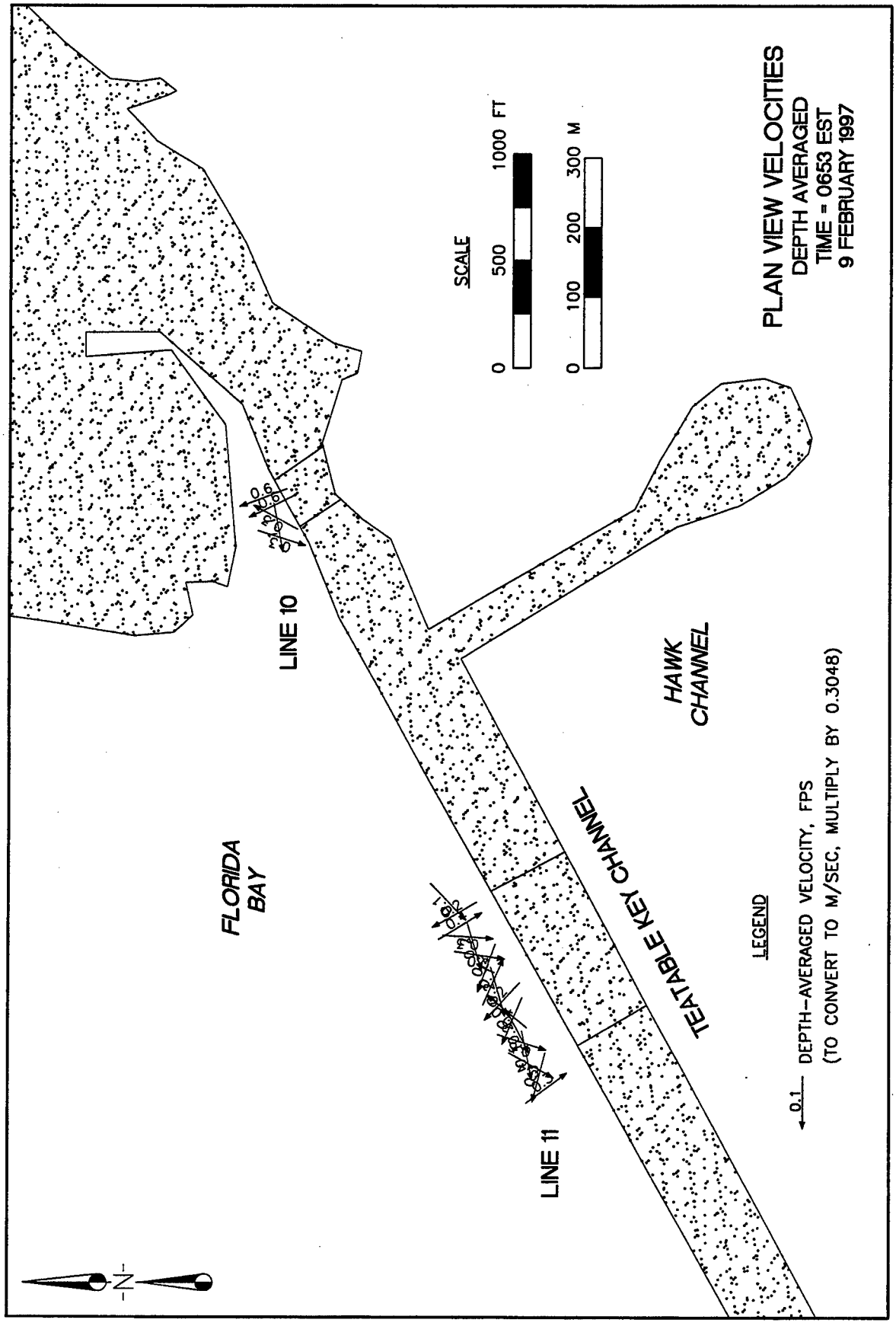
PLAN VIEW VELOCITIES
DEPTH AVERAGED
TIME = 0653 EST
9 FEBRUARY 1997
SCALE
0
500
1000 FT
0
100
200
300 M
FLORIDA BAY
LINE 10
LINE 11
HAWK CHANNEL
TEATABLE KEY CHANNEL
LEGEND
0.1
DEPTH-AVERAGED VELOCITY, FPS
(TO CONVERT TO M/SEC, MULTIPLY BY 0.3048)
N

Figure 12

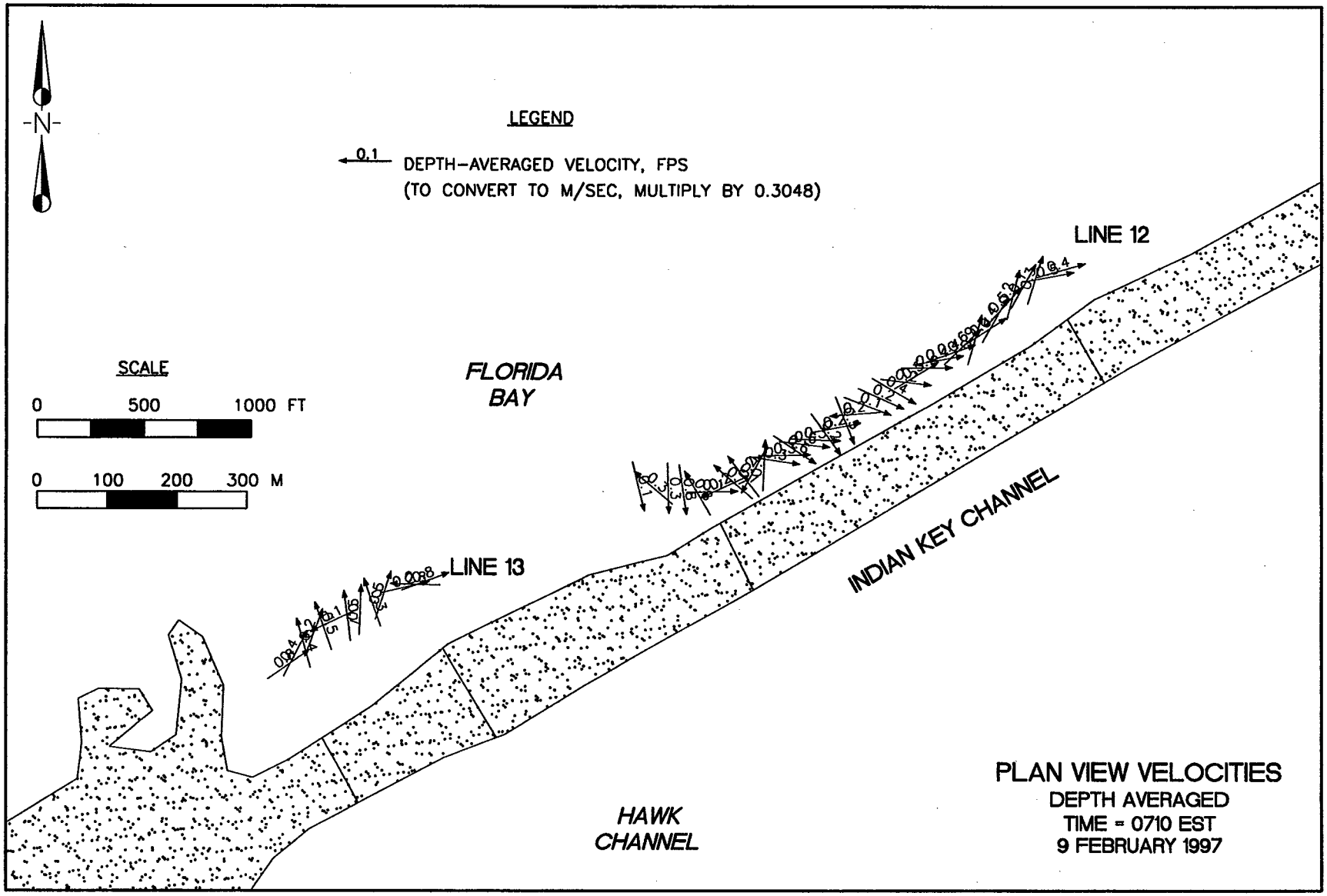
-N-
LEGEND
0.1
DEPTH-AVERAGED VELOCITY, FPS
(TO CONVERT TO M/SEC, MULTIPLY BY 0.3048)
SCALE
0 500 1000 FT
0 100 200 300 M
FLORIDA BAY
LINE 12
LINE 13
INDIAN KEY CHANNEL
HAWK CHANNEL
PLAN VIEW VELOCITIES
DEPTH AVERAGED
TIME = 0710 EST
9 FEBRUARY 1997

Figure 13

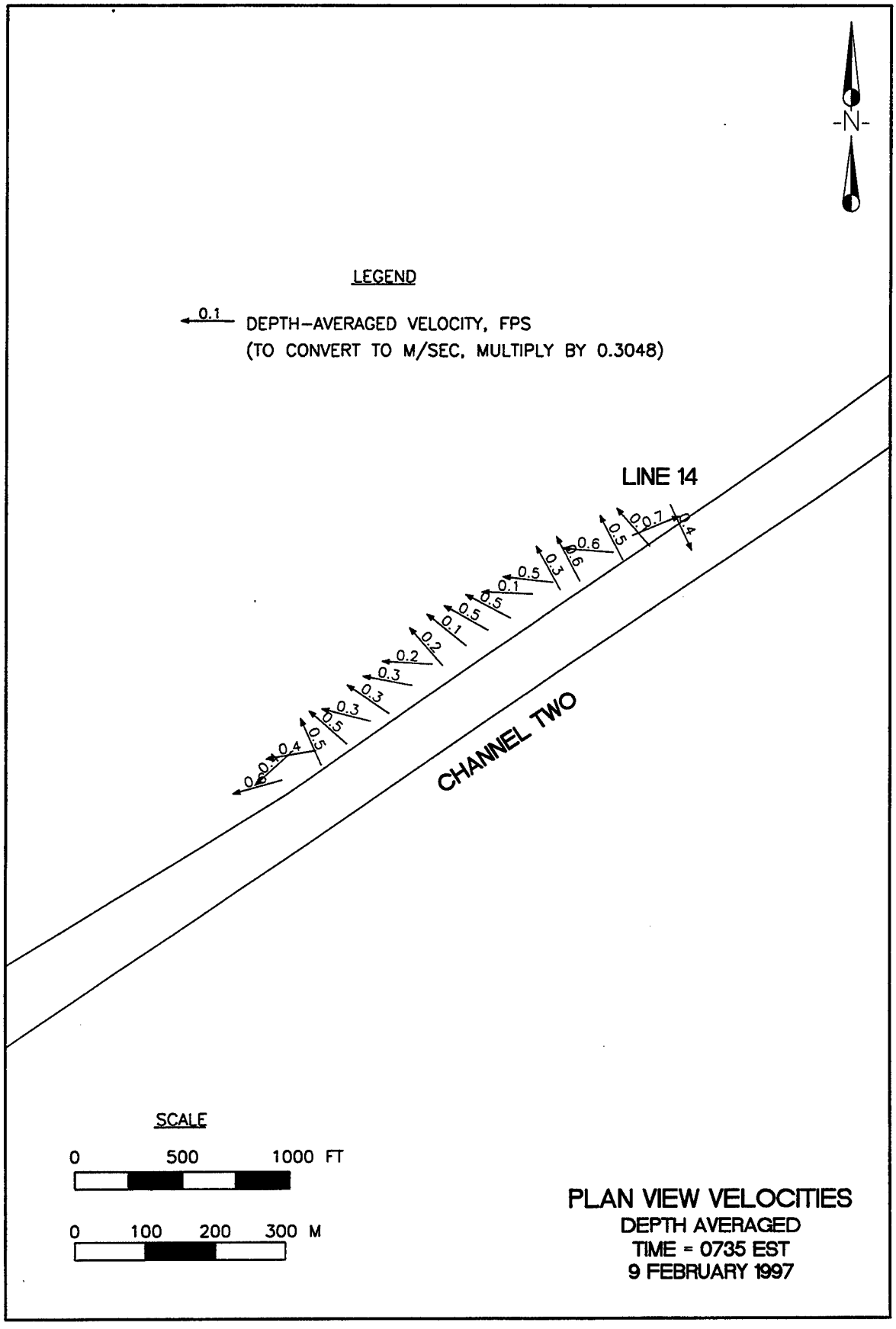
-N-
LEGEND
0.1
DEPTH-AVERAGED VELOCITY, FPS
(TO CONVERT TO M/SEC, MULTIPLY BY 0.3048)
LINE 14
CHANNEL TWO
SCALE
0 500 1000 FT
0 100 200 300 M
PLAN VIEW VELOCITIES
DEPTH AVERAGED
TIME = 0735 EST
9 FEBRUARY 1997

Figure 14

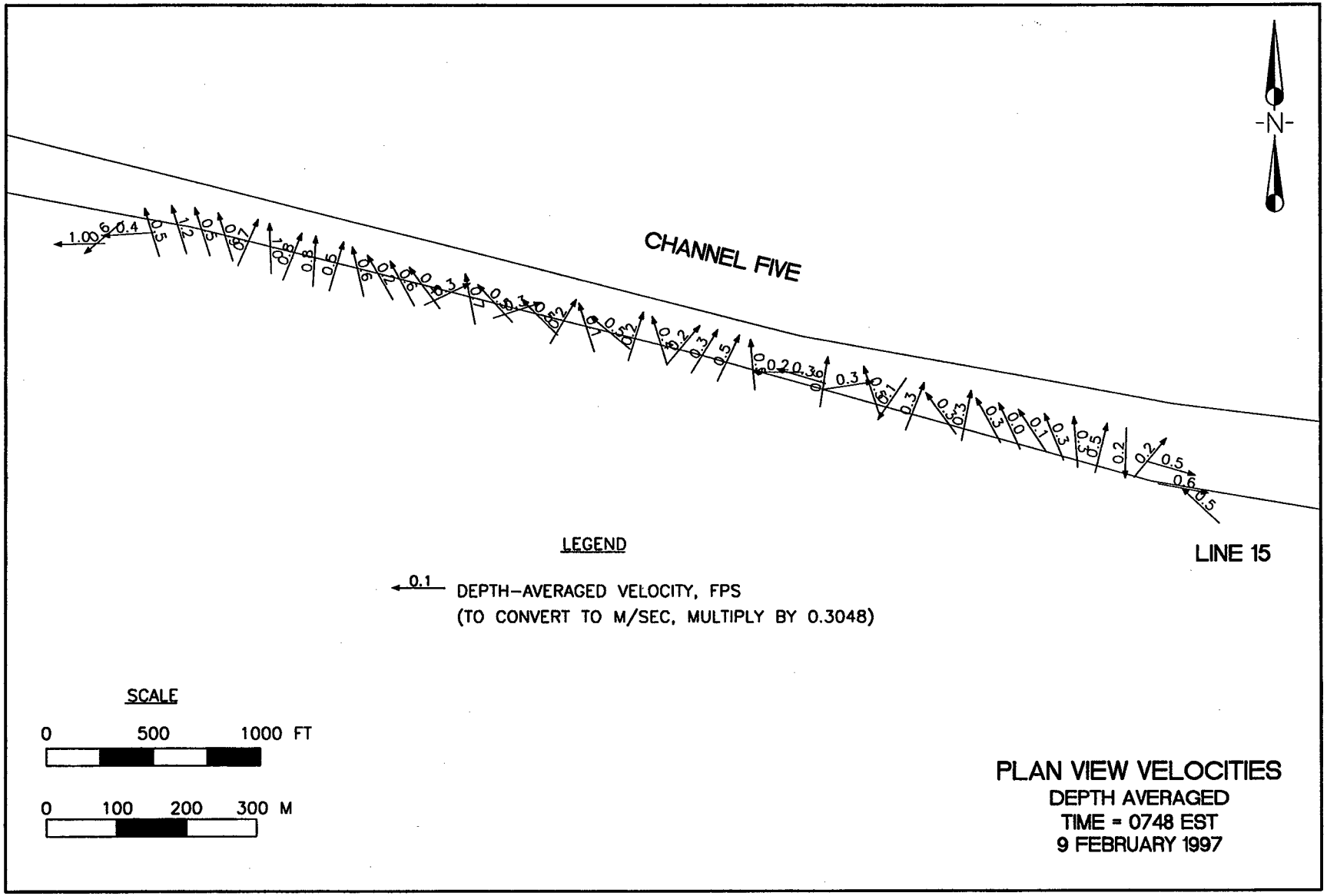
-N-
CHANNEL FIVE
LINE 15
LEGEND
0.1 DEPTH-AVERAGED VELOCITY, FPS
(TO CONVERT TO M/SEC, MULTIPLY BY 0.3048)
SCALE
0 500 1000 FT
0 100 200 300 M
PLAN VIEW VELOCITIES
DEPTH AVERAGED
TIME = 0748 EST
9 FEBRUARY 1997

Figure 15

Figure 16

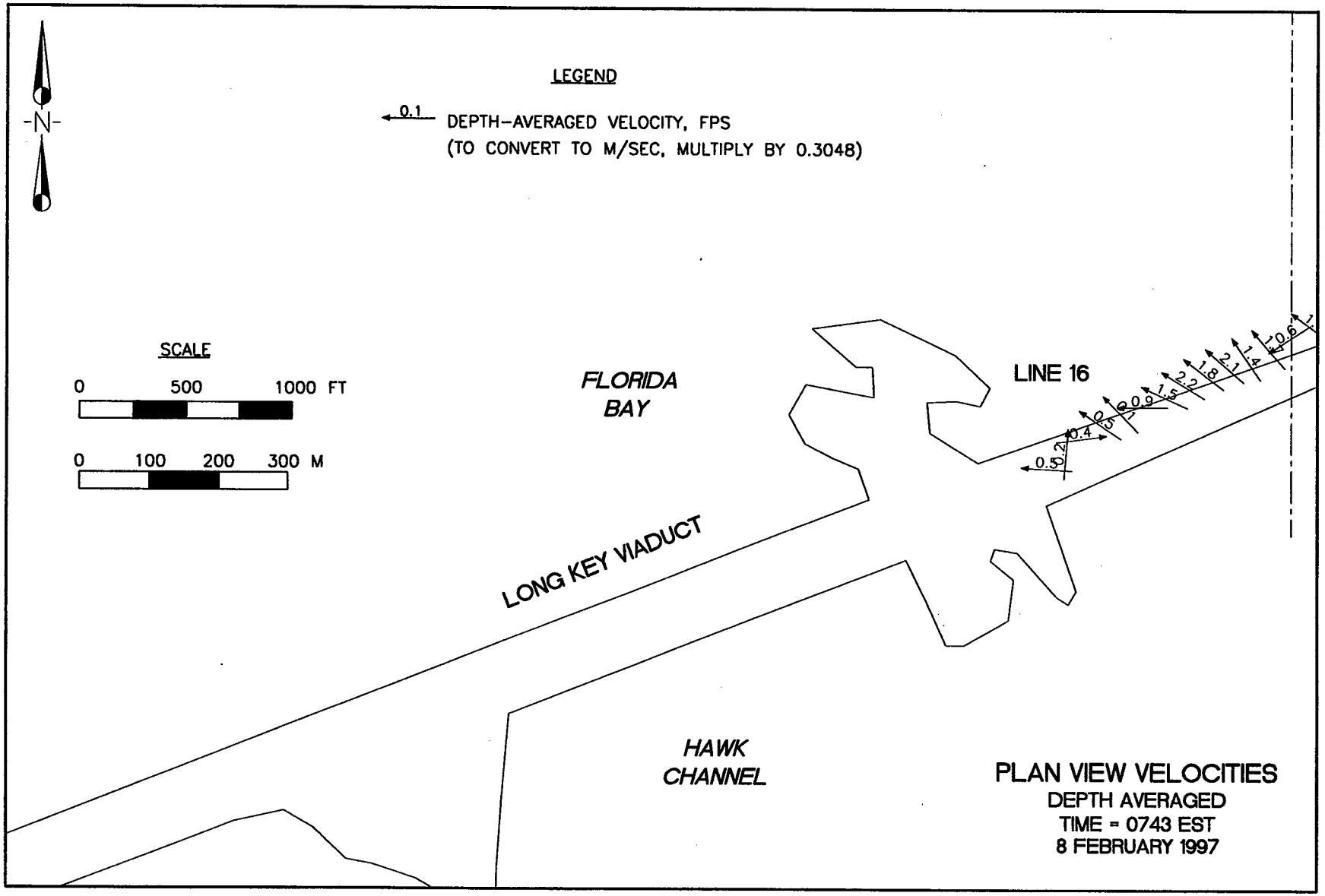
LEGEND
0.1
DEPTH-AVERAGED VELOCITY, FPS
(TO CONVERT TO M/SEC, MULTIPLY BY 0.3048)
-N-
SCALE
0 500 1000 FT
0 100 200 300 M
FLORIDA BAY
LINE 16
LONG KEY VIADUCT
HAWK CHANNEL
PLAN VIEW VELOCITIES
DEPTH AVERAGED
TIME = 0743 EST
8 FEBRUARY 1997

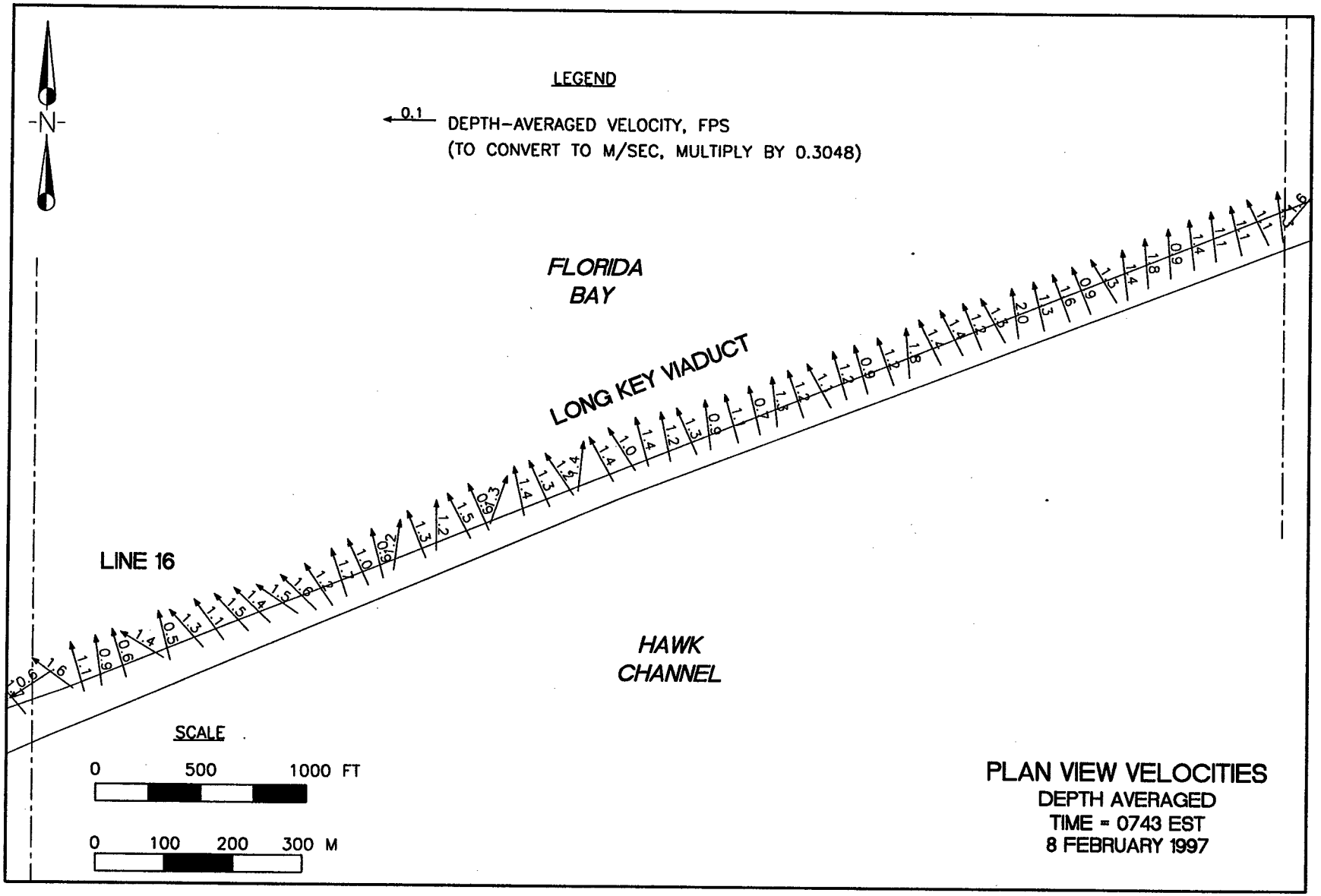
LEGEND
0.1
DEPTH-AVERAGED VELOCITY, FPS
(TO CONVERT TO M/SEC, MULTIPLY BY 0.3048)
-N-
FLORIDA
BAY
LONG KEY VIADUCT
LINE 16
HAWK
CHANNEL
SCALE
0 500 1000 FT
0 100 200 300 M
PLAN VIEW VELOCITIES
DEPTH AVERAGED
TIME = 0743 EST
8 FEBRUARY 1997

Figure 17

Figure 18

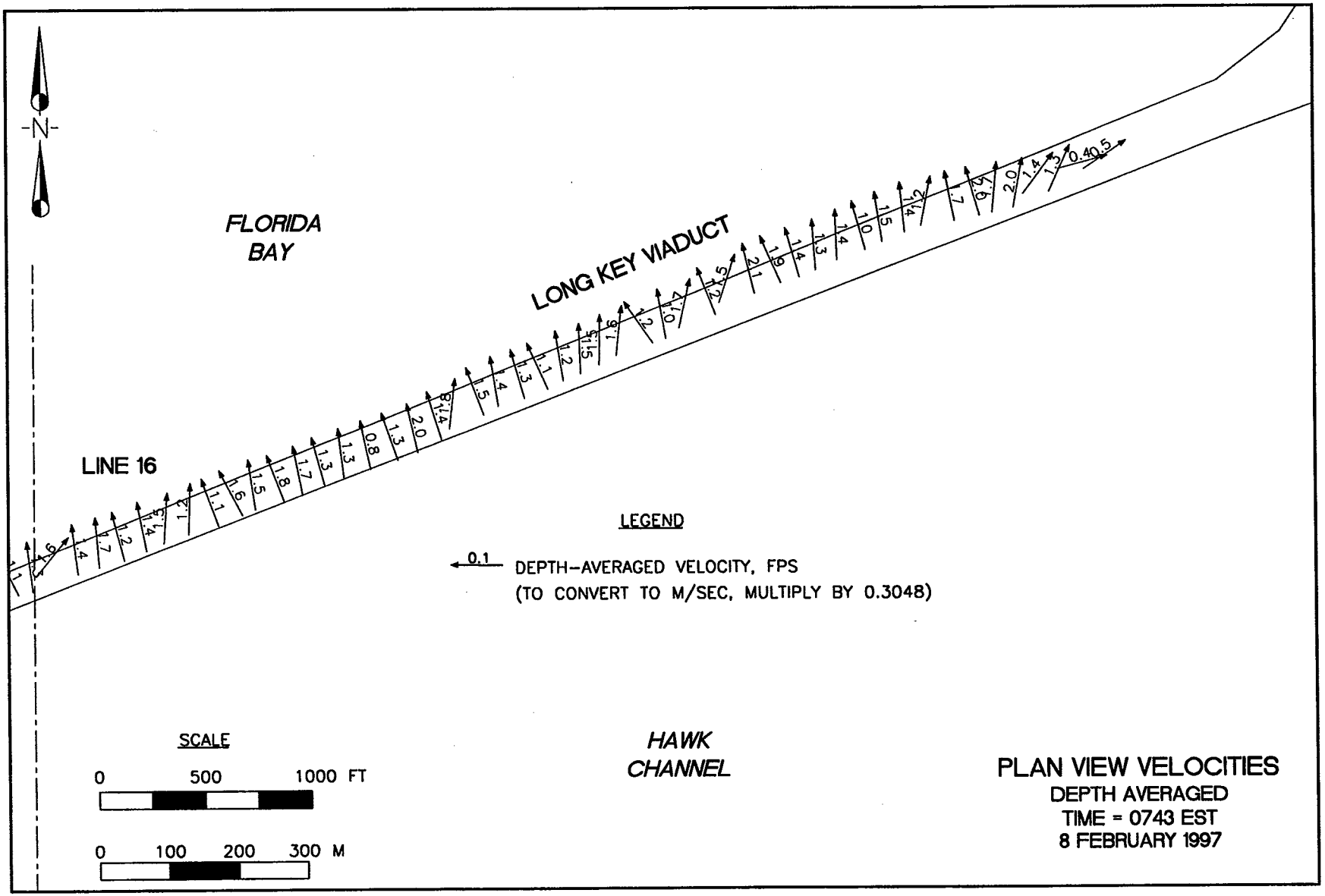
N
FLORIDA BAY
LONG KEY VIADUCT
LINE 16
LEGEND
0.1 DEPTH-AVERAGED VELOCITY, FPS
(TO CONVERT TO M/SEC, MULTIPLY BY 0.3048)
SCALE
0 500 1000 FT
0 100 200 300 M
HAWK CHANNEL
PLAN VIEW VELOCITIES
DEPTH AVERAGED
TIME = 0743 EST
8 FEBRUARY 1997

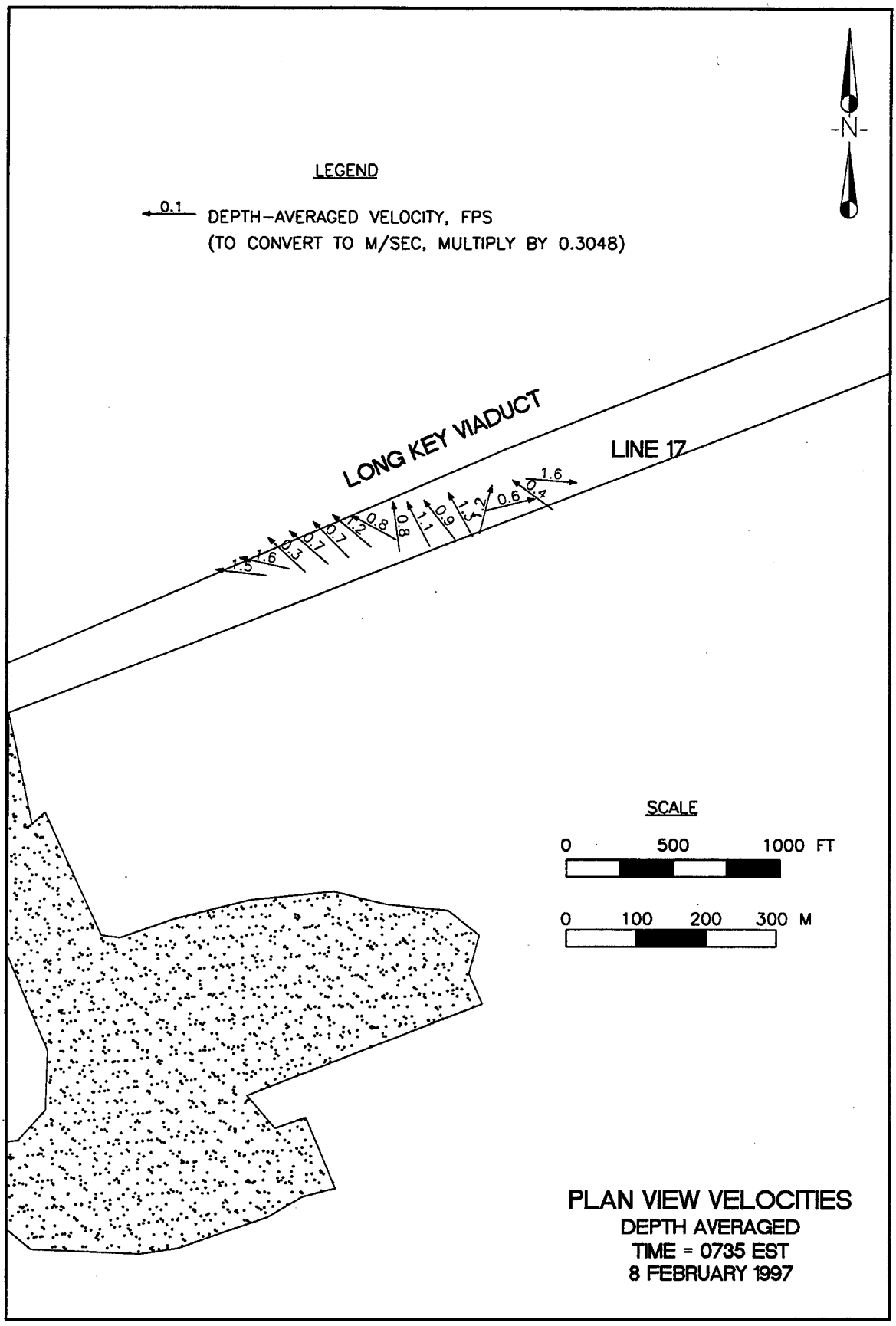
LEGEND
0.1 DEPTH-AVERAGED VELOCITY, FPS
(TO CONVERT TO M/SEC, MULTIPLY BY 0.3048)
-N-
LONG KEY VIADUCT
LINE 17
1.5
1.6
0.3
0.7
0.7
1.2
0.8
0.8
1.1
0.9
1.3
1.2
0.6
0.4
1.6
SCALE
0 500 1000 FT
0 100 200 300 M
PLAN VIEW VELOCITIES
DEPTH AVERAGED
TIME = 0735 EST
8 FEBRUARY 1997

Figure 19

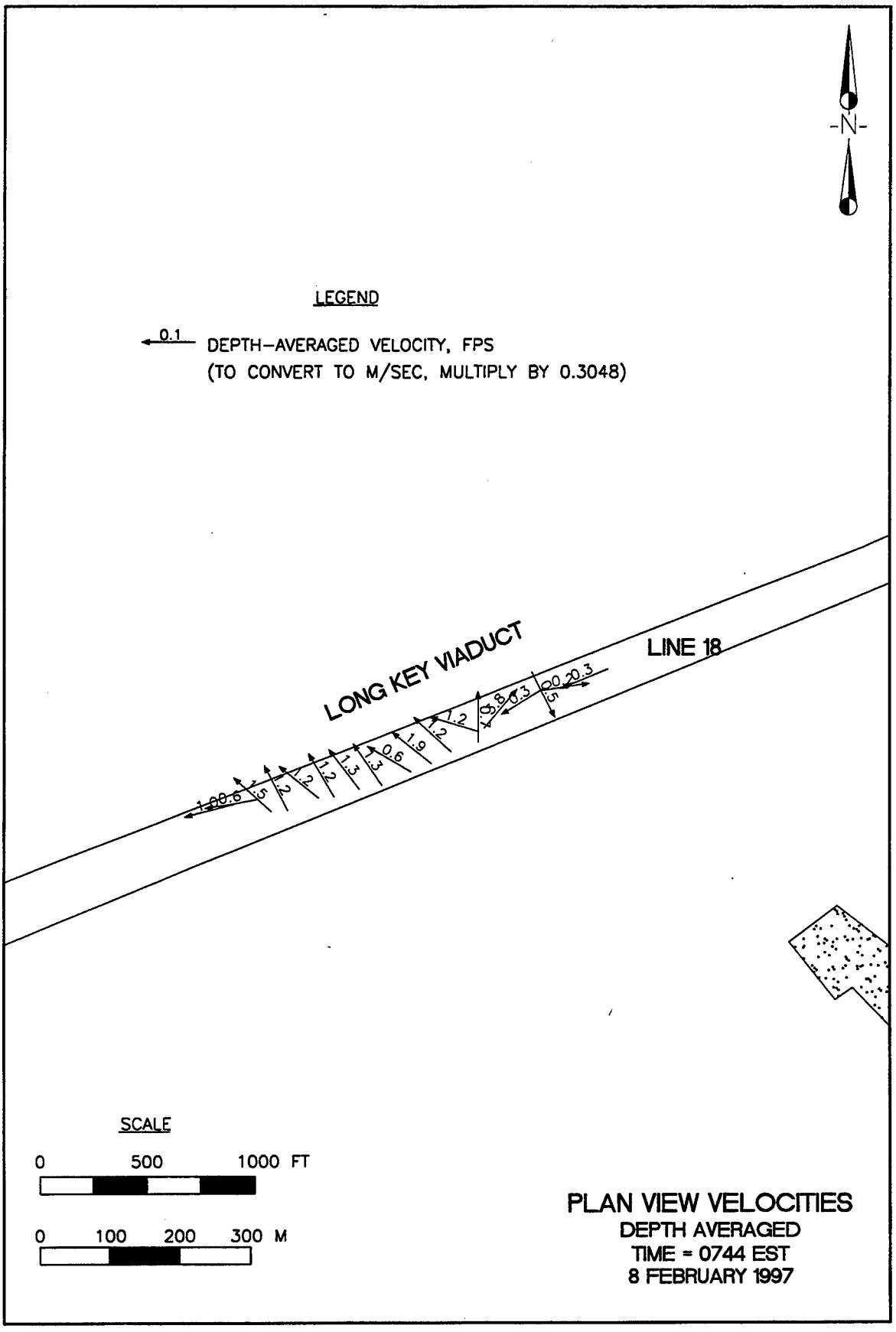
-N-
LEGEND
0.1
DEPTH-AVERAGED VELOCITY, FPS
(TO CONVERT TO M/SEC, MULTIPLY BY 0.3048)
LONG KEY VIADUCT
LINE 18
1.0
0.6
1.5
1.2
1.2
1.2
1.3
1.3
0.6
1.9
1.2
1.2
0.8
0.3
0.2
0.3
5
SCALE
0
500
1000 FT
0
100
200
300 M
PLAN VIEW VELOCITIES
DEPTH AVERAGED
TIME = 0744 EST
8 FEBRUARY 1997

Figure 20

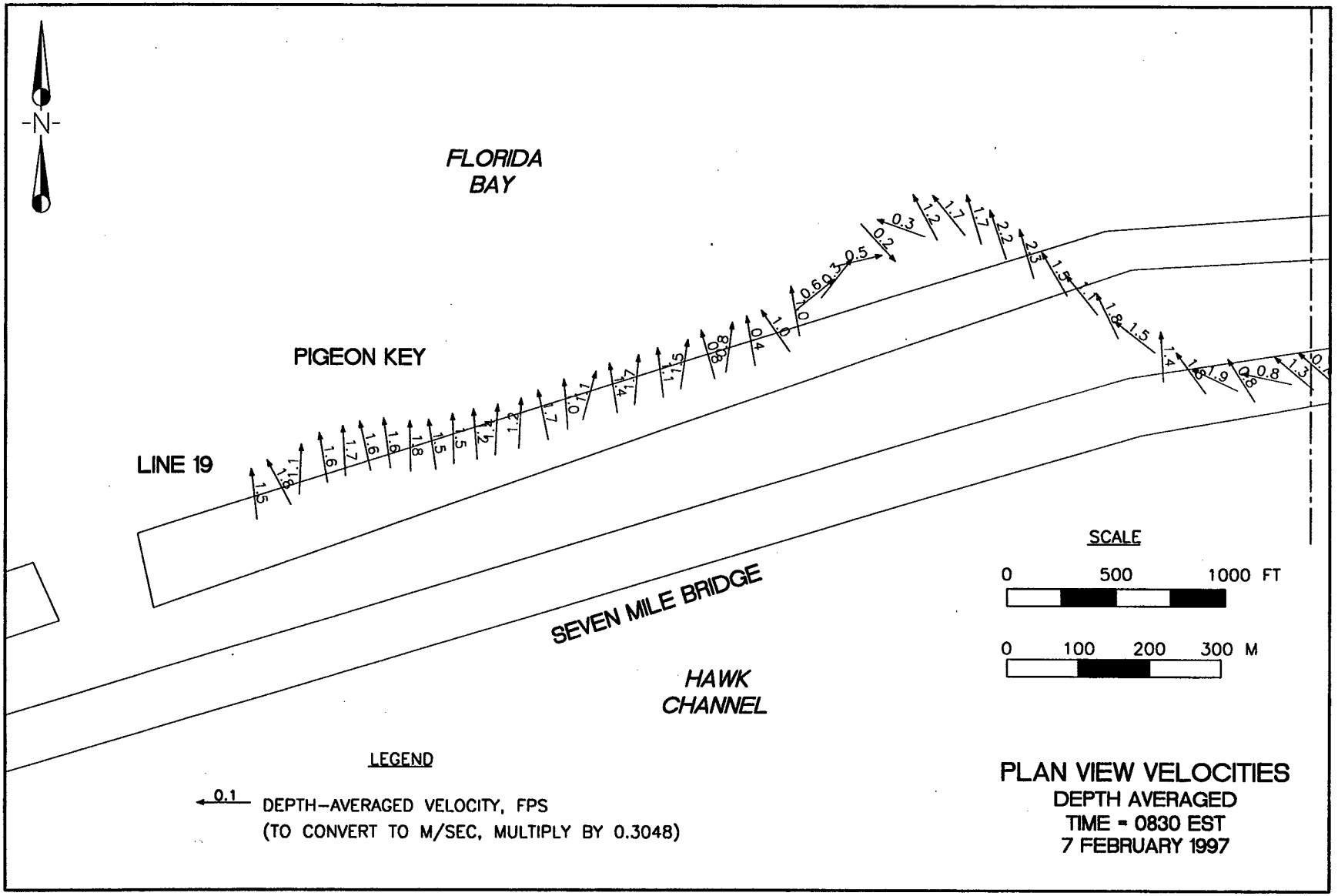
-N-
FLORIDA BAY
PIGEON KEY
LINE 19
SEVEN MILE BRIDGE
HAWK CHANNEL
SCALE
0 500 1000 FT
0 100 200 300 M
LEGEND
0.1 DEPTH-AVERAGED VELOCITY, FPS
(TO CONVERT TO M/SEC, MULTIPLY BY 0.3048)
PLAN VIEW VELOCITIES
DEPTH AVERAGED
TIME = 0830 EST
7 FEBRUARY 1997

Figure 21

Figure 22

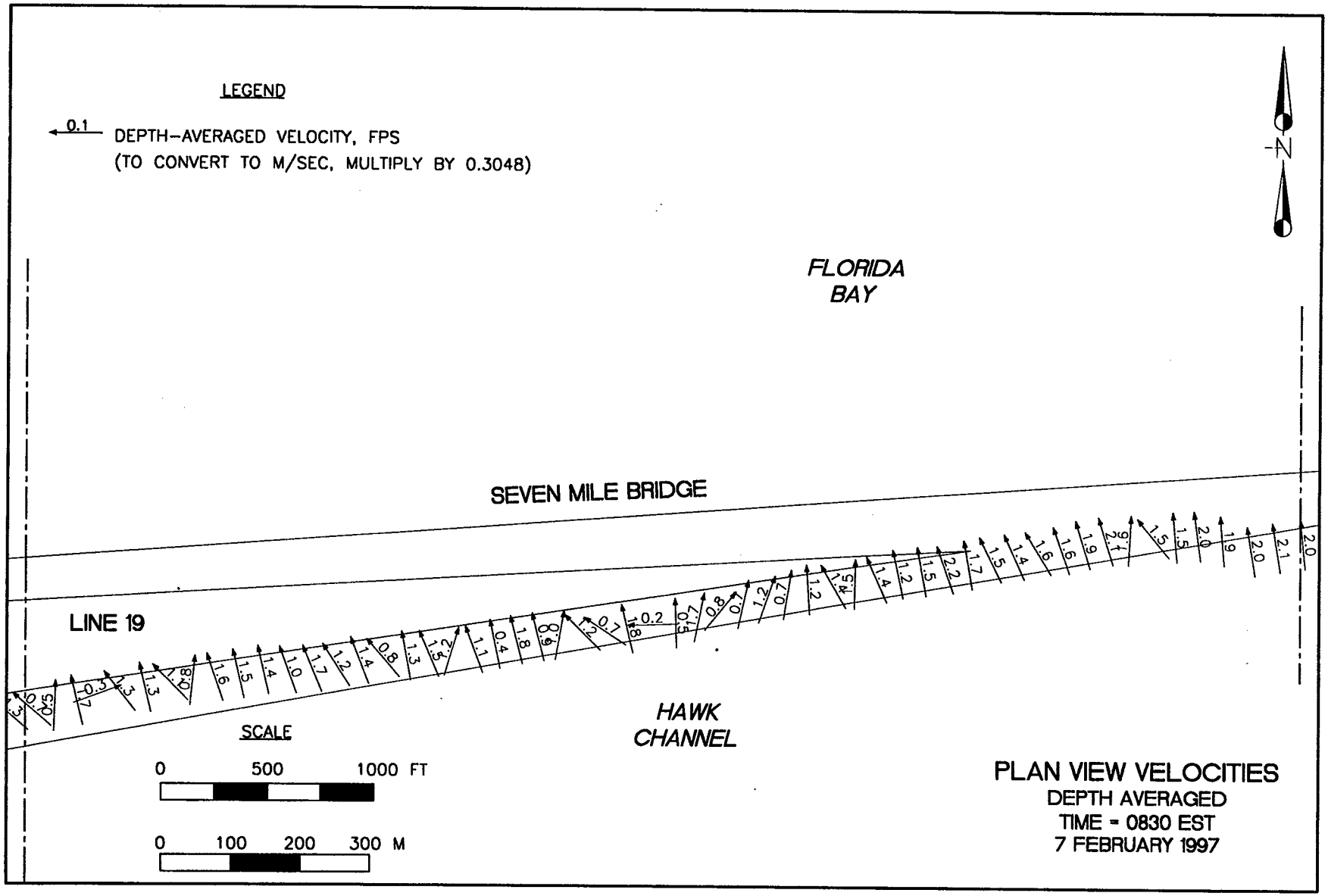
LEGEND
0.1
DEPTH–AVERAGED VELOCITY, FPS
(TO CONVERT TO M/SEC, MULTIPLY BY 0.3048)
N
FLORIDA BAY
SEVEN MILE BRIDGE
LINE 19
HAWK CHANNEL
SCALE
0 500 1000 FT
0 100 200 300 M
PLAN VIEW VELOCITIES
DEPTH AVERAGED
TIME = 0830 EST
7 FEBRUARY 1997

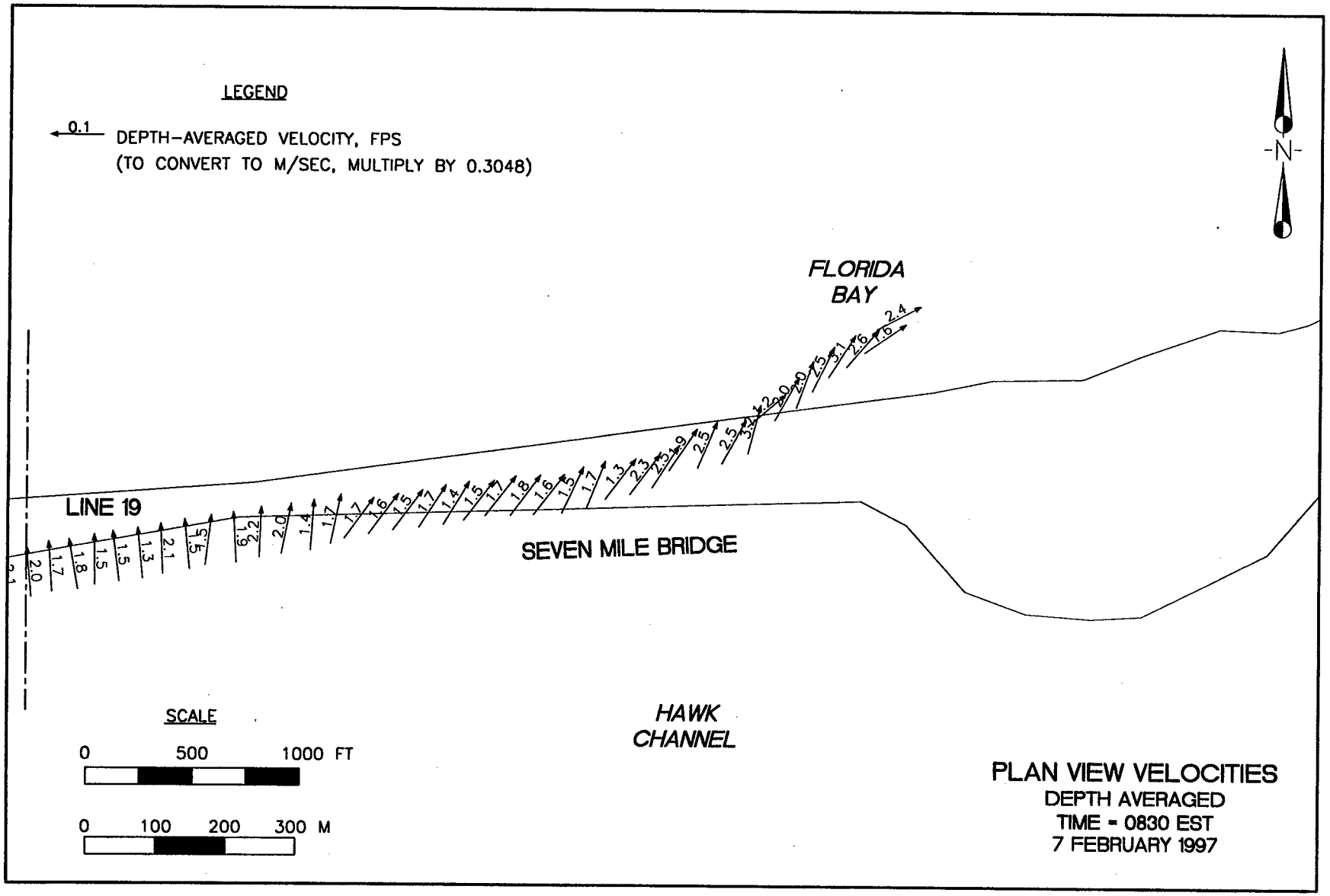
LEGEND
0.1
DEPTH-AVERAGED VELOCITY, FPS
(TO CONVERT TO M/SEC, MULTIPLY BY 0.3048)
N
FLORIDA BAY
LINE 19
SEVEN MILE BRIDGE
HAWK CHANNEL
SCALE
0 500 1000 FT
0 100 200 300 M
PLAN VIEW VELOCITIES
DEPTH AVERAGED
TIME = 0830 EST
7 FEBRUARY 1997

Figure 23

Figure 24

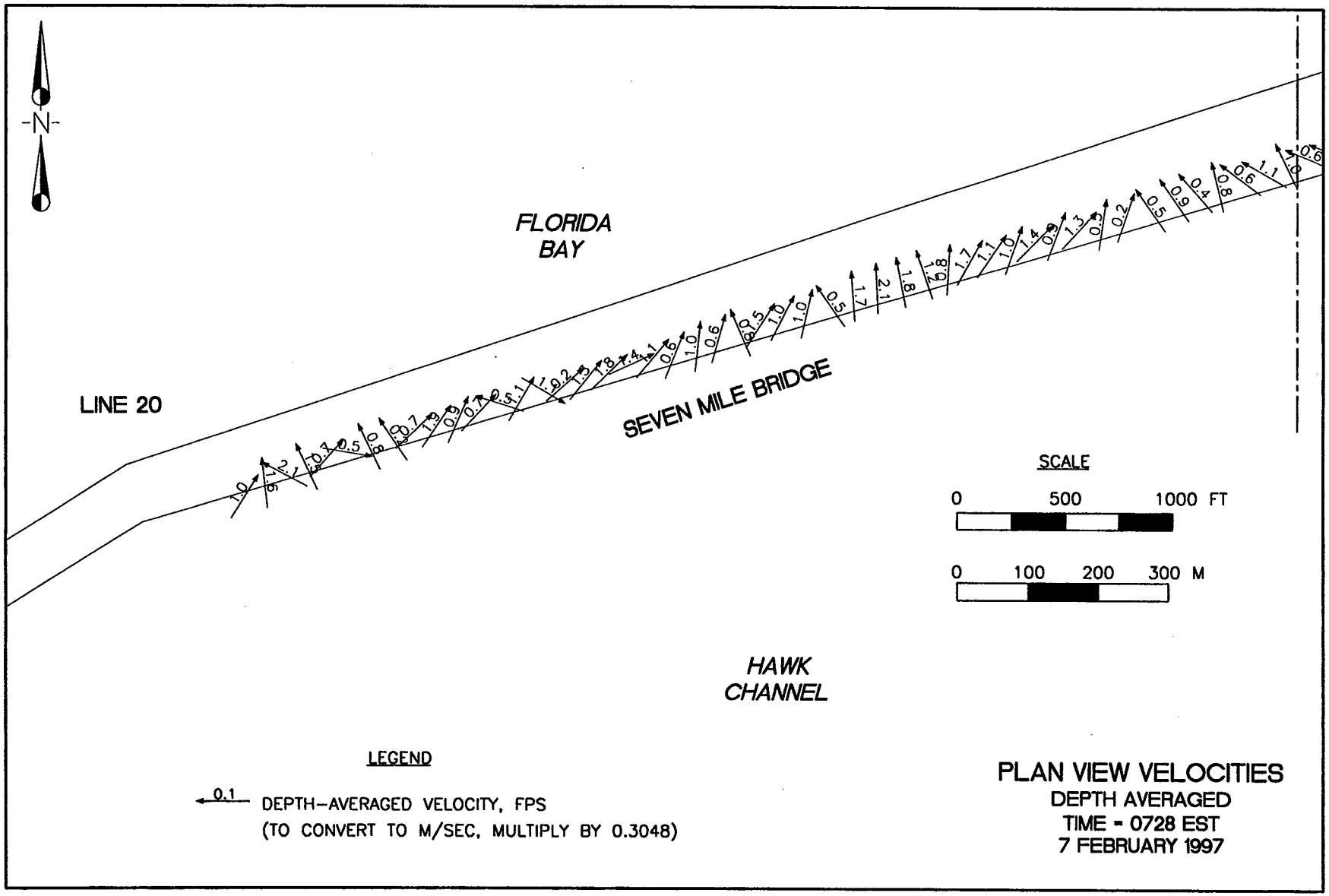
N
FLORIDA BAY
LINE 20
SEVEN MILE BRIDGE
HAWK CHANNEL
SCALE
0 500 1000 FT
0 100 200 300 M
LEGEND
0.1 DEPTH-AVERAGED VELOCITY, FPS
(TO CONVERT TO M/SEC, MULTIPLY BY 0.3048)
PLAN VIEW VELOCITIES
DEPTH AVERAGED
TIME = 0728 EST
7 FEBRUARY 1997

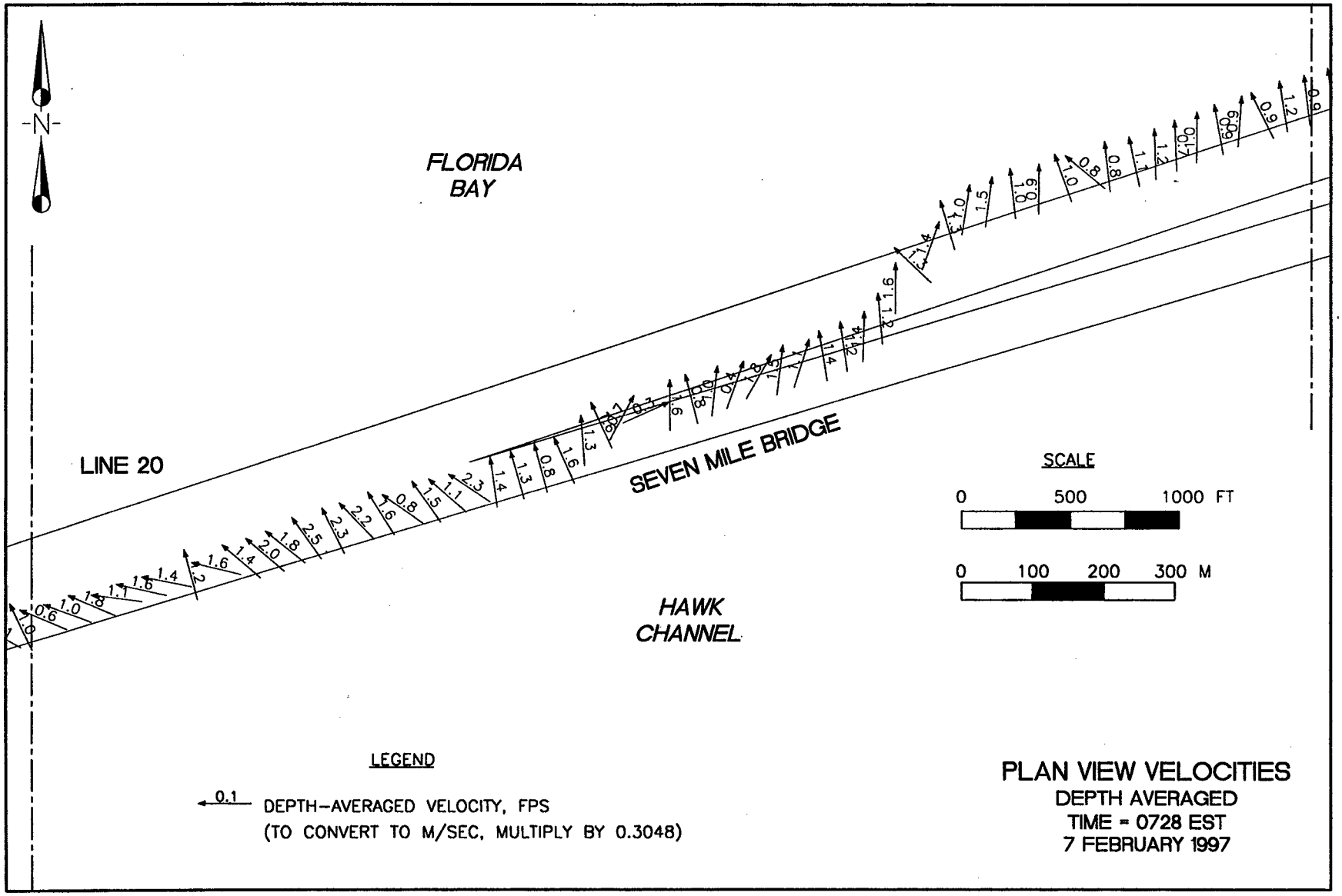
N
FLORIDA BAY
LINE 20
SEVEN MILE BRIDGE
HAWK CHANNEL
SCALE
0 500 1000 FT
0 100 200 300 M
LEGEND
0.1 DEPTH-AVERAGED VELOCITY, FPS
(TO CONVERT TO M/SEC, MULTIPLY BY 0.3048)
PLAN VIEW VELOCITIES
DEPTH AVERAGED
TIME = 0728 EST
7 FEBRUARY 1997

Figure 25

Figure 26

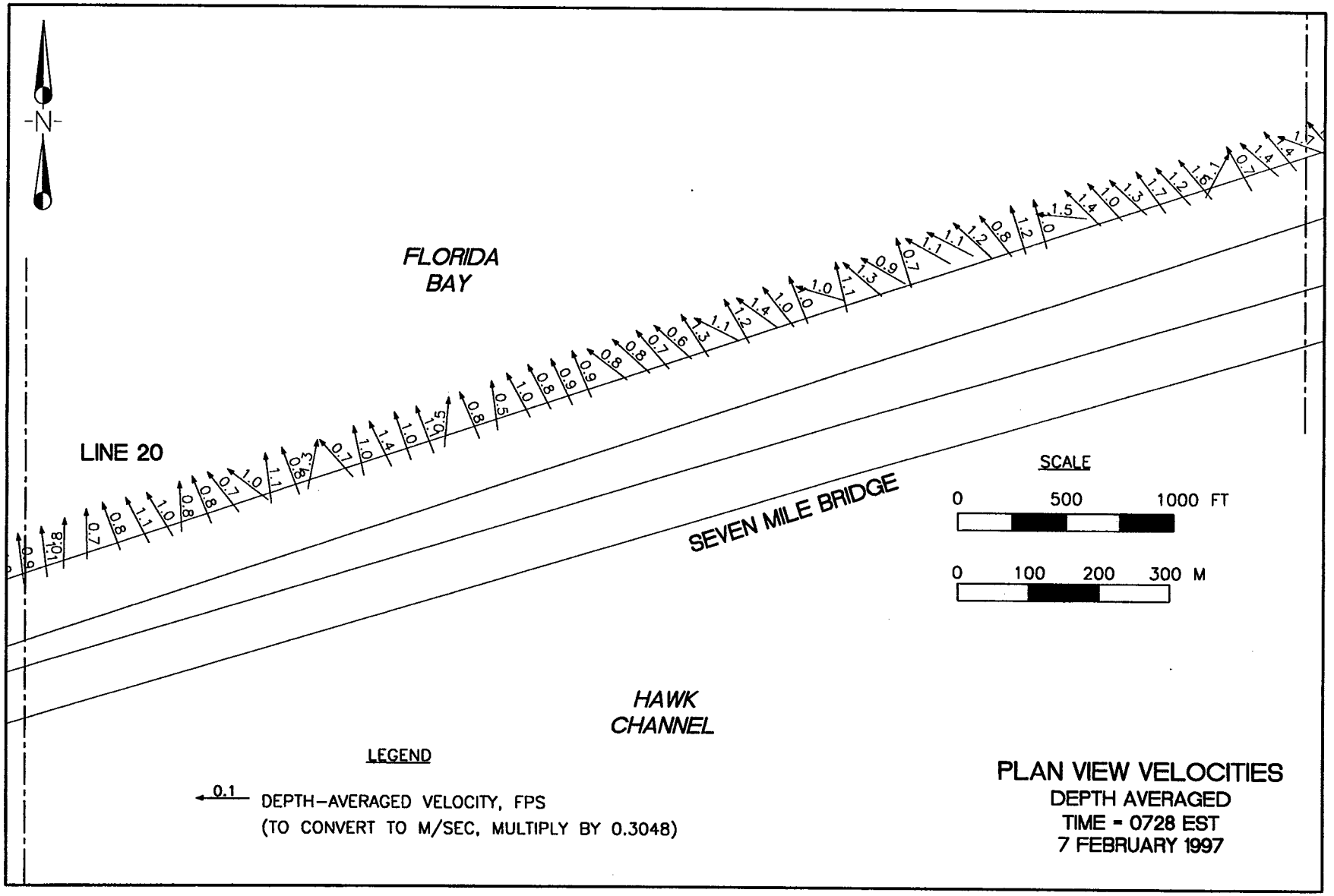
N
FLORIDA BAY
LINE 20
SEVEN MILE BRIDGE
HAWK CHANNEL
SCALE
0 500 1000 FT
0 100 200 300 M
LEGEND
0.1 DEPTH-AVERAGED VELOCITY, FPS
(TO CONVERT TO M/SEC, MULTIPLY BY 0.3048)
PLAN VIEW VELOCITIES
DEPTH AVERAGED
TIME - 0728 EST
7 FEBRUARY 1997

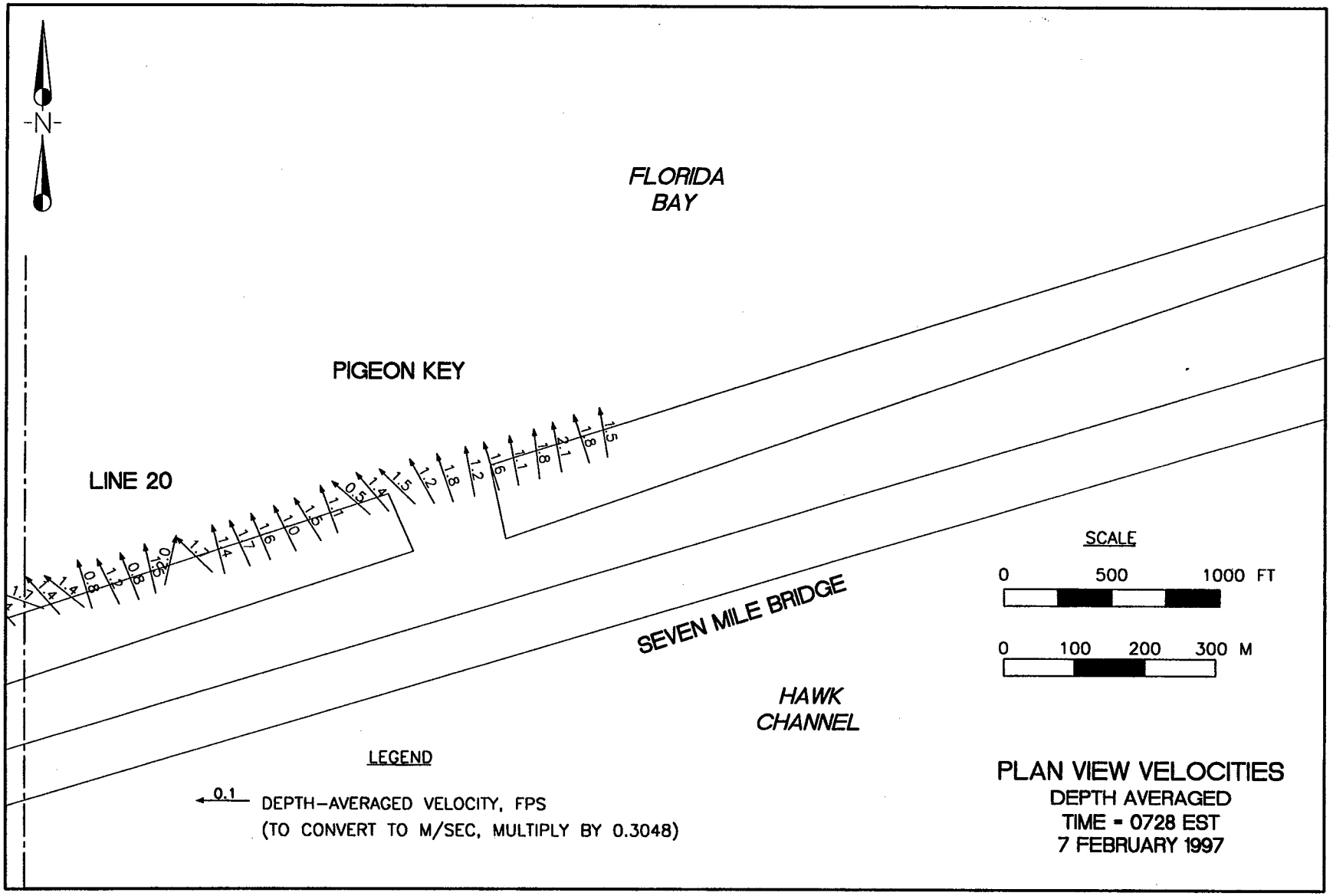
-N-
FLORIDA
BAY
PIGEON KEY
LINE 20
SEVEN MILE BRIDGE
HAWK
CHANNEL
SCALE
0 500 1000 FT
0 100 200 300 M
LEGEND
0.1 DEPTH-AVERAGED VELOCITY, FPS
(TO CONVERT TO M/SEC, MULTIPLY BY 0.3048)
PLAN VIEW VELOCITIES
DEPTH AVERAGED
TIME = 0728 EST
7 FEBRUARY 1997

Figure 27

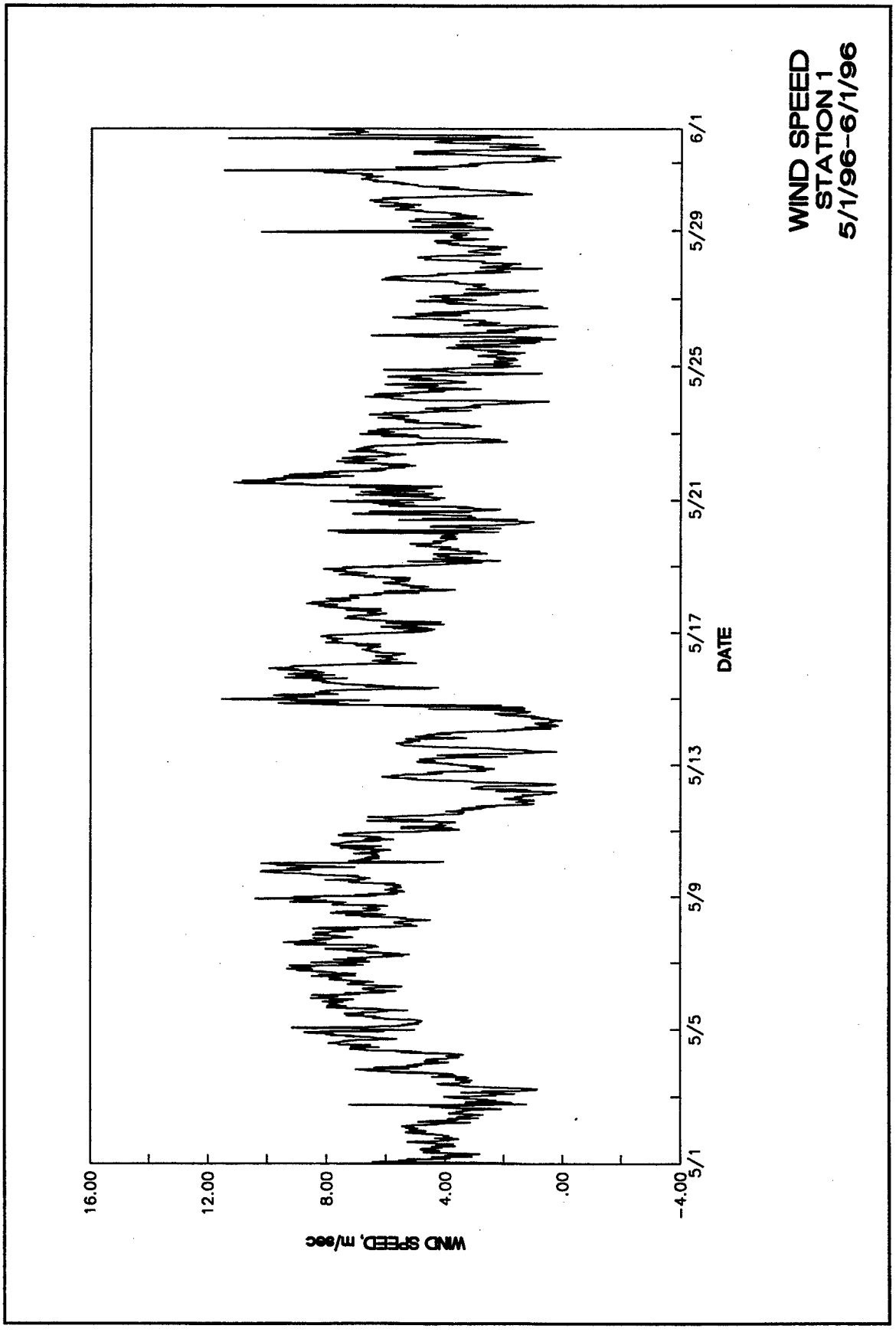
WIND SPEED
STATION 1
5/1/96-6/1/96
WIND SPEED, m/sec
16.00
12.00
8.00
4.00
.00
-4.00
5/1
5/5
5/9
5/13
5/17
5/21
5/25
5/29
6/1
DATE

Plate 1

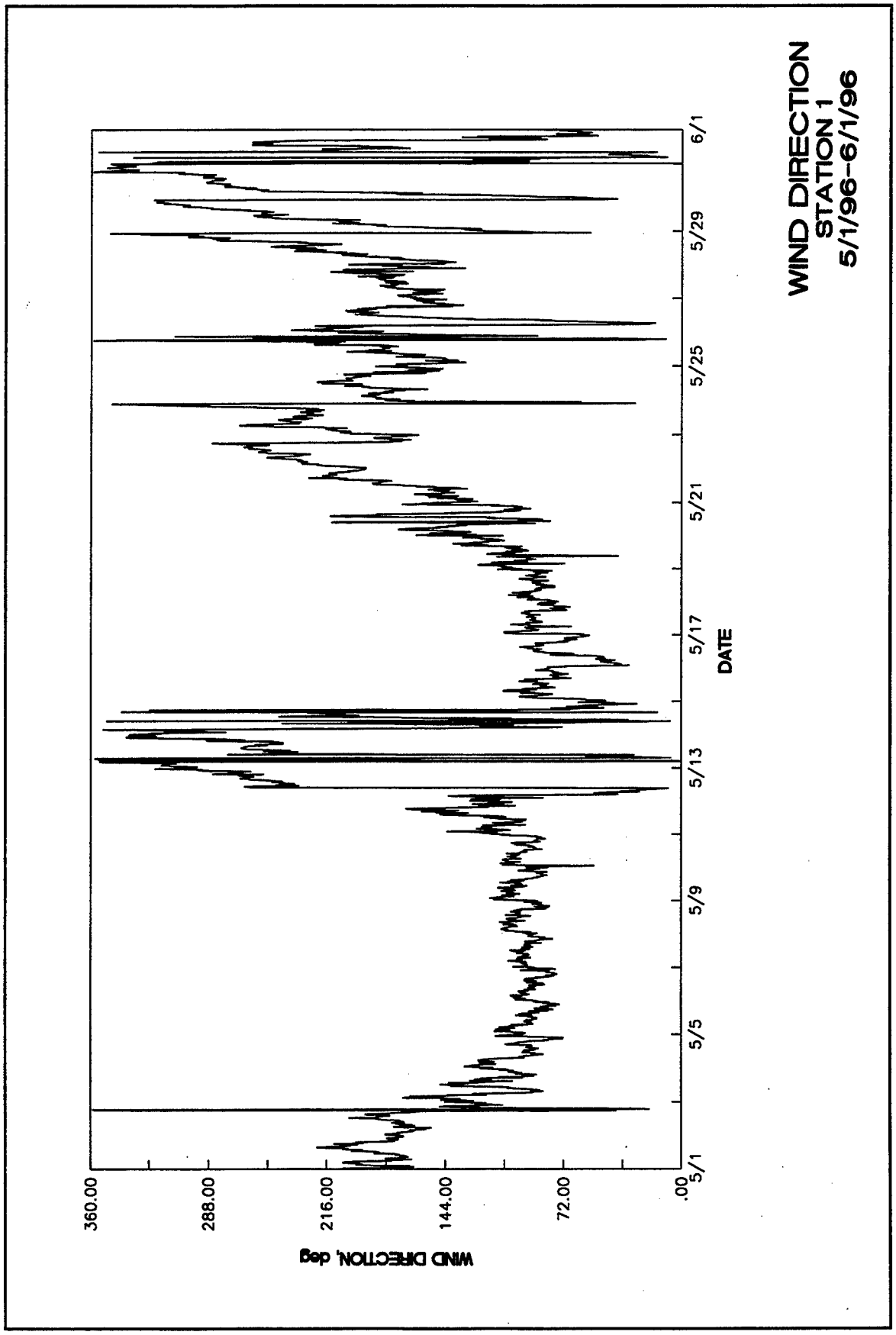
WIND DIRECTION
STATION 1
5/1/96-6/1/96
WIND DIRECTION, deg
360.00
288.00
216.00
144.00
72.00
.00
5/1
5/5
5/9
5/13
5/17
5/21
5/25
5/29
6/1
DATE

Plate 2

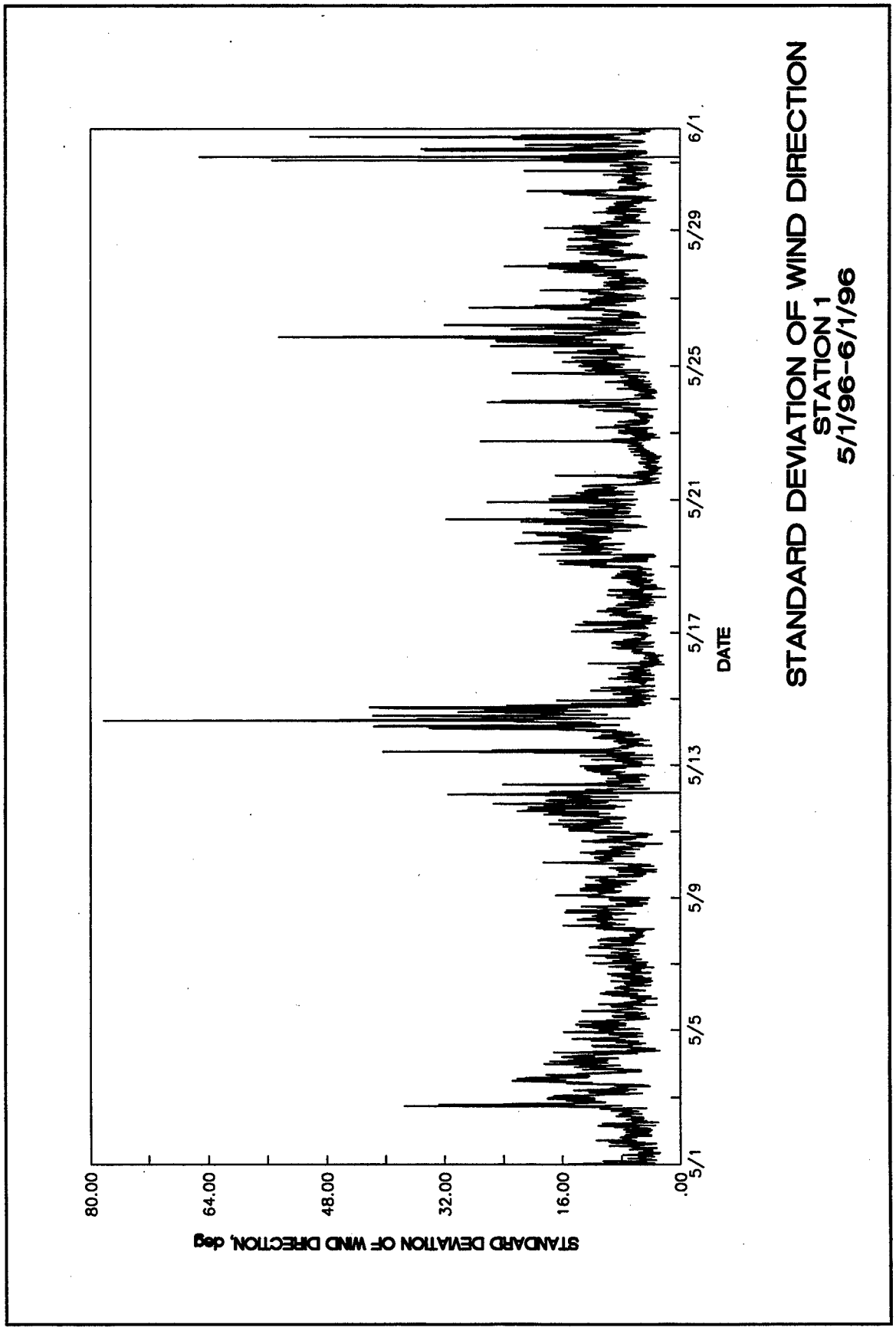
STANDARD DEVIATION OF WIND DIRECTION
STATION 1
5/1/96-6/1/96
STANDARD DEVIATION OF WIND DIRECTION, deg
80.00
64.00
48.00
32.00
16.00
.00
5/1
5/5
5/9
5/13
5/17
5/21
5/25
5/29
6/1
DATE

Plate 3

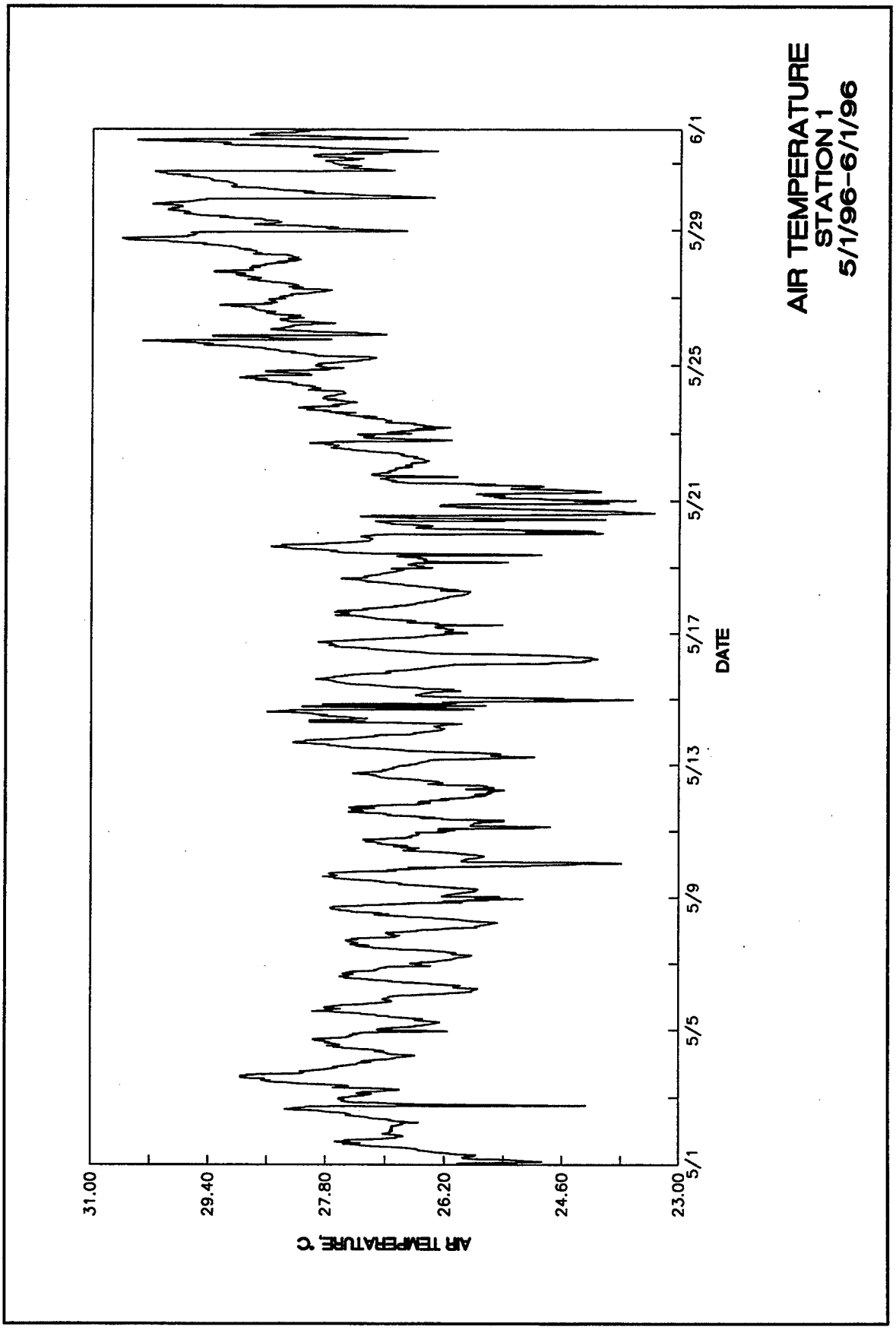
AIR TEMPERATURE
STATION 1
5/1/96-6/1/96
AIR TEMPERATURE, °C
31.00
29.40
27.80
26.20
24.60
23.00
5/1
5/5
5/9
5/13
5/17
5/21
5/25
5/29
6/1
DATE

Plate 4

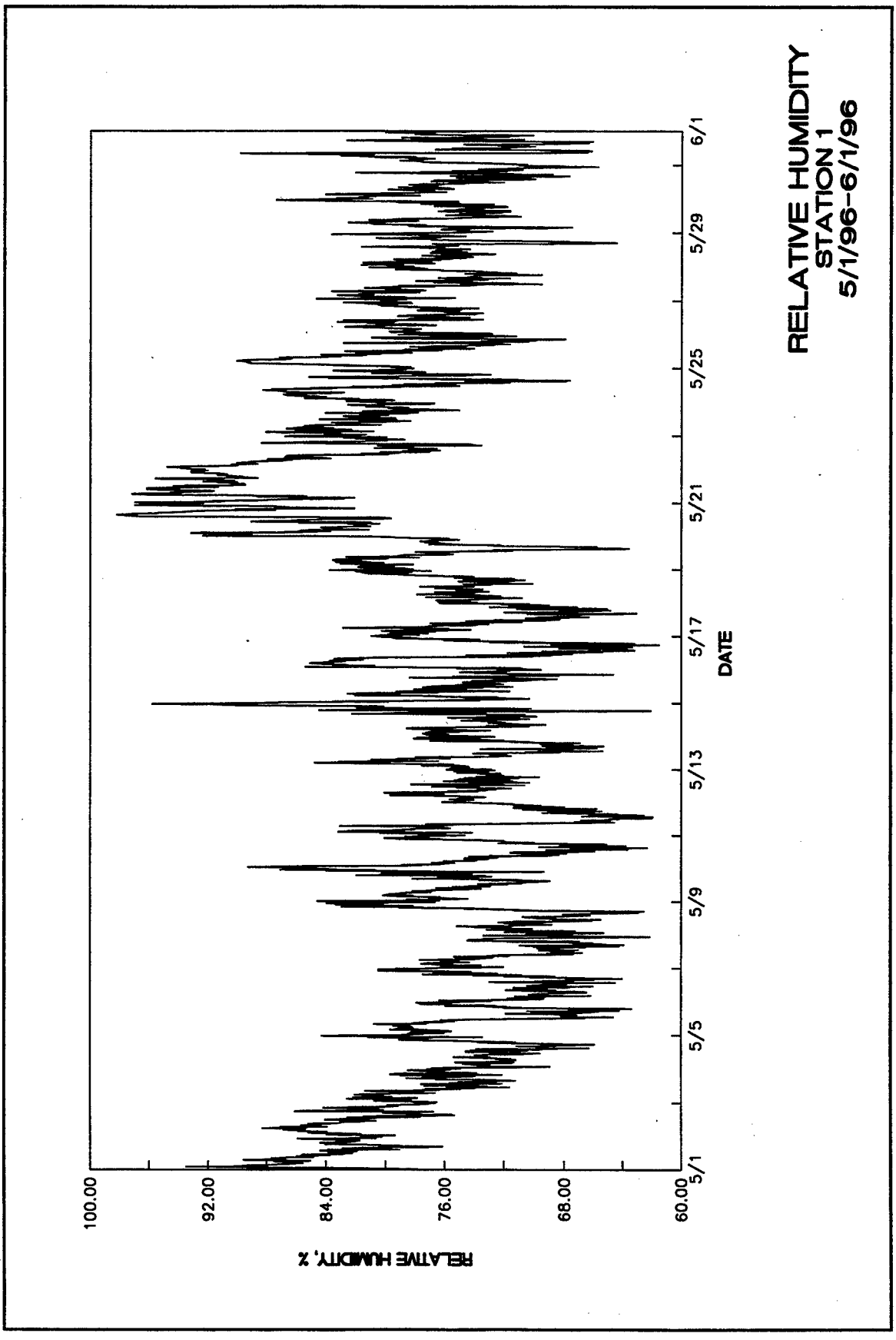
RELATIVE HUMIDITY
STATION 1
5/1/96-6/1/96
RELATIVE HUMIDITY, %
100.00
92.00
84.00
76.00
68.00
60.00
5/1
5/5
5/9
5/13
5/17
5/21
5/25
5/29
6/1
DATE

Plate 5

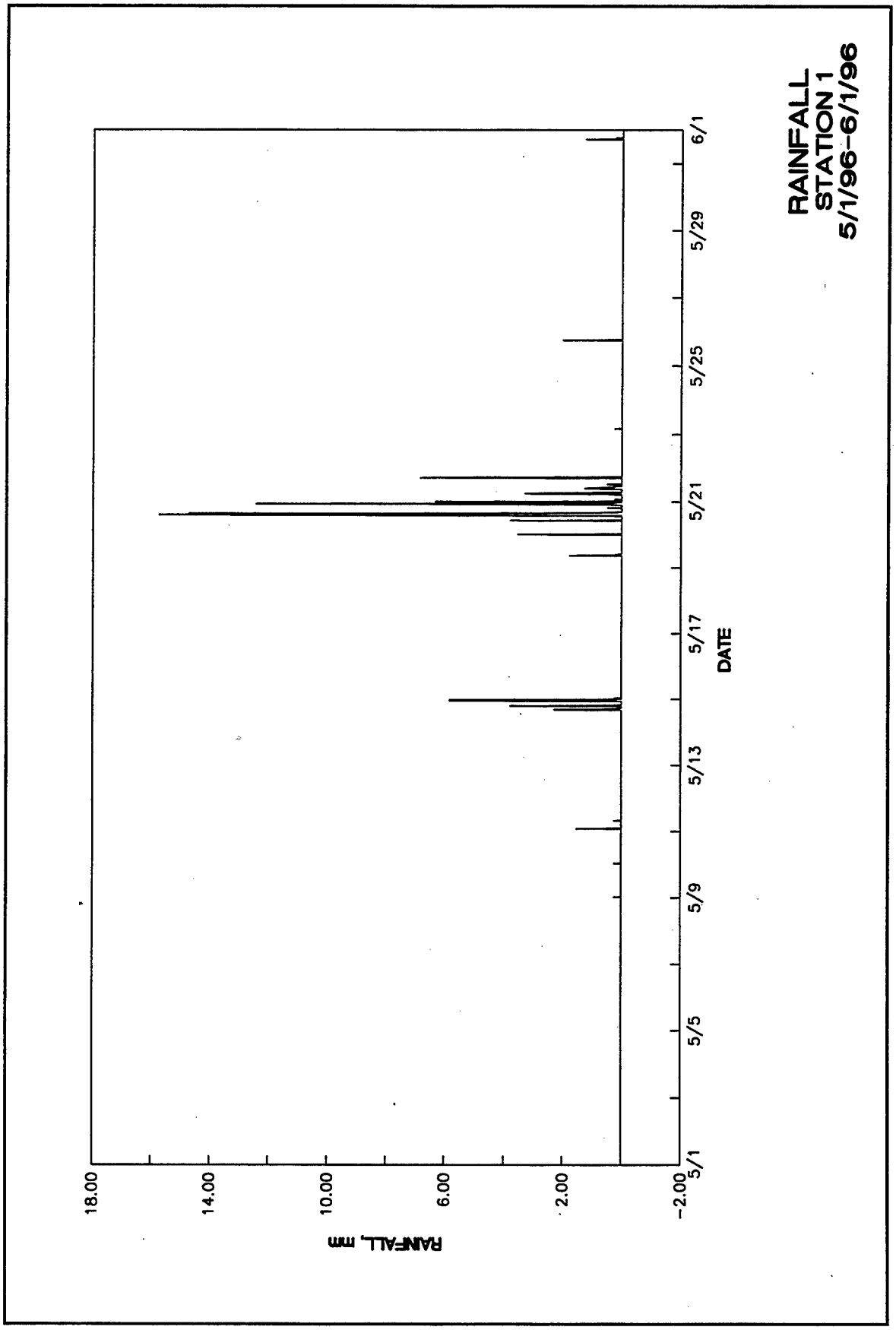
RAINFALL
STATION 1
5/1/96-6/1/96
RAINFALL, mm
18.00
14.00
10.00
6.00
2.00
-2.00
5/1
5/5
5/9
5/13
5/17
5/21
5/25
5/29
6/1
DATE

Plate 6

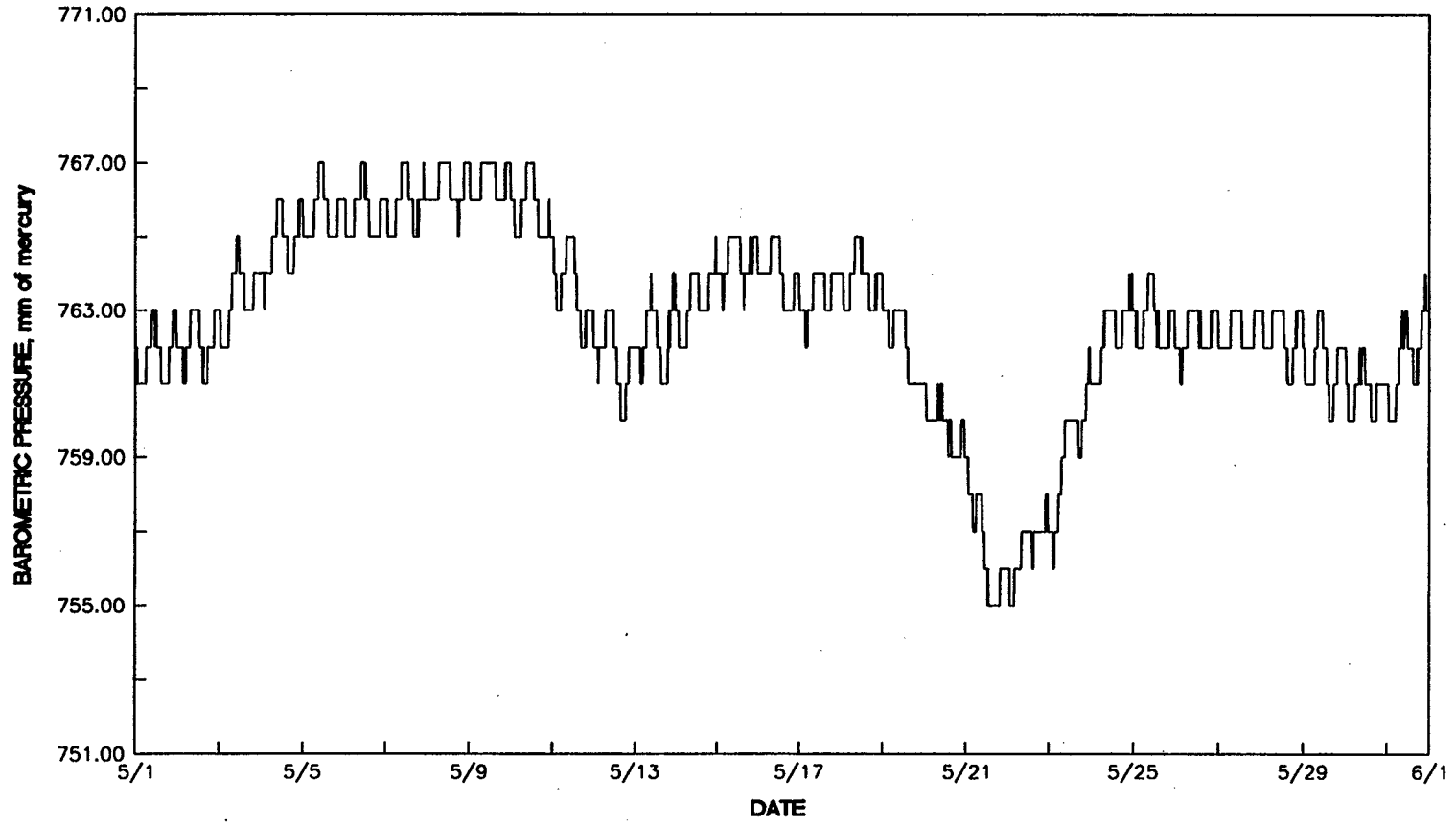

BAROMETRIC PRESSURE
STATION 1
5/1/96-6/1/96

Plate 7

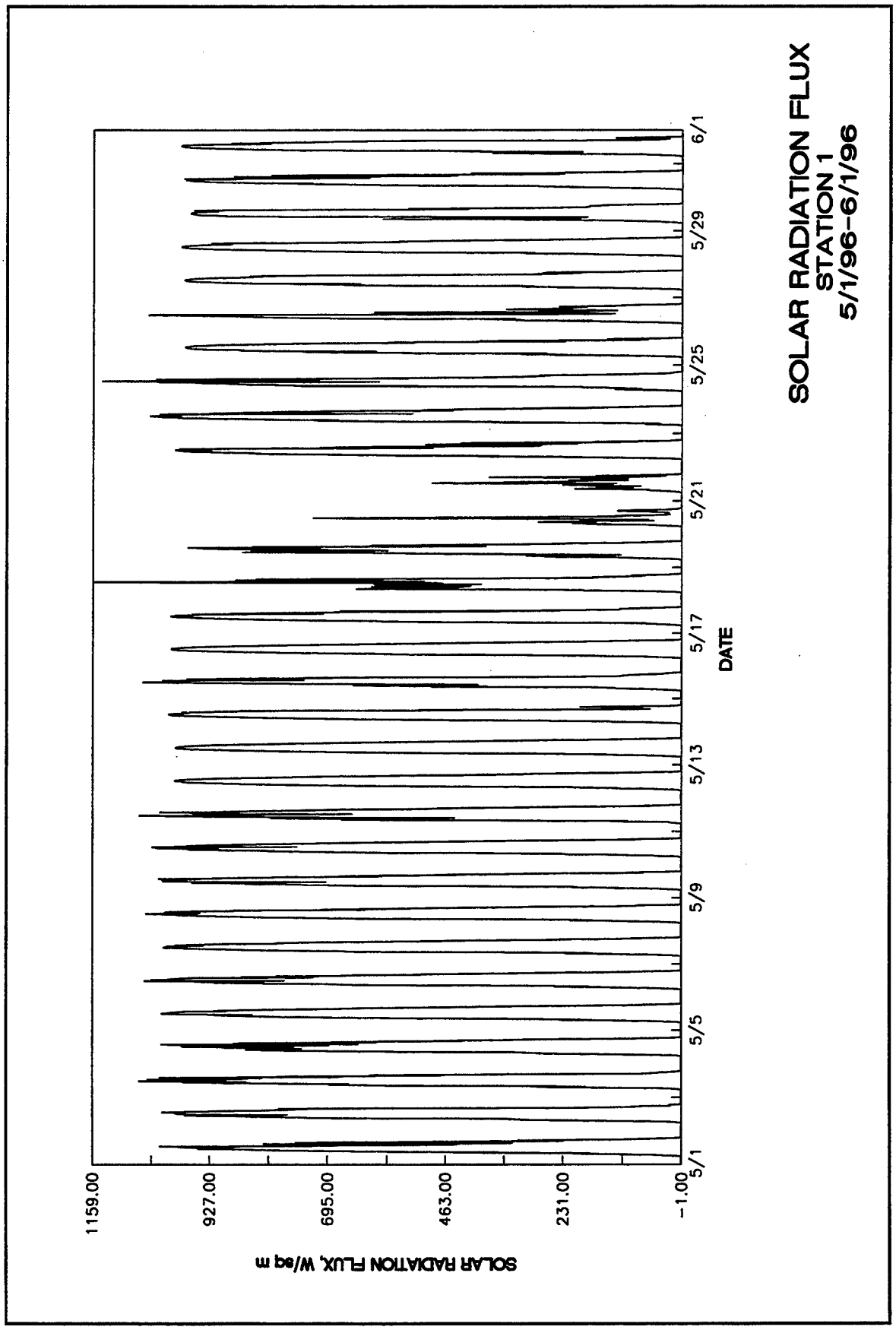
SOLAR RADIATION FLUX
STATION 1
5/1/96-6/1/96
SOLAR RADIATION FLUX, W/sq m
1159.00
927.00
695.00
463.00
231.00
-1.00
5/1
5/5
5/9
5/13
5/17
5/21
5/25
5/29
6/1
DATE

Plate 8

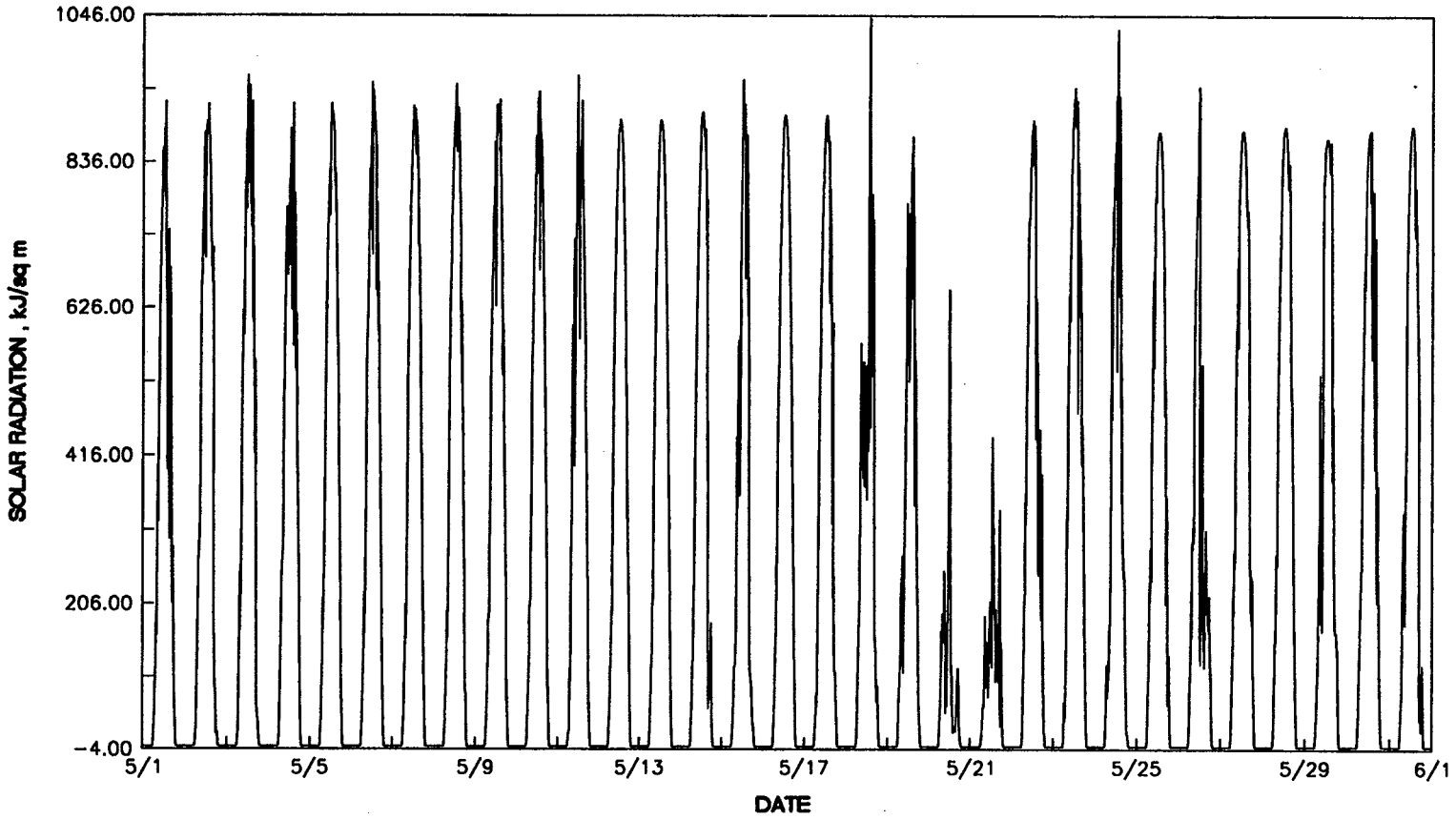

SOLAR RADIATION
STATION 1
5/1/96-6/1/96

Plate 9

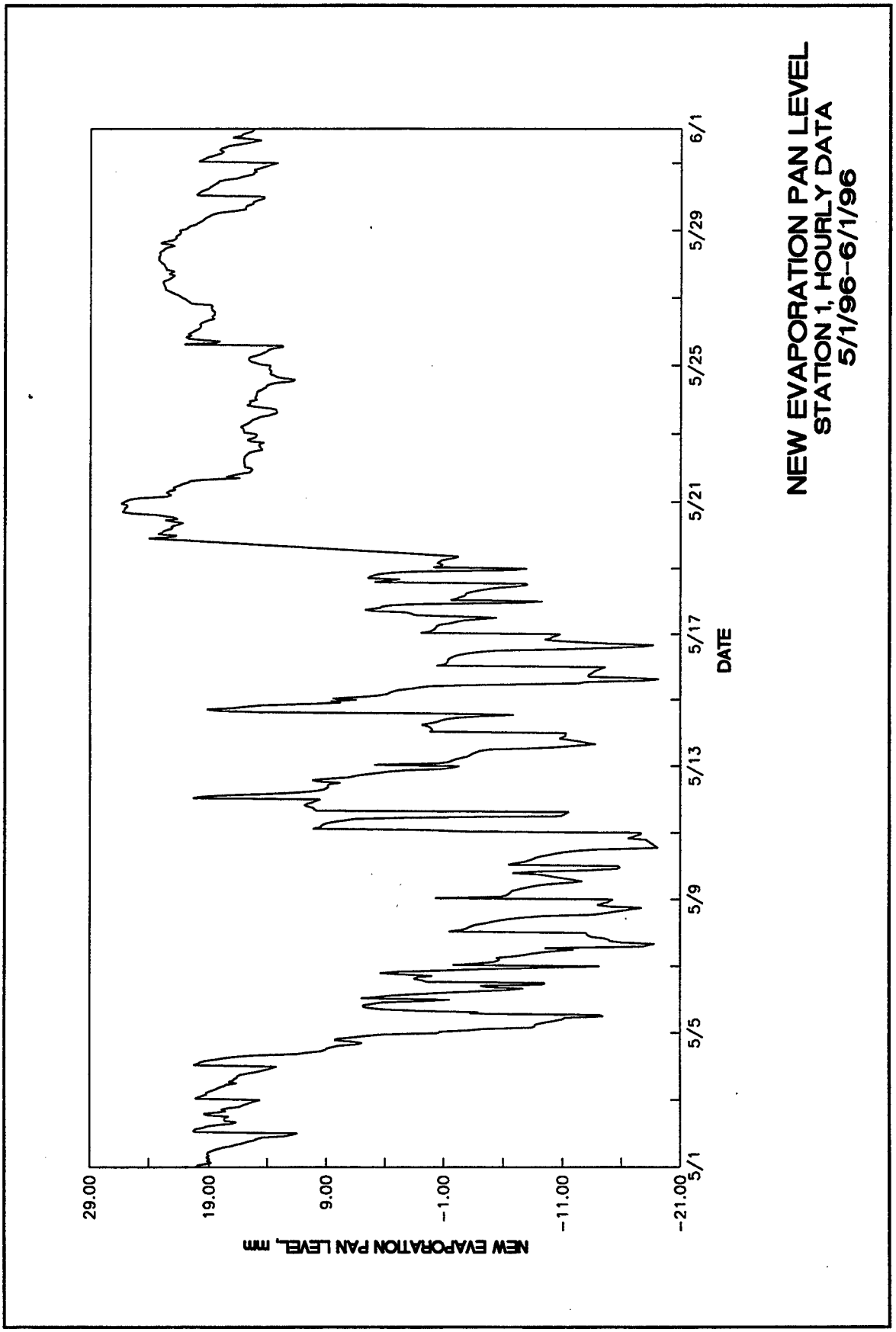
NEW EVAPORATION PAN LEVEL
STATION 1, HOURLY DATA
5/1/96-6/1/96
NEW EVAPORATION PAN LEVEL, mm
29.00
19.00
9.00
-1.00
-11.00
-21.00
5/1
5/5
5/9
5/13
5/17
5/21
5/25
5/29
6/1
DATE

Plate 10

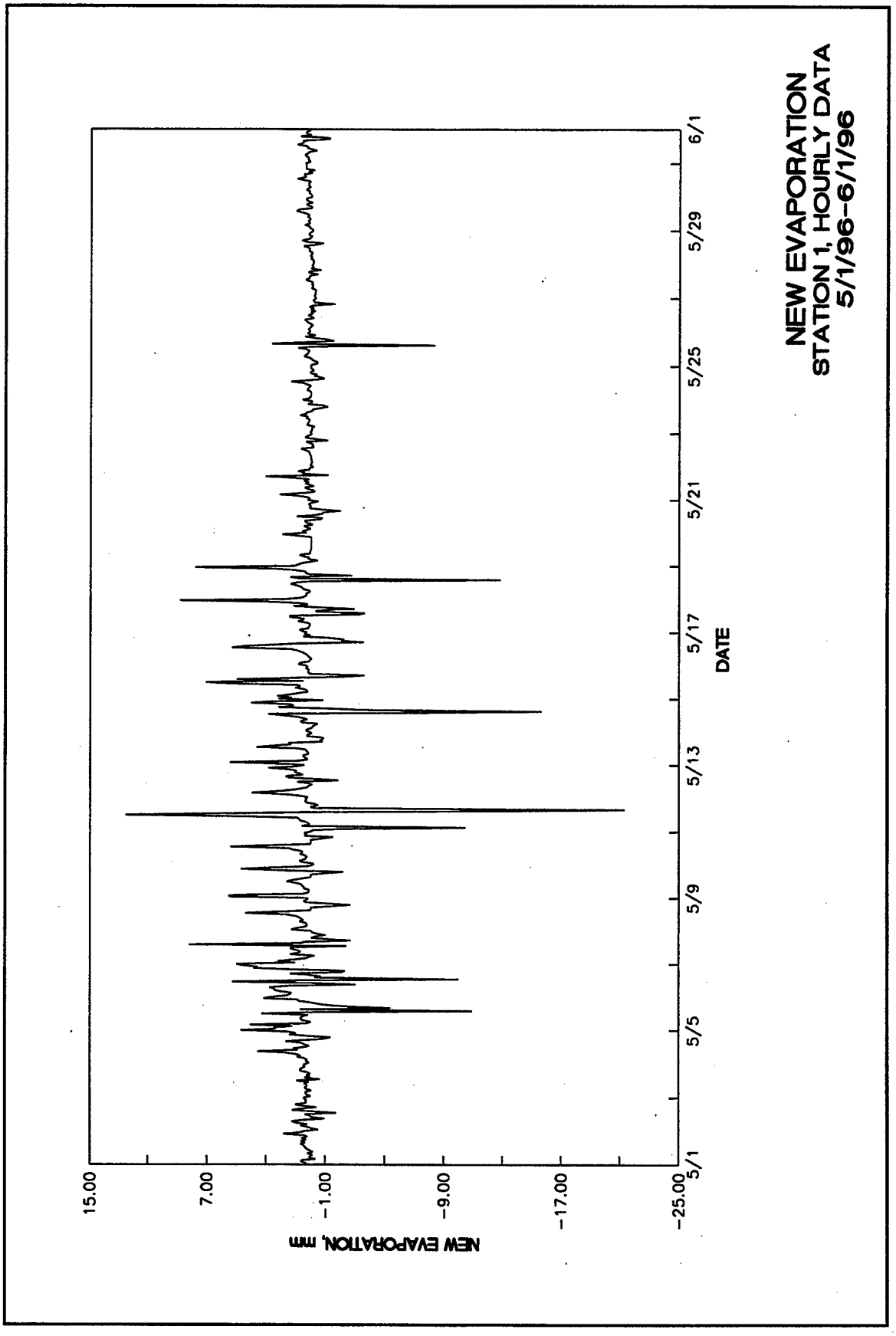
NEW EVAPORATION
STATION 1, HOURLY DATA
5/1/96-6/1/96
NEW EVAPORATION, mm
15.00
7.00
-1.00
-9.00
-17.00
-25.00
5/1
5/5
5/9
5/13
5/17
5/21
5/25
5/29
6/1
DATE

Plate 11

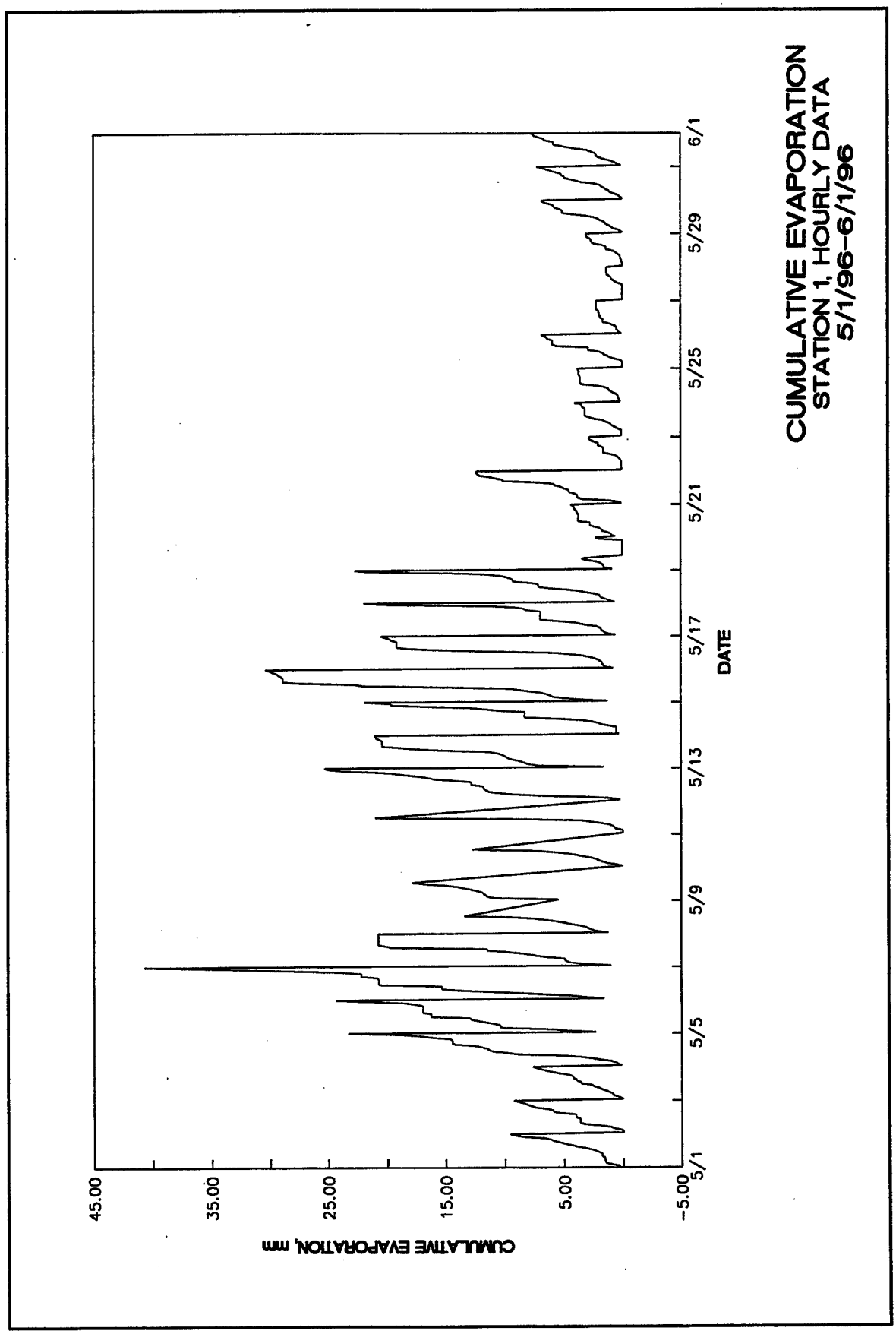
CUMULATIVE EVAPORATION
STATION 1, HOURLY DATA
5/1/96-6/1/96
CUMULATIVE EVAPORATION, mm
45.00
35.00
25.00
15.00
5.00
-5.00
5/1
5/5
5/9
5/13
5/17
5/21
5/25
5/29
6/1
DATE

Plate 12

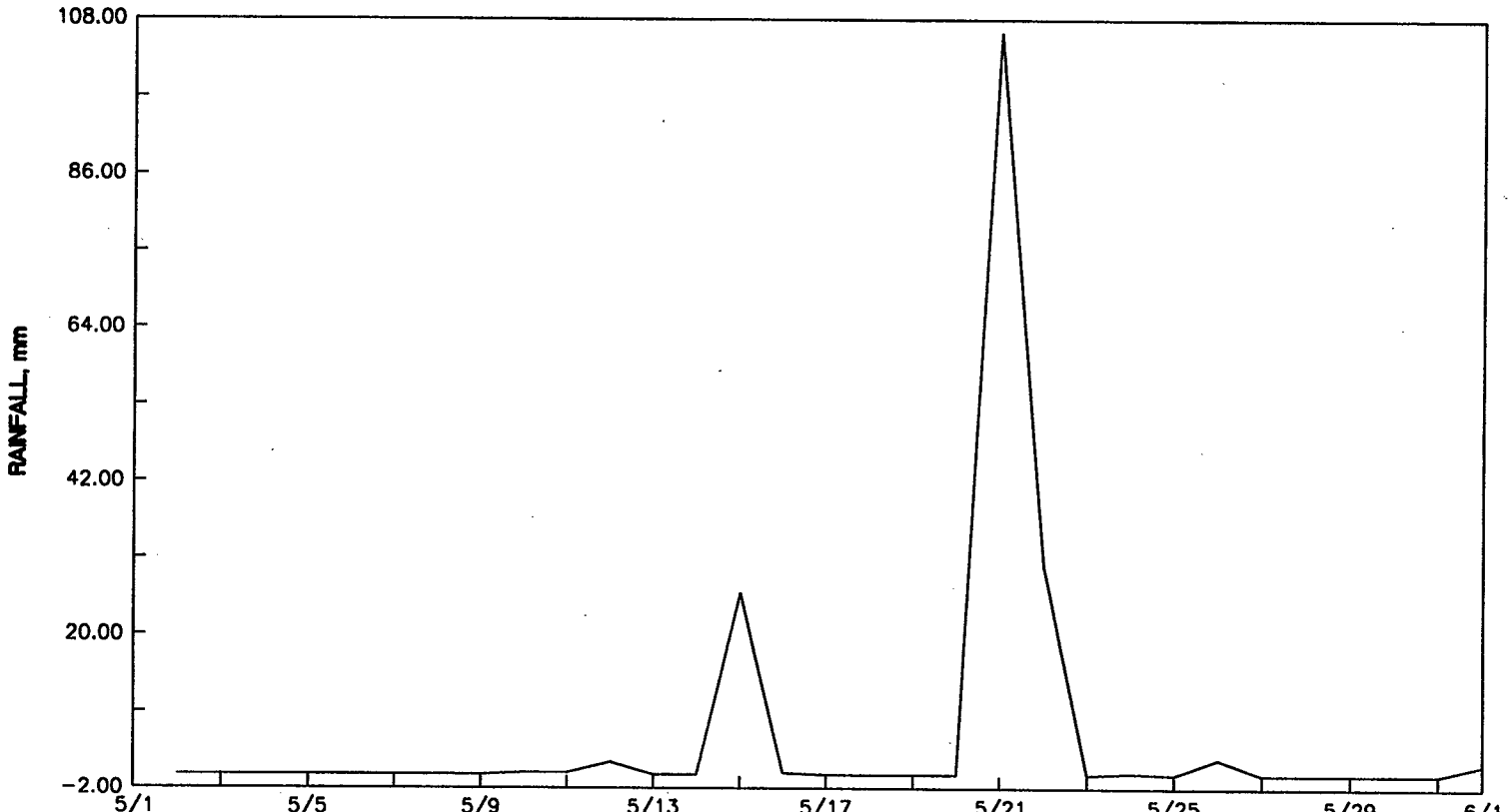

RAINFALL
STATION 1, DAILY DATA
5/1/96-6/1/96

Plate 13

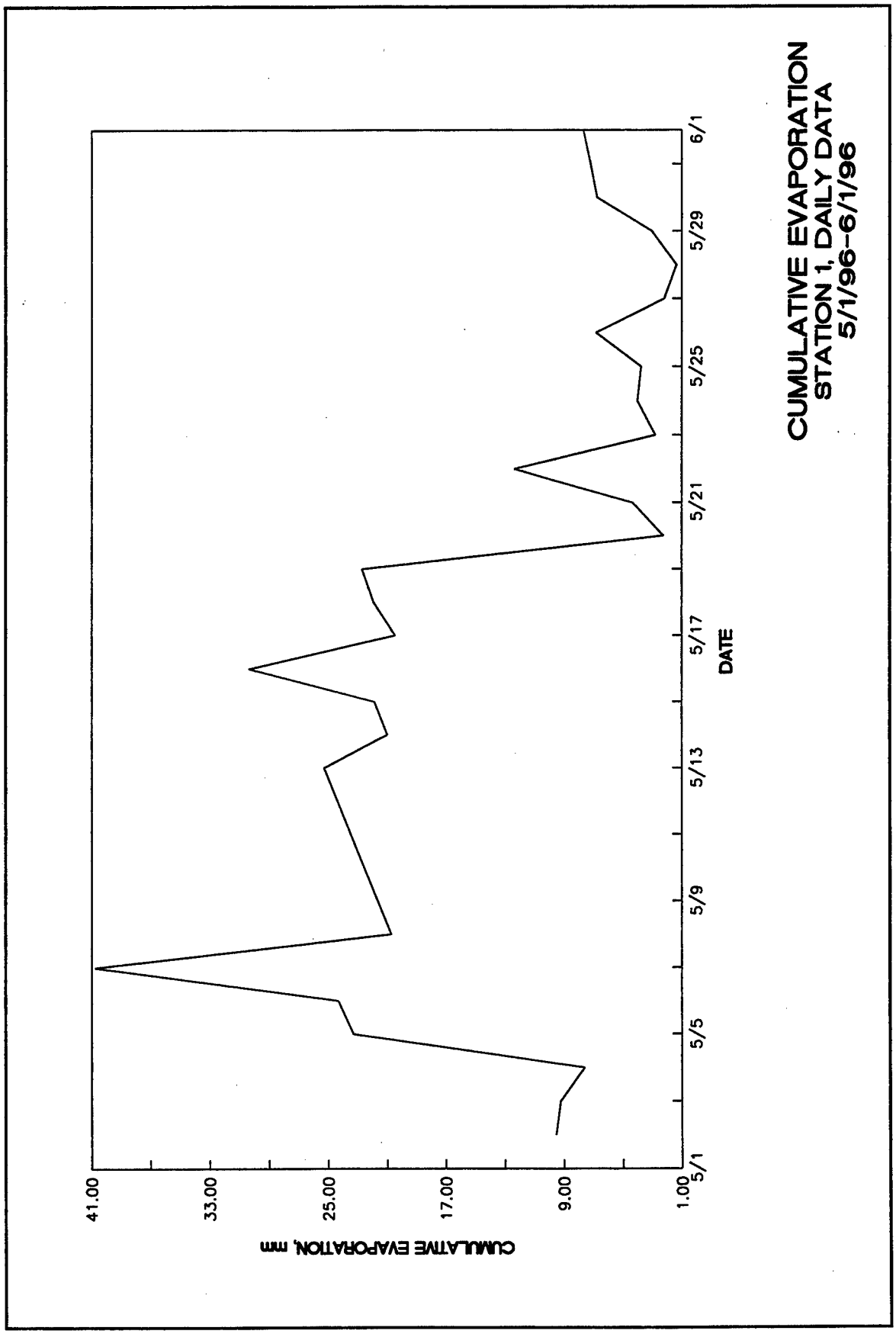
CUMULATIVE EVAPORATION
STATION 1, DAILY DATA
5/1/96-6/1/96
CUMULATIVE EVAPORATION, mm
41.00
33.00
25.00
17.00
9.00
1.00
5/1
5/5
5/9
5/13
5/17
5/21
5/25
5/29
6/1
DATE

Plate 14

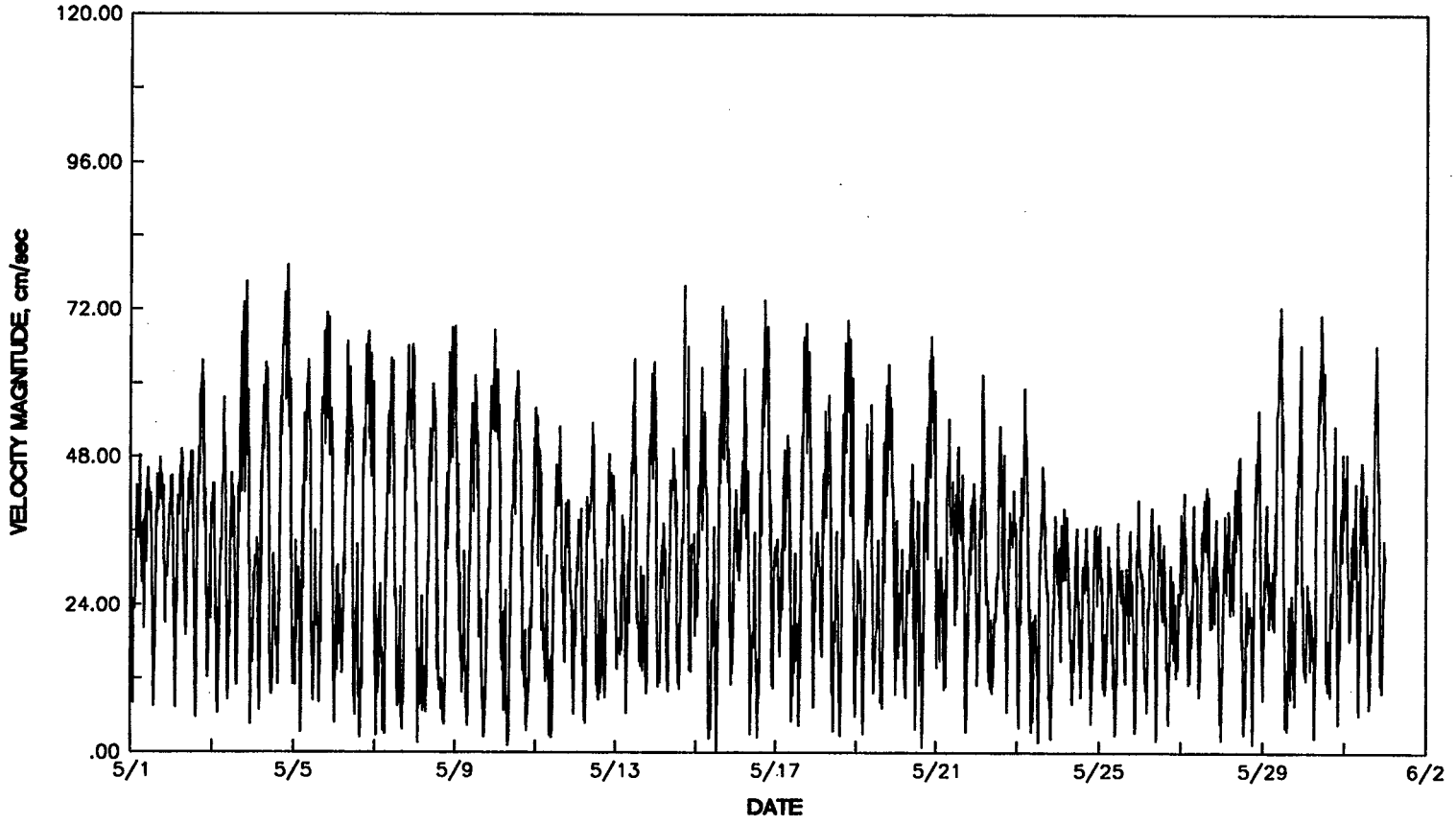

NOTE: SURFACE DATA

VELOCITY MAGNITUDE
STATION 1, 15 MINUTE DATA
5/1/96-6/2/96

Plate 15

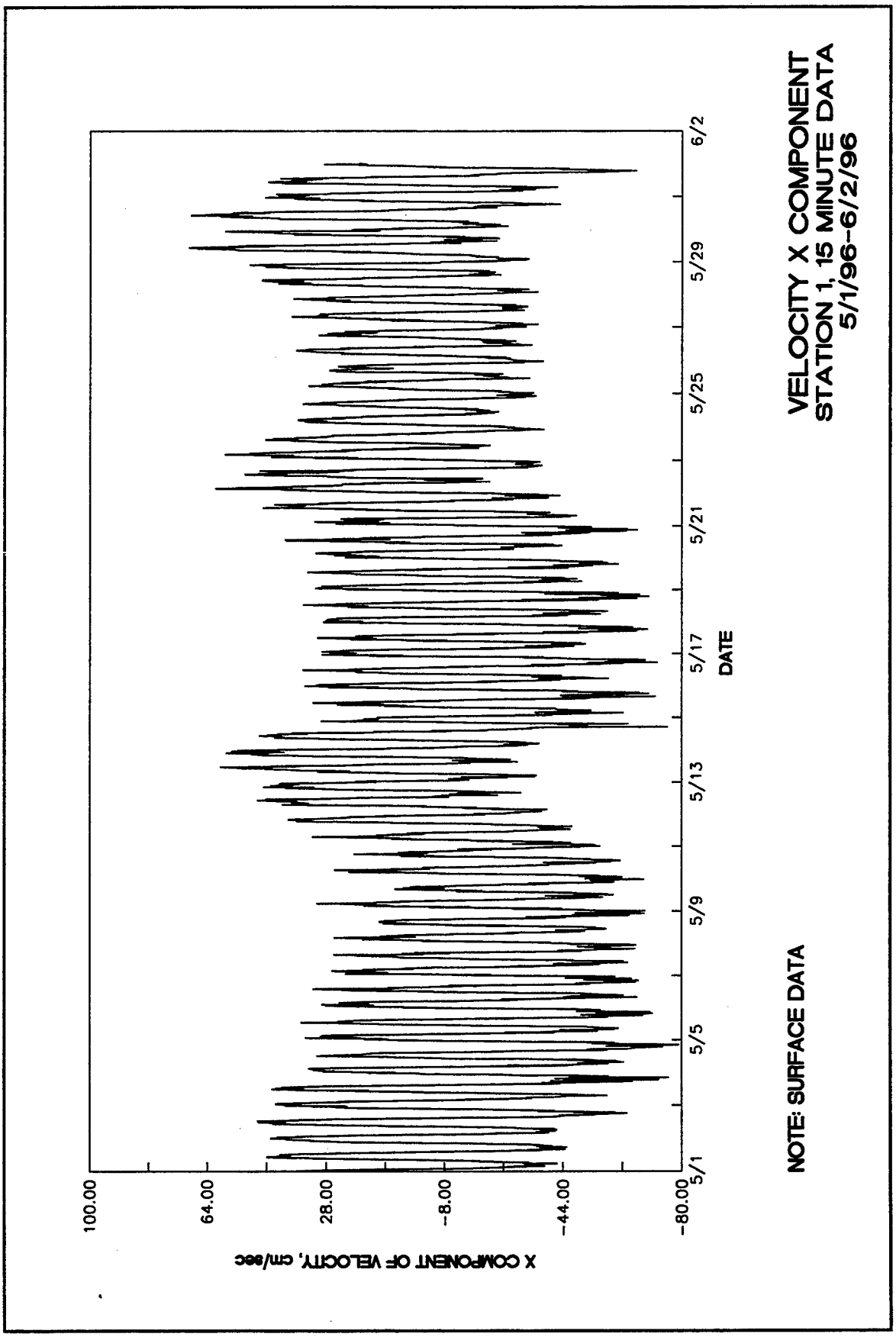
VELOCITY X COMPONENT
STATION 1, 15 MINUTE DATA
5/1/96-6/2/96
NOTE: SURFACE DATA
X COMPONENT OF VELOCITY, cm/sec
100.00
64.00
28.00
-8.00
-44.00
-80.00
5/1
5/5
5/9
5/13
5/17
5/21
5/25
5/29
6/2
DATE

Plate 16

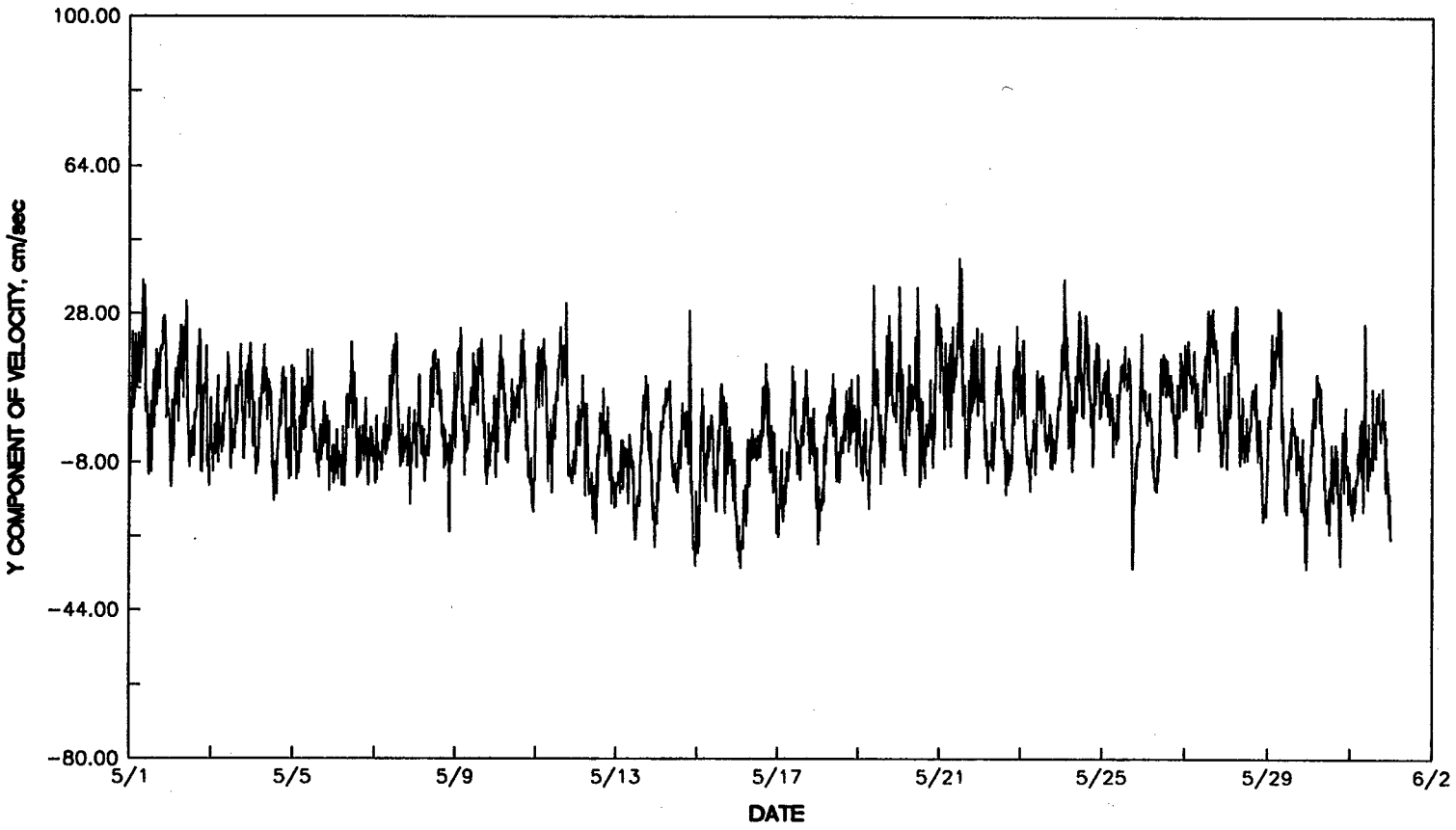

NOTE: SURFACE DATA

VELOCITY Y COMPONENT
STATION 1, 15 MINUTE DATA
5/1/96-6/2/96

Plate 17

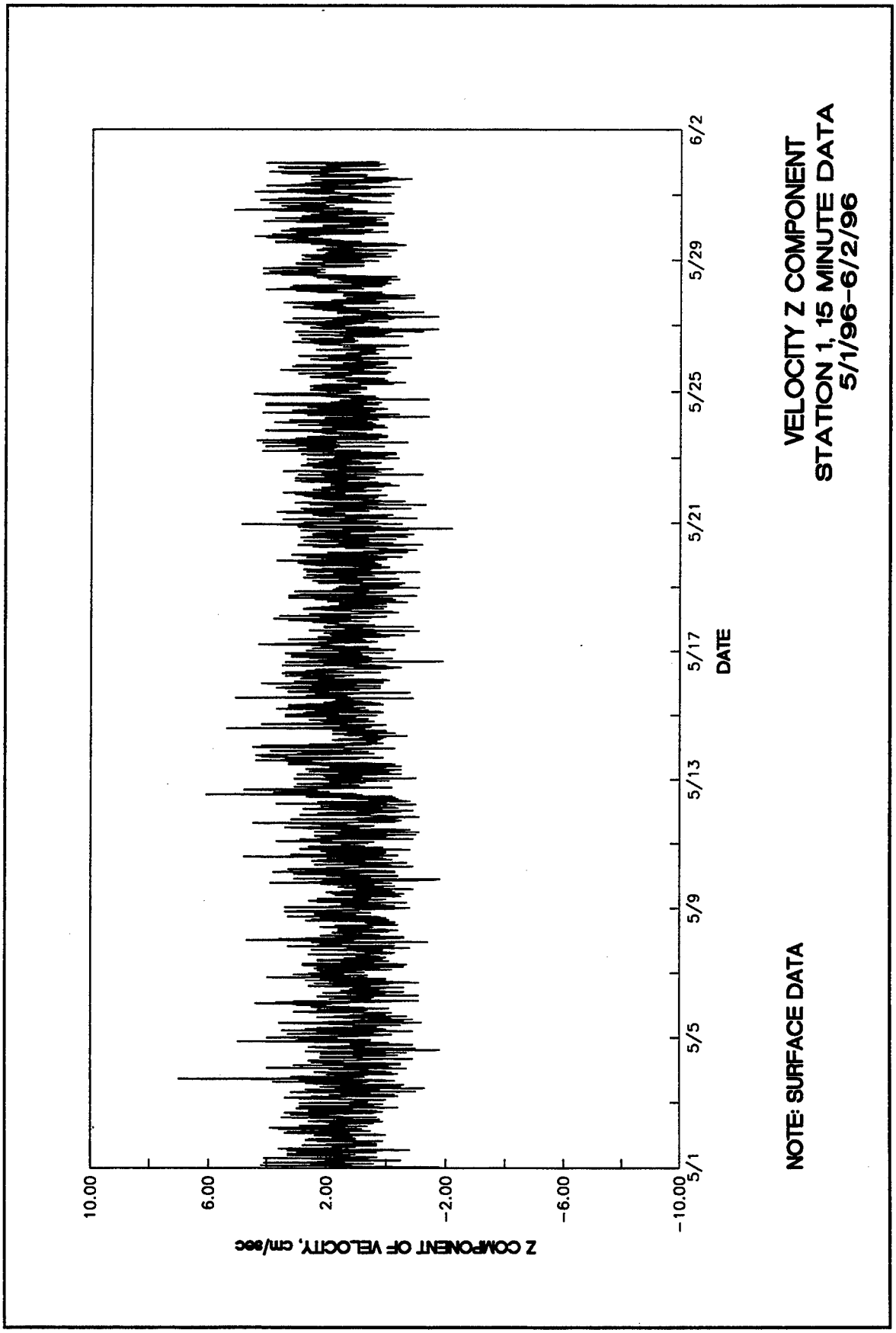
VELOCITY Z COMPONENT
STATION 1, 15 MINUTE DATA
5/1/96-6/2/96
NOTE: SURFACE DATA
Z COMPONENT OF VELOCITY, cm/sec
10.00
6.00
2.00
-2.00
-6.00
-10.00
5/1
5/5
5/9
5/13
5/17
5/21
5/25
5/29
6/2
DATE

Plate 18

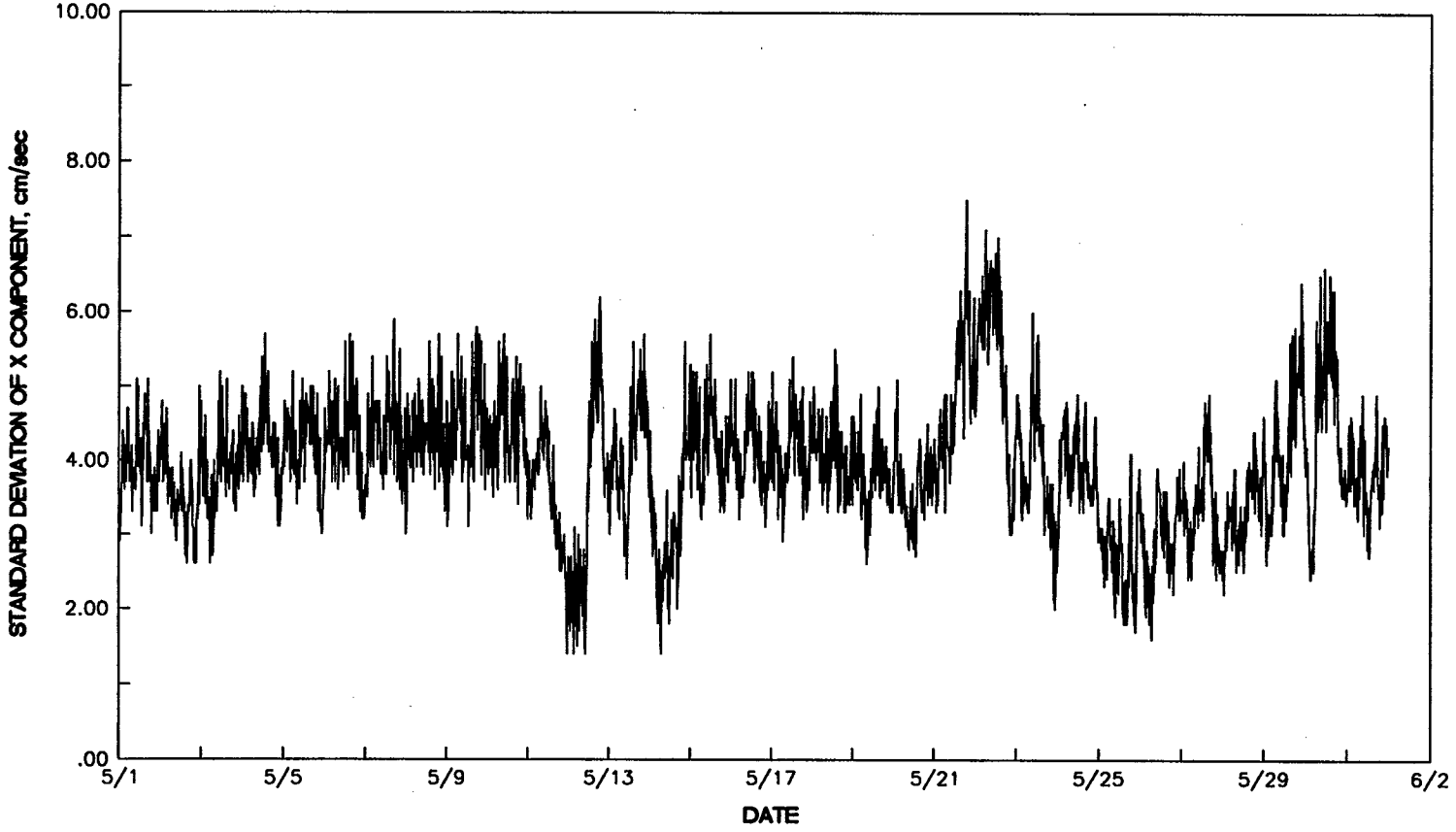

NOTE: SURFACE DATA

STANDARD DEVIATION OF X COMPONENT
STATION 1, 15 MINUTE DATA
5/1/96-6/2/96

Plate 19

Plate 20

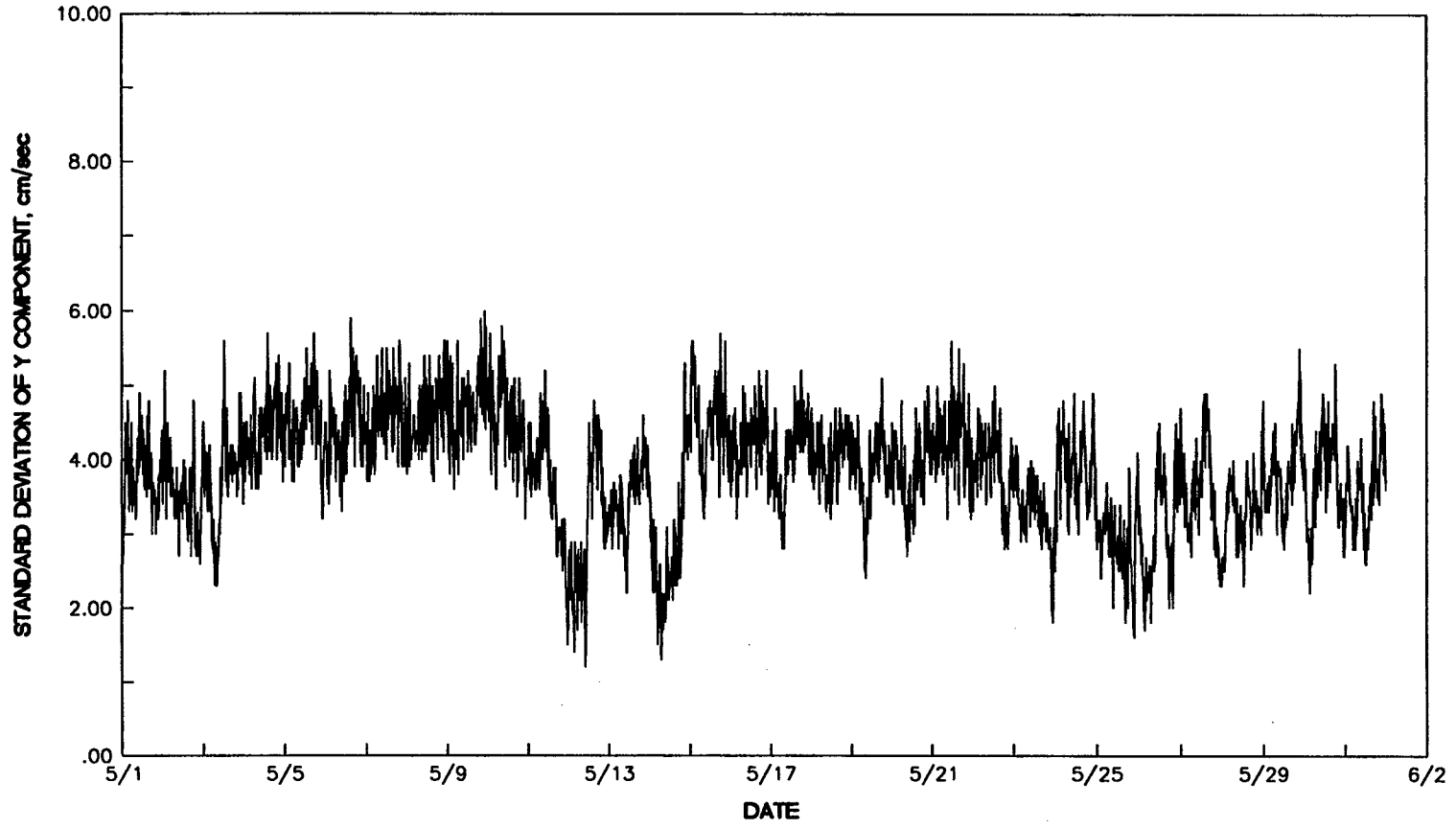

NOTE: SURFACE DATA

STANDARD DEVIATION OF Y COMPONENT
STATION 1, 15 MINUTE DATA
5/1/96-6/2/96

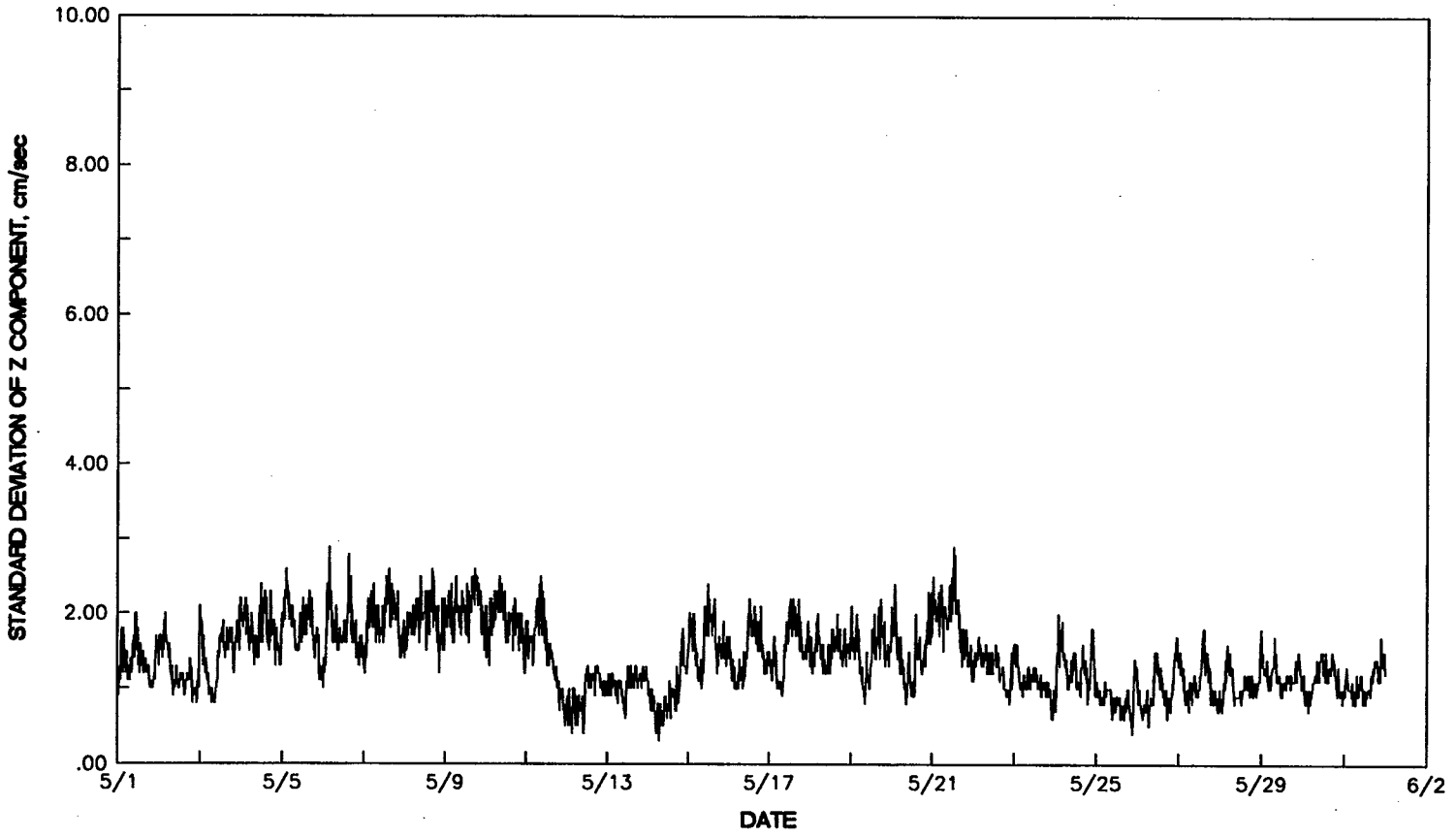

NOTE: SURFACE DATA

STANDARD DEVIATION OF Z COMPONENT
STATION 1, 15 MINUTE DATA
5/1/96-6/2/96

Plate 21

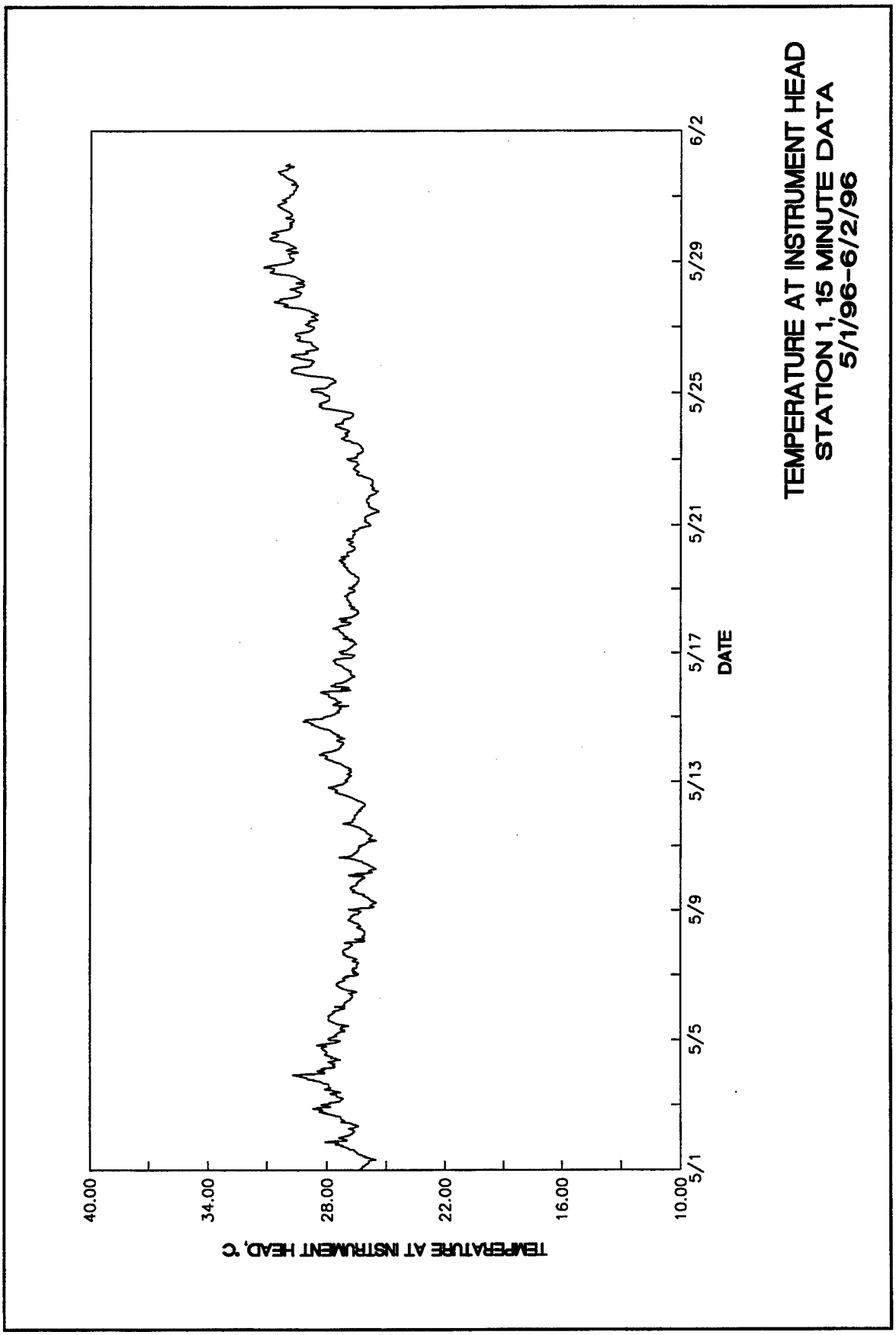
TEMPERATURE AT INSTRUMENT HEAD
STATION 1, 15 MINUTE DATA
5/1/96-6/2/96
TEMPERATURE AT INSTRUMENT HEAD, °C
40.00
34.00
28.00
22.00
16.00
10.00
5/1
5/5
5/9
5/13
5/17
5/21
5/25
5/29
6/2
DATE

Plate 22

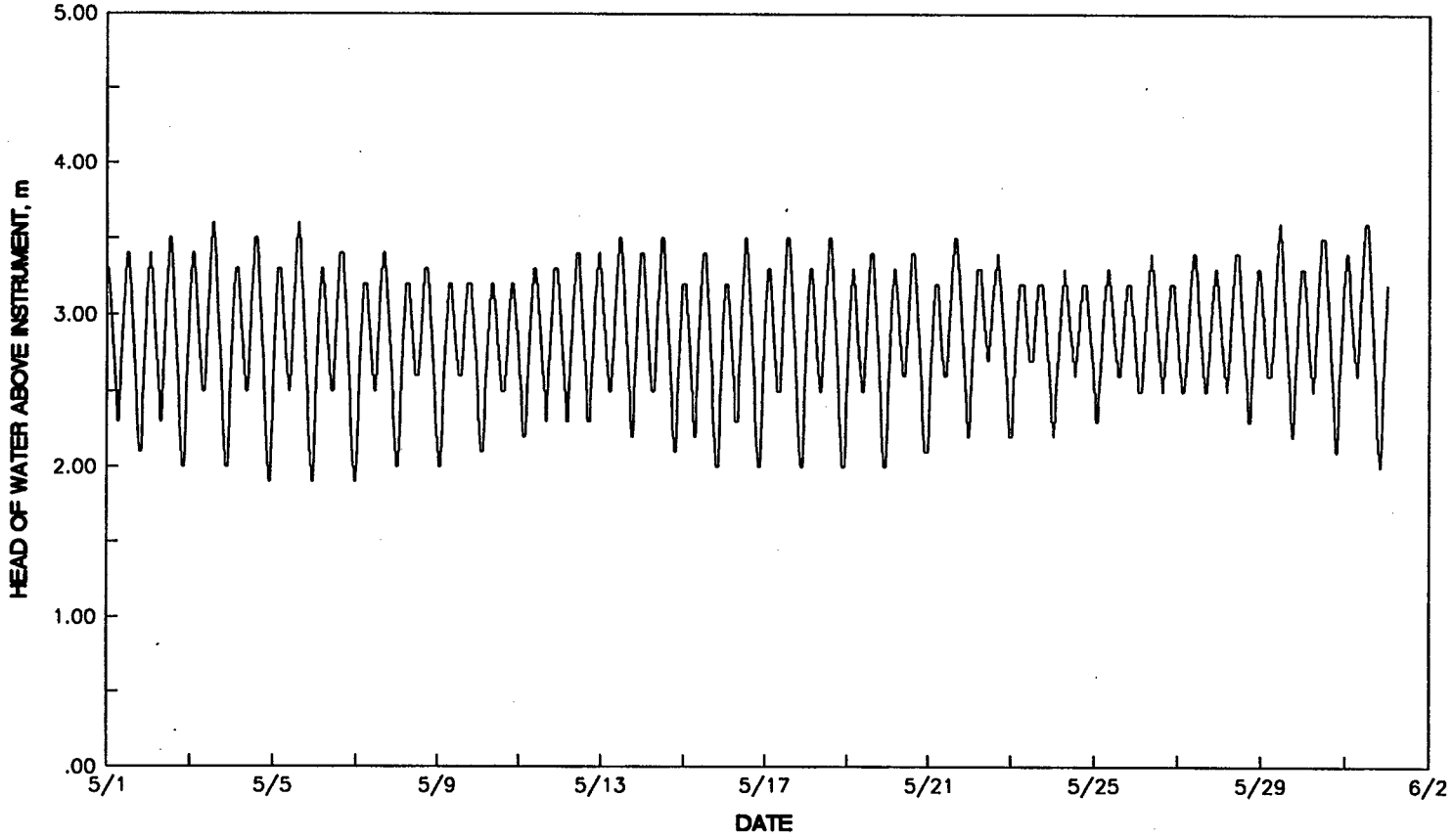

HEAD OF WATER ABOVE INSTRUMENT
STATION 1, 15 MINUTE DATA
5/1/96-6/2/96

Plate 23

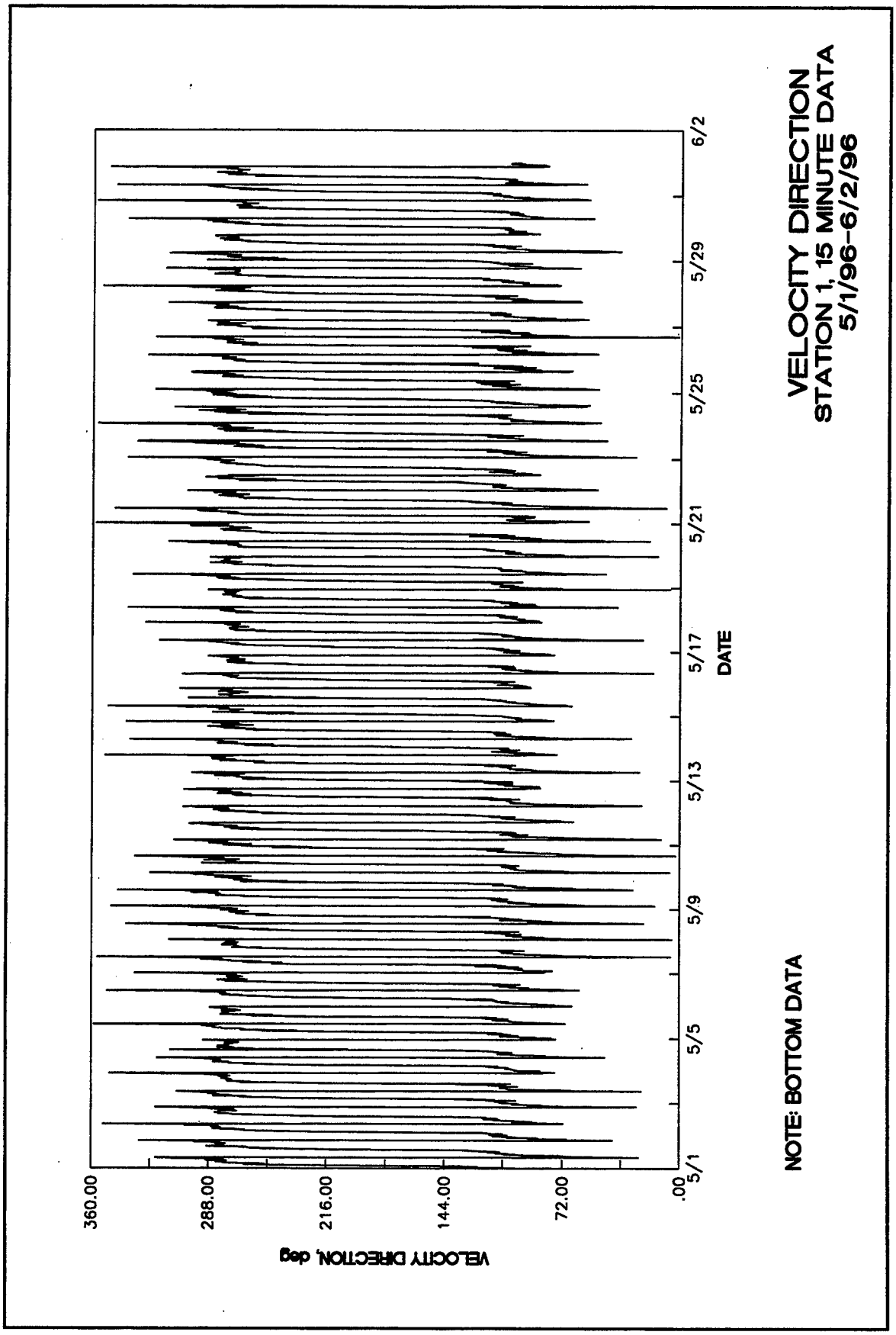
VELOCITY DIRECTION
STATION 1, 15 MINUTE DATA
5/1/96-6/2/96
NOTE: BOTTOM DATA
VELOCITY DIRECTION, deg
360.00
288.00
216.00
144.00
72.00
.00
5/1
5/5
5/9
5/13
5/17
5/21
5/25
5/29
6/2
DATE

Plate 24

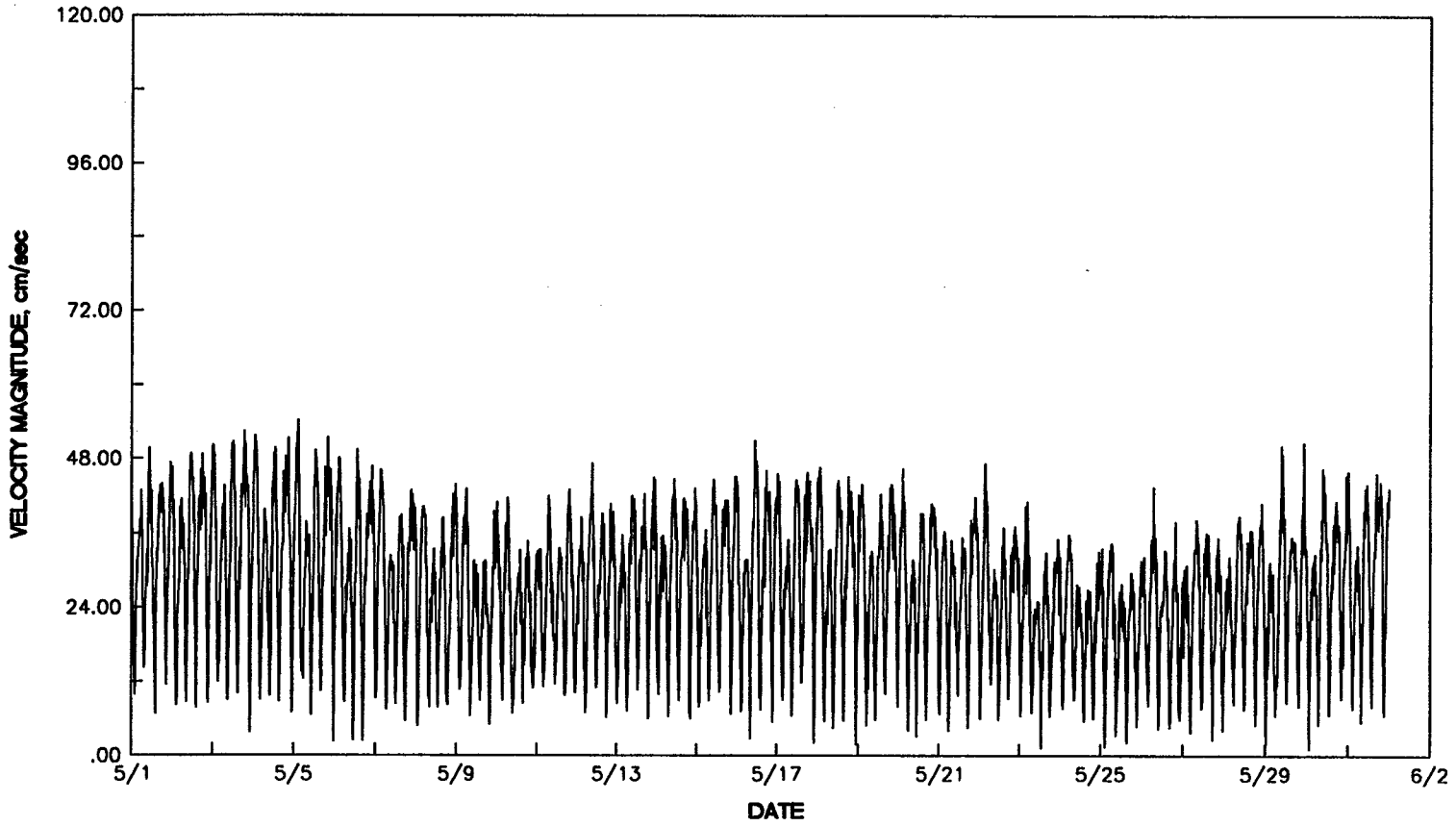

NOTE: MIDDEPTH DATA

VELOCITY MAGNITUDE
STATION 1, 15 MINUTE DATA
5/1/96-6/2/96

Plate 25

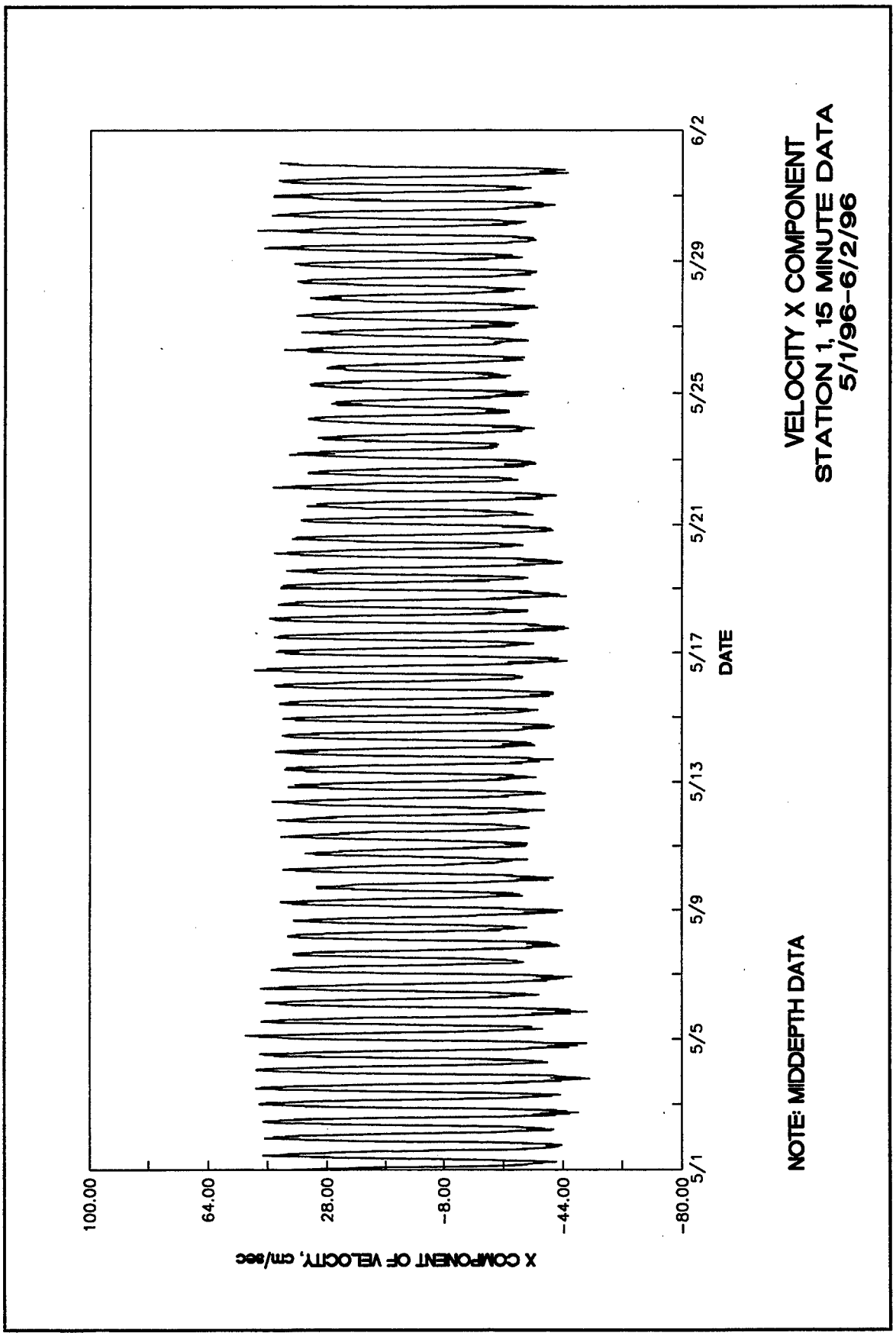
VELOCITY X COMPONENT
STATION 1, 15 MINUTE DATA
5/1/96-6/2/96
NOTE: MIDDEPTH DATA
X COMPONENT OF VELOCITY, cm/sec
100.00
64.00
28.00
-8.00
-44.00
-80.00
5/1
5/5
5/9
5/13
5/17
5/21
5/25
5/29
6/2
DATE

Plate 26

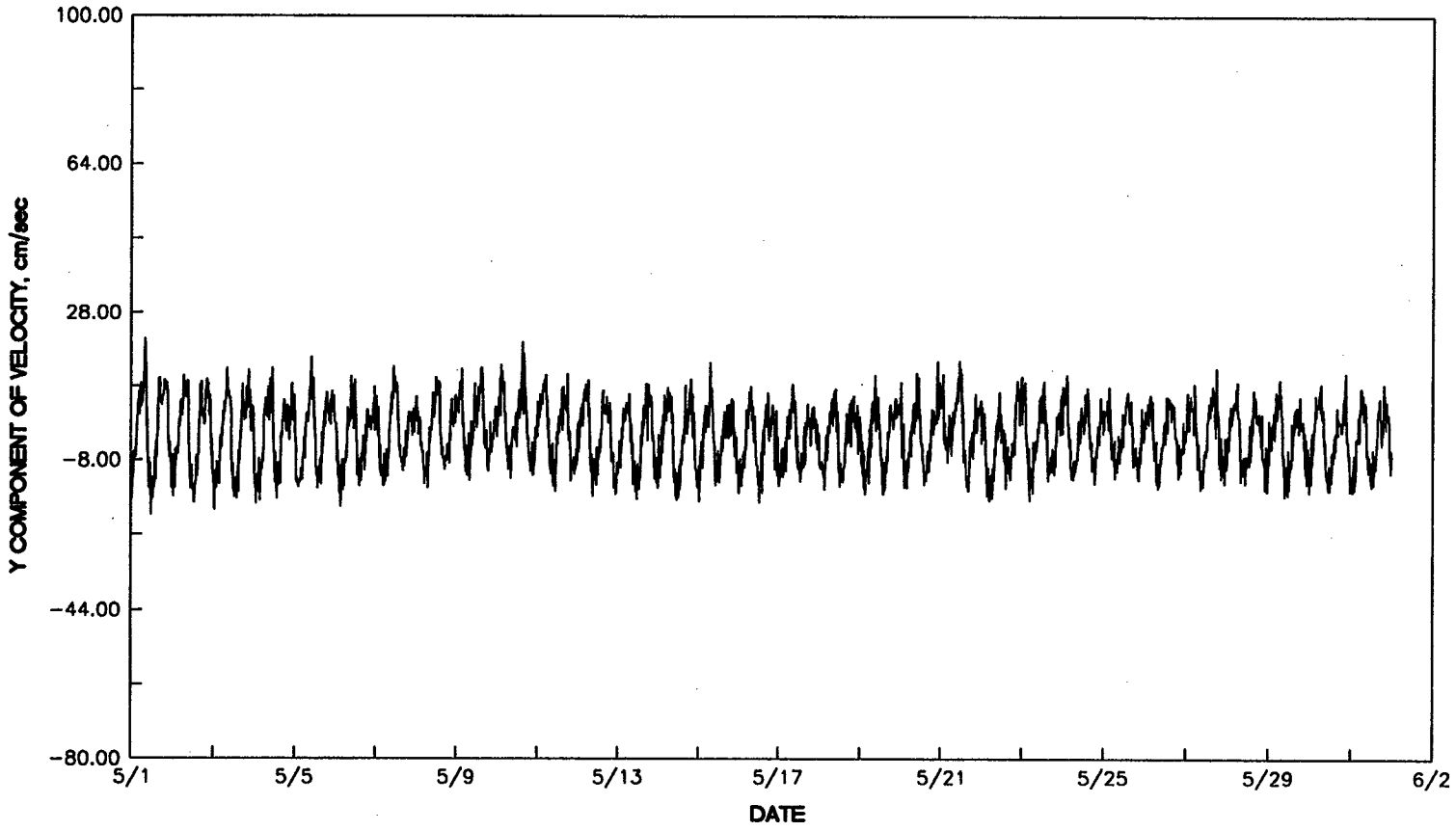

NOTE: MIDDEPTH DATA

VELOCITY Y COMPONENT
STATION 1, 15 MINUTE DATA
5/1/96-6/2/96

Plate 27

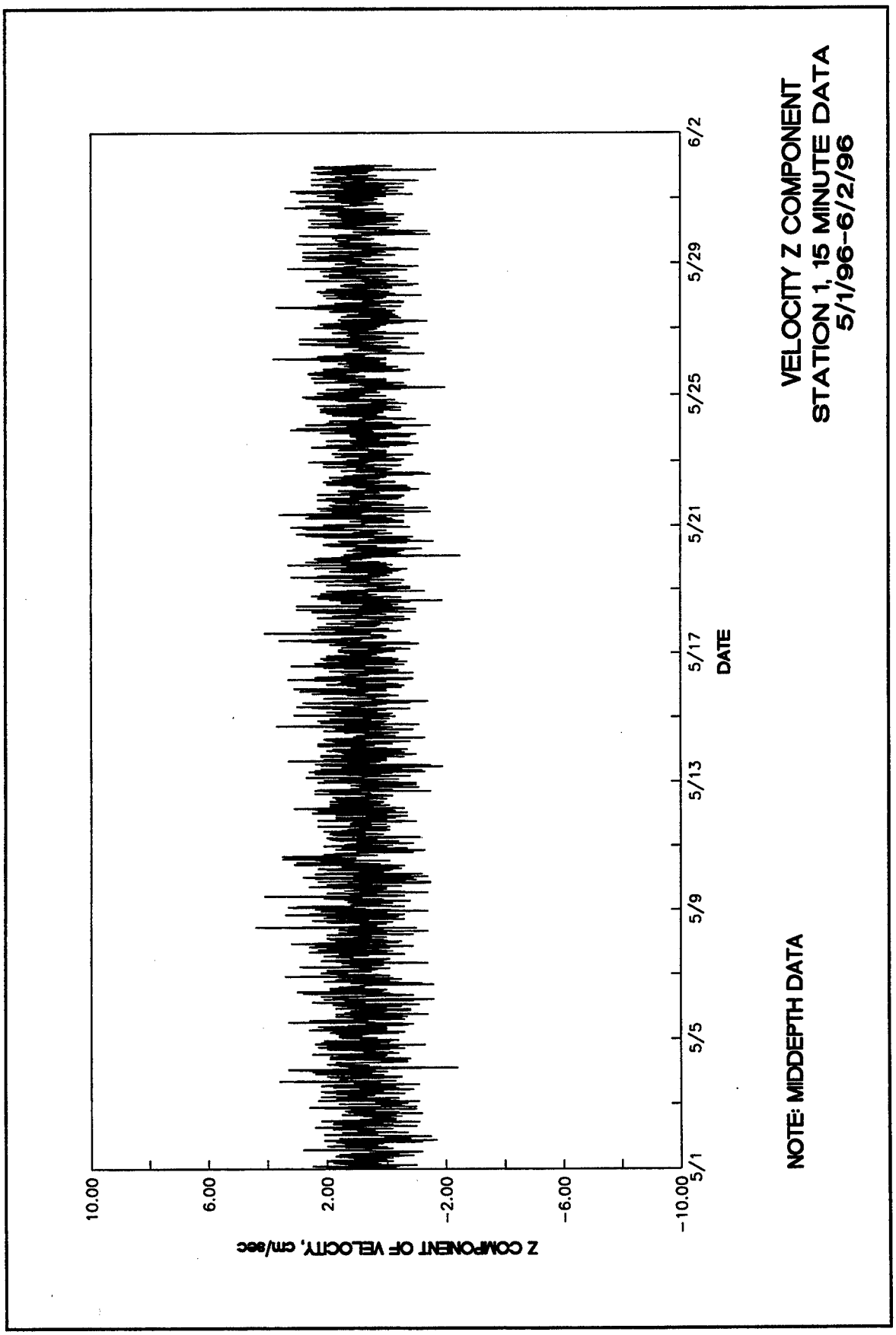
VELOCITY Z COMPONENT
STATION 1, 15 MINUTE DATA
5/1/96-6/2/96
NOTE: MIDDEPTH DATA
Z COMPONENT OF VELOCITY, cm/sec
10.00
6.00
2.00
-2.00
-6.00
-10.00
5/1
5/5
5/9
5/13
5/17
5/21
5/25
5/29
6/2
DATE

Plate 28

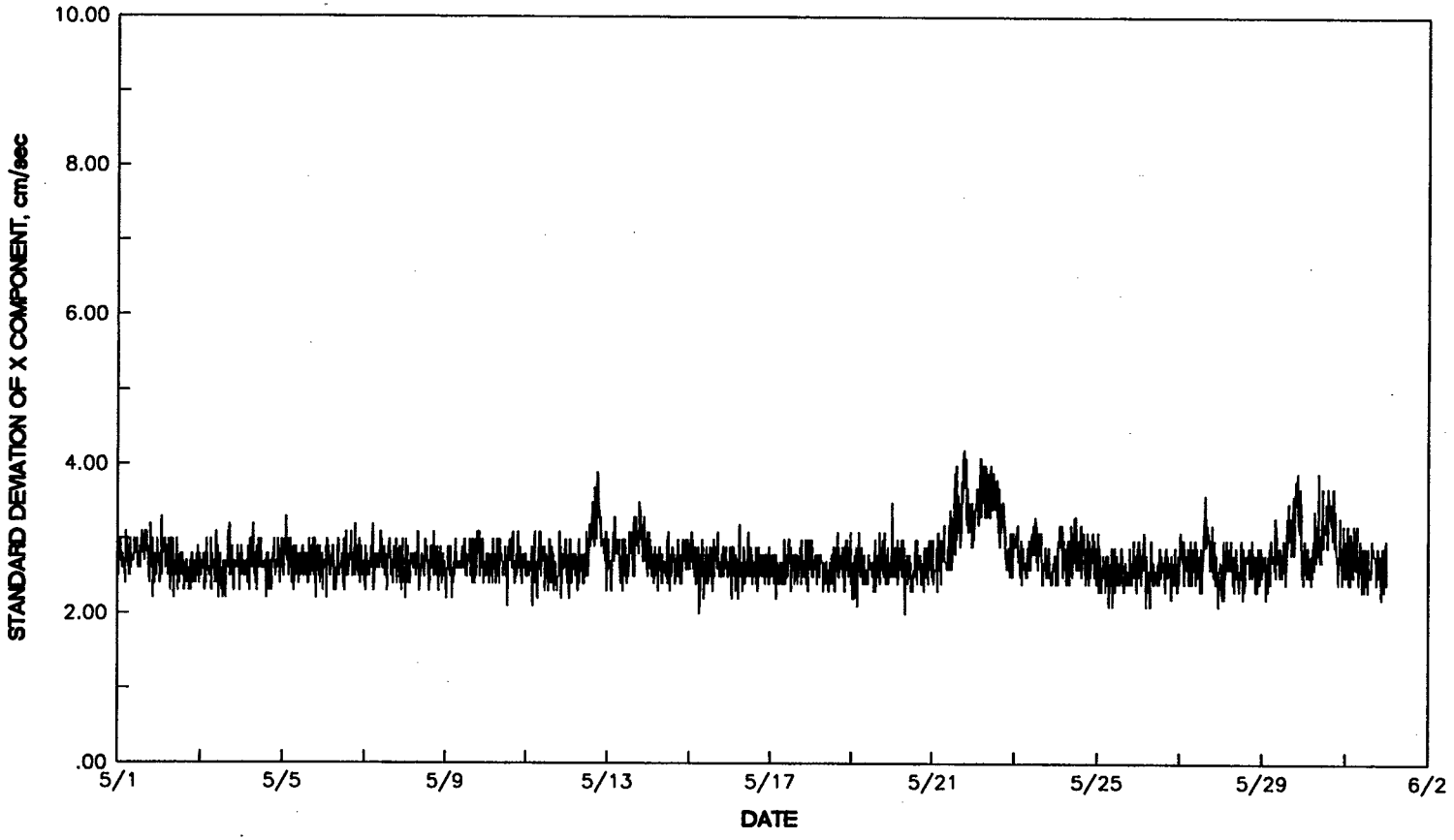

NOTE: MIDDEPTH DATA

STANDARD DEVIATION OF X COMPONENT
STATION 1, 15 MINUTE DATA
5/1/96-6/2/96

Plate 29

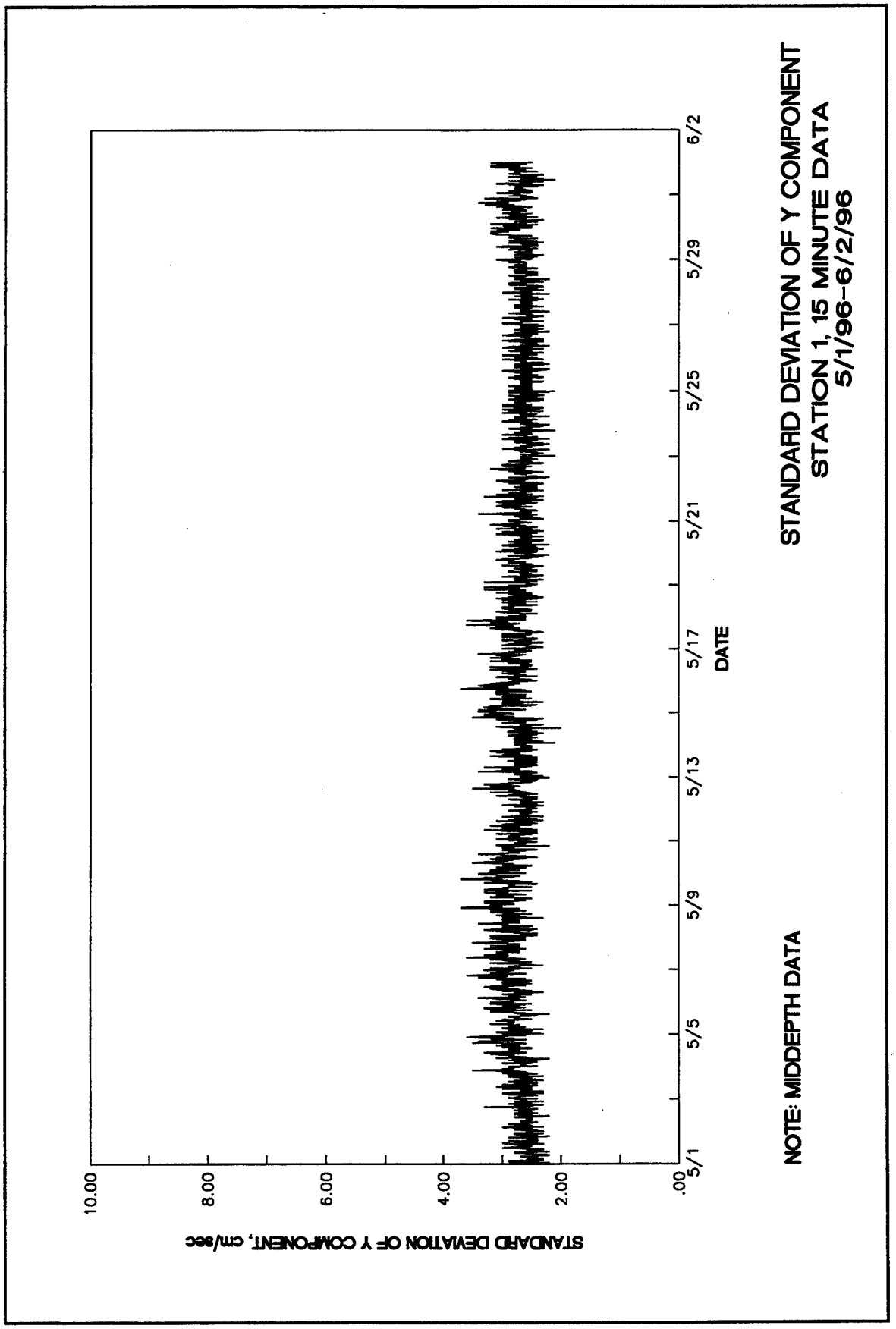
STANDARD DEVIATION OF Y COMPONENT
STATION 1, 15 MINUTE DATA
5/1/96-6/2/96
NOTE: MIDDEPTH DATA
STANDARD DEVIATION OF Y COMPONENT, cm/sec
10.00
8.00
6.00
4.00
2.00
.00
5/1
5/5
5/9
5/13
5/17
5/21
5/25
5/29
6/2
DATE

Plate 30

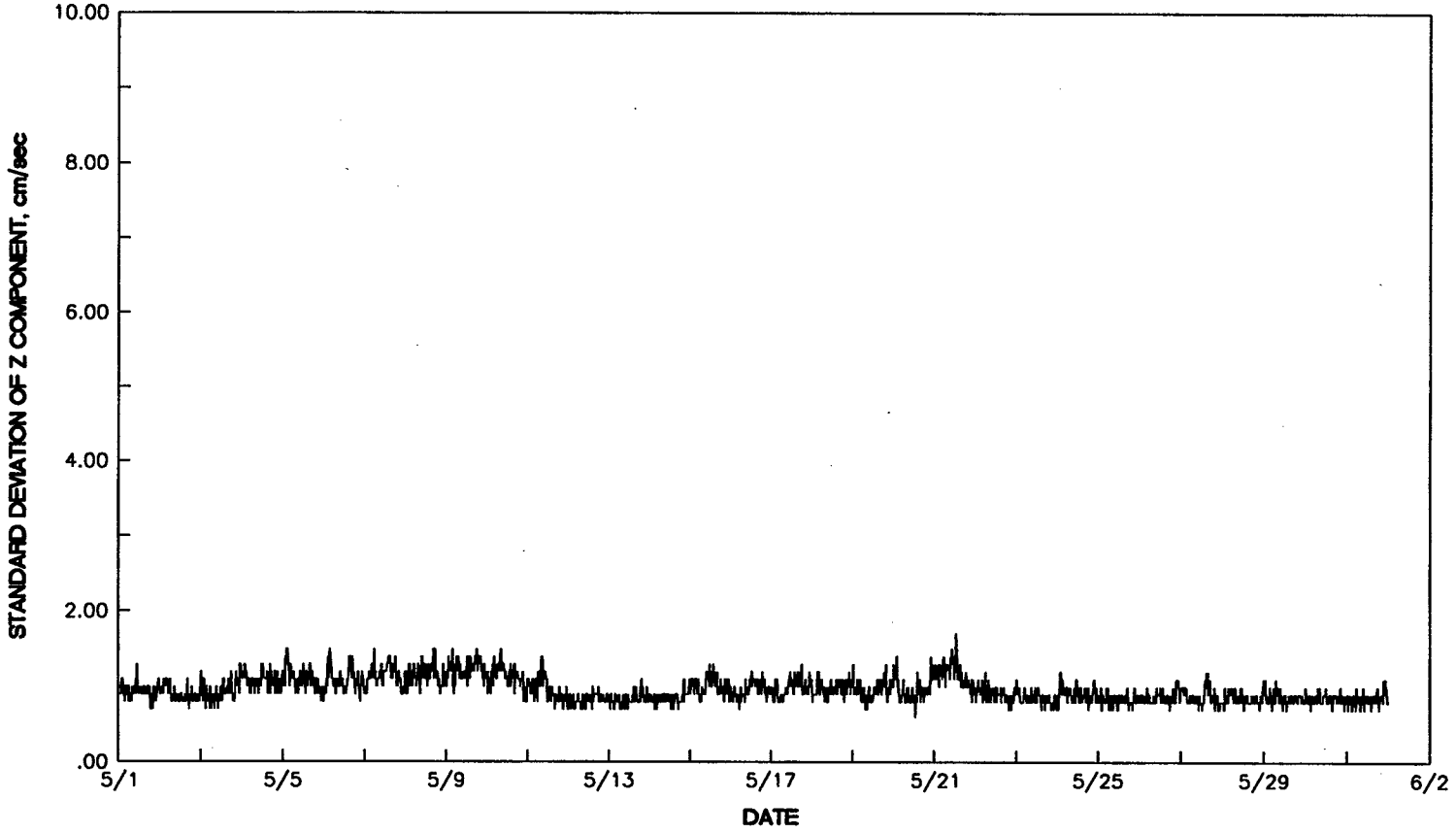

NOTE: MIDDEPTH DATA

STANDARD DEVIATION OF Z COMPONENT
STATION 1, 15 MINUTE DATA
5/1/96-6/2/96

Plate 31

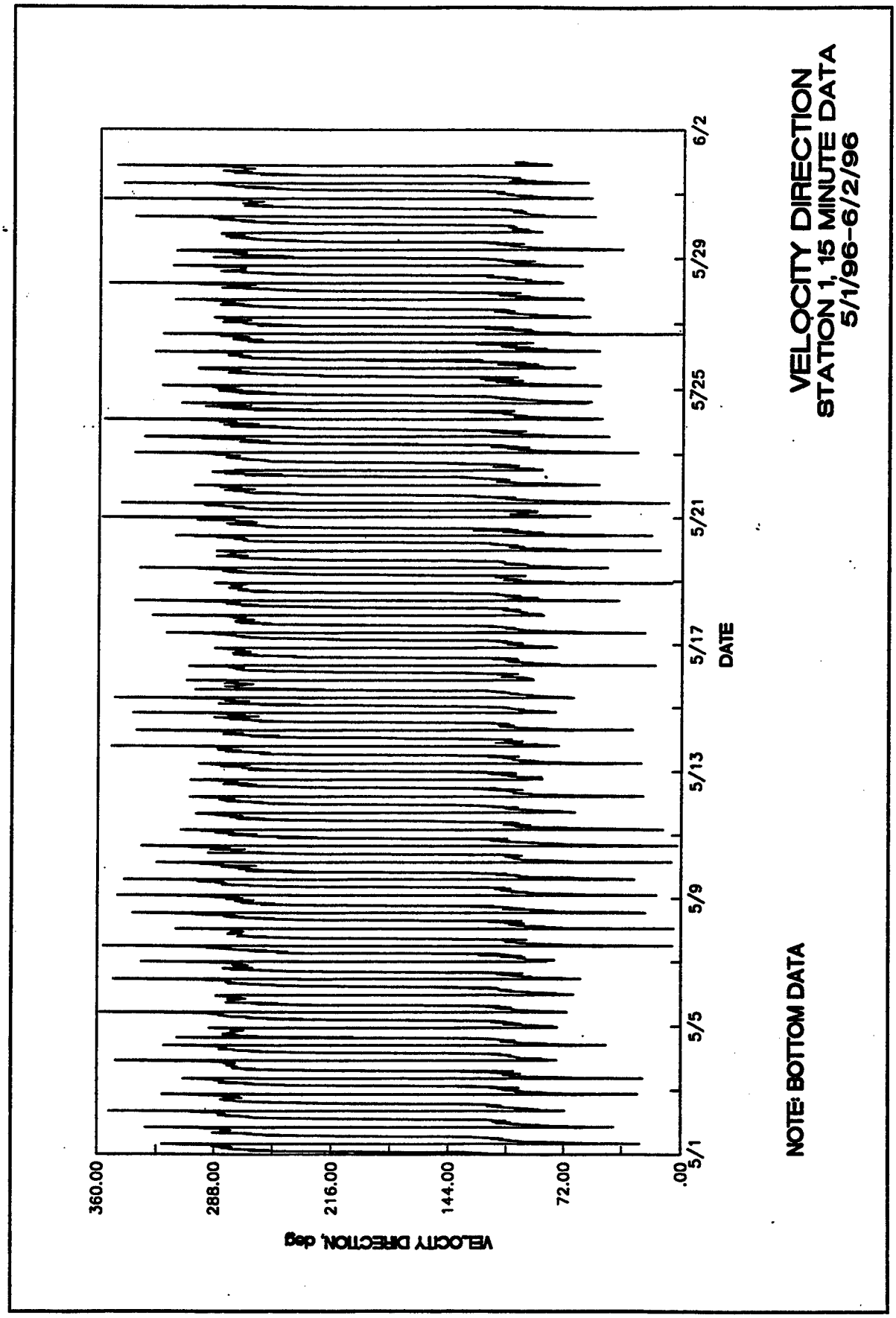
VELOCITY DIRECTION
STATION 1, 15 MINUTE DATA
5/1/96-6/2/96
NOTE: BOTTOM DATA
VELOCITY DIRECTION, deg
360.00
288.00
216.00
144.00
72.00
.00
5/1
5/5
5/9
5/13
5/17
5/21
5/25
5/29
6/2
DATE

Plate 32

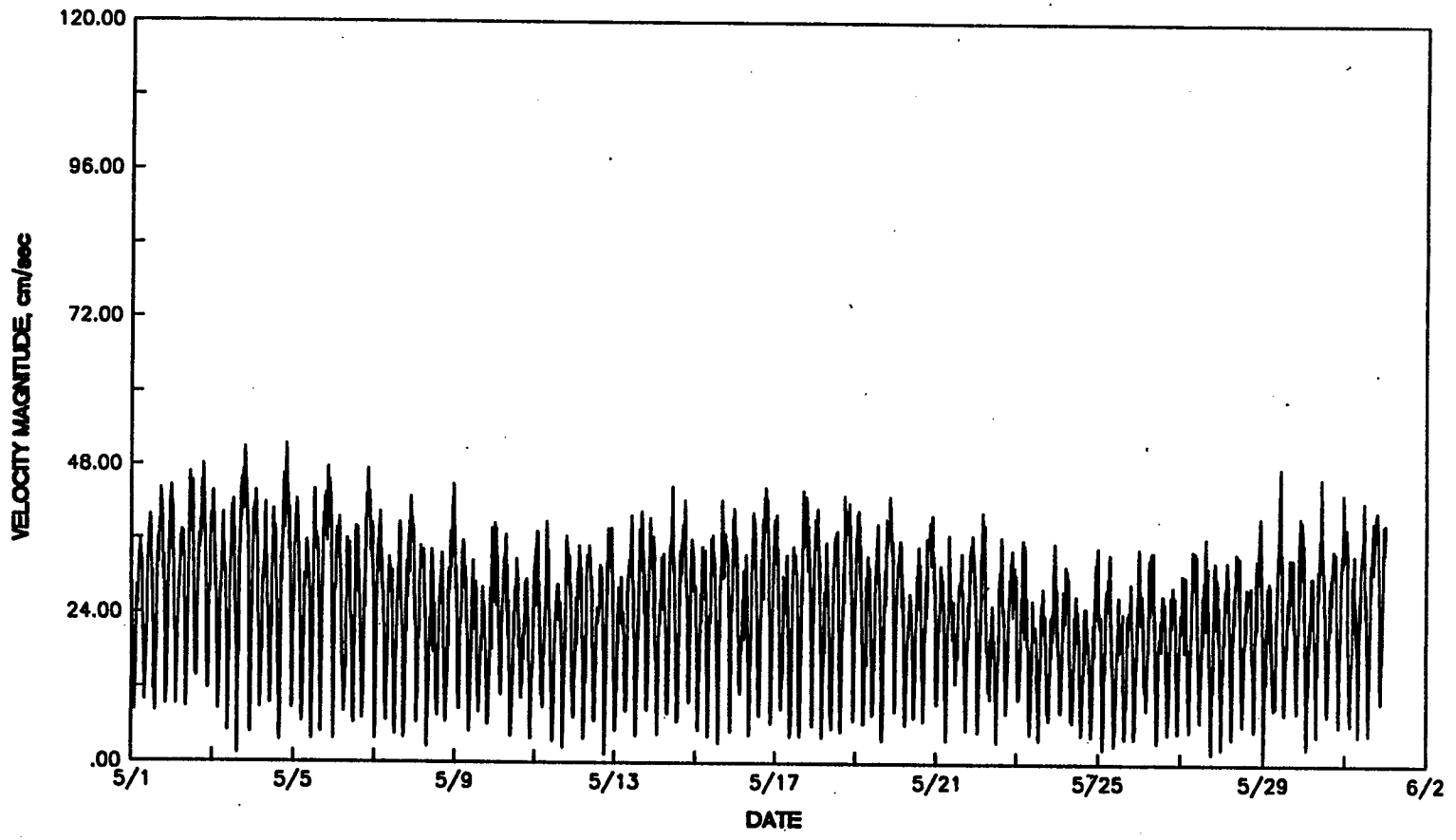

NOTE: BOTTOM DATA

VELOCITY MAGNITUDE
STATION 1, 15 MINUTE DATA
5/1/96-6/2/96

Plate 33

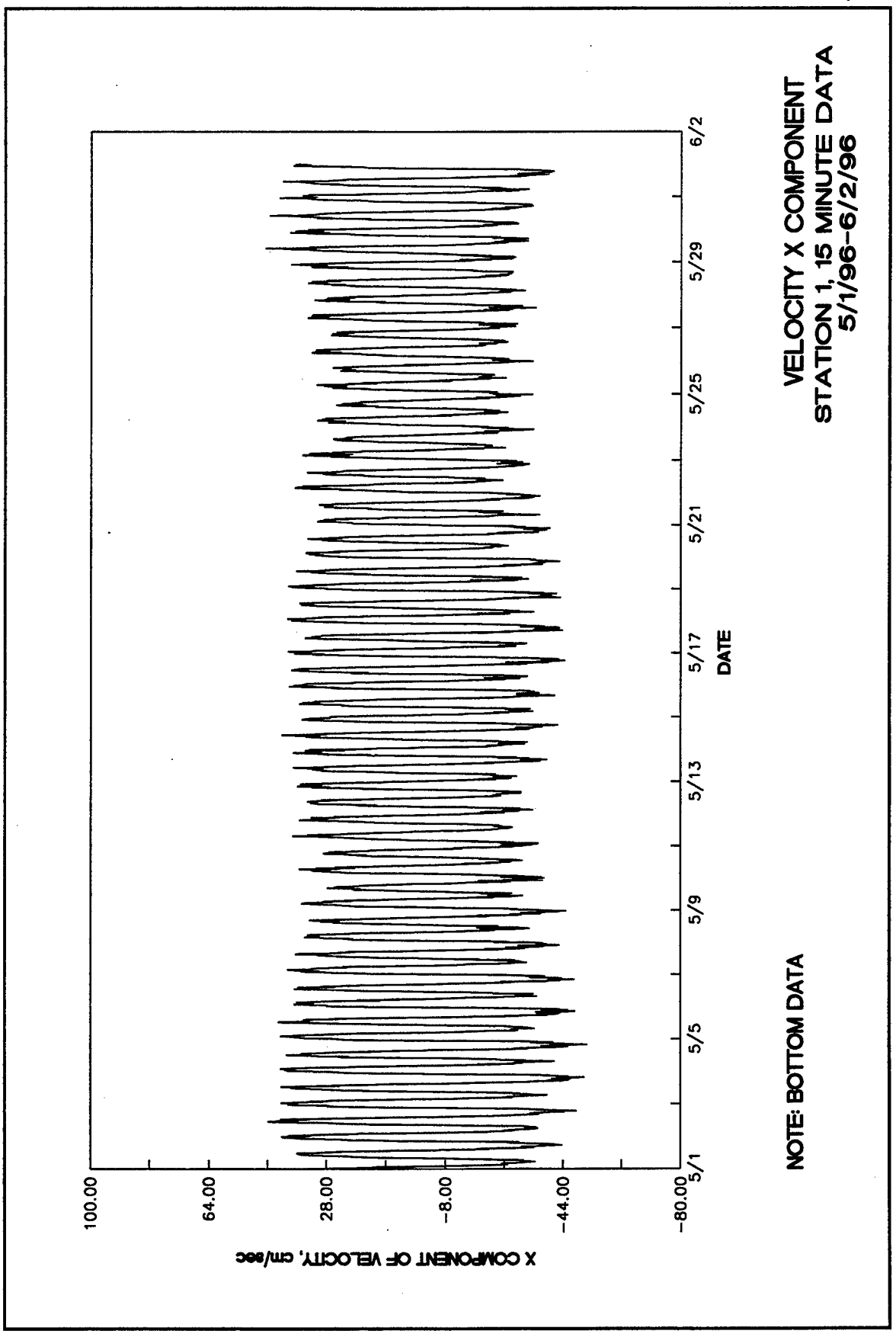
VELOCITY X COMPONENT
STATION 1, 15 MINUTE DATA
5/1/96-6/2/96
NOTE: BOTTOM DATA
X COMPONENT OF VELOCITY, cm/sec
100.00
64.00
28.00
-8.00
-44.00
-80.00
5/1
5/5
5/9
5/13
5/17
5/21
5/25
5/29
6/2
DATE

Plate 34

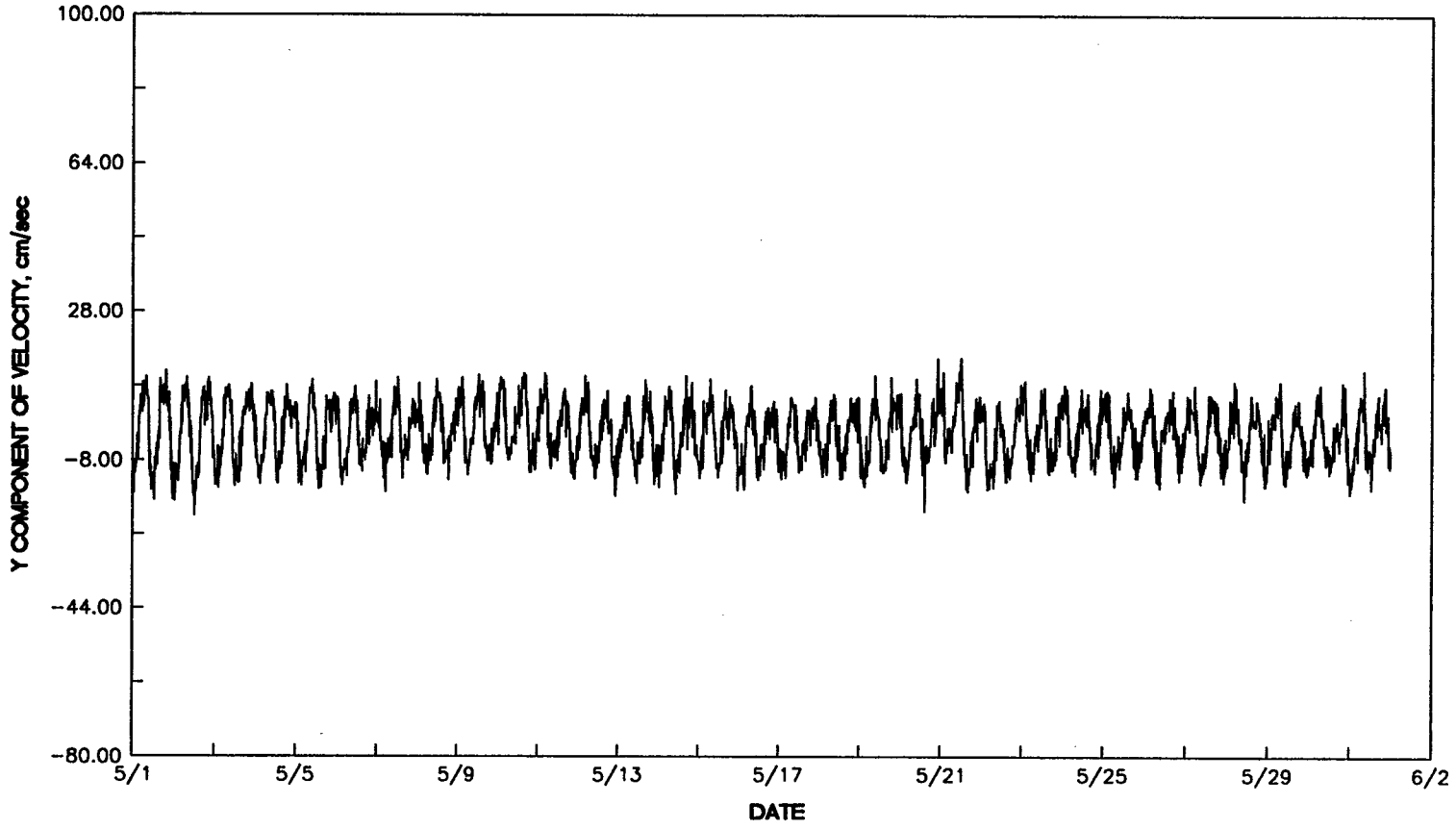

NOTE: BOTTOM DATA

VELOCITY Y COMPONENT
STATION 1, 15 MINUTE DATA
5/1/96-6/2/96

Plate 35

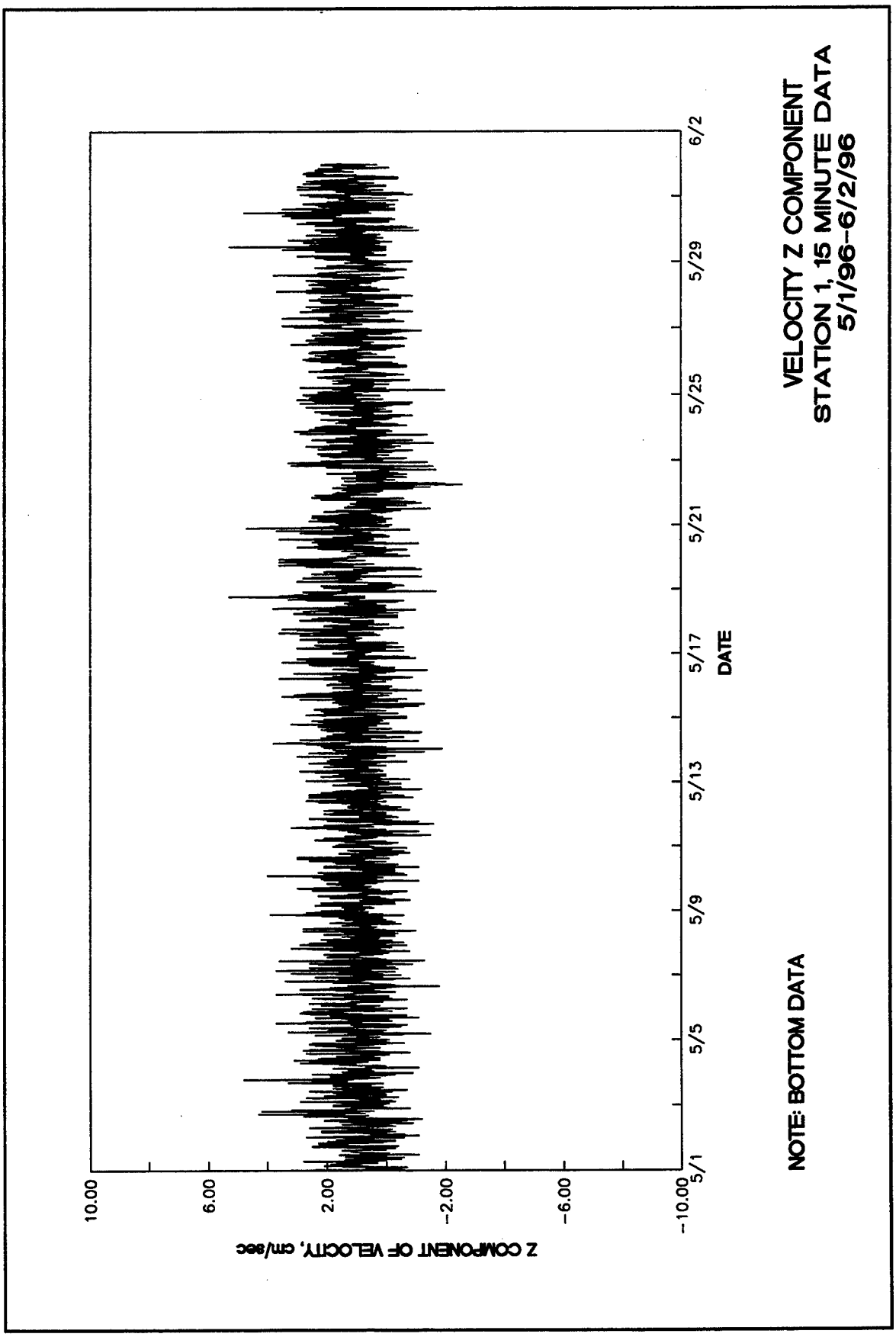
VELOCITY Z COMPONENT
STATION 1, 15 MINUTE DATA
5/1/96-6/2/96
NOTE: BOTTOM DATA
Z COMPONENT OF VELOCITY, cm/sec
10.00
6.00
2.00
-2.00
-6.00
-10.00
5/1
5/5
5/9
5/13
5/17
5/21
5/25
5/29
6/2
DATE

Plate 36

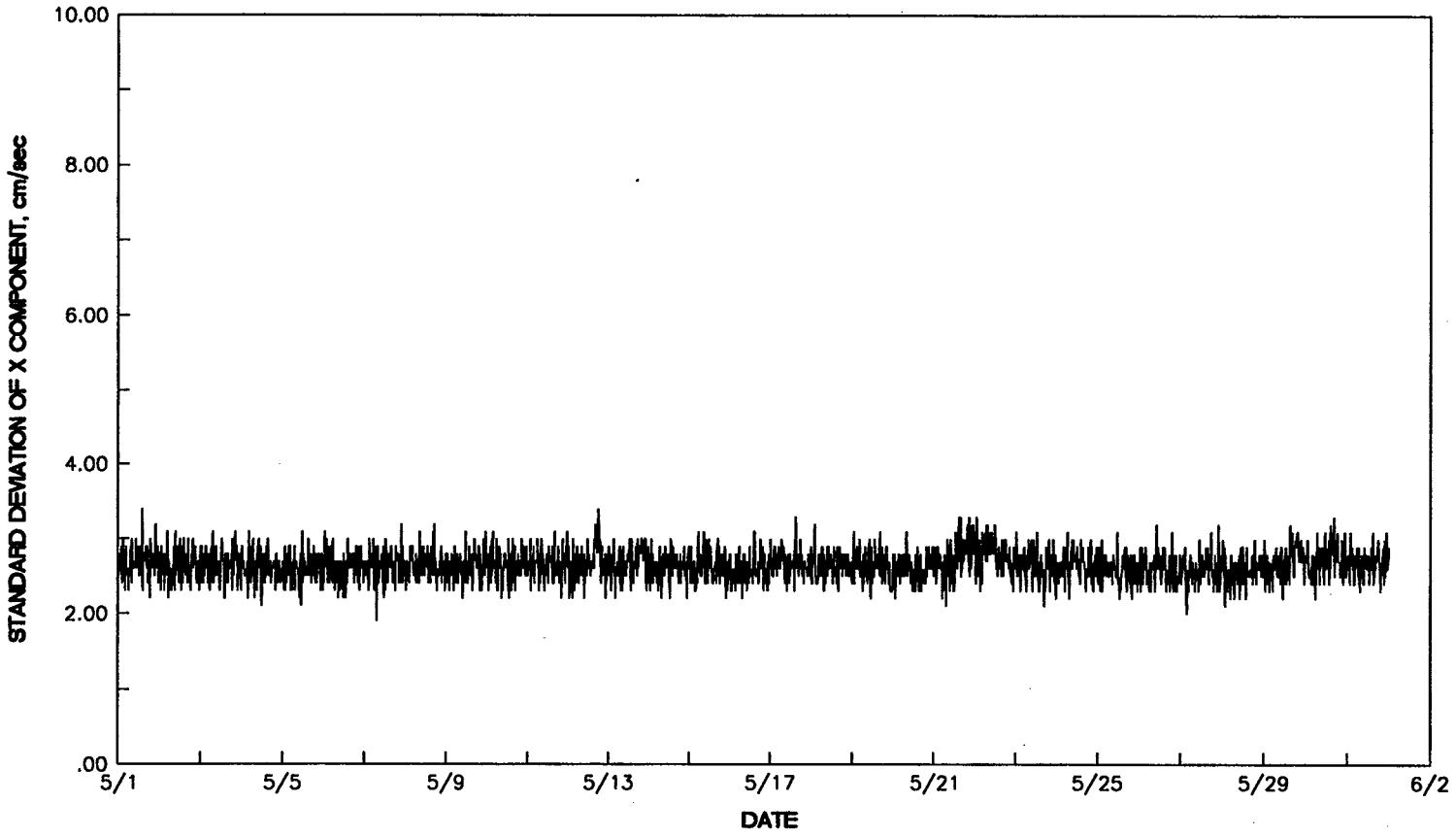

NOTE: BOTTOM DATA

STANDARD DEVIATION OF X COMPONENT
STATION 1, 15 MINUTE DATA
5/1/96-6/2/96

Plate 37

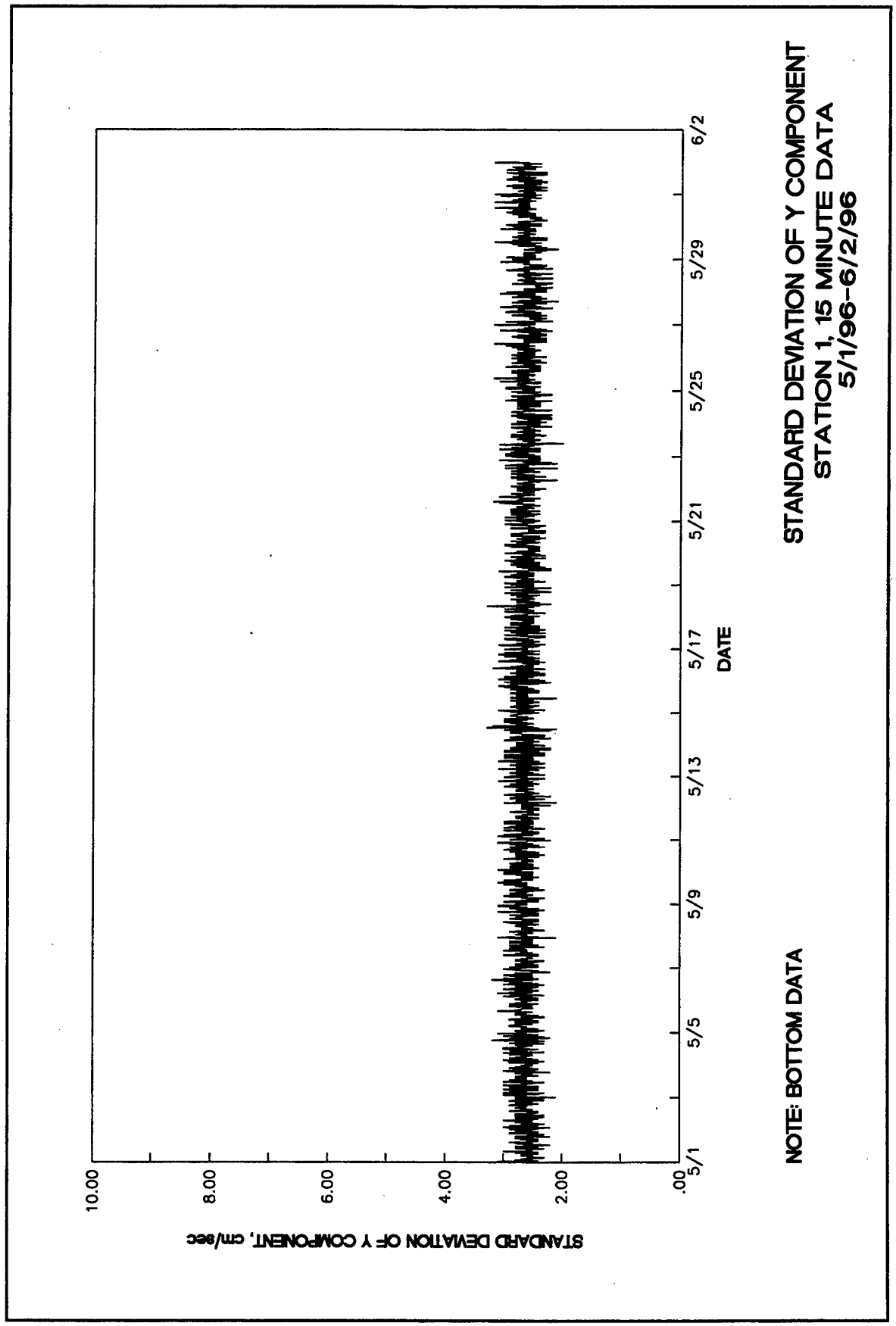
STANDARD DEVIATION OF Y COMPONENT
STATION 1, 15 MINUTE DATA
5/1/96-6/2/96
NOTE: BOTTOM DATA
STANDARD DEVIATION OF Y COMPONENT, cm/sec
10.00
8.00
6.00
4.00
2.00
.00
5/1
5/5
5/9
5/13
5/17
5/21
5/25
5/29
6/2
DATE

Plate 38

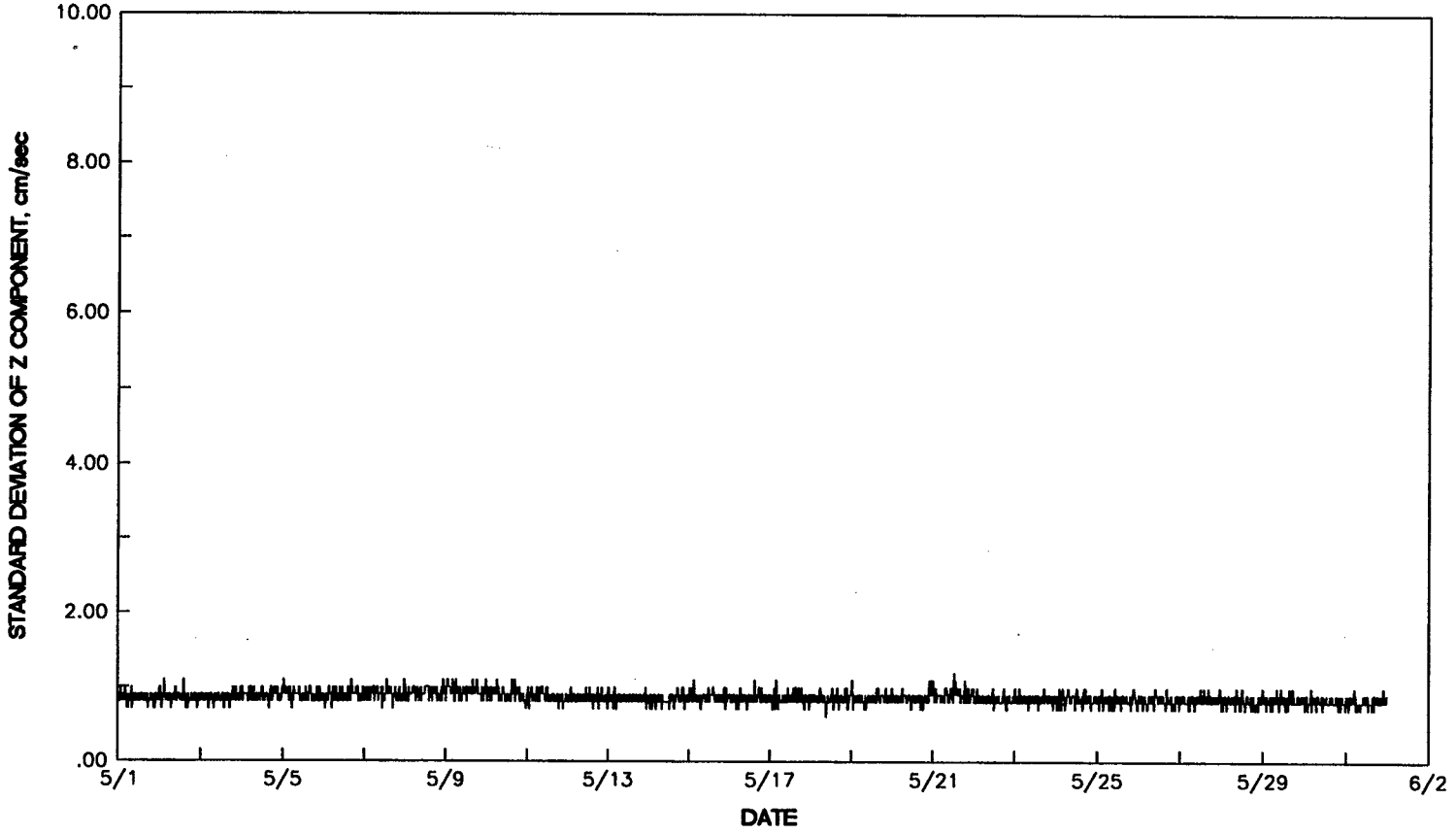

NOTE: BOTTOM DATA

STANDARD DEVIATION OF Z COMPONENT
STATION 1, 15 MINUTE DATA
5/1/96-6/2/96

Plate 39

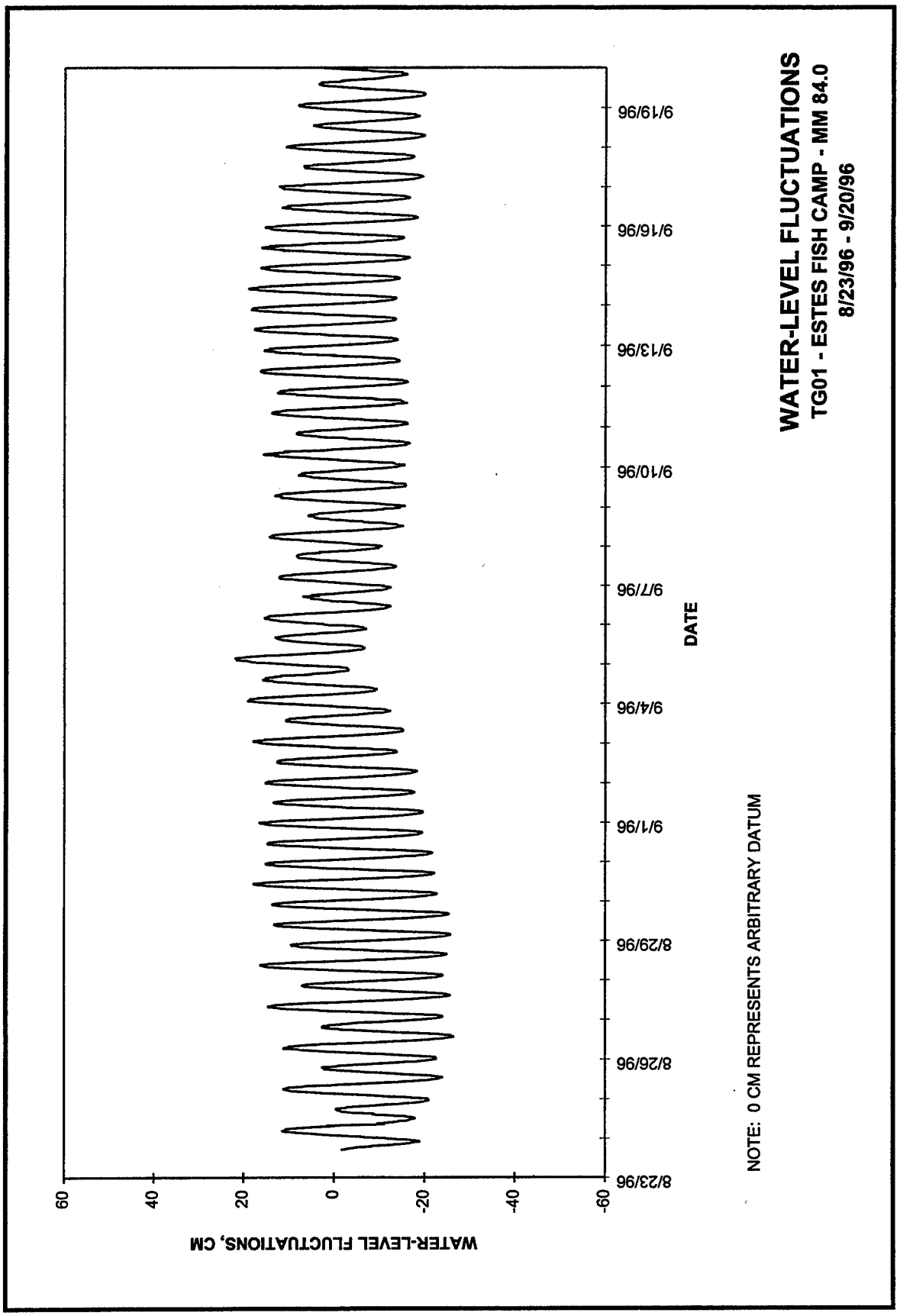
WATER-LEVEL FLUCTUATIONS
TG01 - ESTES FISH CAMP - MM 84.0
8/23/96 - 9/20/96
WATER-LEVEL FLUCTUATIONS, CM
60
40
20
0
-20
-40
-60
8/23/96
8/26/96
8/29/96
9/1/96
9/4/96
9/7/96
9/10/96
9/13/96
9/16/96
9/19/96
DATE
NOTE: 0 CM REPRESENTS ARBITRARY DATUM

Plate 40

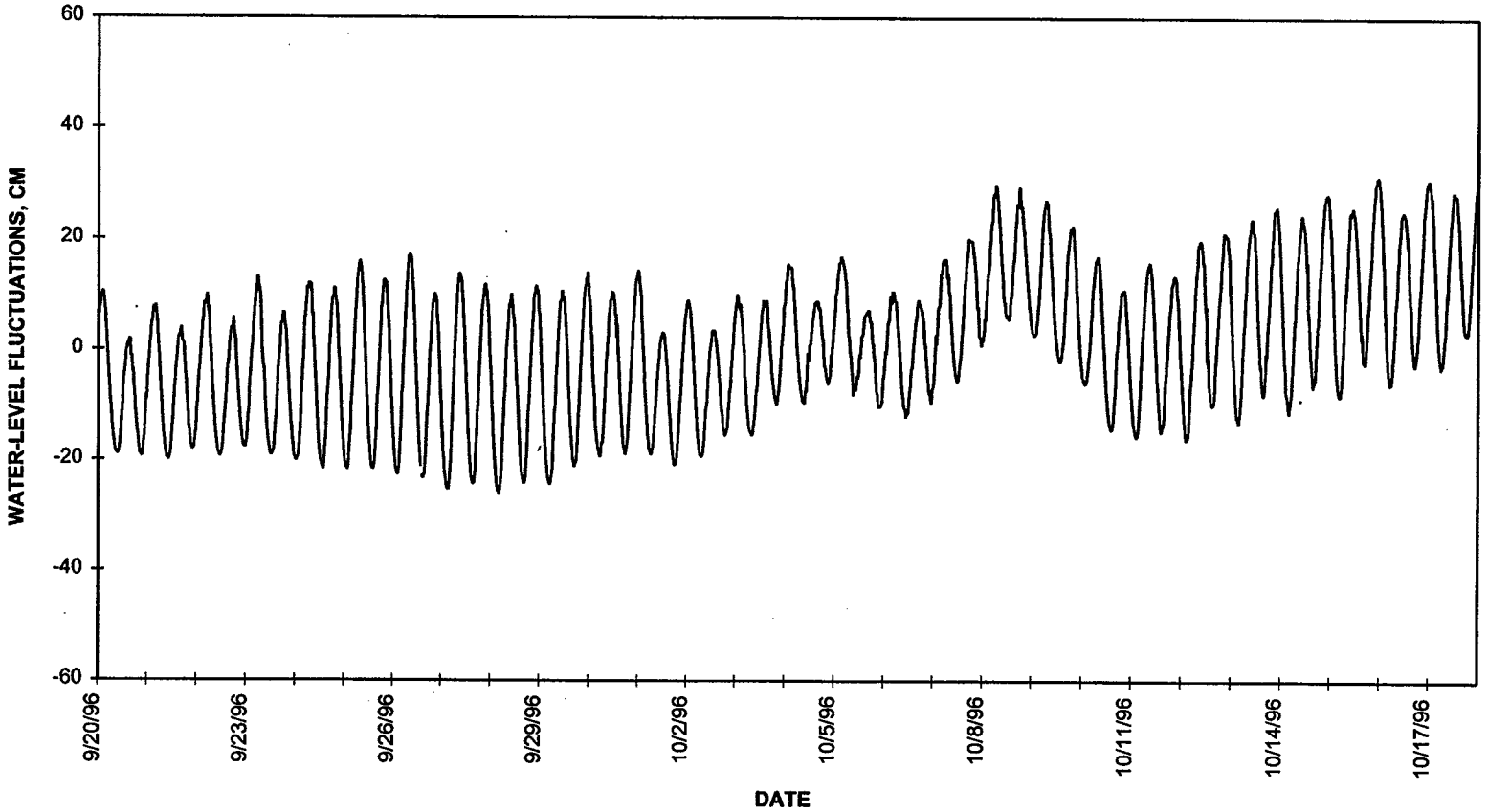

NOTE: 0 CM REPRESENTS ARBITRARY DATUM

WATER-LEVEL FLUCTUATIONS
TG01 - ESTES FISH CAMP - MM 84.0
9/20/96 - 10/18/96

Plate 41

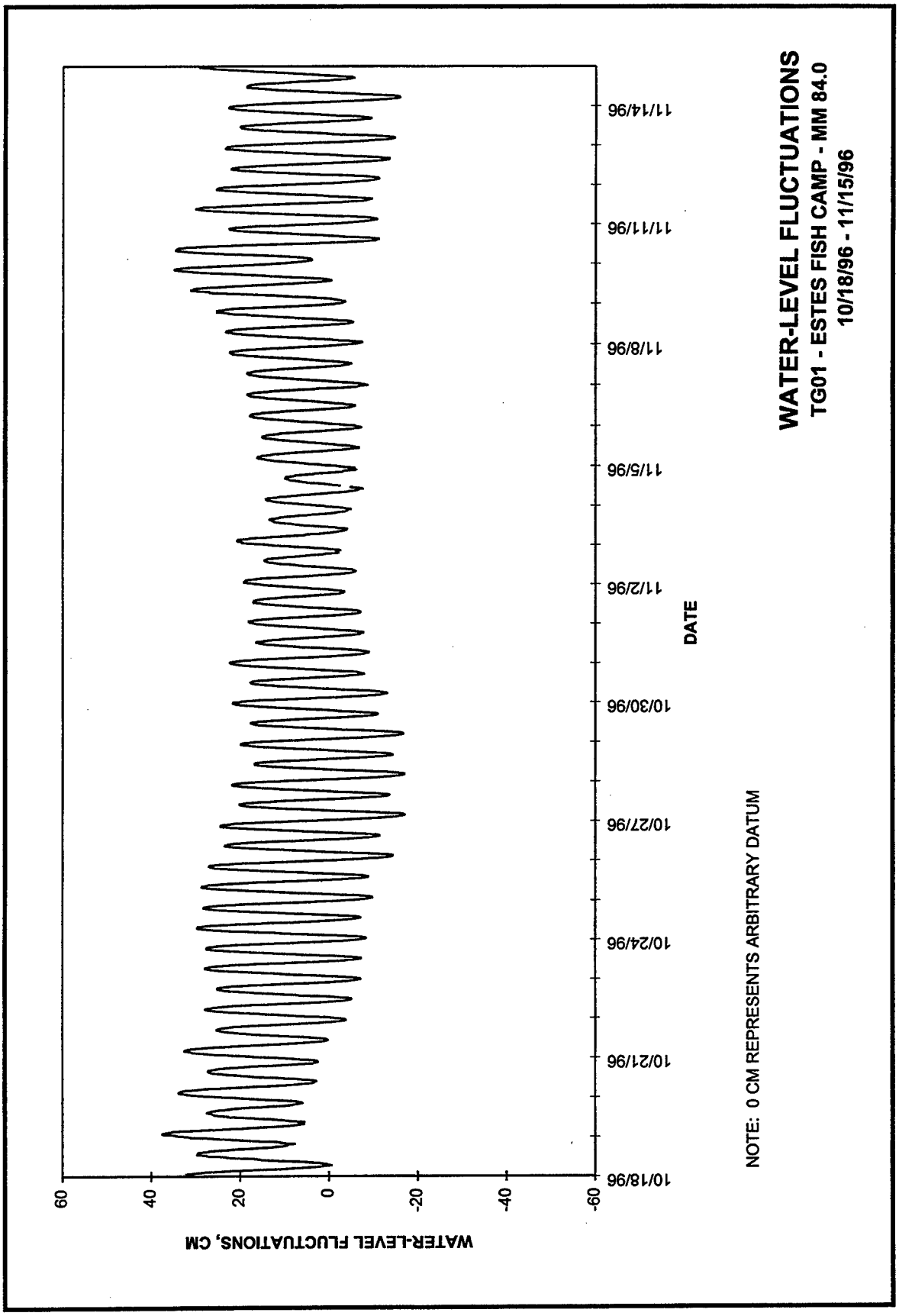
WATER-LEVEL FLUCTUATIONS
TG01 - ESTES FISH CAMP - MM 84.0
10/18/96 - 11/15/96
WATER-LEVEL FLUCTUATIONS, CM
60
40
20
0
-20
-40
-60
10/18/96
10/21/96
10/24/96
10/27/96
10/30/96
11/2/96
11/5/96
11/8/96
11/11/96
11/14/96
DATE
NOTE: 0 CM REPRESENTS ARBITRARY DATUM

Plate 42

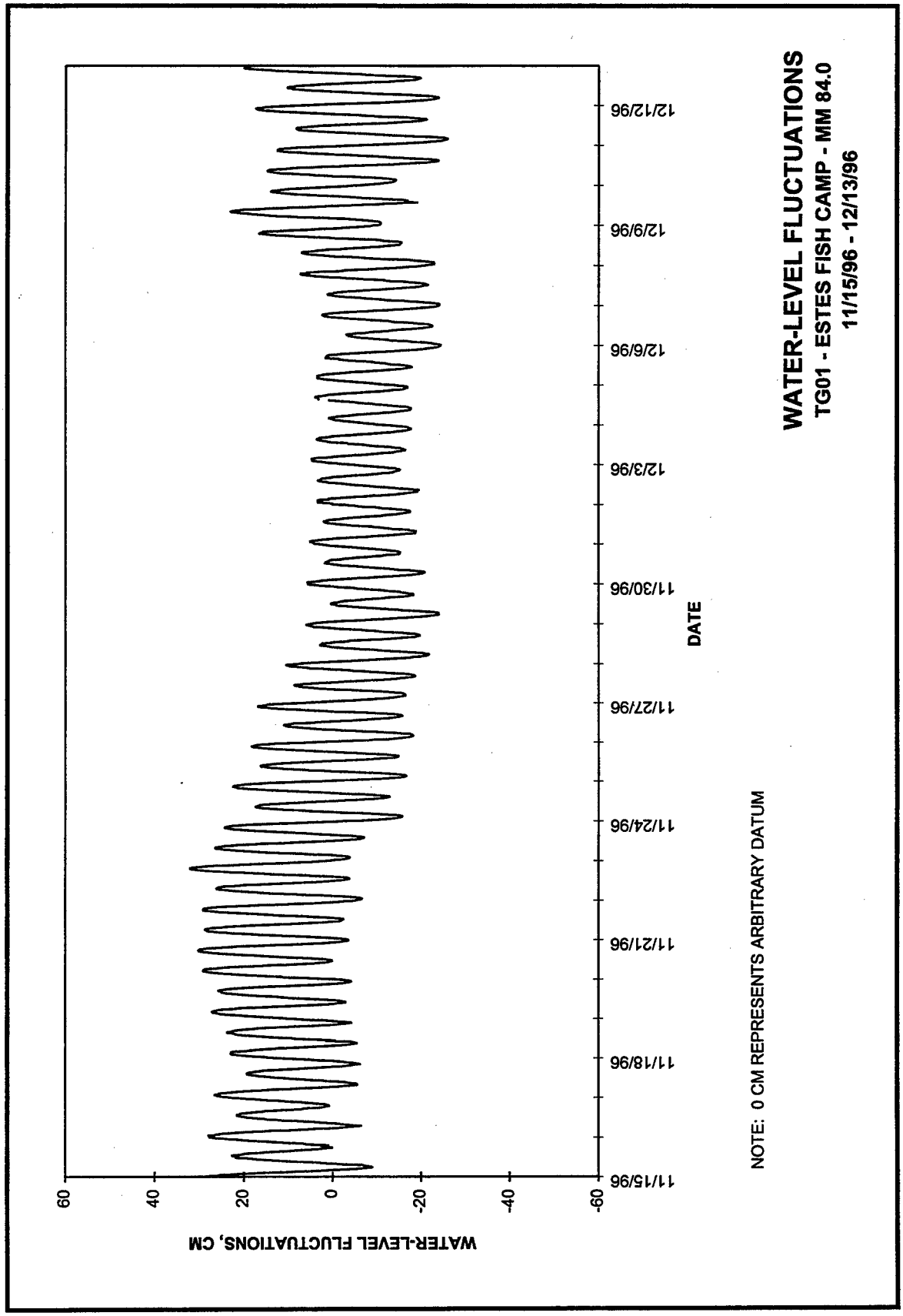
WATER-LEVEL FLUCTUATIONS
TG01 - ESTES FISH CAMP - MM 84.0
11/15/96 - 12/13/96
WATER-LEVEL FLUCTUATIONS, CM
60
40
20
0
-20
-40
-60
11/15/96
11/18/96
11/21/96
11/24/96
11/27/96
11/30/96
12/3/96
12/6/96
12/9/96
12/12/96
DATE
NOTE: 0 CM REPRESENTS ARBITRARY DATUM

Plate 43

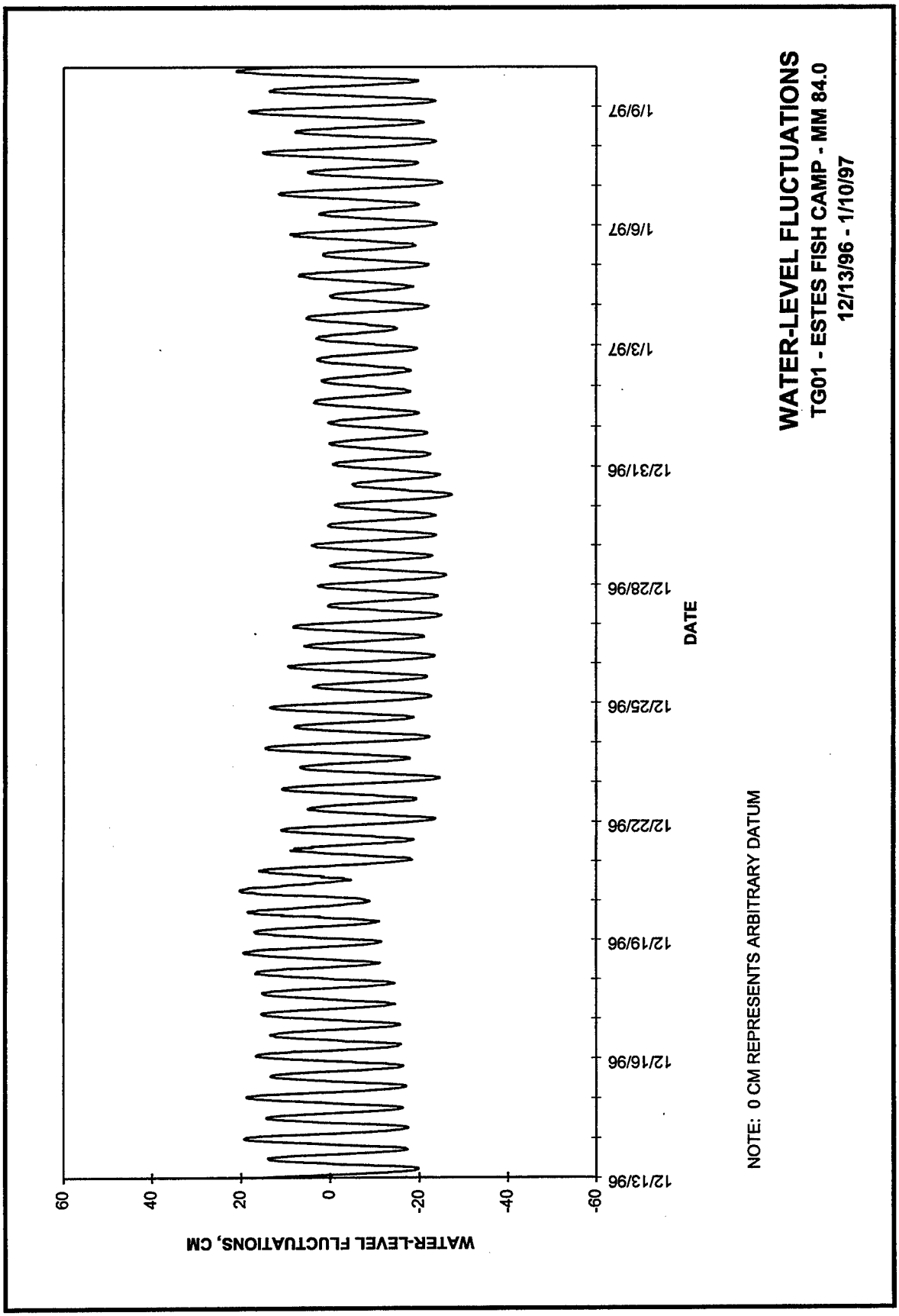
WATER-LEVEL FLUCTUATIONS
TG01 - ESTES FISH CAMP - MM 84.0
12/13/96 - 1/10/97
NOTE: 0 CM REPRESENTS ARBITRARY DATUM
DATE
12/13/96
12/16/96
12/19/96
12/22/96
12/25/96
12/28/96
12/31/96
1/3/97
1/6/97
1/9/97
WATER-LEVEL FLUCTUATIONS, CM
60
40
20
0
-20
-40
-60

Plate 44

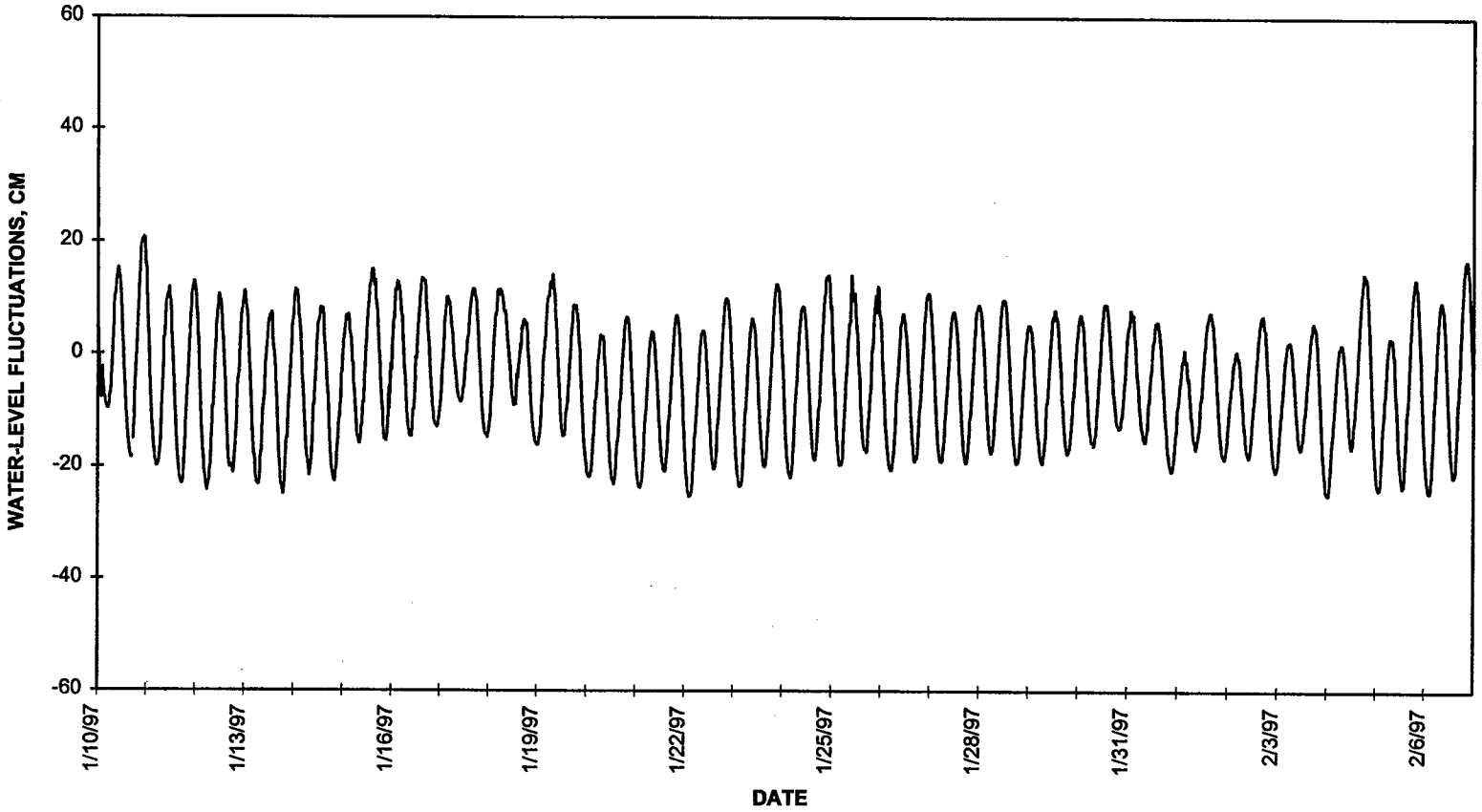

NOTE: 0 CM REPRESENTS ARBITRARY DATUM

WATER-LEVEL FLUCTUATIONS
TG01 - ESTES FISH CAMP - MM 84.0
1/10/97 - 2/7/97

Plate 45

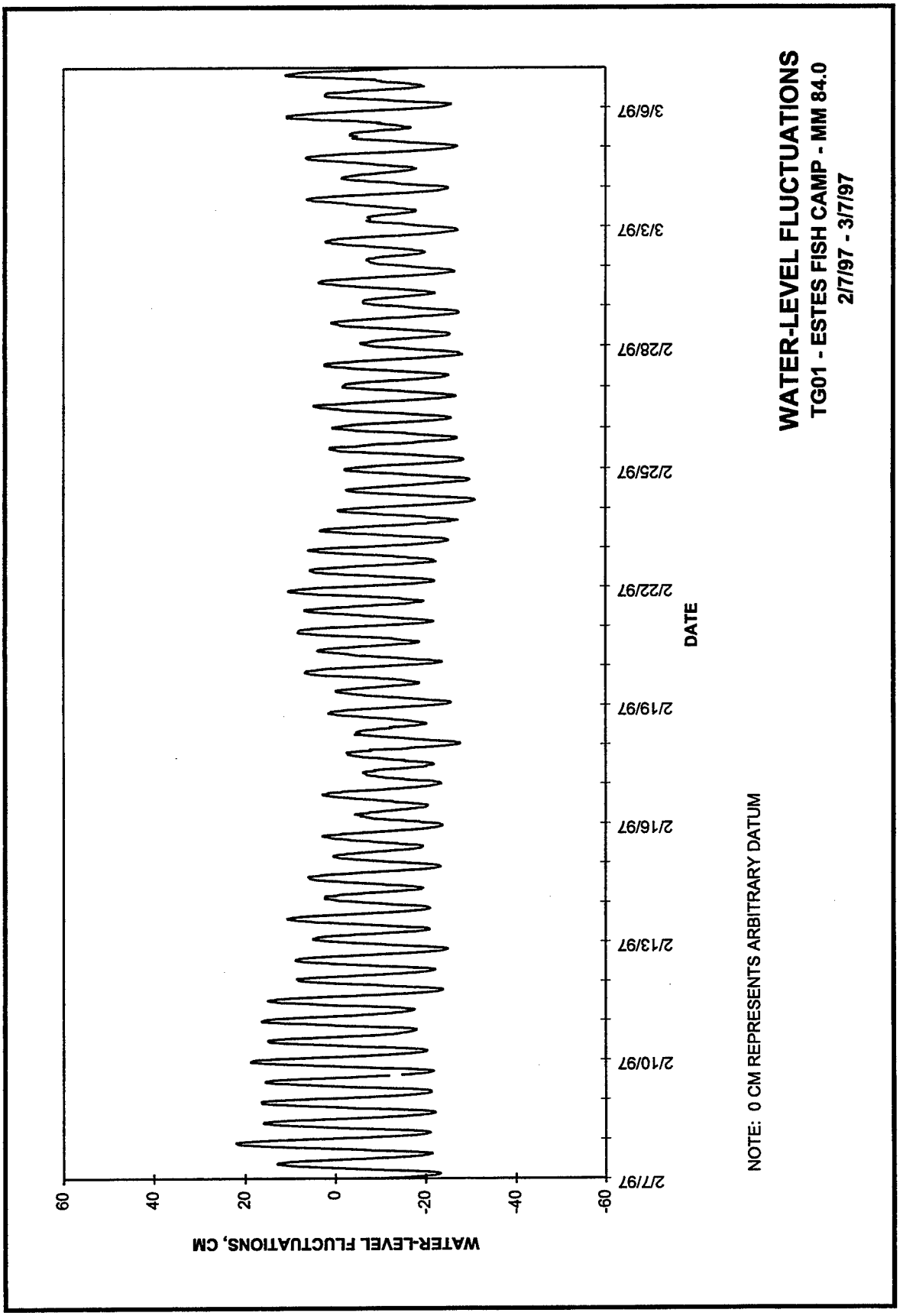
WATER-LEVEL FLUCTUATIONS
TG01 - ESTES FISH CAMP - MM 84.0
2/7/97 - 3/7/97
WATER-LEVEL FLUCTUATIONS, CM
60
40
20
0
-20
-40
-60
2/7/97
2/10/97
2/13/97
2/16/97
2/19/97
2/22/97
2/25/97
2/28/97
3/3/97
3/6/97
DATE
NOTE: 0 CM REPRESENTS ARBITRARY DATUM

Plate 46

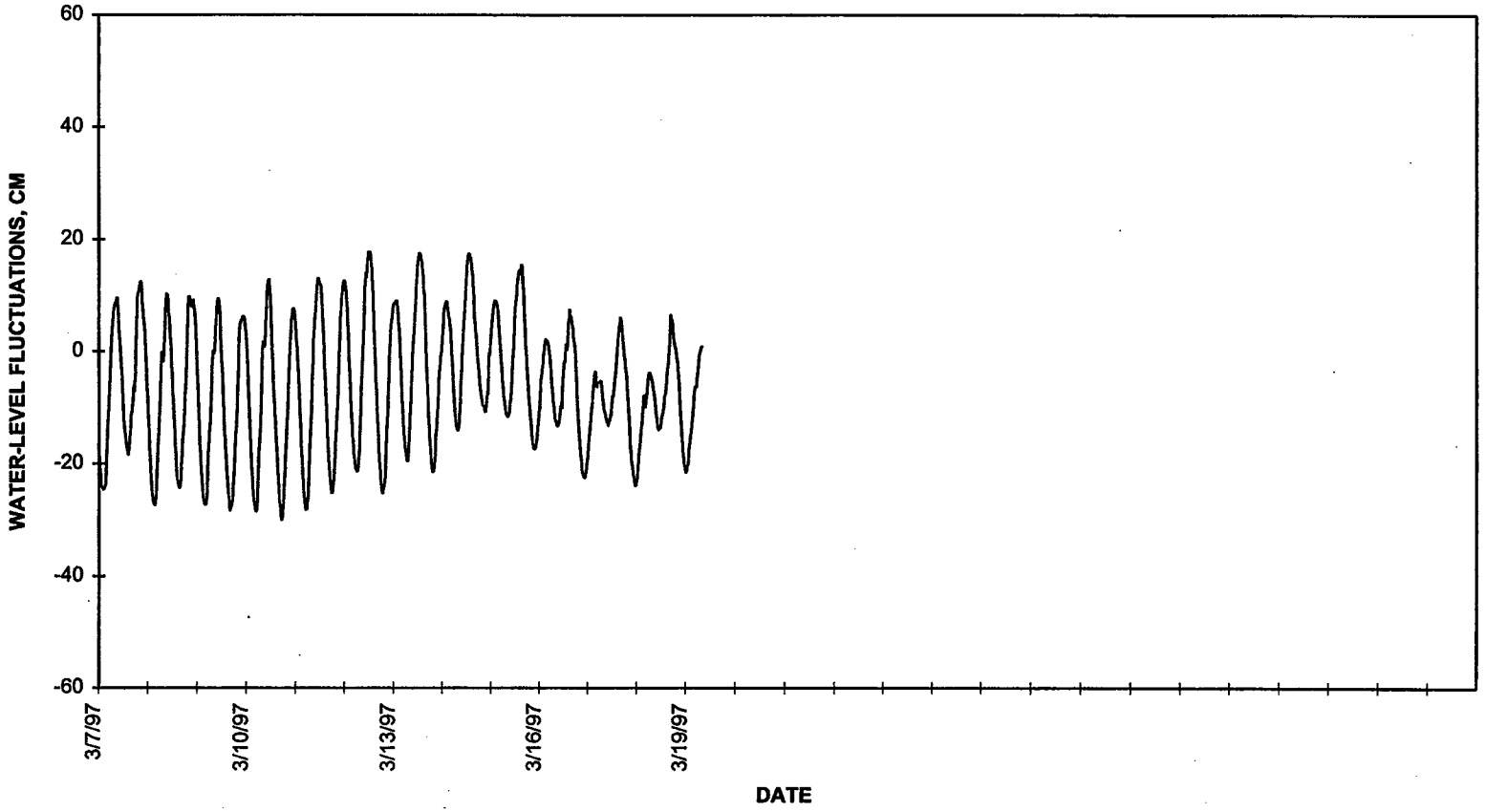

NOTE: 0 CM REPRESENTS ARBITRARY DATUM

WATER-LEVEL FLUCTUATIONS
TG01 - ESTES FISH CAMP - MM 84.0
3/7/97 - 3/19/97

Plate 47

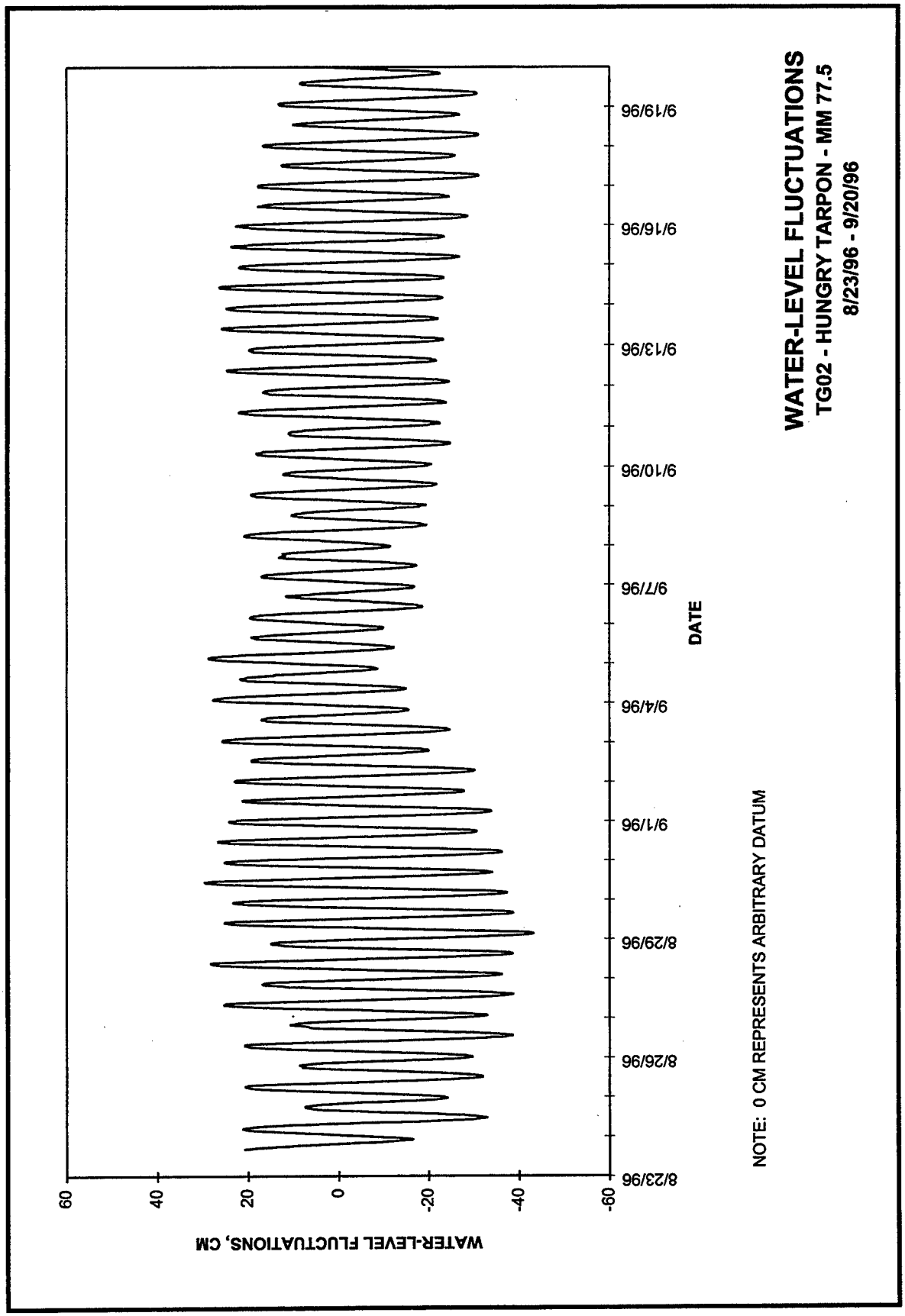
WATER-LEVEL FLUCTUATIONS
TG02 - HUNGRY TARPON - MM 77.5
8/23/96 - 9/20/96
WATER-LEVEL FLUCTUATIONS, CM
60
40
20
0
-20
-40
-60
8/23/96
8/26/96
8/29/96
9/1/96
9/4/96
9/7/96
9/10/96
9/13/96
9/16/96
9/19/96
DATE
NOTE: 0 CM REPRESENTS ARBITRARY DATUM

Plate 48

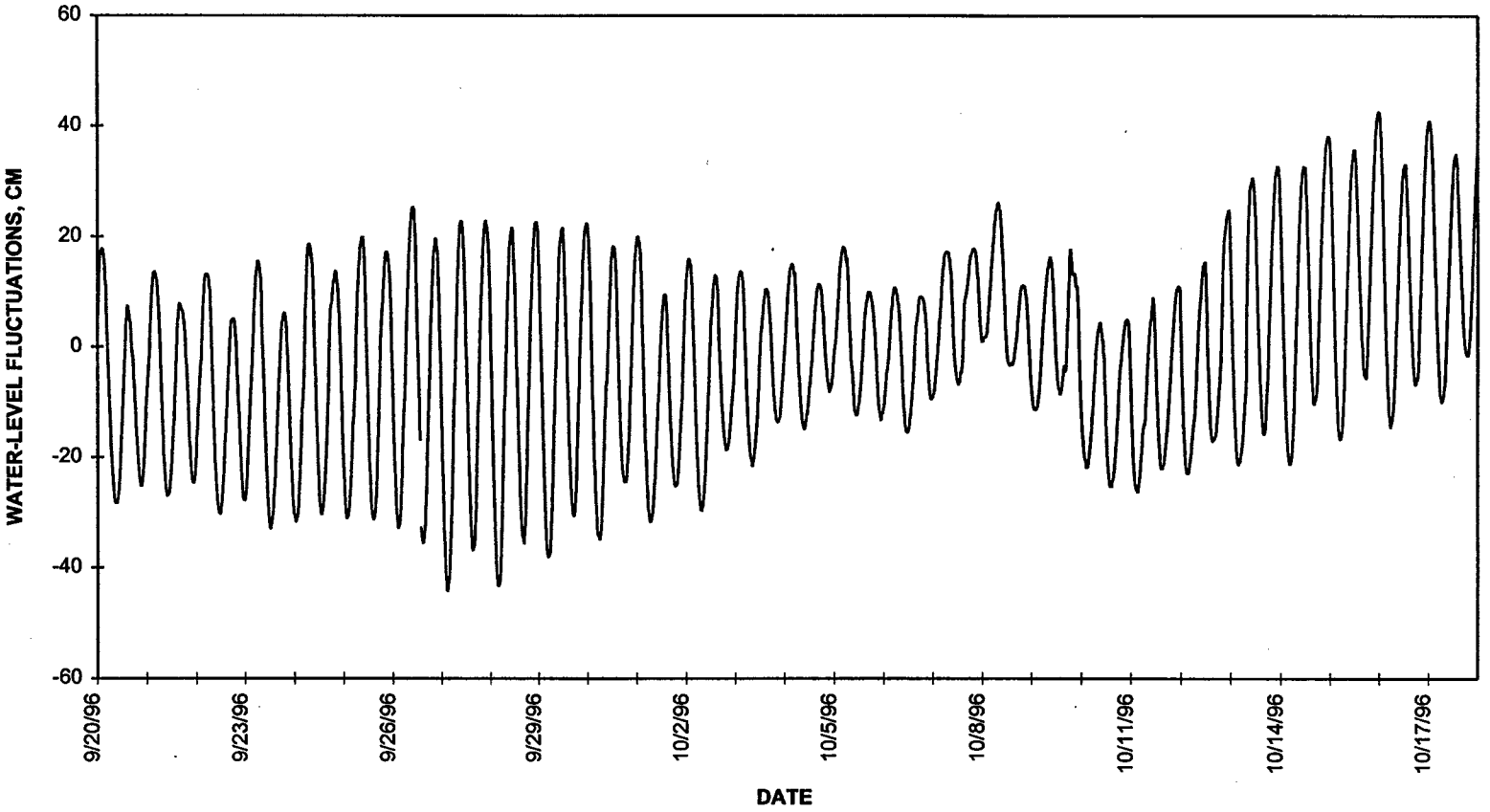

NOTE: 0 CM REPRESENTS ARBITRARY DATUM

WATER-LEVEL FLUCTUATIONS
TG02 - HUNGRY TARPON - MM 77.5
9/20/96 - 10/18/96

Plate 49

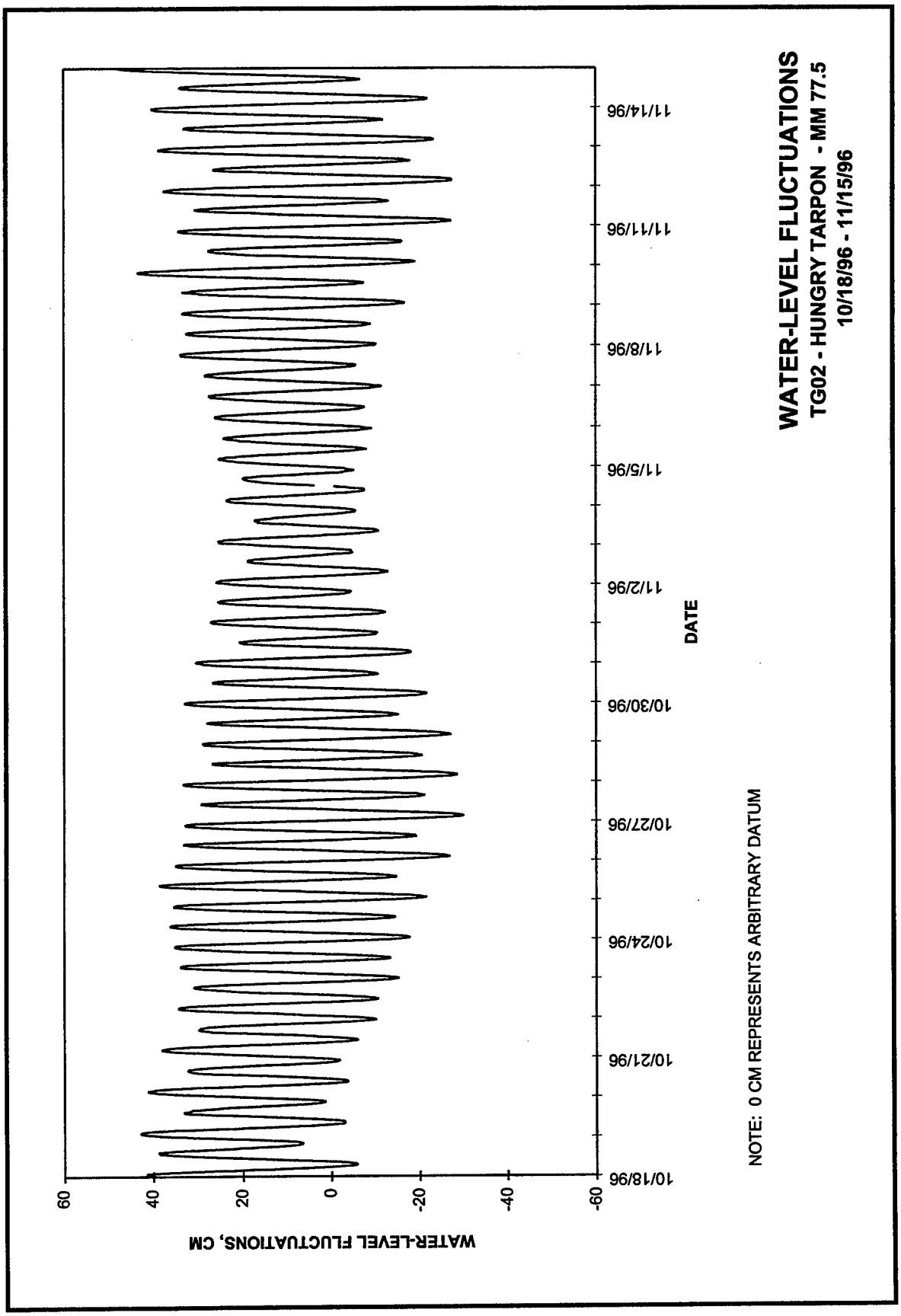
WATER-LEVEL FLUCTUATIONS
TG02 - HUNGRY TARPON - MM 77.5
10/18/96 - 11/15/96
WATER-LEVEL FLUCTUATIONS, CM
60
40
20
0
-20
-40
-60
10/18/96
10/21/96
10/24/96
10/27/96
10/30/96
11/2/96
11/5/96
11/8/96
11/11/96
11/14/96
DATE
NOTE: 0 CM REPRESENTS ARBITRARY DATUM

Plate 50

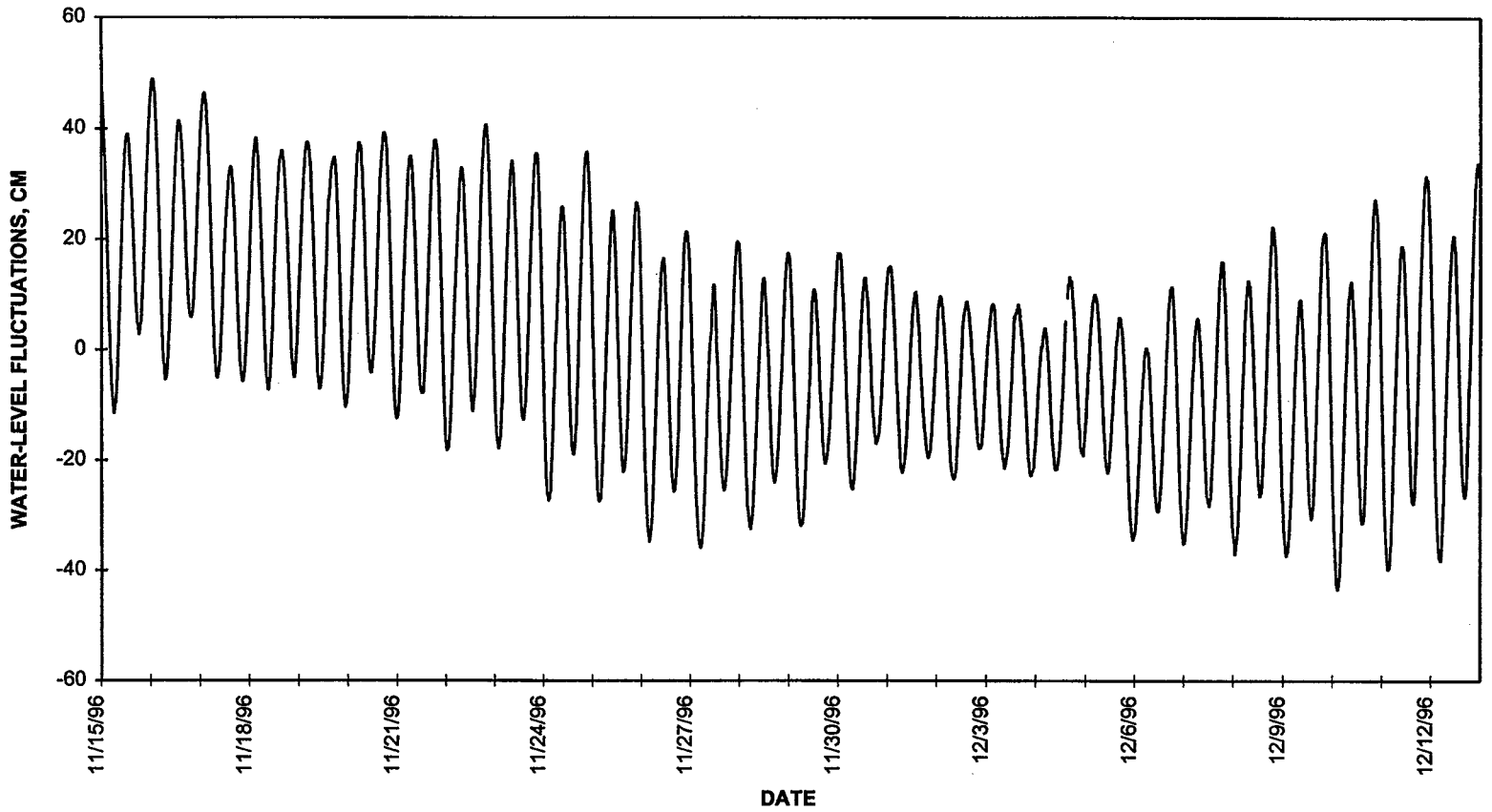

NOTE: 0 CM REPRESENTS ARBITRARY DATUM

WATER-LEVEL FLUCTUATIONS
TG02 - HUNGRY TARPON - MM 77.5
11/15/96 - 12/13/96

Plate 51

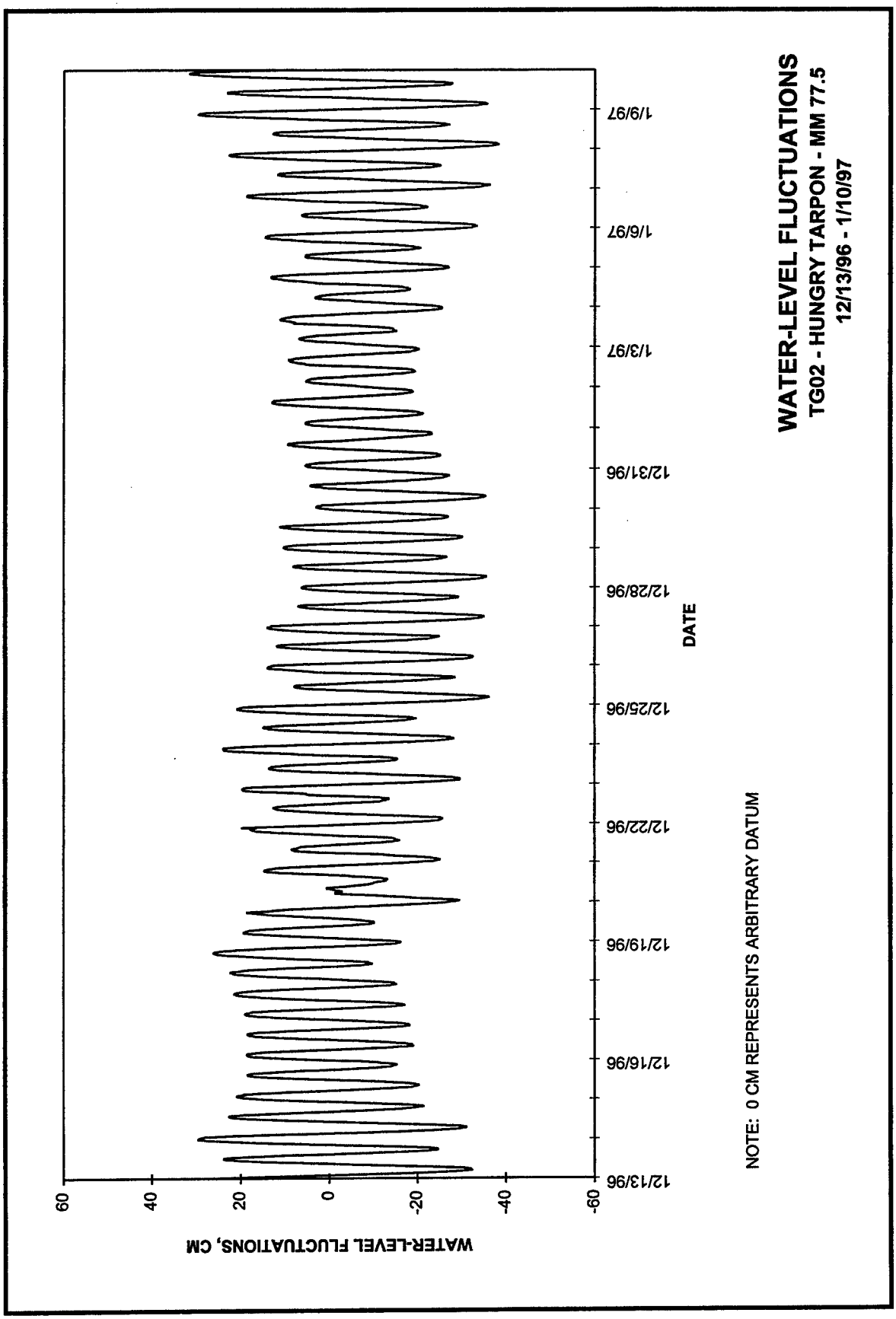
WATER-LEVEL FLUCTUATIONS
TG02 - HUNGRY TARPON - MM 77.5
12/13/96 - 1/10/97
WATER-LEVEL FLUCTUATIONS, CM
60
40
20
0
-20
-40
-60
12/13/96
12/16/96
12/19/96
12/22/96
12/25/96
12/28/96
12/31/96
1/3/97
1/6/97
1/9/97
DATE
NOTE: 0 CM REPRESENTS ARBITRARY DATUM

Plate 52

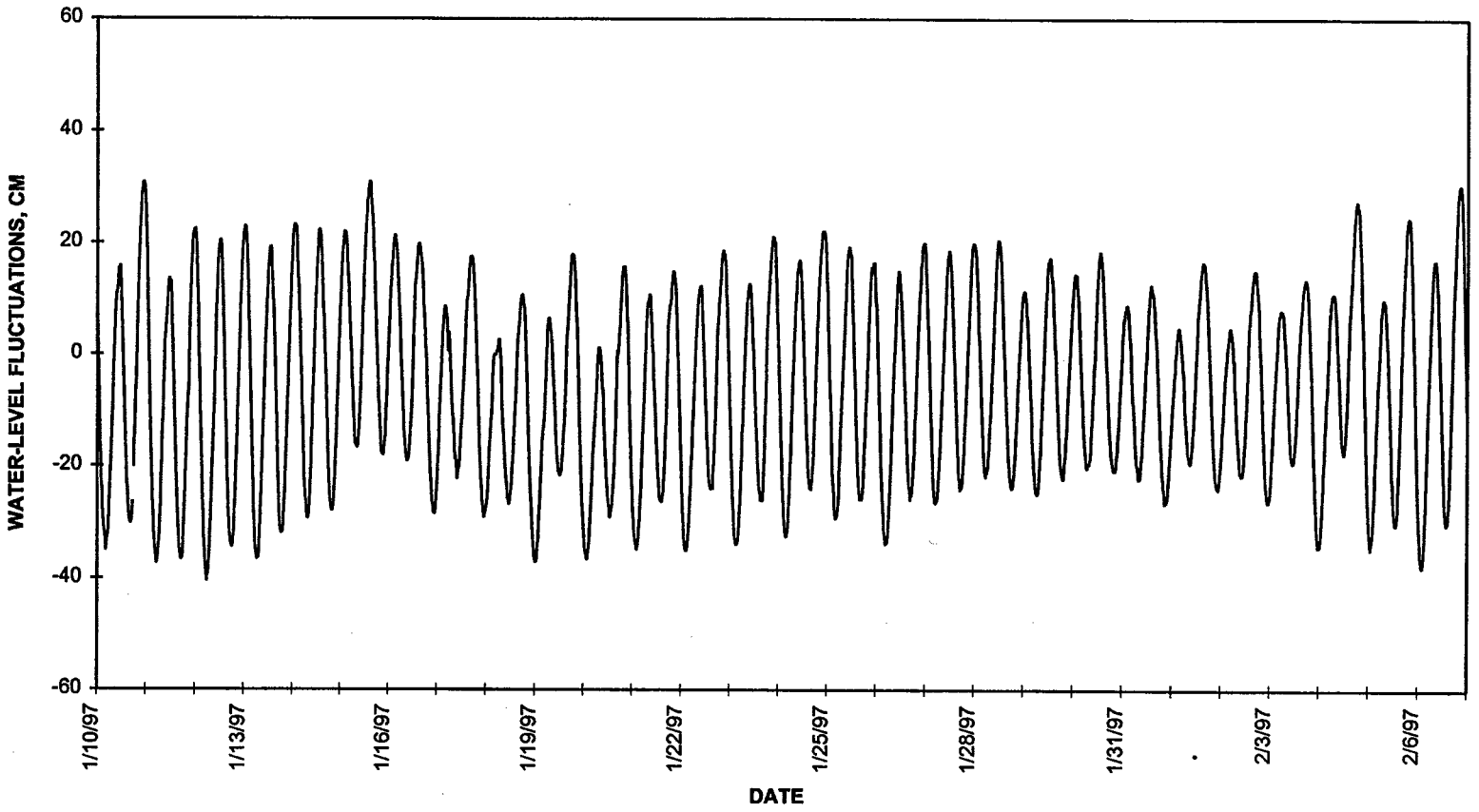

NOTE: 0 CM REPRESENTS ARBITRARY DATUM

WATER-LEVEL FLUCTUATIONS
TG02 - HUNGRY TARPON - MM 77.5
1/10/97 - 2/7/97

Plate 53

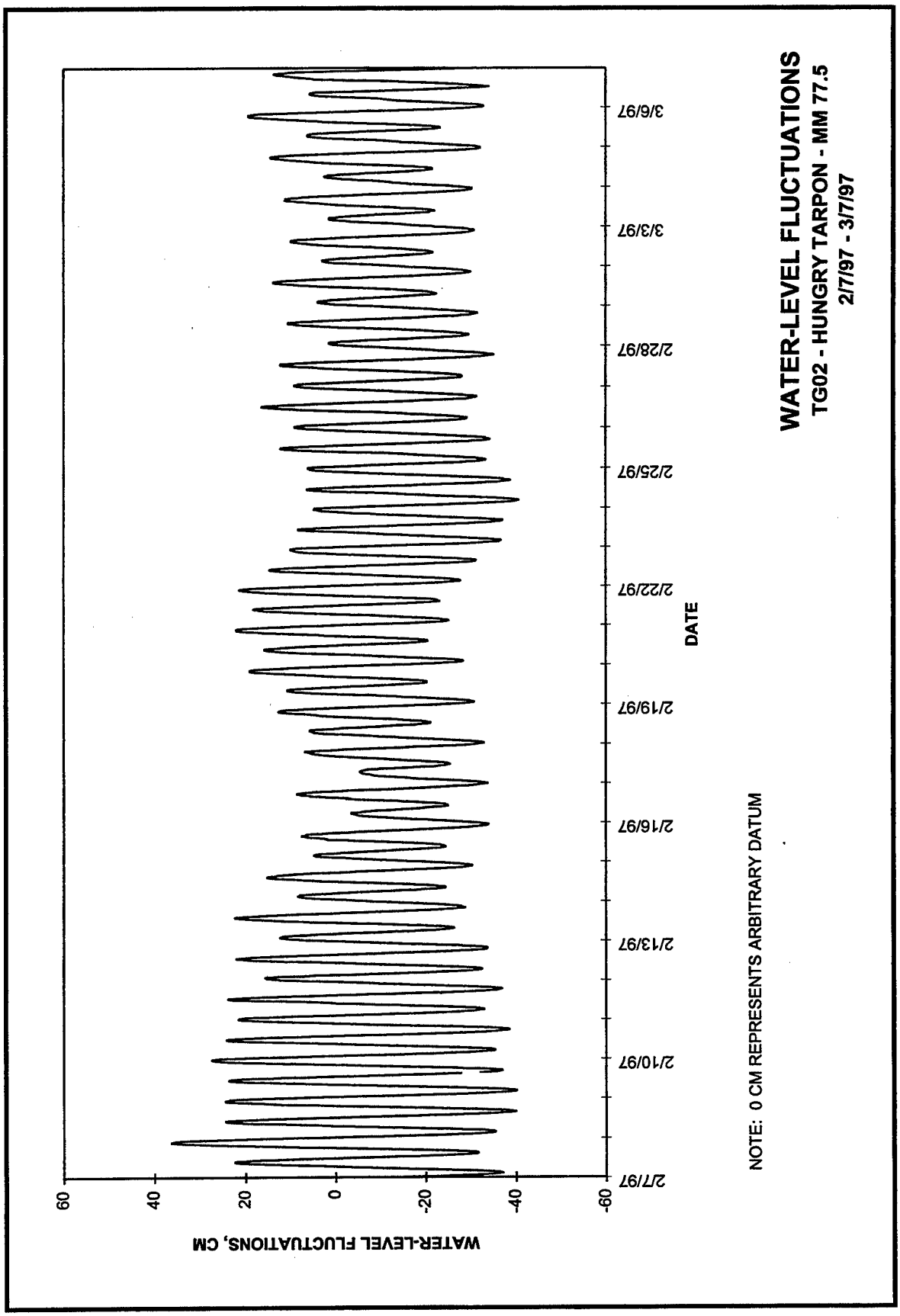
WATER-LEVEL FLUCTUATIONS
TG02 - HUNGRY TARPON - MM 77.5
2/7/97 - 3/7/97
WATER-LEVEL FLUCTUATIONS, CM
60
40
20
0
-20
-40
-60
2/7/97
2/10/97
2/13/97
2/16/97
2/19/97
2/22/97
2/25/97
2/28/97
3/3/97
3/6/97
DATE
NOTE: 0 CM REPRESENTS ARBITRARY DATUM

Plate 54

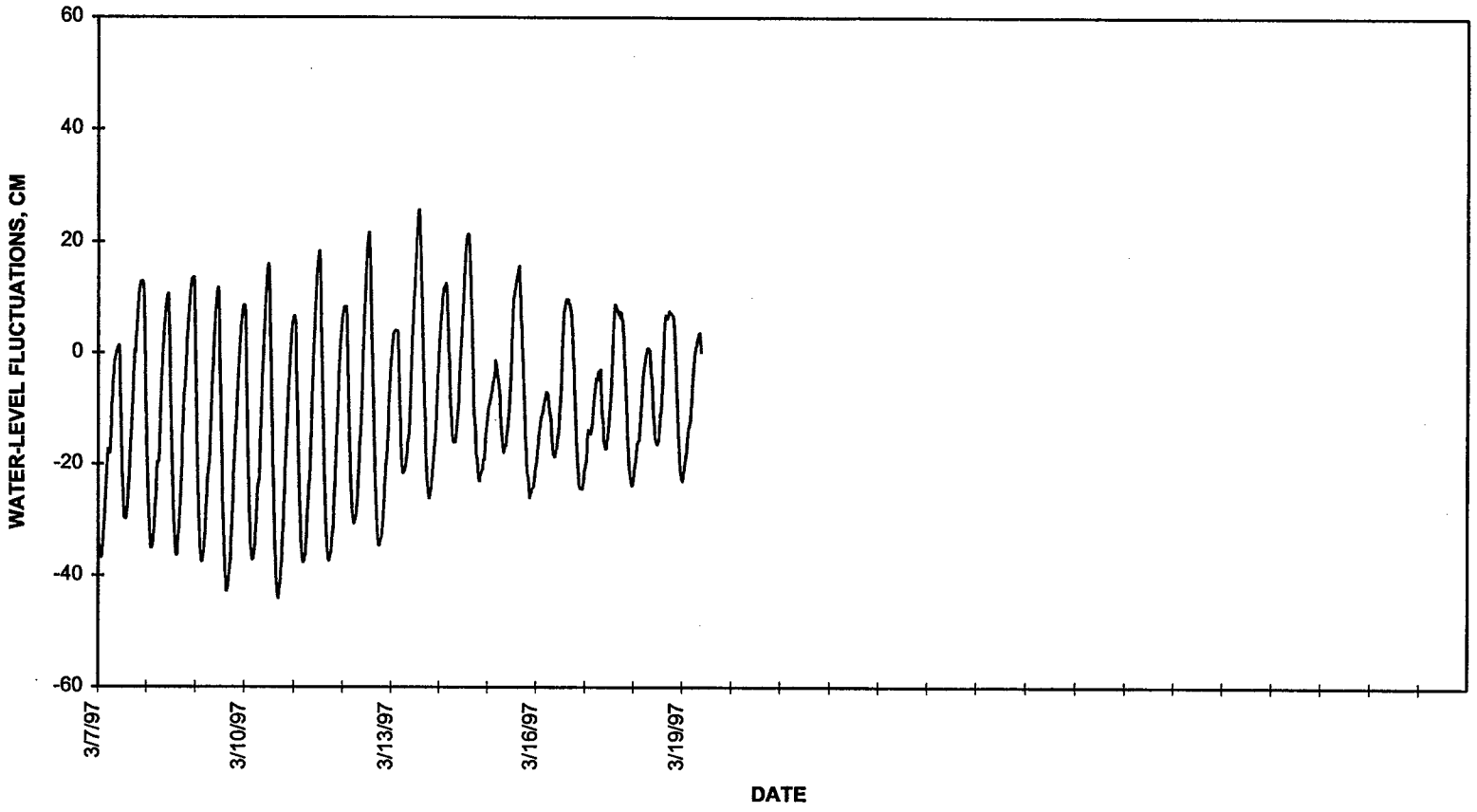

NOTE: 0 CM REPRESENTS ARBITRARY DATUM

WATER-LEVEL FLUCTUATIONS
TG02 - HUNGRY TARPON - MM 77.5
3/7/97 - 3/19/97

Plate 55

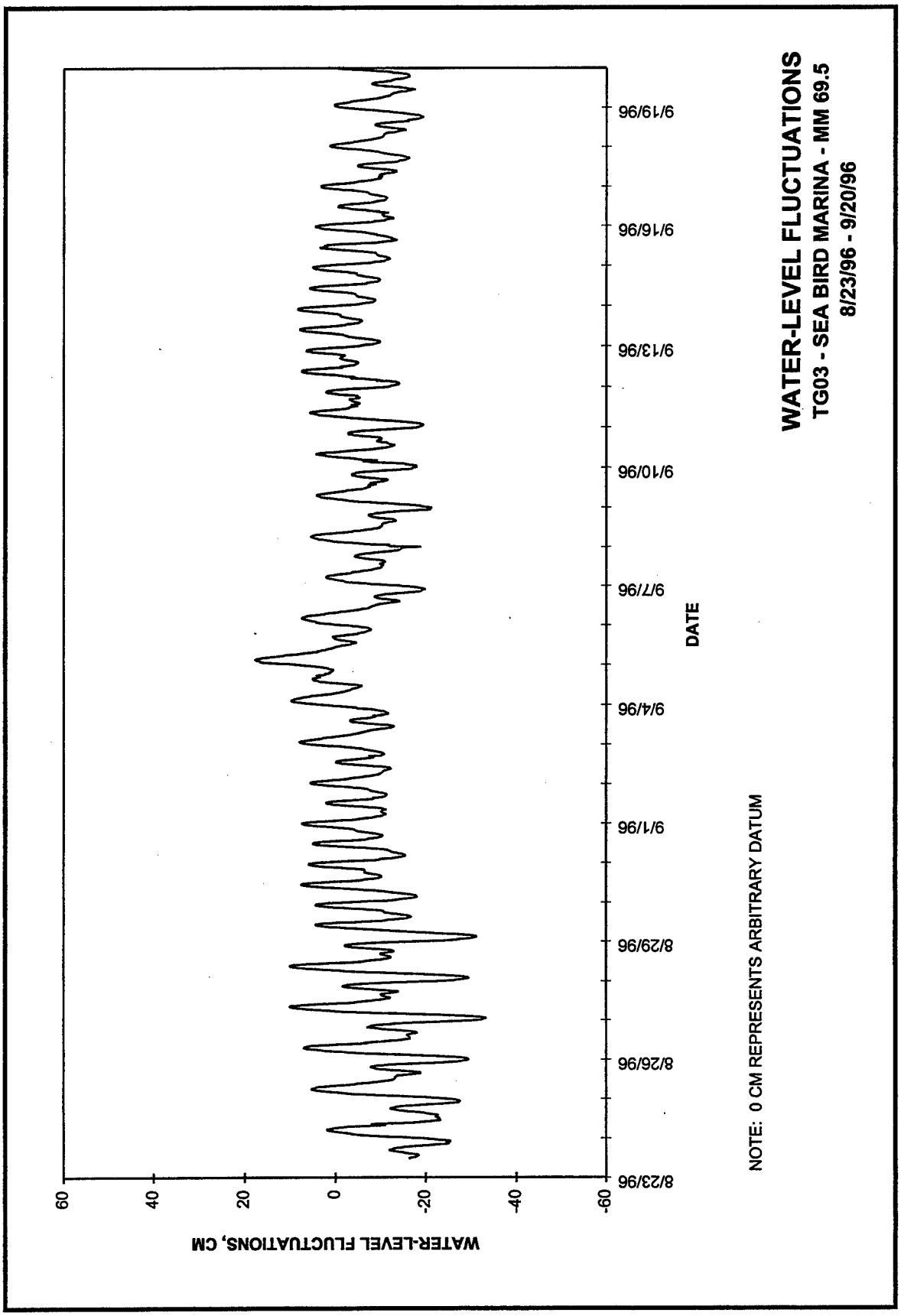
WATER-LEVEL FLUCTUATIONS
TG03 - SEA BIRD MARINA - MM 69.5
8/23/96 - 9/20/96
WATER-LEVEL FLUCTUATIONS, CM
60
40
20
0
-20
-40
-60
8/23/96
8/26/96
8/29/96
9/1/96
9/4/96
9/7/96
9/10/96
9/13/96
9/16/96
9/19/96
DATE
NOTE: 0 CM REPRESENTS ARBITRARY DATUM

Plate 56

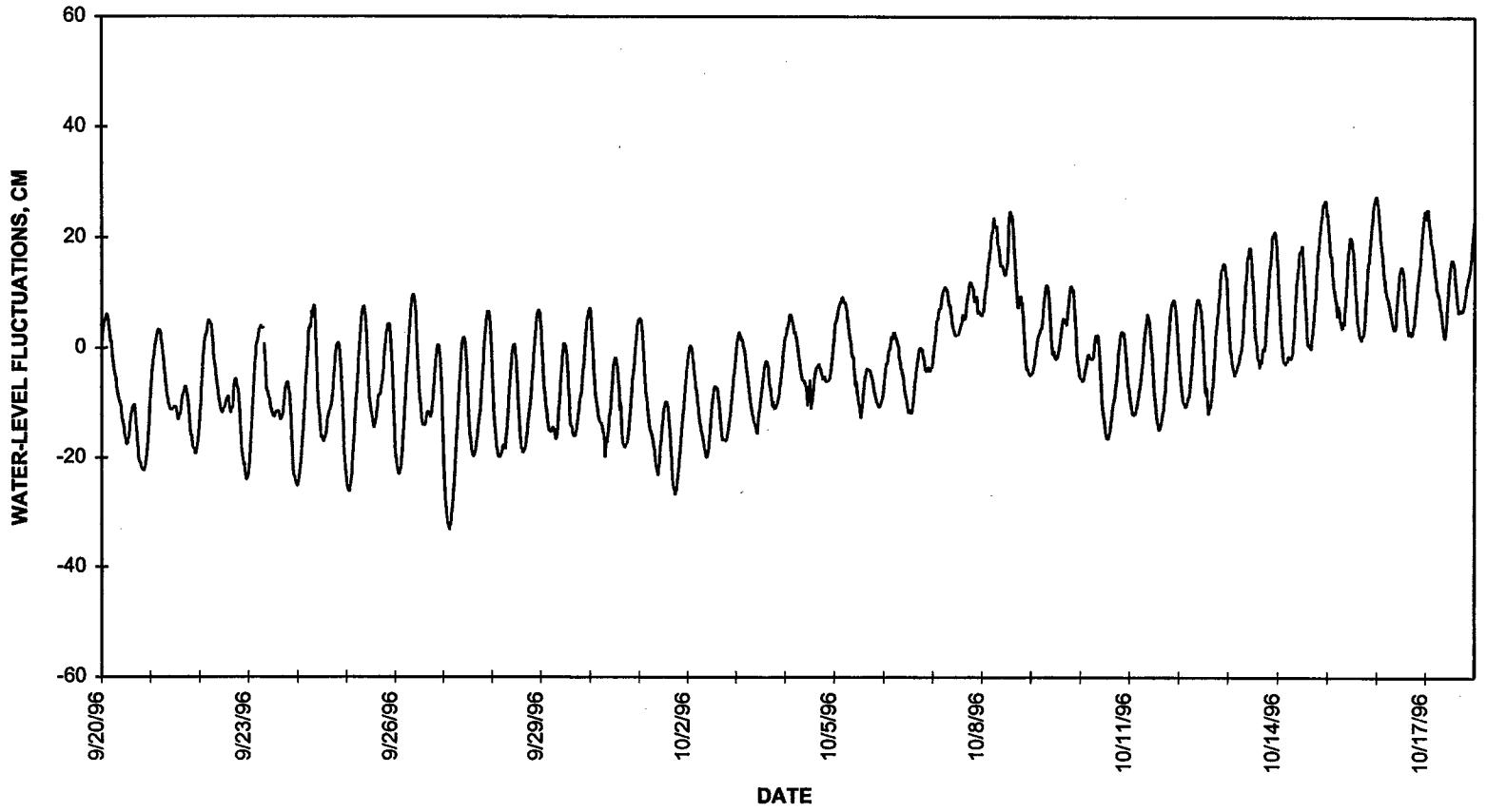

NOTE: 0 CM REPRESENTS ARBITRARY DATUM

WATER-LEVEL FLUCTUATIONS
TG03 - SEA BIRD MARINA - MM 69.5
9/20/96 - 10/18/96

Plate 57

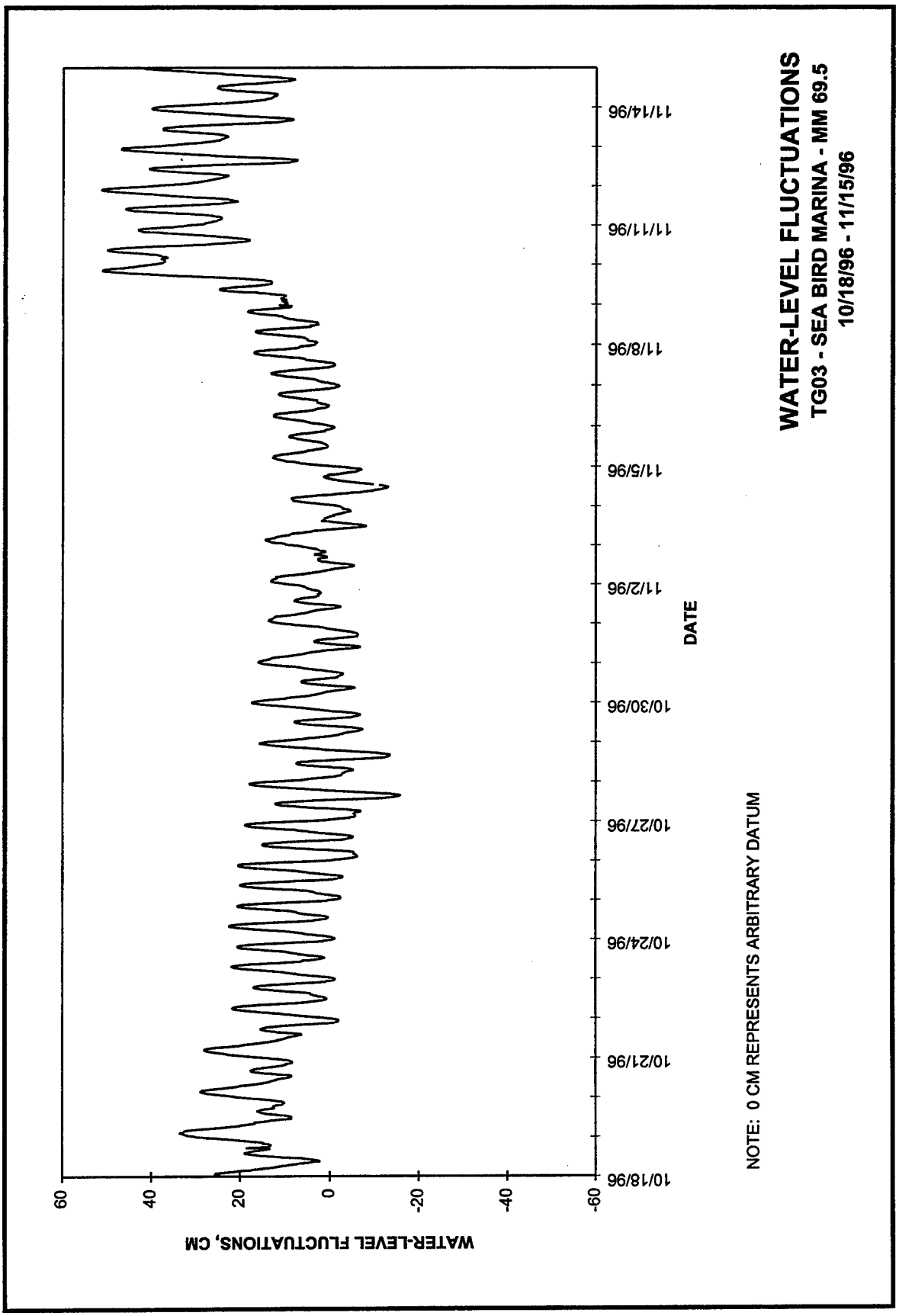
WATER-LEVEL FLUCTUATIONS
TG03 - SEA BIRD MARINA - MM 69.5
10/18/96 - 11/15/96
WATER-LEVEL FLUCTUATIONS, CM
60
40
20
0
-20
-40
-60
10/18/96
10/21/96
10/24/96
10/27/96
10/30/96
11/2/96
11/5/96
11/8/96
11/11/96
11/14/96
DATE
NOTE: 0 CM REPRESENTS ARBITRARY DATUM

Plate 58

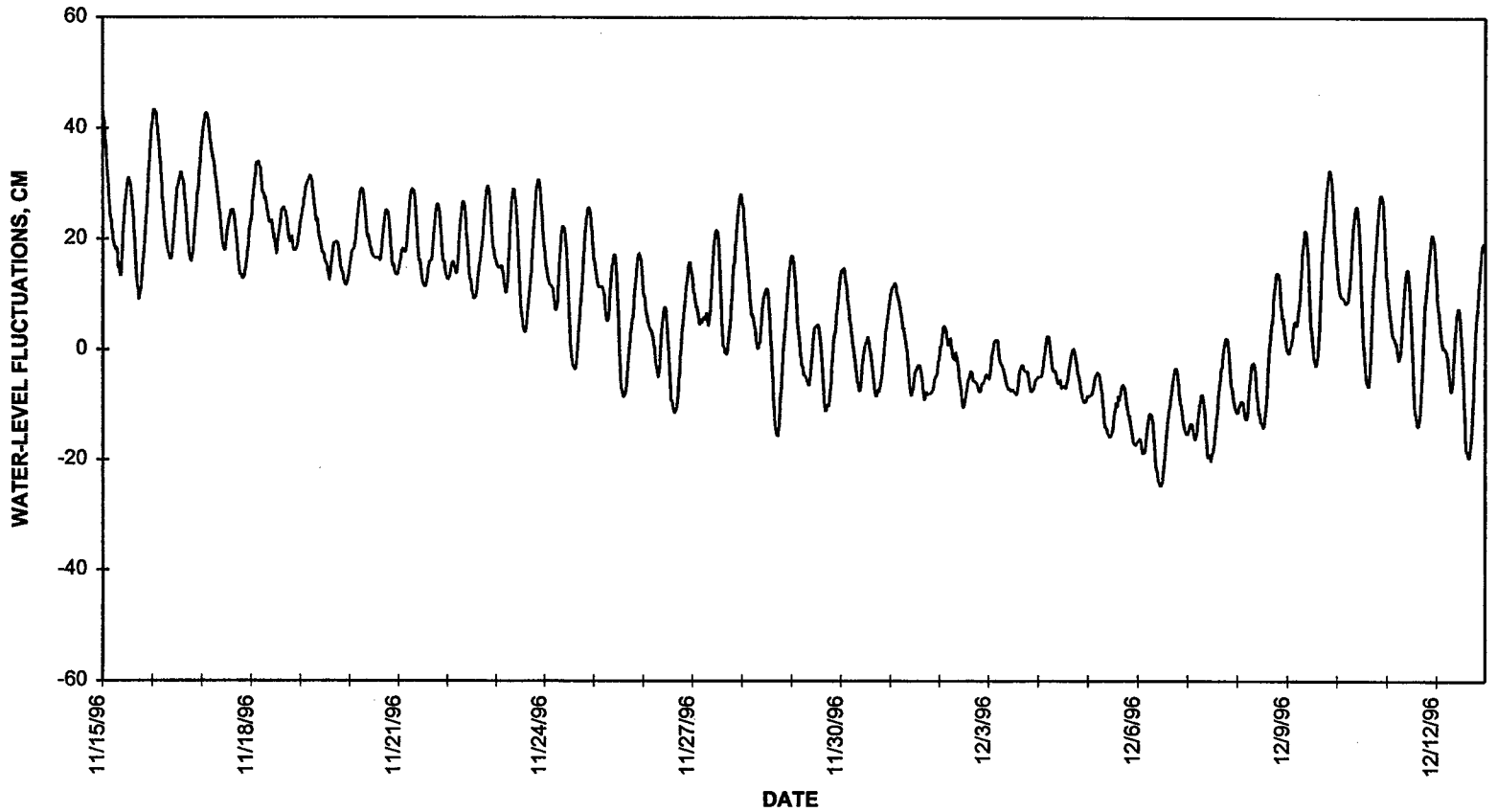

NOTE: 0 CM REPRESENTS ARBITRARY DATUM

WATER-LEVEL FLUCTUATIONS
TG03 - SEA BIRD MARINA - MM 69.5
11/15/96 - 12/13/96

Plate 59

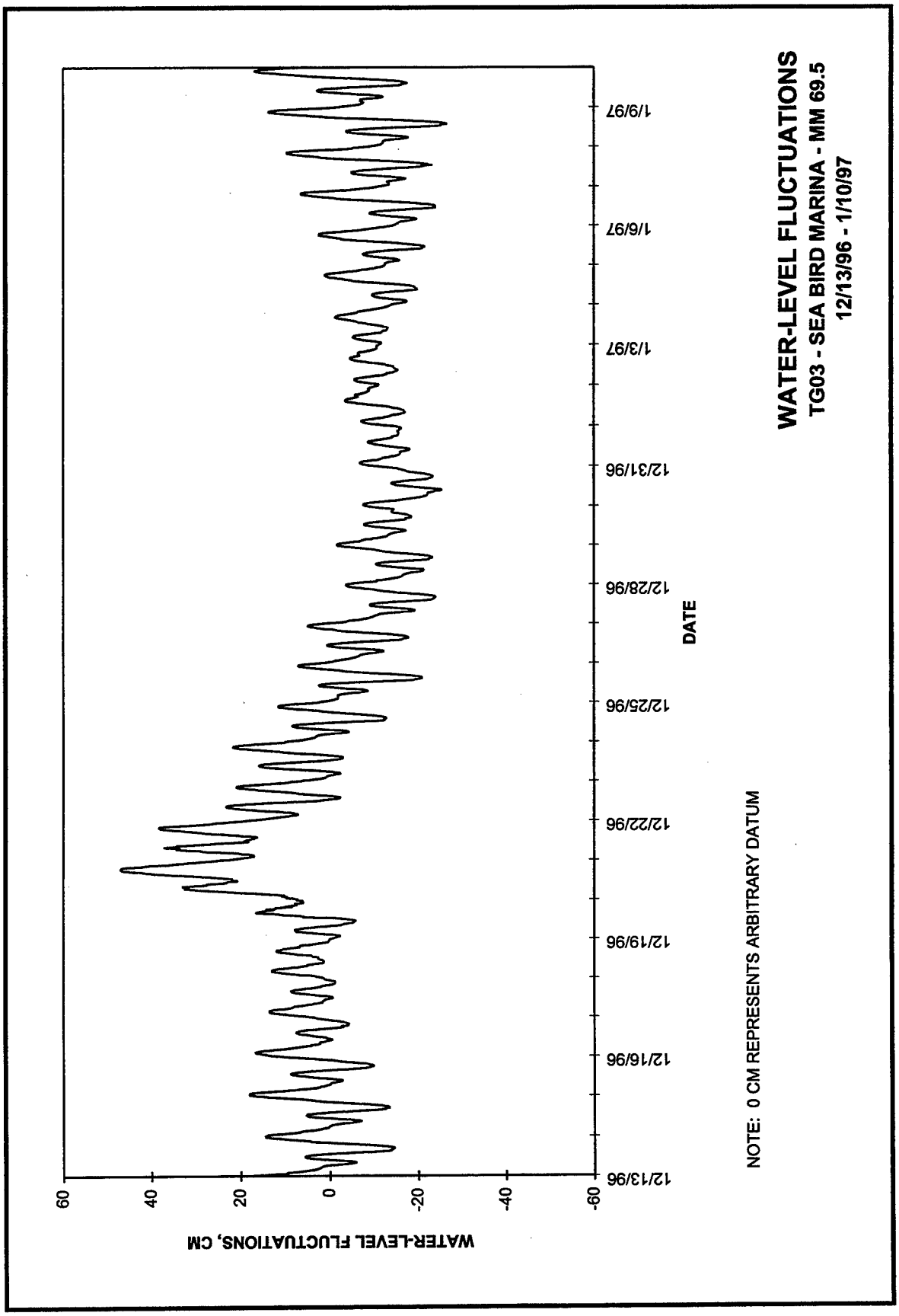
WATER-LEVEL FLUCTUATIONS
TG03 - SEA BIRD MARINA - MM 69.5
12/13/96 - 1/10/97
NOTE: 0 CM REPRESENTS ARBITRARY DATUM
WATER-LEVEL FLUCTUATIONS, CM
60
40
20
0
-20
-40
-60
DATE
12/13/96
12/16/96
12/19/96
12/22/96
12/25/96
12/28/96
12/31/96
1/3/97
1/6/97
1/9/97

Plate 60

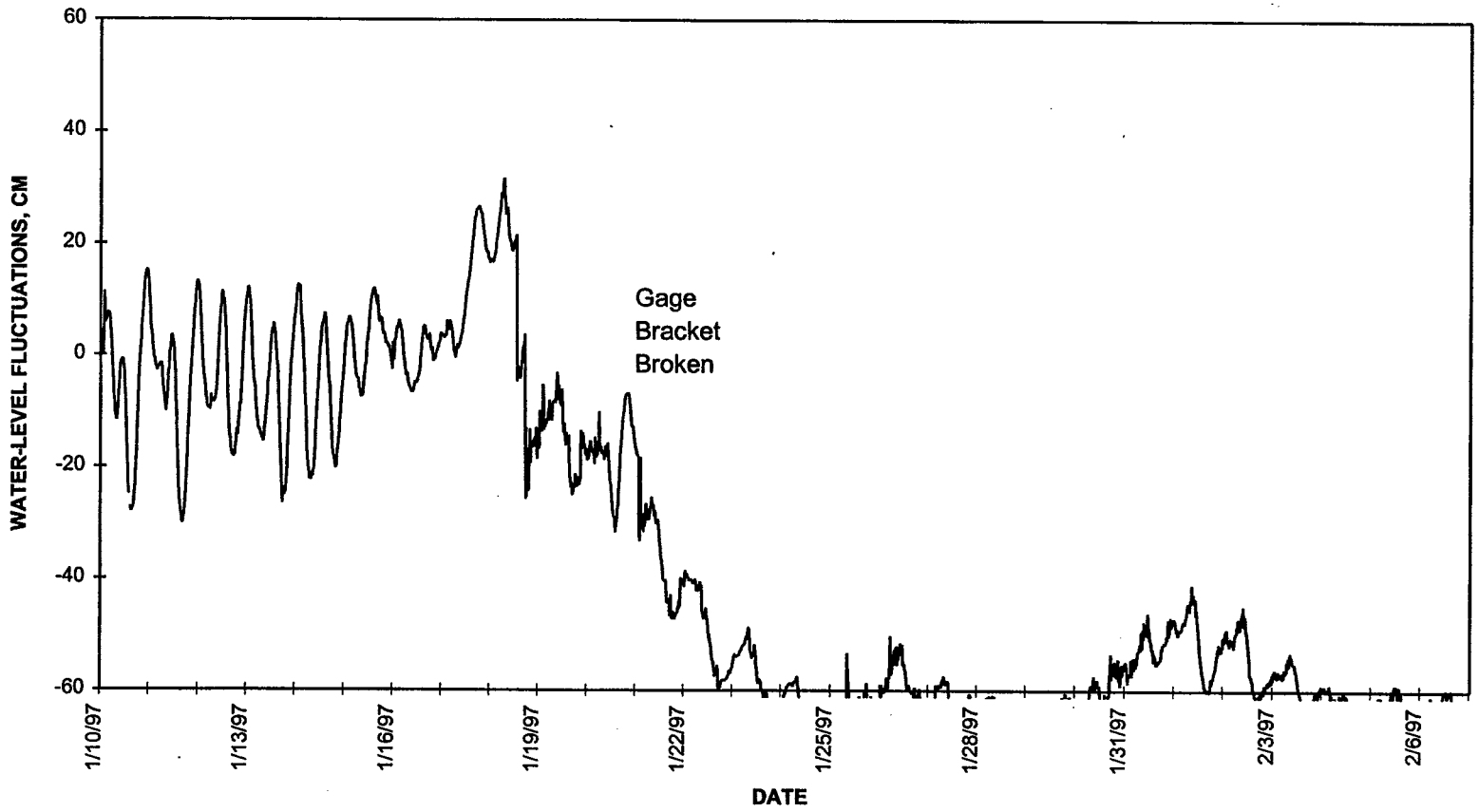

NOTE: 0 CM REPRESENTS ARBITRARY DATUM

WATER-LEVEL FLUCTUATIONS
TG03 - SEA BIRD MARINA - MM 69.5
1/10/97 - 2/7/97

Plate 61

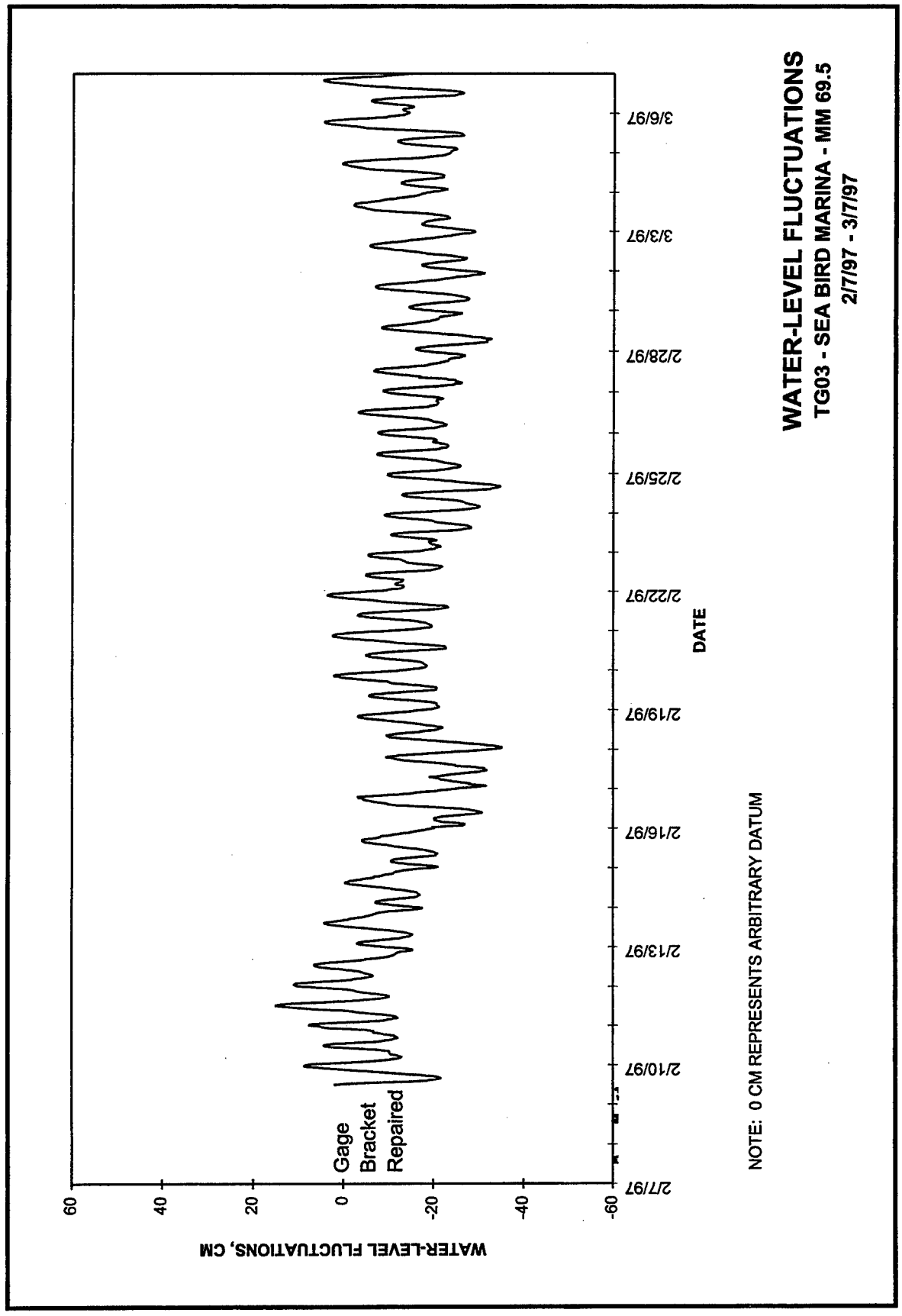
WATER-LEVEL FLUCTUATIONS
TG03 - SEA BIRD MARINA - MM 69.5
2/7/97 - 3/7/97
WATER-LEVEL FLUCTUATIONS, CM
60
40
20
0
-20
-40
-60
2/7/97
2/10/97
2/13/97
2/16/97
2/19/97
2/22/97
2/25/97
2/28/97
3/3/97
3/6/97
DATE
Gage
Bracket
Repaired
NOTE: 0 CM REPRESENTS ARBITRARY DATUM

Plate 62

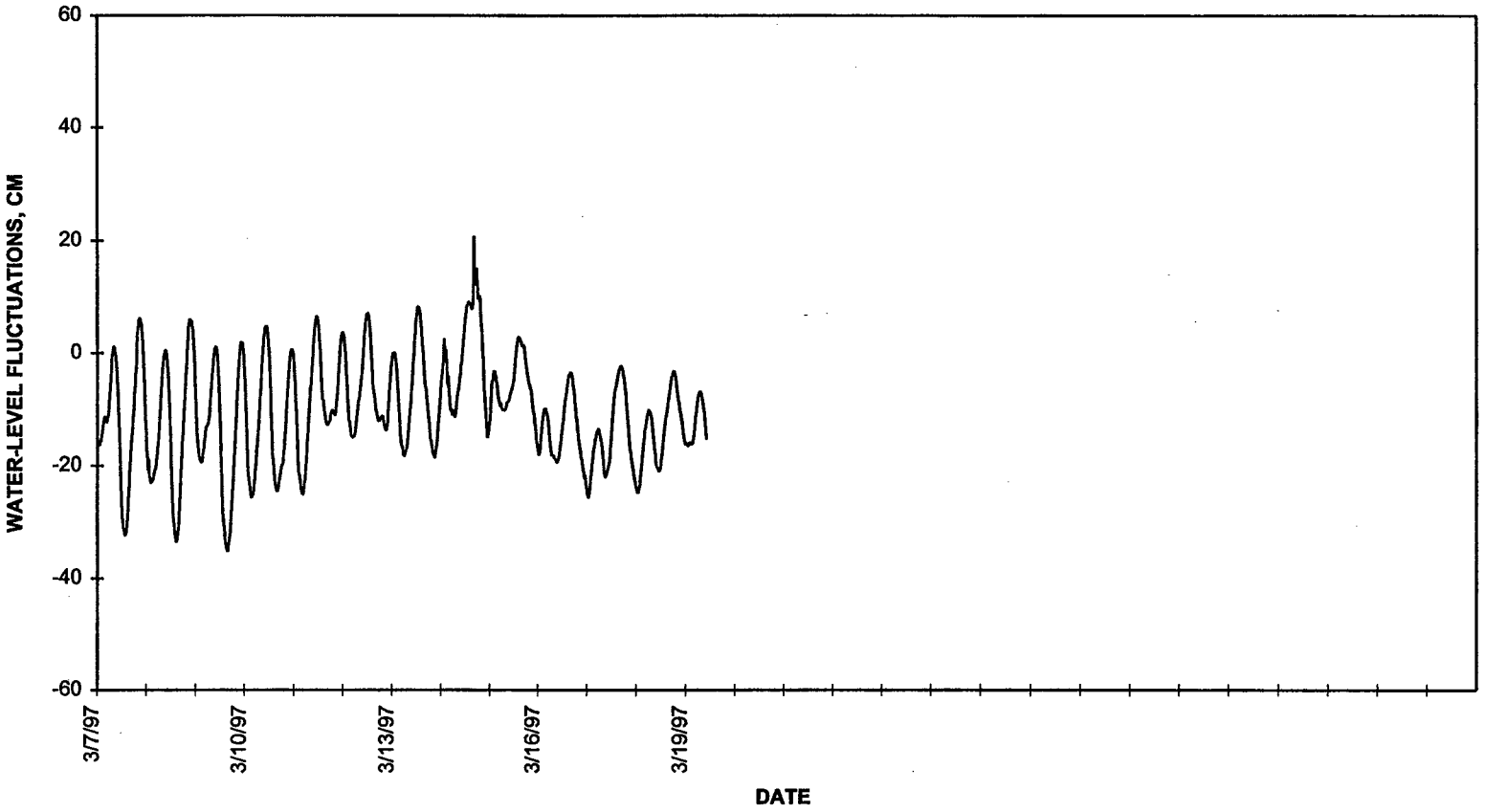

NOTE: 0 CM REPRESENTS ARBITRARY DATUM

WATER-LEVEL FLUCTUATIONS
TG03 - SEA BIRD MARINA - MM 69.5
3/7/97 - 3/19/97

Plate 63

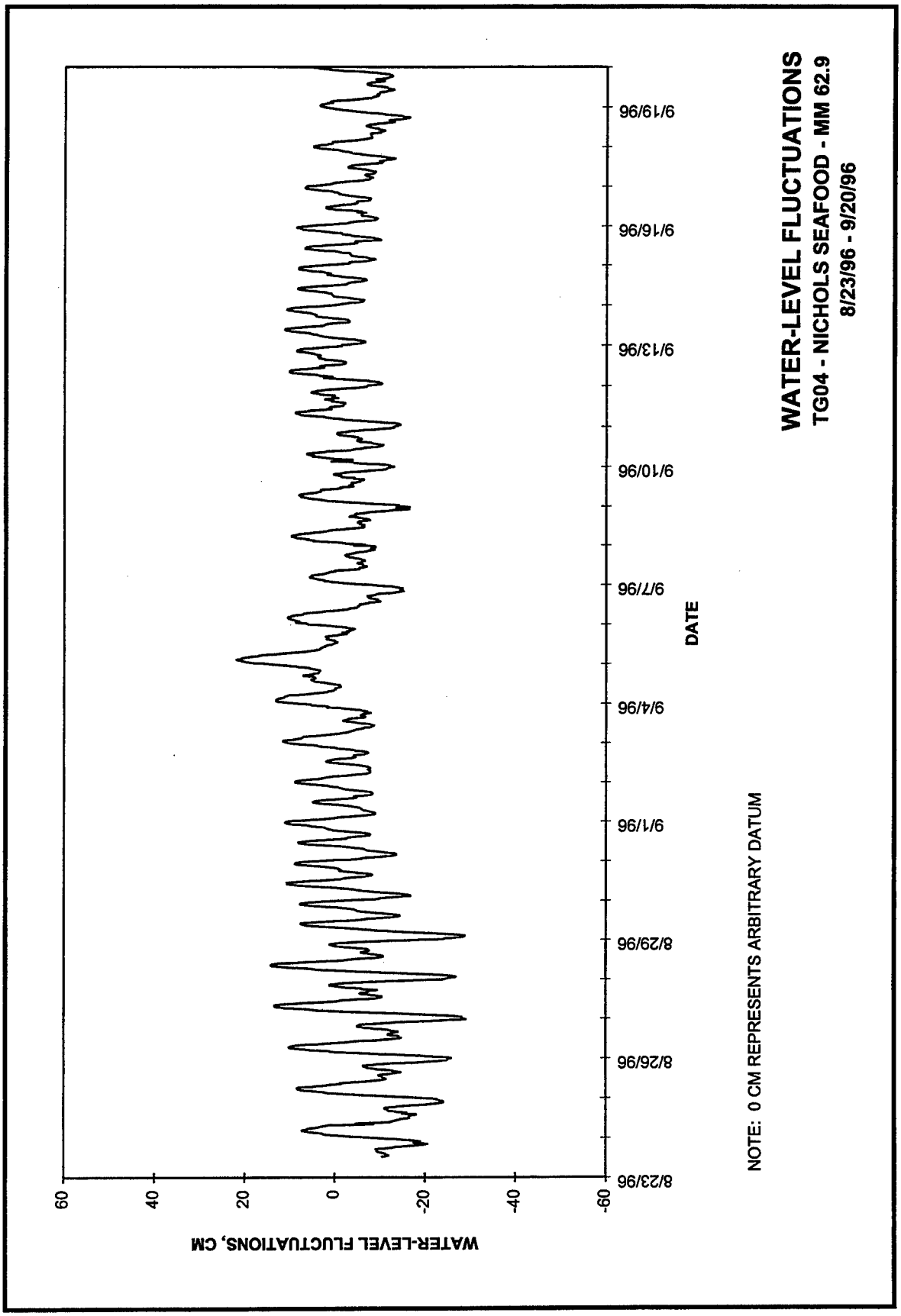
WATER-LEVEL FLUCTUATIONS
TG04 - NICHOLS SEAFOOD - MM 62.9
8/23/96 - 9/20/96
NOTE: 0 CM REPRESENTS ARBITRARY DATUM
WATER-LEVEL FLUCTUATIONS, CM
60
40
20
0
-20
-40
-60
8/23/96
8/26/96
8/29/96
9/1/96
9/4/96
9/7/96
9/10/96
9/13/96
9/16/96
9/19/96
DATE

Plate 64

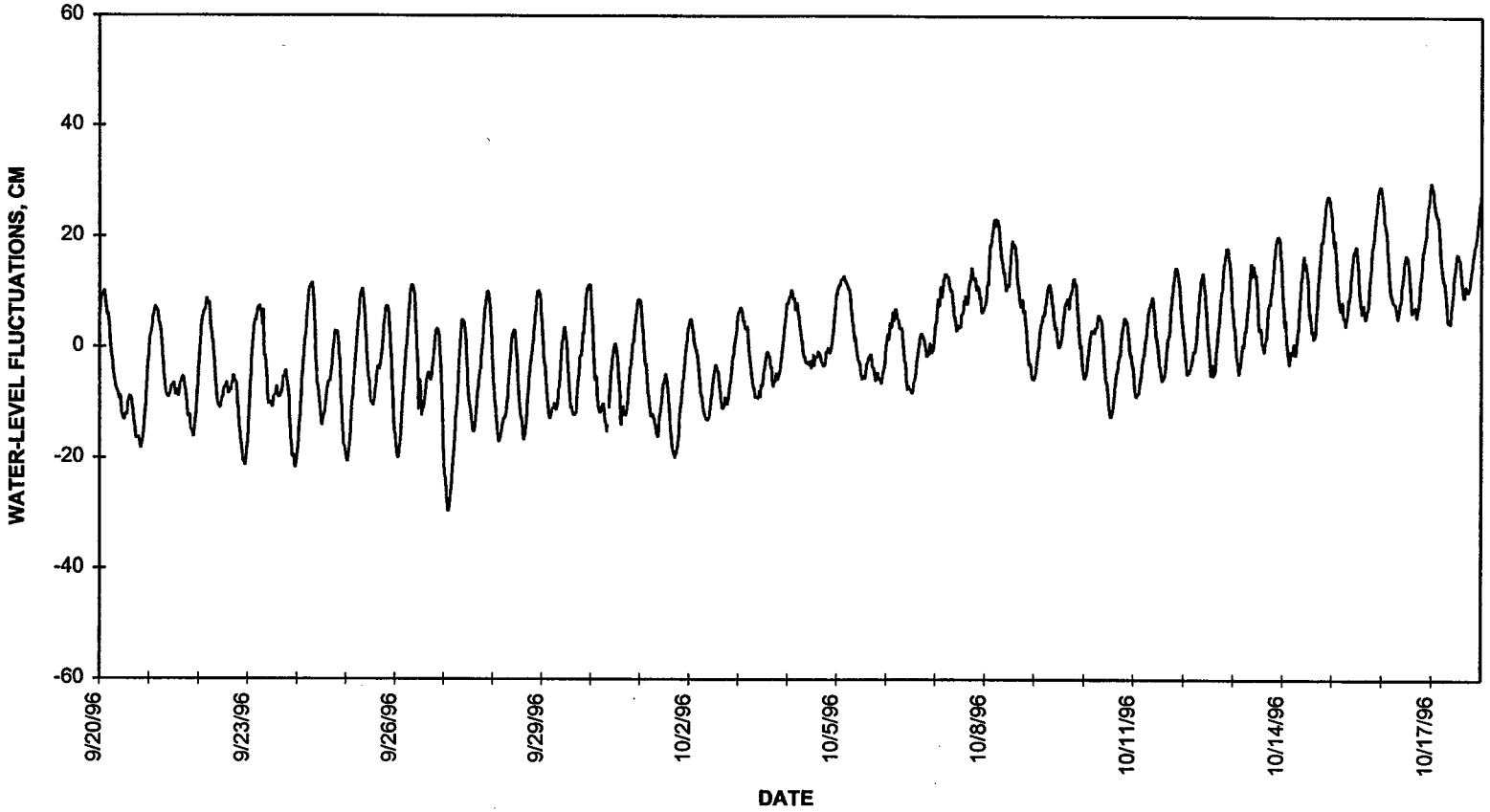

NOTE: 0 CM REPRESENTS ARBITRARY DATUM

WATER-LEVEL FLUCTUATIONS
TG04 - NICHOLS SEAFOOD - MM 62.9
9/20/96 - 10/18/96

Plate 65

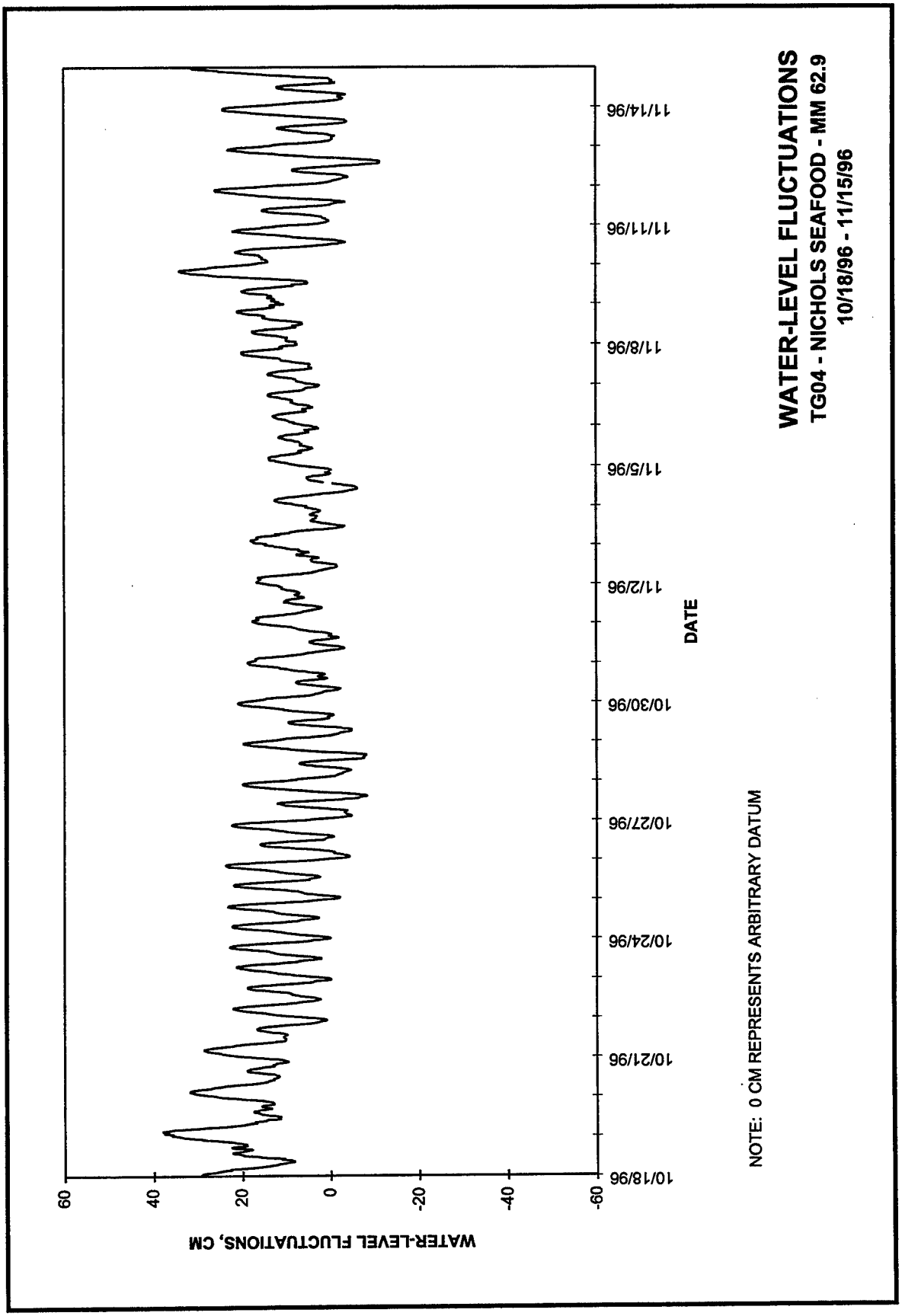
WATER-LEVEL FLUCTUATIONS
TG04 - NICHOLS SEAFOOD - MM 62.9
10/18/96 - 11/15/96
WATER-LEVEL FLUCTUATIONS, CM
60
40
20
0
-20
-40
-60
10/18/96
10/21/96
10/24/96
10/27/96
10/30/96
11/2/96
11/5/96
11/8/96
11/11/96
11/14/96
DATE
NOTE: 0 CM REPRESENTS ARBITRARY DATUM

Plate 66

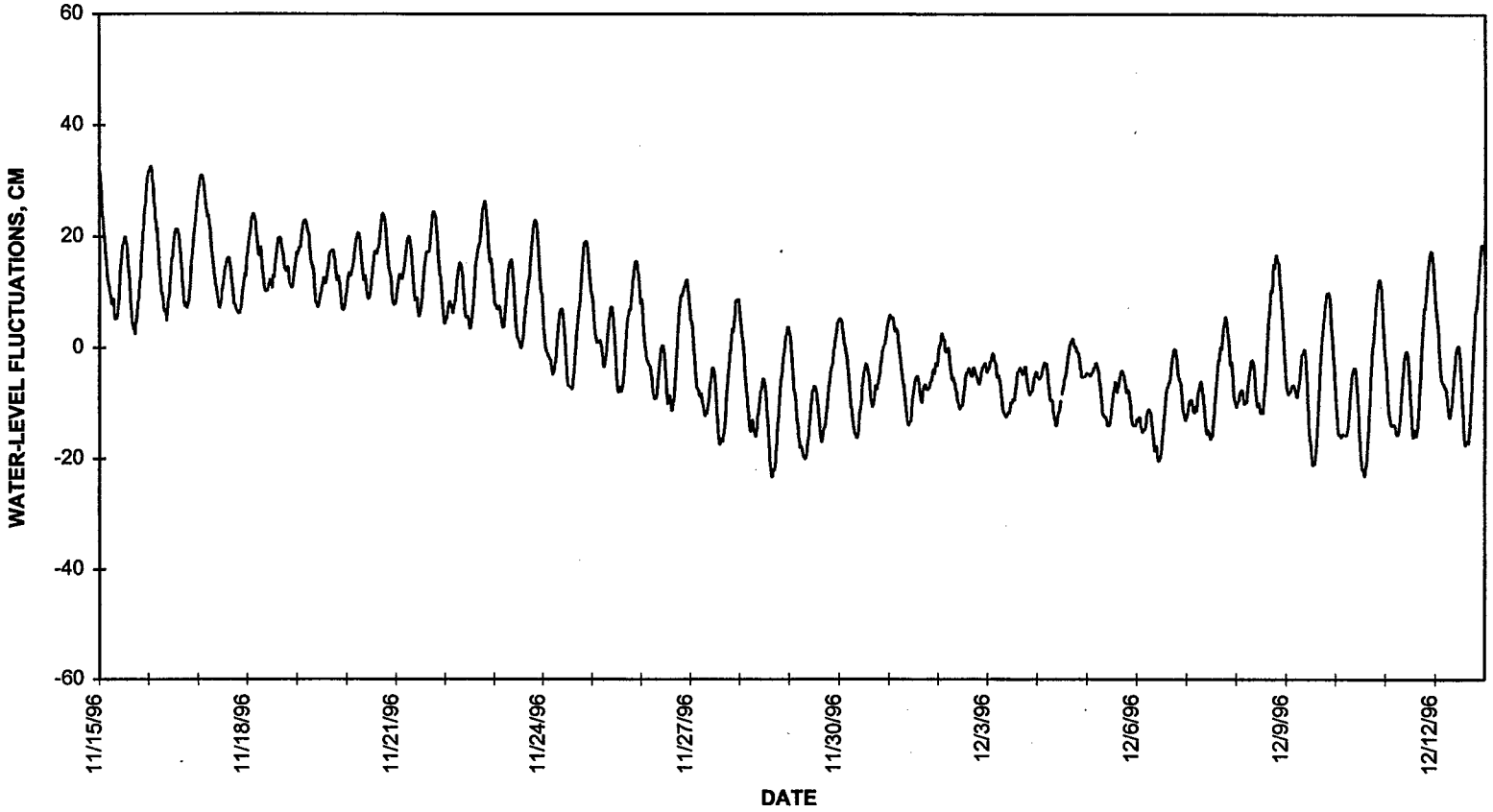

NOTE: 0 CM REPRESENTS ARBITRARY DATUM

WATER-LEVEL FLUCTUATIONS
TG04 - NICHOLS SEAFOOD - MM 62.9
11/15/96 - 12/13/96

Plate 67

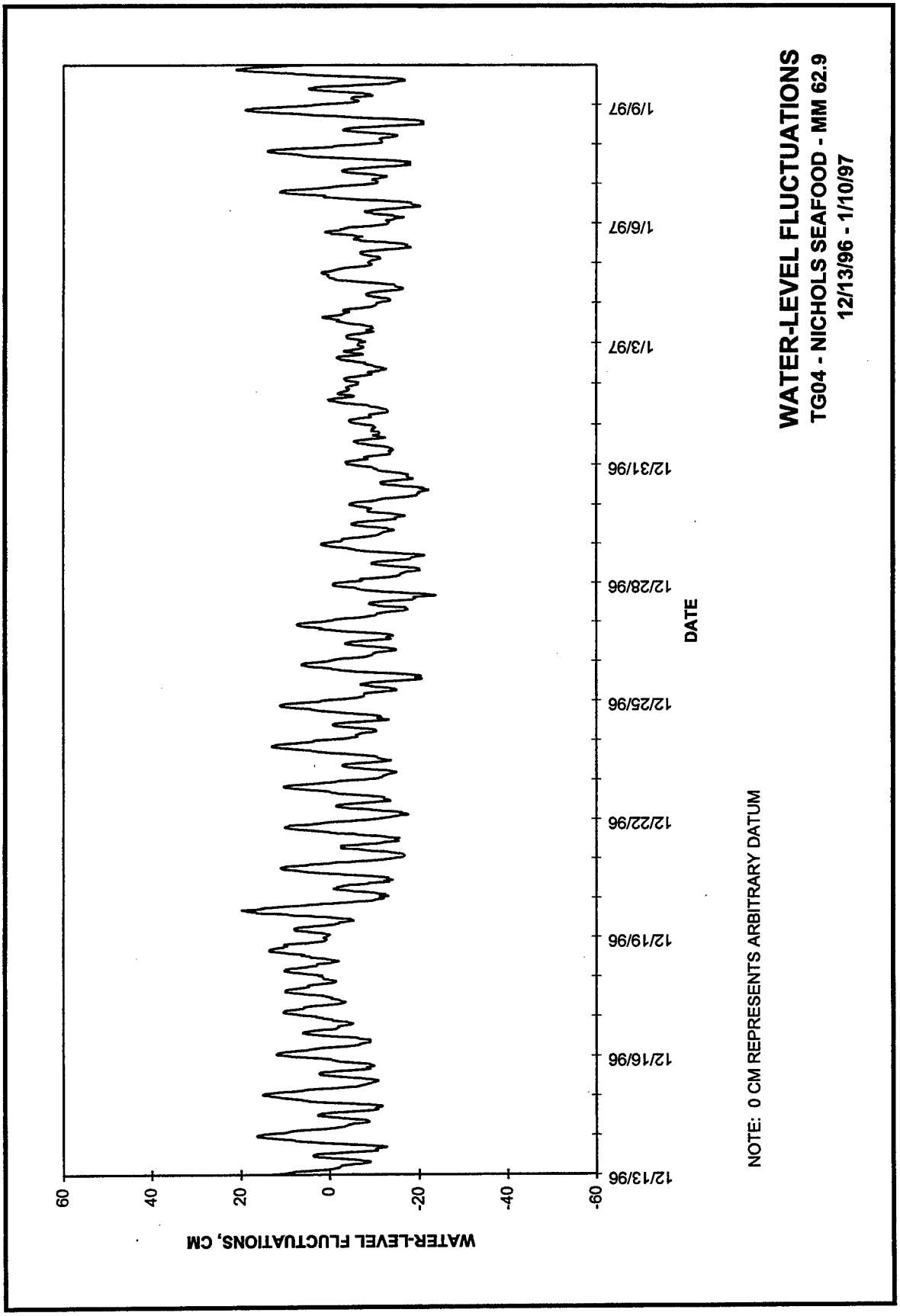
WATER-LEVEL FLUCTUATIONS
TG04 - NICHOLS SEAFOOD - MM 62.9
12/13/96 - 1/10/97
WATER-LEVEL FLUCTUATIONS, CM
60
40
20
0
-20
-40
-60
12/13/96
12/16/96
12/19/96
12/22/96
12/25/96
12/28/96
12/31/96
1/3/97
1/6/97
1/9/97
DATE
NOTE: 0 CM REPRESENTS ARBITRARY DATUM

Plate 68

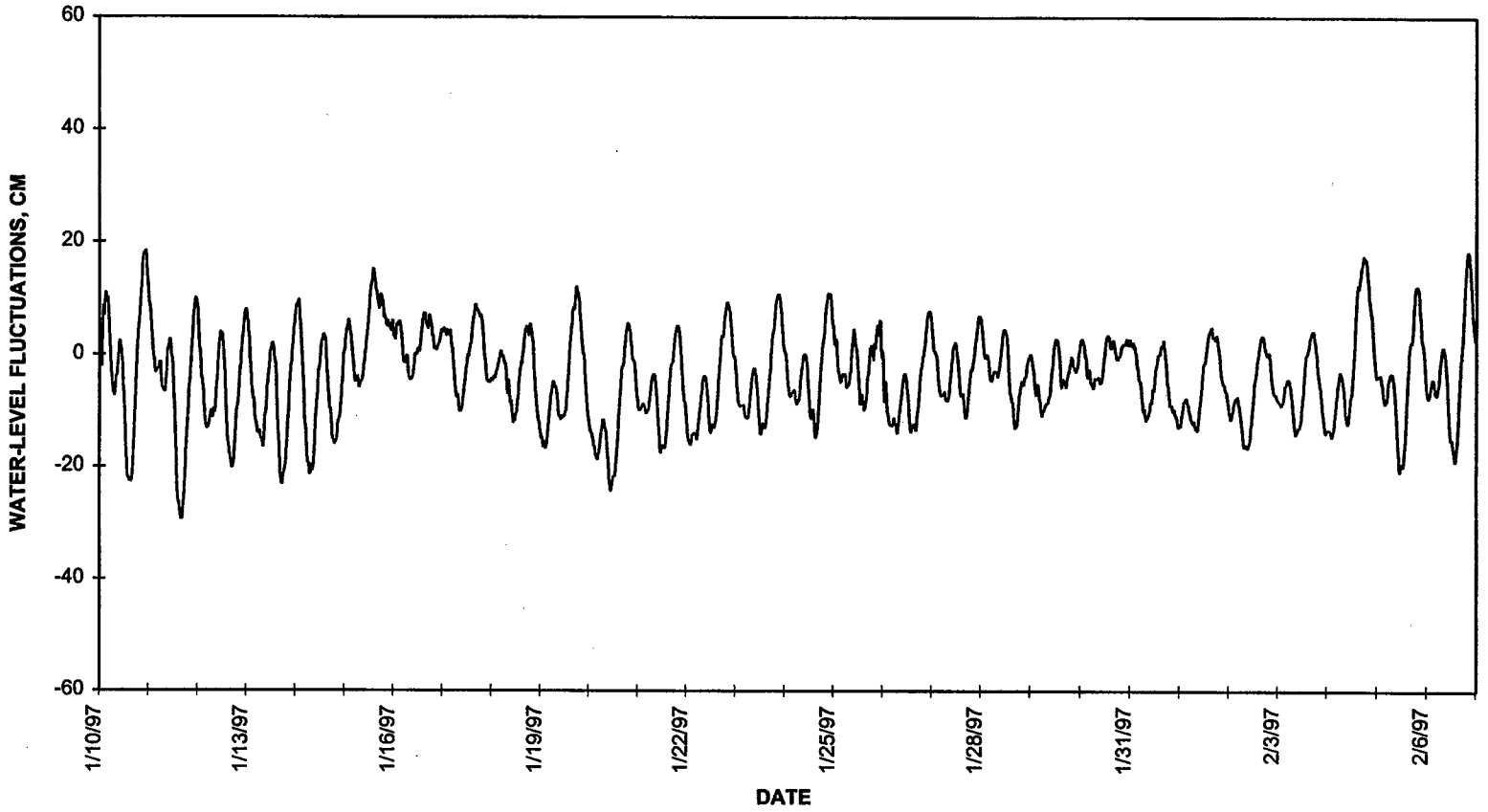

NOTE: 0 CM REPRESENTS ARBITRARY DATUM

WATER-LEVEL FLUCTUATIONS
TG04 - NICHOLS SEAFOOD - MM 62.9
1/10/97 - 2/7/97

Plate 69

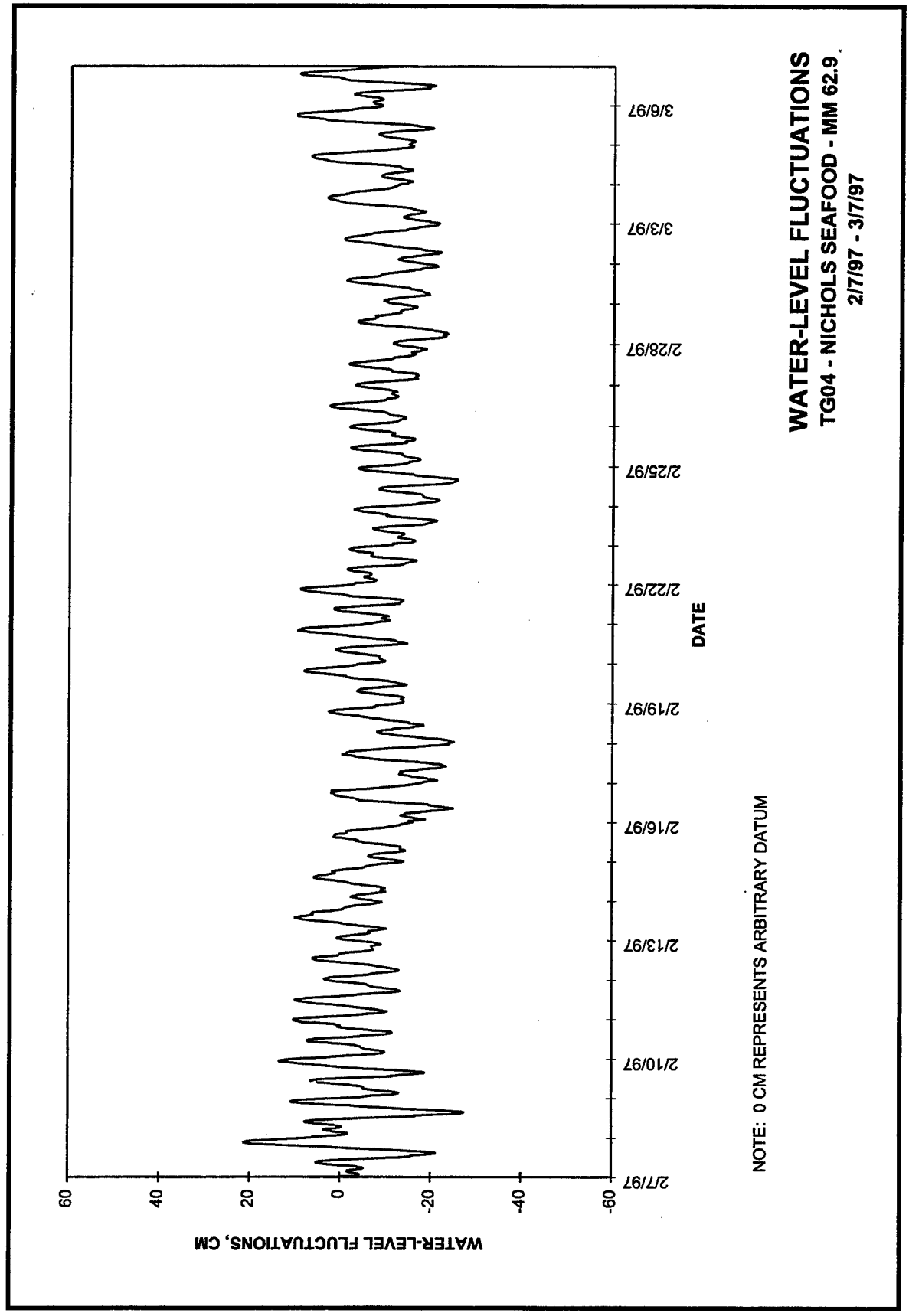
WATER-LEVEL FLUCTUATIONS
TG04 - NICHOLS SEAFOOD - MM 62.9
2/7/97 - 3/7/97
WATER-LEVEL FLUCTUATIONS, CM
60
40
20
0
-20
-40
-60
2/7/97
2/10/97
2/13/97
2/16/97
2/19/97
2/22/97
2/25/97
2/28/97
3/3/97
3/6/97
DATE
NOTE: 0 CM REPRESENTS ARBITRARY DATUM

Plate 70

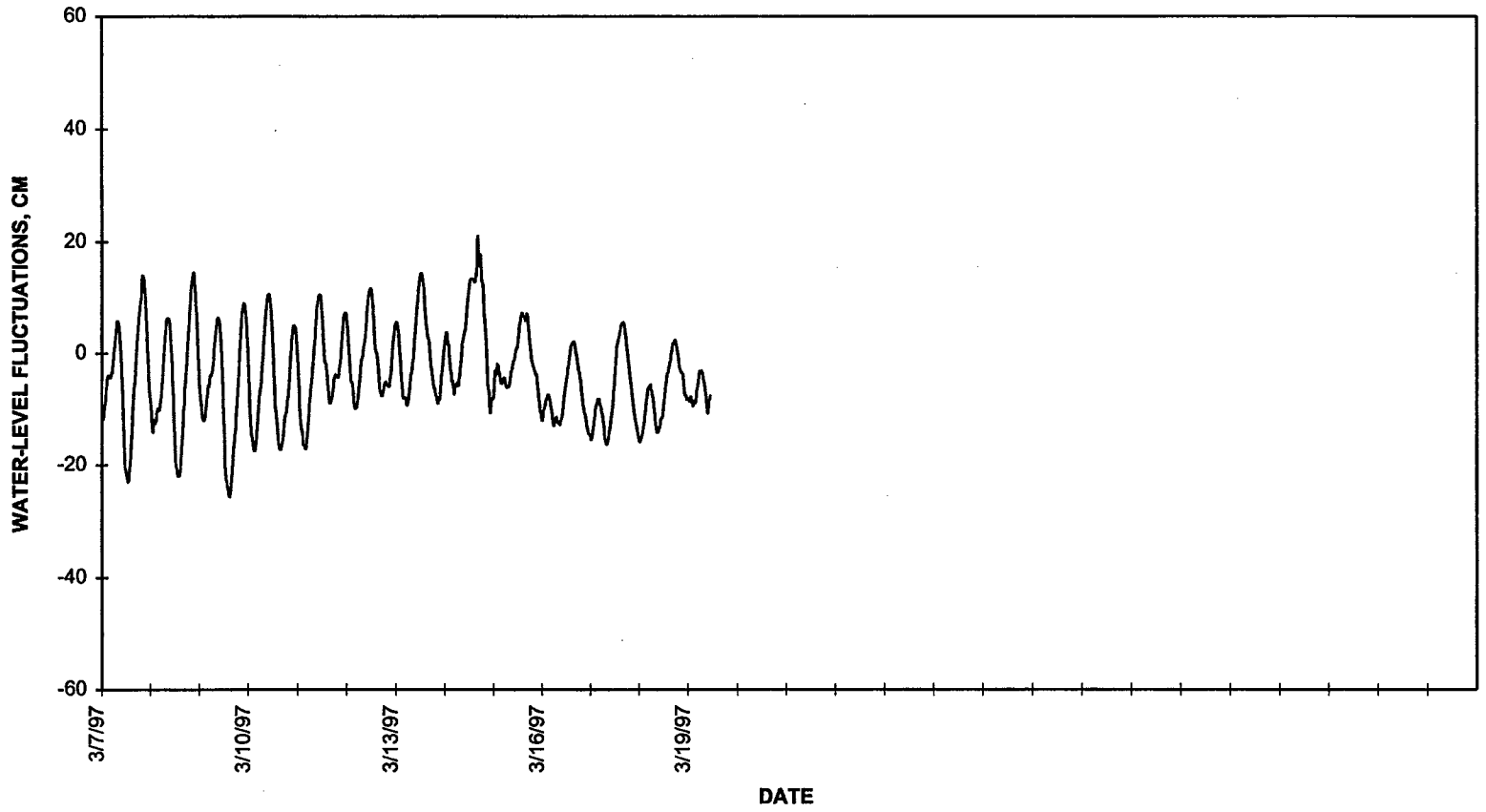

NOTE: 0 CM REPRESENTS ARBITRARY DATUM

WATER-LEVEL FLUCTUATIONS
TG04 - NICHOLS SEAFOOD - MM 62.9
3/7/97 - 3/19/97

Plate 71

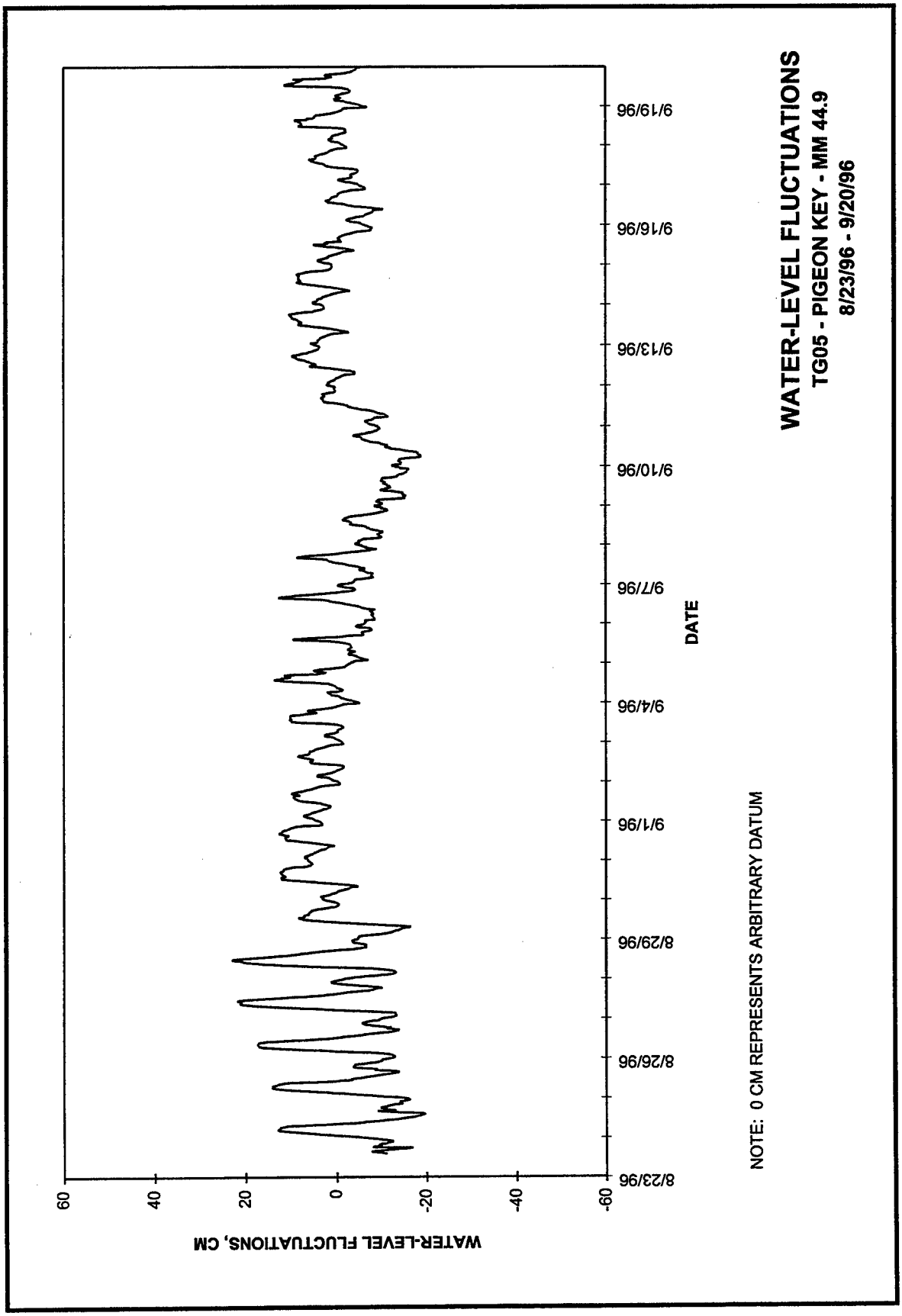
WATER-LEVEL FLUCTUATIONS
TG05 - PIGEON KEY - MM 44.9
8/23/96 - 9/20/96
WATER-LEVEL FLUCTUATIONS, CM
60
40
20
0
-20
-40
-60
8/23/96
8/26/96
8/29/96
9/1/96
9/4/96
9/7/96
9/10/96
9/13/96
9/16/96
9/19/96
DATE
NOTE: 0 CM REPRESENTS ARBITRARY DATUM

Plate 72

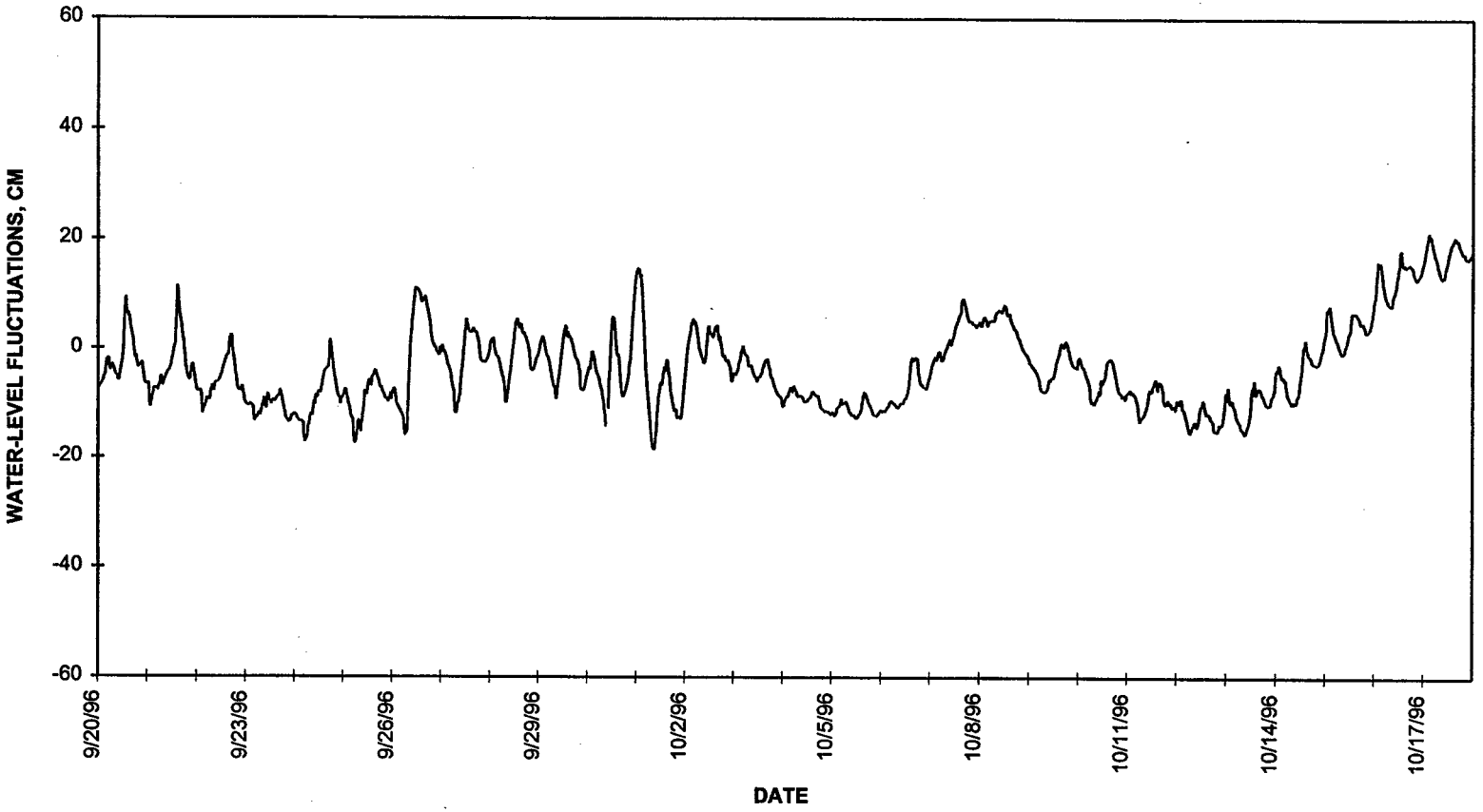

NOTE: 0 CM REPRESENTS ARBITRARY DATUM

WATER-LEVEL FLUCTUATIONS
TG05 - PIGEON KEY - MM 44.9
9/20/96 - 10/18/96

Plate 73

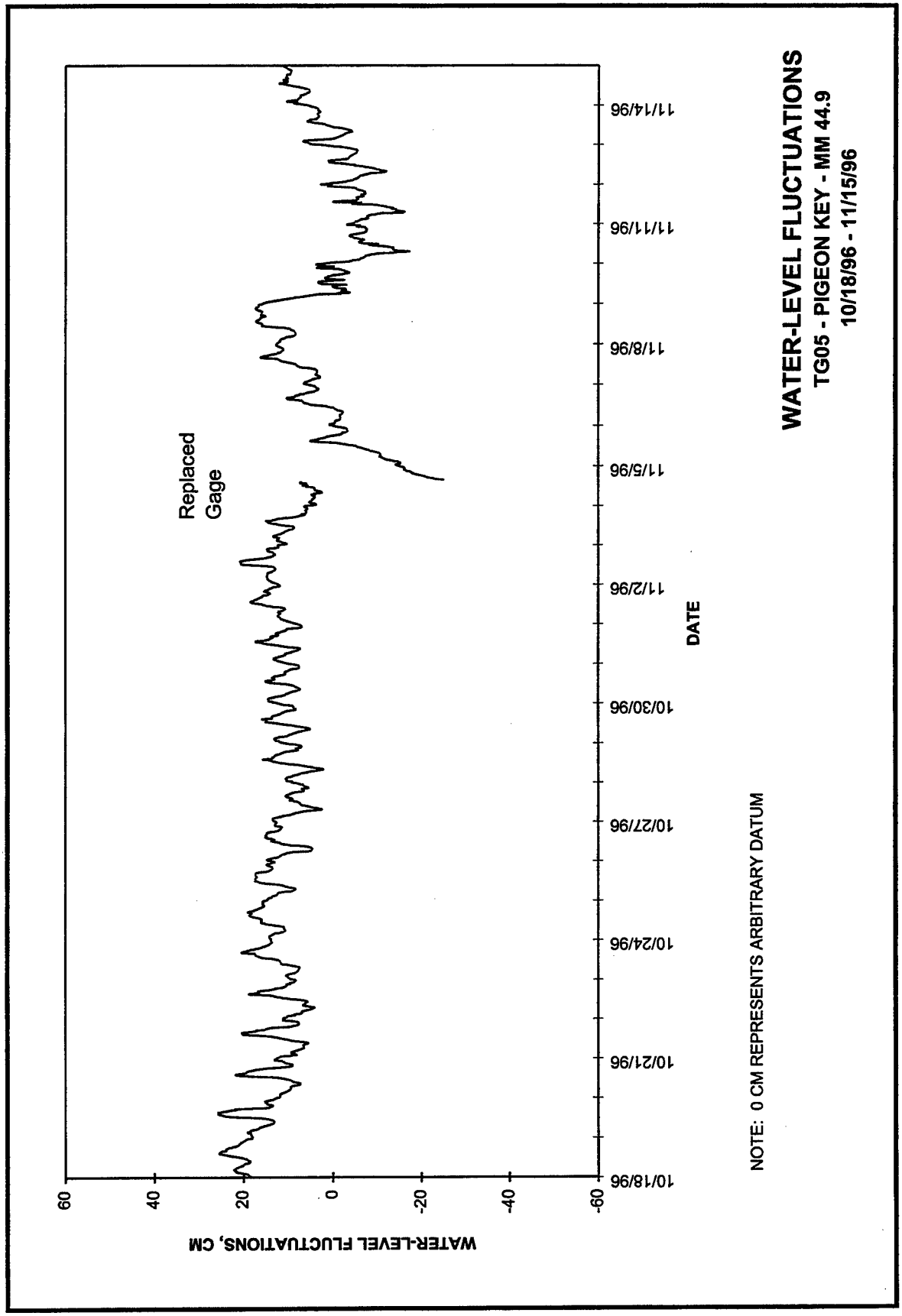
WATER-LEVEL FLUCTUATIONS
TG05 - PIGEON KEY - MM 44.9
10/18/96 - 11/15/96
Replaced
Gage
WATER-LEVEL FLUCTUATIONS, CM
60
40
20
0
-20
-40
-60
10/18/96
10/21/96
10/24/96
10/27/96
10/30/96
11/2/96
11/5/96
11/8/96
11/11/96
11/14/96
DATE
NOTE: 0 CM REPRESENTS ARBITRARY DATUM

Plate 74

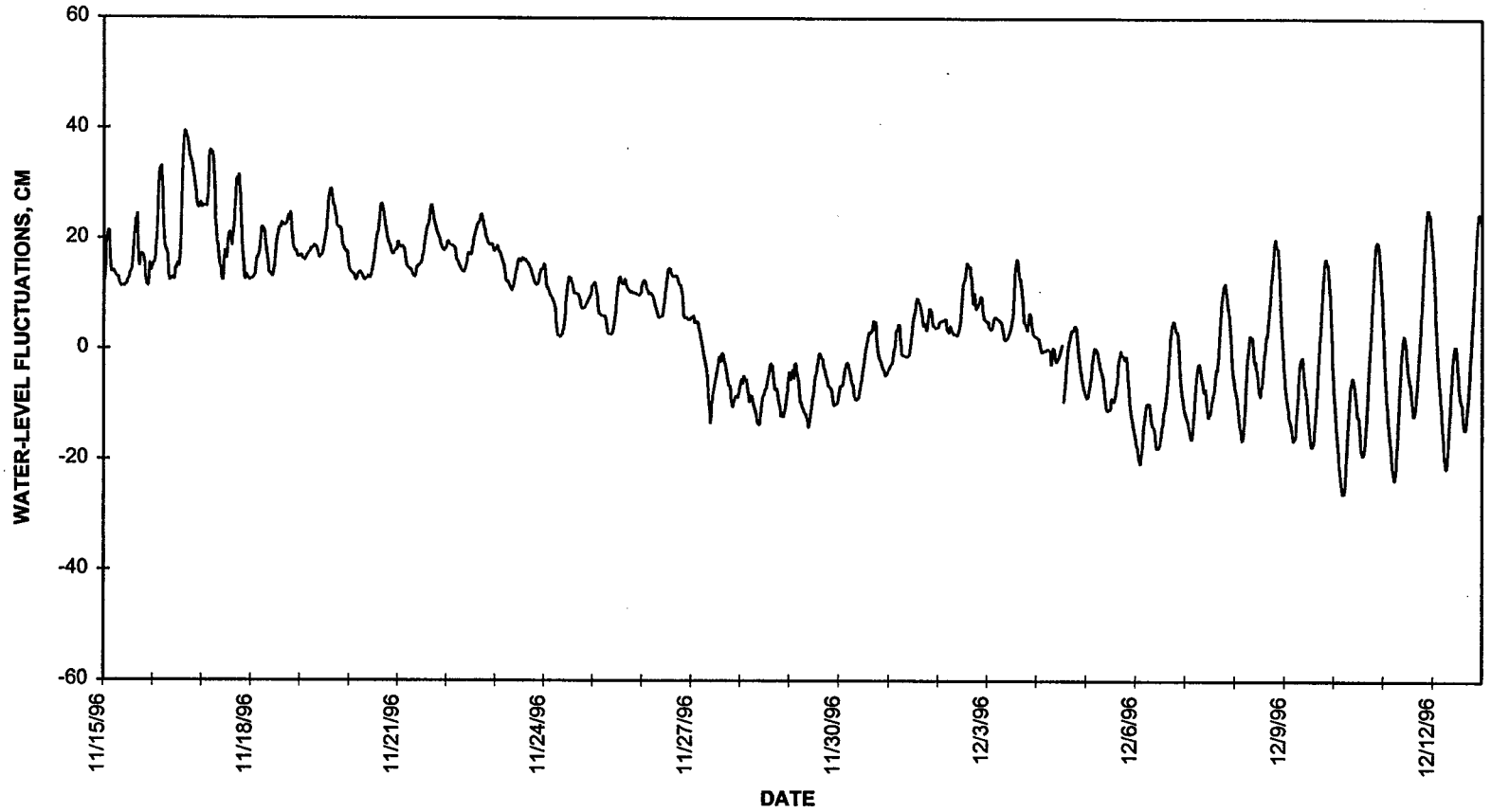

NOTE: 0 CM REPRESENTS ARBITRARY DATUM

WATER-LEVEL FLUCTUATIONS
TG05 - PIGEON KEY - MM 44.9
11/15/96 - 12/13/96

Plate 75

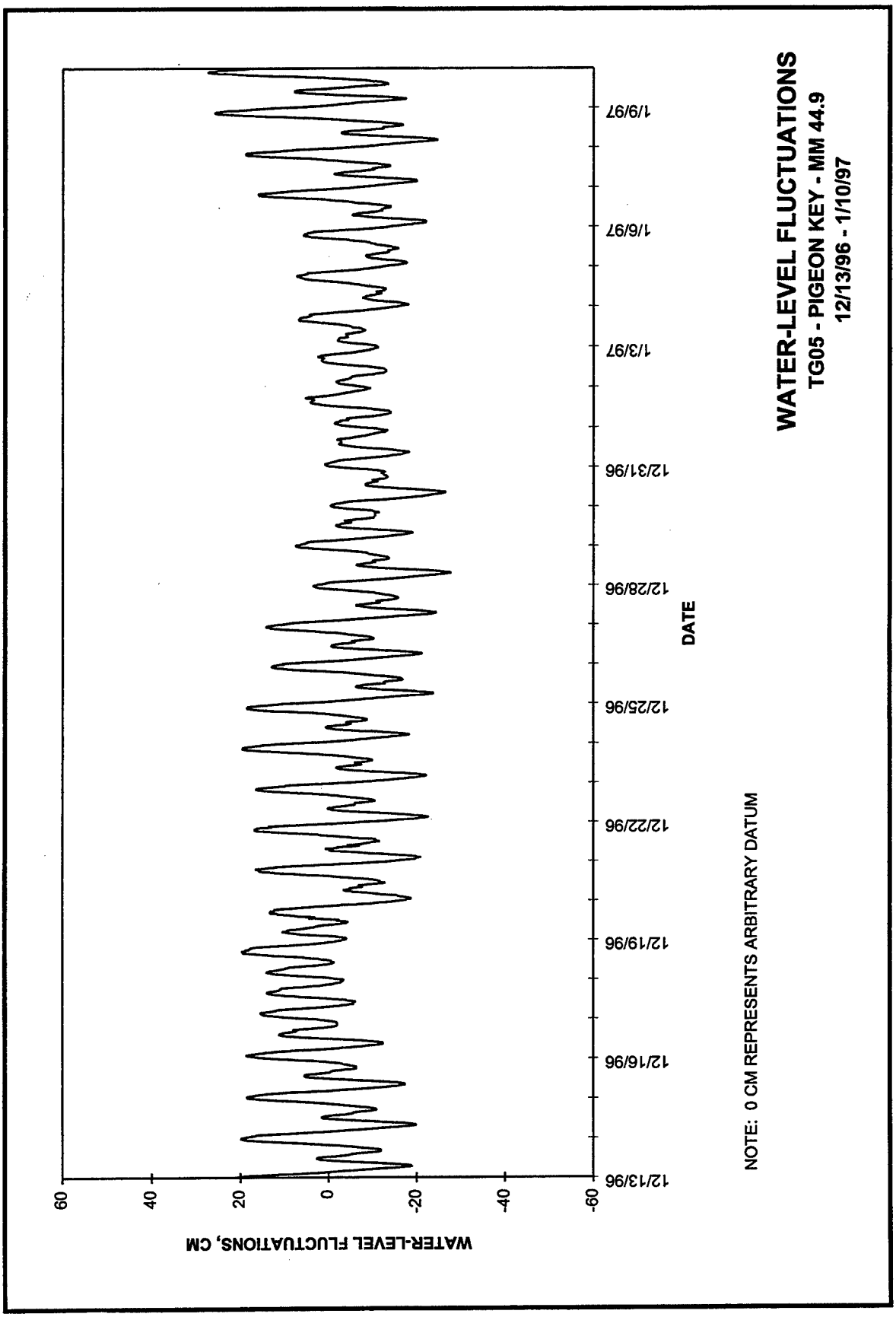
WATER-LEVEL FLUCTUATIONS
TG05 - PIGEON KEY - MM 44.9
12/13/96 - 1/10/97
WATER-LEVEL FLUCTUATIONS, CM
60
40
20
0
-20
-40
-60
12/13/96
12/16/96
12/19/96
12/22/96
12/25/96
12/28/96
12/31/96
1/3/97
1/6/97
1/9/97
DATE
NOTE: 0 CM REPRESENTS ARBITRARY DATUM

Plate 76

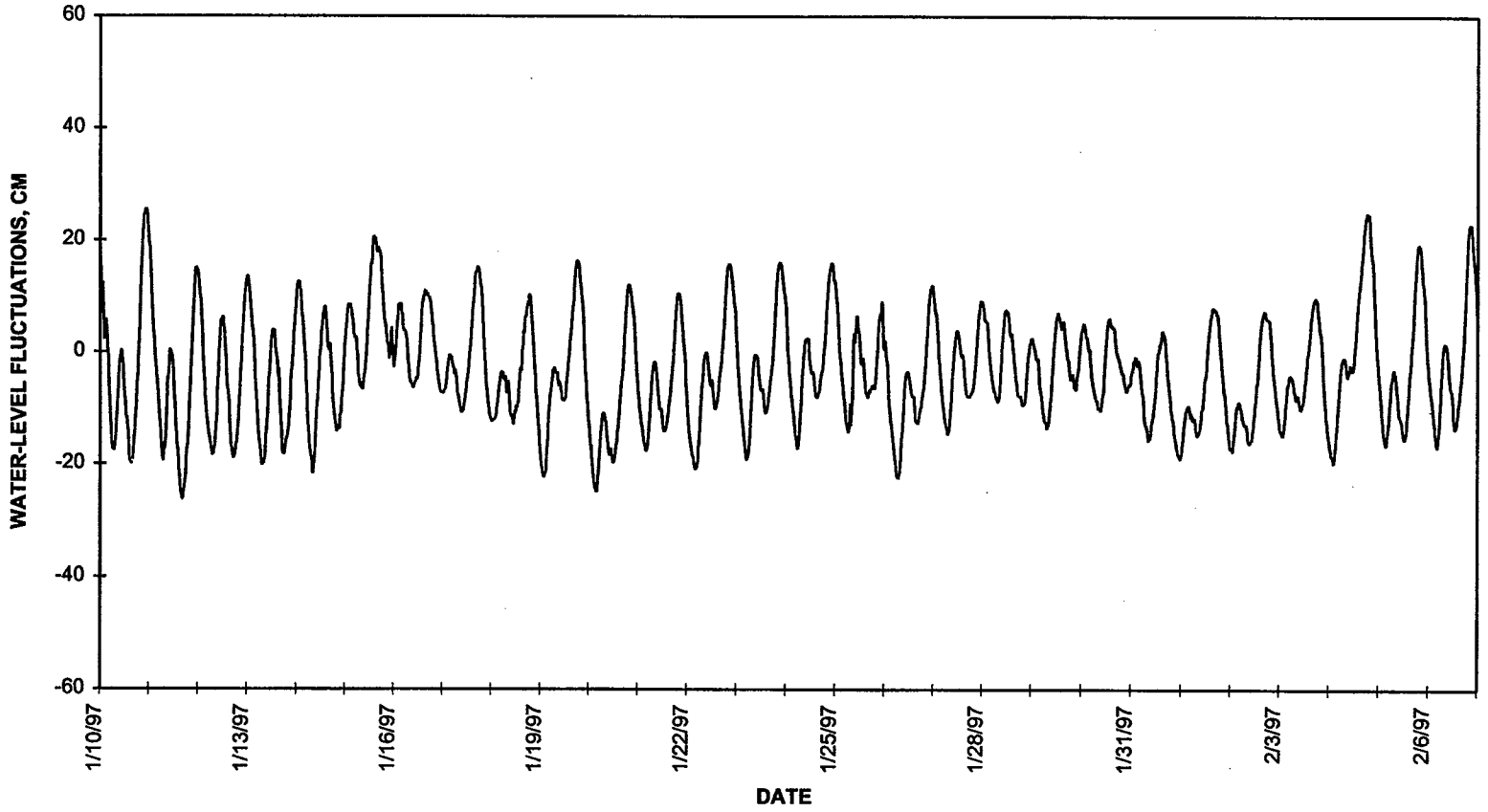

NOTE: 0 CM REPRESENTS ARBITRARY DATUM

WATER-LEVEL FLUCTUATIONS
TG05 - PIGEON KEY - MM 44.9
1/10/97 - 2/7/97

Plate 77

Plate 78

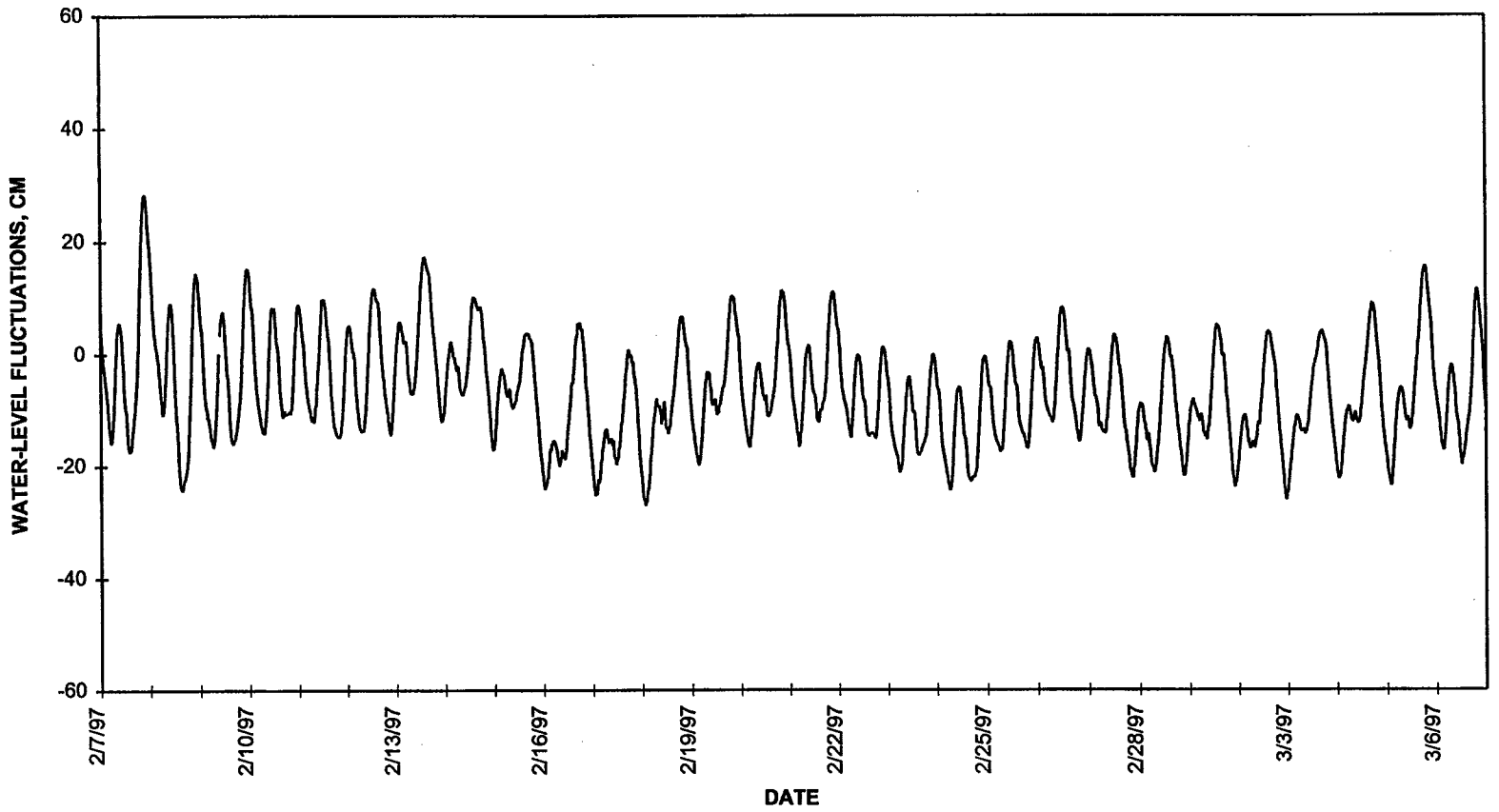

NOTE: 0 CM REPRESENTS ARBITRARY DATUM

WATER-LEVEL FLUCTUATIONS
TG05 - PIGEON KEY- MM 44.9
2/7/97 - 3/7/97

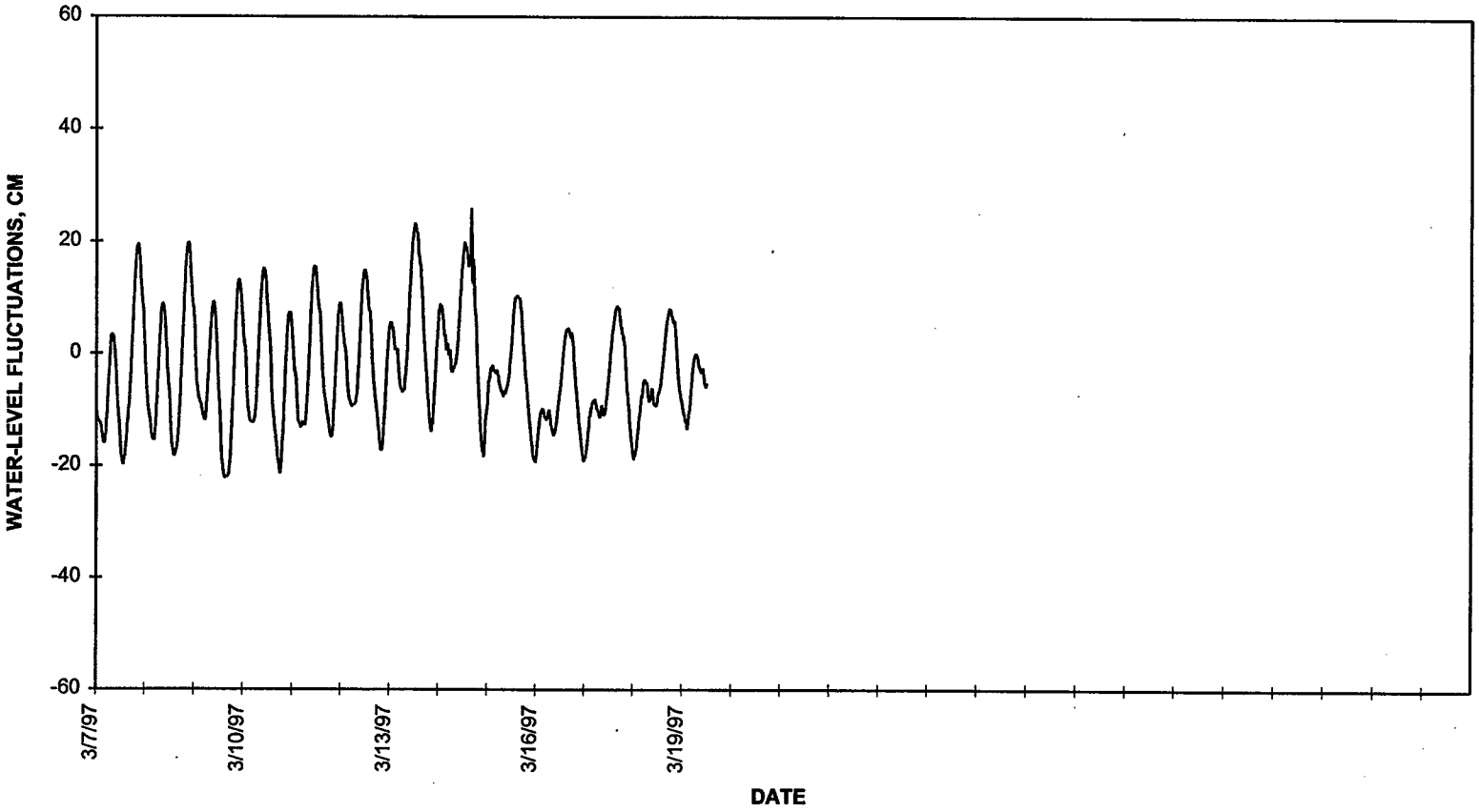

NOTE: 0 CM REPRESENTS ARBITRARY DATUM

WATER-LEVEL FLUCTUATIONS
TG05 - PIGEON KEY - MM 44.9
3/7/97 - 3/19/97

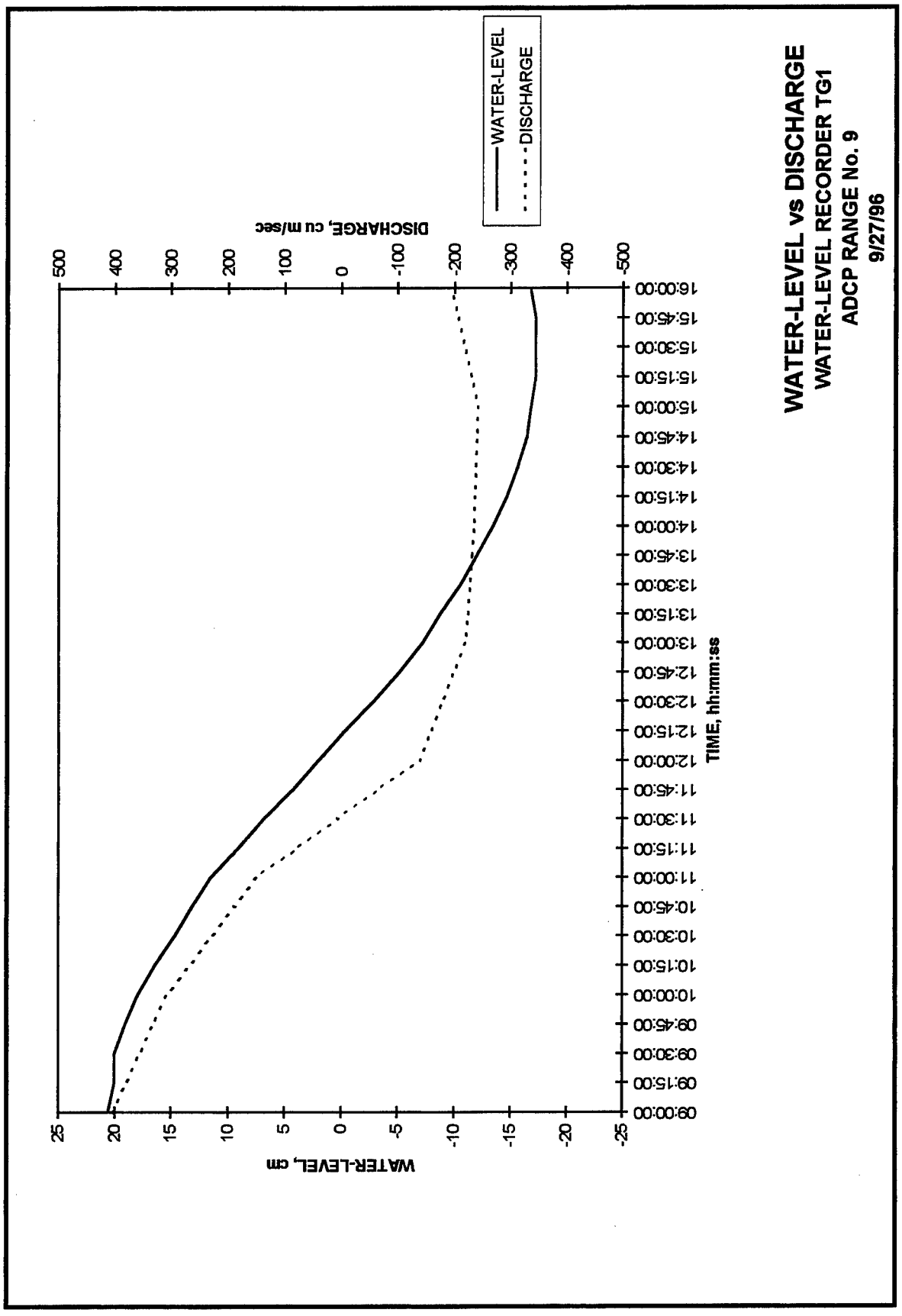
WATER-LEVEL vs DISCHARGE
WATER-LEVEL RECORDER TG1
ADCP RANGE No. 9
9/27/96
WATER-LEVEL
DISCHARGE
WATER-LEVEL, cm
DISCHARGE, cu m/sec
TIME, hh:mm:ss
25
20
15
10
5
0
-5
-10
-15
-20
-25
500
400
300
200
100
0
-100
-200
-300
-400
-500
09:00:00
09:15:00
09:30:00
09:45:00
10:00:00
10:15:00
10:30:00
10:45:00
11:00:00
11:15:00
11:30:00
11:45:00
12:00:00
12:15:00
12:30:00
12:45:00
13:00:00
13:15:00
13:30:00
13:45:00
14:00:00
14:15:00
14:30:00
14:45:00
15:00:00
15:15:00
15:30:00
15:45:00
16:00:00

Plate 80

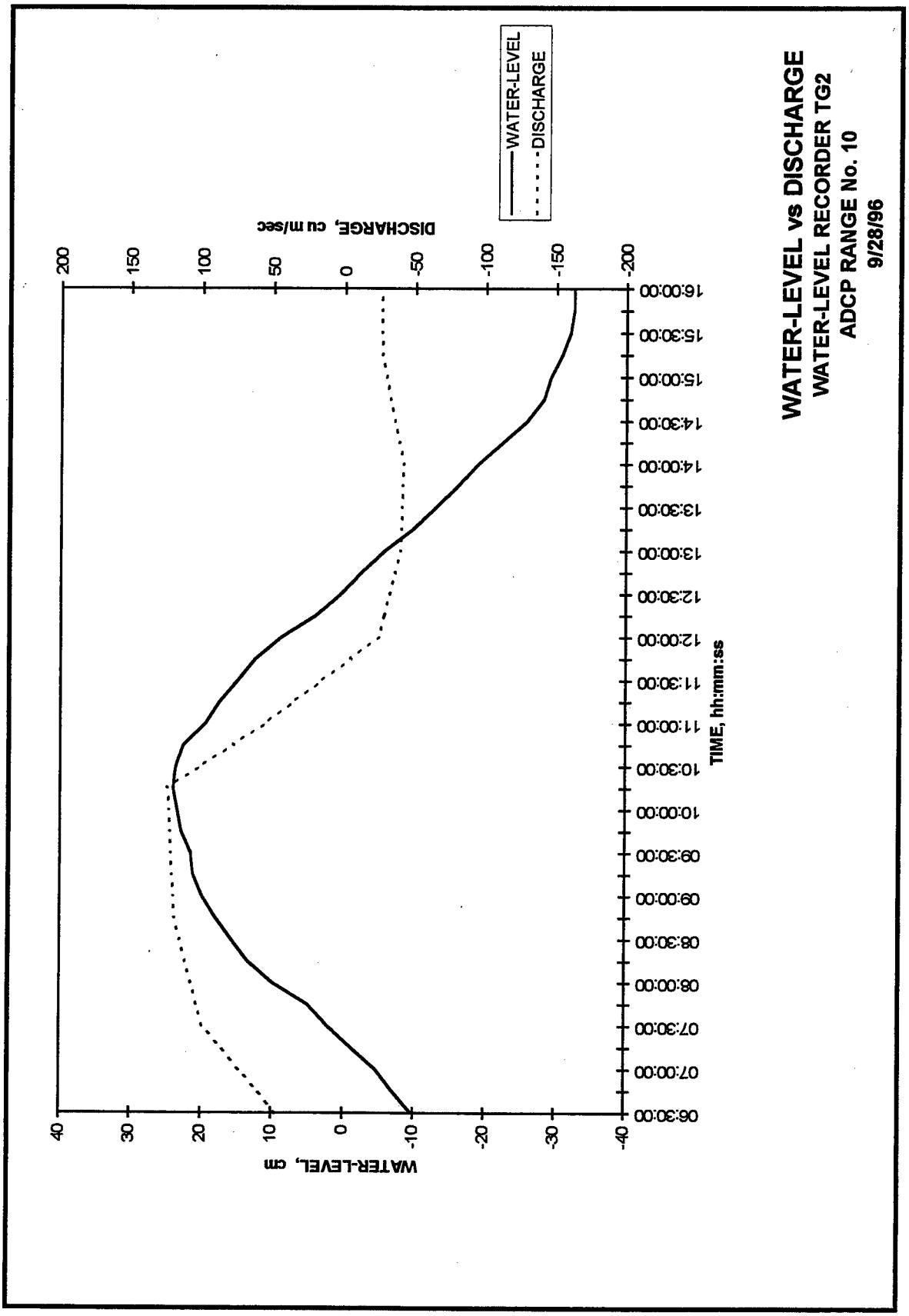
WATER-LEVEL vs DISCHARGE
WATER-LEVEL RECORDER TG2
ADCP RANGE No. 10
9/28/96
WATER-LEVEL
DISCHARGE
WATER-LEVEL, cm
DISCHARGE, cu m/sec
TIME, hh:mm:ss
40
30
20
10
0
-10
-20
-30
-40
200
150
100
50
0
-50
-100
-150
-200
06:30:00
07:00:00
07:30:00
08:00:00
08:30:00
09:00:00
09:30:00
10:00:00
10:30:00
11:00:00
11:30:00
12:00:00
12:30:00
13:00:00
13:30:00
14:00:00
14:30:00
15:00:00
15:30:00
16:00:00

Plate 81

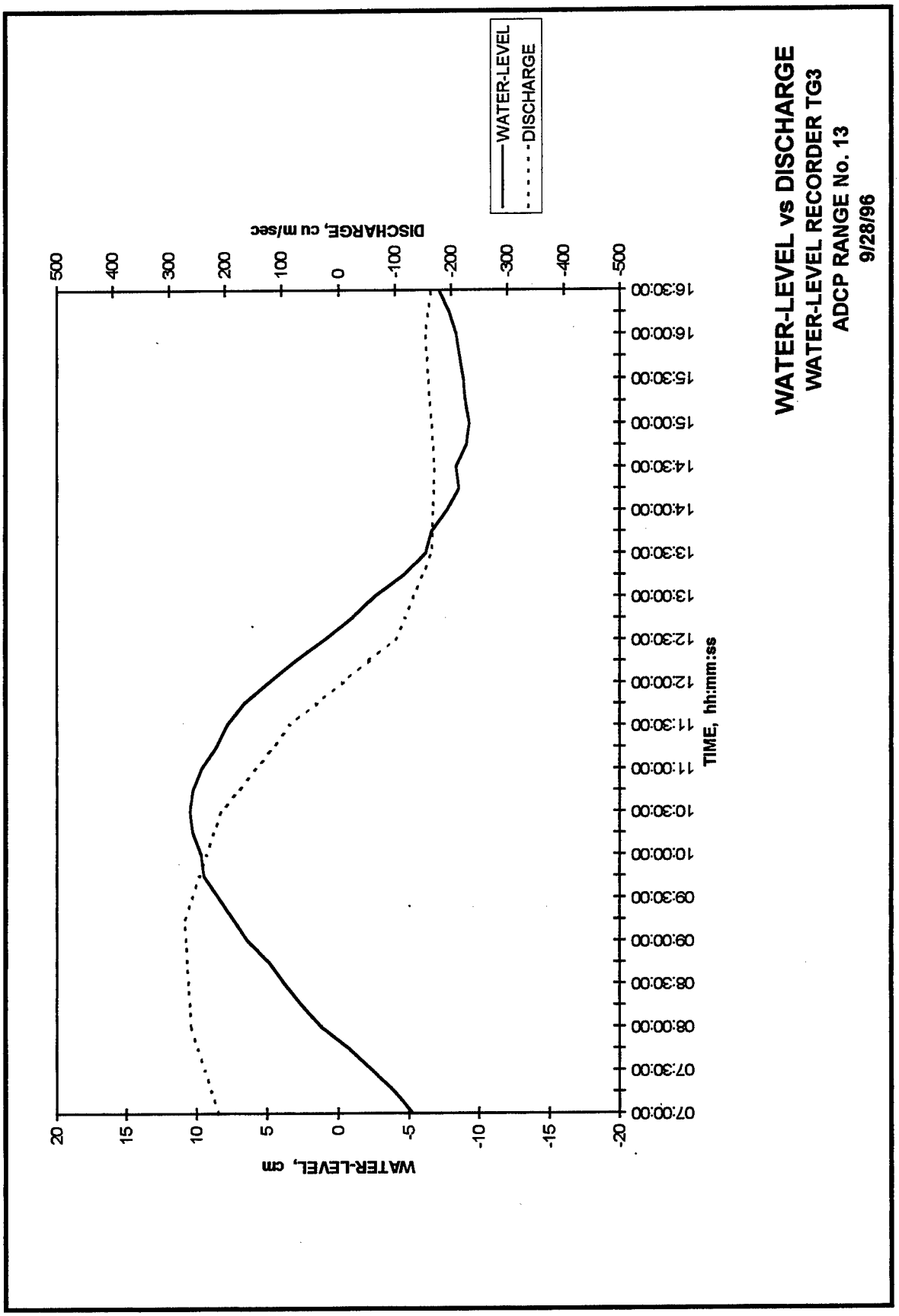
WATER-LEVEL vs DISCHARGE
WATER-LEVEL RECORDER TG3
ADCP RANGE No. 13
9/28/96
WATER-LEVEL
DISCHARGE
WATER-LEVEL, cm
DISCHARGE, cu m/sec
TIME, hh:mm:ss
20
15
10
5
0
-5
-10
-15
-20
500
400
300
200
100
0
-100
-200
-300
-400
-500
07:00:00
07:30:00
08:00:00
08:30:00
09:00:00
09:30:00
10:00:00
10:30:00
11:00:00
11:30:00
12:00:00
12:30:00
13:00:00
13:30:00
14:00:00
14:30:00
15:00:00
15:30:00
16:00:00
16:30:00

Plate 82

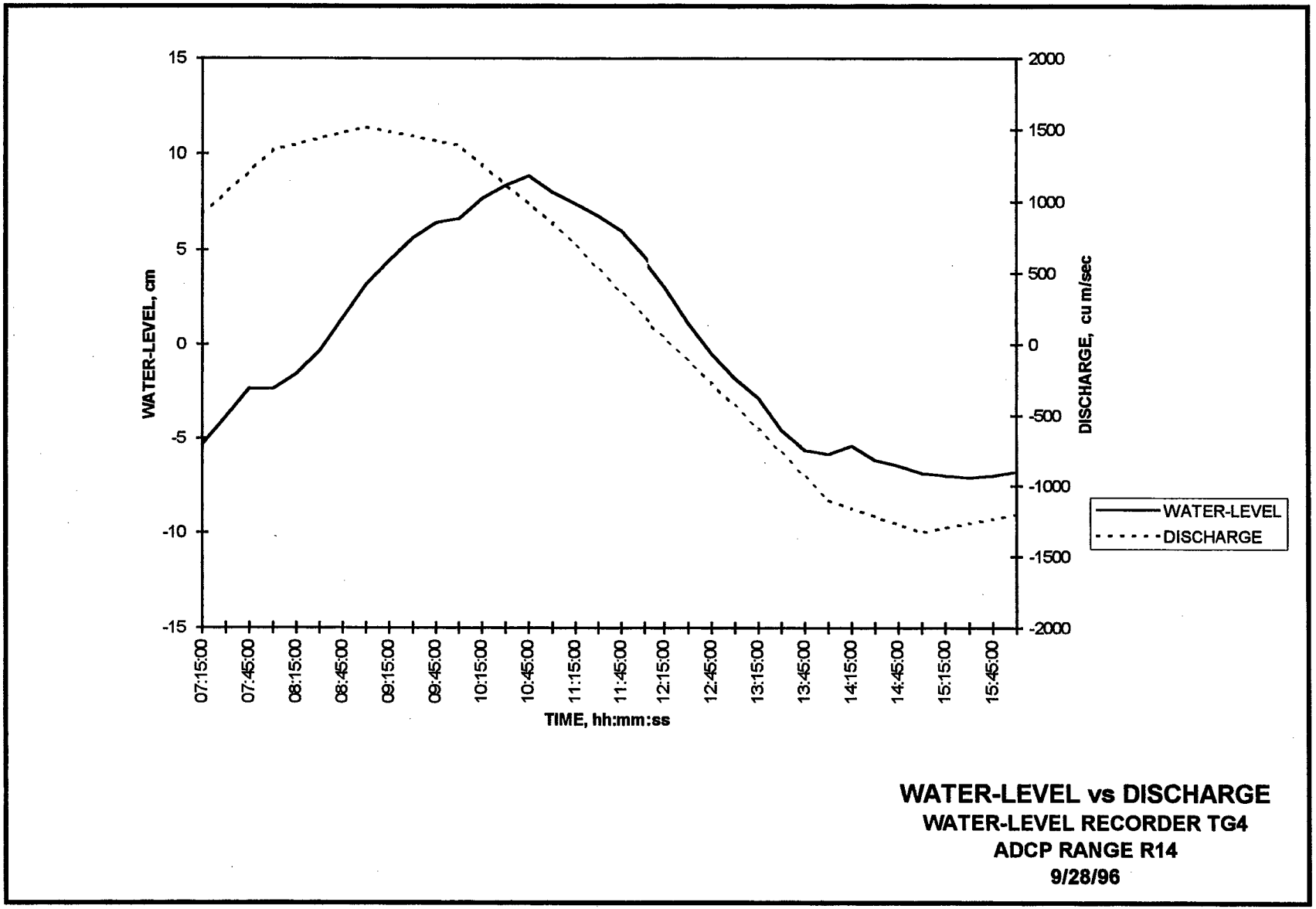

WATER-LEVEL vs DISCHARGE
WATER-LEVEL RECORDER TG4
ADCP RANGE R14
9/28/96

Plate 83

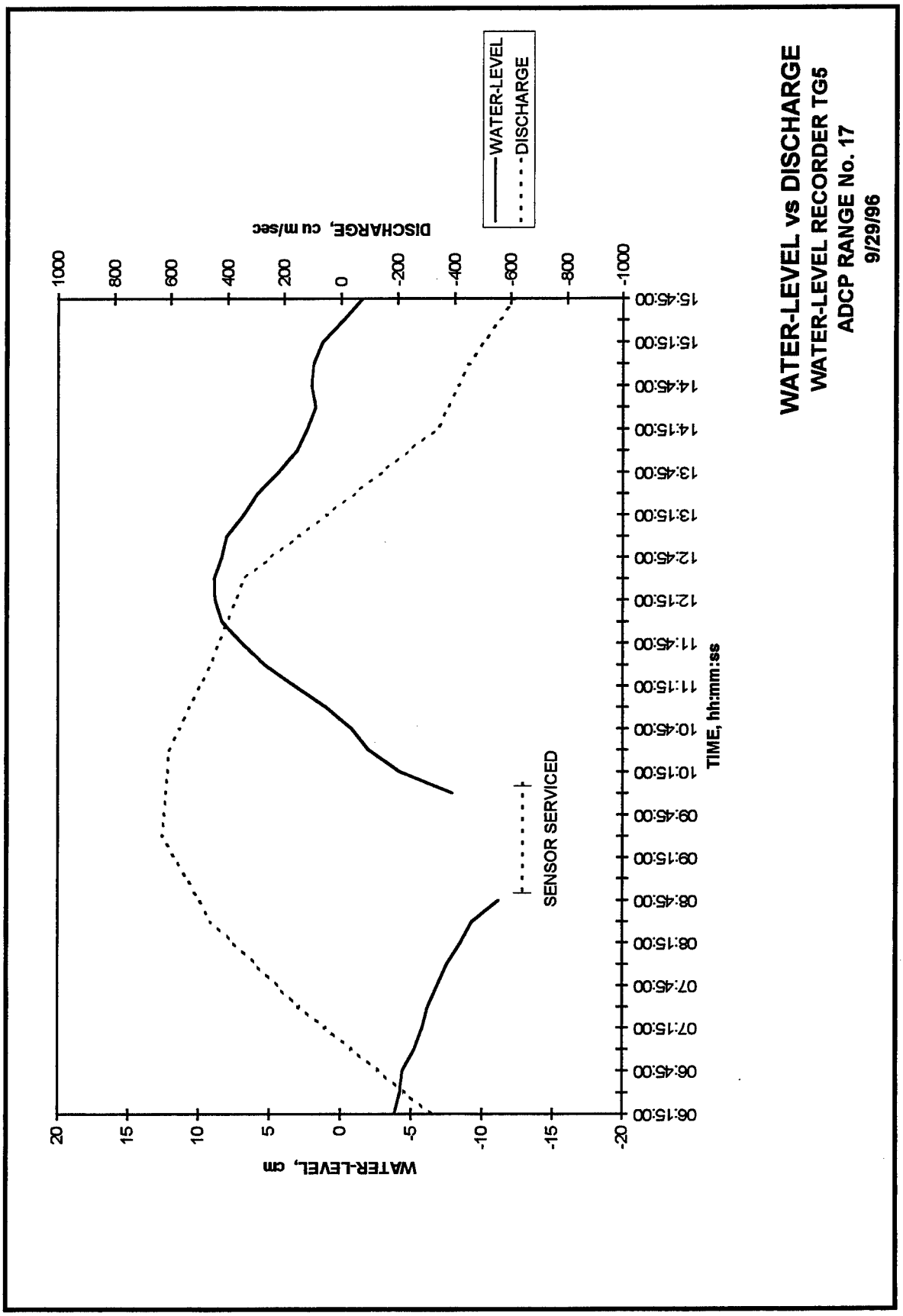
WATER-LEVEL vs DISCHARGE
WATER-LEVEL RECORDER TG5
ADCP RANGE No. 17
9/29/96
WATER-LEVEL
DISCHARGE
DISCHARGE, cu m/sec
1000
800
600
400
200
0
-200
-400
-600
-800
-1000
WATER-LEVEL, cm
20
15
10
5
0
-5
-10
-15
-20
SENSOR SERVICED
TIME, hh:mm:ss
06:15:00
06:45:00
07:15:00
07:45:00
08:15:00
08:45:00
09:15:00
09:45:00
10:15:00
10:45:00
11:15:00
11:45:00
12:15:00
12:45:00
13:15:00
13:45:00
14:15:00
14:45:00
15:15:00
15:45:00

Plate 84

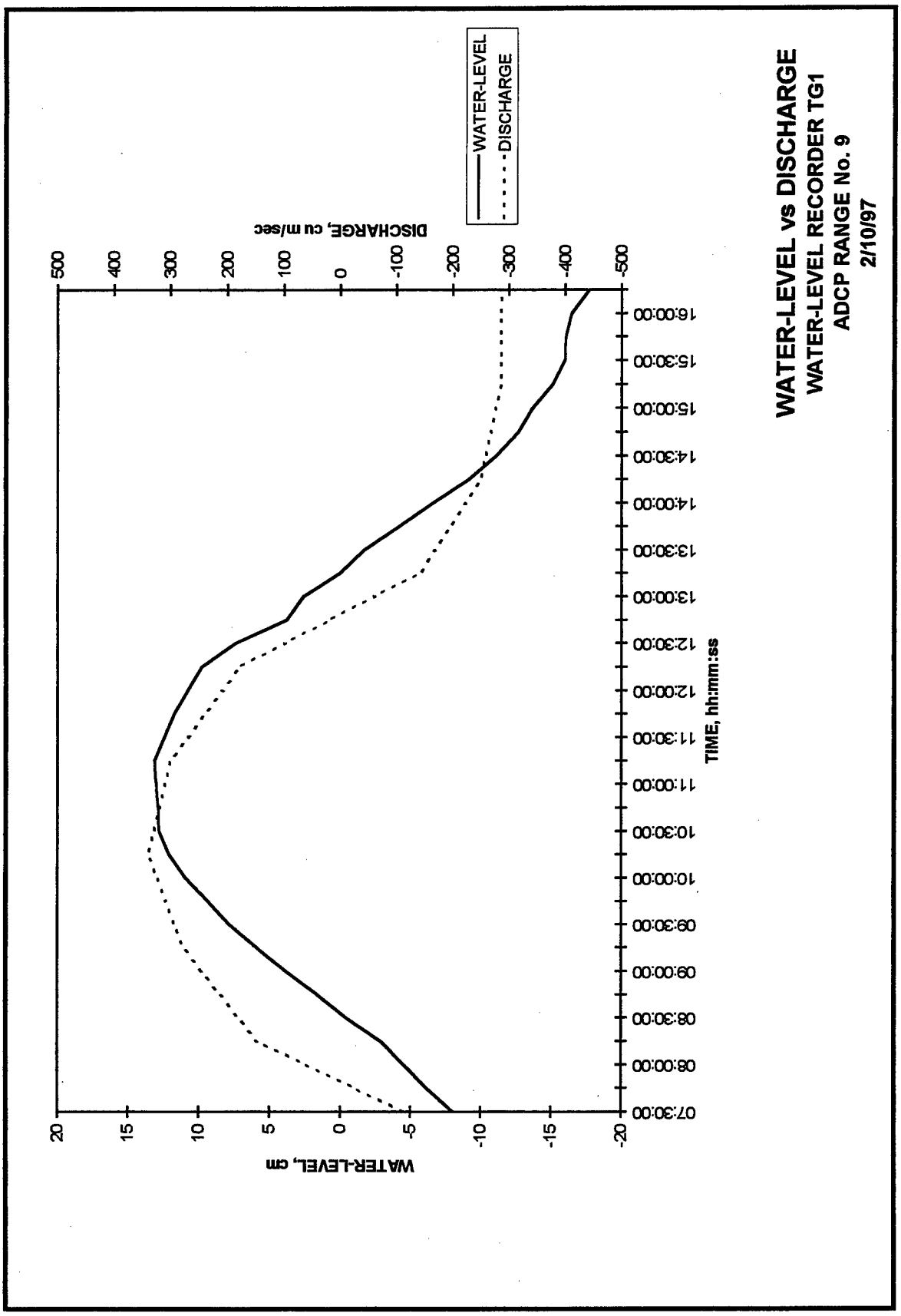
WATER-LEVEL vs DISCHARGE
WATER-LEVEL RECORDER TG1
ADCP RANGE No. 9
2/10/97
WATER-LEVEL
DISCHARGE
WATER-LEVEL, cm
DISCHARGE, cu m/sec
TIME, hh:mm:ss
20
15
10
5
0
-5
-10
-15
-20
500
400
300
200
100
0
-100
-200
-300
-400
-500
07:30:00
08:00:00
08:30:00
09:00:00
09:30:00
10:00:00
10:30:00
11:00:00
11:30:00
12:00:00
12:30:00
13:00:00
13:30:00
14:00:00
14:30:00
15:00:00
15:30:00
16:00:00

Plate 85

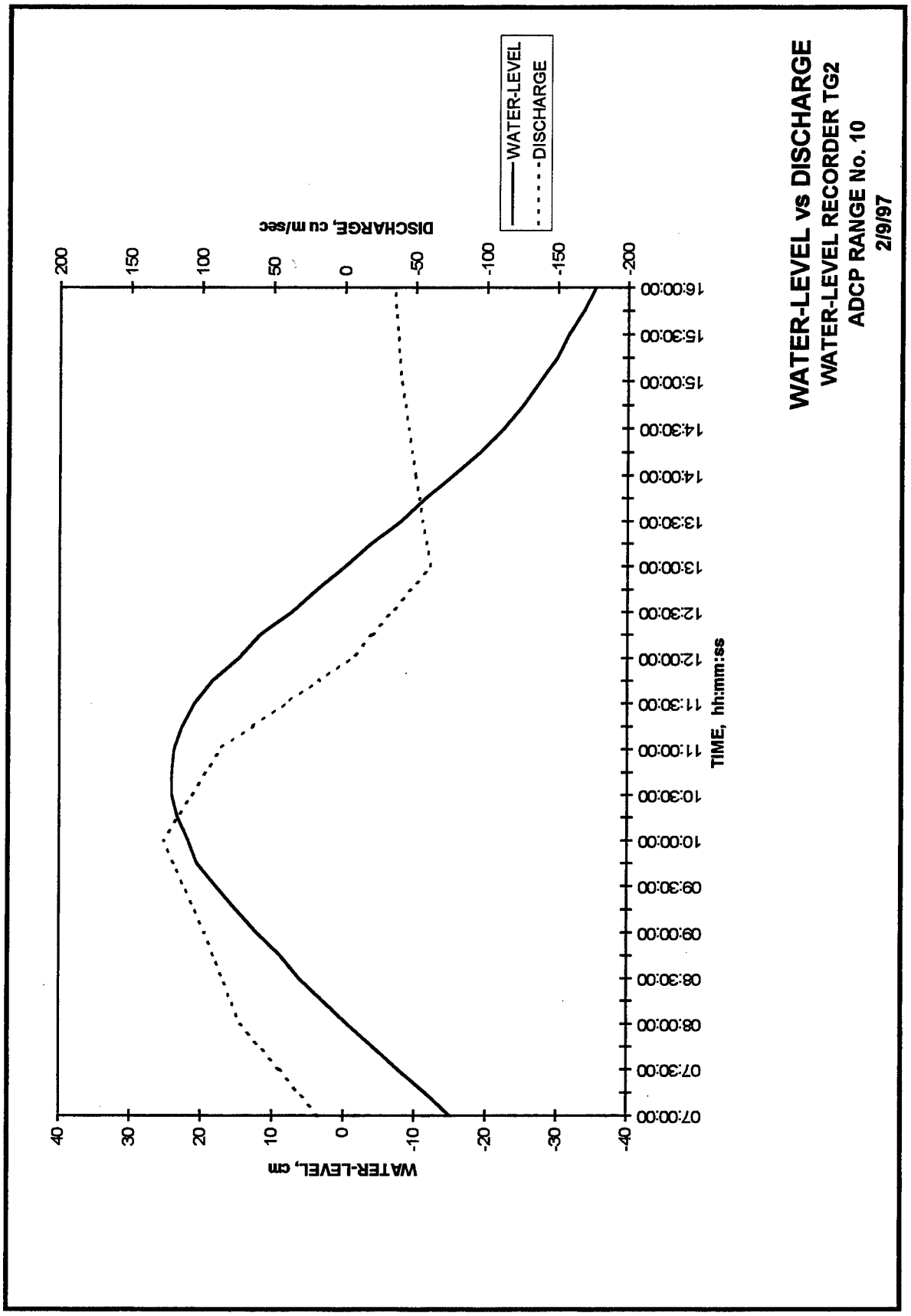
WATER-LEVEL vs DISCHARGE
WATER-LEVEL RECORDER TG2
ADCP RANGE No. 10
2/9/97
WATER-LEVEL
DISCHARGE
DISCHARGE, cu m/sec
WATER-LEVEL, cm
TIME, hh:mm:ss
200
150
100
50
0
-50
-100
-150
-200
40
30
20
10
0
-10
-20
-30
-40
07:00:00
07:30:00
08:00:00
08:30:00
09:00:00
09:30:00
10:00:00
10:30:00
11:00:00
11:30:00
12:00:00
12:30:00
13:00:00
13:30:00
14:00:00
14:30:00
15:00:00
15:30:00
16:00:00

Plate 86

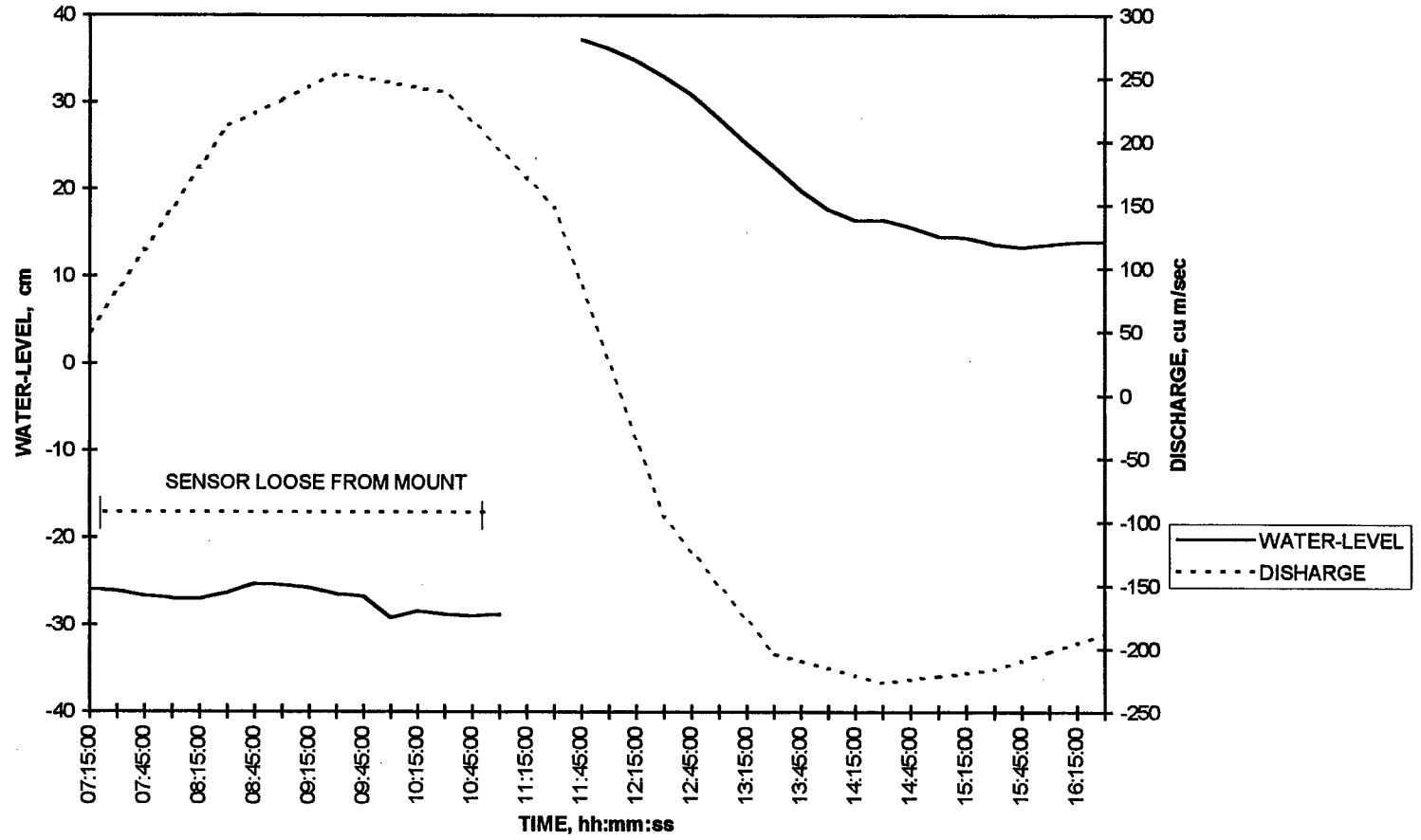

WATER-LEVEL vs DISCHARGE
WATER-LEVEL RECORDER TG3
ADCP RANGE No. 13
2/9/97

Plate 87

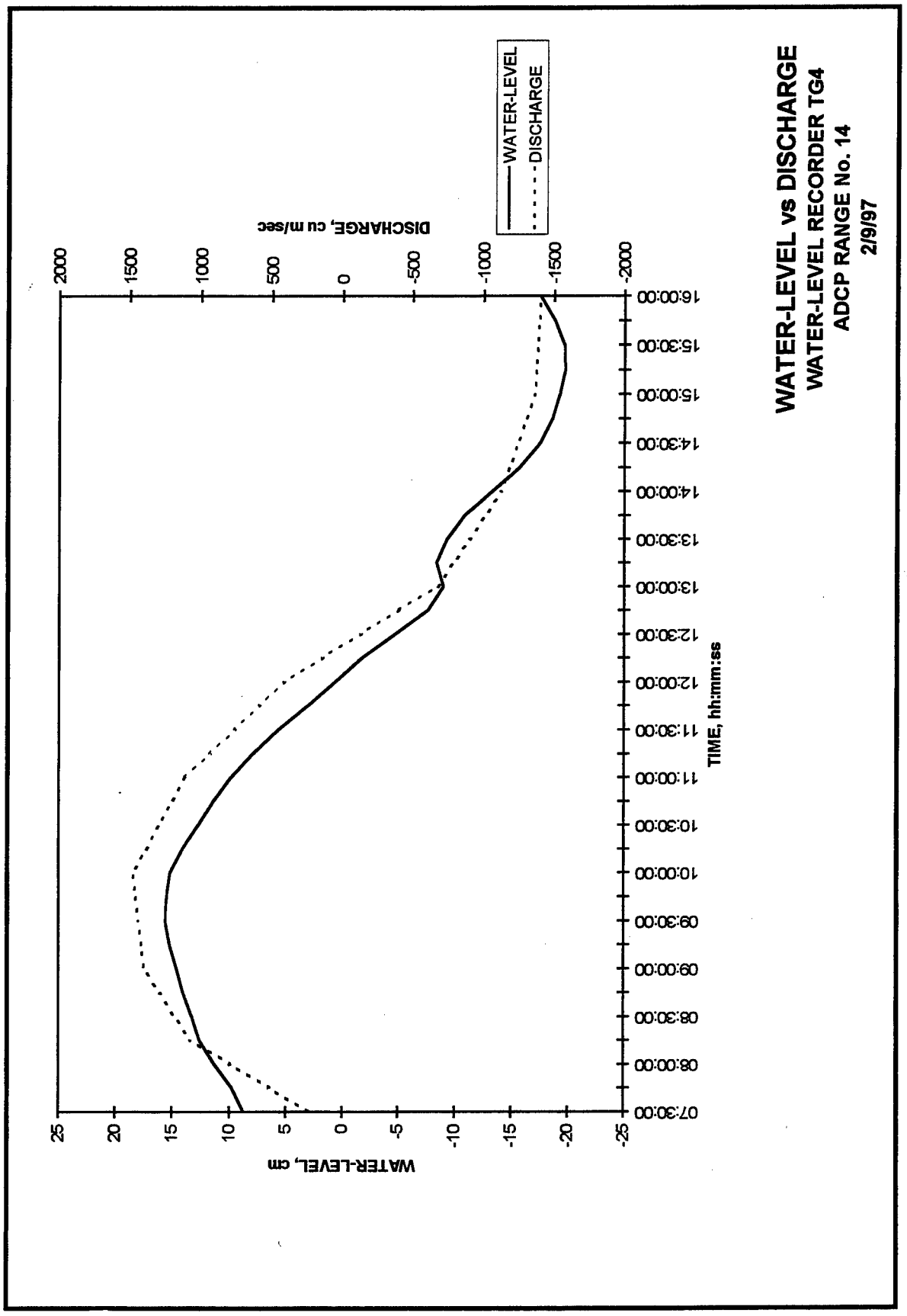
WATER-LEVEL vs DISCHARGE
WATER-LEVEL RECORDER TG4
ADCP RANGE No. 14
2/9/97
WATER-LEVEL
DISCHARGE
WATER-LEVEL, cm
DISCHARGE, cu m/sec
TIME, hh:mm:ss
25
20
15
10
5
0
-5
-10
-15
-20
-25
2000
1500
1000
500
0
-500
-1000
-1500
-2000
07:30:00
08:00:00
08:30:00
09:00:00
09:30:00
10:00:00
10:30:00
11:00:00
11:30:00
12:00:00
12:30:00
13:00:00
13:30:00
14:00:00
14:30:00
15:00:00
15:30:00
16:00:00

Plate 88

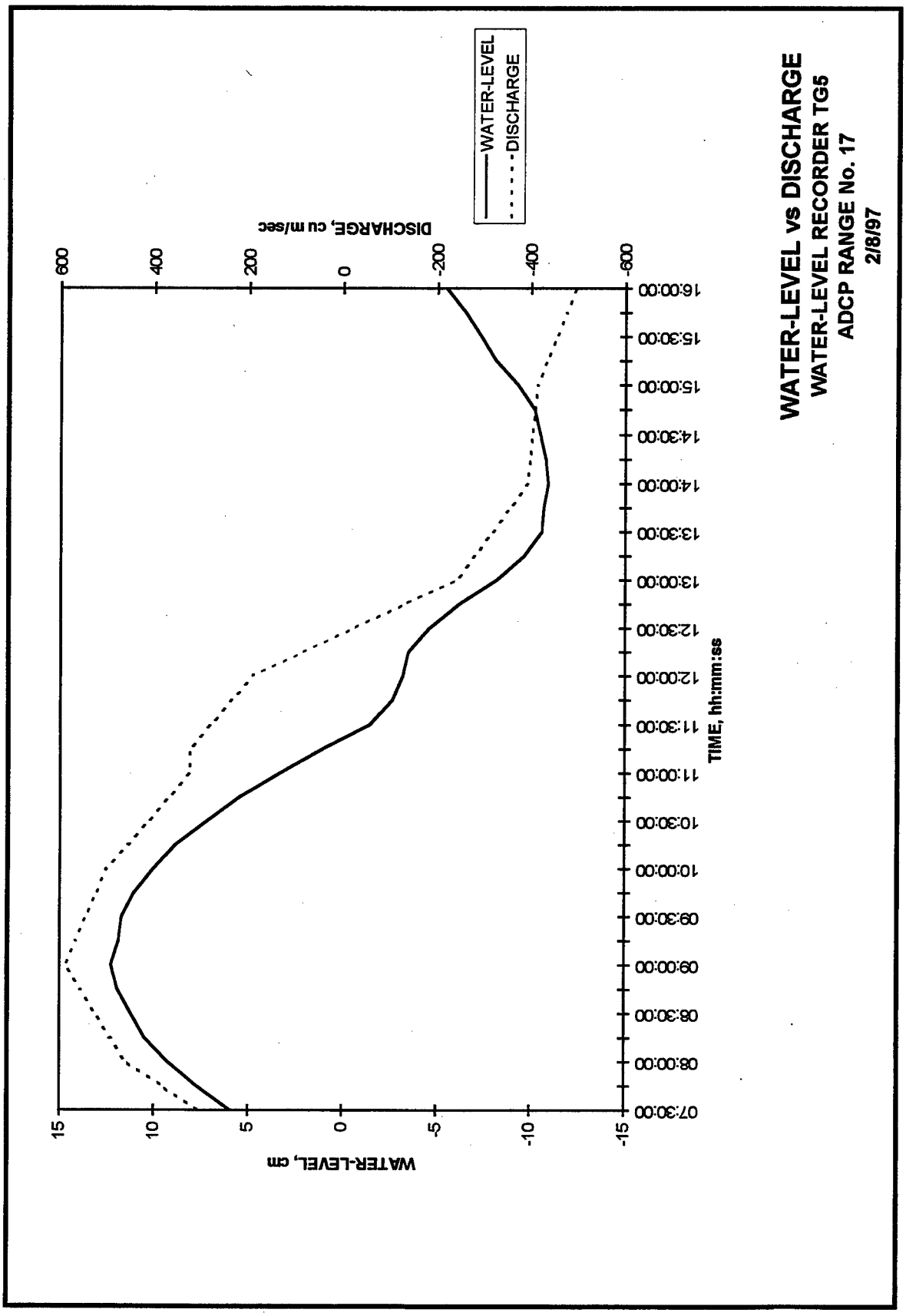
WATER-LEVEL vs DISCHARGE
WATER-LEVEL RECORDER TG5
ADCP RANGE No. 17
2/8/97
WATER-LEVEL
DISCHARGE
DISCHARGE, cu m/sec
600
400
200
0
-200
-400
-600
WATER-LEVEL, cm
15
10
5
0
-5
-10
-15
TIME, hh:mm:ss
07:30:00
08:00:00
08:30:00
09:00:00
09:30:00
10:00:00
10:30:00
11:00:00
11:30:00
12:00:00
12:30:00
13:00:00
13:30:00
14:00:00
14:30:00
15:00:00
15:30:00
16:00:00

Plate 89

APPENDIX A

HYDRAULIC ANALYSIS GROUP DATA COLLECTION EQUIPMENT AND LABORATORY ANALYSIS PROCEDURES

The contents of this appendix are to provide detailed information on the types of data collection and laboratory equipment used in a majority of the field investigations performed by the Hydraulic Analysis Group (HAG), Coastal and Hydraulics Laboratory (CHL), of the US Army Engineer Waterways Experiment Station (USAEWES). The following table is provided to identify the parameters most commonly measured and the types of instruments which can provide these measurements.

	Page No.
Current Velocity and Direction Measurements	
Acoustic Doppler current meters	2
Fixed-depth recording current meters	5
Suspended Sediment Sampling	
Pumped water samples	8
Automatic water samplers	8
Optical backscatterance (OBS) sensors	10
Salinity Measurements	
Hydrolab DataSonde 3 water quality data loggers	11
Wave Height Measurements	
Electronic wave height recorders	12
Water Level Measurements	
Electronic water level recorders	13

Bottom Sediment Sampling

Push-core samplers 16
Petite ponar samplers 17
Box-core samplers 18
Tethered drag samplers 18

Meteorological Measurements

Digital data acquisition of meteorological data 19

Laboratory Equipment and Sample Analysis

Laboratory analysis for salinity concentrations 21
Laboratory analysis for total suspended materials 22
Density analysis 22

Current Velocity and Direction Measurements

Acoustic Doppler current meters

Acoustic techniques are used to obtain current velocity and direction measurements for fast and accurate profiling in the field. The equipment used is RD Instruments BroadBand Acoustic Doppler Current Profilers (ADCPs) and SonTek Acoustic Doppler Profilers (ADPs), as shown in Figures A1 and A2, respectively. The RDI instruments vary in operating frequency ranges from 150-1200 kHz, whereas the SonTek instruments have frequency ranges from 75-3000 kHz. The equipment can be mounted over the side of boat with the acoustic transducers submerged, and data are collected while the vessel is underway as shown in Figure A3. It can also be mounted on a stable platform and placed on the riverbed or seabed as shown in Figure A4.

The ADCP and ADP transmit sound bursts into the water column which are scattered back to the instrument by particulate matter suspended in the flowing water. The ADCP and ADP sensors listen for the returning signal and assign depth and velocity to the received signal based on the change in the frequency caused by the moving particles. This change in frequency is referred to as a Doppler shift. The ADCP is also capable of measuring vessel direction, current direction, water temperature, and bottom depth. Communication with the instrument for setup and data recording are performed with a portable computer using manufacturer-supplied software, hardware, and communication cables. The

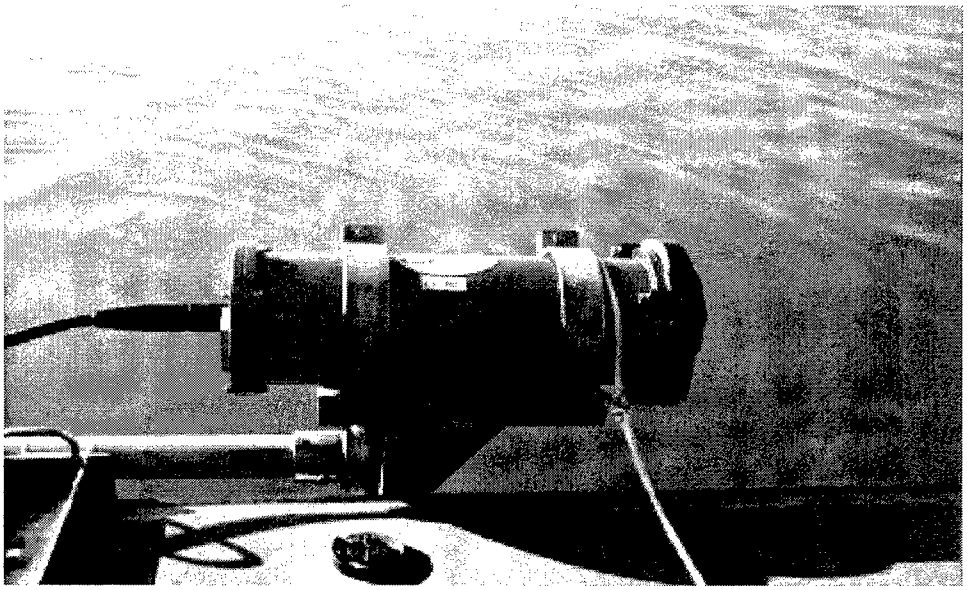

Figure A1. Acoustic Doppler current profiler (ADCP).

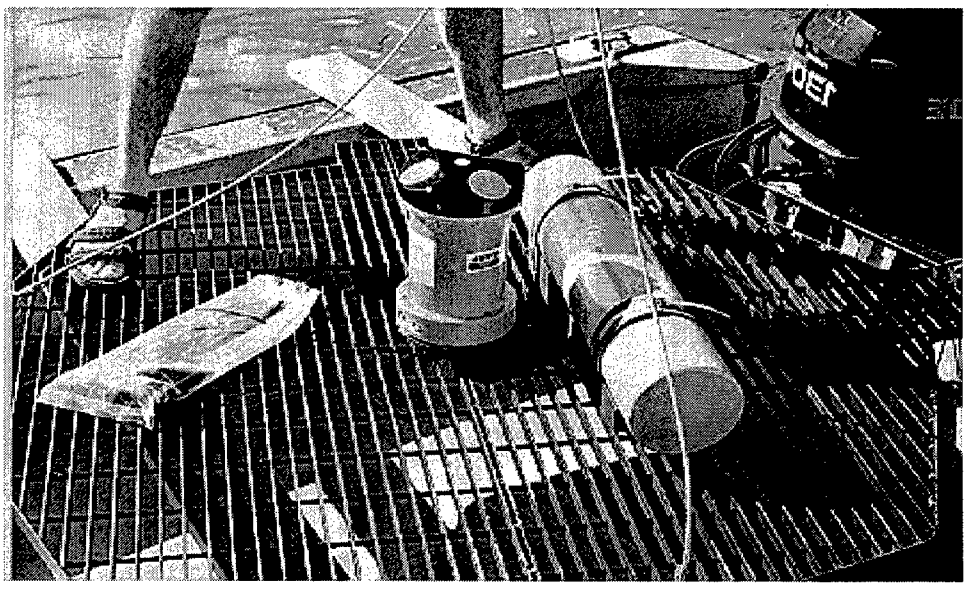

Figure A2. Acoustic doppler profiler (ADP).

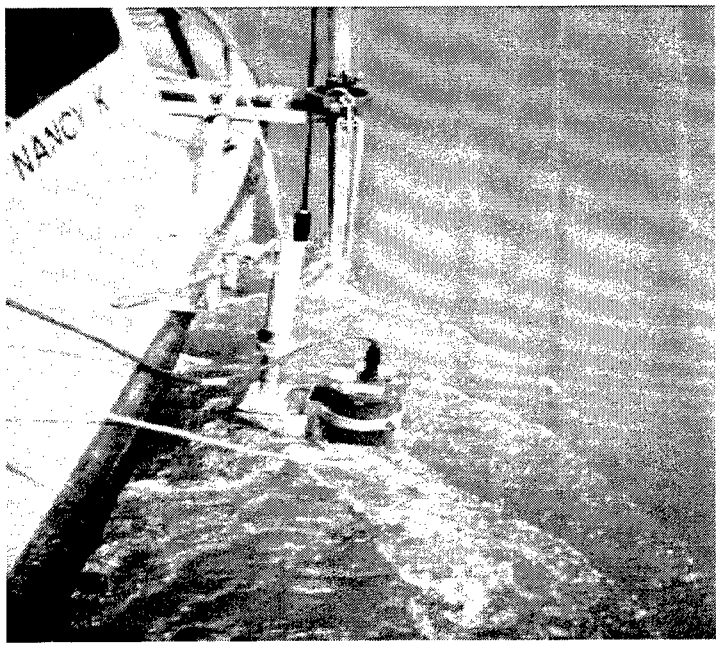

Figure A3. Vessel-mounted ADCP.

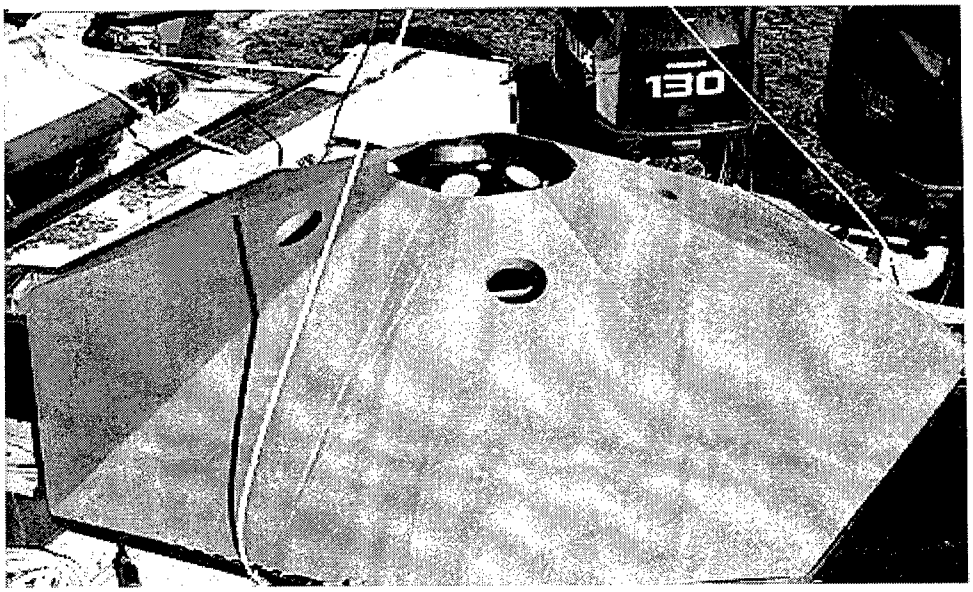

Figure A4. Bottom-mounted ADP unit.

manufacturer-stated accuracies are ±0.2 cm/sec for current speed measurement; ±2 deg* for vessel direction; and ±5 °F for temperature.

Fixed-depth recording current meters

Self-contained recording current meters are used to obtain current velocity and direction measurements for both profiling and for long-term fixed-depth deployment. The Environmental Device Corporation (ENDECO) Type 174 SSM current meter, shown in Figure A5, is tethered to a stationary line or structure and floats in a horizontal position at the end of the tether (as shown in Figure A6). It measures current speed with a ducted impeller and current direction with an internal compass. It also measures temperature with a thermilinear thermistor and conductivity with an induction-type probe. Data are recorded on an internal solid-state memory data logger. Data are offloaded from the meter data logger by means of a communication cable connected between the meter and a computer. The threshold speed is less than 2.5 cm/sec, maximum speed of the unit is about 2.5 m/sec (10 knots), and stated speed accuracy is ±2 percent of full scale. The manufacturer states that direction accuracy is ±7.2 deg above 2.5 cm/sec. Time accuracy is ±4 sec/day.

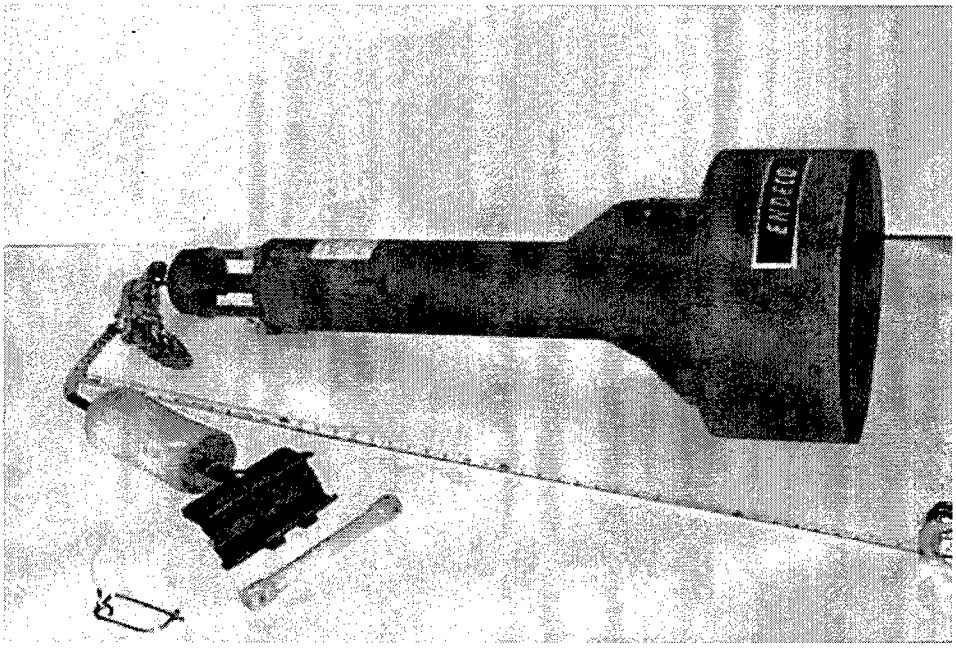

Figure A5. ENDECO Type 174 SSM current meter.

*All angles are given in degrees. To convert to radians, multiply by 0.01745.

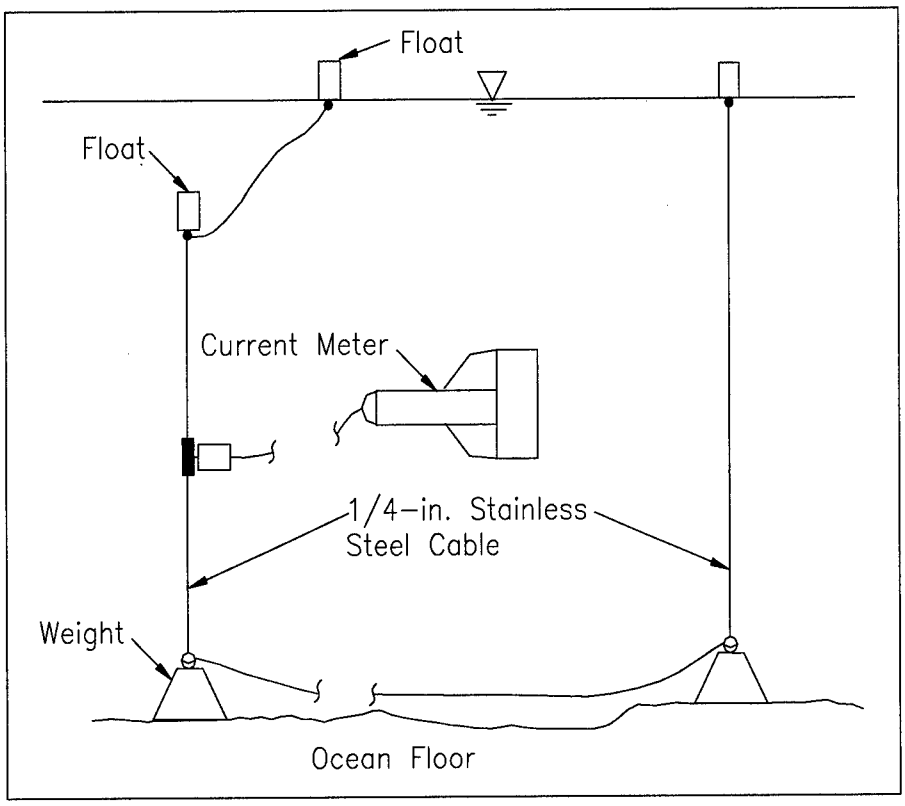

Figure A6. ENDECO 174 SSM current meter as deployed in the field.

The InterOcean Model S4 electromagnetic current meter, shown in Figure A7, can obtain continuous recording of current velocity and direction at fixed depths or can be used to profile the water column for current velocity and direction. The S4 meter is a 10-in.-diameter sphere that is suspended vertically in the water column with a submerged flotation device and anchored to the bottom by a heavy block and anchor arrangement. This deployment technique is illustrated in Figure A8. The S4 meter measures the current velocity using an electromagnetic microprocessor coupled with an internal flux-gate compass and computes the velocity vectors, which are then stored in the solid-state memory. The accuracy of the S4 meter current speed is ±0.2 cm/sec.

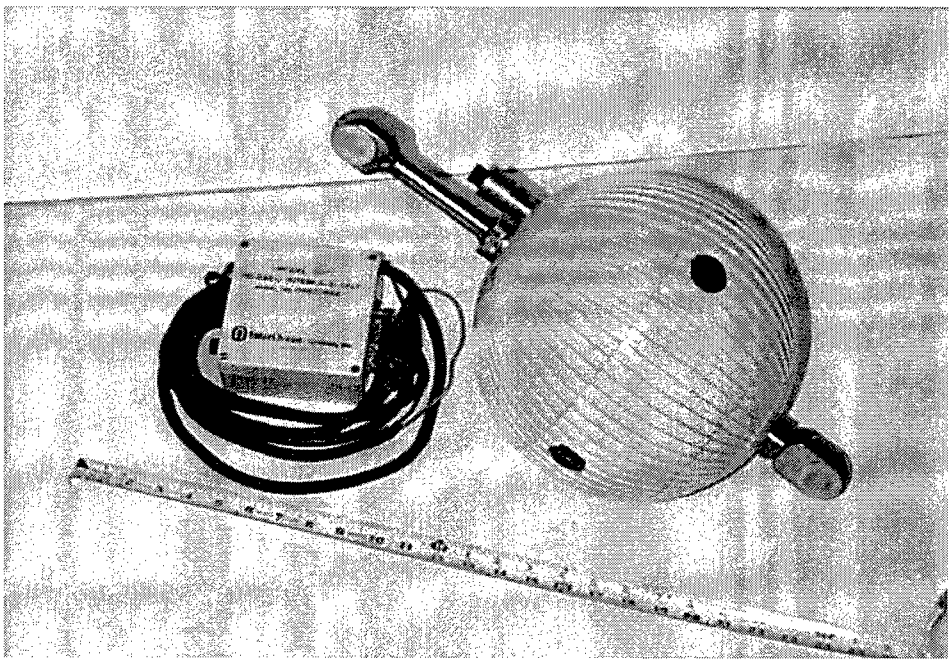

Figure A7. InterOcean S4 electromagnetic current meter.

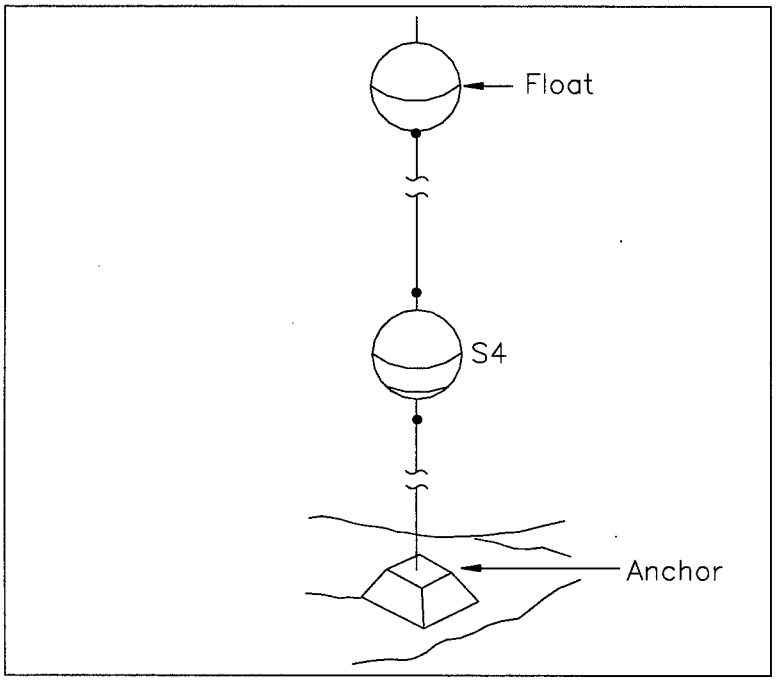

Figure A8. Electromagnetic current meter deployment technique.

Suspended Sediment Sampling

Pumped water samples

In combination with the over-the-side velocity measuring equipment, water samples for analysis of suspended sediment concentrations and total suspended solids are obtained by pumping the sample from the desired depth to the surface collection point. The pumping system consists of a 1/4-in.-ID plastic tubing attached to the current meter signal cables for support. The opening of the sampling tubing is attached to the solid suspension bar at the same elevation as the current meter and is pointed into the flow. A 12-V d-c pump is used to pump the water through the tubing to the deck of the boat where each sample is then collected in individual 8-oz plastic bottles. The pump and tubing are flushed for approximately 1 min at each depth before collecting the sample.

Automatic water samplers

The ISCO Model 6700 automatic water sampler, shown in Figure A9, and the American Sigma Models 700 and 2000 are employed to provide unattended sampling. A typical field installation of these

Figure A9. ISCO Model 6700 automatic water sampler.

water samplers is shown in Figure A10. Discrete water samples are collected in 1-liter plastic bottles located inside the sampler. The samplers are fully programmable, operating from a 12-V d-c power source, for obtaining any volume of sample desired up to the maximum size of the bottle, for obtaining composite samples, for setting different intervals between samples, and for setting times to begin the sampling routine. During servicing, the sample bottles are replaced with empty bottles to begin a new sampling period.

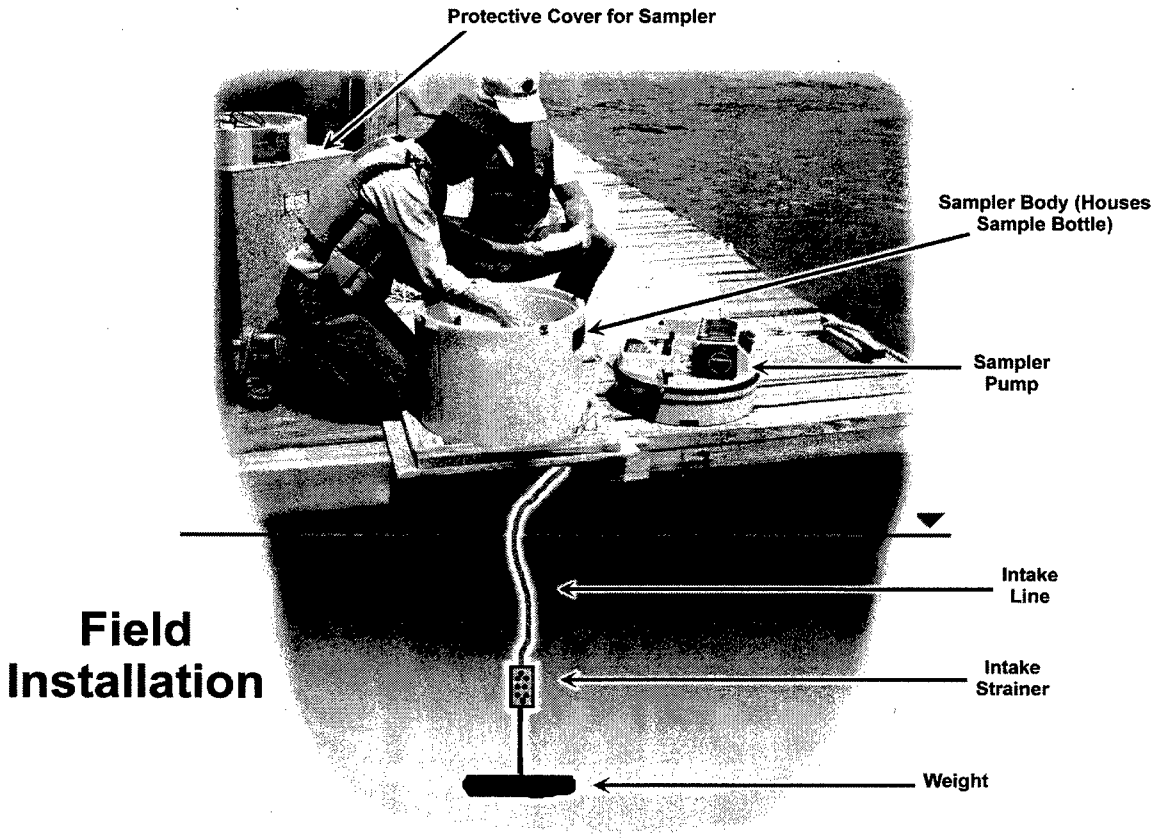

Figure A10. Typical field installation of automatic water samplers.

Optical backscatterance (OBS) sensors

The OBS sensor, a product of D&A Instruments and Engineering, is a type of nephelometer for measuring turbidity and solids concentrations by detecting scattered infrared light from suspended matter. It consists of a high-intensity infrared emitting diode (IRED), a series of silicon photodiodes as detectors, and a linear solid-state temperature transducer. The IRED emits a beam, at angles 50 deg in the axial plane and 30 deg in the radial plane, to detect suspended particles by sensing the radiation they scatter, as shown in Figure A11. Scattering by particles is a strong function of the angle between the path of radiation from the sensor through the water and the signal return to the detector. OBS sensors detect only radiation scattered at angles greater than 140 deg. As with other optical turbidity sensors, the response of the OBS sensor depends on the size distribution, composition, and shape of particles suspended in the medium being monitored. For this reason, sensors must be calibrated with suspended solids from the waters being monitored. The OBS sensor can be interfaced with "smart" data loggers that are capable of powering the sensor during sampling intervals.

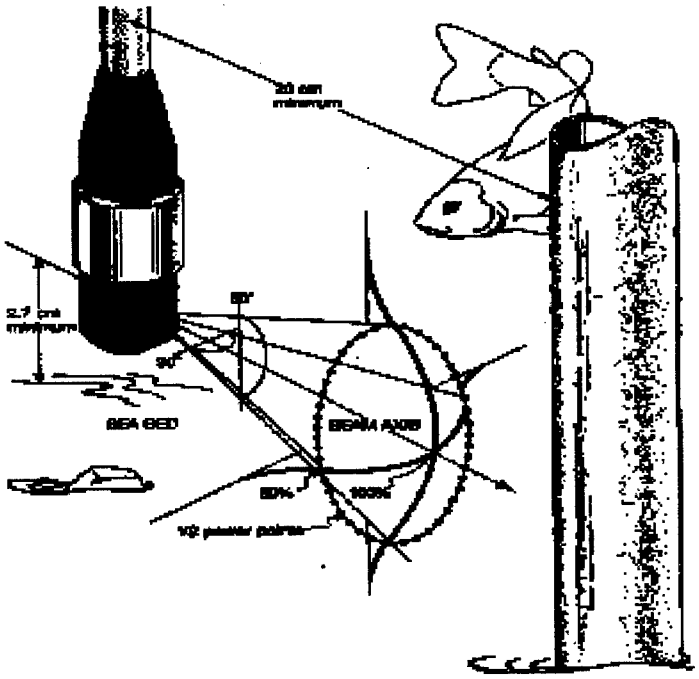

Figure A11. OBS sensor beam pattern.

Salinity Measurements

Hydrolab DataSonde 3 water quality data loggers

The Hydrolab Datasonde 3 water quality data logger, shown in Figure A12, provides conductivity and temperature with a computed salinity concentrations measurement corrected to a known calibration standard at 25 °C. The recorder housing is a high-density PVC case with a specific conductance cell and temperature sensor. The specific conductance probe is a six-electrode cell having a measurement range of 0.0 to 100 mS/cm with an accuracy of ±1 mS/cm. The salinity concentration range is from 0.0 to 40 ppt with an accuracy of ±0.2 ppt (calculated from the conductivity). The temperature probe is a thermistor type sensor with a measurement range of -5 ° to 50 °C with an accuracy of ±0.15 °C. The data sampling intervals range from 1-59 sec, 1-59 min, or 1-23 hr. Data are stored on non-volatile EPROM chips. Internal or external batteries provide the power requirements for sensor operation and data storage. Data are offloaded from the instrument via an industry standard RS-232 port to a portable computer using standard communication software.

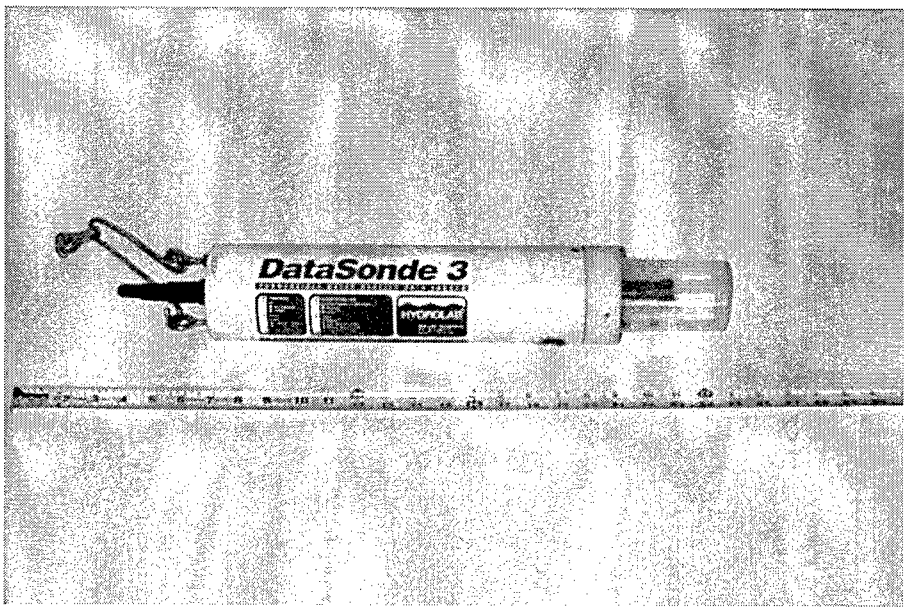

Figure A12. Hydrolab Datasonde 3 water quality data logger.

Wave Height Measurements

Electronic wave height recorders

The Microtide water level recorders, shown in Figure A13, contain a strain-gage type pressure transducer in a subsurface case which records the absolute pressure of the column of water above the case. The pressure transducer is not vented to the atmosphere; therefore, an extra unit is positioned in the study area to record atmospheric pressure changes. Water pressure is measured for the desired sample interval and an average value is computed and stored on the internal RAM data logger. The stated accuracy is ±0.6 cm. The sampling time interval can be set from 0.25 sec to 24 hr. The Microtide also measures temperature by means of a Yellow Springs Instruments (YSI) thermilinear thermistor built into the water level recorder. The thermistor has a range of -5 ° to +45 °C, with a stated accuracy of ±0.1 °C. The data from each recorder are stored on an accessible RAM located in the waterproof subsurface unit which also contains the d-c power supply.

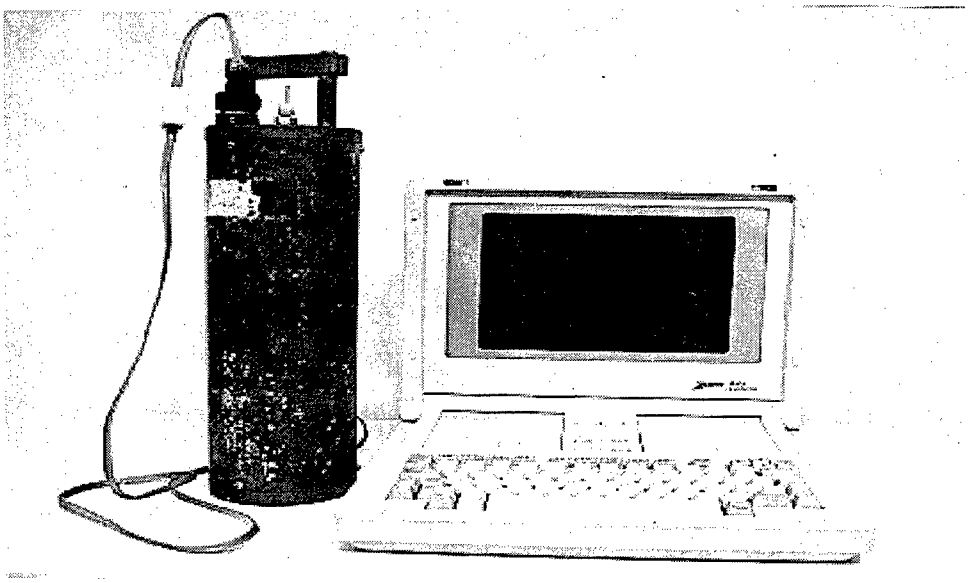

Figure A13. Microtide electronic wave height recorder.

Water Level Measurements

Electronic water level recorders

Water level elevation measurements can also be recorded using solid-state electronic recorders, such as Microtide, YSI, and ENDECO water level recorders. Water level elevations, temperature, conductivity, salinity, and dissolved oxygen (DO) concentration measurements are recorded using YSI Model 6000 water level recorders and ENDECO Models 1152 and 1029 SSM (solid-state measurement) water level recorders (excluding the DO measurements). The ENDECO Model 1152 SSM, shown in Figure A14, and Model 1029 SSM recorders, contain a strain-gage type pressure transducer located in a subsurface case which records the absolute pressure of the column of water above the case. The pressure transducer is vented to the atmosphere by a small tube in the signal cable to compensate for atmospheric pressure. The pressure is measured for 49 sec of each minute of the recording interval with a frequency of 5-55 kHz to filter out surface waves, therefore eliminating the need for a stilling well. The accuracy is ±1.5 cm. The sampling time interval can be set from 1 min to 1 hr. The Models 1152 and 1029 also measure temperatures by means of a thermilinear thermistor built into the recorders. The thermistor has a range of -5 ° to +45 °C, with an accuracy of ±0.2 °C. The Model 1152 measures conductivity by an inductively coupled probe installed on the meter. These measurements and the measurements of temperature are used to calculate salinity concentrations in units of parts per thousand (ppt). The salinity concentrations are computed with an accuracy of ±0.2 ppt.

The sampling time interval for conductivity and temperature cannot be set independently from the water level measurements. The data from each recorder are stored on a removable EPROM solid-state memory cartridge located in a waterproof surface unit which also contains the d-c power supply.

The YSI/ENDECO Model 6000 recorder also uses a strain-gage type pressure transducer located in a subsurface case and records the absolute pressure of the water column above the case. The Model 6000 is not vented to compensate for atmospheric pressure; therefore, after the sensor is initially calibrated, any changes in barometric pressure will appear as changes in depth. This is particularly significant in shallow water. For example, a change of 1 mm of Hg in barometric pressure will change the apparent depth by approximately 1.37 cm. The range of 0-9.14 m of water has an accuracy of ±1.83 cm and a resolution of 0.03 cm. The Model 6000 utilizes a thermistor of sintered metallic oxide which changes predictably in resistance with temperature variations. The thermistor has a range of -5 ° to +45 °C, with an accuracy of ±0.15 °C and a resolution of 0.01 °C. The Model 6000 measures conductivity using a four nickel electrode cell in the range of 0-100 mS/cm with an accuracy of ±0.5 percent and a four digit resolution. Salinity is calculated based on the conductivity and temperature measurements in the range of 0-70 ppt with an accuracy of ±0.1 ppt and a resolution of 0.01 ppt. The Model 6000 uses a dissolved oxygen (DO) sensor that employs a patented "Rapid-Pulse" measuring technique. Its range is 0-20 mg/ℓ with an accuracy of ±0.2 mg/ℓ and 0-200 percent saturation with an accuracy of ±2 percent.

Figure A14. ENDECO Model 1152 SSM water level recorder.

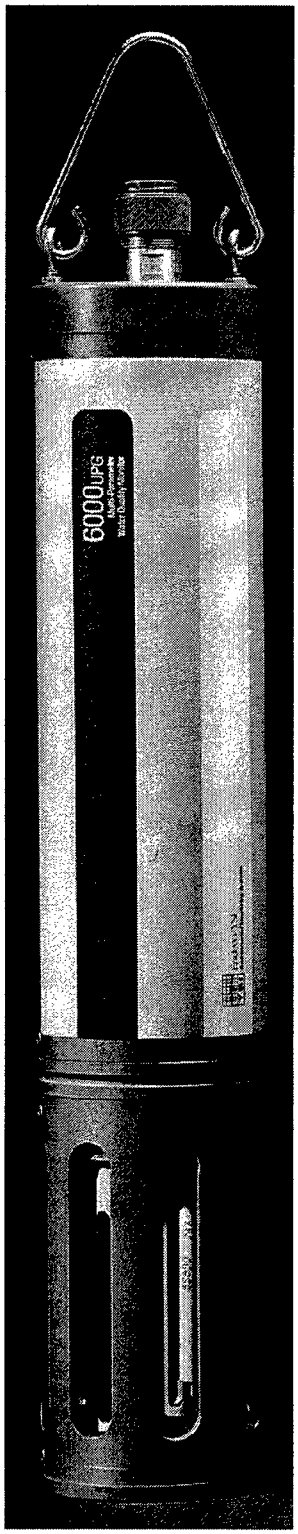

Figure A15. YSI/ENDECO Model 6000 water level recorder

Bottom Sediment Sampling

Push-core samplers

Bottom sediments are obtained using a push-core type sampler. The sampler consists of a 1.5-in.-diam PVC pipe, 18 in. in length. Attached to this is a smaller section of pipe with a valve attached at the upper end. The purpose of the valve is to create a reduced pressure holding the sample in the larger-diameter pipe. The samples are then brought to the surface and classified by visual inspection or transported back to WES for more detailed analysis. The push-core sampler is displayed in Figure A16.

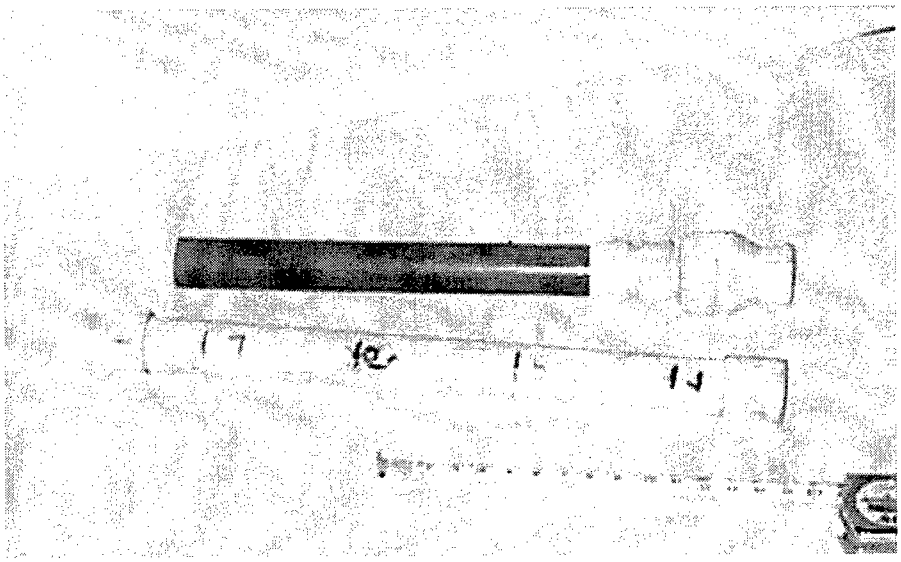

Figure A16. Push-core sampler.

Petite Ponar samplers

The petite Ponar sampler is basically a clam-shell type sampler. The sampler is cocked on the surface before lowering to the bottom. When the sampler makes contact with the bottom, the trigger pin releases allowing the sampler to close. As the sampler is raised to the surface, it closes around the captured sediment until it is opened at the surface. Samples are removed, inspected, and packaged in plastic bags or jars for further analysis once returned to WES. The petite Ponar is displayed in Figure A17.

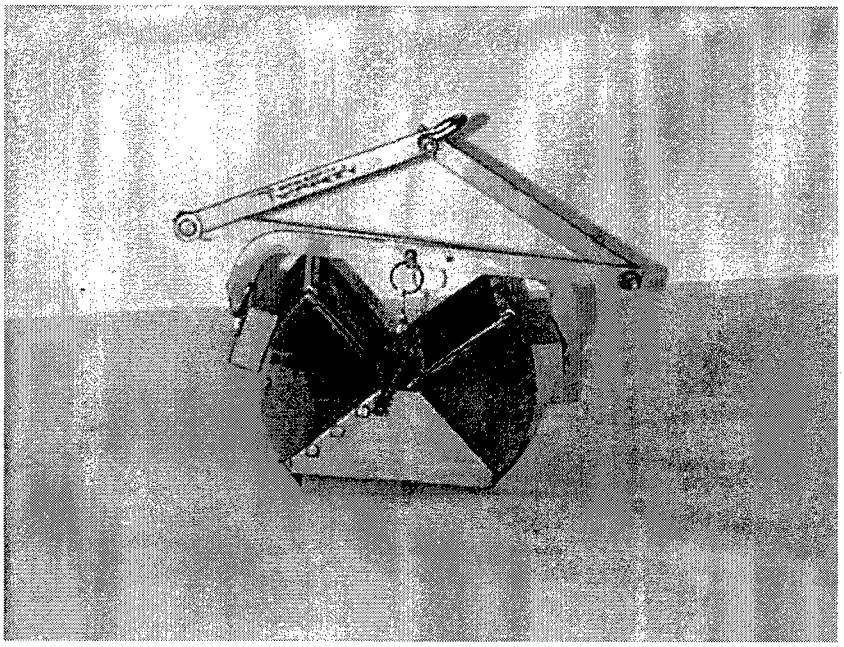

Figure A17. Petite Ponar sampler.

Box- core samplers

The box-core sampler is very similar to the petite Ponar in its triggering mechanism and sampling technique. The main difference in the two samplers is where the sample is trapped. The box-core has clam-shell jaws that scoop the sediment into a clear plastic square tube. When the sampler is opened at the surface, the sample is visible from a top door on the sampler. From this top door, the trapped sample can be sub-sampled for more detailed analysis. Figure A18 is a picture of the box-core sampler.

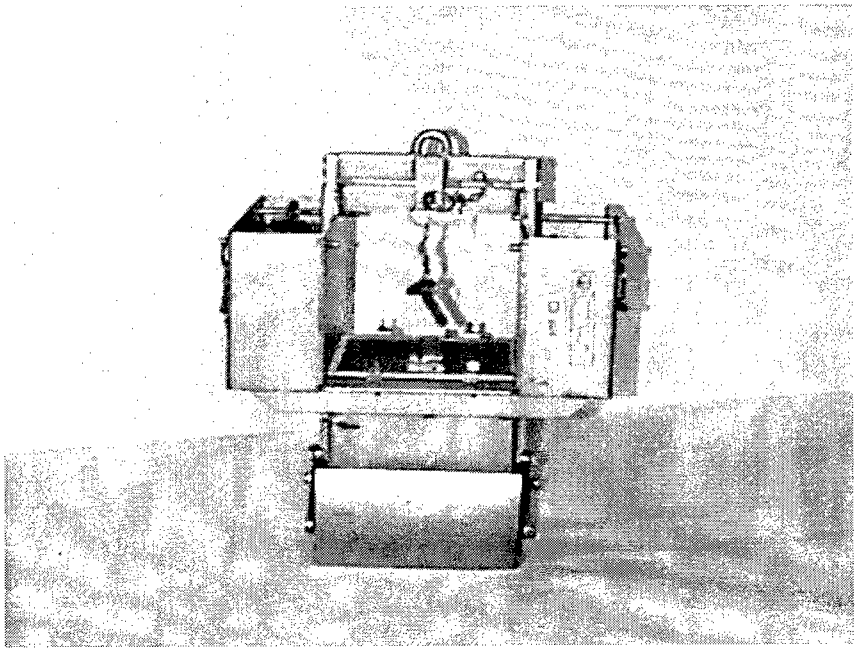

Figure A18. Box-core sampler.

Tethered-drag samplers

The Tethered-drag sampler is basically a 3-in.-diam pipe cut on a 45-deg angle with a shackle mounted on one side. The sampler is thrown over the side and dragged along the bottom. The sample accumulates inside the pipe. Samples are removed, inspected and packaged in plastic bags or jars for further analysis once returned to WES. The tethered-drag sampler is displayed in Figure A19.

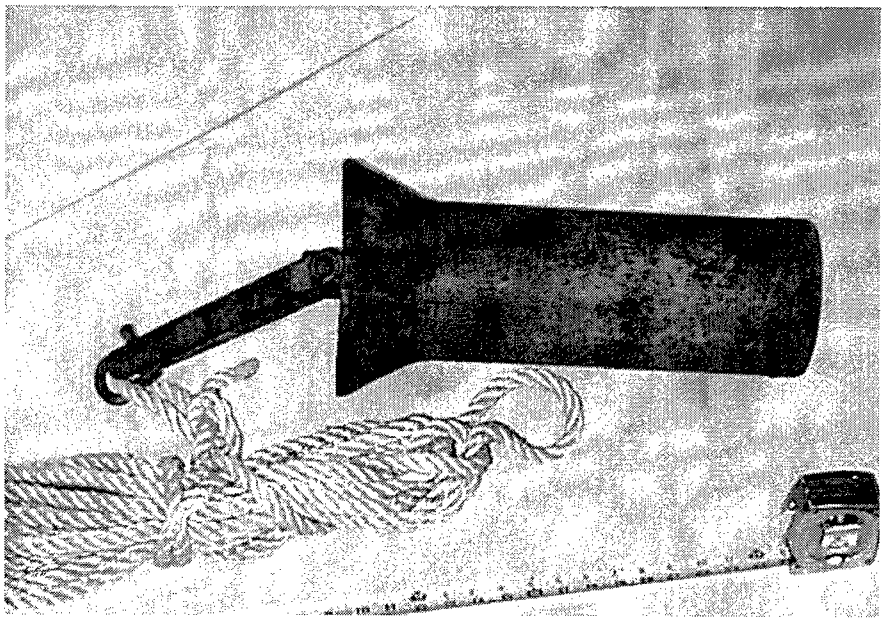

Figure A19. Tethered-drag sampler.

Meteorological Measurements

Digital data acquisition of meteorological data

Continuous wind speed and direction measurements are recorded using a Campbell Scientific Model W2000 Data Acquisition system (see Figure A20). The data collection platform is typically located at some central location in the study area and mounted approximately 5 m above the water. The data acquisition system is a battery-powered microcomputer with a real-time clock, a serial data interface, and programmable analog-to-digital converter. The battery is constantly charged using a solar panel charging system located near the system. Various programming options are available for setting the sampling interval of the system for the input signals from the wind speed and direction sensors. The system can be programmed to sample the input signals each second over a set period of time to determine the mean wind speed, mean direction, maximum wind gust speed, and maximum wind gust direction. The data are processed internally and stored in formats specified in a user-entered output table. The accuracy of the analog input of the wind speed and direction sensors is ±1.0 mph and ±3.0 deg, respectively. The barometric pressure sensor, Model CS105, has an accuracy of ±0.5 mb for a range from 600-1060 mb. The tipping bucket rain gage has an resolution of 0.01 in. for each tip. The calibrated accuracy is ±1 tip or 1 percent at 2 in./hr or less. The relative humidity sensor has an accuracy of ±2-percent RH within the range of 0-90 percent and ±3-percent RH within the range of 90-100 percent.

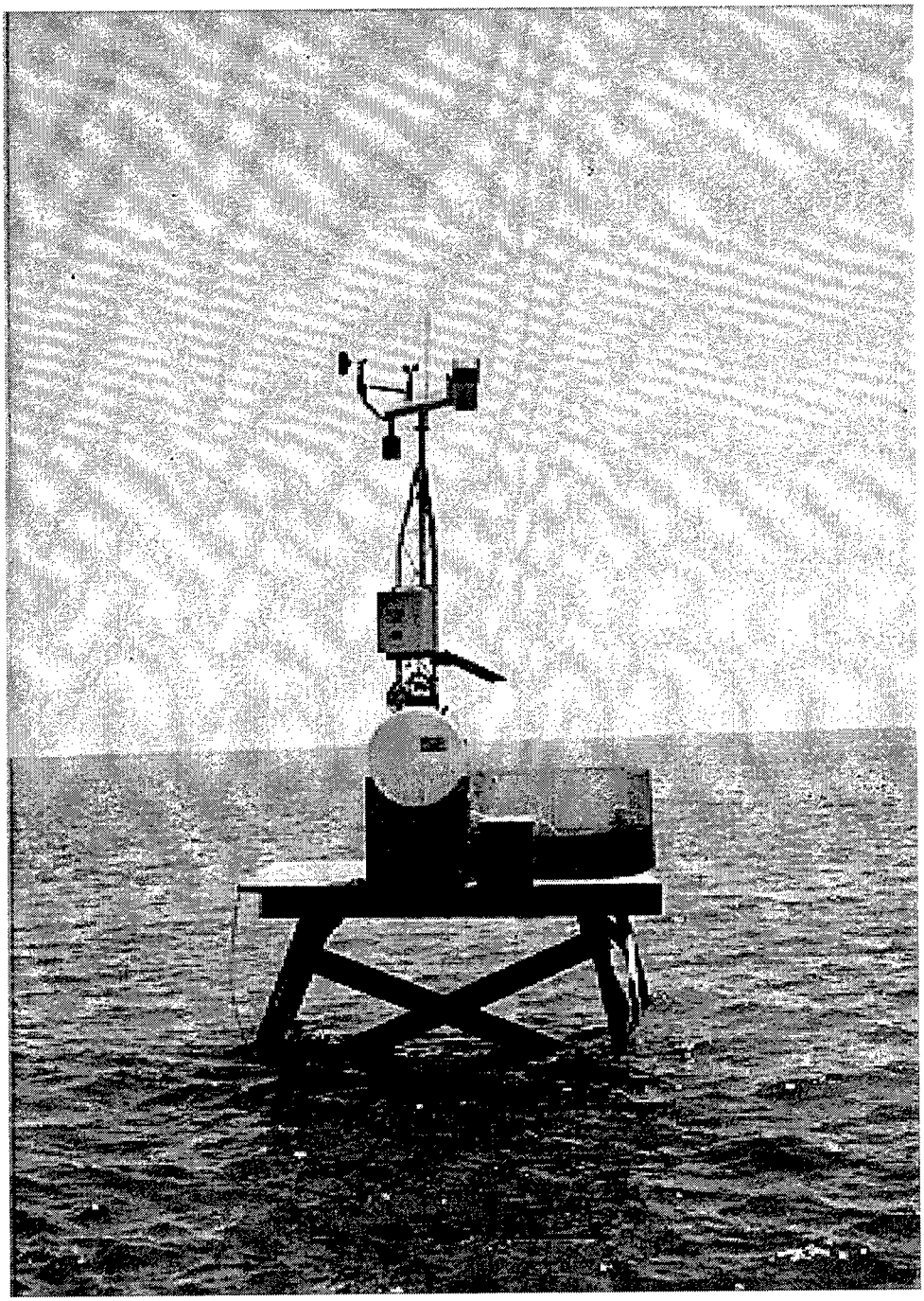

Figure A20. Weather Station Model W2000

Laboratory Equipment and Sample Analysis

Laboratory analysis for salinity concentrations

An AGE Instruments Incorporated Model 2100 MINISAL salinometer (Figure A21) with automatic temperature compensation is used for the determination of suspended sediment concentrations in the individual samples. The salinometer is a fully automated system, calibrated with standard seawater, and the manufacturer's stated accuracy is ±0.003 ppt on samples ranging from 2 to 42 ppt.

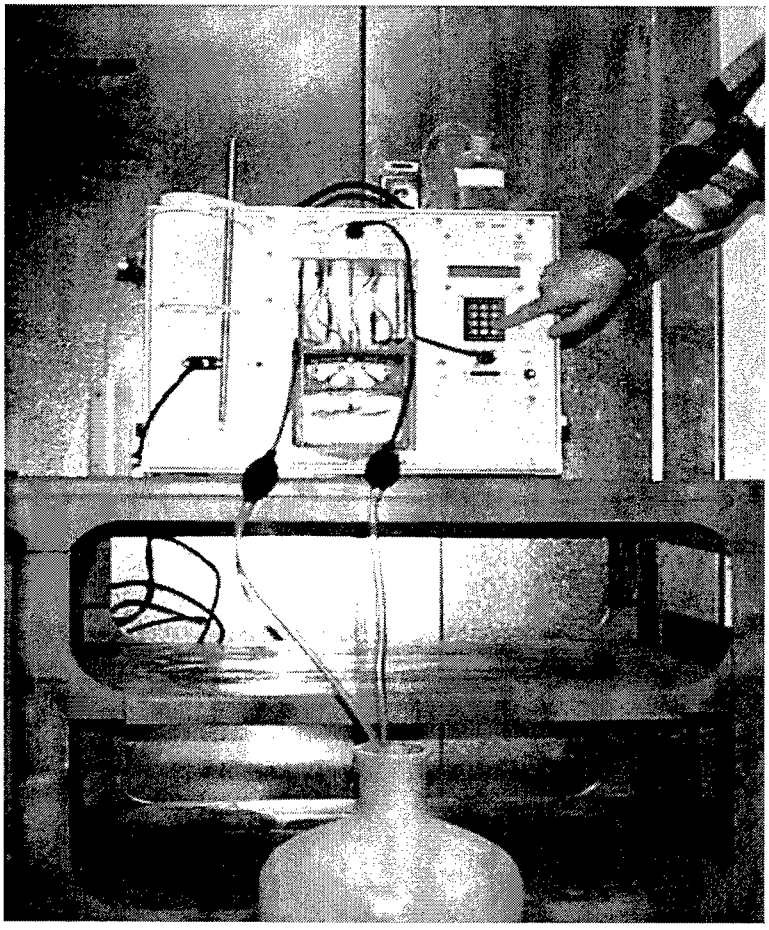

Figure A21. AGE MINISAL salinometer.

Laboratory analysis for total suspended materials

Total suspended materials (TSM) are determined by filtration of samples. Nuclepore (Registered Trademark) polycarbonate filters with 0.40 micron pore size are used. They are desiccated and preweighed, then a vacuum system (8-lb vacuum maximum) is used to draw the sample through the filter. After the filters and holders are washed with distilled water, the filters are dried at 105 °C for 1 hr and reweighed. The TSM are calculated based on the weight of the filter and the volume of the filtered sample.

Density analysis

A density analysis is done using wide-mouth, 25-cm constant-volume pycnometers. They are calibrated for tare weight and volume. A pycnometer is partially filled with sediment and weighed, then topped off with distilled water. Care is taken to remove any bubbles before the pycnometer is reweighed. The bulk density (BSG) of the sediment is then calculated by the equation:

$$BSG = \frac{(\rho)(sedwt - tarewt)}{(\rho)(volpyc) + (sedwt) - (sed + waterwt)} \quad \text{(A1)}$$

where:

ρ = density of water at temperature of analysis
sedwt = Total weight of pycnometer and sediment
tarewt = tare weight of pycnometer
volpyc = volume of pycnometer
sed + *waterwt* = Total weight of pycnometer, sediment, and water

APPENDIX B

AN ANALYSIS OF WEATHER DATA FROM NORTHERN FLORIDA BAY

The contents of this appendix are to provide information on the additional analysis of the weather data performed by the Harbor Branch Oceanographic Institution (HBOI). The results of these analyses were useful in quantifying the spatial correlation of wind stress and precipitation-evaporation balances across the northern part of the bay. A detailed summary of the HBOI analyses of the weather data is provided herein.

An Analysis of Weather Data from Northern Florida Bay

Ned P. Smith
Harbor Branch Oceanographic Institution
5600 U.S. Highway 1, North
Fort Pierce, Florida 34946

INTRODUCTION

In mid-March 1996, the U. S. Army Engineer Waterways Experiment Station (WES) initiated a field study that included three weather stations across northern Florida Bay, near Johnson Key, Buttonwood Key, and Butternut Key (Stations A-C, respectively, in Figure B1). Each weather station recorded wind speed and direction, air temperature, air pressure, relative humidity, rainfall, and incoming solar radiation (insolation). Each platform contained an evaporation pan.

The Johnson Key station (A) was at latitude 25° 03' 09.29"N, 80° 54' 22.11"W; the Buttonwood Key station (B) was at 25° 04' 39.40"N, 80° 43' 04.24"W; and the Butternut Key station (C) was at 25° 05' 12.86"N, 80° 31' 12.09"W. The three study sites provide good spatial coverage across the northern part of the bay and, together with the CMAN weather station just north of Long Key, provide good spatial coverage of Florida Bay in general.

In a February 29, 1996, response to a Request for Quotations issued by the Jacksonville District Office, Harbor Branch Oceanographic Institution (HBOI) offered to analyze the weather data in support of a parallel modeling effort that was underway at WES. Included in the Scope of Work was Task 4: "Develop a methodology to quantify evaporative water loss as a function of wind speed, humidity and air and water temperature from the weather stations. Compare with pan evaporation data." A later (October 7, 1996) and more specific listing of the collaborative research effort included the following under "Other Data Analysis Tasks of Interest:"

a. WES will make all weather station data available to HBOI for analysis (first 6 months of data by Oct/Nov 1996; second 6 months of data by Mar/Apr 1997).

b. HBOI analysis of the weather station data may include some or all of the following:

1. Comparison of pan evaporation rates with calculated rates.
2. Correlation between wind fields and ADCP measurements.
3. Spatial correlation of wind fields across the bay.

c. HBOI may choose whether or not to prepare a report on the weather station analyses, depending upon the time and resources available.

This final report contains the analysis and interpretation of selected parts of the weather station data. The purpose is to describe in some detail the methodology used to quantify wind stress and evaporation and to summarize results of the analysis of the data from these three stations. Results from individual stations are useful for characterizing local weather conditions in that part of Florida Bay. Comparison of results from any two stations provide information relating to spatial gradients. An understanding of spatial variations in weather will help guide the placement of future weather stations for specific studies or for long-term monitoring. The data used in this report come from all three stations, but they are not continuous over the 406-day time period from March 14, 1996, to April 24, 1997. This is a result of gaps in the records (see Table B1 for time periods of available and missing data).

Throughout the field study, WES personnel have plotted weather data in relatively short segments. Variables such as wind speed, relative humidity, solar radiation flux, air temperature, and barometric pressure, etc., have been plotted over approximately one-month intervals, and additional analog plots are not needed. The methodology utilized for this report is intentionally confined to that which is needed to provide the bigger picture in a temporal sense and to quantify gradients in a spatial sense. The relationship between wind forcing and transport through the open western boundary of the bay has not been included in this report. This subject was covered in some detail in Appendix C (Smith 1997).

The primary application for the results of the analysis of the wind data is the hydrodynamic model that is under development at WES. Specifically, the methodology is intended to (a) provide information needed to characterize the magnitude and temporal variability of wind forcing in Florida Bay;and (b) provide information on the spatial correlation of wind stress across the northern part of the bay. Apart from hydrodynamic modeling applications, the methodology is intended to (c) provide information relating to the precipitation-evaporation balance of the bay that will be needed in water budget studies. All results presented here contribute to an understanding of the climatology of Florida Bay.

THE DATA

Weather data are available from three study sites along an east-west line across northern Florida Bay (see Figure B1). The westernmost study site was approximately 100 yards northwest of Johnson Key, and "wind shadow effects" (a local reduction in wind speed and/or deflection of the wind direction when the weather station is downwind of the key) might be expected for wind directions between approximately 90 and 160°. The central station was southeast of Buttonwood Key, and "wind shadow effects" might occur for wind directions from about 270 to 360°. The easternmost station was at the western tip of Butternut Key, and some "wind shadow effects" might be expected for wind directions between about 90 and 160°.

At all three study sites, measurements were made from a platform that had a base nominally 2-3 m above the water surface. The height of the anemometers was estimated to be 5.2 m (17 feet) above the surface.

Time series began on March 14 (Johnson Key), March 15 (Buttonwood Key), or March 16 (Butternut Key). Data available for analysis continue through April 23 (Johnson Key), April 11 (Buttonwood Key), and April 24, 1997 (Butternut Key), although gaps appear in all three records. The Johnson Key data base has gaps from June 13 to July 23 and from November 5 to December 6, 1996. The Buttonwood Key data base has gaps from April 20 to May 30, from June 12 to July 22, and from November 5 to December 6, 1996. The Butternut Key data base has gaps from April 20 to May 30, from June 12 to July 22, and from November 5 to December 6. Data gaps are summarized in Table B1.

At all study sites, weather variables were recorded at 15-min intervals, with a time stamp indicating the end of the 15-min averaging period. Weather variables include the scalar average wind speed (m s^{-1}), resultant (vector average) wind speed (m s^{-1}), resultant wind direction (°), 15-min average air temperature (°C), relative humidity (%), 15-min accumulated rainfall (mm), barometric pressure (mm Hg), average solar radiation rate (W m^{-2}), and accumulated solar radiation flux during the 15-min sampling interval (kJ m^{-2}).

METHODOLOGY

(a) Wind-Stress Calculations

The most important weather variables recorded at the three weather stations are wind speed and direction, because they provide the basis for the wind-stress calculations. While weather variables such as air temperature, incoming solar radiation, and humidity may be of primary importance for ecological studies, they are of secondary importance in calculating wind stress. Air temperature and humidity are needed for calculating air density, however, which is used in quantifying wind stress.

As a preliminary step in the calculation of wind stress, wind speeds recorded approximately 5.2 m above the water surface were adjusted to represent the wind speed that would have been recorded 10 m above the surface, the standard reference height. To make this adjustment, it was assumed that a power law could be used to describe the wind profile. With an exponent of 0.1, the 10-m level wind, V_{10}, can be estimated from the recorded wind speed, V_r, by

$$V_{10} = 1.068\, V_r \qquad \text{(B1)}$$

Using an exponent of 0.1 (see Kourafalou et al. 1996), the 1.068 correction factor is virtually identical to the 1.066 value one would use assuming a logarithmic profile with a dynamic roughness of 0.025 cm (Brocks 1962).

The calculation of wind stress, τ, uses a quadratic formula. The general form of the expression is

$$\tau = \rho_a C_D V^2 \tag{B2}$$

where ρ_a is the density of the overlying air, C_D is a drag coefficient, and V is the magnitude of the wind vector, in m s^{-1}. The drag coefficient is the one suggested by Wu (1980), namely

$$C_D = (0.8 + 0.065 V_{10}) \times 10^{-3} \tag{B3}$$

for wind speeds greater than 1 m s^{-1}. To calculate an approximate wind stress, one can use a constant value for air density. For example, density is 1.1884 kg m^{-3} for dry air with a temperature of 20°C at a pressure of 1000 mb. The actual density of air varies inversely with temperature and humidity and directly with pressure. Because all these variables are available from the WES weather stations, all have been used to calculate wind stress more precisely.

Tables of air density (List 1963) give values as a function of pressure and virtual temperature. Virtual temperature is the temperature that dry air must have at a given pressure to have the same density as moist air at pressure p, temperature T, and mixing ratio w. The mixing ratio is the dimensionless ratio of the mass of water vapor per unit mass of dry air. Thus, to determine the density of air, one calculates the virtual temperature--after calculating the mixing ratio to determine the moisture content of the air. The mixing ratio is given by

$$w = \frac{0.622 e}{p - e} \tag{B4}$$

where p is the surface pressure, in millibars, and e is the vapor pressure (the partial pressure exerted by water vapor in the atmosphere). One calculates the vapor pressure using the observed relative humidity, r, which is the ratio of the vapor pressure to the saturation vapor pressure, e_s. The saturation vapor pressure is given by Murray (1967) as

$$e_s = 6.1078 \exp\left[\frac{17.2694 T_C}{T_K - 35.86}\right] \tag{B5}$$

where T_K and T_C are the Kelvin and Centigrade air temperatures, respectively. Then, the vapor pressure is given by

$$e = r e_s \tag{B6}$$

Starting with the vapor pressure, one calculates the mixing ratio, then the virtual temperature.

With the virtual temperature, one then calculates air density, using

$$\rho = \frac{p}{R\ T} \qquad \text{(B7)}$$

where R is the gas constant for dry air, p is the air pressure in millibars, and T_v is the virtual temperature. With air density, one is then in a position to calculate the wind stress that is needed to drive the hydrodynamic model of Florida Bay circulation.

Wind stress has been calculated using the weather records from all three weather stations. No particular emphasis is placed on results from the Johnson Key weather station, but these calculations are especially significant for two reasons. First, the Johnson Key weather station has the longest uninterrupted time series; therefore, it provides the best data base for comparison with the Acoustic Doppler Profiler (ADP) time series along the 81°05'W meridian. Second, the Johnson Key study site is the closest of the WES weather stations to the three ADP study sites. For the purpose of comparing wind forcing (wind stress) with wind-driven currents (ADP data), it is best to consider only the weather station that is closest to the ADP stations.

Wind stress will be emphasized in this report. Because the wind-driven current is proportional to the square of the wind speed, characteristics of wind speed can be misleading. It is assumed that only wind stress will be used by the model for forcing Florida Bay circulation.

(b) Evaporation Calculations

The weather stations in Florida Bay provided an opportunity to quantify evaporation from empirical formulas as well as from evaporation pan measurements. Results presented here will be restricted to calculations that involve the bulk aerodynamic formulas. Emphasis is on evaporation calculations because this allows one to track evaporative water losses over shorter time scales. Over time scales on the order of a few hours, it is impossible to detect the very small water losses by measuring water levels in an evaporation pan.

Several methods are available for calculating evaporative water losses, and the decision to use one over another is generally made in view of available data. In this study, the principal limitation is the unavailability of water temperature data from the three weather stations. The missing water temperature data can be supplied in two ways. First, one can use measured values from the ADP time series. Alternately, one can look for a relationship using the CMAN data recorded near Long Key. The drawback of using ADP data is that temperatures were measured just above the bottom, while evaporation is fueled by surface temperatures. Also, ADP water temperatures were recorded in 2-3 m of water, while most of Florida Bay is on the order of 0.5 to 1 m deep. The drawback of using the CMAN data is that the platform is in 2-3 m of water. While the temperature sensor is about 1 m below the surface, a water column of this depth will warm and cool more slowly than a shallower water

column over the mud banks.

The approach used for calculating evaporative water losses ("moisture flux," E) using measurements of atmospheric conditions is the one described by Pond, et al. (1974):

$$E = \rho_a C_q V \Delta q \qquad \text{(B8)}$$

where ρ_a is the density of the air, in g cm^{-3}, C_q is a nondimensional bulk aerodynamic coefficient (sometimes referred to as the Dalton Number), V is the scalar average wind speed, in cm s^{-1}, and Δq is the specific humidity difference between the water surface and the level at which the weather observations are recorded. Calculating evaporative water losses (or latent heat losses) therefore has many of the same equations needed for the calculation of wind stress. Specifically, one must first calculate air density, which is a function of surface pressure (measured), surface temperature (measured), and atmospheric moisture (calculated from the saturation vapor pressure, the mixing ratio, and the virtual temperature, as described above). The advantage of this approach is that one can calculate evaporative water losses over the same 15-min time intervals for which atmospheric variables are recorded. While there is uncertainty in the evaporative water loss calculations, plots of water loss versus time make it clear that there are significant variations over time scales on the order of a few hours as winds fluctuate over the course of a day.

The greatest source of uncertainty in the evaporative water loss calculations is the surface water temperature needed to calculate the specific humidity at the air-water interface. A 356-day weather record (January 1 to December 22, 1994) from the CMAN station was used to obtain a relationship between CMAN water temperature and weather station air temperature. The linear correlation coefficient (+0.9692) for air temperature and water temperature was highly significant. The regression equation is

$$T_w = 0.9759 T_a + 1.44°C \qquad \text{(B9)}$$

where T_w and T_a are the water temperature and air temperature, respectively. In practice, for each 15-min observation, Δq was calculated from the air temperature, the estimated water temperature, and the relative humidity; and ρ_a was calculated from the observed air pressure and the virtual temperature. The extrapolated 10-m level wind speed was used in the product, and C_q was assigned a constant value of 1.4×10^{-3} (Hsu 1978). Humidity values were checked in mid-March 1997. Errors were assumed to accumulate linearly from the start of the study.

To present evaporative water-loss calculations, two approaches are used. To emphasize the short-term variability, quarter-hourly E values are plotted as a function of time; to emphasize the longer time scales, cumulative E values were calculated. The slope of the least-squares regression line quantifies the mean evaporative water loss over the time interval covered by the plot. For ecological applications, the precipitation-evaporation difference is of primary concern, because it is the net gain or loss of water that will lower or raise salinity. Thus, plots of P-E are presented. These plots are conceptually similar to water-level time

series that would be obtained from evaporation pan measurements.

(c) Persistence and Autocorrelation Calculations

Data from a single study site can provide information that is directly related to the temporal variability of the wind at that location--how "steady" or "unsteady" the wind is. In this report, persistence is calculated to quantify the extent to which "steady-state" conditions occurred at the time and place that the wind records were obtained. Persistence is defined as the ratio of the resultant wind speed to the scalar average wind speed:

$$P = \frac{V_R}{V_S} \tag{B10}$$

The quotient will range from 0 to 1.0. At the low end, a value of 0 indicates that over the averaging period the east-west and north-south components canceled themselves completely. At the high end, a value of 1.0 indicates that the wind and direction never varied. It should be noted that persistence can be calculated for each 15-min observation using the scalar average and resultant wind speeds that are stored by the data logger. Over longer time periods, persistence is calculated by averaging the east-west and north-south wind components (for the numerator) and dividing by the average of the scalar means (the denominator).

When winds are not perfectly steady, questions may arise regarding periodic or quasi-periodic fluctuations in the time series. To quantify the correlation of wind speed with wind speed from the same location but at a later time, we calculate autocorrelation coefficients, r_L, where L refers to the "lag," or time interval over which the two observations are separated:

$$r_L = \frac{\sum_{i=1}^{N-L} (x_i - X)\ (x_{i+L} - X)}{s_1 s_2 N} \tag{B11}$$

where x_i are the 15-min observations, X is the mean of the N observations, and s_1 and s_2 are the standard deviations of the lagged and unlagged series. Autocorrelation is calculated over time scales of up to six hours to examine the decision to sample quarter-hourly. The square of the autocorrelation values can be used to quantify the fraction of the variance occurring in the time-lagged measurements. If strong autocorrelation (a value near 1.00) is calculated over time scales on the order of one hour and shorter, then it might be concluded that a single hourly sample represents four quarter-hour samples adequately.

(d) Progressive Vector Diagrams

One of the best ways to summarize long time series of wind stress is by calculating and plotting progressive vector diagrams (PVDs). The PVD is constructed by plotting wind-stress vectors (magnitude and direction) in a head-to-tail manner. The resulting pattern shows how wind stress varied at the weather station. PVDs are best suited for characterizing wind forcing over the longer time scales. For example, seasonal variations in wind direction stand out

clearly. Information on the hour-by-hour fluctuations of wind stress is largely lost, however, and thus the PVD is not suitable for investigations that emphasize shorter time scales. The PVD, constructed from many hours of observations, is analogous to a 15-min resultant wind speed that is constructed from the one-second readings that the weather station takes over the quarter-hour averaging period. The end points of the PVD, together with the time interval that separates them, can be used to calculate the resultant wind stress. When two PVDs constructed from observations recorded at different study sites during a given time interval are compared, one sees immediately if the two stations had similar wind speeds and/or directions. Information of this kind is directly related to the decision to occupy two or more weather stations.

(e) Horizontal Coherence and Shear

Another way one can summarize long time series of wind stress from two locations is by calculating the linear correlation and the mean directional shear (Kundu 1976). Using the east-west (u-component) and north-south (v-component) currents from weather stations A and B, two correlation components, κ_1 and κ_2, are calculated:

$$\kappa_1 = \frac{<u_A u_B + v_A v_B>}{<u_A^2 + v_A^2>^{1/2} <u_B^2 + v_B^2>^{1/2}}, \kappa_2 = \frac{<u_A v_B - v_A u_B>}{<u_A^2 + v_A^2>^{1/2} <u_B^2 + v_B^2>^{1/2}} \quad \text{(B12)}$$

where the angle brackets, $< >$, represent a time average. The correlation coefficient is then given by

$$\kappa = (\kappa_1^2 + \kappa_2^2)^{1/2} \quad \text{(B13)}$$

The average counterclockwise angle, α, at the second station relative to the heading at the first, is given by

$$\alpha = \tan^{-1} \frac{<u_A v_B - v_A u_B>}{<u_A u_B + v_A v_B>} \quad \text{(B14)}$$

An important difference between using this approach and using PVDs constructed from two neighboring weather stations, is that α equally weights all observations in the time series, whereas the PVD weights observations in direct proportion to the magnitude of the wind stress vectors.

RESULTS

Results presented in this report for the weather data are fundamentally different from results that were presented in Appendices C and D. When describing the ADP data from the 81°05'W meridian (taken to be the western boundary of Florida Bay) and when describing the boat-mounted ADCP data from the two intensive surveys of the tidal channels along the eastern, southeastern, and southern sides of the bay, plots and tabular data represented

dependent variables (the response to wind and tidal forcing, for example) that are to be reproduced to a close approximation by the hydrodynamic model. In this report, the plots and tables of wind stress and evaporation represent independent variables. Wind stress in particular will be specified as model input and will not be reproduced as model output.

Four of the shorter records (March 15 to April 20 and May 30 to June 12 from Station 2, Buttonwood Key, and March 16 to June 20 and May 30 to June 12 from Station 3, Butternut Key) have not been included, because it is felt that they do not contribute anything in addition to what is brought out by the longer records.

Results are grouped in two subsections. The first subsection contains results of analyses of data from individual weather stations. Results include information related to wind-stress patterns (presented as progressive vector diagrams), persistence, autocorrelation, and evaporation (presented as quarter-hourly and cumulative values). The second subsection compares wind stress recorded at pairs of weather stations. Results include information related to the coherence and phase of variations in north-south and east-west wind-stress components, as well as information related to the correlation and mean veering of the instantaneous wind vectors. Also included, though perhaps of lesser interest, are plots of hourly air temperature and total daily light. Plots from all three stations are combined, because they describe virtually the same weather conditions. Similarities in total daily accumulated insolation are quantified by calculating linear regression coefficients.

1. INDIVIDUAL WEATHER STATIONS

a. Johnson Key

Figure B2 shows the PVD of wind stress calculated from weather data recorded at Johnson Key (Station A in Figure B1). The time period is March 14 to June 13, 1996. As noted above, the PVD is not well suited for describing wind forcing over time scales on the order of hours, but it is well suited for summarizing the "big picture." During this 91-day time period, the resultant wind-stress vector was nearly directly westward (275°), although especially early in this time period wind directions were highly erratic, tracing several clockwise loops before becoming more steadily westward. The wind observations from which wind stress was calculated had a resultant speed of 2.29 m s^{-1} and a resultant direction toward 276°.

As noted above, the persistence statistic quantifies the steadiness of the wind speeds and directions that were used in the wind-stress calculations. The persistence calculated from the 8,720 quarter-hour observations is 0.448. This is about at the midpoint between totally random wind vectors (persistence = 0.0) and completely steady winds (1.0).

Autocorrelation coefficients provide another measure of steadiness, but they apply to much shorter time scales. For the March-June Johnson Key data, the east-west component of the wind had an autocorrelation coefficient of +0.949 for a one-hour time lag. Squaring the

autocorrelation coefficient quantifies the percent of the variance occurring at a later time that can be explained by any observation. For example, for this one-hour time lag, an observation at a given time will explain 90% of the variance occurring an hour later. Calculations show that autocorrelation coefficients decrease with greater lag times, as would be expected. For example, for lags of three hours the autocorrelation coefficient is +0.863, indicating that an observation at a given time explains 74% of the variance occurring three hours later. Information of this kind is useful for deciding the necessary sampling interval. The autocorrelation coefficient for a lag of one-half hour is +0.974.

Figure B3 shows the PVD calculated from wind observations recorded at the Johnson Key weather station from July 23 to November 5, 1996. With the exception of a brief period of light and variable winds in the middle of the plot (occurring during the first three weeks of September and a large clockwise loop formed by southerly and then northeasterly winds during the second week of October, wind stress was relatively steady toward the southwest. The resultant wind-stress heading was toward 255°; wind stress was directed more toward the southwest later in this 105-day time period, indicating a slight seasonal shift in direction. The resultant wind was toward 257° with a speed of 2.54 m s^{-1}.

Persistence during this late summer and early fall time period was 0.551, suggesting that winds might be somewhat steadier at this time of year. Autocorrelation coefficients were slightly lower, however. The autocorrelation of east-west wind components for a time lag of one hour was +0.924, indicating that just over 85% of the variance occurring an hour later could be explained by measurements made at a given time. Autocorrelation coefficients were also calculated from the north-south wind components, and they were generally slightly lower. For example, north-south components of Johnson Key wind vectors for this time period had an autocorrelation coefficient of +0.889 for a time lag of one hour. Because autocorrelation coefficients are similar for east-west and north-south components and because autocorrelation is not of primary interest in this study, only the autocorrelation of east-west components will be included in the results from the other two weather stations.

Figure B4 is the final figure showing long time scale wind-stress patterns at the Johnson Key study site. The curve consists of two relatively well-defined components. During about the first two-thirds of the plot, the resultant wind stress is directed southwestward; during the final third of the plot, wind stress is directed west-southwestward. These are two parts of the seasonal variation in wind stress affecting Florida Bay. The erratic behavior that occurs from time to time throughout the record is a result of frontal passages. Generally speaking, winds are out of the southeasterly quadrant prior to the frontal passage, then swing sharply into the northerly quadrant following the passage of the cold front. For the 138-day time period as a whole, the resultant wind-stress direction is toward 231°. The wind observations themselves had a resultant speed of 2.41 m s^{-1} and a resultant heading toward 244°.

Autocorrelation calculations produced results similar to those noted above.

Autocorrelation coefficients for half-hour, one-hour, two-hour, and three-hour time lags were +0.977, +0.956, +0.918, and +0.882, respectively. Thus, for example, wind observations at a given time can be used to explain 91% of the variance in the winds occurring an hour later and 78% of the variance occurring three hours later. Persistence in the December-April Johnson Key wind record was similar to the persistence calculated at that location for the two earlier time periods. In this case, the persistence value was 0.452, slightly lower than the 0.551 value obtained from the July-November time period. It is likely that the lower persistence in winter months is a result of cold fronts, which have a dramatic effect on both wind speeds and directions.

Evaporation from the surface of Florida Bay at the Johnson Key study site is shown in Figure B5. The curve is divided into three parts as a result of breaks in the record from June 13 to July 23 and again from November 5 to December 6. All three curves are characterized by highly variable evaporation rates over time scales on the order of quarter-hours to weeks. Generally speaking, evaporation rates vary from 0 to 0.03 cm h^{-1}, with occasional rates as high as 0.04 cm h^{-1}. A representative mean value would be approximately 0.01 cm h^{-1}, or about a quarter of a centimeter per day. Greatest variability occurs over the diurnal time scales, as a result of diurnal variations in air and water temperature, humidity, and wind speed. Evaporative water losses also vary significantly over time scales of several days, as weather systems move through the study area, effecting changes in wind speed, air temperature, and humidity. Over the seasonal time scales--the longest that can be resolved in this study--variations in evaporative losses are relatively subtle. Lowest evaporation rates appear late in the record, during winter months (December-February), as a result of lower water temperatures, and in spite of stronger winds and lower humidity values following frontal passages. The cumulative water loss during the 298 days represented by these three records was 61.4 cm. If evaporation during the two time periods of missing data was similar, the annual evaporative water loss would be 75.2 cm.

b. Buttonwood Key

Results from Station B (see Figure B1), Buttonwood Key, are intentionally restricted to the analyses of data from the two longer records--July 22 to November 5, 1996, and December 6, 1996, to March 18, 1997. It is felt that the two shorter time series at the beginning of the study (March 14 to April 20 and May 30 to June 12) do not contribute enough information to justify additional figures.

Figure B6 shows the PVD for wind stress at the Buttonwood Key study site from July 22 to November 5, 1996. As one would expect, there is great similarity between the pattern obtained at Buttonwood Key and that found at Johnson Key (see Figure B3). Prominent features include the period of light and variable wind stress just before the midpoint of the curve and the elongated clockwise loop just after the midpoint. The resultant direction for wind stress during this 106-day time period was toward 269°; the resultant wind had a speed of 3.04 m s^{-1} and a heading of 269°.

The persistence calculated from the wind-stress record is 0.577--the highest value obtained for any of the seven long records. Over shorter time periods, autocorrelation calculations produced values similar to those found at Johnson Key. For time lags of 1, 2, and 3 hours, autocorrelation values were +0.931, +0.892, and +0.855. Thus, for example, sampling could have been reduced to hourly and 87% or more of the variance within the hour would have been accounted for by the hourly readings.

Figure B7 is the continuation of the Buttonwood Key wind stress PVD, covering the time period from December 6, 1996, to March 18, 1997. For comparison, see Figure B4, which covers the same time period at Johnson Key. Again, the pattern shows the seasonal transition from southwestward to west-northwestward wind stress that begins in late winter. From the start of the record and through about the midpoint of the plot (not necessarily the midpoint of the time period, however), the erratic meandering of the curve is a result of frontal passages moving across northern Florida Bay every 1-2 weeks. The approximately 90° clockwise veering of the wind-stress vector occurs around February 19, although this information is not available directly from the plot. For the remaining eight weeks of he plot, wind stress is relatively strong and generally toward the west-northwest.

Persistence calculated from the wind-stress record is similar to the value obtained at other locations and over other time intervals: 0.548. Like other persistence values, this suggests neither unusually steady winds nor unusually variable wind conditions. Similarly, autocorrelation coefficients are similar to those obtained from other time periods and at other study sites. For one-hour time lags, the autocorrelation coefficient was +0.947, and this decreased to +0.870 for time lags of three hours.

Evaporative water losses from the Buttonwood Key study site are shown in Figure B8. The plot is broken into four parts as a result of two data gaps early in the record followed by another between November 5 and December 6, 1996. A qualitative comparison of this plot with the plot for Johnson Key (see Figure B5) brings out several similar features. Again, the most obvious feature of the Buttonwood Key plot is the amount of high-frequency variability (time scales of up to a few days), resulting from short-period variations in wind speed, relative humidity, air temperature, and water temperature. Evaporation rates of 0.02 cm h^{-1} are attained often, values of 0.03 cm h^{-1} are reached occasionally, and 0.04 cm s^{-1} is approached three times. On average, the hourly evaporative loss is 0.0087 cm, which is equivalent to 0.21 cm day^{-1}. A seasonal signal is difficult to detect. Transient periods of high evaporation appear throughout the record. The calculations suggest that condensation can occur under the right conditions. For example, during the third week of August and again in mid October, negative values suggest that water vapor is condensing on the surface of the bay. It appears that during periods of high humidity water vapor can condense if the water temperature cools slightly. Condensation is also indicated in mid-January and mid-February.

c. Butternut Key

Butternut Key is the easternmost of the three WES weather stations, located less than 5

km from the keys at the nearest point. Water depths are somewhat shallower than those surrounding the other two sites, and thus the water should be somewhat more responsive to warming and cooling over the year. Water temperature data are not available from the weather station, but it is assumed that evaporation in summer and winter seasons might be alternately enhanced and suppressed as a result of the greater, then lesser heat energy available for evaporation. Data from Butternut Key are also divided into four parts as a result of breaks in the data throughout the study. Results of wind stress calculations, as well as estimates of evaporative water losses, are similar to those already discussed for Johnson Key and Buttonwood Key.

The PVD constructed from wind data recorded between July 22 and November 5, 1996, is shown in Figure B9. The same two prominent features appear just before and just after the midpoint of the curve. From about August 30 to September 24, sustained light and variable winds result in a nearly one-month period with little net movement in the PVD. Two weeks later, on October 7, a two-day period of strong northward wind stress results in the first part of the clockwise loop. The turnaround occurs on October 9, with the arrival of the first cold front of the 1996-1997 winter season. The heading of the resultant wind-stress vector during this 106-day time period was 264°; the resultant wind vector for the same time period was 2.69 m s^{-1} with a heading of 269°. Before and after the seasonal shift in early October, however, the resultant wind-stress vectors have headings of about 275° and 235°.

The persistence value calculated from the July-November Butternut Key wind record is 0.547, which is similar to values found at the other study sites. Again, this value makes it difficult to characterize the Butternut Key winds as either unusually steady or unusually variable. Autocorrelation is also similar to autocorrelation found elsewhere for the same time period. For time lags of 1, 2, and 3 hours, autocorrelation coefficients decreased nearly uniformly from +0.933 to +0.891 and then to +0.855.

Figure B10 is the continuation of the wind stress PVD from Butternut Key, covering the time period from December 6, 1996, to April 24, 1997. The seasonal shift from southwestward to westward, or west-northwestward wind stress occurs in mid February. This is unusually early for a transition from the winter pattern to the spring pattern. Prior to the seasonal wind shift, the signatures of several frontal passages appear as rapid changes in wind direction, sometimes involving a complete clockwise loop. Even very late in the record, however, several such loops identify the final cold fronts of the 1996-97 winter season. The last part of the plot, from late March through the end of the record, is a time of unusually variable wind directions. The resultant wind stress vector for this time period is directed toward 235°. The resultant wind stress before and after the seasonal shift is approximately 210° and 280°, respectively. The resultant wind vector for the full time period had a speed of 2.48 m s^{-1} and a direction of 252°.

Persistence and autocorrelation calculations do not offer anything new. The persistence of the quarter-hourly wind readings was 0.516, and the autocorrelation coefficients for time

lags of 1, 2, and 3 hours were +0.949, +0.912, and +0.880, respectively.

Figure B11 summarizes results of the evaporation calculations using the Butternut Key weather data. The three data gaps in April-May, June-July, and November-December divide the plot into four parts, but the two short records contribute useful information regarding evaporation rates in spring and early summer months. An unusual feature of the plot is the brief period of very high evaporation at the start of the second week in December. Values of just over 0.05 cm h^{-1} were attained. Inspection of the raw weather data reveals that this was a result of the combined effect of wind speeds that were as high as 10-11 m s^{-1} and humidities as low as 35-40%. For the record as a whole, however, evaporation rates varied generally between 0 and 0.02 cm h^{-1}, and the average was approximately 0.008 cm h^{-1}, which is equivalent to 0.19 cm d^{-1} and 70 cm y^{-1}. As is the case at the other two stations, subtle seasonal variations are apparent, although they have not been quantified with calculations based on shorter periods of the total record. Aside from the transient high values noted above, greatest evaporative losses appear to occur in late August and early September and again at the end of the record.

As was noted at the other two stations, brief periods of condensation are suggested by the calculations, but they are infrequent and do not appear to be restricted to any particular time of year. The combination of sufficiently high humidity and/or sufficiently cold water results in cooling of the air at the air-water interface and the deposition of water vapor. Over brief periods, Florida Bay appears to gain water from the atmosphere, but it is important to recall that the water temperature data used in the calculations were obtained from the Long Key CMAN station.

2. INTER-STATION COMPARISONS

a. Analysis of Wind-Stress Vectors

The availability of weather data from three study sites makes possible a direct comparison of differences in the magnitude and direction of wind stress at Stations A, B, and C. In this subsection of the report, data from pairs of weather stations are compared to quantify the similarity of wind-stress values calculated across the northern part of the bay. Similarity would be expected to increase as the station separation decreases. Thus, one would expect greater similarities between Stations A and B (Johnson Key and Buttonwood Key, separated by 19.4 km) and between Stations B and C (Buttonwood Key and Butternut Key, separated by 20.4 km) than between A and C (separated by 39.1 km).

Wind-stress vectors from pairs of stations were decomposed into north-south and east-west components then compared using Kundu's method, as described in the METHODOLOGY section. Calculations were made for Stations A and B, B and C, and A and C. Because of breaks in the record, the first set of calculations covered the time period from 0000 EST July 24 to 0000 EST November 5, 1996. The second set of calculations was restricted to the time period from 0000 EST December 7, 1996, to 0000 EST April 12, 1997,

because the data from Buttonwood Key ended at that time.

Results presented here are summarized in Table B2. For all pairs of stations, the mean deflection was less than 2.0°, and these small differences are similar to the accuracy of the wind vane. This suggests that all three anemometers were aligned properly relative to true north. Improper orientation of the wind vane would introduce a systematic error in direction that might suggest that winds in northern Florida Bay are converging or diverging. The high correlation coefficients suggest that for most purposes one weather station would have provided sufficient information for characterizing wind forcing. As noted in the introduction, however, each study site had a key relatively close by through some range of directions. Thus, there remains the possibility that under some wind conditions data from one of the stations would include wind shadow effects and thus not represent wind forcing well for Florida Bay as a whole.

Correlation coefficients are all within the range of 0.91 to 0.95, indicating that between 83 and 90% of the variance in wind speed and direction at one location can be explained by observations made at a neighboring location. As might be expected, lowest correlation coefficients were calculated when Station A (Johnson Key) was compared with Station C (Butternut Key). Correlation coefficients were highest and about equal when Stations A and B and when Stations B and C were compared. These stations are separated by only 19 and 20 km, respectively.

b. Precipitation-Evaporation Balance

Of greater importance than the evaporative water losses described above is the net freshwater gain or loss obtained from the difference between the rainfall recorded at a given station and the evaporation calculated for the same time interval--precipitation minus evaporation, or P-E. The cumulative net gain or loss is the primary variable for controlling increases or decreases in salinity in the poorly flushed interior of the bay.

Figure B12 shows the P-E balance for all three weather stations. Because of the gaps in the records, the P-E balance has to be reset to zero following each break. Nevertheless, net gains and losses are apparent even for the shorter segments of each plot. The curves that appear when precipitation and evaporation data are combined consist of relatively sharp increases separated by relatively slow decreases. Effects of rain showers generally occur over time periods that are between a few minutes and a few hours. Evaporation, on the other hand, produces a relatively slow but persistent freshwater loss. While rain showers can produce a gain of 1 cm over a time period of an hour or less, calculations described in the previous subsection indicate that evaporation removes fresh water at a rate on the order of 0.01 cm h^{-1}, which is two orders of magnitude less. Thus, for the hypothetical rain shower that drops 1 cm of rain in one hour, it would take over three days to remove the same amount of water through evaporation.

The top plot in Figure B12 contains P-E for Johnson Key in three parts. The first

segment, lasting 91 days, results in a near balance as a result of a rainy period in mid-May that contributes approximately 13 cm of rainfall. Smaller rain shower events from mid-March through mid-May mitigate the effects of chronic evaporation, however. The second segment of the record indicates a net gain of fresh water from late July through early November, following a net loss through much of August. This is the rainy season, and a net gain is expected during summer and fall months. Conversely, the final segment of the Johnson Key data, covering the time period from early December through late April, shows a net freshwater loss. Again, because this corresponds with the dry season, one would expect the cumulative P-E value to be negative. The net loss of about 14 cm would have been considerably greater if it were not for two rainy periods in mid-January and mid-March that probably coincide with frontal passages during the 1996-97 winter season.

The plot in the middle of Figure B12 contains cumulative P-E values calculated from the Buttonwood Key data. The first two segments of the record are too short for a meaningful comparison with the Johnson Key data, but the final two segments offer some insight regarding spatial variability in the P-E balance. The net freshwater gain during midsummer and autumn months is similar in some respects to the gain recorded at Johnson Key, but about 50% more rain was recorded at Buttonwood Key. Also, over shorter time scales, rainfall events appearing in one curve are not mirrored in the other. This could be a result of the development or dissipation of rain showers as they moved from one location to the other, or it could be because Johnson Key was not downwind of Buttonwood Key. During the December 1996 to April 1997 period, the two curves are similar, but heavier rainfall amounts at Buttonwood Key reduce the net freshwater loss to 10 cm, as opposed to 14 cm at Johnson Key.

It is immediately apparent from the plot at the bottom of Figure B12 that the rain gauge at Butternut Key was not recording rainfall from the start of the study through the data gap that ended in early December. What should be a plot of the net freshwater gain or loss is a plot of cumulative evaporative losses. For the final segment, however, the pattern is similar to that recorded at the other two locations, though the net freshwater loss at Buttonwood Key was the largest of the three stations.

c. Total Daily Insolation

Weather records from Johnson Key, Buttonwood Key, and Butternut Key also provided time series of air temperature and incoming solar radiation (insolation). While these two variables are not in themselves of primary concern within the context of wind forcing and evaporative water loss, they are of fundamental importance within the broader context of the ecology of Florida Bay. Insolation in the form of daily accumulations (millions of Joules per square meter per day) is summarized in Figure B13. All three plots trace a sinusoidal pattern that results from the seasonally varying zenith angle of the sun at local noon. Maximum insolation values are those that occur on cloud-free days. Maximum daily accumulations at the time of the winter solstice are 55-60% of the maximum accumulations in early summer, when the sun at local noon is nearly directly overhead (zenith angle is near 0°) at the latitude of

northern Florida Bay. Clearly, the minimum values are more variable as a result of the type and amount of cloud cover from one day to the next. A seasonal pattern in the day-to-day variability is poorly defined, and very cloudy days can reduce insolation to 10-15% of the total possible value throughout the year. Although individual cumulus clouds affecting one of the weather stations would rarely if ever affect insolation being recorded at the other weather stations, the daily averages plotted in Figure B13 are quite similar at these three locations.

d. Air Temperature

Finally, air temperatures recorded during the 406-day study are summarized in Figure B14. The annual cycle appears as a sinusoidal variation with maximum values from late August through mid-September, and minimum values during the month of January. Comparison of the annual temperature cycle with the plot of total daily insolation (Figure B13) shows clearly the approximately two-month time lag of warmest water relative to maximum solar heating. The temperature plot is similar to the insolation plot in the sense that the day-to-day variation in maximum temperatures is considerably smoother than the day-to-day variation of minimum values. Unlike the insolation data, however, the temperature plot is noticeably less variable in midsummer months than it is in winter months. In all three plots, midsummer temperatures range from about 26° to about 32°. In midwinter months, on the other hand, temperatures vary from about 24° down to as low as 8-12°C.

DISCUSSION

The data base available for this report proved to be quite well suited for characterizing many aspects of the weather affecting Florida Bay, as well as for quantifying spatial coherence. While gaps in the record reduced the longest time series to 3327 hours, this time period is long enough for investigating the response to meteorological forcing over time scales on the order of 1-2 weeks. Also, by piecing together data obtained from before and after the gaps, one can get a feeling for seasonal scale variations in wind stress, evaporation, air temperature, and insolation.

The WES data base is also well suited for characterizing east-west spatial coherence across the northern part of Florida Bay. Both the PVD plots of wind stress and the calculations of the correlation and mean veering of wind vectors suggest that wind forcing across the entire northern part of the bay is very similar. High correlations were found in spite of station-to-station differences in locations relative to the nearest keys. One can therefore tentatively conclude that "wind shadow effects" were not a serious problem. Calculations have not been made to compare WES data with the CMAN data in the southern part of the bay, but this would constitute a useful follow-up to the work done for this report.

A shortcoming in the data base was the lack of water temperature needed for quantifying evaporative losses. Two alternatives were available (ADP bottom temperatures and CMAN middepth temperatures), but neither was an entirely acceptable alternative for surface temperature at the study site. The availability of CMAN air temperatures and water

temperatures provided a regression equation for estimating water temperature at the WES stations, but the 1.44°C standard error introduced an error in the relative humidity calculations. It is likely, however, that a greater source of error is the absence of surface temperature data from the extensive mud flats that are found throughout Florida Bay. Water temperatures over mud flats are probably significantly higher in summer and lower in winter. If so, evaporative losses in summer and winter would be correspondingly higher and lower. This might not change the cumulative annual water loss, but it could affect the seasonal cycle. Without a better indication of surface temperature in both shallow and "deep" water throughout the bay, the seasonal variation in evaporative water loss and the evaporation rate within any given season are subjects for follow-up studies.

Wind data obtained during the March 1996 to April 1997 one-year period support in a general way the annual cycle that has been found in previous one-year weather records from throughout the keys. The pattern consists of easterly winds (westward wind stress) during spring and summer months, followed by northeasterly winds (southwestward wind stress) during fall and winter months. The change from one pattern to another can be surprisingly abrupt. Some interannual--or perhaps spatial--variability is apparent with each new plot, but basically the same pattern emerges from one year to the next.

Annual evaporation totals result in large annual evaporative losses. Combining the 75 cm y^{-1} local water loss with the 2,140-km^2 surface area of Florida Bay east of the 81°05'W meridian, one obtains a total water loss of 1,605 x 10^6 m^3 per year, which is equivalent to just over 68 m^3 s^{-1}. This is an important result obtained from the WES data base, because it is one of the components needed for an understanding of the water balance of Florida Bay.

LITERATURE CITED

Brocks, K. 1962. Results of wind profile measurements above the sea. Proc. Symp. Math. Hydrodyn. Methods of Phys. Oceanogr., Hamburg, 1961, pp. 409-410.

Hsu, S.A. 1978. Micrometeorological fluxes in estuaries. Pages 125-134 in: Estuarine Transport Processes (B.J. Kjerfve, ed.), Univ. of South Carolina Press, Columbia, SC.

Kourafalou, V.H., T.N. Lee and L-Y Oey. 1996. The fate of river discharge on the continental shelf, 2. Transport of coastal low-salinity saters under realistic wind and tidal forcing. Journ. of Geophys. Research 101:3435-3455.

Kundu, P. 1976. Ekman veering observed near the ocean bottom. J. Phys. Ocean. 6:238-242.

List, R.J. 1963. Smithsonian Meteorological Tables (6th rev. ed.). Smithsonian Institution, Washington, D.C., 527 pp.

Murray, F.W. 1967. On the computation of saturation vapor pressure. Journ. of Applied Meteorology 6:203-204.

Pond, S., D. Fissel and C. Paulson. 1974. A note on bulk aerodynamic coefficients for sensible heat and moisture fluxes. Boundary-Layer Meteorology 6:333-339.

Smith, N.P. 1997. An analysis of acoustic doppler profiler data from Western Florida Bay. Final Report (Appendix C) to the U.S. Army Engineer Waterways Experiment Station, for Contract DACW17-96-M-0420, 30 pages.

Wu, J. 1980. Wind-stress coefficients over sea surface near neutral conditions--a revisit. Journ. of Physical Oceanography 10:727-740.

Table B1
Time Periods of Available and Missing Weather Data
March 1996 to April 1997

Station No.	Location	Dates Available	Dates Missing
A	Johnson Key Station	March 14 to June 13, 1996	June 13 to July 23, 1996
		July 23 to November 5, 1996	November 5 to December 6, 1996
		December 6, 1996 to April 23, 1997	
B	Buttonwood Key Station	March 15 to April 20, 1996	April 20 t0 May 30, 1996
		May 30 to June 12, 1996	June 12 to July 22, 1996
		July 22 to November 5, 1996	November 5 to December 6, 1996
		December 6, 1996 to April 11, 1997	April 12 to April 24, 1997
C	Butternut Key Station	March 16 to April 20, 1996	April 20 to May 30, 1996
		May 30 to June 12, 1996	June 12 to July 22, 1996
		July 22 to November 5, 1996	November 5 to December 6, 1996
		December 6, 1996 to April 24, 1997	

Table B2
Correlation Values (Upper Right) and Mean Deflections (Lower Left) of Hourly Wind Values Recorded at Stations A, B, and C December 7, 1996-April 11, 1997

Station No.	Location	Weather Station		
		A	B	C
A	Johnson Key	-	0.947	0.917
B	Buttonwood Key	-1.6^0	-	0.946
C	Butternut Key	-0.8^0	$+1.0^0$	-

Note: Deflections indicate the mean counterclockwise veering at the station identified along the left side of the matrix relative to the station identified along the top of the matrix.

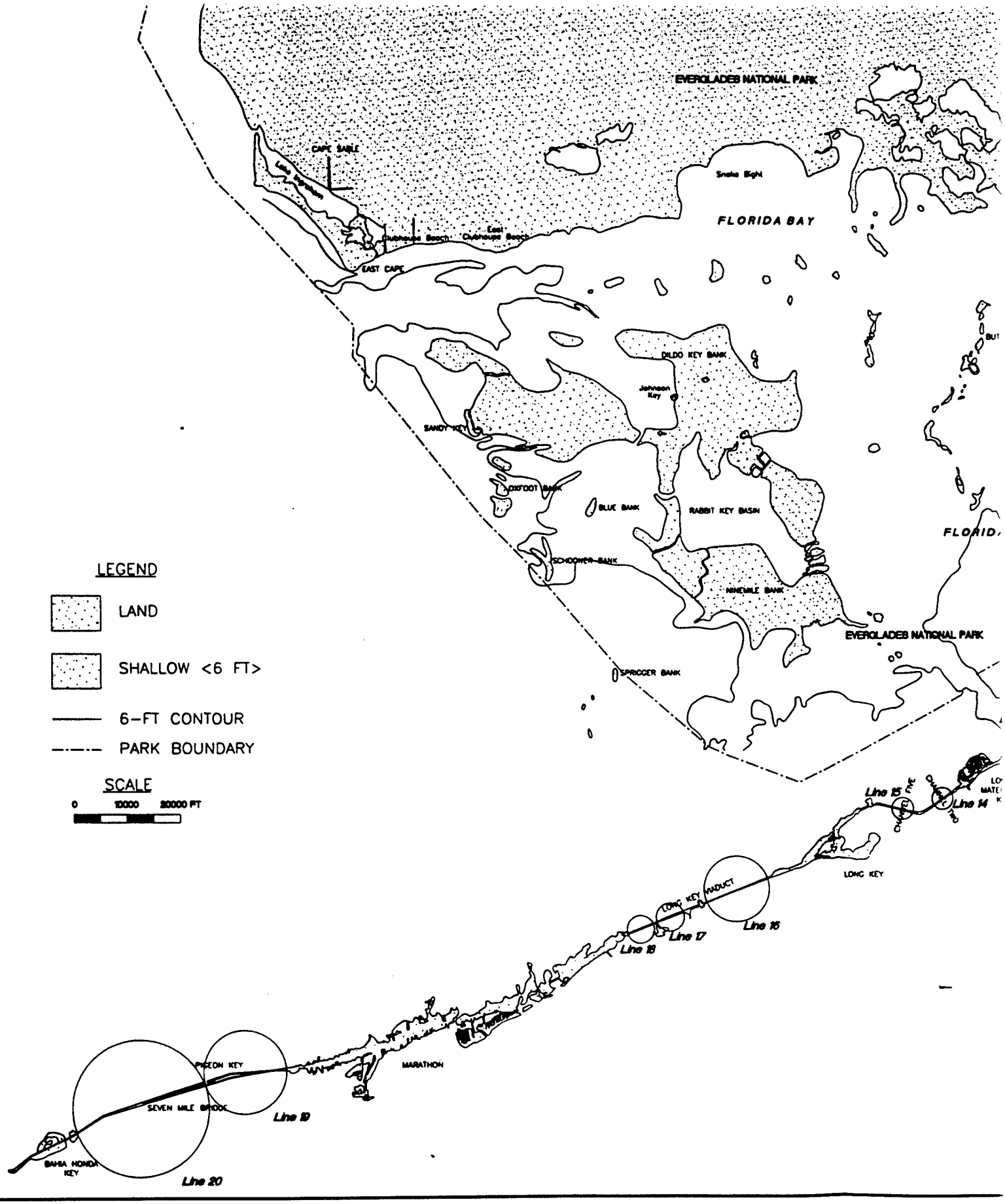

Appendix B An Analysis of Weather Data from Northern Florida Bay

1

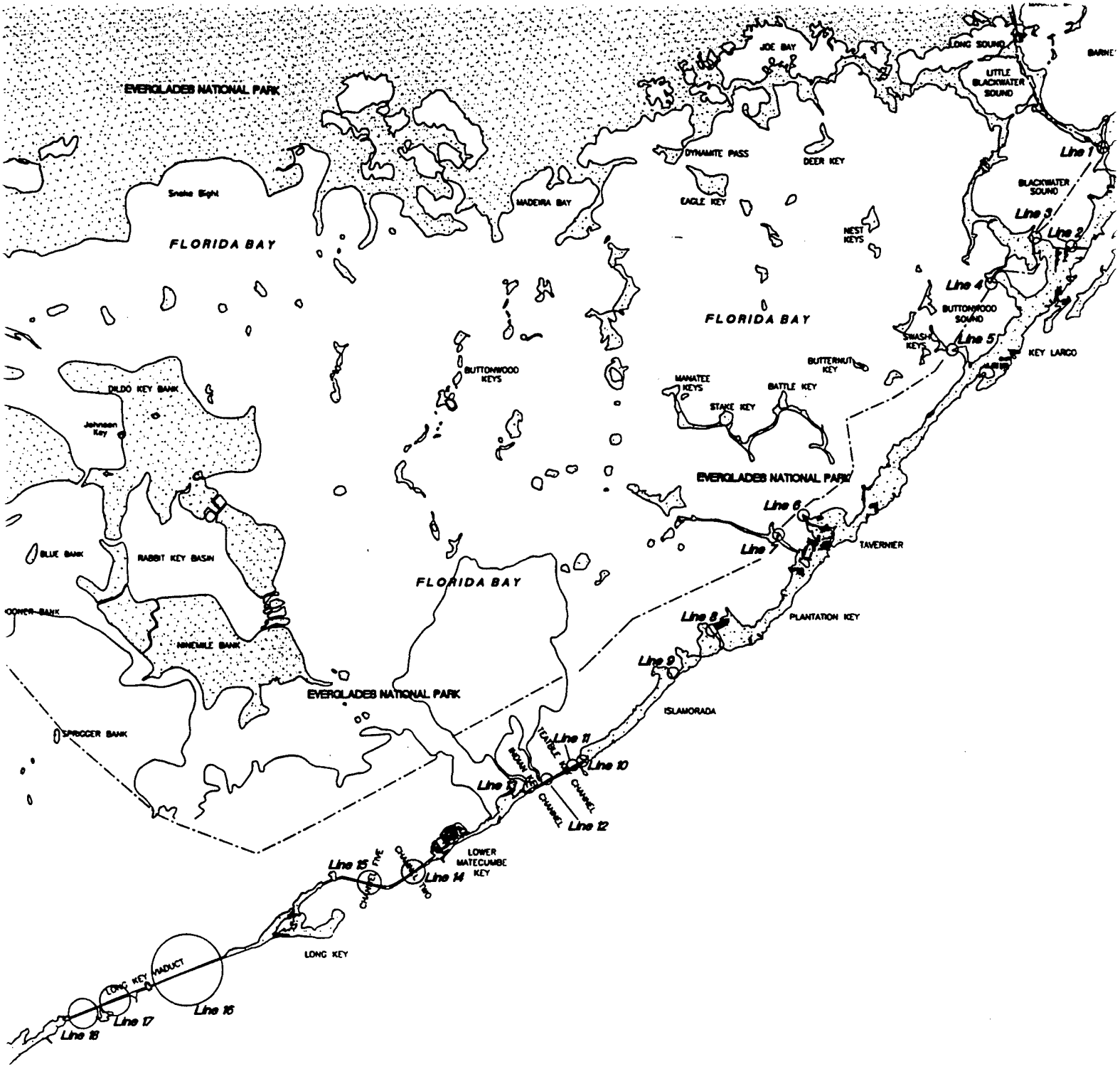

INTENSIVE SURVEY TR
LOCATION MA

(2)

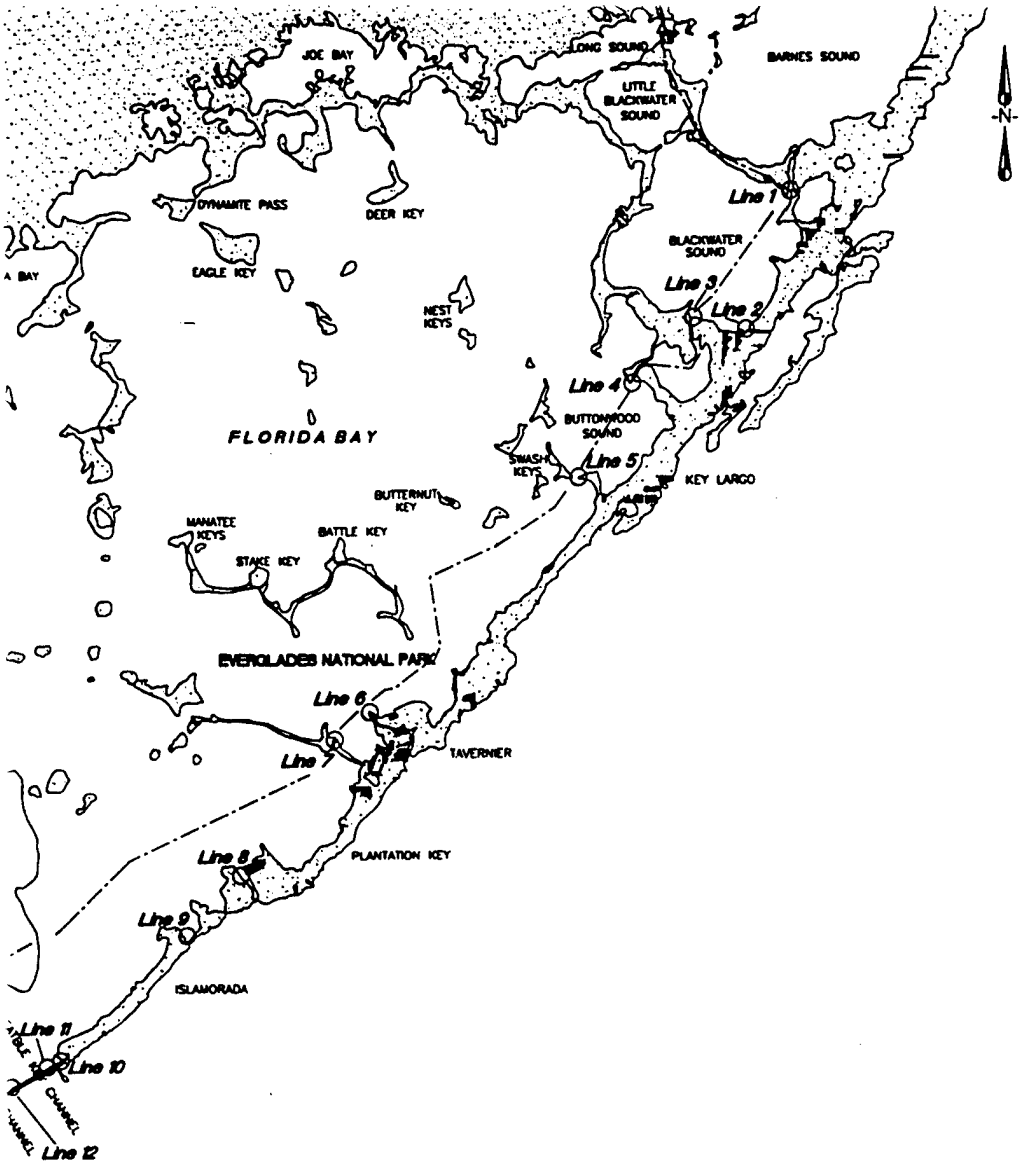

INTENSIVE SURVEY TRANSECT
LOCATION MAP

Figure B1

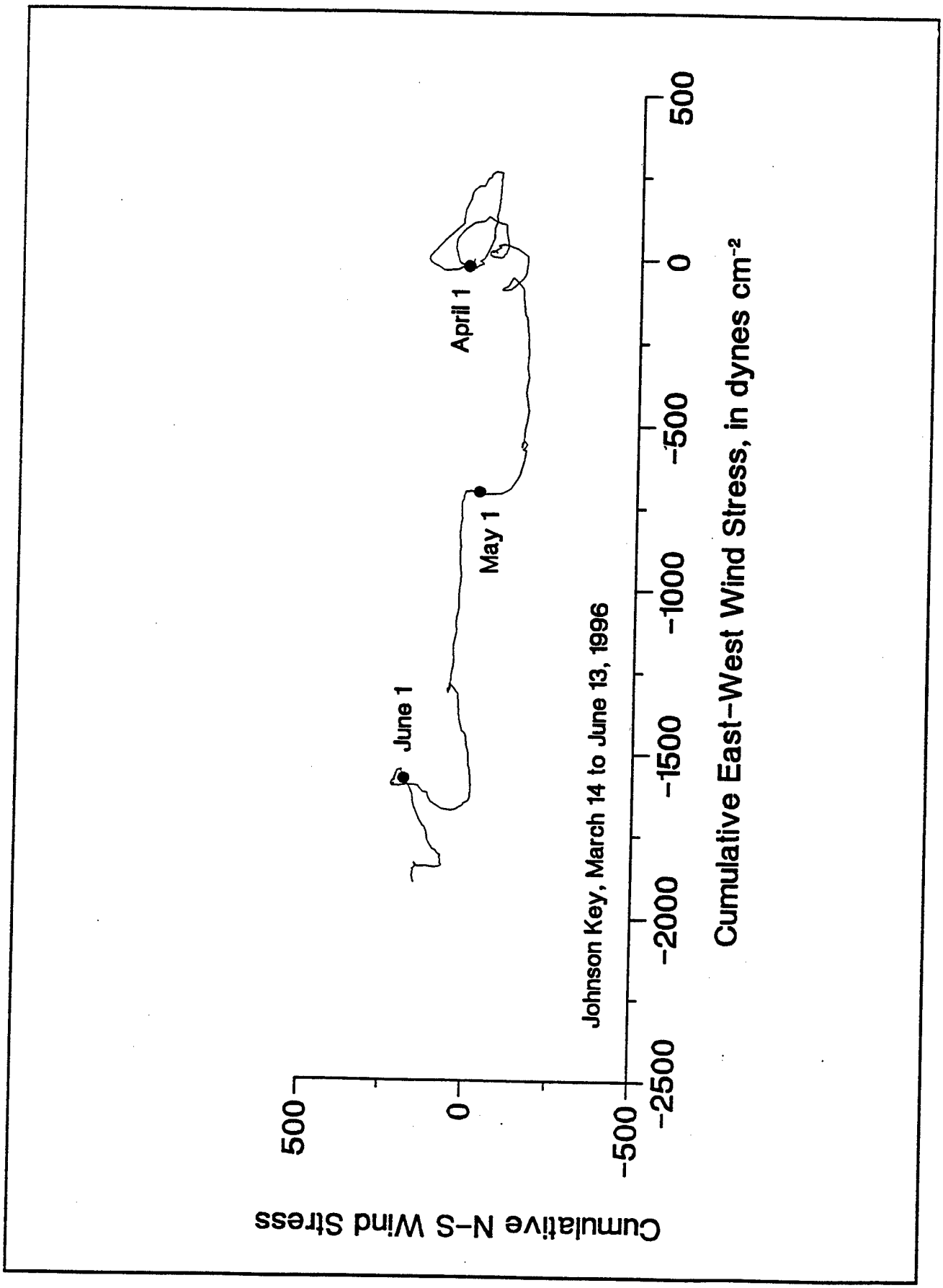
Cumulative N-S Wind Stress
500
0
-500
-2500
-2000
-1500
-1000
-500
0
500
Cumulative East-West Wind Stress, in dynes cm⁻²
Johnson Key, March 14 to June 13, 1996
June 1
May 1
April 1

Figure B2

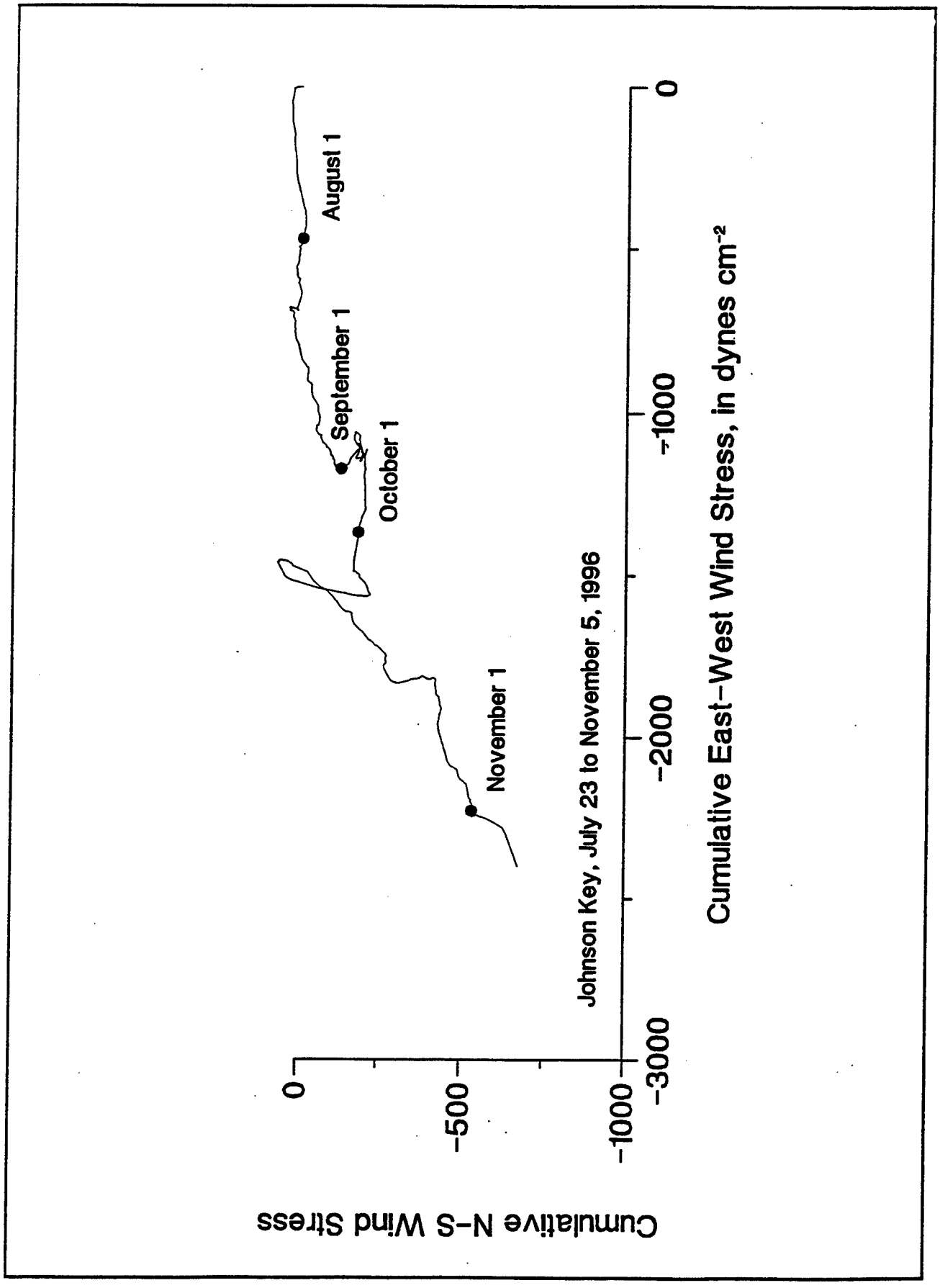
Cumulative N-S Wind Stress
0
-500
-1000
-3000
-2000
-1000
0
Cumulative East-West Wind Stress, in dynes cm⁻²
Johnson Key, July 23 to November 5, 1996
August 1
September 1
October 1
November 1

Figure B3

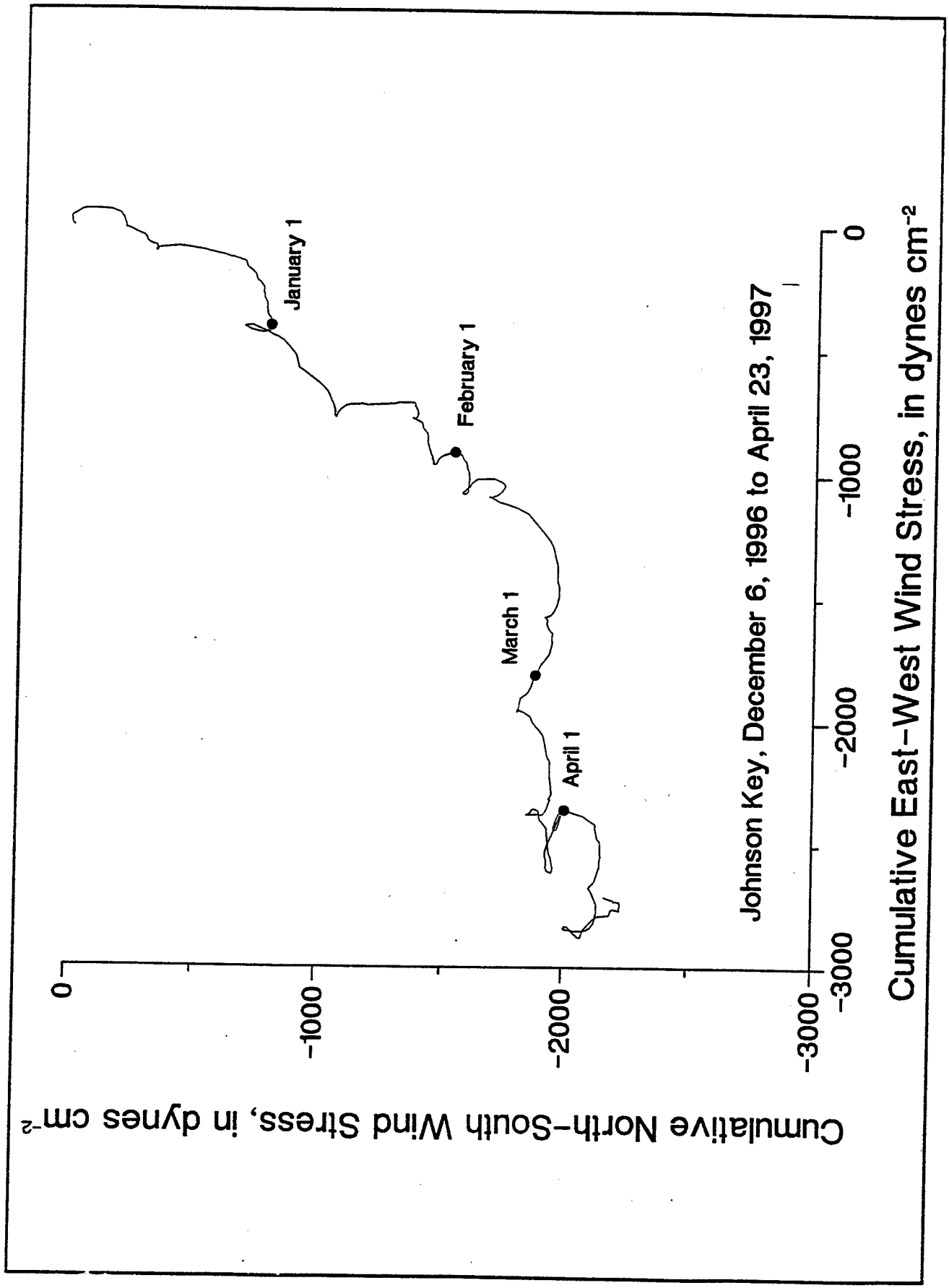
Johnson Key, December 6, 1996 to April 23, 1997
Cumulative East-West Wind Stress, in dynes cm-2
Cumulative North-South Wind Stress, in dynes cm-2
0
-1000
-2000
-3000
January 1
February 1
March 1
April 1

Figure B4

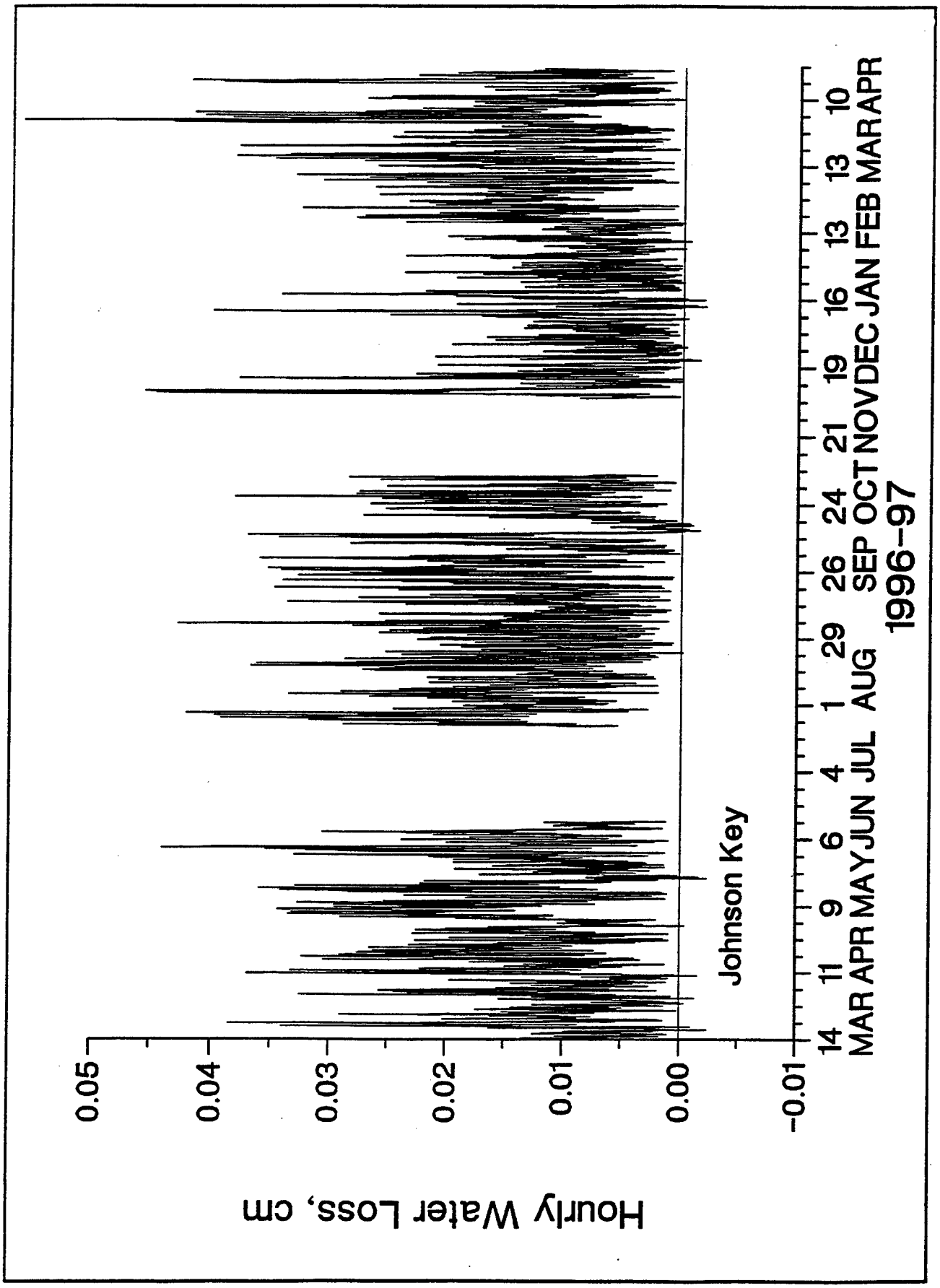
Hourly Water Loss, cm
0.05
0.04
0.03
0.02
0.01
0.00
-0.01
Johnson Key
14 11 9 6 4 1 29 26 24 21 19 16 13 13 10
MAR APR MAY JUN JUL AUG SEP OCT NOV DEC JAN FEB MAR APR
1996-97

Figure B5

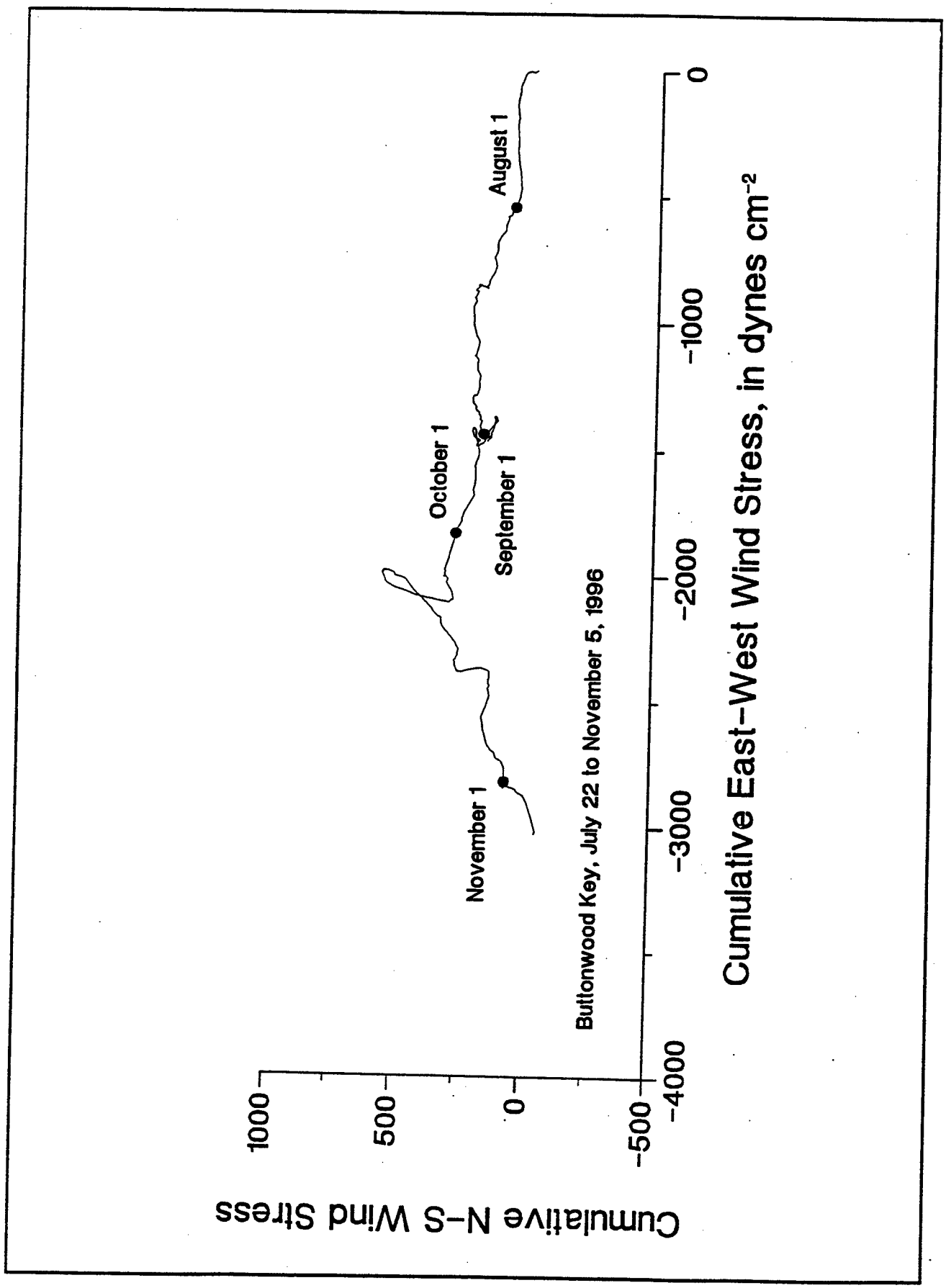
Cumulative N–S Wind Stress
1000
500
0
-500
Cumulative East–West Wind Stress, in dynes cm^{-2}
0
-1000
-2000
-3000
-4000
August 1
September 1
October 1
November 1
Buttonwood Key, July 22 to November 5, 1996

Figure B6

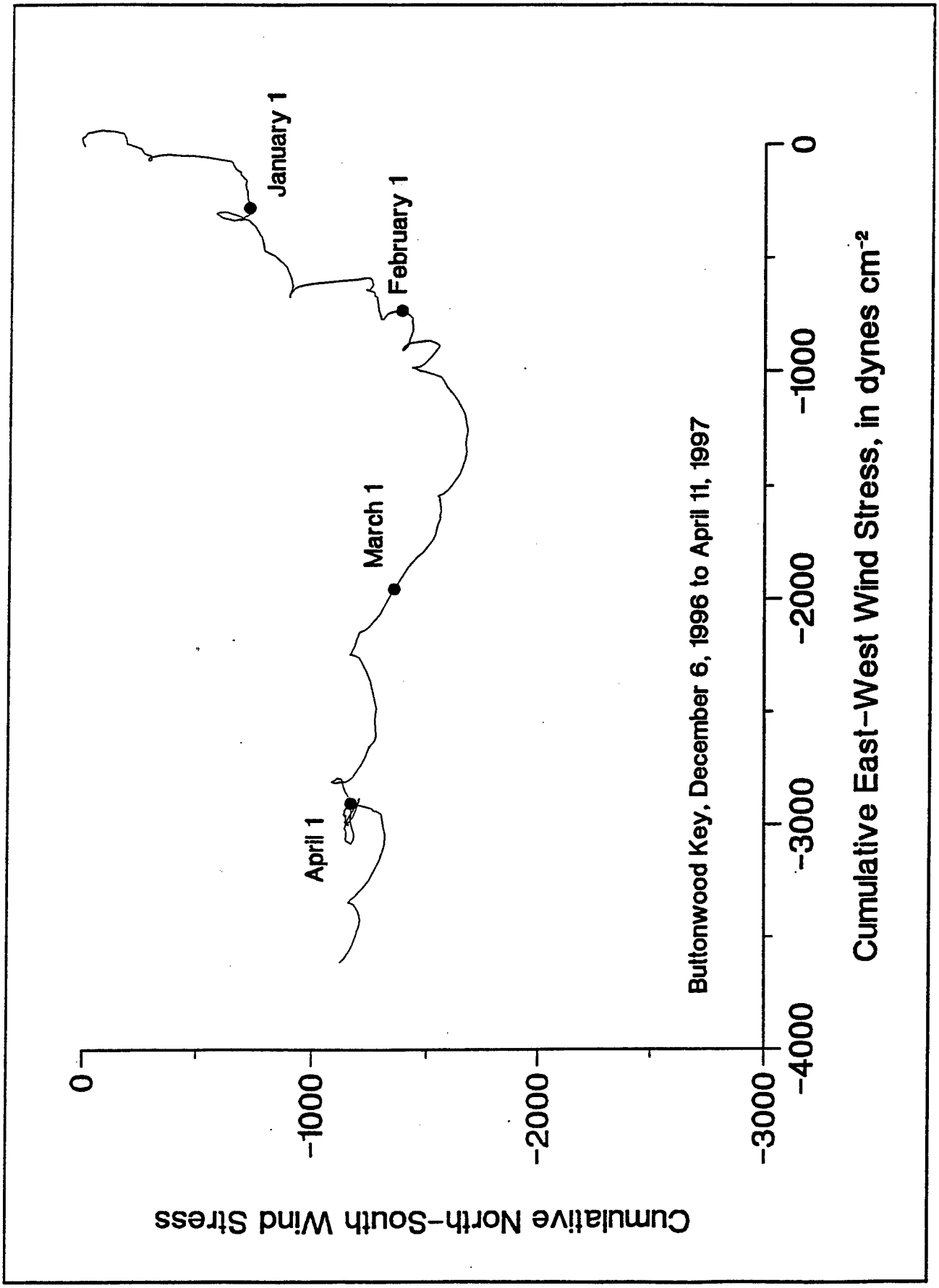
Cumulative North-South Wind Stress
0
-1000
-2000
-3000
Cumulative East-West Wind Stress, in dynes cm-2
0
-1000
-2000
-3000
-4000
Buttonwood Key, December 6, 1996 to April 11, 1997
January 1
February 1
March 1
April 1

Figure B7

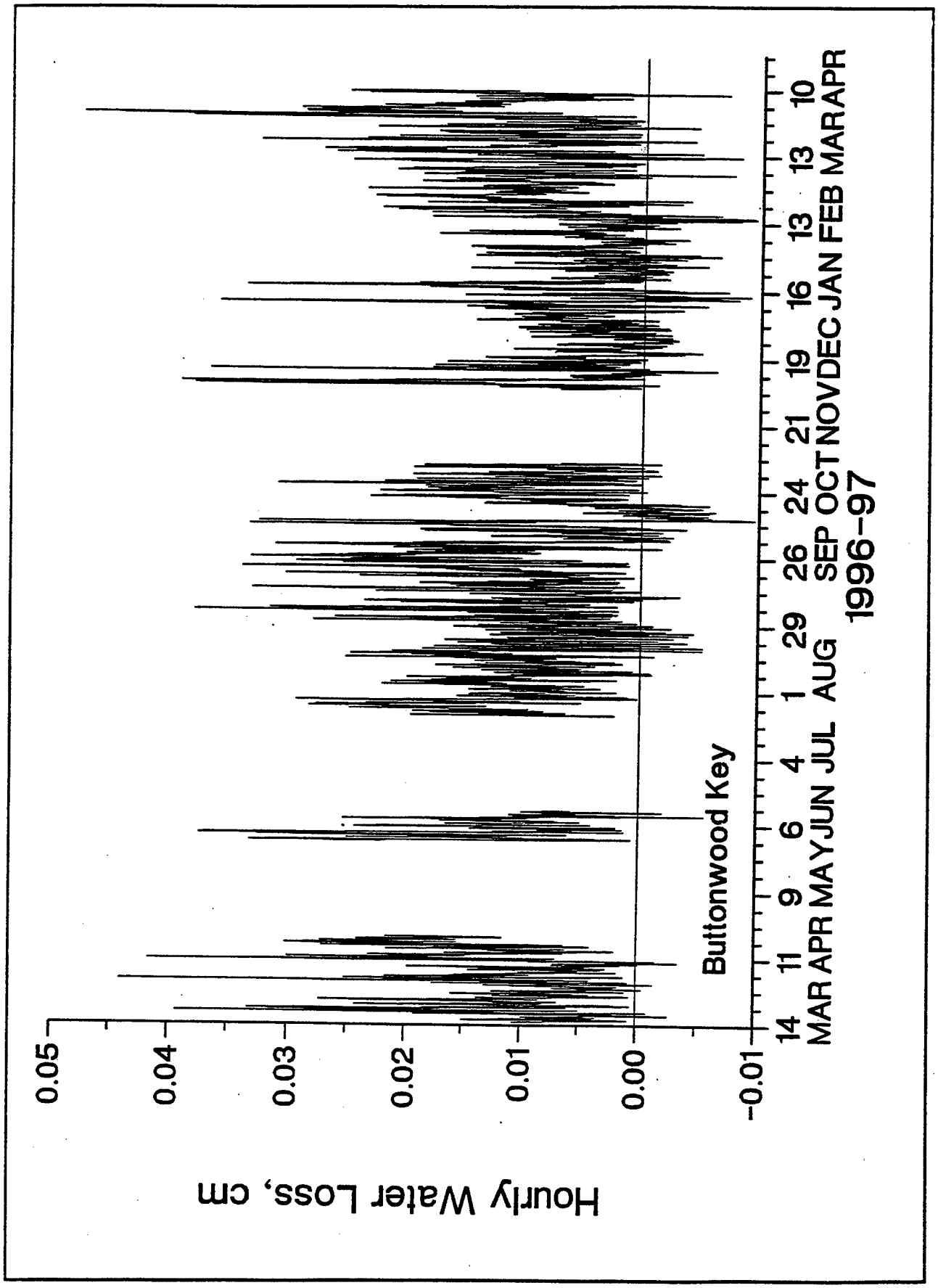
Hourly Water Loss, cm
0.05
0.04
0.03
0.02
0.01
0.00
-0.01
Buttonwood Key
14 11 9 6 4 1 29 26 24 21 19 16 13 13 10
MAR APR MAY JUN JUL AUG SEP OCT NOV DEC JAN FEB MAR APR
1996-97

Figure B8

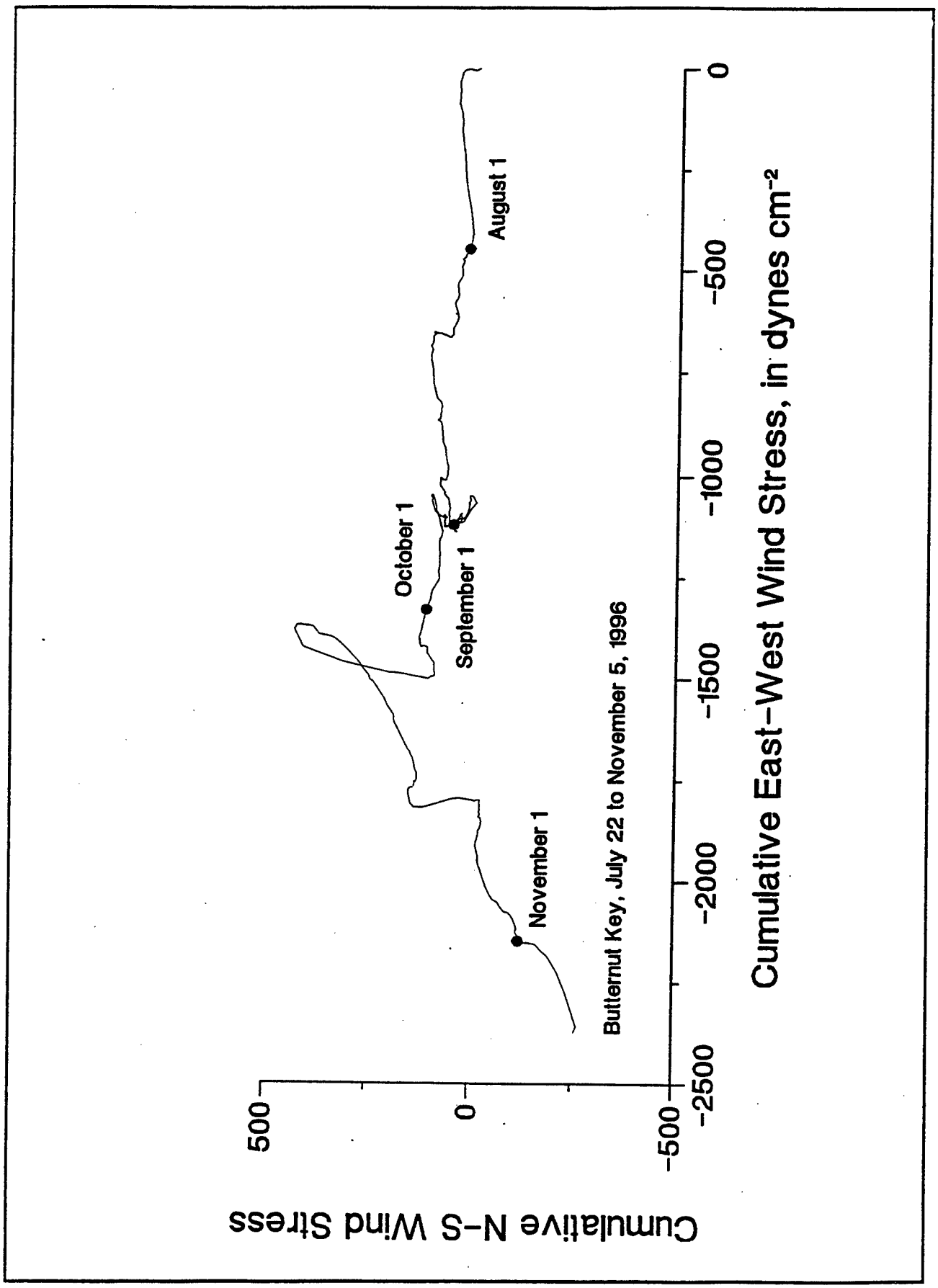
Cumulative East-West Wind Stress, in dynes cm⁻²
0
-500
-1000
-1500
-2000
-2500
Cumulative N-S Wind Stress
500
0
-500
August 1
September 1
October 1
November 1
Buttermut Key, July 22 to November 5, 1996

Figure B9

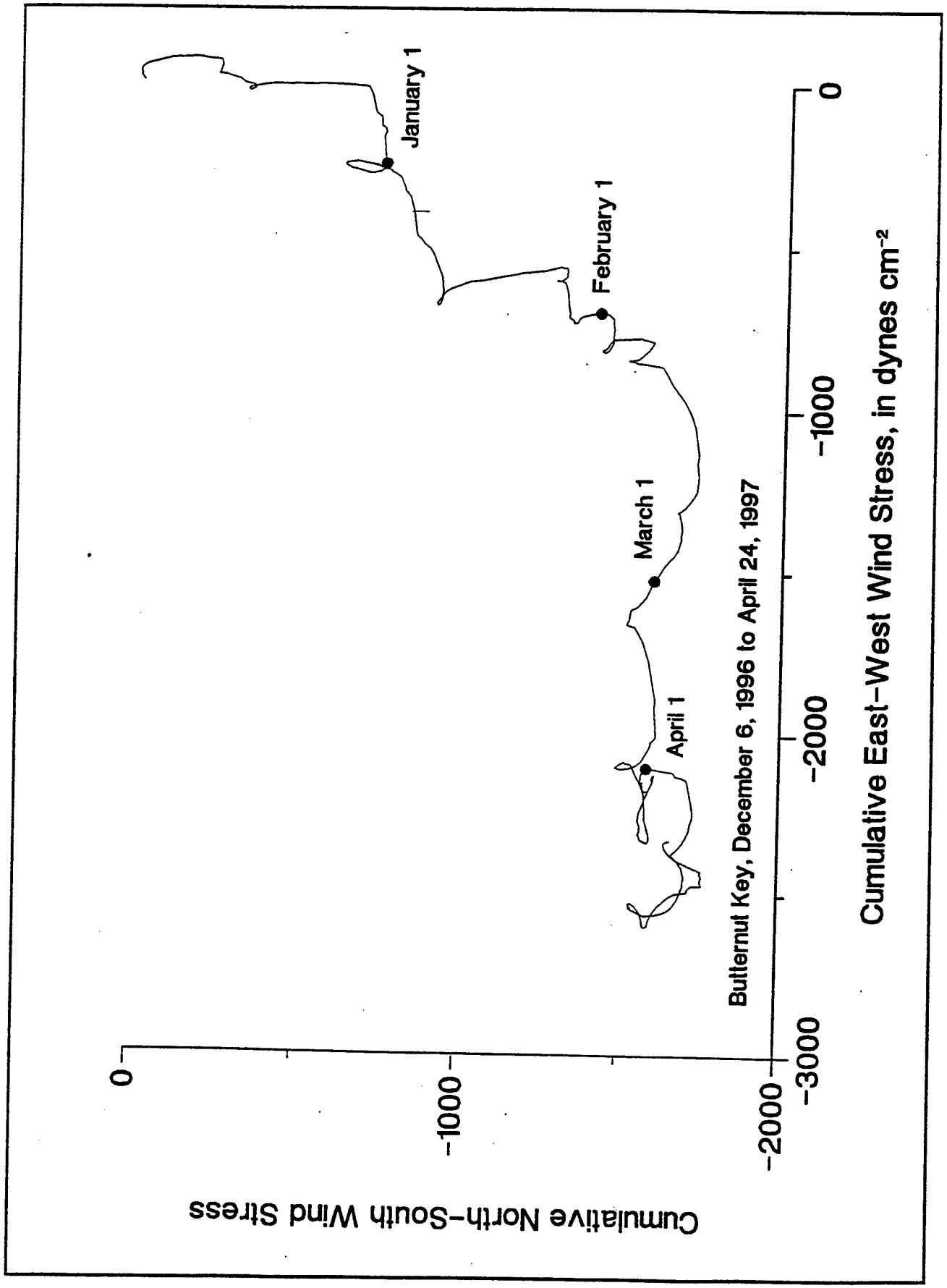
Cumulative North–South Wind Stress
0
-1000
-2000
Cumulative East–West Wind Stress, in dynes cm⁻²
0
-1000
-2000
-3000
January 1
February 1
March 1
April 1
Butternut Key, December 6, 1996 to April 24, 1997

Figure B10

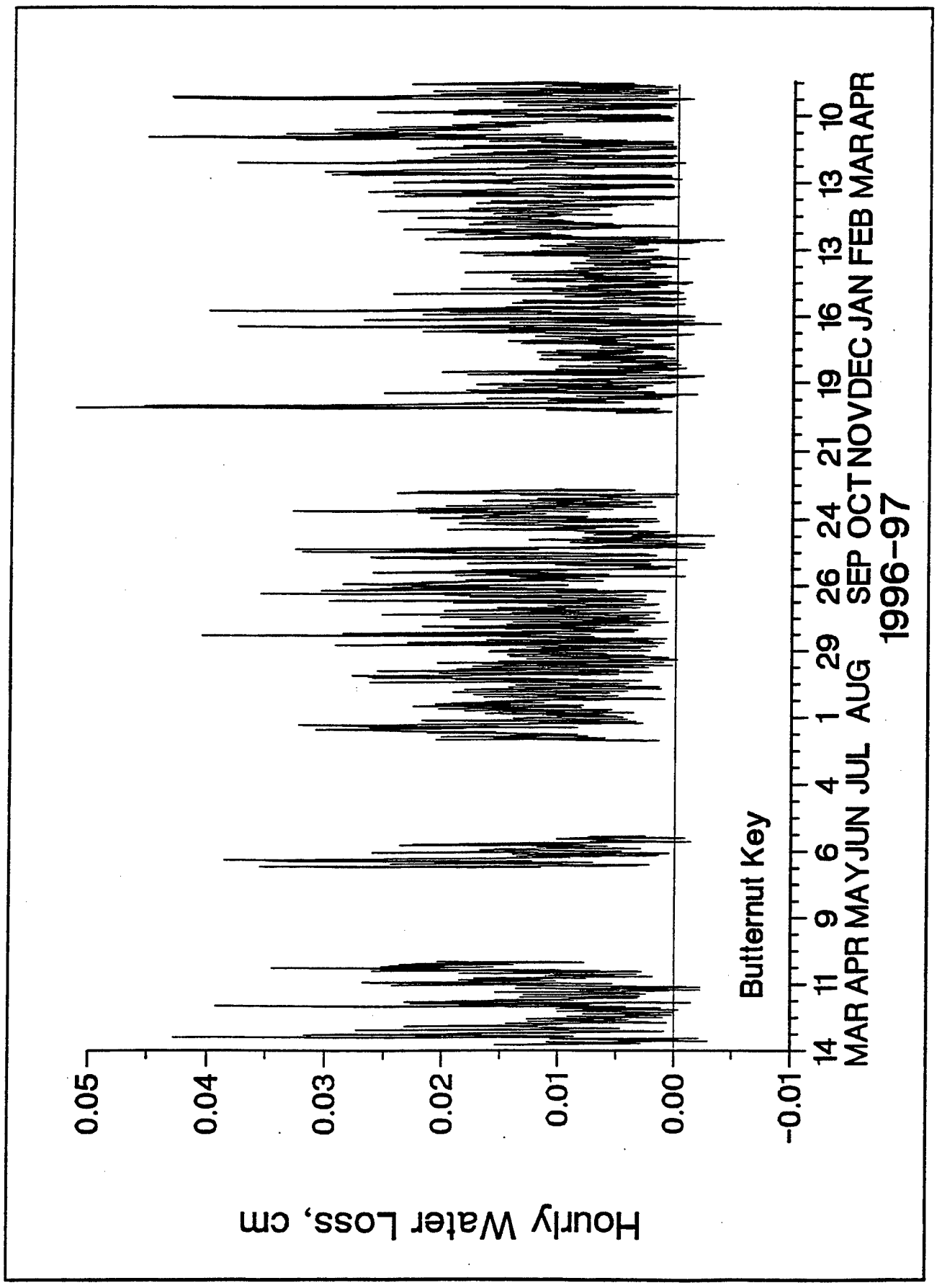
Hourly Water Loss, cm
0.05
0.04
0.03
0.02
0.01
0.00
-0.01
Butternut Key
14 11 9 6 4 1 29 26 24 21 19 16 13 13 10
MAR APR MAY JUN JUL AUG SEP OCT NOV DEC JAN FEB MAR APR
1996-97

Figure B11

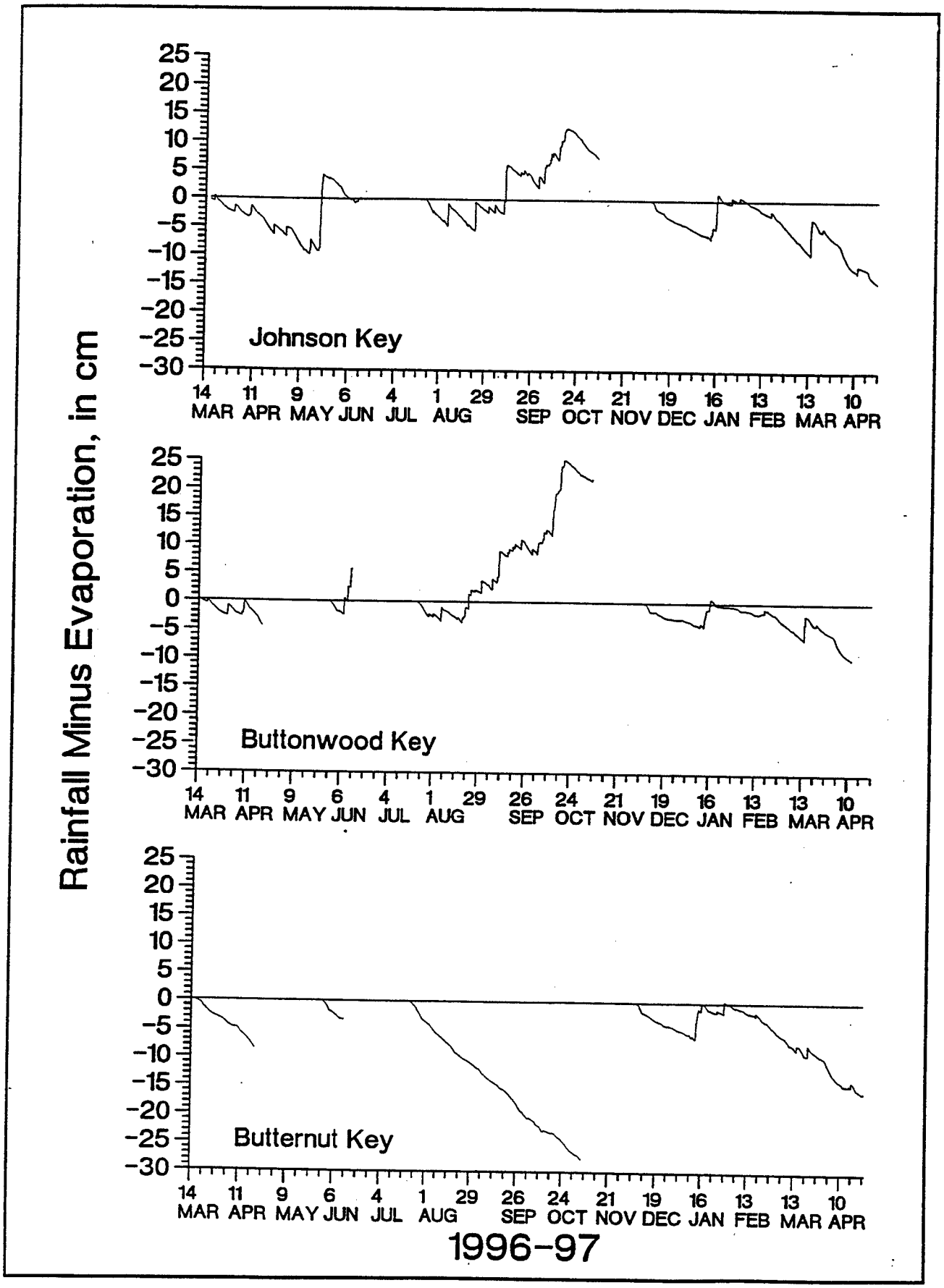
Rainfall Minus Evaporation, in cm
25
20
15
10
5
0
-5
-10
-15
-20
-25
-30
Johnson Key
Buttonwood Key
Butternut Key
14 MAR
11 APR
9 MAY
6 JUN
4 JUL
1 AUG
29 AUG
26 SEP
24 OCT
21 NOV
19 DEC
16 JAN
13 FEB
13 MAR
10 APR
1996-97

Figure B12

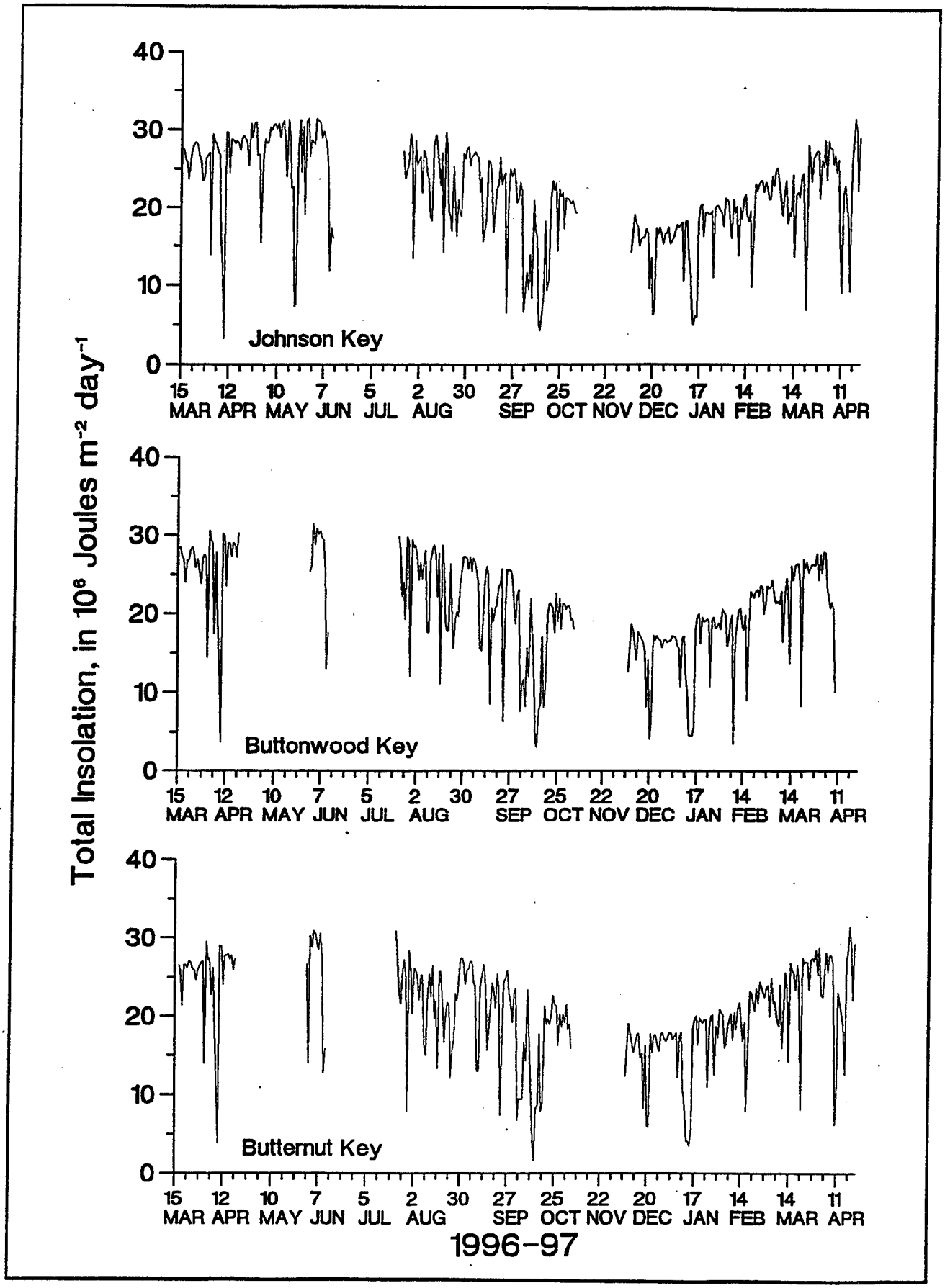
Total Insolation, in 10^6 Joules m^{-2} day^{-1}
Johnson Key
Buttonwood Key
Butternut Key
0
10
20
30
40
15 MAR
12 APR
10 MAY
7 JUN
5 JUL
2 AUG
30 SEP
27 OCT
25 NOV
22 DEC
20 JAN
17 FEB
14 MAR
14 APR
11 APR
1996-97

Figure B13

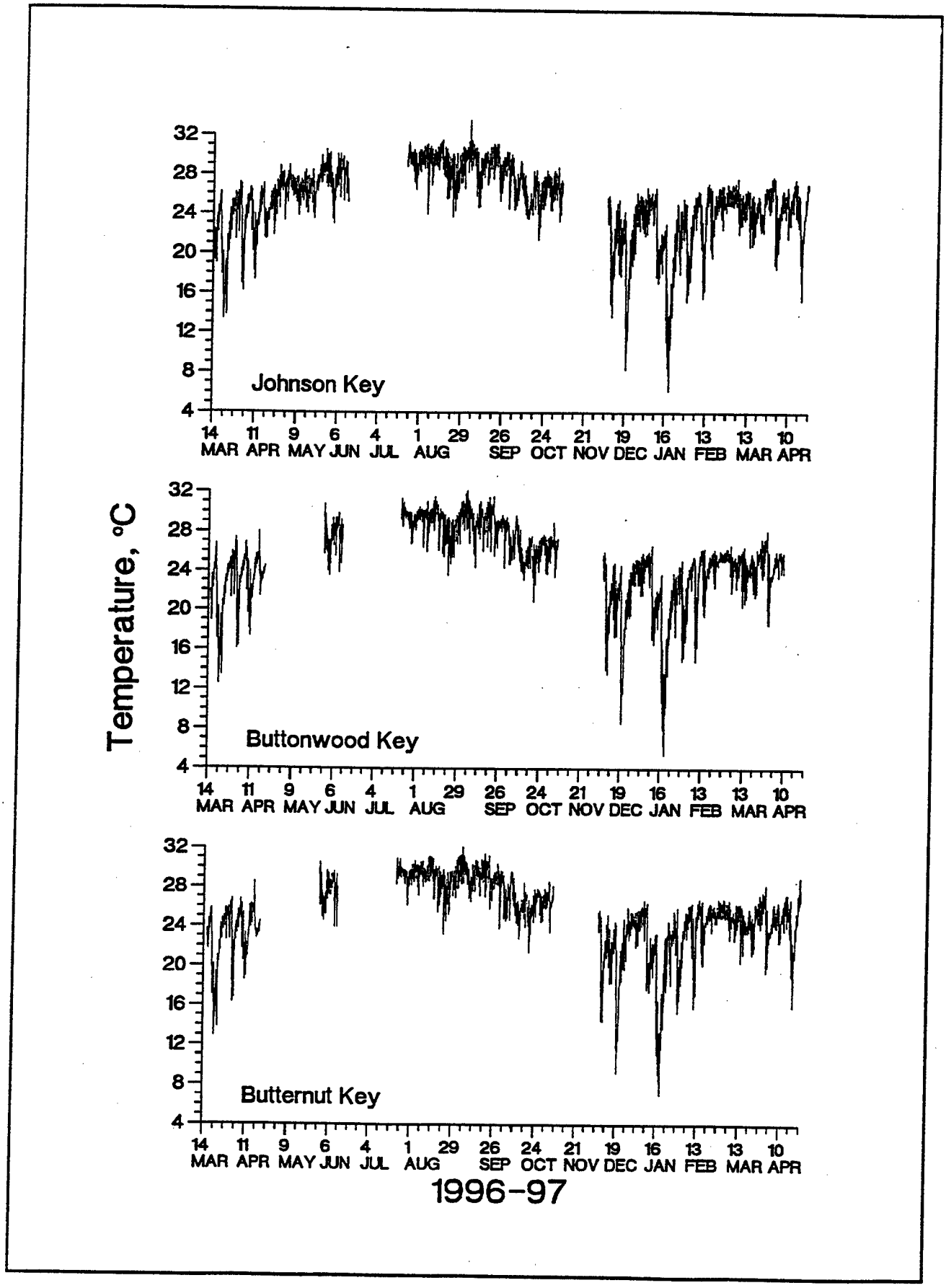
Temperature, °C
32
28
24
20
16
12
8
4
Johnson Key
Buttonwood Key
Butternut Key
14 11 9 6 4 1 29 26 24 21 19 16 13 13 10
MAR APR MAY JUN JUL AUG SEP OCT NOV DEC JAN FEB MAR APR
1996-97

Figure B14

APPENDIX C

AN ANALYSIS OF ACOUSTIC DOPPLER PROFILER DATA FROM WESTERN FLORIDA BAY

The contents of this appendix are to provide information on the additional analysis of the ADP data provided by the Harbor Branch Oceanographic Institution (HBOI) in support of the hydrodynamic numerical modeling effort. The result of this analysis is to provide various harmonic constituents (amplitude and phase) of the vertically averaged currents, cumulative net transport (inflow or outflow), and wind-drift speeds and directions. A detailed summary of the HBOI analyses of the ADP data is provided herein.

An Analysis of Acoustic Doppler Profiler Data from Western Florida Bay

Ned P. Smith
Harbor Branch Oceanographic Institution
5600 U.S. Highway 1, North
Fort Pierce, Florida 34946

INTRODUCTION

In mid-March 1996, the U. S. Army Engineer Waterways Experiment Station (WES) initiated a field study that included three study sites along the 81°05'W meridian, a north-south line from East Cape on the southwest tip of the Florida Peninsula to the west end of Vaca Key (Stations 1-3 in Figure C1). The 81°05'W meridian is often taken to represent the western boundary of Florida Bay. The same boundary was used in an earlier (mid-March 1994 to early April 1994) Harbor Branch Oceanographic Institution (HBOI) study designed to investigate east-west exchanges between Florida Bay and the inner shelf of the eastern Gulf of Mexico.

The northern station (Station 1) was at latitude 25°04' 59.78"N, the central station (Station 2) was at 24°54' 59.51"N, and the southern station (Station 3) was at 24°46' 59.51"N. The northern study site was 0.12 n.m. south of the northernmost HBOI study site, the central study site was 2.51 n.m. south of the central HBOI site, and the southern study site was 3.07 n.m. south of the southernmost HBOI site. Both studies, however, provide data from stations that are approximately equally spaced along the open western boundary of Florida Bay.

In a February 29, 1996, response to a Request for Quotations issued by the Jacksonville District Office, HBOI offered to analyze the Acoustic Doppler Profiler (ADP) data in support of a parallel modeling effort that was underway at WES. Included in the Scope of Work was Task 1: "Develop the methodology to quantify the total and tidal transport at long-term ADP stations in the western bay." A later (October 7, 1996), more specific listing of the collaborative research effort included the following:

a. WES will provide HBOI with bottom anchored ADP data from three stations in western Florida Bay. The format of the data will be mutually agreed upon and WES will provide initial data reduction as required to meet format specifications (first 6 months of data - Oct/Nov 1996; second 6 months of data - Mar/Apr 1997).

b. HBOI will prepare analysis and report.

This report contains the analysis and interpretation of the ADP data. The purpose of the report is to provide an overview of the methodology used in the analysis, as well as to describe the results of the analysis.

Throughout the field study, WES personnel have plotted ADP data in relatively short-term segments. Variables such as current speed (x-, y-, and z-components) and direction, standard deviation of the current speed, etc., have been plotted over approximately one-month intervals. Thus, additional analog plots are not needed, and the methodology utilized for this report is intentionally confined to that which provides the bigger picture in a temporal sense and the vertically-averaged flow in a spatial sense. In some cases, ADP data have been combined with weather data collected nearby to establish relationships between the speed and direction of the current that arises in response to wind stress of a given magnitude and direction.

The application for the results of the analysis of the ADP data is the hydrodynamic model that is under development at WES. Specifically, the methodology is intended to:

(a) provide harmonic constants (amplitudes and local phase angles) of the vertically averaged current at the three study sites for comparison with model output from corresponding grid points in the model domain;

(b) provide cumulative net transport past each study site for comparison with model output from corresponding grid points in the model domain; and

(c) provide wind-drift speeds and directions past each study site for comparison with model output from corresponding grid points in the model domain under similar wind conditions.

Because the ADPs provide current speeds and directions at anywhere from four to twelve levels through the water column, the data are well suited for examining the fundamental decision to use a two-dimensional (2-D) model to simulate Florida Bay circulation. Comparison of flow patterns from the top and bottom levels will reveal a degree of similarity that quantifies the extent to which top and bottom layers move along with a similar speed and direction. To quantify top-to-bottom differences in current speed and direction, the report includes progressive vector diagrams (PVDs), harmonic constants, and correlation coefficients for top and bottom levels. To quantify the response to wind forcing, spectral analysis is used to calculate the gain (also known as the magnitude of the transfer function). The gain gives the current speed that arises in response to wind-stress forcing of a given magnitude.

THE DATA

The data used to characterize flow patterns at the three WES study sites are summarized in Table C1. The ADPs were programmed to record current speed and direction

every 15 min. Current profiles begin with a reading 69 cm above the instrument. Because the instrument has a height of about 14 cm, and assuming that the base of the instrument is flush with the sea floor, the midpoint of the first layer is approximately 83 cm above the bottom. The number of layers depends upon the water depth. Each layer above the bottom layer has a thickness of 29 cm, i.e., the indicated height ± 14.5 cm. Thus, the first layer extends from the sea floor to a height of 97.5 cm above the bottom. The speed assigned to the top layer rarely represents a full 29-cm layer, but the thickness can be determined from the water level that is recorded (to the nearest 10 cm) with each quarter-hour sample. In calculating transport, two assumptions were made regarding the current profile. First, it was assumed that the current profile in the lowest part of the water column was logarithmic. Second, it was assumed that the current speed remained constant above the highest level reported in the profile. The first assumption is probably a good one; because of wind forcing on the top layer, the second assumption is probably a poor one, but wind shear was not estimated to provide this refinement.

For unknown reasons, all three ADPs did not store data from time to time. Missing data occurred randomly, resulting in a serious problem, but one that could be handled given the scope of the study. Table C1 summarizes the data that were lost over the course of the study at each location. For example, at Station 1, 3,013 quarter-hour observations were lost out of a possible 38,820 15-min sampling periods. This represents a 7.76% loss. The treatment of the data is described in the following section, but it should be noted here that this data loss presented special difficulties when top-of-the-hour values were needed for harmonic analysis to identify the principal tidal constituents. Fortunately, about 80% of the time the dropped observations were single missing values within a given hour. But in about 9% of the cases, two observations were missing within a single hour, and occasionally an hour had three of the four values missing. All three ADPs performed similarly. It is felt, however, that the available data base is satisfactory for all intended purposes (tidal analyses, spectral analyses, and progressive vector diagram plots) of this report.

A second problem, unique to Station 3, was detected in the data from December 5, 1996, to January 8, 1997. Following a data gap that may coincide with a periodic servicing of the instrument, current speeds became very erratic and generally higher. A plot of current speeds (not shown) confirmed that the data contained unacceptable errors in three forms. First, many current speeds were in the 100- to 200-cm s^{-1} range--nearly an order of magnitude higher than anything seen before December 5 or following January 8. Second, current speeds often increased and decreased erratically from one 15-min observation to the next. Third, the current profiles sometimes showed current speeds decreasing dramatically with height above the bottom. One would logically expect current speeds to increase with height above the sea floor. For these reasons, this 34-day segment of the data from the southern station was not included in the analysis.

Data from Station 2 recorded between June 26 and July 1, 1996, were also contaminated. Thus, data available for comparison with wind data vary from one station to

the next. The longest time interval for comparing flow patterns at all three study sites is the 105-day period from July 23 to November 5, 1996.

METHODOLOGY

(a) Vertical Integration of Current Profiles

The important first step in the analysis of the ADP data was the vertical integration of the current speeds and directions to obtain a single speed and direction that represents the entire water column. This vertically-integrated value will be directly comparable with the current speed and direction simulated by the 2-D model. As noted above, it was assumed that the current in the lowest part of the water column (below the first reported level) varied logarithmically in speed and did not vary in direction. Current speeds in a logarithmic profile will increase with height according to

$$u(z) = \frac{u_*}{k} \log_e \frac{z}{z_o} \qquad \text{(C1)}$$

where u(z) is the speed at height z above the bottom, u_* is the friction velocity, k is the von Kármán constant (0.41), and z_o is the roughness length. As a rule of thumb, z_o is 1/30th the size of the roughness elements (clam shells, sponges, sand grains, etc.) at the study site. A value of 0.1 cm was used here as a compromise representing the combined effect of sand grains, sand ripples, sea grasses, and an occasional sponge or sea fan. With an assumed value for z_o, the friction velocity can be determined from the current measured at the first level in the profile. The vertically integrated form of this expression gives the mean current speed, U:

$$U = \frac{u_*}{k(Z - z_o)} [Z \log_e \frac{Z}{z_o} - (Z - z_o)] \qquad \text{(C2)}$$

where Z in this case is the height of the water column to the top of the first layer reported by the ADP (83 + 14.5 = 97.5 cm). Incorporating known values for Z, z_o, and k, one obtains

$$U = 14.351 u_* = 0.875 u_{ref} \qquad \text{(C3)}$$

where u_{ref} is the current speed recorded for the first level by the ADP.

At higher levels in the profile, it is assumed that the current remains constant through the layer. At the top of the profile, it is assumed that the current speed remains constant above the last reported value. The thickness of the top layer is 29 cm plus the difference between the total water depth (which is recorded to within 5 cm) and the height above the bottom of the uppermost layer.

Given the current speed as a function of height above the bottom and the thickness of

the layer that each speed represents, two-dimensional transport, in $m^2 s^{-1}$, is given by the product of the speed and the thickness. The total 2-D transport is then the sum of the contributions from each of the n layers:

$$T_{2\text{-}D} = \sum_{i=1}^{n} U_i \, \Delta z_i \tag{C4}$$

Given the 2-D transport associated with any given quarter-hour observation, one can then calculate transport, analyze the time series to identify and quantify the principal tidal constituents, and compare transport with wind stress to investigate wind forcing. Because anywhere from 7 to 9% of the data were missing, padding was needed to fill incomplete hours (those with less than four observations), and interpolation was required to provide the top-of-the-hour value when that was missing.

Padding to fill incomplete hours was done by counting the number of observations that accumulated before the hour counter (appearing on the first line of the output) changed. Once the hour changed, indicating that no further data would be accumulated for the hour in question, the transport was multiplied by 4/m, where m is the number of observations accumulated for the hour. For example, if two quarter hours were recorded, m = 2, and 4/m = 2. Thus the transport that was accumulated for the hour from the two hours that were recorded was multiplied by 2 to approximate the transport that would have been accumulated from all four observations.

Determining the top-of-the-hour values was made difficult by the fact that occasionally two or even three successive 15-min values, including the top-of-the-hour observation, might be missing in a given part of the time series. To interpolate through a single missing value (C), given the two values preceding the gap (A and B) and the value following the gap (D), the missing value was estimated from

$$C = B + 0.5[(B-A) + (D-B)] = B + 0.5(D-A)] \tag{C5}$$

This value is midway between a continuation of the A-to-B slope and a direct interpolation from B to D. If two adjacent 15-min values were missing and observations A, B, and E were available to estimate C and D, the missing values were estimated from

$$C = B + 0.5\left[3B - A + \frac{1}{3}(E-B)\right]; \quad D = \frac{1}{3}[B + 2(B-A)] + \frac{2}{3}\left[B + \frac{2}{3}(E-B)\right] \tag{C6}$$

Interpolations were of course degraded when A was an interpolated value, but instances in which missing values were clustered in this way were rare. When six or more consecutive 15-min observations were missing, such as when an ADP was recovered for servicing, interpolation through the gap was by linear interpolation.

(b) Tidal Analysis

To identify the principal tidal constituents, the harmonic analysis program used by the

National Ocean Service on 29-day time series was used (Dennis and Long 1971). For both currents and vertically-integrated transport, the vectors were broken into east-west and north-south components. Within the context of this study, the east-west component is clearly of greater interest, because it is the east-west movement of water through the 81°05'W meridian that describes the exchange of water between Florida Bay and the inner shelf of the eastern Gulf of Mexico. When time series are considerably longer than 29 days, multiple harmonic analyses can provide several pairs of amplitudes and local phase angles for each of the principal tidal constituents. In these cases, harmonic constants are vector averaged to provide values more representative of the entire time series.

Given the amplitudes of the principal tidal constituents, one can calculate the tide-induced movement of water back and forth past the study site. For the ith constituent with amplitude A_i, the tidal excursion, T, is given by

$$T_i = \frac{A_i P_i}{\pi} \qquad \text{(C7)}$$

where P_i is the period of the constituent. If the amplitude is in km h^{-1} and the period, P, is in hours, the tidal excursion will be in km. One must be cautious when interpreting the tidal excursion in terms of how far a water parcel moves after passing the study site, but T_i is an accurate representation of flow at the study site itself.

Tidal analysis can involve model output as easily as it can involve field observations. Model output from a grid point corresponding to one of the ADP study sites can be analyzed to show which tidal constituents the model is reproducing. For transport calculations, it is crucially important that both amplitudes and local phase angles are being reproduced accurately for both the rise and fall of the water surface and the ebb and flood of the tide.

(c) Spectral Analysis

Although wind and current meter records were broken into relatively short segments, it was possible to use spectral analysis to quantify the relationship between wind forcing and the resulting wind-driven current (wind drift). Spectral analysis (Little and Schure 1988) provides energy density spectra (showing the time scales at which fluctuations of wind stress and current speed are most energetic), coherence spectra (showing the time scales at which wind stress and current are most tightly coupled), phase spectra (showing the time lead of wind-stress variations over the responding current), and gain spectra (quantifying the current speed that results from a given amount of wind-stress forcing). The coherence, phase, and gain spectra are all relevant within the context of model verification. Coherence spectra will confirm that wind drift does in fact exist at a given location in the bay, and they will reveal the band of time scales over which this coupling occurs. Phase spectra will then quantify the time lag of the wind-driven current, following an increase in wind speed or shift in wind direction. Both coherence spectra and phase spectra can be computed from model output as well as from field observations. Perhaps of greatest significance are the gain spectra, which will show the current speed that arises in response to a wind stress of, say, 1 dyne cm^{-2}. Again, comparison

with model output for the same wind forcing will show if the model is over- or underestimating wind-drift current speeds.

(d) Progressive Vector Diagrams

One of the best ways to summarize long time series of current speed and direction, or of 2-D (vertically integrated) transport, is with the PVD. The PVD is constructed by plotting current or transport vectors (magnitude and direction) in a head-to-tail manner. The resulting pattern shows how water moved past the study site, and it should not be interpreted as the movement of a water parcel (such as a drogue drift) away from the study site. The end points of the PVD, together with the time interval that separates them, can be used to calculate the resultant flow. The PVD is not especially well suited for tracking flow patterns over the shorter time scales of hours to days, but it summarizes general flow patterns nicely. When two PVDs, constructed from observations recorded in different parts of the water column, are plotted on the same x- and y-axes, one sees immediately if those two parts of the water column had similar current speeds and/or directions. Information of this kind is directly related to the decision to use a 2-D model.

(e) Vertical Coherence and Shear

Another way to summarize long time series of current speed from top and bottom layers in the water column--and thus to test the suitability of a 2-D model--is by calculating vertical correlation and the mean directional shear (Kundu 1976). Using the east-west (u-component) and north-south (v-component) currents from surface (subscript s) and bottom (subscript b) levels, two correlation components, κ_1 and κ_2, are calculated:

$$\kappa_1 = \frac{< u_s u_b + v_s v_b >}{< u_s^2 + v_s^2 >^{1/2} < u_b^2 + v_b^2 >^{1/2}}, \quad \kappa_2 = \frac{< u_s v_b - v_s u_b >}{< u_s^2 + v_s^2 >^{1/2} < u_b^2 + v_b^2 >^{1/2}} \tag{C8}$$

where the angle brackets, $< >$, represent a time average. The correlation coefficient is then given by

$$\kappa = (\kappa_1^2 + \kappa_2^2)^{1/2} \tag{C9}$$

The average counterclockwise angle, α, of the near-bottom current relative to the heading of the near-surface current is given by

$$\alpha = \tan^{-1} \frac{< u_s v_b - v_s u_b >}{< u_s u_b + v_s v_b >} \tag{C10}$$

An important difference between this approach and a comparison of PVDs constructed from top- and bottom-level currents is that α equally weights all the observations in the time series, whereas the PVD weights observations in direct relation to the magnitude of the vectors.

RESULTS

Results are grouped in four subsections dealing with (a) vertically integrated transport past each study site, (b) the tidal component of the total current, (c) vertical correlation and shear through the water column, and (d) the local response to wind forcing.

a. Two-dimensional Transport

Figure C2 shows the PVD of vertically integrated transport constructed from ADP data recorded at Station 1, just south of East Cape, from March 14, 1996, to April 22, 1997. The plot shows the movement of water past the study site, taking into account vertical differences in speed and direction throughout the water column, as well as the rise and fall in sea level. At this location, flow is tightly constrained by regional topographic features, including the southwest tip of the Florida Peninsula, and possibly by local topographic features that deflect near-bottom currents in a more southerly direction on both the flood and ebb (see DISCUSSION). Units of m^2 are obtained by summing the horizontal flow in each layer from surface to bottom.

The figure shows a relatively steady movement of water toward the southeast (a resultant direction of 140°). The cumulative net transport of approximately 3.93×10^6 m^2 during the 9,705 hours of the time series is equivalent to a depth-averaged transport of 0.113 $m^2\ s^{-1}$. Given the 3.07-m average water depth at the study site during that time period, this is also equivalent to an average current speed of 3.7 cm s^{-1}. The spacing of the dots that have been entered every two months provide a qualitative indication of the rate at which water moves past the study. The greater spacing from August to February suggests that inflow is somewhat greater from late summer through mid-winter.

The east-west component of the transport can be isolated from the ADP profiles to look specifically at inflow and outflow across the 81°05'W meridian. Figure C3 is a plot of 2-D transport into and out of Florida Bay just south of East Cape as a function of time during the 9,705-hr study. The positive slope indicates an inflow, and the relatively constant slope shows that the seasonal deviations from the mean 0.07 $m^2\ s^{-1}$ surface-to-bottom transport are correspondingly subtle. Given the mean water depth at the study site, the data indicate a long-term average inflow of 2.3 cm s^{-1}. Only during late April 1996 and from mid-February through mid-March 1997 does inflow into the bay decrease to negligible levels. The quasi-steady inflow, combined with the net outflow in the surface layer (see Figure C10), suggests that the movement of water into Florida Bay at this location is a result of a tidal pumping mechanism.

Figure C4 shows vertically integrated transport past the central study site, Station 2, from March 14 to June 27, 1996, before the four-day break in the record. The plot is basically similar to the one representing data collected at Station 1 for the same time period. The pattern shows a quasi-steady flow angling into Florida Bay. At this location, the resultant heading is toward 143°, and the magnitude of the resultant transport is 0.057 $m^2\ s^{-1}$. Again,

incorporating the 2.64-m average depth recorded during this time period, the vertically integrated transport is equivalent to a mean current speed of 2.2 cm s^{-1}. The east-west component of the total transport (not shown), representing the flow of water across the 81°05'W meridian and into Florida Bay, is 0.034 m^2 s^{-1}, and the resultant eastward speed is 1.3 cm s^{-1}.

Figure C5 is the continuation of Figure C4, showing transport past the central study site from July 1, 1996, to the end of the record on February 8, 1997. Inflow during the months of August and September is remarkably steady, and the resultant direction remains virtually unchanged during this two-month period. Transport from early October through mid-November, however, differs significantly from the quasi-steady southeastward transport recorded both before and after that time period. During this approximately six-week period, little net east-west transport is recorded. The transport vectors indicate a net southward movement of water past the study site. When inflow resumes in mid-November, it occurs at a slightly slower rate than that recorded during the first half of the plot. Because of the six-week period of anomalous transport, the long-term net value is reduced somewhat. During the full time period, the resultant transport is 0.05 m^2 s^{-1}, and the resultant speed is 1.9 cm s^{-1} along a heading of 140°.

A plot of the cumulative east-west transport as a function of time (Figure C6) shows clearly the temporary reduction in the net advective import of Gulf water to Florida Bay. The change in slope provides a clearer indication that the tide-induced movement of water into the bay is temporarily opposed by a nearly equal transport mechanism that by itself would act to remove water from the bay. The cause of this temporary balance is not entirely clear, but it is likely that wind forcing plays an important role. Wind stress recorded during October (see Figure C15) indicates that the first cold front of the 1996-97 winter season arrived on October 8th and that a distinct seasonal change in wind forcing occurred at that time.

Other fluctuations in the transport of Gulf shelf water into Florida Bay are relatively minor. In mid-January, a temporary reversal in transport occurs, but effects last only a few days. This, too, is presumably related to the passage of a cold front. A close look at the cumulative net eastward transport of water in the absence of perturbing effects suggests that a vertically integrated transport rate of about 0.047 m^2 s^{-1}. Dividing by the mean water depth of 2.6 m, this corresponds to a quasi-steady inflow of about 1.8 cm s^{-1} during the first part of the plot, and a value of about 0.33 m^2 s^{-1}, corresponding to a quasi-steady inflow of about 1.3 cm s^{-1}. The values obtained early and late in the record may represent components of a seasonal cycle.

Figure C7 is the PVD of vertically integrated transport at Station 3, the southern study site, from March 14 to December 5, 1996. The noteworthy feature in this plot is the net outflow from Florida Bay (negative east-west transport) as a result of relatively brief periods of westward transport that occurred during May and June, and again starting in early October. At other times, and for most of the study period, transport is directed southward, sometimes

with a slight eastward component, suggesting that Florida Bay experiences neither advective filling nor draining at this location for time periods of several weeks. For this 242-day time period, the resultant transport had a heading of 210°, and the resultant transport rate was 0.039 $m^2 s^{-1}$. Given the 1.88-m mean water depth at Station 3 during this time period, this corresponds to a mean current speed of 2.1 cm s^{-1}. For the the east-west component of the transport in particular, the net transport through the 81°05'W meridian during this time period was -0.018 $m^2 s^{-1}$, which is equivalent to an outflow of 1.0 cm s^{-1}.

It is noteworthy that the start of the period of most rapid outflow coincides closely in time with the October 8th frontal passage. It is reasonable to assume that distinct changes in regional circulation patterns will arise from seasonal changes in wind forcing, and this change from inflow to outflow across the 81°05'W meridian may be an example of such a change.

Figure C8 is the 1997 continuation of the progressive vectors computed from the 1996 transport data at Station 3. Because of the expanded scales on the x- and y-axes, the tidal ellipses are a prominent feature of the plot. The ellipses are relatively circular when wind forcing is minimal, but they lose their elliptical appearance completely when wind forcing is producing a strong nontidal current. The pattern during this second, 104-day pattern is similar to the pattern obtained between mid-March and early December. Net transport is in a west-southwestward direction, with a heading of 255°. The magnitude is 0.036 $m^2 s^{-1}$, which corresponds to a depth-averaged current speed of 1.9 cm s^{-1}.

Figure C9 shows the cumulative east-west transport past the study site at Station 3. This representation of the data suggests that periods of inflow into the bay are infrequent and relatively short-lived. Inflow is in progress in mid-March, at the start of the study, and it is not known how long this had been in progress when the ADP went into the water. The only other period of sustained inflow occurs during the month of September. Because it is followed by a period of unusually strong outflow, the eastward transport is little more than a short-term interruption of a quasi-steady transport that averages -0.019 $m^2 s^{-1}$, or -1.0 cm s^{-1}.

The general pattern suggested by the three ADP study sites includes a broad region of net inflow into Florida Bay, extending southward approximately 30 km from East Cape. The southernmost 15 km appears to be a region of net outflow. In the southern region, however, advective transport can be negligible for extended periods of time, or even reverse for shorter periods ranging from days to a few weeks. The quasi-steady inflow into the bay through the northern part of the open western boundary may be partly due to the larger tidal amplitudes in both currents and water levels (see the following section and Tables C2-C4).

b. Tidal Characteristics

Given the baseline role that tides play in forcing water into and through Florida Bay, an ability to reproduce tidal ebbs and floods closely will be an important capability of any hydrodynamic model. For this reason, tidal characteristics are presented in several forms and discussed at length. Tidal information presented here will provide crucial information in one

of two ways, depending on where the western boundary of Florida Bay is defined for the hydrodynamic model. First, if the 81°05'W meridian is used as the western boundary of the model, then the harmonic constants presented here represent the boundary conditions. They can be used directly to provide the predicted tide needed for the tidal component of the exchange of water between the inner shelf of the eastern Gulf of Mexico and the western fringe of Florida Bay. Alternately, they can be compared to the boundary conditions provided by the Gulf of Mexico model to determine if tidal ebbs and floods are being specified with sufficient accuracy. Second, tidal computations can also be used as a test of the Florida Bay model near, but not along, its western boundary. If the western boundary of the model lies west of the 81°05'W meridian, these harmonic constants can be used for comparison with simulated ebbs and floods as model tidal waves enter the bay. If simulated tides are not properly represented near the western boundary of the bay, it is likely that simulations will be a poor representation of tidal conditions in the interior of the bay as well.

Table C2 includes harmonic constants of the principal tidal constituents at Station 1. As noted in the METHODOLOGY section, amplitudes indicate the east-west and north-south components of the maximum flood and ebb current speeds attained during any half tidal cycle. Alternately, amplitudes expressed in units of km h^{-1} can be used to estimate the tidal excursion--the horizontal distance that water is transported over either the flood or ebb half of the tidal cycle. Results from Table C2 indicate that maximum M_2 tidal currents at Station 1 reach speeds of 39.3 cm s^{-1} (the square root of the sum of the squares of the north-south and east-west component amplitudes), or 1.415 km h^{-1}. Given the 12.421-hr period of the M_2 constituent, the tidal excursion is 5.6 km. More meaningful within the context of bay-shelf exchanges is the 5.4 km tidal excursion computed from the east-west component of the current that passes through the 81°05'W meridian. As noted above, however, this value has to be treated with caution, because measurements from any given location provide no information regarding how far a water parcel moves as it approaches or leaves the study site. The two component speeds are directly comparable with the east-west and north-south current components that should be simulated by the model at that location, however. Results from Stations 2 and 3 show that the ebb and flood of the tide decrease dramatically from north to south. Amplitudes decrease by 50% from Station 1 to Station 2 (Table C3) and by another 50% from Station 2 to Station 3 (Table C4).

Not included in Table C2 are the harmonic constants of four additional tidal constituents that had slightly lower amplitudes. The K_2, P_1, M_4, and M_6 constituents, with amplitudes of 3.1, 2.6, 2.4, and 2.1 cm s^{-1}, respectively, might be significant for some purposes, but they will not be mentioned further in this report.

Comparing phase angles of the east-west and north-south tidal constituents included in Tables C2-C4, one can determine the sense of rotation of the tidal ellipses. Using the M_2 constituent as Station 1 as an example, the 220.4° and 351.9° phase angles for the north-south and east-west components reveal that northward flow leads eastward flow by 131.5°, and the rotation must be clockwise. For the M_2 constituent, with a period of 12.421 hr, a 131.5°

phase lead is equivalent to a 4 hr, 32 min time lead. The closer the phase difference is to 180°, the more elliptical the motion. In this case, the 131.5° phase difference is a result of the nearby southern tip of the Florida Peninsula (East Cape), which inhibits the northeastward and southwestward flow needed for circular motion.

The interpretation of Section (b) of Tables C2-C4, containing vertically-integrated surface-to-bottom transport, is similar to the interpretation of Section (a) above. Again, the M_2 constituent stands out as the principal tidal constituent. The 1.082-m^2 s^{-1} amplitude at Station 1 indicates that at maximum flood or ebb the volume of water passing the study site reaches this value. This is consistent with the vertically-averaged current speed: Dividing 1.082 m^2 s^{-1} by the mean water depth and converting to cm s^{-1}, one gets a value of 36.2 cm s^{-1}, providing a check on the calculations.

Comparison of the amplitudes of the three semidiurnal tidal constituents (M_2, S_2, and N_2) provides information on the spring-neap tide differences. Interaction of the M_2 and S_2 tidal constituents results in a 14.77-day variation in tidal range that corresponds to the transition from full moon to new moon (and vice versa). Interaction of the M_2 and N_2 tidal constituents results in a 27.55-day variation in tidal range that corresponds to the moon's elliptical orbit around the earth (e.g., apogee to apogee). At Station 1, for example, the interaction of M_2 and S_2 will result in flood and ebb tide currents varying between 26.7 and 49.7 cm s^{-1} (38.2 $\pm$11.5 cm s^{-1}). Similarly, over any 27.55-day period, tidal currents will vary between 32.2 and 44.2 cm s^{-1} in response to the interaction of M_2 and N_2. With all three constituents interacting, semidiurnal tidal currents can vary between 15.3 and 55.7 cm s^{-1}. These are clearly important differences that should be kept in mind when tuning the hydrodynamic model.

Interaction of semidiurnal constituents and the K_1 and O_1 diurnal constituents produce diurnal inequalities that result in distinctly different maximum flood or ebb current speeds on successive semidiurnal tidal cycles. For example, at Station 1 when the K_1 and/or O_1 flood coincides with the M_2 flood, results will be additive. But on the following semidiurnal tidal cycle, the M_2 flood will coincide with the K_1 and/or O_1 ebb and the result will be the difference rather than the sum. Again, these features of the tide along the western boundary of Florida Bay should be kept in mind, whether observations are used for boundary conditions or for the verification of model simulations. As noted above, variation in tidal current speed range is directly related to variation in tidal excursion. Thus, by closely approximating tidal conditions along the western fringe of the bay, the direct effects of tidal exchanges with the inner shelf of the eastern Gulf of Mexico will be reproduced with greater accuracy.

Sections (c) and (d) of Tables C2-C4 compare tidal motions recorded in the top and bottom layers of the water column. Amplitudes for the bottom layer (83 cm above the bottom) are generally 80-90% of the amplitudes in the surface layer (which was anywhere from 2.1 to 4.0 m above the pressure sensor during the time of the study). Phase angles, which can be translated into times of slack water, maximum flood, etc., show substantial differences in

some cases. This will be discussed further later in this subsection.

Comparing results from Tables C2, C3, and C4, one can begin to see how tidal conditions vary in a north-to-south direction. North-to-south differences in harmonic constants make it clear that boundary conditions for the western fringe of the bay must be spatially variable as well. Forcing by unvarying tidal conditions would be unrealistic. Comparison of Tables C2 and C3 indicate that tidal rotations are still highly elliptical, but that the axes of the ellipses have rotated clockwise. East-west and north-south components are nearly equal for Station 2, sections (c) and (d), meaning that the major axis of the ellipse is oriented approximately northwest-southeast. Strongest M_2 tidal currents (without regard to direction) are 25.9 cm s^{-1} at Station 2, and the east-west tidal excursion is 2.74 km. Other semidiurnal and diurnal constituents contribute similar highly elliptical rotations, and they are rotated similarly in a clockwise direction.

Comparison of east-west component amplitudes calculated for Stations 1 and 2 indicates that the east-west current components, and thus the transport into and out of Florida Bay by the M_2 constituent, decreases by about 50% in the approximately 15 km from Station 1 to Station 2. Other tidal constituents decrease similarly. As mentioned above, this is partly a result of the clockwise rotation of the tidal ellipses. Nevertheless, it represents a significant reduction in the magnitude of the tide-induced exchange between the bay and shelf waters of the eastern Gulf of Mexico.

Table C4 concludes the north-to-south comparison of tidal conditions at the three ADP stations, and both the decrease in tidal amplitude and the clockwise rotation of the ellipse continue for the semidiurnal and diurnal constituents at Station 3. Strongest M_2 currents, for example, are just under 18 cm s^{-1}. Section (a) of Table C4 shows that the east-west component of the M_2 constituent has decreased to 9.2 cm s^{-1}, indicating an east-west tidal excursion of 1.3 km. Other semidiurnal and diurnal constituents can contribute to the tidal excursion as they cycle in and out of phase, but the total remains below 2.5 km. At Station 3, the north-south components of most of the constituent current speeds are significantly stronger than the east-west components.

c. Vertical Coherence and Vertical Shear

The availability of ADP data makes possible a direct comparison of near-surface and near-bottom currents to investigate top-to-bottom differences in current speed and direction. Also included in Sections (c) and (d) of Tables C2-C4 are results of harmonic analyses of east-west and north-south current components. Differences in amplitudes and phase angles are directly related to the extent to which the ebb and flood of the tide at this location move as a single current.. Results from all three study sites can be summarized quite easily. Especially for the dominant M_2 constituent, phase differences for the east-west current components are only a few degrees. The physical interpretation is that strongest floods and ebbs, as well as slack water conditions, occur nearly simultaneously throughout the water column. In such shallow water, this is not surprising. The only case in which large phase differences are found

is in the north-south current at Station 1. As discussed later in this report, it is likely that local topographic features affecting the near-bottom current have only negligible impact on the near-surface flow.

The correlation coefficients, representing the association of near-surface and near-bottom flow at any instant of time, are logically influenced by the high degree of similarity of the tidal currents. Thus, even at Station 1, where near-bottom flow may be influenced by local topography, the correlation coefficient is +0.854. At Stations 2 and 3, where bottom topography does not seem to be a factor, correlation coefficients are +0.966 and +0.929, respectively. Mean top-to-bottom counterclockwise deflections are -0.2, +0.4, and +0.2°, respectively. These small angles are within the resolution of the ADP's current direction (reported to the nearest 1°), and these results suggest that there is no physically significant variation with depth in the direction of the instantaneous current.

A second and graphical way of visualizing vertical shear in the water column involves a comparison of cumulative net displacement diagrams constructed from top-level and bottom-level current observations. Unlike the calculations of κ and α, which weigh individual hourly observations equally, PVDs weigh individual current vectors in direct proportion to the magnitude of the current speed. Thus, even a few hours with anomalously strong or weak currents at one level, or unusually large directional shear, can separate the two curves and leave one offset from the other through the rest of the plot.

Figure C10 shows PVDs constructed from surface layer (top) and bottom layer currents recorded at Station 1 from March 14, 1996, to April 22, 1997. The two plots trace out significantly different patterns. Surface-layer flow results in a net west-southwestward displacement (250°) with a resultant speed of 8.5 cm s^{-1}. Some evidence of a seasonal variation is evident, with westward flow from the start of the record through mid-July, and again from mid-February through the end of the study period. From mid-July through mid-February, the resultant flow is southwestward. Surface displacement is undoubtedly influenced by the westward directed resultant wind stress (see Figure C15 in the following section), and it is hypothesized that westward wind stress sets down water levels in the northwest corner of the bay. This, in turn, would maintain an eastward-directed slope in the surface of the bay. The associated pressure gradient would oppose a wind-driven outflow in near-bottom layers.

At the bottom level, the east-west tidal oscillations are very nearly equal, and little net east-west displacement occurs during the 404-day study. With each tidal exchange, however, a slight southward offset occurs, perhaps related to the curvature of the isobaths south of East Cape. The result is a quasi-steady southward displacement of water past the study site. It is important to keep in mind that this is a feature of the local flow only, and it does not indicate that dissolved or suspended material would have oscillated slowly to the south along the 81°05'W meridian, even though there is open water south of the Station 1 study site.

Figure C11 shows the PVDs constructed from top-layer (left) and bottom-layer (right) currents recorded at Station 2 from the start of the study to the break in the record that occurred in late June. The situation depicted here is somewhat unusual in the sense that the movement past the study site in the lowest layer resolved by the ADP is greater than the movement in the top layer. In both layers, both the ebb and flood of the tide and the long-term net movement is tightly constrained to southeastward and northwestward headings. This may be due to local topographic steering, although it is unusual to see this in the top, wind-influenced layer as much as in the bottom layer. Because the flow is largely rectilinear, it is difficult to track the net movement as a function of time. Nevertheless, it is apparent that there is a significant degree of similarity in the near-surface and near-bottom layers.

Figure C12 is the continuation of the record from Station 2 following the data gap that ended on July 1, 1996. For this longer time period, the progressive vectors constructed from top and bottom levels show a greater degree of dissimilarity, and for several periods within the 223-day segment the surface currents are clearly decoupled from near-bottom currents. For example, early in the record, surface layer flow starts toward the southeast, while bottom layer flow starts in a southward direction, then continues toward the northwest. Surface layer flow reverses on October 9th, and for the remainder of the study period resultant flow in both surface and bottom layers is northwestward. During a substantial part of this time period, then, the water column does indeed move as a single layer.

Figure C13 shows the cumulative net displacement plots from Station 3 for the time period from March 14 to December 5, 1996. At this location, surface-layer and bottom-layer flow patterns are very similar. Virtually all of the features seen in one plot are represented in the other, and the progressive vector plots trace similar patterns. Both curves start off in a south-southeastward direction, then turn clockwise into a northwestward heading. About two-thirds of the way through the record, both curves make similar clockwise loops before continuing southwestward at the end of the study period. At this location, except for somewhat stronger current speeds in the surface layer, the water column acts very much like a single layer. On average, current speeds at the lower layer are 80% of the speeds recorded for the upper layer. This is in good agreement with the amplitudes recorded for the principal tidal constituents at these two levels (Tables C2-C4).

Figure C14, containing the PVDs of current data recorded at Station 3 following the break from December 5, 1996, to January 8, 1997, is similar to results presented in Figure C13 in the sense that flow in the lowest layer resolved by the ADP is similar to flow in the top layer of the water column. For this 104-day time period, however, the net displacement in the bottom layer is only 50% of the net displacement in the top layer. In both plots, net movement is northwestward, although the tidal ellipses suggest that the ebb and flood of the tide is largely in a north-south direction. Together, the two records from Station 3 indicate that the southern part of the open western boundary of Florida Bay is a region of net outflow. Only rarely during the 13-month study was the flow past the study site into the bay for time periods in excess of a few days. The dissimilarity of net flow patterns at the three ADP study

sites suggests a complex pattern of inflow and outflow across the western boundary of Florida Bay.

It is noteworthy that the general shape of the PVDs can be distinctly different from the patterns seen in the vertically-integrated two-dimensional transport (e.g., compare Figures C2 and C10 for Station 1 and Figures C5 and C12 for Station 2). This is because 2-D transport calculations take time-varying water depth into account, while PVDs represent only the flow past the current meter. In the case of Station 3, however, vertically-integrated transport (see Figure C6) traces a pattern that is similar to that seen for both surface and bottom levels (e.g., Figure C13). Apparently, either the tide-induced transport is relatively small, or tide-induced transport is in the general direction of the resultant current, and thus tidal transport acts more to reinforce the current than to oppose or deflect it. At Station 3, a single current meter in the water column would represent the flow throughout the water column, and it would represent total transport to a close approximation as well.

d. Response to Wind Forcing

To examine the response to wind forcing, hourly wind observations from the Johnson Key weather station are paired with vertically-integrated east-west transport values. The time period for the comparison was the 2,526-hour interval from July 23 to November 5, 1996. The Johnson Key weather station was selected because it was the westernmost weather station, and therefore the closest to the ADP study sites. Also, it provided data for the longest overlap period for ADP Stations 1-3. Station 1 is 10 n.m. (18.5 km) from the Johnson Key weather station along a heading of 280°; Station 2 is 12.9 n.m. (23.8 km) from Johnson Key along a heading of 230°; and Station 3 is 19 n.m. (35.2 km) from Johnson Key along a heading of 210°. The three-and-a-half month weather record prevented a spectral analysis of the response to wind stress over seasonal time scales, but it is well suited for exploring cause-and-effect relationships over the 3- to 5-day time periods characteristic of meteorological forcing.

The PVD of hourly wind-stress values (Figure C15) provides a good overview of wind conditions from July 23 to November 5. The figure can be broken into two components. From the start of the record to October 8th (the clockwise loop near the middle of the plot), winds over Florida Bay were headed in a generally west-southwestward direction. With the passage of the first cold front of the 1996-97 winter season on October 8th, a seasonal wind shift occurred as well. For the remainder of the record, wind stress acting on Florida Bay was directed more southwestward. The PVD is not well suited for characterizing temporal variability over shorter time scales, but these features are discussed in greater detail in the report that focuses upon wind data. Throughout the plot, relatively high-frequency fluctuations in direction are apparent. Similar variations in the magnitude of wind stress are equally probable, but the PVD is not well suited for showing variations in the magnitude of wind forcing. Figure C15 therefore suggests not only that variations in east-west transport across the western boundary of Florida Bay occur over time scales on the order of several days, but that more subtle, seasonal changes in regional flow patterns might be expected as well.

The investigation of wind forcing in western Florida Bay began by determining the wind stress component to which east-west transport at each ADP study site was most responsive. To isolate the wind conditions for which east-west transport is most responsive, low-pass filtered wind-stress components were compared with low-pass filtered east-west transport. By filtering both time series, tidal fluctuations in the transport record as well as seabreeze effects in the wind-stress record were removed. East-west transport at Station 1, the ADP study site closest to Johnson Key, was most highly correlated with the 123-303° wind-stress component. At Station 2, east-west transport was most highly correlated with the 064-244° component, and at Station 3, east-west transport was most highly correlated with the 055-235° wind-stress component at Johnson Key. All three of these wind-stress components are within 35° of a heading that is directly into the bay, suggesting a direct filling and draining mechanism acting along the open western boundary to the bay. With this as the basis for selecting a single wind-stress component for investigating the coupling of transport to wind stress, analysis continued with a spectral analysis of the transport from the three ADP study sites, and using hourly data that had not been low-pass filtered.

Plots of the spectral analyses are not presented, because results, summarized in Table C5, can be described easily. Of primary interest are the coherence and gain spectra, which show the time scales over which wind forcing and transport are most highly coupled, and which quantify the relative magnitudes of transport and wind stress. For modeling purposes, the gain, coherence and, to a lesser extent, phase relationships are of particular significance.

The coherence spectrum of east-west transport past Station 1 and the 123-303° wind-stress component shows surprisingly low coherence. Highest coherence values were less than 0.3, suggesting an only marginally coherent relationship. Highest coherence levels occur for the longest time scales--longer than 65 hours, or about two and a half days. Over these time scales, variations in wind forcing are very nearly in phase with the resulting transport into and out of the bay. The gain spectrum indicates that a 1 dyne cm^{-1} wind stress (corresponding to a wind speed of 8 m s^{-1}, or 18 miles hr^{-1}) will produce a transport of 0.105 m^2 s^{-1}. Given the 3.1-m mean depth of the water at Station 1 during the study period, a depth-integrated transport of 0.105 m^2 s^{-1} is equivalent to a depth-averaged current speed of 3.4 cm s^{-1}. While this seems like a small response to such a strong wind, one must keep in mind that this is mean value for the entire water column. Also, in practice, a wind-driven outflow will set down water levels within the bay, producing a barotropic pressure gradient that will oppose the wind-stress force.

The coherence spectrum for east-west transport at Station 2 and the 064-244° wind-stress component reveals a coherence level of just under 0.6 at a periodicity of 65 hr. Variations in wind forcing lead variations in east-west transport by approximately 30°, corresponding to a time lead of 5-6 hr. The gain spectrum indicates that a 1 dyne cm^{-2} wind stress will produce a 0.07 m^2 s^{-1} transport. At Station 2, the mean depth during the study was 2.6 m, and thus a vertically integrated transport of 0.07 m^2 s^{-1} corresponds to a depth-averaged current speed of 2.7 cm s^{-1}.

At Station 3, the coherence of east-west transport and the 055-235° component wind stress was the highest found for all three stations, in spite of the fact that the separation of the ADP study site and the weather station was greatest of the three. Highest coherence is 0.74 at a period of 130 hours, or about five and a half days. The phase spectrum indicates a 25-40° phase lead, which is equivalent to a time lead of anywhere from 5-9 hr. The gain varies from 0.08 to 0.10 $m^2 s^{-1}$ per dyne cm^{-2}. With a mean depth of 1.9 m during the study, the corresponding depth-averaged current speed is 4.1 to 5.1 cm s^{-1}.

DISCUSSION

The ADP data summarized in this report provide the best information to date for describing tidal and long-term nontidal exchanges across the open western boundary of Florida Bay. The picture that emerges suggests that the central and especially the northern part of the 81° 05'W meridian, from East Cape to Marathon, is a region of net inflow, while the southern part of the western boundary appears to be a region of net outflow. Most of the eastward transport across the boundary appears to be tide induced, but wind effects become important in the south, where tidal current speed amplitudes are reduced in both water level and current data. At Station 3, for example, tide-induced transport by itself would produce a gradual inflow across the boundary. Adding the effects of a generally westward-directed wind stress (see Figure C15), however, deflects the total transport to a more south-southwestward direction and makes it an outflow. Comparing inflow at Stations 1 and 2 (see Figures C2, C4, and C5), it appears that the region just south of East Cape is a primary source of strong and persistent inflow into the bay.

Although Johnson Key wind data were used to describe wind-driven transport at ADP Stations 1-3, follow-up studies should include similar investigations using CMAN data from the weather station northwest of Long Key. The Long Key weather station will be maintained as a long-term monitoring site, thus any relationships between wind forcing and transport established with CMAN data can be applied for other time periods, when the Long Key weather station will still be in operation. Data from Stations A, B and C will be useful for looking at spatial coherence across the northern part of Florida Bay, but this is a topic to be explored in the report dealing specifically with the weather data.

The need to consider the water column in multiple layers seems to depend upon the questions being asked. The ebb and flood of the tide varies little with depth at Stations 1-3. Amplitudes of the principal tidal constituents in the near-bottom layer are generally 80-85% of those in the near-surface layer, and phase angles often differ by 1° or less. Only when one considers cumulative effects, and over longer time scales, do the top-to-bottom differences become apparent and significant--and then only at two of the three stations investigated here. At Station 3, except for stronger currents in the top layer, both the top and bottom parts of the water column appear to be moving as a single unit (Figures C13 and C14). A degree of similarity appears in portions of the plots of data from Station 2, but only for carefully selected parts of the record. For much of the first part of the one-year study, resultant flow in the

surface layer is quite different from resultant flow in near-bottom levels. At Station 1, on the other hand, there is virtually no similarity in the plots of top-level and bottom-level currents (Figure C10). The available database does not represent Florida Bay as a whole, but for the western boundary one must keep in mind that vertically integrated transport may poorly represent transport in near-surface or near-bottom layers individually.

LITERATURE CITED

Dennis, R.E. and E.E. Long. 1971. A user's guide to a computer program for harmonic analysis of data at tidal frequencies. NOAA Tech. Rept. 41, U.S. Dept. of Comm., Rockville, MD.

Kundu, P. 1976. Ekman veering observed near the ocean bottom. Journ. of Phys. Oceanogr. 6:238-242.

Little, J.N. and L. Schure. 1988. Signal processing toolbox. 167 pp., MathWorks, Natick, MA.

Table C1
Florida Bay, Stations 1-3, ADP Collection Summary

Station	Start Date	End Date	Quarter Hours[1]	Number Missing[2]	Percent Missing
ADP1	3/14/96	4/22/97	38,820	3,013	7.76
ADP2[3]	3/14/96	2/8/97	31,814	2,651	8.33
ADP3[4]	3/14/96	4/22/97	38,844	3,668	9.44

[1]Maximum possible number of observations between start and end dates.
[2]Number of quarter-hour observations randomly dropped during study period.
[3]Data recorded 6/26/96-7/1/96 contain spurious values; this part of record not used to characterize general flow patterns, including tidal currents, nor to quantify the response to wind forcing.
[4]Data recorded 12/5/96-2/8/97 contain spurious values; this part of record not used to characterize general flow patterns, including tidal currents, nor to quantify the response to wind forcing.

Table C2
Florida Bay, Station 1, ADP Amplitudes and Local Phase Angles

		M_2	S_2	N_2	K_1	O_1
(a) Vertically Averaged Current Speed						
EW Comp	η	38.2	11.5	6.0	7.9	6.1
	κ	351.9	14.3	321.8	260.1	238.8
NS Comp	η	9.2	2.6	1.6	0.9	1.5
	κ	220.4	221.2	176.3	118.9	50.9
(b) Vertically Integrated Two-dimensional Transport						
EW Comp	η	1.082	0.341	0.186	0.202	0.149
	κ	351.3	13.9	322.3	260.0	237.6
NS Comp	η	0.278	0.080	0.051	0.023	0.035
	κ	219.0	221.1	176.4	109.9	46.4
(c) Top-layer Current Speed						
EW Comp	η	41.9	13.3	7.1	8.0	6.4
	κ	352.0	15.0	321.8	262.0	232.8
NS Comp	η	10.5	2.7	2.4	2.5	1.3
	κ	217.1	235.7	184.5	2.3	44.8
(d) Bottom-layer Current Speed						
EW Comp	η	37.1	11.0	5.4	7.8	6.4
	κ	352.3	13.8	322.8	262.9	241.7
NS Comp	η	9.2	2.6	1.4	0.8	1.8
	κ	221.8	223.4	161.2	144.1	57.2

Note: Amplitudes (η) and local phase angles (κ) of the principal tidal constituents calculated from ADP data at Station 1. Harmonic constants are from a single 29-day calculation, starting at 0000 EST, 3/14/96. Section (a) contains vertically averaged east-west and north-south current components. Amplitudes are in cm/sec. Section (b) contains vertically integrated east-west and north-south 2-D transport. Amplitudes are in sq m/sec. Sections (c) and (d) contain harmonic constants for top and bottom levels of the water column that can be used to examine vertical differences in amplitude or phase that might be lost in a single-layered model. Amplitudes are in cm/sec. Local phase angles throughout the table are in degrees.

Table C3
Florida Bay, Station 2, ADP Amplitudes and Local Phase Angles

		M_2	S_2	N_2	K_1	O_1
(a) Vertically Averaged Current Speed						
EW Comp	η	19.27	5.88	2.79	4.25	3.32
	κ	358.7	18.9	331.8	271.1	253.4
NS Comp	η	17.32	5.17	2.45	3.33	2.53
	κ	199.9	215.9	172.7	101.9	85.8
(b) Vertically Integrated Two-dimensional Transport						
EW Comp	η	0.528	0.167	0.086	0.106	0.079
	κ	358.1	18.6	330.8	270.7	253.3
NS Comp	η	0.475	0.146	0.076	0.080	0.058
	κ	199.1	215.8	170.7	101.7	86.0
(c) Top-layer Current Speed						
EW Comp	η	22.8	7.0	3.5	5.2	3.7
	κ	358.9	18.3	335.4	268.6	253.8
NS Comp	η	20.6	5.8	2.9	4.1	3.3
	κ	200.9	218.4	176.5	93.5	90.0
(d) Bottom-layer Current Speed						
EW Comp	η	17.9	5.5	2.4	3.6	3.2
	κ	358.9	20.6	330.7	271.7	249.4
NS Comp	η	16.1	5.0	2.4	3.2	2.4
	κ	199.8	214.9	176.0	105.3	89.1

Note: Amplitudes (η) and local phase angles (κ) of the principal tidal constituents calculated from ADP data at Station 2. Harmonic constants are from a single 29-day calculation, starting at 0000 EST, 3/14/96. Section (a) contains vertically averaged east-west and north-south current components. Amplitudes are in cm/sec. Section (b) contains vertically integrated east-west and north-south 2-D transport. Amplitudes are in sq m/sec. Sections (c) and (d) contain harmonic constants for top and bottom levels of the water column that can be used to examine vertical differences in amplitude or phase that might be lost in a single-layered model. Amplitudes are in cm/sec. Local phase angles throughout the table are in degrees.

Table C4
Florida Bay, Station 3, ADP Amplitudes and Local Phase Angles

		M_2	S_2	N_2	K_1	O_1
(a) Vertically Averaged Current Speed						
EW Comp	η	9.2	2.9	1.7	2.8	2.0
	κ	330.5	357.1	292.8	256.1	234.2
NS Comp	η	15.2	4.0	2.2	2.3	1.7
	κ	233.8	250.6	205.7	157.9	136.9
(b) Vertically Integrated Two-dimensional Transport						
EW Comp	η	0.170	0.055	0.034	0.049	0.037
	κ	330.6	359.1	298.1	259.9	236.4
NS Comp	η	0.286	0.078	0.046	0.042	0.031
	κ	233.1	250.8	206.9	166.3	147.5
(c) Top-layer Current Speed						
EW Comp	η	10.8	3.1	1.6	3.1	2.6
	κ	329.6	359.5	298.8	256.3	225.4
NS Comp	η	17.7	4.5	2.5	2.8	1.9
	κ	234.2	248.6	205.1	153.2	134.7
(d) Bottom-layer Current Speed						
EW Comp	η	9.4	3.0	1.9	2.9	1.8
	κ	331.4	357.3	295.2	257.2	237.4
NS Comp	η	15.5	4.1	2.2	2.5	1.9
	κ	233.9	252.0	200.5	158.0	134.4

Note: Amplitudes (η) and local phase angles (κ) of the principal tidal constituents calculated from ADP data at Station 3. Harmonic constants are from a single 29-day calculation, starting at 0000 EST, 3/14/96. Section (a) contains vertically averaged east-west and north-south current components. Amplitudes are in cm/sec. Section (b) contains vertically integrated east-west and north-south 2-D transport. Amplitudes are in sq m/sec. Sections (c) and (d) contain harmonic constants for top and bottom levels of the water column that can be used to examine vertical differences in amplitude or phase that might be lost in a single-layered model. Amplitudes are in cm/sec. Local phase angles throughout the table are in degrees.

Table C5
Summary of Spectral Analyses of Wind Stress and East-West Transport at ADP Stations 1-3

	Station 1	Station 2	Station 3
Time Interval	7/23-11/5/96	7/23-11/5/96	7/23-11/5/96
Wind Stress[1]	123 - 303^0	64 - 244^0	55 - 235^0
Highest Coherence	0.3 at >65 hr	0.6 at 65 hr	0.7 at 130 hr
Phase Lead of Wind	$\pm 5^0$	30^0	25 - 40^0
Gain	0.105	0.07	0.08 - 0.10

[1]Refers to the component of the low-pass filtered wind-stress vector to which low-pass filtered east-west transport was most highly correlated. The gain has units of m^2s^{-1} per dyne cm^{-2}.

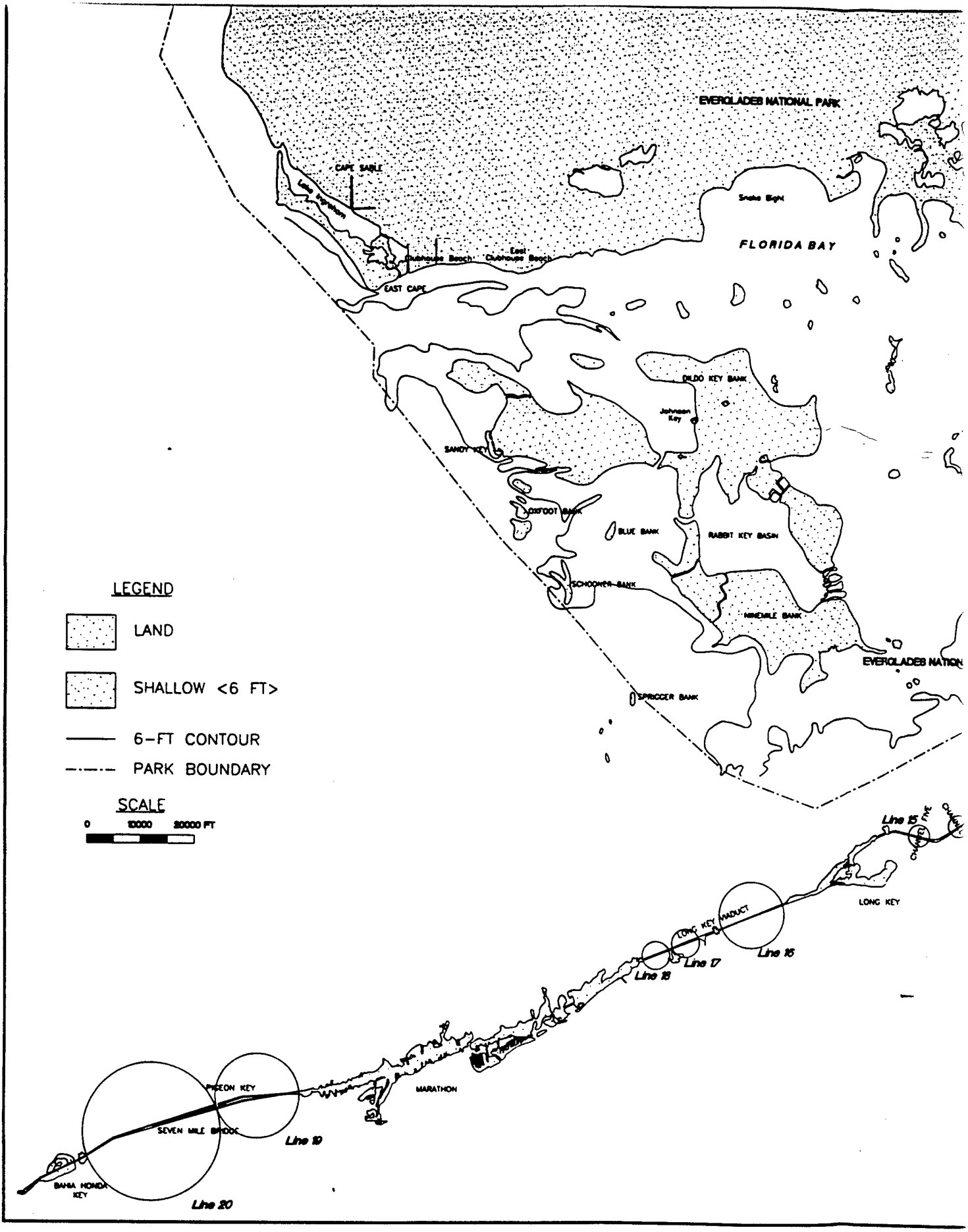
EVERGLADES NATIONAL PARK
CAPE SABLE
Lake Ingraham
Snake Bight
FLORIDA BAY
Clubhouse Beach
East Clubhouse Beach
EAST CAPE
DILDO KEY BANK
Johnson Key
SANDY KEY
OXFOOT BANK
BLUE BANK
RABBIT KEY BASIN
SCHOONER BANK
NINEMILE BANK
EVERGLADES NATION
SPRIGGER BANK
LEGEND
LAND
SHALLOW <6 FT>
6-FT CONTOUR
PARK BOUNDARY
SCALE
0 10000 20000 FT
Line 15
LONG KEY
LONG KEY VIADUCT
Line 16
Line 17
Line 18
PIGEON KEY
MARATHON
SEVEN MILE BRIDGE
Line 19
BAHIA HONDA KEY
Line 20

Figure C1

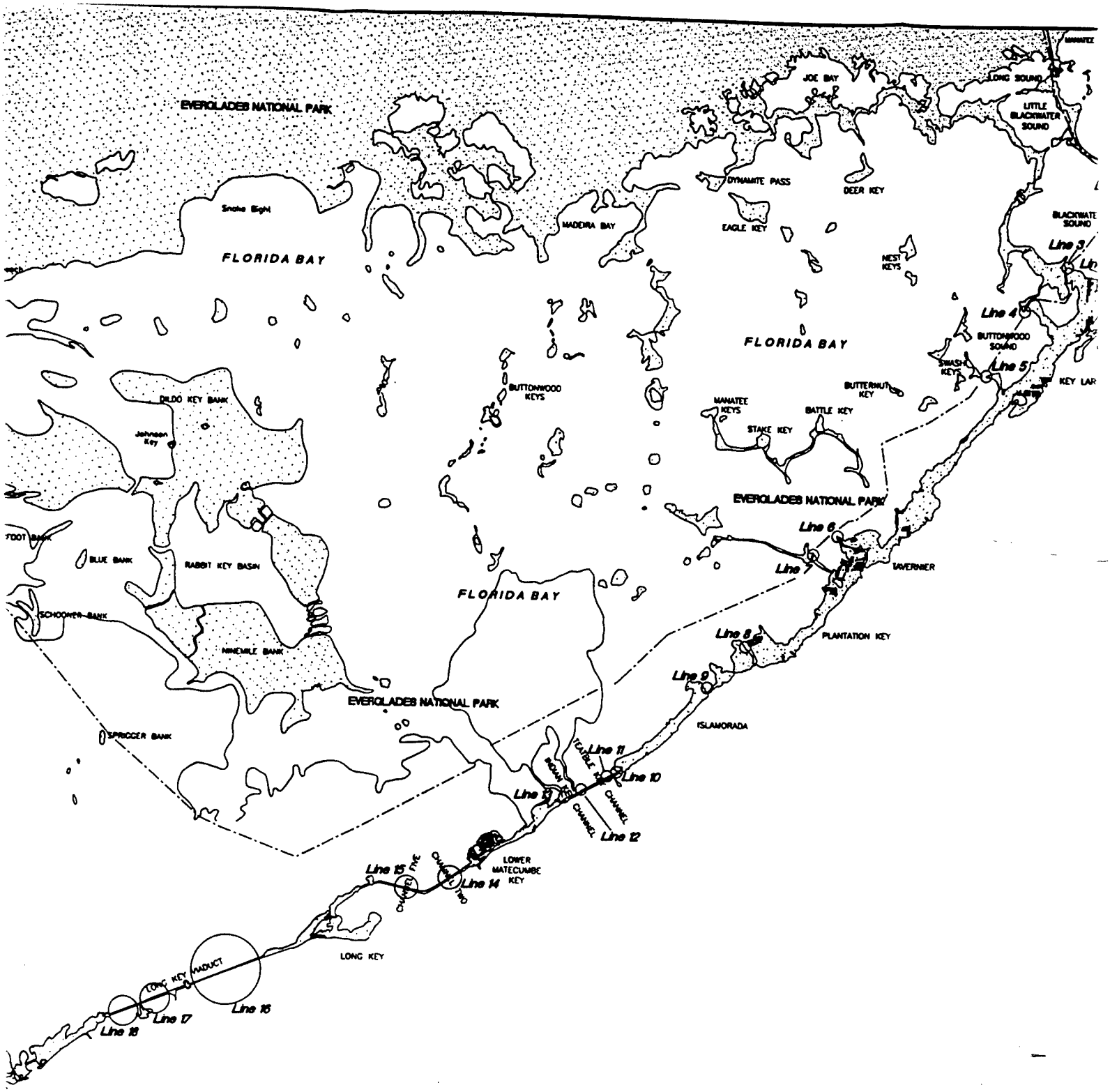

INTENSIVE SURVEY LOCATION

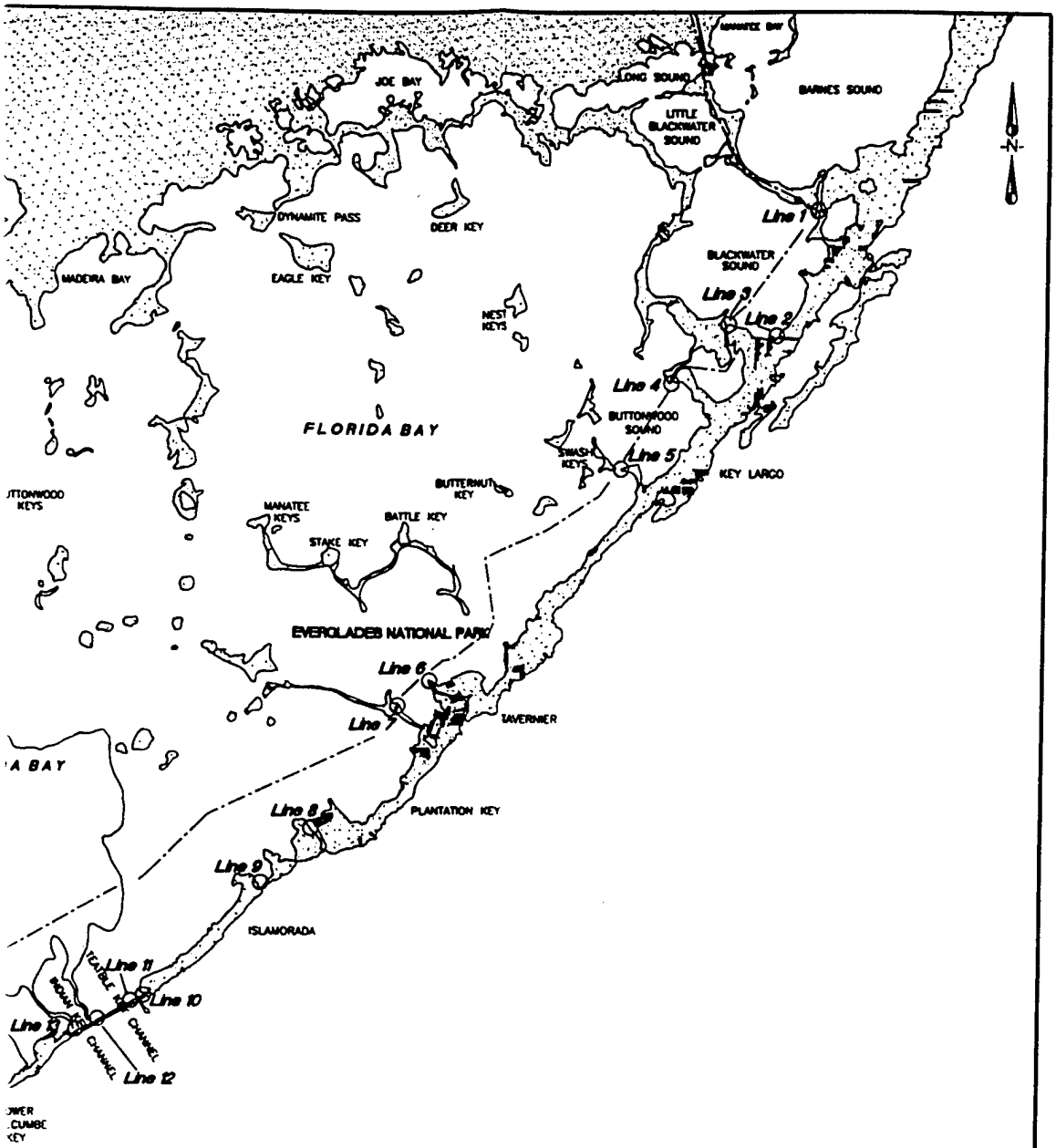

INTENSIVE SURVEY TRANSECT
LOCATION MAP

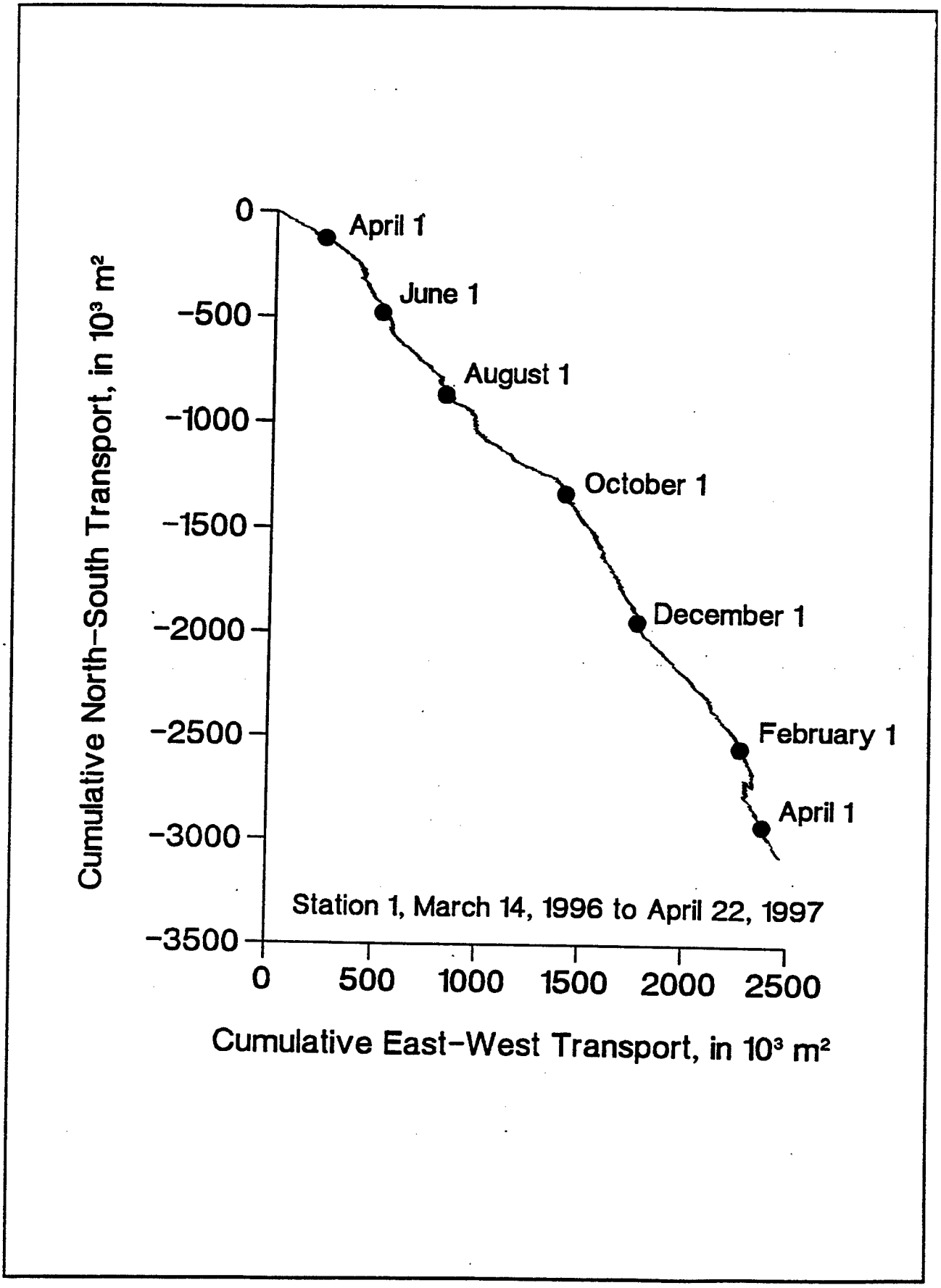
0
-500
-1000
-1500
-2000
-2500
-3000
-3500
April 1
June 1
August 1
October 1
December 1
February 1
April 1
Station 1, March 14, 1996 to April 22, 1997
0
500
1000
1500
2000
2500
Cumulative North–South Transport, in 10³ m²
Cumulative East–West Transport, in 10³ m²

Figure C2

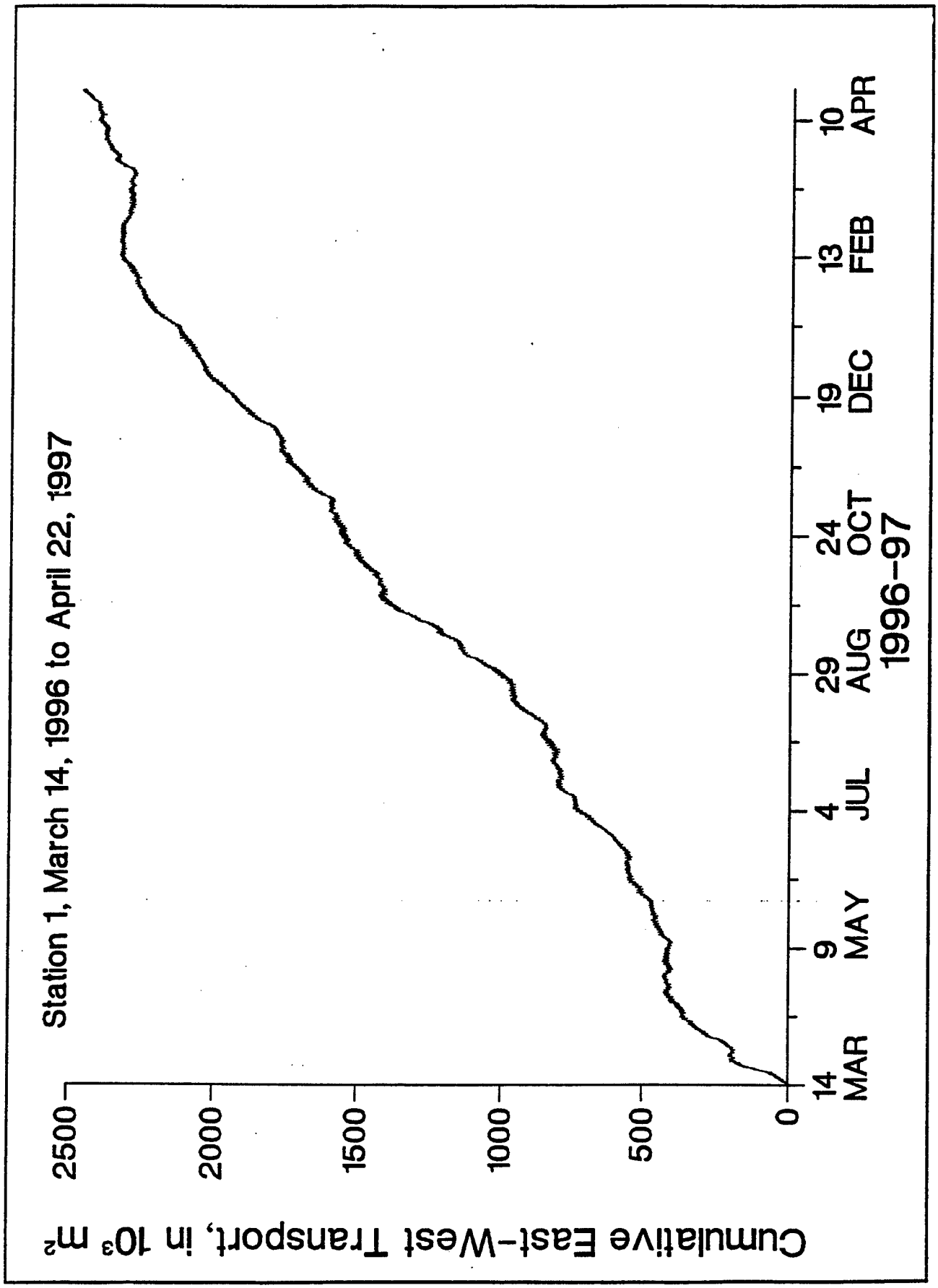
Station 1, March 14, 1996 to April 22, 1997
Cumulative East–West Transport, in 10^3 m^2
2500
2000
1500
1000
500
0
14 MAR
9 MAY
4 JUL
29 AUG
24 OCT
19 DEC
13 FEB
10 APR
1996–97

Figure C3

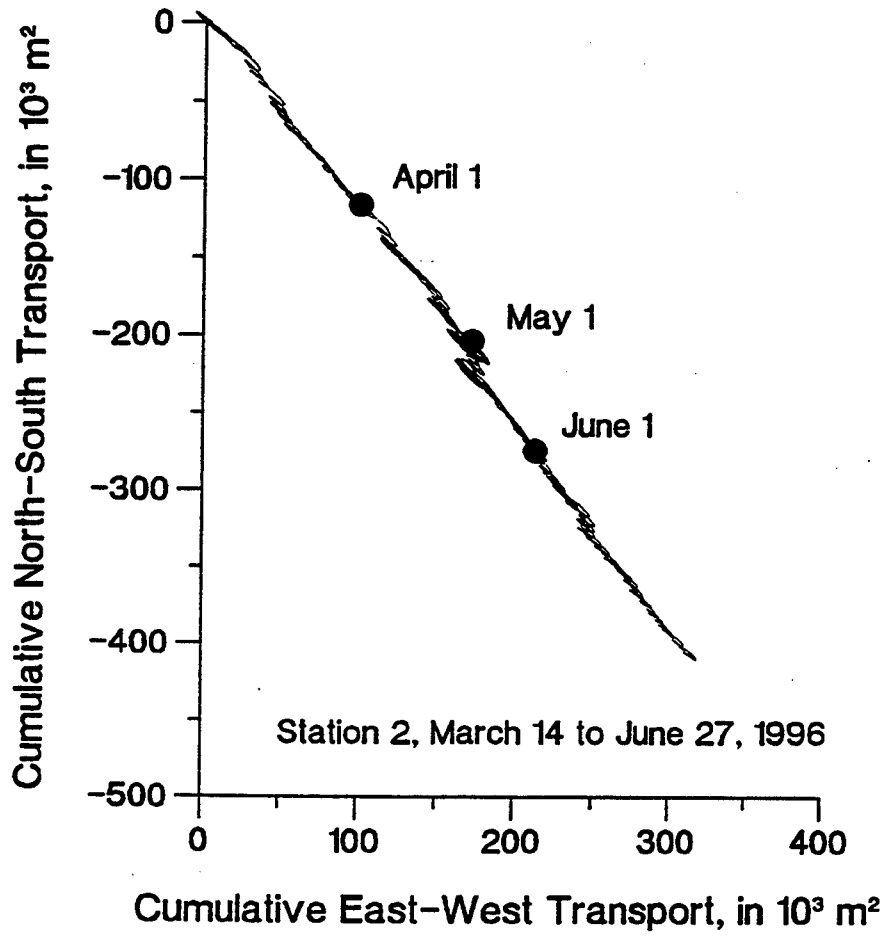
0
-100
-200
-300
-400
-500
April 1
May 1
June 1
Station 2, March 14 to June 27, 1996
0
100
200
300
400
Cumulative North-South Transport, in 10³ m²
Cumulative East-West Transport, in 10³ m²

Figure C4

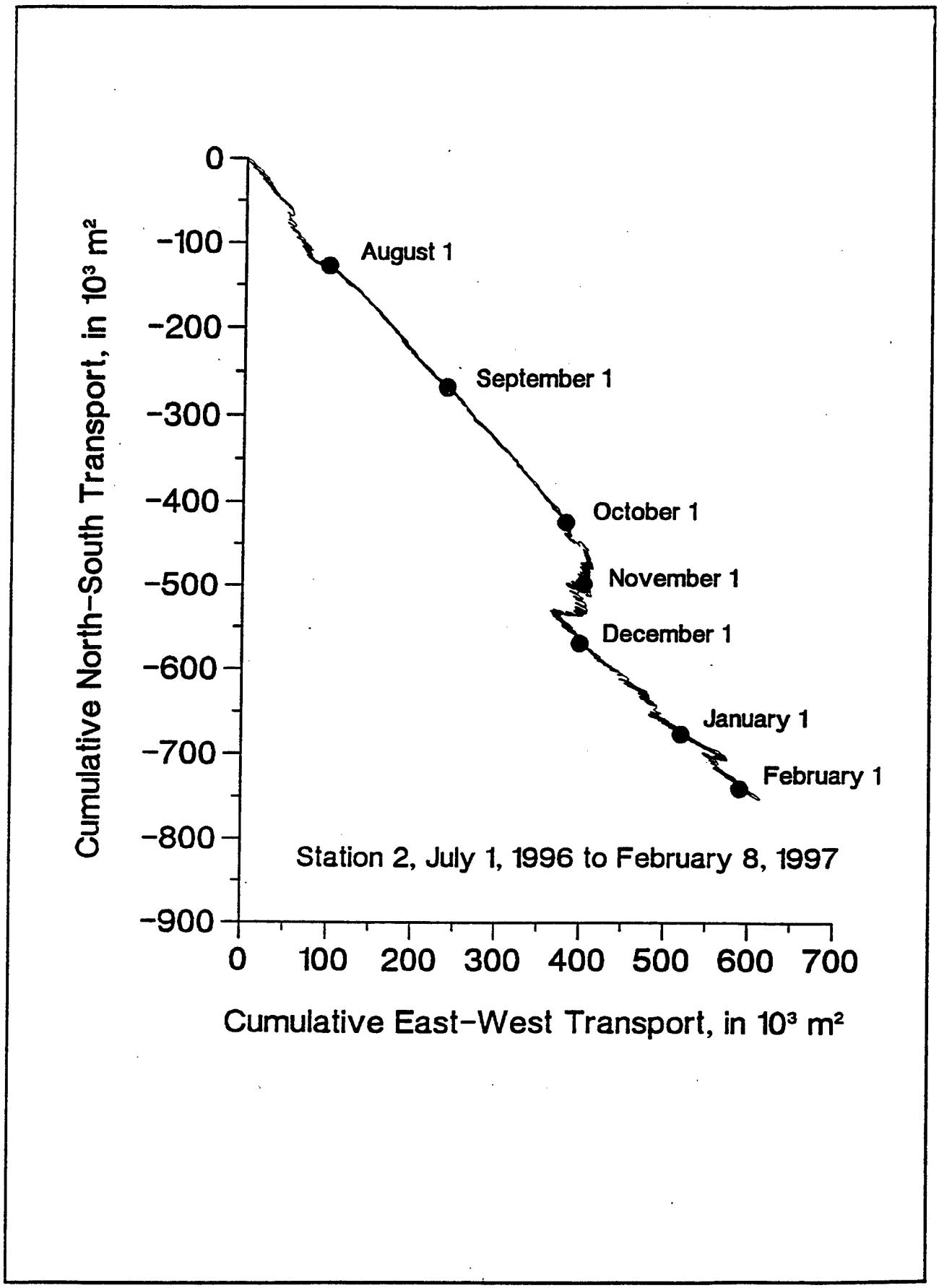
0
-100
-200
-300
-400
-500
-600
-700
-800
-900
Cumulative North-South Transport, in 10³ m²
August 1
September 1
October 1
November 1
December 1
January 1
February 1
Station 2, July 1, 1996 to February 8, 1997
0
100
200
300
400
500
600
700
Cumulative East-West Transport, in 10³ m²

Figure C5

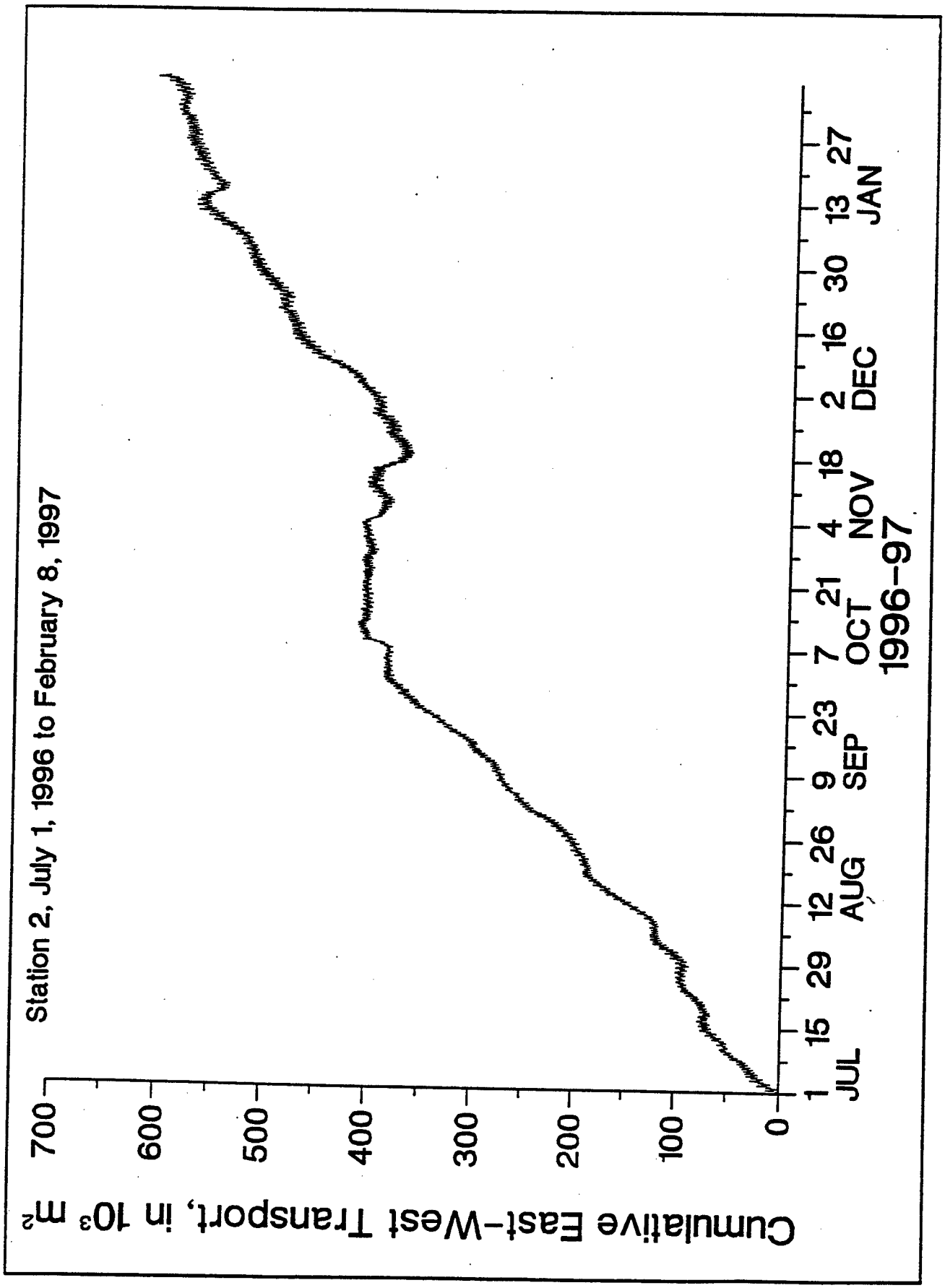
Cumulative East–West Transport, in 10³ m²
700
600
500
400
300
200
100
0
Station 2, July 1, 1996 to February 8, 1997
1 JUL 15 29 AUG 12 26 SEP 9 23 OCT 7 21 NOV 4 18 DEC 2 16 30 JAN 13 27
1996–97

Figure C6

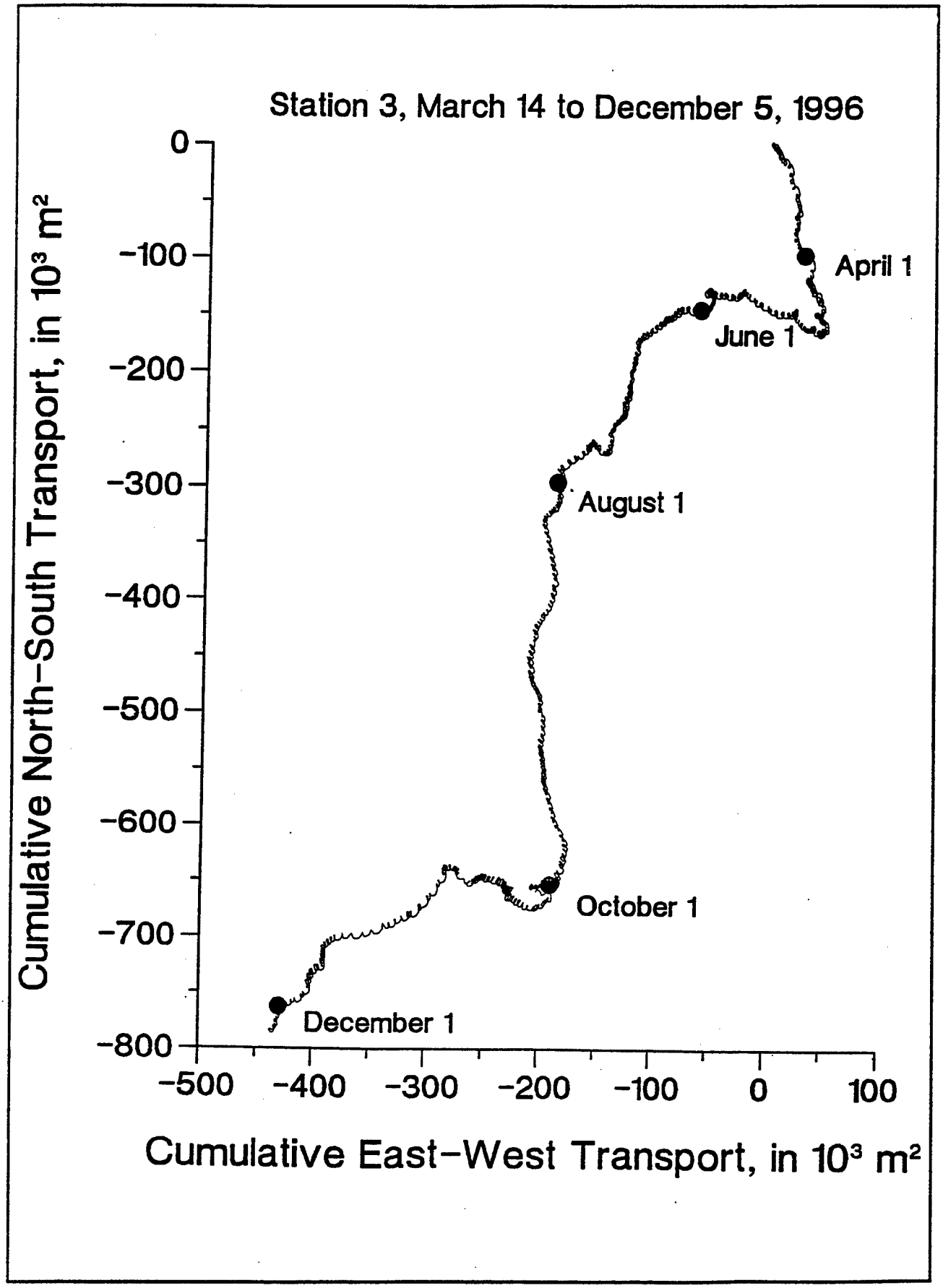
Station 3, March 14 to December 5, 1996
Cumulative North–South Transport, in 10³ m²
0
-100
-200
-300
-400
-500
-600
-700
-800
April 1
June 1
August 1
October 1
December 1
-500
-400
-300
-200
-100
0
100
Cumulative East–West Transport, in 10³ m²

Figure C7

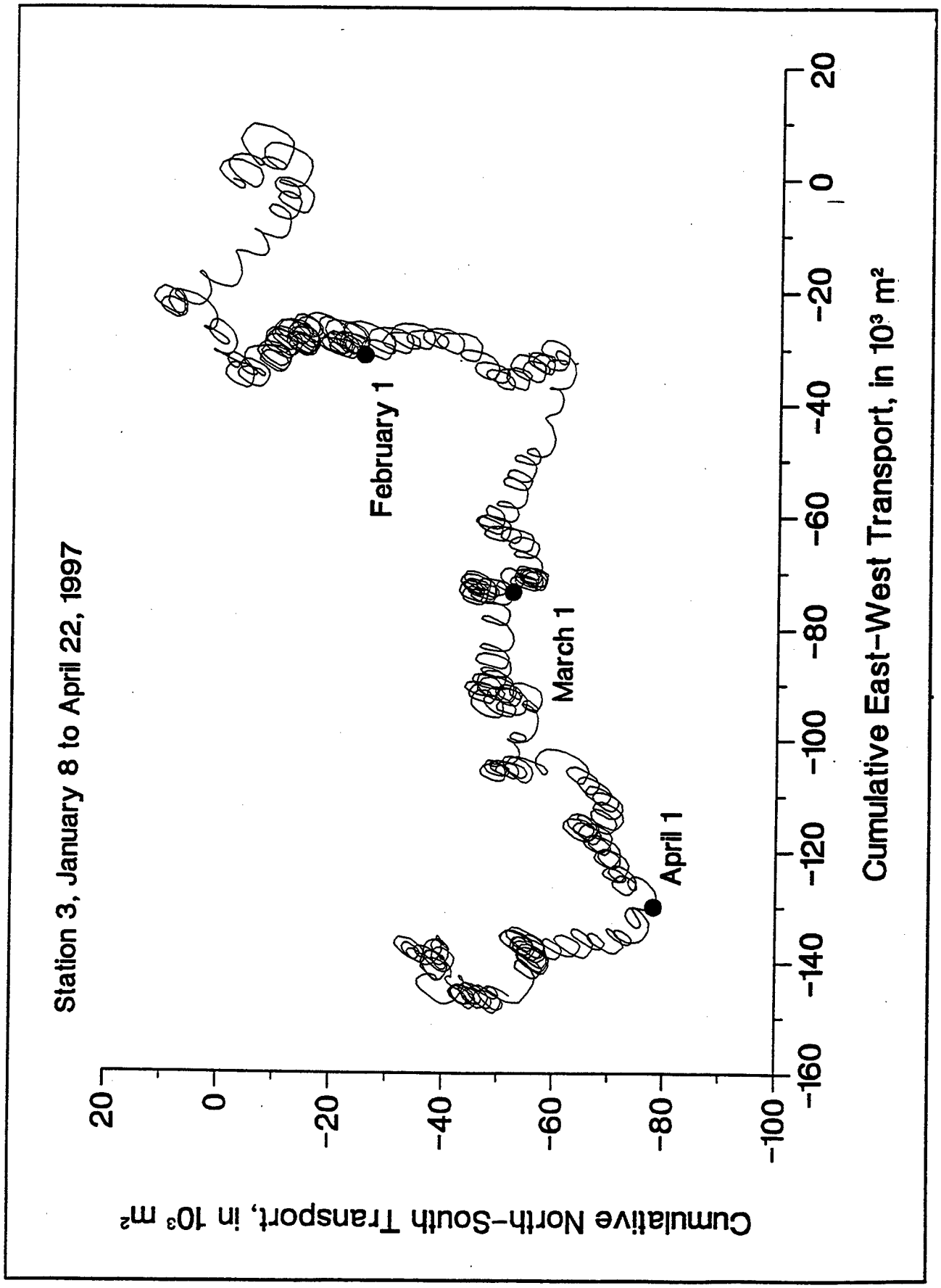
Station 3, January 8 to April 22, 1997
February 1
March 1
April 1
Cumulative East-West Transport, in 10³ m²
Cumulative North-South Transport, in 10³ m²
20
0
-20
-40
-60
-80
-100
-160
-140
-120
-100
-80
-60
-40
-20
0
20

Figure C8

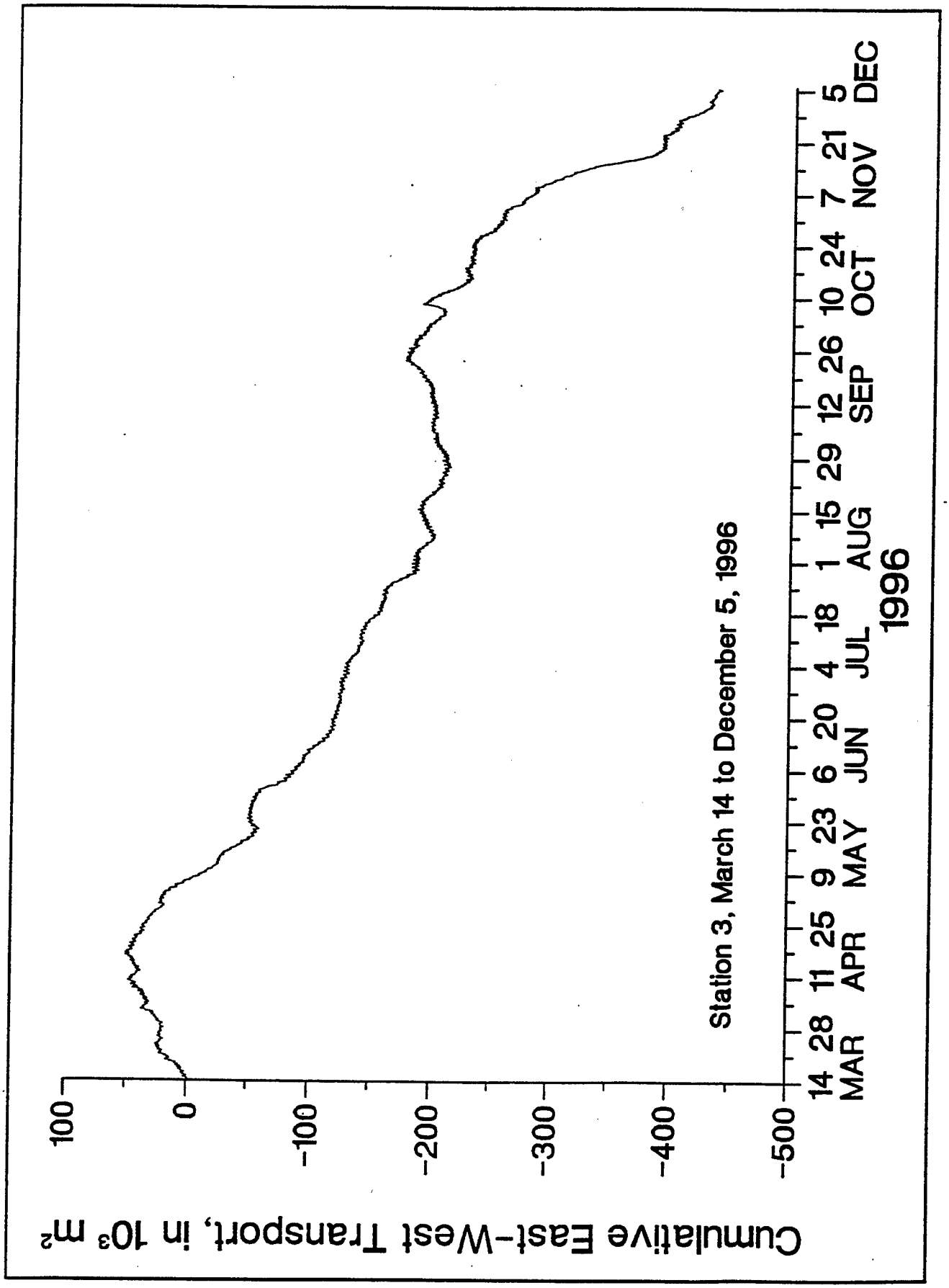
Cumulative East–West Transport, in 10^3 m^2
100
0
-100
-200
-300
-400
-500
Station 3, March 14 to December 5, 1996
14 28 11 25 9 23 6 20 4 18 1 15 29 12 26 10 24 7 21 5
MAR APR MAY JUN JUL AUG SEP OCT NOV DEC
1996

Figure C9

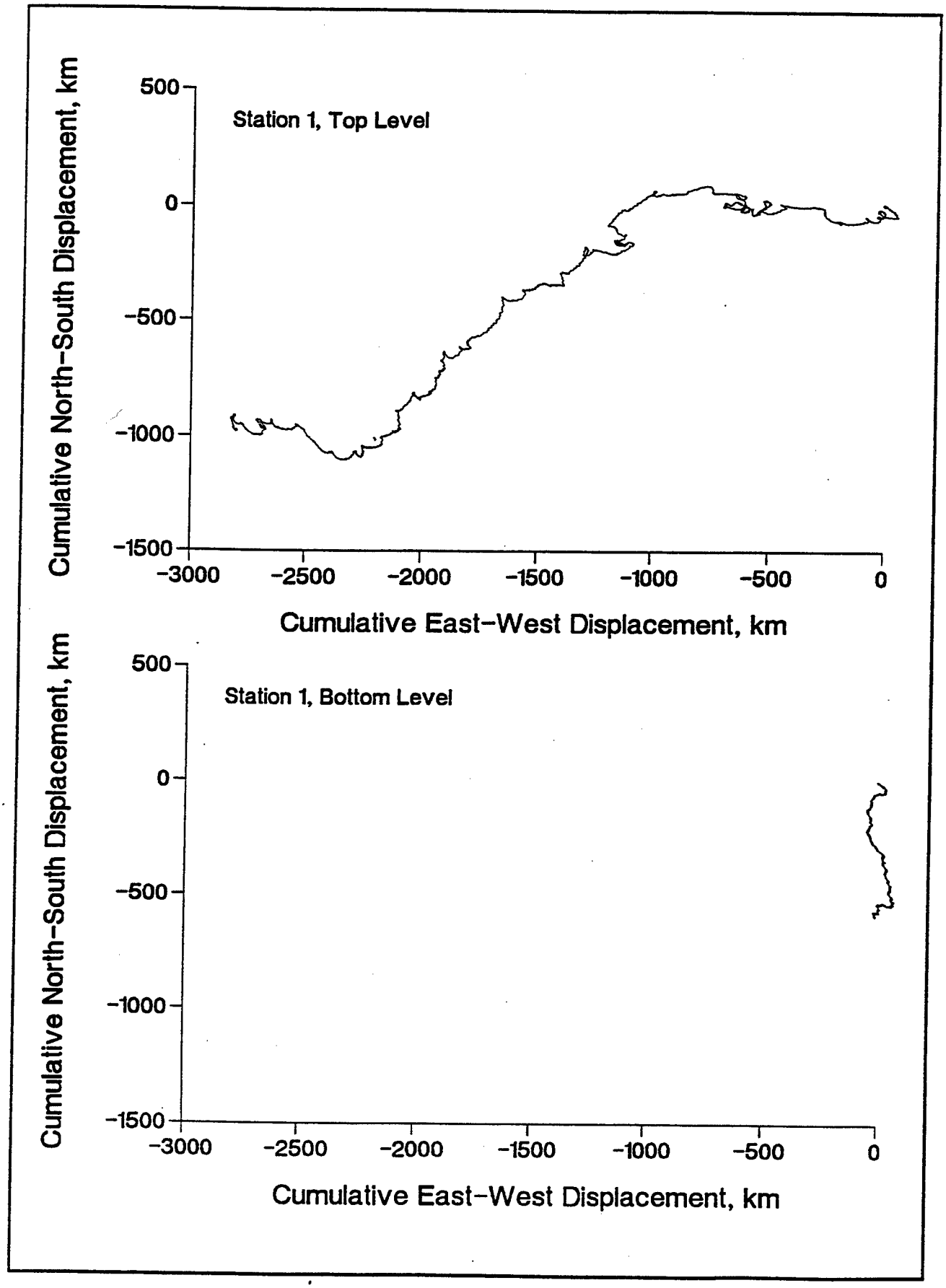
Station 1, Top Level
Cumulative North-South Displacement, km
500
0
-500
-1000
-1500
-3000
-2500
-2000
-1500
-1000
-500
0
Cumulative East-West Displacement, km
Station 1, Bottom Level
Cumulative North-South Displacement, km
500
0
-500
-1000
-1500
-3000
-2500
-2000
-1500
-1000
-500
0
Cumulative East-West Displacement, km

Figure C10

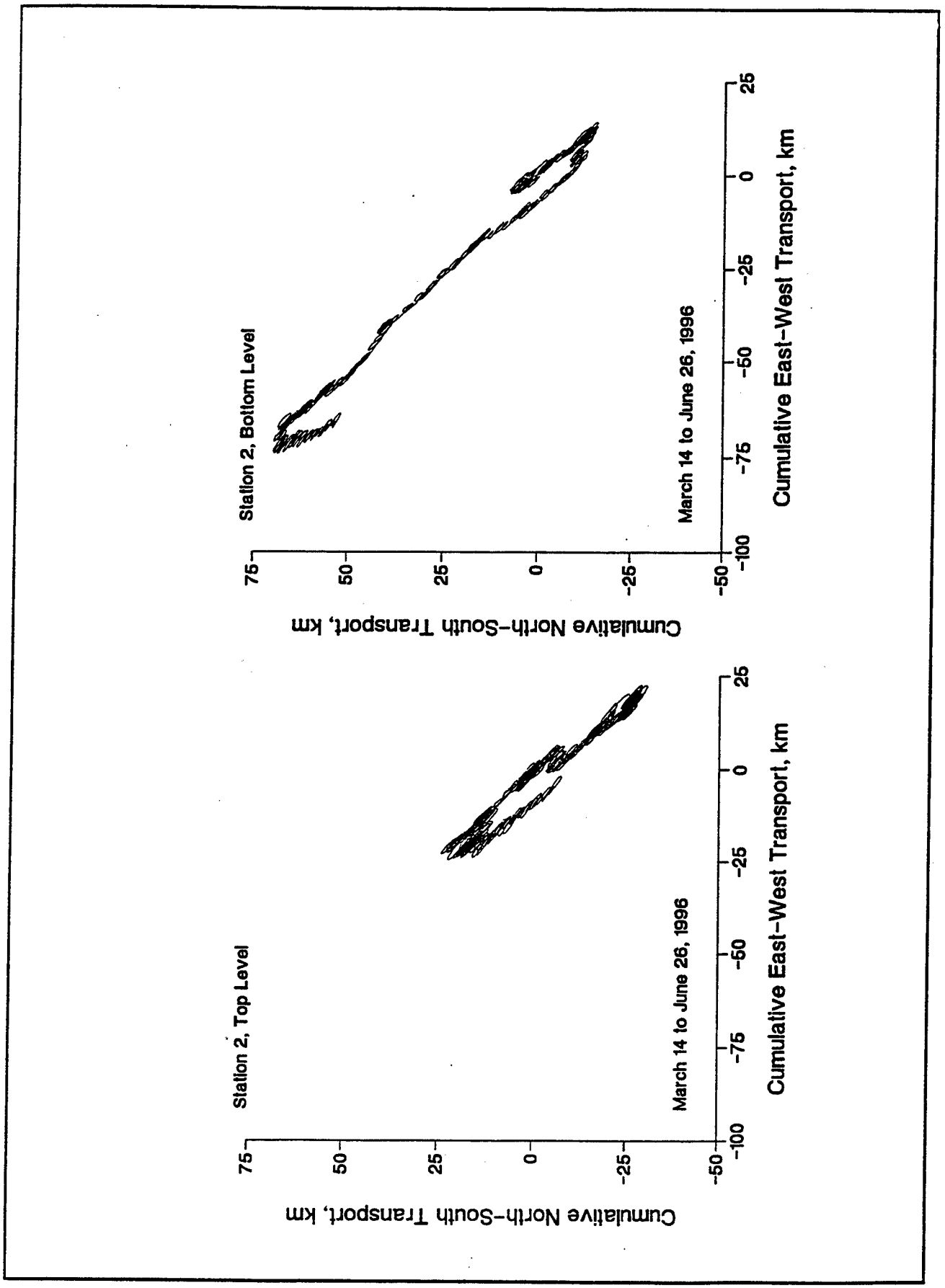
Station 2, Top Level
March 14 to June 26, 1996
Cumulative North-South Transport, km
Cumulative East-West Transport, km
75
50
25
0
-25
-50
-100
-75
-50
-25
0
25
Station 2, Bottom Level
March 14 to June 26, 1996
Cumulative North-South Transport, km
Cumulative East-West Transport, km

Figure C11

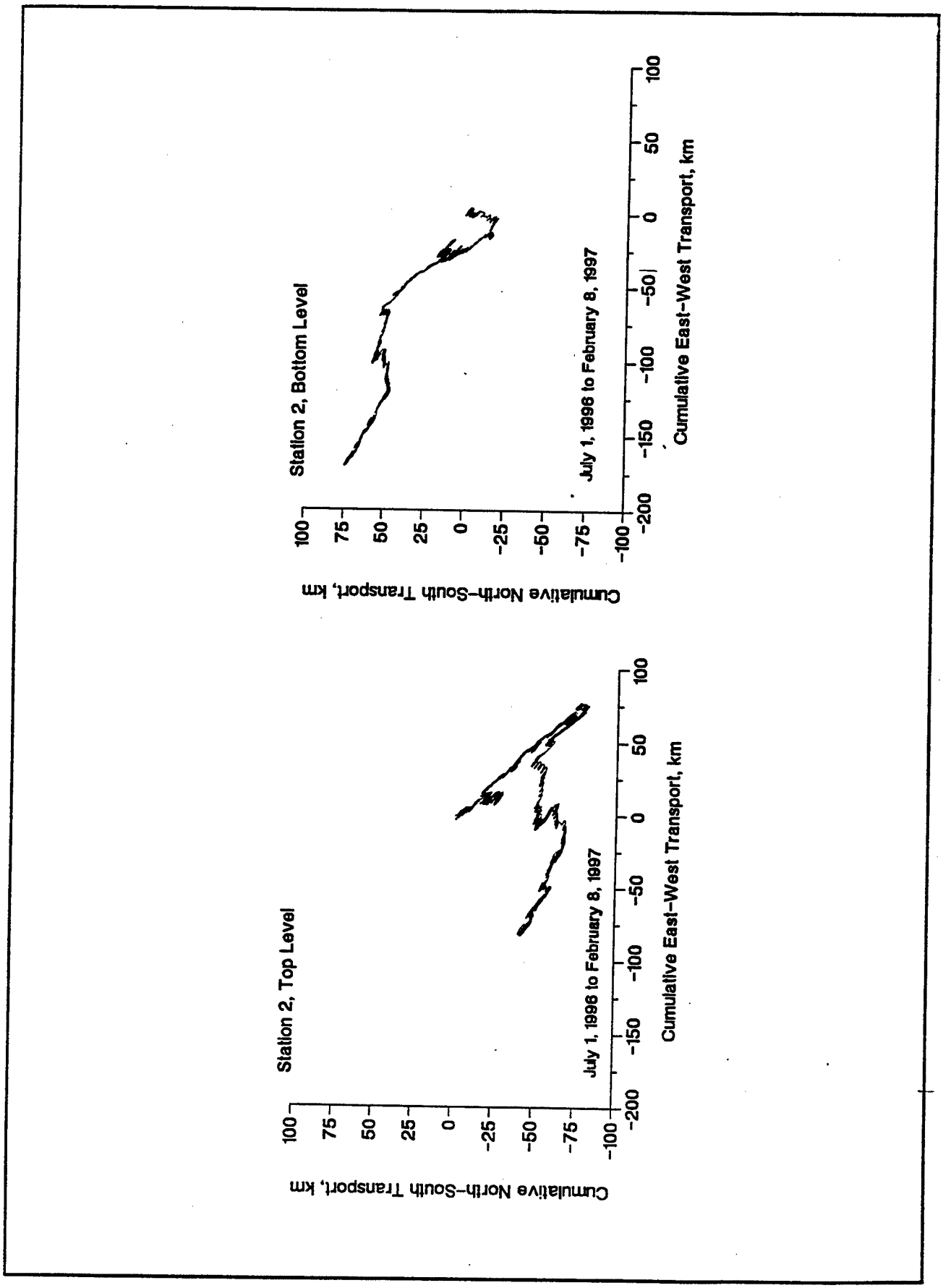
Station 2, Bottom Level
July 1, 1996 to February 8, 1997
Cumulative East-West Transport, km
Cumulative North-South Transport, km
100
75
50
25
0
-25
-50
-75
-100
-200
-150
-100
-50
0
50
100
Station 2, Top Level
July 1, 1996 to February 8, 1997
Cumulative East-West Transport, km
Cumulative North-South Transport, km

Figure C12

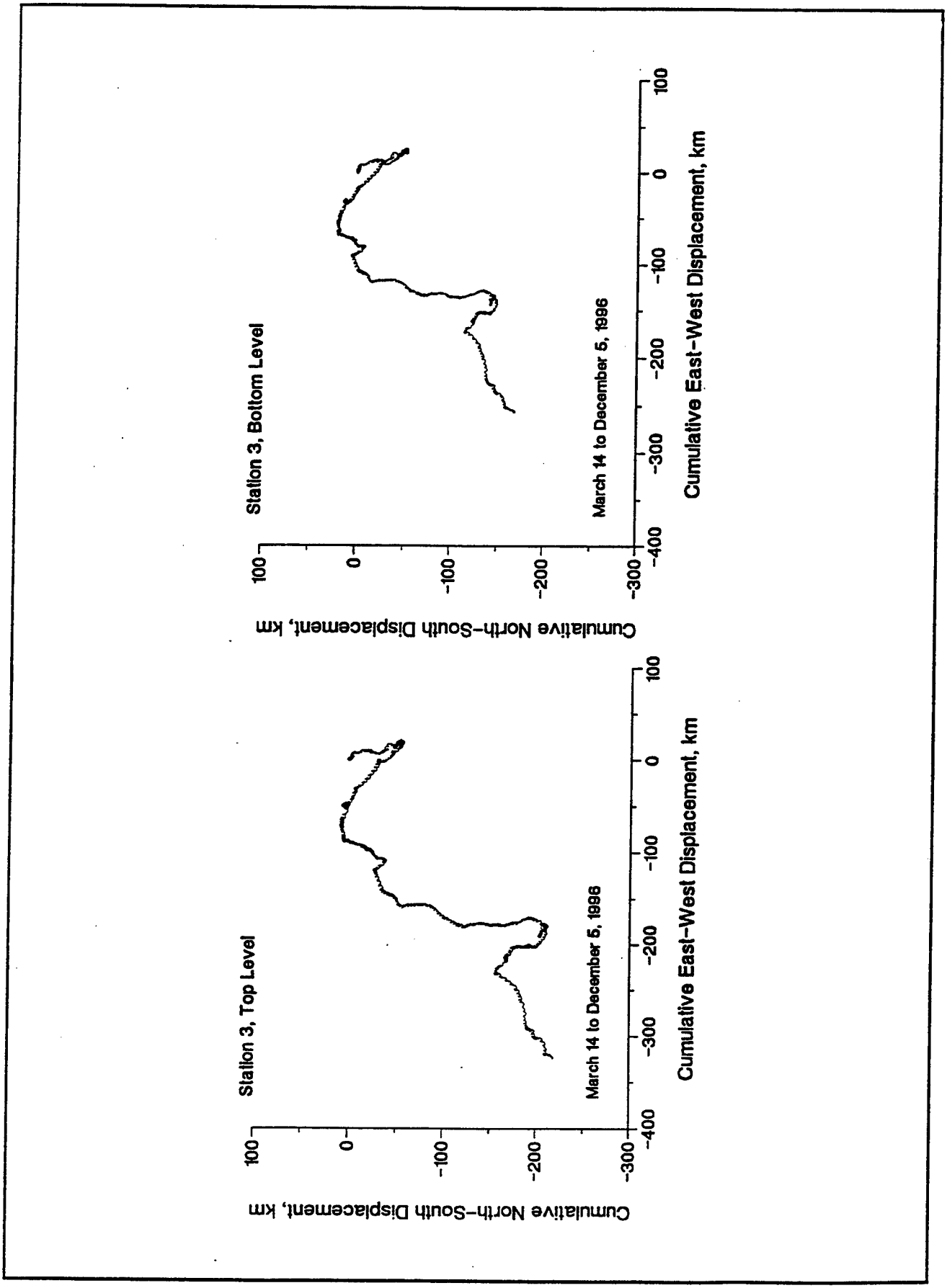
Station 3, Top Level
March 14 to December 5, 1996
Cumulative North–South Displacement, km
Cumulative East–West Displacement, km
100
0
-100
-200
-300
-400
Station 3, Bottom Level
March 14 to December 5, 1996
Cumulative North–South Displacement, km
Cumulative East–West Displacement, km
100
0
-100
-200
-300
-400

Figure C13

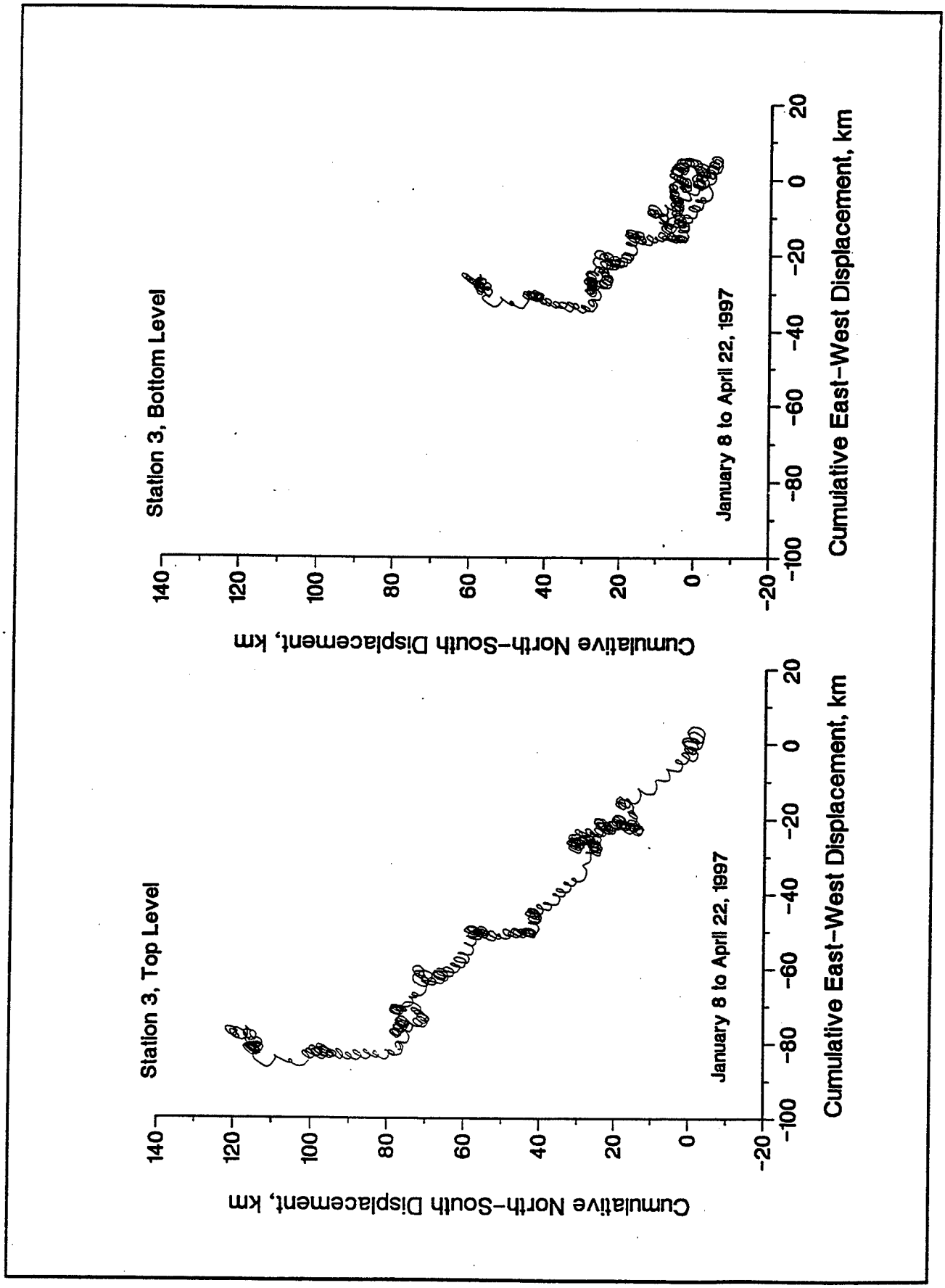
Station 3, Top Level
Station 3, Bottom Level
Cumulative North–South Displacement, km
Cumulative East–West Displacement, km
January 8 to April 22, 1997
140
120
100
80
60
40
20
0
-20
-100
-80
-60
-40
-20
0
20

Figure C14

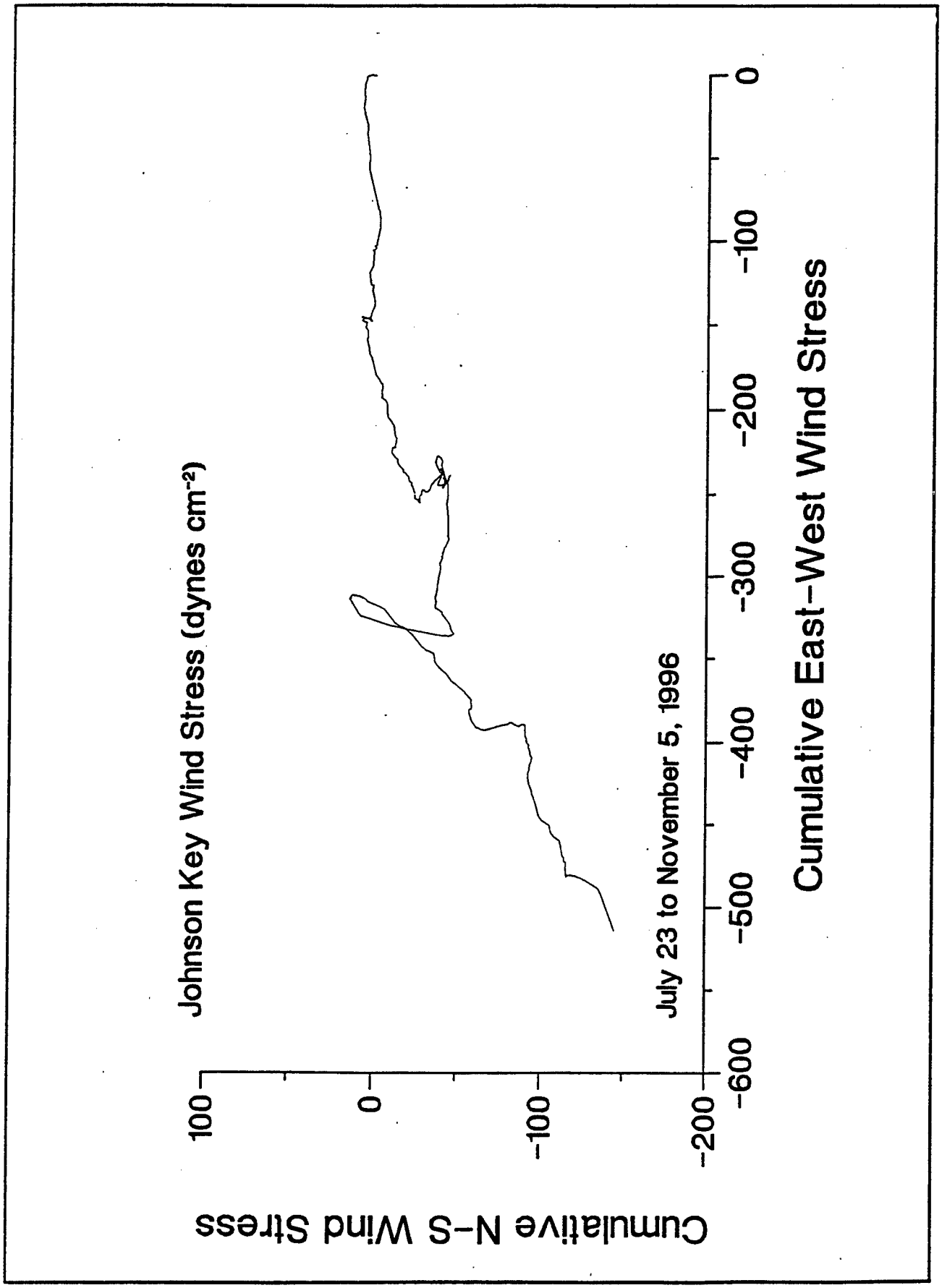
Johnson Key Wind Stress (dynes cm-2)
July 23 to November 5, 1996
Cumulative East-West Wind Stress
Cumulative N-S Wind Stress
100
0
-100
-200
0
-100
-200
-300
-400
-500
-600

Figure C15

APPENDIX D

AN ANALYSIS OF ACOUSTIC DOPPLER CURRENT PROFILER DATA FROM TIDAL CHANNELS IN EASTERN FLORIDA BAY

The contents of this appendix are to provide information on the additional analysis of the ADCP data provided by the Harbor Branch Oceanographic Institution (HBOI) in support of the hydrodynamic numerical modeling effort. The results of this analysis is to provide maximum discharge values and cumulative half-tidal-cycle discharge values for each of the principal tidal constituents. In addition, analysis results will provide the time series cumulative total discharge through each of the tidal channels monitored and a determination of the relative importance of transient wind events. A detailed summary of the HBOI analyses of the ADCP data is provided herein.

An Analysis of Acoustic Doppler Current Profiler Data from Tidal Channels in Eastern Florida Bay

Ned P. Smith
Harbor Branch Oceanographic Institution
5600 U.S. Highway 1, North
Fort Pierce, Florida 34946

INTRODUCTION

In September 1996 and February 1997, the U. S. Army Engineer Waterways Experiment Station (WES) conducted field studies to record tidal and nontidal discharges through 19 channels along the eastern and southern sides of Florida Bay. Two intensive studies were scheduled to coincide with wet season and dry season times of year. The channels were crossed repeatedly (Table D1) during a single semidiurnal tidal cycle using a boat-mounted acoustic doppler current profiler (ADCP). Five of the channels were in the interior of Florida Bay (Jewfish Creek connects Blackwater Sound with Barnes Sound.); the remaining 14 channels connect Florida Bay with Hawk Channel on the Atlantic side of the Keys. The survey included channels as far south as the Seven Mile Bridge Channel on the Key West side of Marathon.

In a February 29, 1996, response to a Request for Quotations issued by the Jacksonville District Office, Harbor Branch Oceanographic Institution (HBOI) offered to analyze the ADCP data in support of a parallel modeling effort that was underway at WES. Included in the Scope of Work was Task 1: "Develop the methodology to calculate transport through tidal channels using data from intensive surveys. In channels where anchor station data exist, compare the transport calculations from each method to develop and/or refine the relationship between anchor station data and tidal transport. Develop methodologies that can be used to compare transport computed by RMA2-WES with measurements" A later (October 7, 1996), more specific listing of the collaborative research effort included the following:

a. WES will provide HBOI with boat-mounted ADCP data from the first intensive survey. The format of the data will be mutually agreed upon and WES will provide initial data reduction as required to meet format specifications (Oct/Nov 1996).

b. WES will provide HBOI with boat-mounted ADCP data from the second intensive survey. The format of the data will be mutually agreed upon and WES will provide initial data reduction as required to meet format specifications (Mar/Apr 1997).

c. HBOI will prepare an analysis and report. Where locations of intensive surveys

coincide with HBOI long-term velocity meters, correlation of the long-term time series with the short-term time series will be examined.

This final report contains the analysis of the ADCP data from the September 1996 and February 1997 intensive surveys. The purpose is to describe the data obtained from the intensive surveys, describe the methodology utilized in the analysis of the data, and describe the results within the context of tidal and nontidal transport at each study site. Where possible, results have been integrated with results that came out of the two other components of the field study: three weather stations were maintained in the northern part of the bay and three acoustic doppler profiler stations were in operation along the open western boundary of the bay.

This report has three subsections, defined by the availability of historical current meter data from the 19 tidal channels. The first subsection includes plots and a brief discussion of WES data collected from nine channels in which Harbor Branch has no historical data: Adams Cut (Range 2), Dusenbury Creek (Range 3), Grouper Creek (Range 4), Baker Cut (Range 5), Cowpens Cut (Range 7), Tea Table Relief Channel (Range 10), Lignumvitae Channel (Range 13), Tom's Harbor Cut (Range 17), and Tom's Harbor Channel (Range 18). In four channels (Tea Table Relief Channel, Lignumvitae Channel, Tom's Harbor Cut, and Tom's Harbor Channel), historical data from nearby channels permit comparisons and estimates of tidal exchanges. The second subsection includes plots from seven channels in which Harbor Branch has historical data, but which were not instrumented at the time of the WES survey: Snake Creek (Range 8), Whale Harbor Channel (Range 9), Indian Key Channel (Range 12), Channel Two (Range 14), Channel Five (Range 15), Long Key Channel (Range 16), and Seven Mile Bridge Channel (Ranges 19 [east part] and 20 [west part]). In all except Seven Mile Bridge Channel, results from Harbor Branch channel calibration exercises are available for comparison with the WES discharge data. The third subsection includes results from three channels in which Harbor Branch studies coincided with the WES intensive study: Jewfish Creek (Range 1), Tavernier Creek (Range 6), and Tea Table Channel (Range 11). For these, the analysis consists of plots, estimates of tidal exchanges, and a translation of historical current meter records into corresponding time series of discharge.

The application for the results of the analysis of the ADCP data is the initialization and/or validation of the hydrodynamic model that is under development at WES. Specifically, the methodology is intended to:

a. provide maximum instantaneous discharge values for each of the principal tidal constituents;

b. provide cumulative half-tidal-cycle discharge values for each of the principal tidal constituents;

c. provide time series of cumulative total discharge through each of the tidal channels

for which Harbor Branch and WES studies were being conducted simultaneously; and

d. provide a measure of the relative importance of transient wind events.

For the purpose of model validation, estimates of discharge that involve tidal exchanges (items a and b above) will probably be most useful.

WES personnel have provided maps of the ADCP transects across each of the channels it investigated. To put these individual study sites in a better geographical perspective, Figure D1 shows all 20 ranges in 19 tidal channels. Also, WES has calculated total channel discharge for each crossing; channel discharge was recorded 8 to 11 times over nearly complete semidiurnal tidal cycles. Thus, the methodology developed for this report is that which is needed to interpret the short-term WES discharge data, using the long time series of bottom pressure and of current speed and direction obtained in the Harbor Branch studies. Several analytical techniques have been used to obtain conversion factors needed to translate the Harbor Branch data into time series of total (tidal and nontidal) volume transport. The 19 channels cannot be treated the same because of differences in the historical data available from Harbor Branch.

THE DATA

The data used to quantify discharge through the 19 tidal channels were obtained from an acoustic doppler current profiler; some of the details of each channel transect are summarized in Table D1. The raw data were not sent to Harbor Branch--only the total discharge values as a function of time. Details of the data collection techniques, as well as details of the instrumentation and study sites, were not available and thus are not included here.

The data used to obtain time series of water level were bottom pressure records obtained at midchannel study sites. Data came from either a Sea Data TDR-3 pressure recorder or a Brancker Model TG-205 pressure recorder. The TDR-3 has an accuracy of 1.2 mb (equivalent to 1.2 cm) and a resolution of 0.5 cm, according to the manufacturer's specifications. The TG-205 has an acccuracy of 2.1 cm and a resolution of 0.6 cm. Thus, both instruments are capable of quantifying tidal constituents with amplitudes as small as 0.5 cm (tidal ranges of 1 cm). An amplitude of 1 cm (tidal range of 2 cm) is used to qualify a tidal constituent as one of the "principal" tidal constituents.

Data used to characterize middepth currents are General Oceanics Mark I and Mark II inclinometer current meters. The stated speed and direction accuracies of the inclinometers are 1 cm s^{-1} and 1°, respectively.

METHODOLOGY

The methodology used for the analysis of the WES data and for the comparison of the WES and HBOI data varied according to the availability and amount of historical data for a given tidal channel. When no historical data were available, the WES data could be described only as it was received, using plots of discharge versus time. When historical data were available from earlier Harbor Branch studies, the tidal component of the WES data could be described. When Harbor Branch studies coincided with the intensive WES studies, both the tidal and nontidal components of the discharge for a given channel could be described.

Several terms are used repeatedly in the RESULTS section, and it is important to define the terminology that is used in this report. Harbor Branch studies, with a current meter in midchannel and just below middepth and with a bottom-mounted pressure recorder to record the rise and fall in water level, permitted calculations of two-dimensional transport. The ebb and flood of the current recorded at a single level were extrapolated to the surface and to the bottom by assuming a logarithmic current profile, and the along-channel current, u, as a function of height above the bottom, z, is given by

$$u_z = \frac{u_*}{k} \log_e \frac{z}{z_o} \qquad \text{(D1)}$$

where u_* is the friction velocity, k is the von Kármán constant (0.41), and z_o is the roughness coefficient. Given the profile, one can integrate over the total water depth to determine the depth-averaged current, U, and the product of the depth-averaged current and the water depth gives the two-dimensional transport in the along-channel direction. The units of the instantaneous transport are $ft^2\ s^{-1}$ or $m^2\ s^{-1}$. Accumulating transport with time, one obtains cumulative net transport in ft^2 or m^2. This can be thought of as the area of the "sheet" of water that moves past the study site over any given time interval. The area will expand and contract over the course of a tidal cycle, but over many tidal cycles it will increase according to the magnitude of the long-term net inflow or outflow through the channel.

Two-dimensional transport can be calculated from any time series of current speed (tidal plus nontidal) and bottom pressure (tidal plus nontidal), and it can be calculated using tidal predictions as input (the predicted ebb and flood of the current and the predicted rise and fall of the water surface). When the analysis is restricted to tidal processes, the calculations quantify a transport mechanism known as "tidal pumping." In most tidal channels, high tide will occur during the flood half of the tidal cycle, and low tide will occur during the ebb. Thus, with high water coinciding with flood tide and low water coinciding with ebb tide, more water enters with the flood than leaves with the ebb. Tidal cycle after tidal cycle, tidal pumping can provide a baseline transport mechanism that is both dependable and predictable. In the case of the tidal channels in the Florida Keys, tidal pumping acts to force water from Hawk Channel into Florida Bay. The local tidal pumping process can be opposed by other regional-scale transport processes that will reverse the net inflow into Florida Bay. If a

similar tidal pumping by Gulf tides entering the bay from the western side is greater than the tidal pumping by Atlantic tidal waves entering through tidal channels, then ebb currents in the tidal channels will be stronger, or last longer, resulting in a net outflow. This appears to be the case in all the tidal channels of the Middle Keys and in nearly all the tidal channels in the Upper Keys.

One of the primary functions of the WES intensive surveys is to provide the data base needed for translating two-dimensional transport at the Harbor Branch study site into discharge for the channel as a whole. Because the HBOI and WES data generally did not coincide in time, however, and because nontidal flow across the WES transect is probably not the same as nontidal flow at the Harbor Branch study site at another place and/or time, the comparison must involve tidal predictions from the Harbor Branch studies with the tidal component of the total discharge recorded by WES. Regressing total discharge against predicted two-dimensional transport provides a regression equation that can be used to translate two-dimensional tidal transport in midchannel to *tidal transport only* for the channel as a whole. It is possible that the y-intercept of the regression line provides additional information on the nontidal discharge onto which the ebb and flood of the tide is superimposed. As discussed later, however, there is some confusion regarding what information the y-intercept provides; thus, any attempt to equate the y-intercept with the nontidal discharge recorded at the same time is accompanied with qualifying remarks. While a regression equation is useful for calibrating a hydrodynamic model, its usefulness for describing long-term net transport through these tidal channels is questionable.

Three-dimensional transport (a term used interchangeably with discharge in this report) is obtained by pairing the slope of the regression equation with the two-dimensional transport. The slope will have units of "$ft^3\ s^{-1}$ per $ft^2\ s^{-1}$" if the two-dimensional transport is calculated in English units or "$ft^3\ s^{-1}$ per $m^2\ s^{-1}$" if the two-dimensional transport is calculated in metric units. The regression equation also quantifies a y-intercept which is needed to reproduce discharge recorded during the intensive survey. As noted above and as will be shown in the following section, however, the y-intercept leads to unrealistic long-term discharge estimates.

The cross section of the channel used to obtain the ADCP discharge data did not include the study site for the Harbor Branch current meter; thus, it is not possible to correlate the point measurement with a specific point in the ADCP transect. This is not felt to be a major qualification, however, because discharge values must be virtually the same along the entire length of a channel. Of greater importance than measurements that coincide in location are measurements that coincide in time. To compare discharge and two-dimensional transport occurring at any given time, tidal predictions are made using the method described by Schureman (1958). At any time, t, the water level associated with the tide is given by

$$h(t) = H_o + \sum_{i=1}^{m} A_n \cos(a_i t + \alpha_i) \qquad \text{(D2)}$$

where H_o is the mean water level (obtained from the time series of bottom pressures), A_n is the node-corrected amplitude of the ith tidal constituent (i.e., corrected for the approximately 19-year variation in the moon's node), a_i is the angular speed of the ith constituent (e.g., 28.9841° hr^{-1} for the M_2 constituent), and α_i is the modified epoch, as defined by Schureman (1958).

To identify the principal tidal constituents, the harmonic analysis program used by the National Ocean Service (NOS) on 29-day time series was used (Dennis and Long, 1971). For currents, vectors were broken into along-channel and across-channel components. Only the along-channel components were used to calculate two-dimensional transport for comparison with the ADCP dis-charge data. When time series are considerably longer than 29 days, multiple harmonic analyses provided several pairs of amplitudes and local phase angles for each of the principal tidal constituents. In these cases, harmonic constants were vector averaged to provide values more representative of the entire time series. Tidal analysis can involve model output as easily as it can involve field observations. Model output from grid points corresponding to the ADCP ranges can be analyzed to show which tidal constituents the model is reproducing. Also, for transport calculations, it is important that for all of the important constituents both amplitudes and local phase angles are being reproduced accurately for the rise and fall of the water surface as well as for the ebb and flood of the tide.

For the three channels investigated simultaneously by WES and Harbor Branch, the ratio of the measured channel discharge to the calculated midchannel two-dimensional transport (the slope of the regression line) can be used to translate any time series of two-dimensional transport into a time series of discharge. The cumulative net transport diagram is one of the best ways to represent long time series of hourly discharge values. The diagram is constructed by plotting cumulative transport as a function of time, with positive and negative flow defined according to the WES convention. The resulting pattern approximates how water moves through the tidal channel at the WES transect. The end points of the plot, together with the time interval that separates them, can be used to calculate the resultant flow. Cumulative net transport diagrams are not well suited for tracking flow patterns over the shorter time scales of hours to days, but they summarize general flow patterns nicely.

RESULTS

In the first part of this section, results from the September 1996 intensive survey are presented, along with descriptions of each study site. In the second part, results from the February 1997 survey are presented, along with some remarks to compare the two seasonal studies.

As noted in the INTRODUCTION, results are grouped in three subsections. In this first subsection, the eight channels that are discussed are those for which there are no historical data from Harbor Branch studies. WES discharge data are presented as plots accompanied by a brief discussion of discharge versus time. The WES discharge data cannot

be interpreted with the aid of longer time series needed to characterize tidal and nontidal exchanges.

1A. TIDAL CHANNELS WITH NO HISTORICAL DATA - September 1996 Survey

a. Range 2, Adams Cut

Adams Cut connects the southeast side of Blackwater Sound with Largo Sound on the Atlantic side of Key Largo. Range 2 was on the Blackwater Sound side of Adams Cut. Figure D2 is a plot of the 11 crossings made on September 26. Positive transport is eastward, by definition, carrying water from Blackwater Sound into Largo Sound. The approximately nine hours of data show a well-defined tidal variation, with flood tides into Blackwater Sound occurring during the first part of the study period. Maximum flood transport of just over 2,700 $ft^3 s^{-1}$ is nearly twice as strong as the maximum ebb transport of 1,375 $ft^3 s^{-1}$. Because historical data are not available from this channel, it is not possible to differentiate between flood dominance resulting from a diurnal equality in the tide and a flood dominance resulting from a nontidal inflow during this time period. The available data can be used for comparison with model output, however, insofar as it shows a well-defined tidal fluctuation and strongest flood/ebb transport within the range of 1000-3000 $ft^3 s^{-1}$.

b. Range 3, Dusenbury Creek

Dusenbury Creek lies on the south side of Blackwater Sound and connects Blackwater Sound with Tarpon Basin. Range 3 was on the Blackwater Sound side of Dusenbury Creek. Figure D3 shows transport recorded during the 10 crossings on September 26. Positive transport is northward, by definition, carrying water out of Tarpon Basin into Blackwater Sound. Because Dusenbury Creek exchanges water between two semi-enclosed basins, the tidal signal in the plot is small and difficult to detect. Throughout the eight-hour study period, transport is into Tarpon Basin, and the flow is both irregular and within a relatively narrow range. Wind observations have not been isolated for this time period, but it is likely that the slow filling of Tarpon Basin represents a response to wind forcing in some form.

c. Range 4, Grouper Creek

Grouper Creek connects the south end of Tarpon Basin with the north side of Buttonwood Sound. Range 4 was on the Buttonwood side of Grouper Creek. Figure D4 shows transport values obtained during 10 crossings on September 26. Negative transport is southward, by definition, carrying water out of Tarpon Basin and into Buttonwood Sound. Because both Tarpon Basin and Buttonwood Sound are relatively isolated, tidal exchanges through Grouper Creek are poorly defined. Throughout the study period, flow is into Buttonwood Sound, and it increases irregularly. As expected, similar transport values were found for Dusenbury Creek and Grouper Creek, at opposite ends of Tarpon Basin. These two channels feed and drain Tarpon Basin. The two channels have roughly the same cross-sectional area, and both constitute segments of the Intracoastal Waterway.

d. Range 5, Baker Cut

Baker Cut lies along the south side of Buttonwood Sound and connects Buttonwood Sound with the northeast corner of Florida Bay proper. This is a very short segment of the Intracoastal Waterway, and Range 5 occurs where Buttonwood Sound meets Florida Bay. Figure D5 is a plot of the 10 crossings made on September 26. Positive transport indicates northward flow into Buttonwood Sound, thus, taken together, the transport recorded in Grouper Creek and Baker Cut represent a convergence of water in Buttonwood Sound. The recorded transport is irregular, with strong northward flow into Buttonwood Sound interrupted for two hours by nearly slack-water conditions. A tidal signal is difficult to detect in the data.

e. Range 7, Cowpens Cut

At Cowpens Cut, the Intracoastal Waterway passes through Cross Bank on the north side of Cotton Key Basin. It is located 1.05 nautical miles (1.94 km) southwest of the Florida Bay end of Tavernier Creek, and it is 3.15 nautical miles (5.83 km) northeast of the bay side of Snake Creek, thus flow through the cut should show a well-defined tidal signal. Range 7 was toward the northern end of Cowpens Cut. Figure D6 is a plot of the 10 crossings on September 27. Positive transport is northward by definition. Transport during this nine-hour time period traces a sinusoidal variation, suggesting that the ebb and flood of the tide is a prominent component of the total current. The southward flow during the first three hours of the survey, together with inflow (northward flow) through Tavernier Creek during the same time, suggests that tidal exchanges through Cowpens Cut are a continuation of flow through Tavernier Creek. It is noteworthy, however, that the flow has reversed in Cowpens Cut by 1000 EST, while the flow in Tavernier Creek does not start to ebb until around 1300 EST. The reversal of the flow through Cowpens Cut may therefore also be influenced by the substantial volumes of water exchanged through Snake Creek.

f. Range 10, Tea Table Relief Channel

Tea Table Relief Channel exchanges water directly between Hawk Channel and Florida Bay. Because of the rise and fall of the tide in Hawk Channel, the transport values in Figure D7 show a well-defined tidal signal. Range 10 was on the bay side of the bridge. Positive values indicate flow into Florida Bay. Harbor Branch has not measured the flow in Tea Table Relief Channel, but historical data are available from Tea Table Channel, just 0.5 nautical mile (0.89 km) to the southwest. Thus, it is possible to use the Tea Table Channel time series to help interpret the Tea Table Relief Channel transport data. Using the predicted tidal current from Tea Table Channel as the independent variable and the measured total transport from Tea Table Relief Channel as the dependent variable, linear regression reveals a highly significant ($p < 0.01$) relationship. The correlation coefficient is $+0.9448$, and $r^2 = 0.8927$. Thus, to a close approximation, the flow through Tea Table Channel can be used to estimate tidal transport through neighboring Tea Table Relief Channel. For example, the amplitude of the M_2 tidal constituent in Tea Table Channel is 44.27 cm s^{-1}, or 1.45 ft s^{-1}. From linear regression, the slope of the regression line that relates transport in Tea Table Relief Channel to current speeds in Tea Table Channel is 1529.7 ft^3 s^{-1} per 1 ft s^{-1}. Thus, the M_2 amplitude translates into maximum flood and ebb transport rates of 2,218 ft^3 s^{-1}. This number would be

useful for model verification purposes, if the model were driven only by M_2 tides. Four other tidal constituents are also significant in Tea Table Channel. The S_2, N_2, K_1, and O_1 constituents, with amplitudes of 8.7, 8.3, 8.5, and 8.2 cm s^{-1}, would transport 439, 417, 374, and 414 ft^3 s^{-1}, respectively, at maximum flood and ebb tide. For any given tidal cycle, the interaction of these five tidal constituents will occur in additive and subtractive ways. Thus, M_2 exchanges can be thought of as a baseline level that will increase or decrease by several hundred cubic feet per second under spring or neap tide conditions. Harmonic analysis of model output for Tea Table Relief Channel will determine whether the model is over- or underestimating tidal exchanges. But the above values may be useful in the early stages of model tuning.

g. Range 13, Lignumvitae Channel

Lignumvitae Channel lies 0.6 nautical mile (1.1 km) southwest of Indian Key Channel, and it exchanges water directly between Florida Bay and Hawk Channel. Figure D8 shows a prominent tidal variation. Range 13 was on the bay side of the bridge. Again, positive values indicate a transport of water into Florida Bay. Here, too, Harbor Branch has not made long-term measurements, but results from flow through nearby Indian Key Channel are strongly correlated with flow through Lignumvitae Channel and therefore provide a basis for comparison. Using predicted tidal currents from Indian Key Channel with measured total transport through Lignumvitae Channel, linear regression indicates a correlation coefficient of +0.9847. The r^2 value of 0.9697 indicates that 97% of the variance in the measured transport can be explained by the predicted ebb and flood of the tide through adjacent Indian Key Channel. Again, the slope of the regression line can be used with the amplitudes of the principal tidal constituents to estimate the volume of water exchanged through Lignumvitae by the ebb and flood of the tide. The M_2 amplitude for Indian Key Channel is 1.44 ft s^{-1}, and the slope of the regression line is 4,798.1 ft^3 s^{-1} per 1 ft s^{-1}. Thus, at maximum flood and ebb, the M_2 constituent is moving 6,930 ft^3 s^{-1} of water through Lignumvitae Channel. For the S_2, N_2, K_1, and O_1 constituents, the maximum flood and ebb volume transports are 1,192, 1,228, 1,182, and 1,294 ft^3 s^{-1}. It follows that significant spring-neap tide differences can occur, as well as significant diurnal inequalities. Nevertheless, for model calibration purposes, discharge values for Lignumvitae Channel should average approximately $\pm$7,000 ft^3 s^{-1} for tidal exchanges.

h. Range 17, Tom's Harbor Cut

Tom's Harbor Cut lies just to the west of Long Key Channel in the Middle Keys, and it exchanges water directly between Hawk Channel and Florida Bay. Range 17 was between the old and new bridges. By definition, positive transport values indicate northward flow into Florida Bay. Harbor Branch has not measured flow through Tom's Harbor Cut, but the similarity of flow through Long Key Channel and flow through Tom's Harbor Cut can be used to quantify the tidal component of the flow through the cut. Figure D9 shows the last part of an ebb tide, all of the following flood, and approximately the first half of the next ebb. Regressing the transport values against the predicted tidal currents for the same times, the correlation coefficient is +0.9767, indicating that the predicted tide in Long Key Channel can

be used to explain 95.4% of the variance in the measured total transport. The slope of the regression line is 10,961.5 $ft^3 s^{-1}$ per 1 ft s^{-1}. Combining this with the amplitude of the M_2 tidal constituent, one gets a maximum flood or ebb tidal transport of 17,341 $ft^3 s^{-1}$, and total transport is 156.01 x 10^6 ft^3 during any half M_2 tidal cycle. From the amplitudes of the other principal tidal constituents, one gets maximum transport values of 3,791, 3,244, 3,841, and 3,906 $ft^3 s^{-1}$ for the S_2, N_2, K_1, and O_1 constituents.

i. Range 18, Tom's Harbor Channel

Tom's Harbor Channel is the last of the tidal channels included in the intensive survey that was not among those investigated at some previous time by Harbor Branch. But again, the proximity of Tom's Harbor Channel to Long Key Channel, together with the availability of historical data from Long Key Channel makes possible estimates of tidal discharge. Tom's Harbor Channel lies 0.9 nautical mile (1.67 km) west of Tom's Harbor Cut. Range 18 was between the old and new bridges of U.S. 1, and positive transport indicates flow into Florida Bay. The similarity of the Tom's Harbor Channel plot (Figure D10) and the Tom's Harbor Cut plot (Figure D9) is not surprising, given the proximity of these two channels, and it suggests that tidal exchanges through Tom's Harbor Channel can be estimated from Long Key Channel data, just as tidal exchanges through Tom's Harbor Cut can. Linear regression of total transport against predicted tidal currents produces a correlation coefficient of +0.8862. This is significantly lower than the correlation coefficient found for Tom's Harbor Cut, and only 78.5% of the variance in the total transport can be explained by tidal variations in the current in Long Key Channel. The lower correlation may be a result of any of several factors. It may be due to the somewhat greater distance from Long Key Channel to Tom's Harbor Channel, or it may be related to the blocking effect that Tom's Harbor Keys have on tidal exchanges on the Atlantic side of the channel. Perhaps more likely, Channel Key Banks on the Florida Bay side of the channel may result in significantly different Gulf tides affecting Tom's Harbor Channel than either Tom's Harbor Cut or Long Key Channel. Topographic barriers such as this may limit the area for which Long Key Channel tidal conditions can be used to estimate tidal transport.

1B. TIDAL CHANNELS WITH HISTORICAL DATA - September 1996 Survey

a. Range 12, Indian Key Channel

Indian Key Channel is one of the five channels included in the WES intensive surveys in which Harbor Branch had carried out studies over the past 10 years, but which did not have a current meter in place during the WES survey. Indian Key Channel, lying between Tea Table Channel and Lignumvitae Channel, exchanges water directly between Hawk Channel and Florida Bay. Harbor Branch has conducted three studies in Indian Key Channel to quantify tidal and nontidal transport: September 1994 to March 1995, May 1995 to July 1995, and October 1995 to June 1996. During the second and third studies, pressure recorders were included to quantify the rise and fall in water level. As noted in the METHODOLOGY section, combining the rise and fall in sea level with the ebb and flood of the tide for the six principal tidal constituents, one can compute tidal transport. Regressing the total transport

against the tidal transport calculated for the same times, the slope of the regression line becomes a transfer function to translate midchannel tidal transport into the tidal discharge for the entire channel. The y-intercept can be thought of as a nontidal residual that remains once the tidal discharge has been accounted for by comparison with the tidal predictions. At best, however, the nontidal discharge obtained during the survey is a "snapshot" of a process that is variable over time scales of several days.

Figure D11 shows the predicted local tidal transport (surface to bottom) and the total discharge values for the intensive survey of Indian Key Channel on September 28, 1996. Positive values of both variables indicate northward flow into Florida Bay. The correlation coefficient for local tidal transport and total channel discharge was +0.9892, indicating that 98% of the variance can be explained by the ebb and flood, together with the coincident rise and fall in sea level. The slope of the regression line is +641 $ft^3 s^{-1}$ per 1 $ft^2 s^{-1}$ of local tidal transport. For example, if the water depth of Indian Key Channel is 10 ft and the vertically averaged current speed is 1 ft s^{-1}, then the local transport would be 10 $ft^2 s^{-1}$, and the channel discharge at that time would be 6410 $ft^3 s^{-1}$. The y-intercept is 487 $ft^3 s^{-1}$. As noted in the METHODOLOGY section, this value can be thought of as the nontidal discharge through the channel that was occurring at the time of the intensive survey.

Apart from the tidal predictions needed to calculate transport at the times of the WES crossings along Range 12, harmonic constants for water levels and tidal currents can be used to calculate the residual tidal transport over a complete tidal cycle for each tidal constituent. For example, the surface-to-bottom (but not laterally extrapolated) transport for the M_2 constituent totaled 468,650 ft^2 into Florida Bay on the flood tide and -434,241 ft^2 into Hawk Channel on the ebb. The residual transport was therefore +34,409 ft^2, and over the 12.421-hour M_2 tidal cycle the average was 0.7695 $ft^2 s^{-1}$. Using the slope obtained from the linear regression, it follows that the M_2 constituent is pumping Hawk Channel water into Florida Bay at a rate of 493 $ft^3 s^{-1}$ (i.e., 22.0 x 10^6 ft^3 per M_2 cycle). The actual discharge of water through Indian Key Channel, of course, will include the effects of the other tidal constituents. More importantly, however, the discharge of water through any tidal channel includes more than local effects. The long-term net outflow observed from Florida Bay through most of the tidal channels of the Middle Keys is evidence that the nonlocal forcing of tidal waves entering the western side of Florida Bay is significantly greater than the local effect of Atlantic tidal waves entering the bay from the east through these relatively small tidal channels. Thus, one should not look for a tidal pumping of water into Florida Bay in model simulations. The most significant results presented here are the maximum M_2 flood and ebb volume transport rates of +21,127 and -19,172 $ft^3 s^{-1}$, and the half-tidal-cycle cumulative transports of +298 and -276 x 10^6 ft^3.

Harbor Branch studies included channel calibration exercises designed to convert midchannel current measurements into channel discharge estimates. The Harbor Branch approach was to determine the surface current distribution across the channel based upon three measurements. Thus, lateral resolution is not good. Also, the vertical current profile is

interpolated from the estimated surface current to the bottom, assuming a logarithmic distribution. The advantage of this approach, however, is that surface currents that are felt to be spurious can be thrown out. Plots of ADCP data contain lateral variations that are undoubtedly related to turbulent eddies, yet these transport vectors are taken to represent all of the approximately one-hour time intervals that they represent. The Harbor Branch M_2 transport (which should be compared with the 22.0 x 10^6 ft^3 per M_2 tidal-cycle value noted above) is 7.33 x 10^6 ft^3 per M_2 tidal cycle. While this is of the same order of magnitude, it is only 33% of the WES value. Part of this is a result of the Harbor Branch channel calibration correction that places greater weight on ebb tide transport along the sides of the channel than on flood tide transport. Calibration data from along the sides of Indian Key Channel suggest that ebb tide currents are consistently stronger than flood currents for a given current speed measured at the midchannel study site. Without a correction for the ebb-dominant fringes of the channel and applying a single slope value to all measurements, discharge estimates will tend to overestimate flow into Florida Bay. It was not expected that the WES estimates of tidal discharge would be three times greater than the Harbor Branch estimates, and the difference does not seem to be consistent with flood- and ebb-dominant parts of the channel.

b. Range 14,Channel Two

Channel Two lies between Indian Key Channel and Channel Five and provides direct exchanges between Hawk Channel and Florida Bay. Harbor Branch maintained a current meter and a pressure recorder in Channel Two from late January to mid-April 1994, and harmonic constants of the rise and fall and the ebb and flood of the tide are available for quantifying tidal transport at the study site. Local tidal transport was calculated at times corresponding to each of the 10 crossings during the September intensive survey. Figure D12 is the plot of discharge as a function of predicted tidal transport. Positive values indicate flow into Florida Bay. Tidal exchanges are the primary component of the total movement of water through Channel Two. The correlation coefficient of the points appearing in Figure D12 is +0.9941, indicating that 98.8% of the variance in the total discharge during the intensive survey can be explained by the predicted tidal transport. The slope of the regression line is 2.104 x 10^3 ft^3 s^{-1} of transport for the entire channel per ft^2 s^{-1} of surface-to-bottom transport at the midchannel study site.

The principal tidal constituents found from an analysis of water-level and current meter data can be used to quantify the tidal pumping effect through Channel Two. For the M_2 constituent, the occurrence of high tide during the flood and low tide during the ebb results in a tidal pumping that averages 25,613 ft^2 s^{-1} over every full 12.4206-hour tidal cycle. This is the result of 296,559 ft^2 passing the study site as it moves into Florida Bay on the flood tide and 270,945 ft^2 returning past the study site on the following ebb. Transport of 25,614 ft^2 through a water column that averages 11.6 ft deep over a 12.42-hour tidal cycle is equivalent to a mean inflow of 53.88 x 10^6 ft^3 for the entire channel. In the case of Channel Two, the Harbor Branch channel calibration suggests a somewhat larger value. For the M_2 constituent, the Harbor Branch data indicate a cumulative net exchange of 93.9 x 10^6 ft^3.

Using the slope of the regression line to estimate the total amount of water entering and leaving Florida Bay on each half M_2 tidal cycle through Channel Two, the product of the slope and the flood tide volume indicates that 623.9 x 10^6 ft^3 of water enters on any M_2 flood tide and 570.0 x 10^6 ft^3 leaves on the M_2 ebb. As noted above, however, this inflow would not be apparent if the model is also reproducing tidal pumping effect of Gulf tidal waves entering Florida Bay from the west. The local M_2-induced tidal pumping would be superimposed onto a net outflow resulting from a regional-scale forcing. The numbers given above are useful as guidance for the magnitude of the tidal exchanges, however.

The y-intercept, representing that part of the total transport that cannot be associated with the tidal exchanges, was -3.743 x 10^6 ft^3 s^{-1}. This suggests a mean outflow during the nine hours of the intensive study. As noted in the third section of this report, however, it is not realistic to think of the nontidal current as constant over periods of time that are long with respect to the time of the intensive survey. The magnitude of this nontidal flow underlines the importance of understanding nontidal transport as well as tidal exchanges through tidal channels along the eastern and southern boundaries of Florida Bay. For this, one must obtain current meter records over the days-to-seasons time scales over which nontidal flow can vary significantly.

c. Range 15, Channel Five

Channel Five is the next channel on the Key West side of Channel Two, and it is considerably larger than Channel Two yet considerably smaller than Long Key Channel. Channel Five connects Florida Bay with Hawk Channel directly and plays a valuable, though perhaps local, role by flushing adjacent waters of Florida Bay. Figure D13 shows total measured transport plotted as a function of predicted tidal transport for Channel Five. The high correlation coefficient, +0.9921, indicates that over 98% of the variance in the total transport can be explained by the predicted tidal exchanges, and confirms that during this time period at least the ebb and flood of the tide comprised virtually all of the variability about the mean. The slope of the regression line is +5.8534 x 10^6 ft^3 s^{-1} of total discharge per 1 ft^2 s^{-1} of tidal transport. Interaction of the rise and fall of the M_2 tide with the ebb and flood of the M_2 tidal current results in a tidal pumping of water into Florida Bay of 21,367 ft^2 at the Harbor Branch study site. The local surface-to-bottom transport at the Harbor Branch study site is slightly less than that calculated for Channel Two. For the M_2 constituent, the flood and ebb tide transport are +172,200 and -150,884 ft^2, respectively. The mean transport is +0.48 ft^2 s^{-1}. The mean water depth at the study site was 8.8 ft, thus the tidal pumping effect is equivalent to a steady inflow of +0.049 ft s^{-1}.

Combining these numbers with the regression slope obtained during the September 1996 intensive survey, one finds that the M_2 constituent carries 873.2 x 10^6 ft^3 of water into Florida Bay on the flood tide, then removes 765.1 x 10^6 ft^3 of water on the following ebb. The net effect is a gain of 125.1 x 10^6 ft^3. For comparison, using the Harbor Branch calibration data, the net M_2 tidal transport was 149.97 x 10^6 ft^3 over a full tidal cycle. Other tidal constituents are relatively small. For example, the S_2 and N_2 constituents pump 6.07 and

4.13 x 10^6 ft^3 of water into the bay, respectively. The K_1 and O_1 constituents pump 5.46 and 4.33 x 10^6 ft^3, respectively. As with the M_2 constituent discussed previously, these numbers are the residuals calculated from much larger flood and ebb tide volumes.

d. Range 16, Long Key Channel

Long Key Channel has emerged as one of the most important channels for exchanging water between Hawk Channel and Florida Bay. Its importance stems from its location in the Middle Keys, as well as from the large cross-sectional area of the channel. Figure D14 contains the measured discharge, in thousands of cubic feet per second, plotted as a function of the predicted tidal transport in midchannel. There is somewhat more scatter in the data, but the correlation coefficient is a highly significant +0.9543, indicating that just over 91% of the variance in the total discharge can be explained by tidal exchanges. The slope of the regression line is +9.182 x 10^3 ft^3 s^{-1} of total transport per 1 ft^2 s^{-1} of midchannel tidal transport. The y-intercept, representing nontidal flow during the intensive survey, was +31.21 x 10^3 ft^3 s^{-1}.

Combining predicted tidal currents with predicted water levels at the midchannel study site, one calculates for the M_2 tidal constituent transports of +288,633 ft^2 during the flood tide and -263,905 ft^2 for the ebb. The net M_2 transport is therefore +24,727 ft^2 into Florida Bay at the study site. Using the slope of the regression line this translates into 227.04 x 10^6 ft^3. At times of maximum flood and ebb, tidal transport reaches +188,413 and -168,121 ft^3 s^{-1}, respectively. The difference between the WES-estimated discharge and the Harbor Branch value is quite large, but the two approaches suggest net discharge in the same direction. The Harbor Branch calibration data suggest that the east side of the channel is ebb dominant. For example, on the Key Largo side of the channel, ebb currents were found to be 103% of the mid-channel values, while flood speeds were only 77% of the mid-channel values. On the Key West side, flood currents were stronger than ebb currents for a given mid-channel value, but the difference was significantly less. As a result of the strong ebb currents along the east side of the channel, the net M_2 transport is an outflow of -58.16 x 10^6 ft^3 over each tidal cycle. The difference between the Habor Branch and the WES values may indicate that either the Harbor Branch calibration data or the WES discharge data, both of which came from a single tidal cycle, can produce results that are not representative of all tidal cycles. The other tidal constituents contribute relatively small amounts to the exchange of water between Hawk Channel and Florida Bay. The WES data suggest that the S_2 and N_2 constituents pump 11.28 and 9.68 x 10^6 ft^3 of water into the bay on each tidal cycle, and the K_1 and O_1 constituents pump 4.75 and 3.77 x 10^6 ft^3 of water into the bay during each diurnal tidal cycle.

e. Ranges 19 and 20, Seven Mile Bridge Channel

Seven Mile Bridge Channel marks the boundary between the northeastern end of the Lower Keys and the southwestern end of the Middle Keys. Harbor Branch had a current meter in Moser Channel, the principal channel connecting Hawk Channel with southern Florida Bay, from early September 1987 to early April 1988, and again from late May to mid-

October 1988. No pressure records are available from the study site, so we use results of analyses made by the National Ocean Service, using data collected at Pigeon Key, just one nautical mile (1.9 km) from the study site. Because the channel is so wide, it was divided into two segments. The procedure for the two segments was the same as for any single-segment channel; however, in this case the sum of the two segments quantifies tidal and nontidal exchanges for the channel as a whole.

Figure D15 shows the measured discharge from the east half (top plot) and west half of the channel, plotted as a function of the tidal transport at the Moser Channel study site. Correlation coefficients are +0.964 and +0.890, respectively, indicating that tidal transport explains 93 and 79% of the variance in the total discharge (both plots have a single point, recorded at about 1435 EST, that seems to be unusually low). When these points are ignored, correlation coefficients increase to +0.975 and +0.929. Using the slope of the regression equations, one can translate tidal transport through the eastern and western parts of Moser Channel into two discharge values. The total is the sum of the two components. For the eastern part of Seven Mile Bridge Channel, with a slope of +3.5274 $ft^3\ s^{-1}$ per 1 $ft^2\ s^{-1}$ of midchannel two-dimensional transport, one calculates an M_2 inflow of 1.701 x 10^9 ft^3, an outflow of 1.588 x 10^9 ft^3, and thus a residual inflow of 112.3 x 10^6 ft^3 over each M_2 tidal cycle. For the western part of Seven Mile Channel, the slope is 6.145 x 10^3 $ft^3\ s^{-1}$ per 1 $ft^2\ s^{-1}$ of transport at the Moser Channel study site. Thus the 31,824 ft^2 of M_2 transport translates into a residual inflow of 195.6 x 10^6 ft^3 over each tidal cycle. Combining the contributions of the eastern and western parts of Seven Mile Bridge Channel, results indicate that the total residual M_2 transport is 307.9 x 10^6 ft^3 from Hawk Channel into Florida Bay. Other tidal constituents contribute substantially less. The semidiurnal S_2 and N_2 constituents contribute 14.94 and 11.65 x 10^6 ft^3, respectively, and the diurnal K_1 and O_1 constituents are less than 5 x 10^6 ft^3 each. Harbor Branch has not calibrated Seven Mile Bridge Channel, thus no values are available for comparison with the WES data obtained from the intensive survey.

f. Range 8, Snake Creek

Snake Creek, along with Whale Harbor Channel, falls into a special category in this report. Both Snake Creek and Whale Harbor Channel have produced data that suggest these channels have a net transport of water into Florida Bay. Topographic features on the Florida Bay side of the channels (e.g., Cross Bank) apparently have a blocking effect that shields this area from the west-to-east transport of water across Florida Bay. While Harbor Branch has obtained current meter data from these channels, no pressure recorder data are available from the study site. To calculate two-dimensional transport at the study site, harmonic constants from NOS time series have been used. In both cases, study sites were close to the Harbor Branch study site. Thus, even though amplitudes and phase angles can vary significantly over relatively short distances in these tidal channels, the values used in the calculations are felt to be adequate for estimating transport.

Figure D16 shows the WES discharge values plotted as a function of the two-dimensional transport calculated for the midchannel study site. The scatter in the data is

small, and the correlation coefficient is +0.9905, indicating that just over 98% of the total discharge can be explained by the tidal component of the transport. The slope of the regression line is 348.1 $ft^3 s^{-1}$ per 1 $ft^2 s^{-1}$. Combining the slope with the cumulative M_2 constituent inflow and outflow (+218,681 and -206,307 ft^2, respectively), one calculates a net inflow of 4.307 x 10^6 ft^3 over each M_2 tidal cycle. Similarly, using the slope, one calculates maximum flood and ebb discharge rates of 5,392 and -5,006 $ft^3 s^{-1}$.

The Harbor Branch channel calibration data, applied to the M_2 current and the NOS M_2 water level, suggests a cumulative M_2 inflow of 2.756 x 10^6 ft^3. This is 63% of the WES value, and surprisingly one of the closest matches occurs when NOS data from near, but not at, the study site have to be substituted into the calculations. As shown in Table D2, the other tidal constituents contribute relatively little to the tide-induced transport of water through Snake Creek. The N_2 constituent, the next largest, exchanges only 5% of the M_2 value.

g. Range 9, Whale Harbor Channel

Whale Harbor Channel has exhibited characteristics similar to those of Snake Creek in terms of tidal exchanges and long-term net transport. Harbor Branch conducted a study of currents through Whale Harbor Channel from September 20 to December 13, 1994. Again, because no pressure data were obtained at the study site, results of an NOS study of tides in the Florida Keys were used.

Figure D17 shows WES discharge as a function of midchannel two-dimensional transport. The correlation coefficient is +0.9923, indicating that over 98% of the variation in discharge can be explained by variations in tidal transport. The slope of the regression line is 483 $ft^3 s^{-1}$ per $ft^2 s^{-1}$. With this value, the cumulative inflow and outflow associated with the M_2 constituent (+316,921 ft^2 and -282,612 ft^2, respectively) translate into +148.9 and -140.8 x 10^6 ft^3, respectively, and the net M_2 transport is an inflow of +8.1 x 10^6 ft^3. Over the course of each M_2 tidal cycle, the strongest inflow and outflow are +10,538 and -9,817 $ft^3 s^{-1}$, respectively.

Using Harbor Branch calibration data with the predicted ebb and flood of the M_2 current and the predicted rise and fall of the M_2 tide, one calculates a net outflow of -11,201 ft^3 over each M_2 tidal cycle. This does not compare well with the WES-derived value. The difference appears to come from ebb-dominated fringes of the channel suggested by the Harbor Branch data.

1C. TIDAL CHANNELS WITH SIMULTANEOUS HARBOR BRANCH STUDIES - September 1996 Survey

Three tidal channels were being investigated by Harbor Branch in late September, during the WES intensive study. For Jewfish Creek, Tavernier Creek, and Tea Table Channel, correlation of WES discharge data with Harbor Branch current meter data makes possible estimates of volume transport over the longer time periods that the Harbor Branch

current meters were in the water. Both the Jewfish Creek and Tavernier Creek studies lasted just over one year; the Tea Table Channel study was conducted for a period of 114 days from August 21 to December 13, 1996. During the entire time of the Tea Table Channel study, a pressure recorder was in operation at the midchannel study site. For the other two studies, pressure records are available for only part of the total time intervals; for Tavernier Creek this time interval did not include the late September WES intensive survey. Thus, only for Jewfish Creek and Tea Table Channel can we make direct comparisons of two-dimensional transport (surface to bottom at the Harbor Branch study site) and three-dimensional transport (entire channel cross section along the WES transect). The analysis is restricted to those time periods when Harbor Branch had both current meters and pressure recorders in operation. When these time intervals did not coincide with the WES intensive surveys, the predicted rise and fall of the tide is added to the mean water depth to calculate the two-dimensional transport needed for comparison with the WES data.

a. Range 1, Jewfish Creek

Jewfish Creek is a relatively small channel, but it plays a role disproportionate to its size by exchanging water between Barnes Sound and Blackwater Sound in the northeast corner of Florida Bay. Together with Adams Cut, Jewfish Creek provides the only direct flushing activity in Florida Bay north of Tavernier Creek. Jewfish Creek is a segment of the Intracoastal Waterway; thus, where it has been cut through the mangroves, it has a relatively constant width (108 ft, or 33 m) and depth (11 ft, or 3.4 m).

Harbor Branch conducted a field study in Jewfish Creek from October 25, 1995, to December 12, 1996. During that time, a pressure recorder was in operation from June 18 to December 12, 1996. It is this 177-day time period when both currents and bottom pressures were being measured, and which overlaps with the WES intensive study, that is used to describe long-term volume transport through Jewfish Creek.

Figure D18 is a plot of three-dimensional discharge values plotted as a function of the two-dimensional transport computed from *in situ* current and pressure data. Hourly two-dimensional transport values were interpolated to coincide in time with the discharge measurements. Linear regression of the 11 pairs of discharge values produced a correlation coefficient of +0.963, indicating that nearly 93% of the variance in the discharge data during the intensive study period can be explained by the calculated two-dimensional transport at the Harbor Branch study site. It is surprising that the correlation is so high, because the WES transect across Jewfish Creek was 0.3 nautical mile from the Harbor Branch study site and on the other side of the entrance to Lake Surprise. Apparently, exchanges involving Lake Surprise that might have influenced measurements through Range 1 were small. The regression equation obtained from the comparison of Harbor Branch calculations and WES measurements was

$$D = -695.534\ ft^3\ s^{-1} + 1312.62\ ft^3\ s^{-1}\ per\ 1\ m^2\ s^{-1} \times T \qquad (D3)$$

where D is the total discharge in $ft^3 s^{-1}$, and T is the calculated two-dimensional (surface-to-bottom) transport past the Harbor Branch study site.

Given this relationship from the intensive survey and given the long time series from the Harbor Branch field study, one can estimate discharge during the full June-December study period. The regression equation again quantifies both the tidal and the nontidal transport. The y-intercept suggests that the nontidal discharge was -695.5 $ft^3 s^{-1}$. Removing tidal exchanges with a low-pass filter suggests that nontidal transport at this location is commonly within the range of ± 1100 $ft^3 s^{-1}$. At this study site, however, it is possible that the y-intercept may be related to flow leaving Lake Surprise, as well as to the flow through Jewfish Creek. Figure D19 shows the cumulative discharge that occurs when the y-intercept is left in the regression equation (implying that the nontidal flow is constant in time). The nearly 13 billion cubic feet of water entering northeastern Florida Bay through Jewfish Creek during the 177-day study seems to be an unrealistically high value. That, together with the high likelihood that nontidal flow alternates between positive and negative values, suggests that a better estimation of discharge through Jewfish Creek would come from the regression equation without the contribution of a constant slope.

Figure D20 is a plot of cumulative discharge calculated from the assumption that the discharge is directly proportional to the surface-to-bottom transport at the Harbor Branch study site, but without the offset provided by the y-intercept. The pattern shows part of an annual curve, with irregular northward flow during the first four months of the study (through mid-October), then strong southward flow from mid-October through mid-December. Although wind data have not been incorporated into the analysis of the Jewfish Creek data at this point, it is reasonable to suspect that significant changes in discharge would accompany seasonally shifting wind patterns. (Wind data from the C-MAN weather station near Long Key show that the first cold front of the 1996-97 winter season arrived on October 8.) Thus, with no y-intercept in the regression equation, the discharge calculations (Figure D20) indicate a response to seasonally changing wind conditions, while with the y-intercept (Figure D19) the calculations suggest that the response is minimal.

The important features in Figure D20, in addition to the seasonal reversal in discharge in early October, are the low-frequency fluctuations that occur at one- to two-week intervals throughout the study. Until wind data can be incorporated into the study, the cause of these variations cannot be confirmed, but comparison of winds recorded nearby at Molasses Reef over the full study period (Patrick Pitts, personal communication) strongly suggests that wind forcing is the dominant forcing mechanism for these long-period exchanges of water through Jewfish Creek.

The two-dimensional transport calculated at the Harbor Branch study site is a good benchmark for gauging the validity of Figures D19 and D20. Because of the small channel cross section and because wind forcing is minimal as a result of mangroves lining both shores, lateral shear in along-channel flow is small, and the assumption of a logarithmic current

profile is a good one. Figure D21 is a plot of cumulative two-dimensional transport calculated from the Harbor Branch data. Current measurements from 3 ft above the bottom have been extrapolated to the surface, but no lateral extrapolations have been incorporated into the calculations. The similarity of Figures D21 and D20 is a direct result of the absence of a y-intercept in the calculations for Figure D20, thus Figure D21 is not independent proof of Figure D20. But Figure D21, combined with the assumption that nontidal exchanges vary significantly with time, points to Figure D20 as the best measure of what a hydrodynamic model should simulate under these wind conditions.

b. Range 2, Tavernier Creek

Tavernier Creek, along with Adams Cut, plays an important role in flushing northeastern Florida Bay by exchanging water with the Atlantic side of the Keys. Only Tavernier Creek, however, exchanges directly with Hawk Channel. Southwest of Tavernier Creek, the next tidal channel that exchanges water directly between Florida Bay and Hawk Channel is Snake Creek, 4.4 nautical miles (8.1 km) away and on the other side of Cross Bank.

Harbor Branch conducted a field study of Tavernier Creek for a period that lasted just over one year and included the late September intensive survey. A pressure recorder was in operation from early December 1995 to mid-June 1996, but this part of the study did not include the intensive study period. Thus, while bottom-pressure measurements are available to convert two-dimensional transport past the study site into channel discharge for a 195-day period of time, the conversion of two-dimensional transport to three-dimensional transport must be based on tidal predictions.

Top-of-the-hour two-dimensional transport values were shifted in time to correspond with times at which discharge values were obtained. Ten data points were available for a linear regression of discharge against two-dimensional transport. Results are shown in Figure D22. The correlation coefficient was +0.9209 using all 10 points. One of the points, however, appears to be an outlier. This could be a result of either spurious current measurements or spurious discharge values; however, the same data point appeared out of place when predicted tidal transport through Tavernier Creek was compared with discharge. Thus, it appears that this is an anomalously high discharge occurring for a transport of -11.16 $ft^2\ s^{-1}$, rather than an unusually strong two-dimensional ebb transport occurring for a discharge of +689 $ft^3\ s^{-1}$. With this data point removed, the correlation coefficient rose to +0.9695. Nine data pairs were used to quantify the slope and the y-intercept. The regression equation obtained for Tavernier Creek was

$$D, \text{ in } ft^3\ s^{-1} = +356.9\ ft^3\ s^{-1} + 82.84\ ft^3\ s^{-1} \text{ per } 1\ ft^2\ s^{-1} \times T, \text{ in } ft^2\ s^{-1} \qquad (D4)$$

where D is the channel discharge, and T is the two-dimensional transport at the midchannel study site. For Jewfish Creek, measured discharge values are compared with two-dimensional transport values that are also based on measurements--not tidal predictions. Thus, a linear

regression of the points shown in Figure D22 should not have a y-intercept that relates to the nontidal flow. The y-intercept in this case arises from errors in the discharge and/or transport measurements. It is unrealistic to believe that a discharge of 357 $ft^3 s^{-1}$ would exist when the current meter in midchannel is indicating a slack tide condition. Tavernier Creek is only 228 ft (69 m) wide at the study site, and slack tide must occur virtually simultaneously everywhere in the cross section through the study site. Figure D23 shows the cumulative net transport that results when the y-intercept is left in the regression equation and discharge is calculated from the regression equation as it appears above. Periods of transient reversals occur throughout the record, but the plot suggests a quasi-steady transport of water northward into Florida Bay, with an accumulation of approximately 4.2×10^9 ft^3 during the 195-day study period.

Again, the alternative to calculations using the regression equation with the y-intercept are calculations that incorporate only the slope. Figure D24 shows results of this alternate approach, using only the slope of 75.1 $ft^3 s^{-1}$ per 1 $ft^2 s^{-1}$ to translate midchannel two-dimensional transport into discharge for the entire channel. The result is significantly different. For the first four months of the study the net flow through the channel is southward into Hawk Channel on the Atlantic side of the Keys. A short period of northward flow is indicated from mid-April through late May, then an irregular outflow continues through the end of the record. Throughout the study period, the nontidal discharge reverses for time periods on the order of a few days to a week. Because the full study lasted on the order of a half year, the pattern cannot be interpreted in terms of the annual cycle, but the periods of outflow and inflow appear to be related loosely to wind forcing. The sustained period of outflow from December to April comes at a time when seasonal winds are characteristically out of the northeast. Wind data from the Molasses Reef C-MAN station (not shown) suggest that the inflow through Tavernier Creek is related to the north-south wind stress component, although the flow through the channel seems to lag variations in wind stress by about one month.

As a check on these calculations, two-dimensional transport at the study site in the middle of Tavernier Creek was calculated, and hourly values were accumulated just as discharge was in the previous figure. Results are shown in Figure D25. The pattern is virtually identical to that found for discharge simulated without the y-intercept, because the only difference is the conversion from two-dimensional transport to three-dimensional transport using the slope of the regression line. As with the Jewfish Creek data, however, this is the plot that involves the fewest assumptions, and therefore this is probably the best representation of the long-term movement of water through Tavernier Creek. The similarity of Figures D25 and D24 suggests that Figure D24 is the approximation of discharge that is best suited for model verification. The only way Figures D25 and D23 could both be correct (i.e., a reversing transport in midchannel *and* a quasi-steady inflow for the channel as a whole) would be if the sides of the channel were flood-dominant relative to the channel as a whole. In that case, measurements in midchannel would overestimate channel discharge during the ebb half of the tidal cycle and/or underestimate channel discharge during the flood half. Field measurements from Tavernier Creek made at the Harbor Branch study site indicate that the

part of the channel in which current measurements were made was neither flood-dominant nor ebb-dominant. A small flood-dominant region was suggested for the Key West side of the study site, however, and three-fifths of the channel on the Key Largo side was slightly ebb-dominant.

Results of the Tavernier Creek study can be used to evaluate model simulations made under the same wind conditions as those recorded during the December 1995 to June 1996 Harbor Branch study period. Specifically, during the mid-December through mid-April period, modeled discharge should be showing a net southward discharge of the order 1.5×10^9 ft^3. Similarly, from mid April through late May, the flow should reverse and a northward discharge of slightly more than 0.5×10^9 ft^3 should be indicated by model simulations.

From the regression equation alone, information is available for tide-induced discharge. Combining the slope with the net transport for each full M_2 tidal cycle, for example, one gets a tidal pumping value of 1.66×10^6 ft^3. This represents the net effect of an inflow of 17.020×10^6 ft^3 from Hawk Channel into Florida Bay, followed by an outflow of 15.356×10^6 ft^3 through Tavernier Creek. The other tidal constituents are relatively small. The S_2, N_2, K_1, and O_1 constituents are all between 50 and 77×10^3 ft^3, and the P_1 constituent is only 5.3×10^3 ft^3. Model simulations should approximate the M_2 pumping effects to a close approximation because of the important baseline level of transport they provide.

c. Range 11, Tea Table Channel

Tea Table Channel was described briefly in Part f of Section 1A of this report, when discharge data from nearby Tea Table Relief Channel were presented. Figure D26 is a plot of the WES discharge data plotted as a function of the two-dimensional transport (here in m^2 s^{-1}) calculated from the midchannel pressure and current measurements. The 10 points that were plotted in Figure D7 to provide an impression of the total discharge as a function of time are plotted here against midchannel transport to provide a qualitative impression of the regression equation.

The task is to use a relationship obtained from Figure D26 to convert two-dimensional transport in midchannel to three-dimensional transport for the entire channel. The 10 points shown in Figure D26 are very highly correlated: The correlation coefficient is +0.9916, indicating that over 98% of the variation in total discharge can be explained by fluctuations in midchannel surface-to-bottom transport. This is encouraging; however, the regression equation contains a large y-intercept as well as the large slope that was expected. The y-intercept for these points is +2533.5 ft^3 s^{-1}. Nevertheless, the analysis of the Tea Table Channel begins with a time series of channel discharge, D, simulated with the regression equation

$$D = +2{,}533.5 \text{ ft}^3 \text{ s}^{-1} + 5{,}648.0 \text{ ft}^3 \text{ s}^{-1} \text{ per ft}^2 \text{ s}^{-1} \text{ x } T \quad \text{(D5)}$$

where all terms are as defined earlier.

Figure D27 shows the cumulative volume transport during the August 21 to December 13 study period. Positive values indicate flow into Florida Bay. Effects of the ebb and flood of the tide appear as a "sawtooth" pattern on the plot. The general features of the plot are of greater interest, because they indicate periods of outflow (descending curve) and inflow (ascending curve). The slope of the ascending or descending curve at a given time is directly proportional to the magnitude of the low-frequency inflow or outflow. From the start of the plot through early October, the curve descends slightly. From then through the end of the record, however, the curve rises sharply, indicating a quasi-steady inflow into Florida Bay. By the end of the 114-day study, the simulation suggests that a total of approximately 10 billion cubic feet of water had moved through Tea Table Channel and entered Florida Bay.

As noted above, however, these calculations were influenced by the y-intercept of 2,533 $ft^3 s^{-1}$. Not only would this value be added to a transport value coming at slack water, it would be added to each hourly calculation of the total flow (tidal plus nontidal) that should have been quantified by the slope of the regression line. Thus, it is not surprising that the curve suggests a net inflow into Florida Bay. Ebb current speeds would have to be well in excess of flood current speeds, on average, to overcome the effect of the y-intercept. A second simulation estimated channel discharge without the y-intercept. The discharge was calculated solely from the slope of the regression line, and results are shown in Figure D28. While some of the features occurring over shorter time scales remain, the significant difference is that Figure D28 suggests a long-term net outflow from Florida Bay. The presence or absence of the y-intercept can totally reverse the long-term flow pattern.

While it is probably more realistic to remove the y-intercept than to leave it in the regression equation, it is also probably more realistic to allow the regression line to vary according to flood or ebb tide conditions. It is common for tidal channels to have flood-dominant and ebb-dominant sections, and it is possible that the center of the channel is flood- or ebb-dominant. If so, then midchannel measurements of current should not use the same slope to estimate flood discharge as to estimate ebb discharge. To determine how the slope might change from flood to ebb conditions, the WES discharge data were subdivided into five flood and five ebb values. Linear regression analysis of these two subsets included forcing the regression lines to pass through zero by padding the input data with 15 zero-zero "data pairs." As one can see from Figure D26, the slope of flood tide discharges is slightly steeper than the slope of ebb discharges. Regression analysis produced slopes of $+7.135 \times 10^3$ and $+4.468 \times 10^3$ $ft^3 s^{-1}$ per 1 $ft^2 s^{-1}$ for floods and ebbs, respectively. Simulating discharge with a tide-varying slope, however, produced unrealistic results (not shown). The effect of the 60% increase in the slope both reversed the plot and removed all periods of outflow. What should be the most realistic simulation (with no y-intercept and a tide-varying slope) produced the most unrealistic results.

Perhaps the best guide for determining what really was happening in Tea Table Channel is the plot of two-dimensional transport shown in Figure D29. These calculations are based on measurements, and the only assumption is that the current profile above the current meter was logarithmic. In view of the protected nature of the study site, this is probably a good assumption. The pattern shown here includes a relatively rapid outflow through most of the study that is interrupted in early October and mid-November. The similarity of Figures D28 and D29 suggests that the best approximation of discharge comes from the slope of the regression line calculated from pooled flood and ebb data points. The matter cannot be resolved satisfactorily, however, from the available data. One must conclude that an intensive survey that results in only five points during any half tidal cycle is insufficient to quantify the relationship between surface-to-bottom flow in midchannel and the total discharge for the channel as a whole.

The remaining parts of the RESULTS section relate specifically to the second intensive survey. In this case, the results are subdivided into two parts. The first part deals with results from channels in which Harbor Branch has collected no historical data (see Figure D30); the second part deals with results from channels in which Harbor Branch has collected current meter and/or pressure data. No Harbor Branch field studies were underway during the second intensive survey; therefore, it is not possible to compare February discharge data with simultaneous current measurements.

2A. TIDAL CHANNELS WITH NO HISTORICAL DATA - February 1997 Survey

a. Range 2, Adams Cut

Discharge measurements from Adams Cut show a well-defined tidal signal, although the amplitude is somewhat lower than the amplitude found during the first intensive survey. It appears that strongest flood discharges were not recorded either at the beginning or at the end of the seven and a half hour study, but the range of +900 to -1900 $ft^3 s^{-1}$ is only 65% of the range recorded during the first intensive survey. The larger ebb discharge is consistent with the diurnal inequalities that were occurring in Hawk Channel shelf waters at this time (see Figure D31).

b. Range 3, Dusenbury Creek

The Dusenbury Creek data show a highly erratic pattern that is lacking a clear tidal signal. Only two of the nine measurements indicate northward (positive) flow, and they are separated in time by a measurement of southward flow of nearly the same magnitude. The net discharge during the second intensive survey was southward, as was the case during the first intensive survey.

c. Range 4, Grouper Creek

Results from Grouper Creek are neither clearly tidal nor clearly nontidal, as was the case during the first intensive survey. The study site is in a part of Florida Bay that has negligible tidal-period variations in water level, but tidal currents and transport may be

apparent nonetheless. The net discharge during this time period was southward (negative), and the range is substantially less than the range recorded during the first survey.

d. Range 5, Baker Cut

Discharge measurements from Baker Cut, the last channel surveyed on February 11, reveal a poorly defined tidal signal at best, because of the transient rise to northward (positive) flow in late morning. Without that, the pattern could be interpreted as a tidal-period fluctuation from southward flow in the morning to northward flow in the afternoon. The primary difference between results from the first and second intensive surveys is the dominance of northward flow in the September data and the alternating flow in the February data.

e. Range 7, Cowpens Cut

Data from Cowpens Cut, through Cross Bank, show a relatively well-defined tidal signal, and they suggest the possibility of a diurnal inequality in the southward (negative) flow. This is consistent with the diurnal inequality in low tide levels predicted in shelf waters during this time (see Figure D31). The most significant difference between the first and second intensive surveys is the magnitude of the northward discharge. Maximum values in February were about 50% higher than maximum values in September.

f. Range 10, Tea Table Relief Channel

Starting with Tea Table Relief Channel, all of the ranges are across channels that provide a direct connection between Florida bay and Hawk Channel, and all of the discharge patterns exhibit a clear tidal signal. The pattern for Tea Table Relief Channel is virtually identical to the pattern that was obtained from the September data. In both cases, flood (positive) discharge values are much greater than ebb discharge values, in response to the diurnal inequalities in the rise and fall of the tide along the outer shelf.

g. Range 13, Lignumvitae Channel

Lignumvitae Channel, lying near Indian Key Channel, shows the clearest tidal signal, with a nearly symmetrical alternation from a midmorning flood (positive values) to a midafternoon ebb. Flood discharges are similar in magnitude to those recorded during the first intensive survey; ebb discharges are slightly weaker.

h. Range 17, Tom's Harbor Cut

The data from Tom's Harbor Cut did not continue long enough to document the strongest ebb flow (negative values), which was also the case for the first intensive survey. The relatively regular variation with time, however, suggests that tides make the primary contribution to exchanges at this location. The magnitude of strongest flood and ebb discharges recorded during the second survey are very similar to the magnitudes recorded during the first survey.

i. Range 18, Tom's Harbor Channel

Data from Tom's Harbor Channel produced a pattern very similar to that pattern obtained during the first intensive survey, including strongest flood (positive) discharges and probably the strongest ebb discharges as well. Maximum flood values in the February data are only about 75% of the maximum values recorded in September, however.

The interpretation of flood and ebb discharges shown in Figure D30 are put in perspective using tidal predictions that span the time period from just before the first intensive survey to just after the second. Figure D31 contains predicted water levels, relative to mean sea level, for Tennessee Reef. The rise and fall of water level at this location along the reef tract is probably representative of the rise and fall elsewhere along the outer shelf that forces exchanges with Florida Bay through the major tidal channels. The predictions show that during this time period diurnal inequalities in successive high water levels were relatively small. On the other hand, diurnal inequalities in low water levels could be substantial. The implication for flood and ebb discharges is that successive floods would be similar in magnitude, while successive ebbs could be quite different. Not only could successive ebb discharges be dissimilar, but the fortnightly range in every second ebb is substantial as well. A plot such as this, based on predictions, would serve as a useful tool for planning field work, as well as for interpreting results once the work is completed.

2B. TIDAL CHANNELS WITH HISTORICAL DATA - February 1997 Survey

Results presented in this subsection also will be in abbreviated form, following a composite figure to summarize the calculations. Figure D32 contains the scatter plots constructed from the measured total discharge, in $ft^3\ s^{-1}$, and the midchannel surface-to-bottom transport, in $ft^2\ s^{-1}$ calculated from predicted tidal currents and water levels. The scatter plots serve a very useful purpose, because they show immediately whether some of the points should be treated as outliers. Data from the second intensive survey appear to be reliable, in spite of some scatter in each plot.

Many results coming out of the second intensive survey are very similar to results that appeared from the first intensive survey. Here, the emphasis will be on differences between the results from the two surveys, and the interpretation will focus on whether the two intensive surveys have brought out seasonal variations, or just helped to quantify errors in sampling. In the discussion, information will be provided to quantify errors associated with estimating tidal discharge from predicted tidal transport. The standard error of the estimate is used for this purpose. Sixty-eight percent of the observations lie within ± 1 standard error.

a. Range 1, Jewfish Creek

The February intensive survey produced data that was much more tide-dominated than did the September survey. The second column of Table D3 shows the r^2 value calculated from the regression of discharge against the two-dimensional transport calculated from tidal harmonic constants. For the second intensive survey, tidal variations in transport explained

95% of the variance in the discharge across Range 1. Using the September discharge data, only 78% of the variance could be explained from tidal variations in vertically integrated transport. The slope used to convert tidal transport (in $ft^2\ s^{-1}$) into tidal discharge (in $ft^3\ s^{-1}$) also changed significantly from the first to the second intensive surveys. From the September data, for example, a 10 $ft^2\ s^{-1}$ transport at the Harbor Branch study site would have corresponded to a 1104 $ft^3\ s^{-1}$ discharge through Range 1; using the relationship obtained from the February data, the same transport would have produced a 1957 $ft^3\ s^{-1}$ discharge. One explanation might involve water entering or leaving Lake Surprise, but the available data neither supports nor contradicts this possibility.

b. Range 6, Tavernier Creek

The two intensive surveys produced slopes (alternately referred to as transfer functions) for Tavernier Creek that were more similar. Nevertheless, the February value was 25% larger than the September value. The difference in values may be related to the presence of a greater amount of nontidal transport in the September data. The September tidal transport can be used to explain only 85% of the variance in the discharge data. The greater amount of nontidal "noise" makes it harder to define the true relationship between transport and discharge, given only 10 data pairs.

c. Range 8, Snake Creek

The second intensive survey across Snake Creek produced results very similar to those obtained from the first survey. In both cases, well over 90% of the variance can be explained in terms of the ebb and flood of the tide, and the transfer function was only 3% larger than the value obtained from the September data. Thus, both surveys suggest that on an average M_2 cycle, 4.44×10^6 ft^3 of water are pumped into Florida Bay by the asymmetry of the flood and ebb tides.

d. Range 9, Whale Harbor Channel

Results from Whale Harbor Channel were also similar for the two intensive surveys, but in this case the transfer function obtained from the February data was 3% smaller. Somewhat more scatter in the discharge values reduced the correlation coefficient to 0.96, but the predicted tidal transport nevertheless explains 93% of the variance in the total discharge.

e. Range 11, Tea Table Channel

Tea Table Channel appears to be the second most tide-dominated channel of those inves-tigated, ranking just below Channel Five and just above Channel Two. On average, 98% of the variance of the total discharge can be explained by the ebb and flood of the tide. Results from the two intensive surveys were similar also in the transfer functions they produced. The value obtained from the February data was just under 5% greater than the value obtained from the September data. Averaging the two, results show, for example, that the M_2 tidal constituent carries approximately 194×10^6 ft^3 of water in on the flood, then removes about 180×10^6 ft^3 on the following ebb, for a net inflow of about 14 million cubic feet of water on each tidal cycle.

f. Range 12, Indian Key Channel

Indian Key Channel produced results that are apparently characteristic of all the major tidal channels of the Middle Keys. Predicted tidal transport explains virtually all of the variance in the total discharge. The r^2 values from the first and second intensive surveys were 0.98 and 0.96, respectively. Also, the transfer functions are very similar. The value obtained from the February data was less than 2% larger than the value obtained from the September data. Combining results from the two studies, one can conclude that approximately 298 x 10^6 ft^3 of water are forced into Florida Bay through this channel on the flood, while 276 x 10^6 ft^3 of water are drawn out on the ebb. The net inflow, based on local tidal predictions, is just over 22 x 10^6 ft^3 for each M_2 tidal cycle. Maximum M_2 flood and ebb discharge rates are 21,127 and -19,172 ft^3 s^{-1}, respectively.

g. Range 14, Channel Two

Beginning with Channel Two, tidal channels of the Middle Keys are exchanging much larger amounts of water between Florida Bay and Hawk Channel. This is evidenced by the significantly larger slope values summarized in Table D3. In view of the importance of tidal exchanges, it is satisfying to note that results of the two intensive surveys are in close agreement. The value obtained from the February data is only 2% higher than the value obtained from the September data. Both surveys indicate that virtually all of the variance is explained by the ebb and flood of the tide.

h. Range 15, Channel Five

Results from Channel Five are somewhat puzzling, because the slopes of the regression equations differ by over 9%, yet the plots from both of the intensive surveys indicate very little scatter about the regression line. The possibility that the nontidal discharge was changing steadily and rapidly during either or both of the intensive surveys cannot be ruled out, but it cannot be confirmed with the available data. It is also possible that the length of the range changed slightly from the first survey to the second.

i. Range 16, Long Key Channel

Results from Long Key Channel are consistent in terms of the slopes of the regression lines, but they differ somewhat in terms of the r^2 values. The slope calculated from the February data is just over 2% larger than the slope calculated from the September data, but considerably more scatter appears in the plot of the September discharge versus tidal transport (see Figure D14). In both intensive surveys, r^2 values were lower than those obtained from neighboring channels.

j. Ranges 19 and 20, Seven Mile Bridge Channel

Some inconsistencies arose in the Seven Mile Bridge Channel results as well. For the east part of the channel, the slope value from the February survey were higher than the value from the September survey, but the reverse was true for the west half of the channel. More significantly, perhaps, the difference between slopes for the east part of the channel is the largest of any channel except Jewfish Creek, where tidal exchanges are very small. The slope

from the February data is over 40% larger than the slope from the September data. Also, the variance explained by tidal exchanges increased from September to February for the west part of the channel, while it decreased for the east part.

DISCUSSION

Results from the WES intensive surveys constitute a valuable addition to an understanding of the circulation of Florida Bay. While the data are restricted to the eastern and southern fringes of the bay (Figure D1), these short time series provide a first look at six channels that play important roles--at least locally--in moving water within the bay or between the bay and Hawk Channel. In other channels, where historical data exist, the WES data base constitutes an alternate approach and thus an independent check on earlier measurements. In all channels, and even though the two surveys were conducted to investigate seasonal differences, results give some indication of the repeatability of these measurements, and therefore of the sufficiency of a single intensive survey.

The primary advantage of the boat-mounted ADCP technique of measuring channel discharge is the excellent spatial resolution that it provides in the lateral (across-channel) and vertical dimensions. Although the details of the sampling were not available, it is clear that having data from several levels in the vertical and from many segments across the channel will greatly minimize errors resulting from interpolation and extrapolation of widely spaced anchor station data (the Harbor Branch approach).

While spatial resolution is improved, both the Harbor Branch and (to a lesser extent) WES approaches provide a snapshot that does not provide good temporal resolution. Harbor Branch anchor stations, occupied at midflood or midebb on single half-tidal cycles, are taken to represent the relationship between midchannel and channel-fringe current speeds throughout the half-tidal cycle--and for all floods or ebbs. Recent follow-up calibration measurements have called into question the suitability of single-tidal-cycle anchor station data. The ADCP data base consists of 9 to 11 channel crossings, but results are still from a single tidal cycle. Extrapolation into the longer time scales is open to question. Plots of the ADCP data from any single crossing reveal substantial spatial variability in the transport vectors. Especially at lower current speeds, adjacent vectors can point in very different directions. The scatter is probably related to turbulence existing at the time and place of the measurement. Even with some spatial and/or temporal averaging, the scatter can be considerable, and the measurement is applied to a much longer time interval than it represents.

Another issue, when calibrating channels to quantify discharge, centers around defining the channel. When the channel is bounded on both sides, the only practical problem is water depth and how close to the shore a boat with an ADCP can go. When the channel is unbounded, then exchanges that occur outside the last measurement on either side of the channel can influence the volume transport calculations. Similarly, when the channel is bounded by mangroves, "leakage" into or out of the channel can result in over- or

underestimates of discharge through the cross section defined for the measurements.

Given the uncertainty that surrounds either or both approaches to volume transport calculations, it is not surprising that comparisons produced different estimates of discharge. Never-theless, it is disappointing that some of the differences (e.g., Whale Harbor Channel, Long Key Channel, and Indian Key Channel) are so large. Given the assumptions inherent in each approach, it is likely that the Harbor Branch results are less reliable than the WES results.

The y-intercept obtained from the regression of WES discharge values against the Harbor Branch two-dimensional transport was an unexpected source of confusion. It is still not clear what the y-intercept tells us, and thus whether the y-intercept is anything more than a curve-fitting variable for correlating discharge with midchannel transport during the time of the intensive survey. It appears, however, that the slope of the regression line provides useful information regarding how two-dimensional transport and total channel discharge are related. The y-intercept may quantify nontidal transport at the time of the survey if discharge is regressed against *tidal* two-dimensional transport. But the y-intercept is nothing more than a curve-fitting variable if discharge is regressed against *total* two-dimensional transport. Even where the y-intercept has some physical meaning, it should not be applied to long time series, because the nontidal flow that it represents can be highly variable over time scales on the order of days to weeks. Studies of midchannel flow in many channels have shown repeatedly that tidal channels separating Florida Bay and Hawk Channel are highly dynamic over a wide range of nontidal time scales. To emphasize this point, Figure D33 shows the low-pass filtered flow past a Harbor Branch study site in Tavernier Creek from October 25, 1995, to December 7, 1996. Tidal ebbs and floods of ± 15 to 20 cm s^{-1} are superimposed onto the nontidal flow, thus the tidal and nontidal exchanges are of the same order of magnitude. It follows that a poor representation of the nontidal exchanges could lead to an equally poor understanding of flow patterns in this part of Florida Bay.

Even in channels where tidal exchanges explain a very large percent of the total variance, regression analysis indicates that simulations of the ebb and flood carry with them a substantial degree of uncertainty. In Tea Table Channel, for example, and using the standard error of the estimate to quantify uncertainty, the regression equation provides tidal discharge values to ± 4127 ft^3 s^{-1} (recall that 68% of the estimates of discharge will lie within ± 1 standard error of the estimate). For comparison, at maximum flood and ebb, the discharge through Tea Table Channel reaches +13,746 and -12,524 ft^3 s^{-1}, respectively. The standard error is therefore 30 to 33% of these values, and thus the calculated flood and ebb discharge values can differ significantly from what should be the tidal signal embedded within the total. For other channels, the standard errors of the estimate can be still larger. In the case of Seven Mile Bridge Channel, the sum of the standard errors of the estimate for the west and east parts is nearly 76,000 ft^3 s^{-1}. Thus, while the ADCP surveys have produced consistent values for tidal exchanges through many of the channels that were investigated, there remains a degree of uncertainty in the individual measurements, as well as in the low-frequency exchanges.

LITERATURE CITED

Dennis, R.E. and E.E. Long. 1971. A user's guide to a computer program for harmonic analysis of data at tidal frequencies. NOAA Tech. Rept. 41, U.S. Dept. of Comm., Rockville, MD, 31 pages.

Pitts, Patrick. Personal communication. Harbor Branch Oceanographic Institution, Inc., 5600 U.S. Highway 1 North, Fort Pierce, FL

Schureman, P. 1958. Manual of harmonic analysis and prediction of tides. Special Publication No.98, rev. ed., U.S. Govt. Printing Office, Washington, D.C., 317 pages.

Table D1
Station Summary for ADCP Transects

Range	Channel Name	Survey 1			Survey 2			Latitude deg	Longitude deg
		Date	No. of Crossings	Hours est	Date	No. of Crossings	Hours est		
1	Jewfish Creek	9/26/96	11	0725-1657	2/11/97	9	0841-1605	25.18	80.39
2	Adams Cut	9/26/96	11	0746-1708	2/11/97	9	0857-1620	25.14	80.41
3	Dusenbury Creek	9/26/96	10	0830-1718	2/11/97	9	0821-1548	25.14	80.43
4	Grouper Creek	9/26/96	10	0712-1602	2/11/97	9	0752-1600	25.12	80.45
5	Baker Cut	9/26/96	10	0722-1614	2/11/97	9	0805-1608	25.09	80.47
6	Tavernier Creek	9/27/96	10	0646-1557	2/10/97	10	0730-1600	25.01	80.55
7	Cowpens Cut	9/27/96	10	0654-1602	2/10/97	10	0733-1605	25.00	80.56
8	Snake Creek	9/27/96	9	0850-1623	2/10/97	10	0709-1555	24.96	80.59
9	Whale Harbor Channel	9/27/96	9	0812-1607	2/10/97	10	0725-1607	24.94	80.61
10	Tea Table Relief	9/28/96	10	0637-1600	2/9/97	10	0653-1606	24.90	80.66
11	Tea Table Channel	9/28/96	10	0645-1609	2/9/97	10	0658-1612	24.90	80.67
12	Indian Key Channel	9/28/96	10	0701-1621	2/9/97	10	0710-1622	24.89	80.68
13	Lignumvitae Channel	9/28/96	10	0708-1630	2/10/97	10	0722-1631	24.89	80.69
14	Channel Two	9/28/96	10	0710-1604	2/9/97	10	0735-1555	24.84	80.75
15	Channel Five	9/28/96	10	0724-1619	2/9/97	10	0748-1609	24.84	80.77
16	Long Key Channel	9/29/96	10	0720-1606	2/8/97	10	0743-1555	24.80	80.87

(Continued)

Table D1 (Concluded)

Range	Channel Name	Survey 1			Survey 2			Latitude deg	Longitude deg
		Date	No. of Crossings	Hours est	Date	No. of Crossings	Hours est		
17	Tom's Harbor Cut	9/29/96	10	0621-1543	2/8/97	10	0735-1558	24.78	80.91
18	Tom's Harbor Channel	9/29/96	10	0633-1608	2/8/97	10	0744-1612	24.78	80.92
19	Seven Mile Bridge, east	9/30/96	8	0720-1530	2/7/97	9	0830-1558	24.71	81.14
20	Seven Mile Bridge, west	9/30/96	8	0730-1439	2/7/97	10	0728-1610	24.70	81.18

Note: Latitudes and longitudes are for the approximate midpoints of each range.

Table D2
Net Discharge of Five Principal Tidal Constituents

Range	Channel Name	Tidal Constituent				
		M_2	S_2	N_2	K_1	O_1
1	Jewfish Creek	0.320	0.019	0.085	0.053	0.071
6	Tavernier Creek	1.742	0.057	0.068	0.044	0.055
8	Snake Creek	4.307	0.138	0.220	0.148	0.185
9	Whale Harbor Channel	8.1	0.496	0.697	0.529	0.616
11	Tea Table Channel	13.35	0.427	0.592	0.487	0.525
12	Indian Key Channel	44.50	1.731	1.779	1.336	3.056
14	Channel Two	53.89	3.133	2.150	4.443	1.775
15	Channel Five	125.1	7.007	4.764	9.290	4.896
16	Long Key Channel	227.0	11.28	9.675	4.754	3.770
19 & 20	Seven Mile Bridge Channel	307.8	14.66	11.66	4.665	1.793

Note: Net discharge for each of the five principal tidal constituents through the 10 channels in which Harbor Branch has historical data. Discharge values are in millions of cubic feet and are the net values after one complete cycle of the tidal constituent in question. Values have been calculated using the slopes of the regression equations obtained from the first intensive survey.

Table D3
Statistics Relating Predicted Tidal Transport to Measured Discharge

Range	Channel Name	Survey	Slope	r^2	Y-int
1	Jewfish Creek	1	110.4	0.78	-02026
		2	195.7	0.95	-00859
6	Tavernier Creek	1	75.1	0.85	+00497
		2	93.8	0.94	-03028
8	Snake Creek	1	348.1	0.98	+01186
		2	358.9	0.94	-01171
9	Whale Harbor Channel	1	483.2	0.98	+01683
		2	467.3	0.93	-01850
11	Tea Table Channel	1	459.9	0.99	+00561
		2	481.4	0.97	+02403
12	Indian Key Channel	1	640.7	0.98	+00487
		2	629.7	0.96	-03171
14	Channel Two	1	2103.8	0.99	-03743
		2	2146.9	0.96	-11535
15	Channel Five	1	5853.4	0.98	-09814
		2	6173.6	0.99	-16684
16	Long Key Channel	1	9181.9	0.89	+31207
		2	9385.2	0.94	-57084
19 & 20	Seven Mile Bridge Channel	1 (East)	3527.4	0.95	+13103
		1 (West)	6145.0	0.86	-47041
		2 (East)	4958.1	0.92	-14772
		2 (West)	5878.5	0.98	-49332

Note: Statistics relating predicted tidal transport to measured discharge for each of the 10 channels for which Harbor Branch has historical data to supplement the intensive survey data. The slopes are the transfer functions needed to convert mid-channel two-dimensional transport, in ft^2s^{-1} (or m^2s^{-1}) to discharge, in ft^3s^{-1} (or m^3s^{-1}).

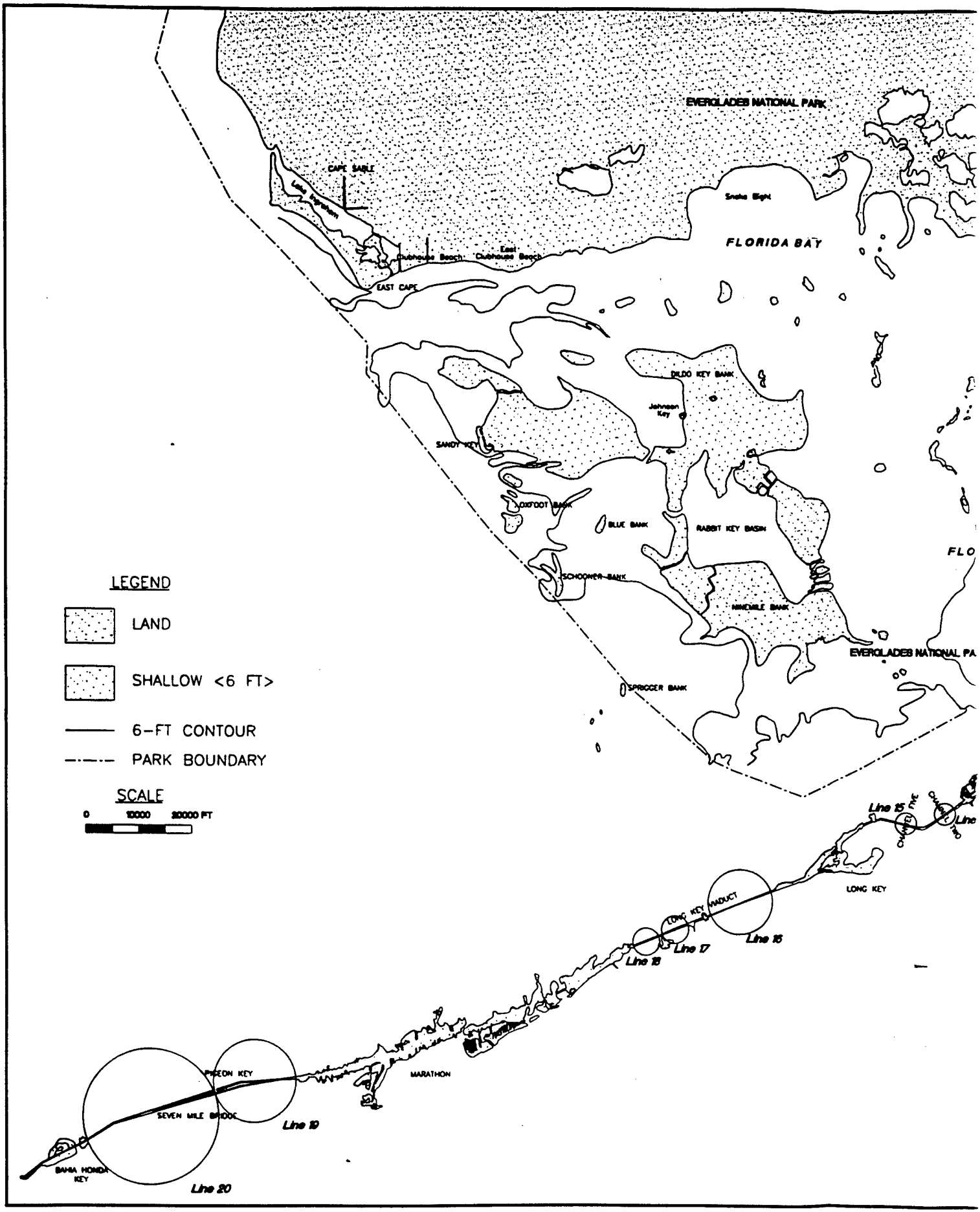
EVERGLADES NATIONAL PARK
CAPE SABLE
Clubhouse Beach
East Clubhouse Beach
EAST CAPE
FLORIDA BAY
DILDO KEY BANK
Johnson Key
SANDY KEY
LOOEOOT BANK
BLUE BANK
RABBIT KEY BASIN
SCHOONER BANK
NINEMILE BANK
SPRIGGER BANK
EVERGLADES NATIONAL PA
LEGEND
LAND
SHALLOW <6 FT>
6-FT CONTOUR
PARK BOUNDARY
SCALE
0 10000 20000 FT
Line 15
LONG KEY
LONG KEY VIADUCT
Line 16
Line 17
Line 18
PIGEON KEY
SEVEN MILE BRIDGE
Line 19
MARATHON
BAHIA HONDA KEY
Line 20

Figure D1

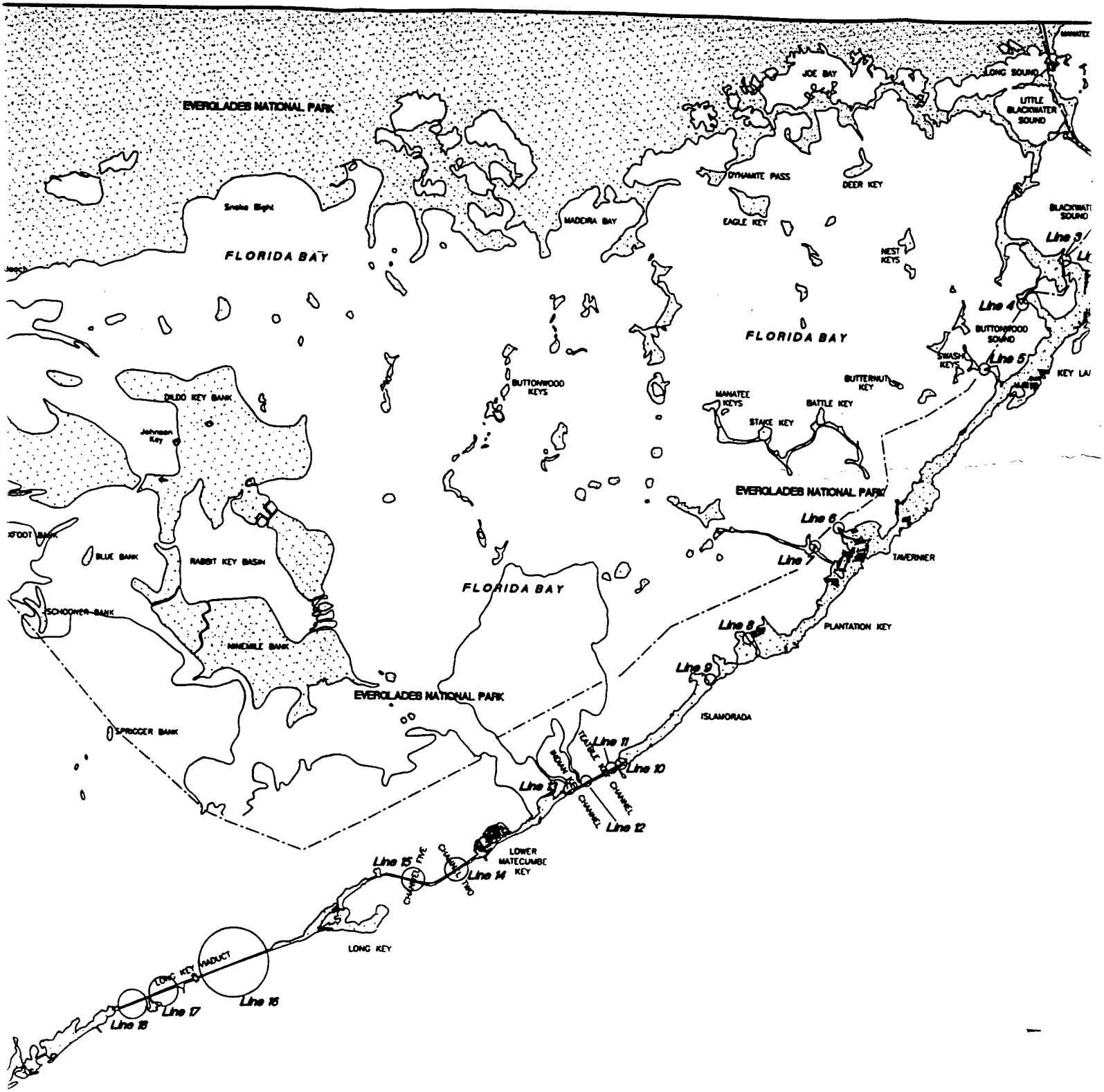

INTENSIVE SURVE
LOCATION

(2)

s in Eastern Florida Bay

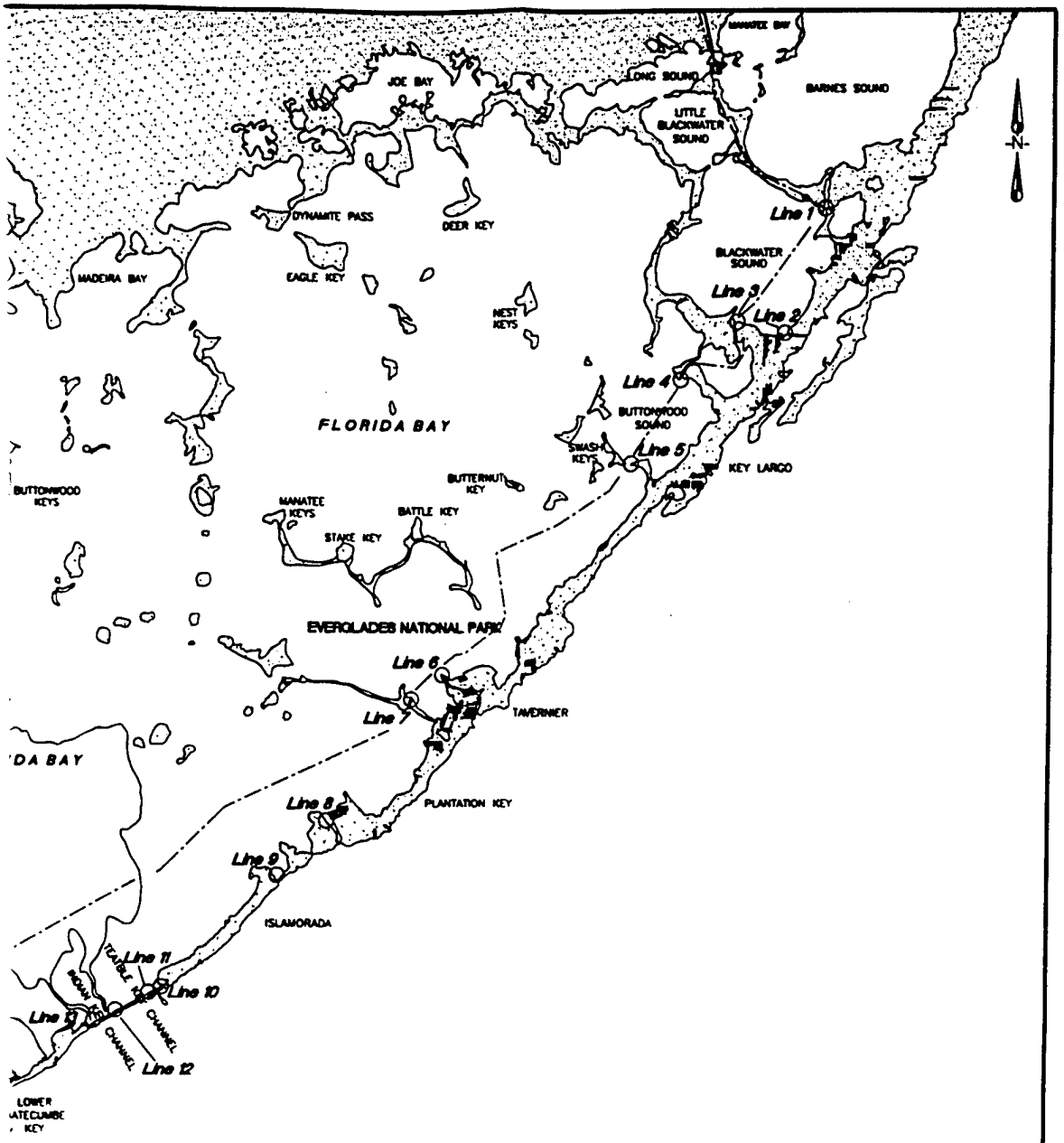

INTENSIVE SURVEY TRANSECT
LOCATION MAP

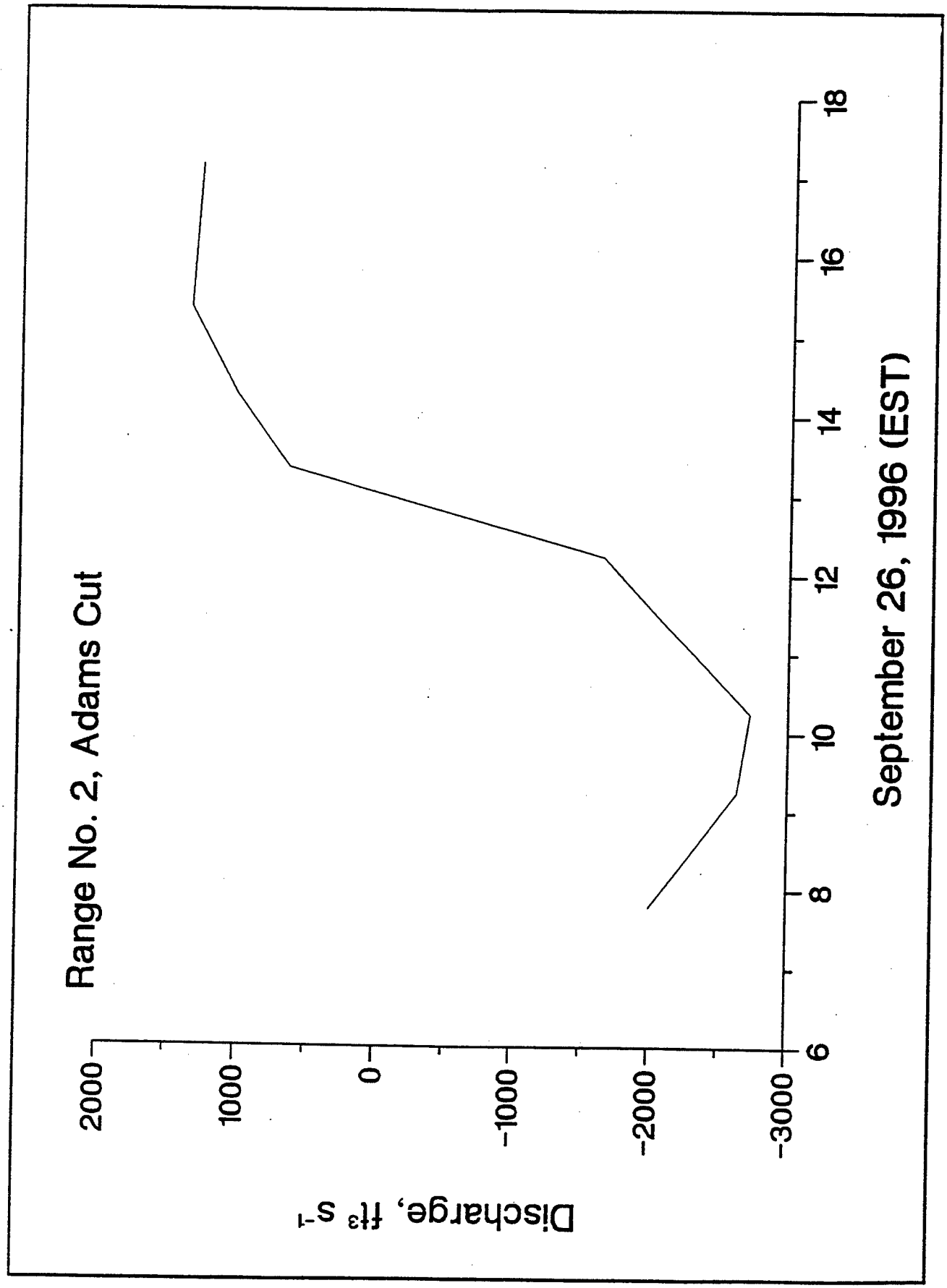
Range No. 2, Adams Cut
September 26, 1996 (EST)
Discharge, ft³ s⁻¹
2000
1000
0
-1000
-2000
-3000
6
8
10
12
14
16
18

Figure D2

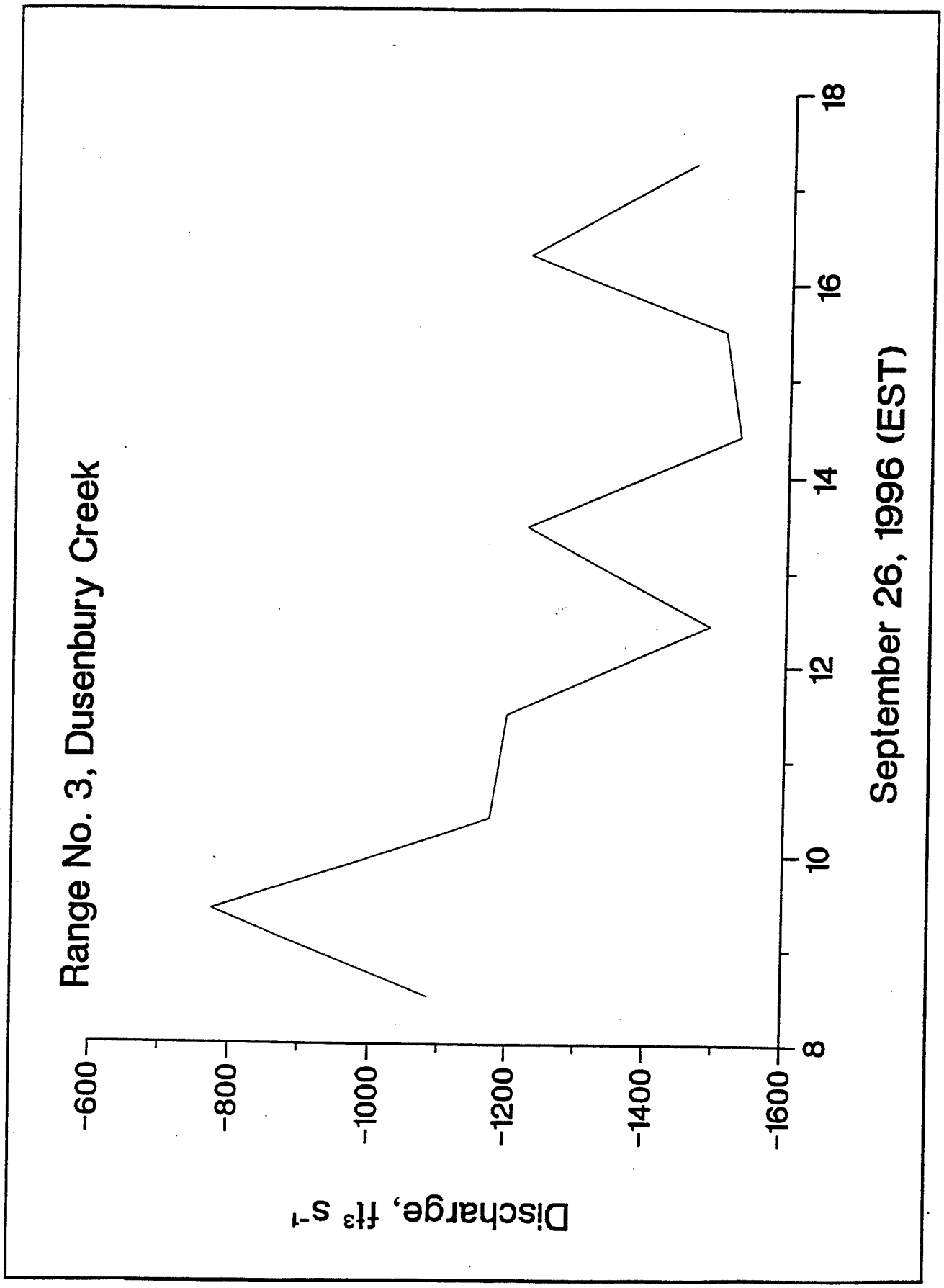
Range No. 3, Dusenbury Creek
Discharge, ft³ s⁻¹
-600
-800
-1000
-1200
-1400
-1600
8
10
12
14
16
18
September 26, 1996 (EST)

Figure D3

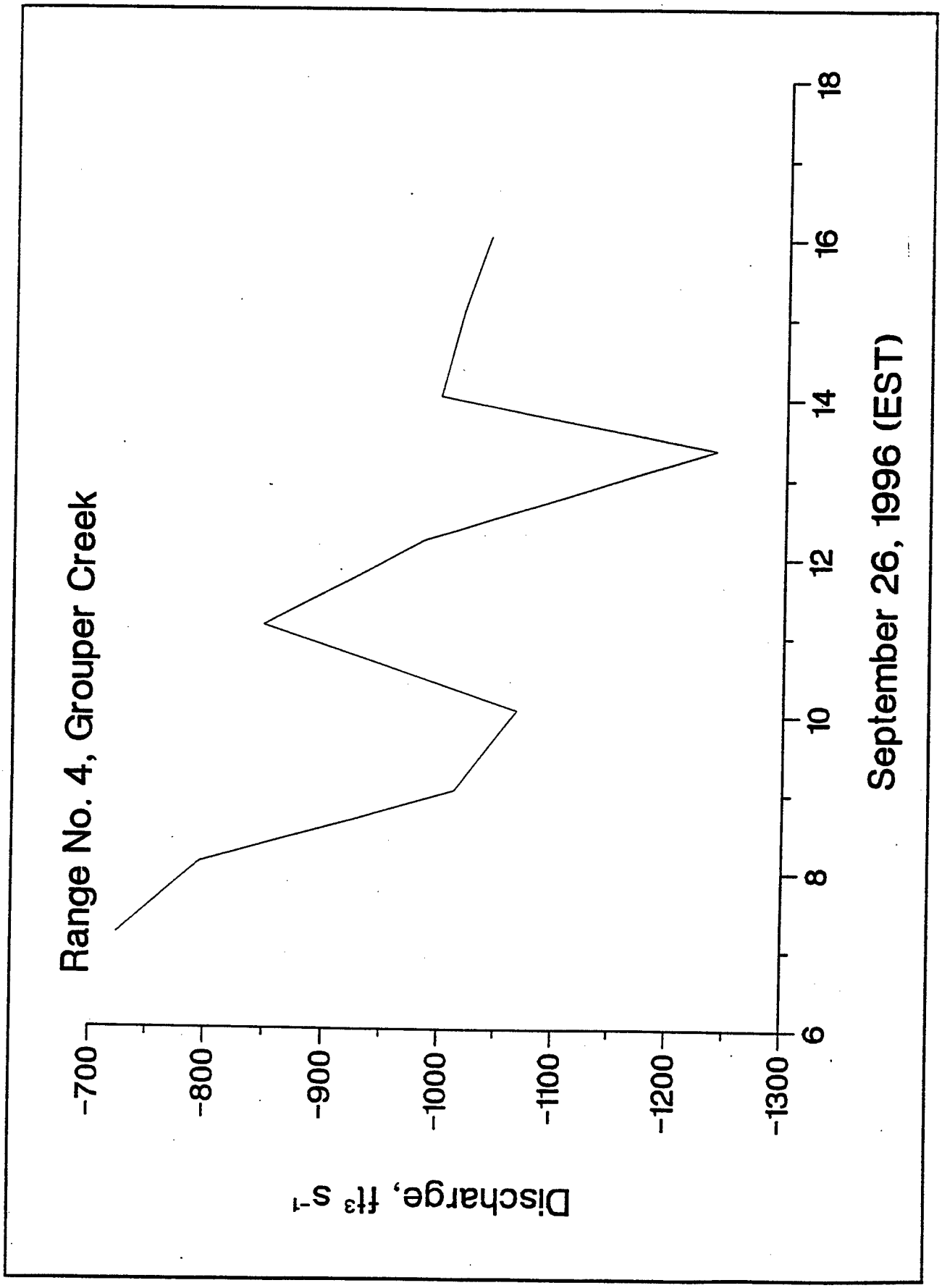
Range No. 4, Grouper Creek
September 26, 1996 (EST)
Discharge, ft³ s⁻¹
-700
-800
-900
-1000
-1100
-1200
-1300
6
8
10
12
14
16
18

Figure D4

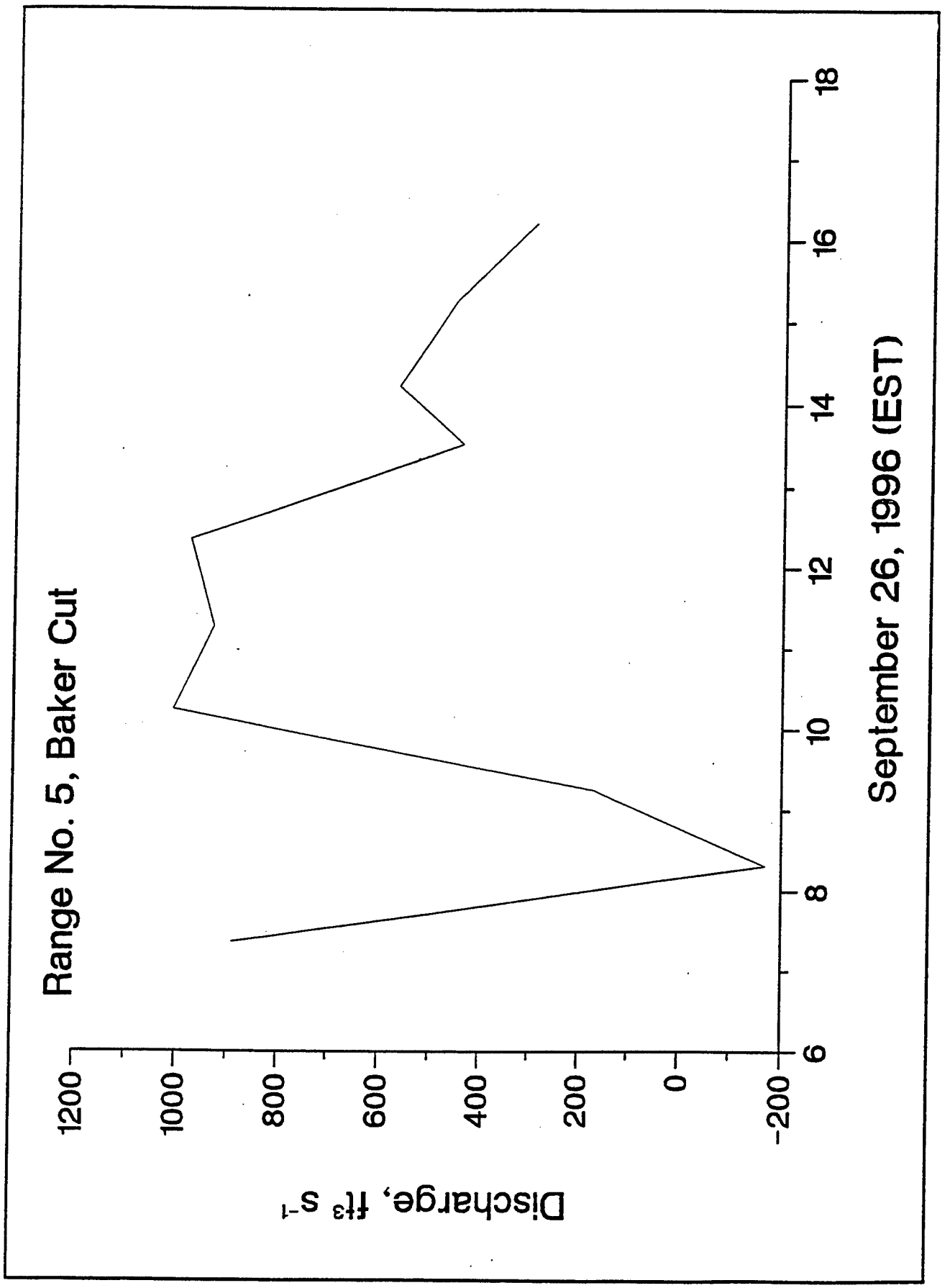
Range No. 5, Baker Cut
September 26, 1996 (EST)
Discharge, ft³ s⁻¹
1200
1000
800
600
400
200
0
-200
6
8
10
12
14
16
18

Figure D5

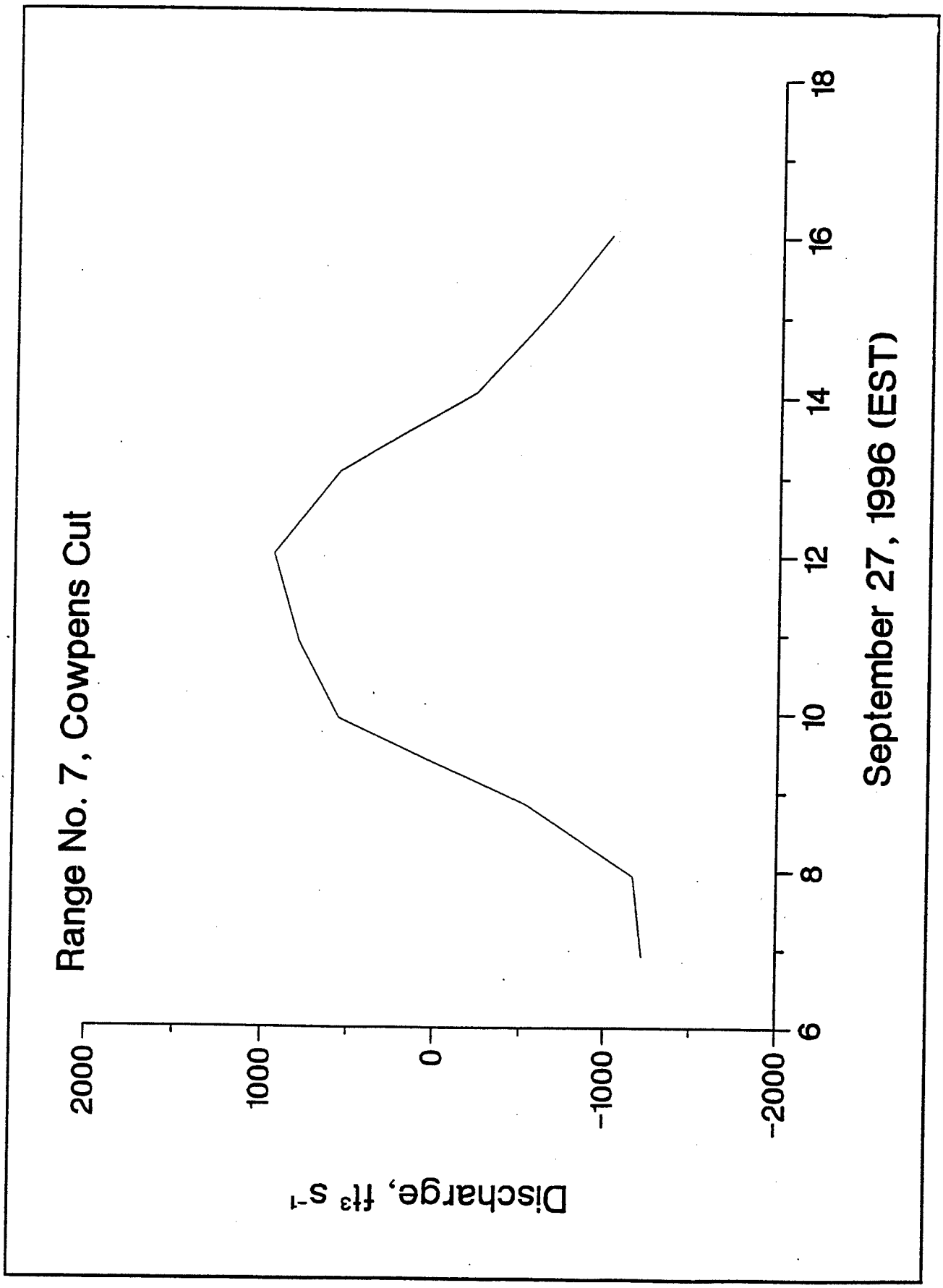
Range No. 7, Cowpens Cut
September 27, 1996 (EST)
Discharge, ft³ s⁻¹
2000
1000
0
-1000
-2000
6
8
10
12
14
16
18

Figure D6

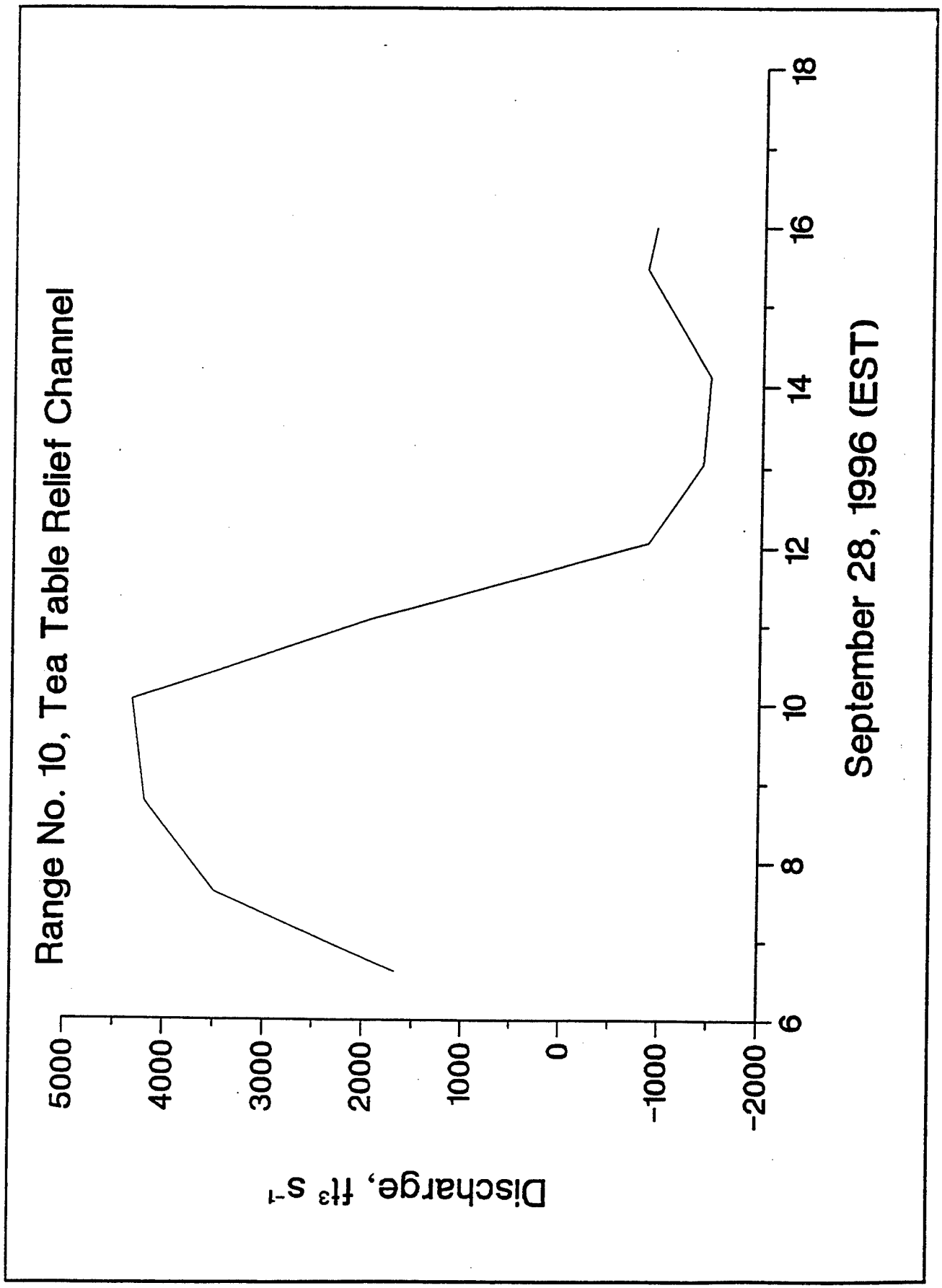
Range No. 10, Tea Table Relief Channel
September 28, 1996 (EST)
Discharge, ft³ s⁻¹
5000
4000
3000
2000
1000
0
-1000
-2000
6
8
10
12
14
16
18

Figure D7

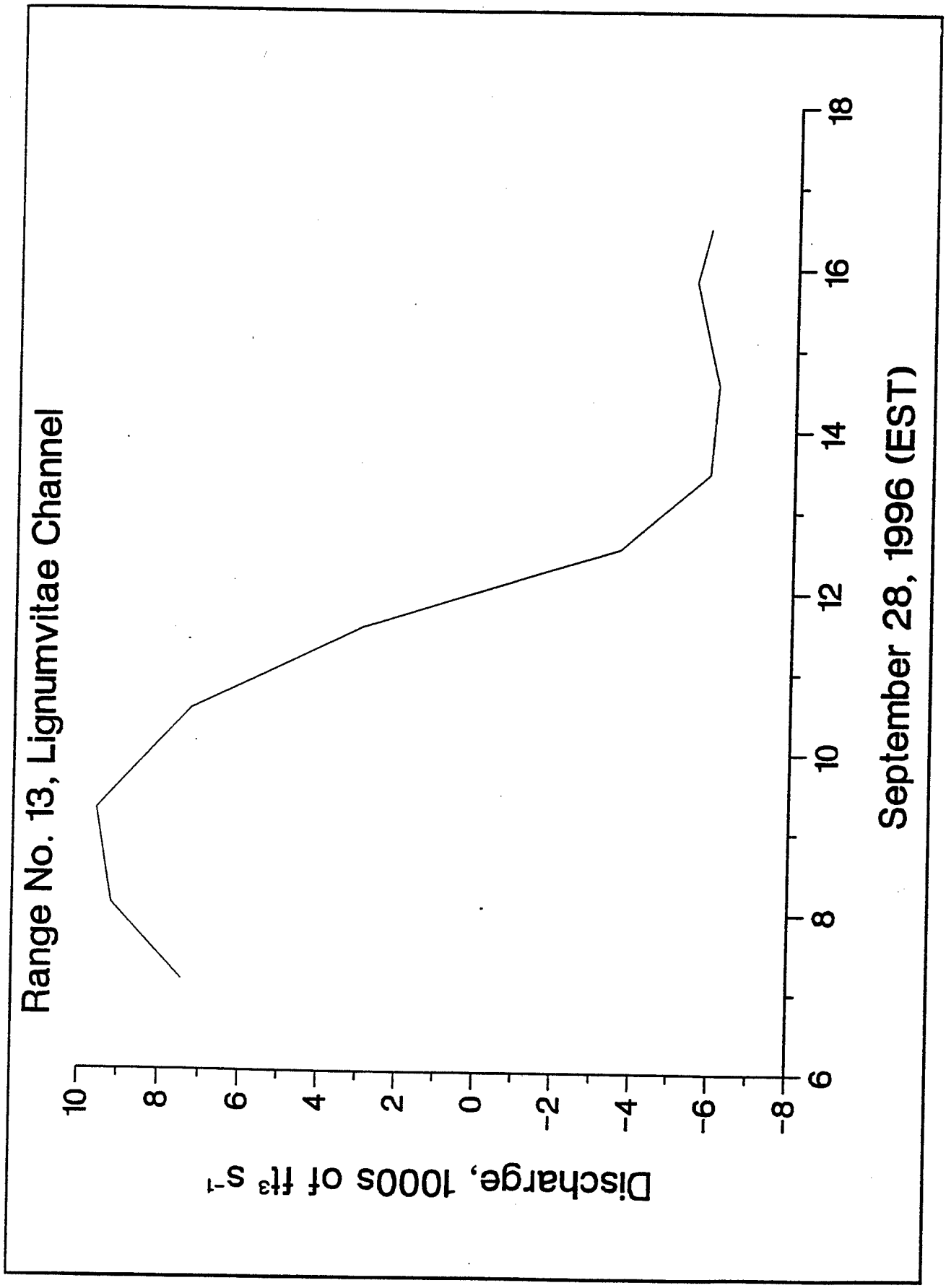
Range No. 13, Lignumvitae Channel
September 28, 1996 (EST)
Discharge, 1000s of ft³ s⁻¹
10
8
6
4
2
0
-2
-4
-6
-8
6
8
10
12
14
16
18

Figure D8

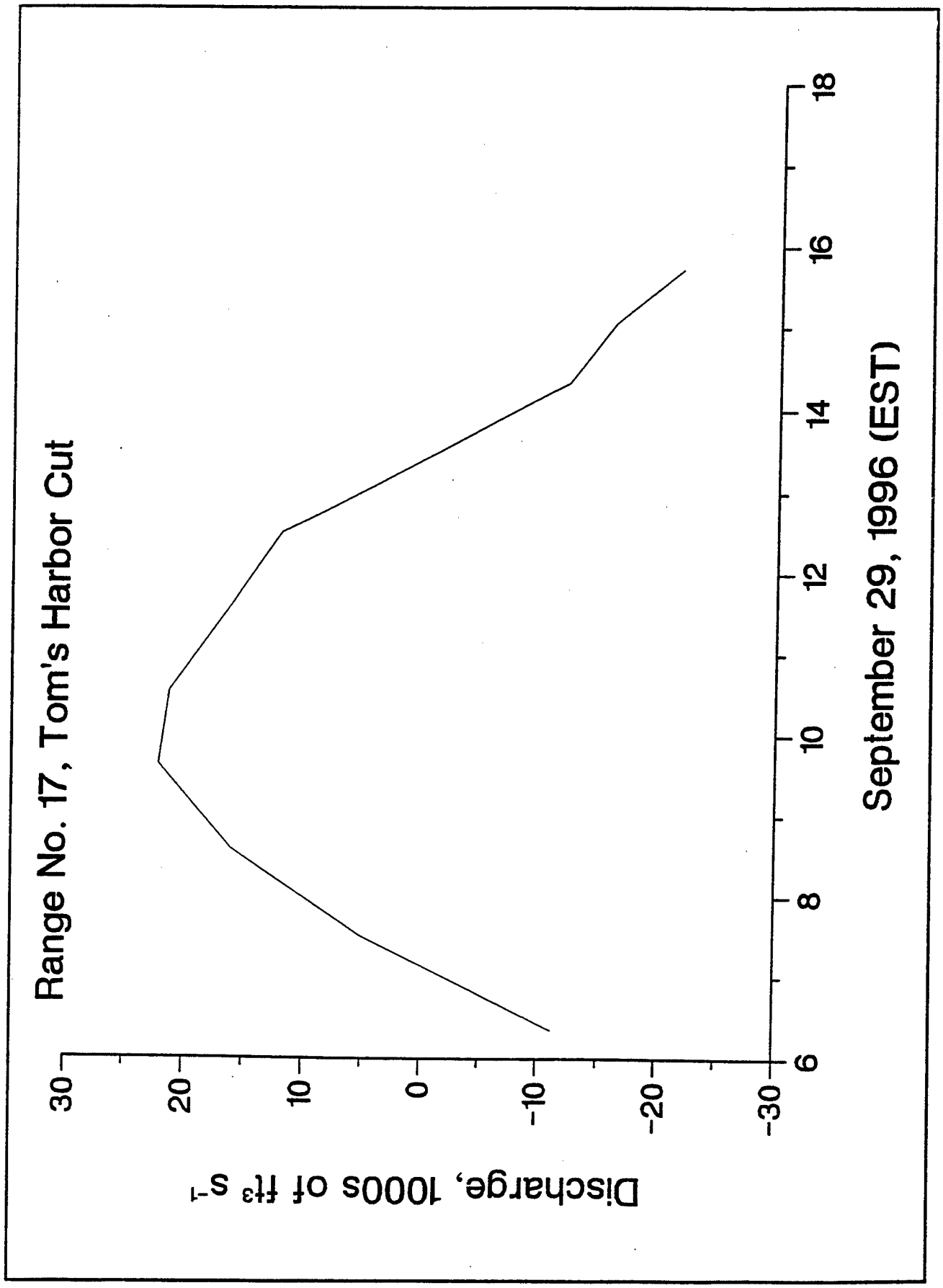
Range No. 17, Tom's Harbor Cut
September 29, 1996 (EST)
Discharge, 1000s of ft³ s⁻¹
30
20
10
0
-10
-20
-30
6
8
10
12
14
16
18

Figure D9

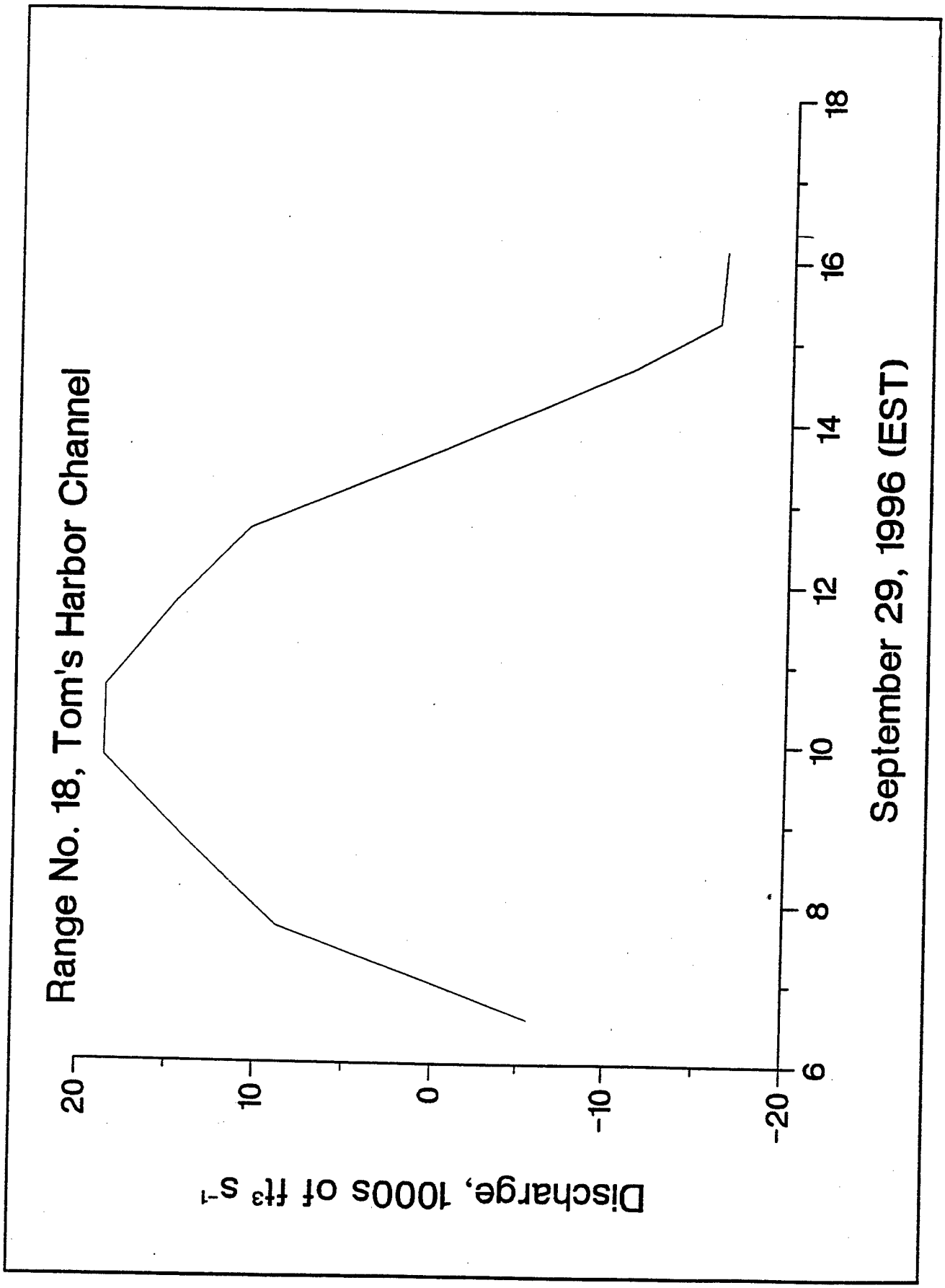
Range No. 18, Tom's Harbor Channel
September 29, 1996 (EST)
Discharge, 1000s of ft³ s⁻¹
20
10
0
-10
-20
6
8
10
12
14
16
18

Figure D10

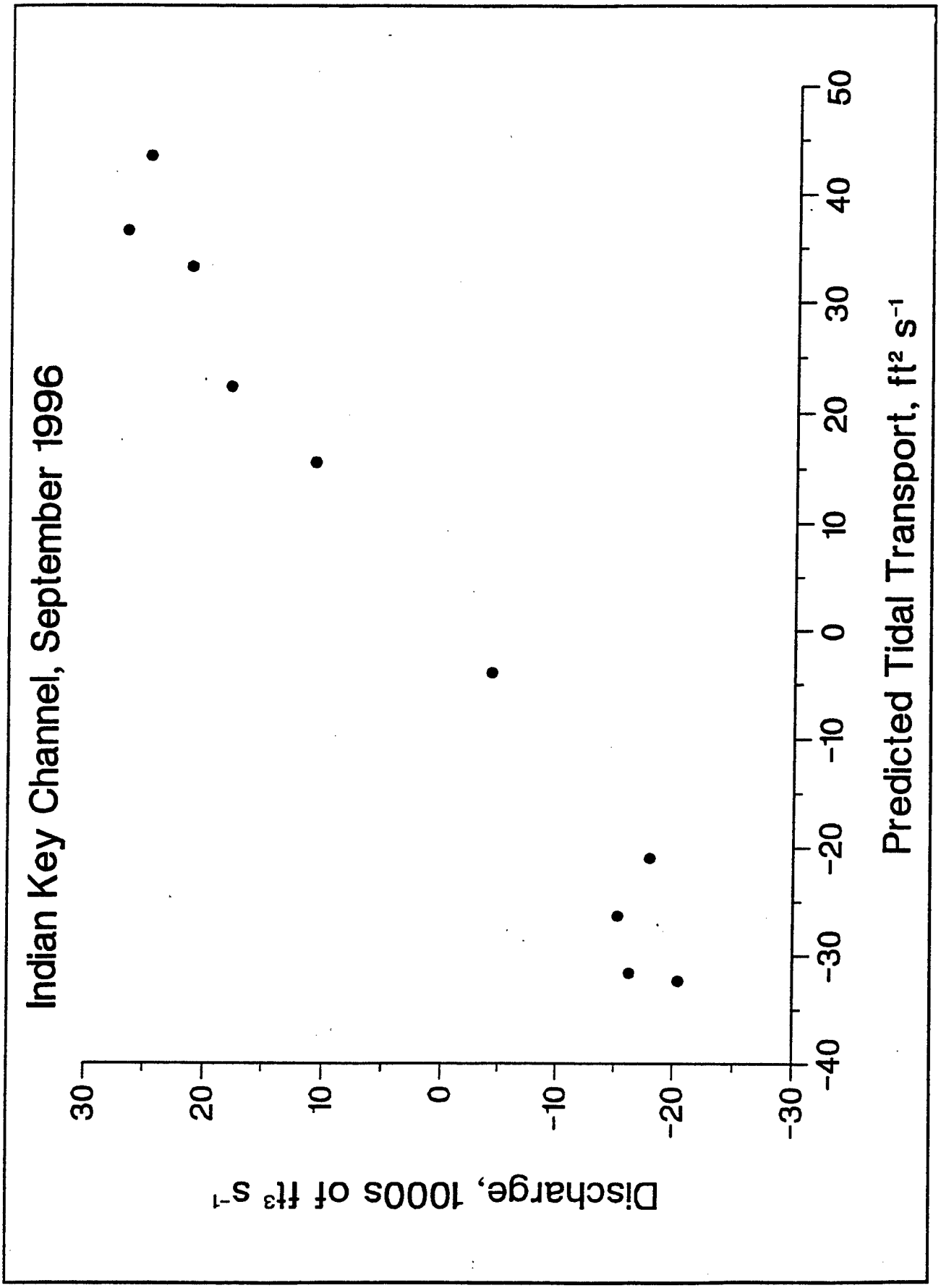
Indian Key Channel, September 1996
Predicted Tidal Transport, ft² s⁻¹
50
40
30
20
10
0
-10
-20
-30
-40
Discharge, 1000s of ft³ s⁻¹
30
20
10
0
-10
-20
-30

Figure D11

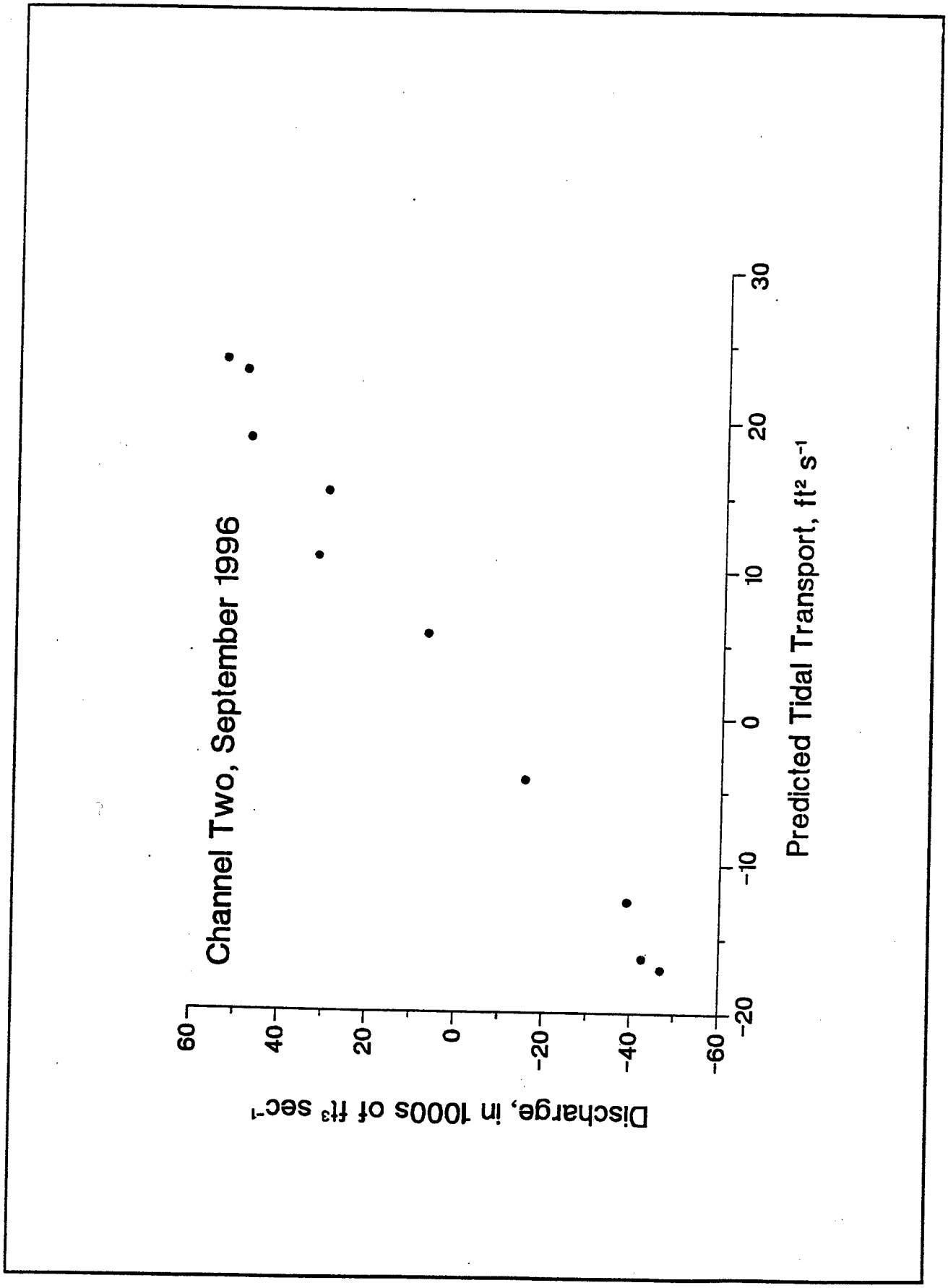
Channel Two, September 1996
Predicted Tidal Transport, ft² s⁻¹
30
20
10
0
-10
-20
Discharge, in 1000s of ft³ sec⁻¹
60
40
20
0
-20
-40
-60

Figure D12

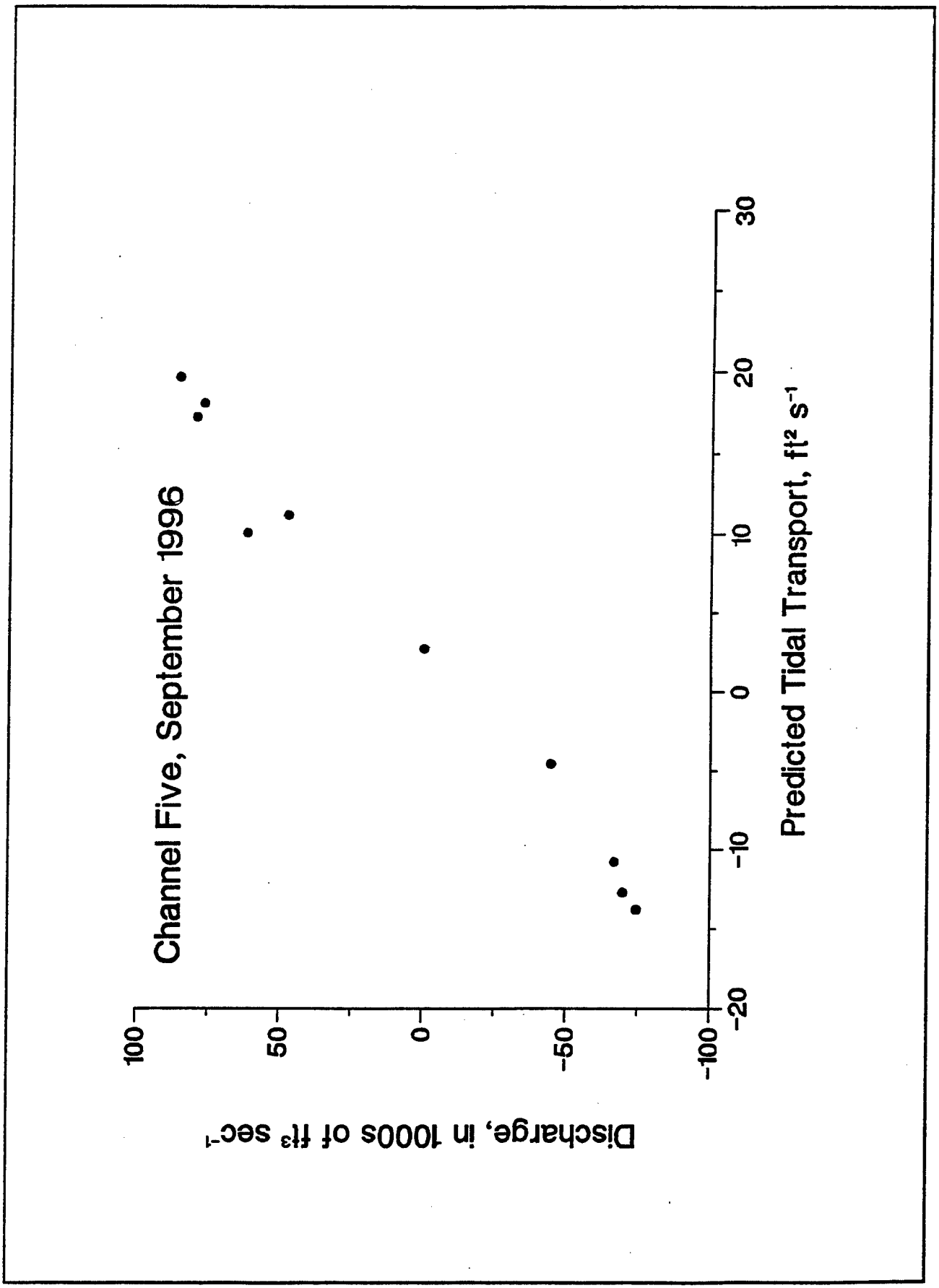
Channel Five, September 1996
Predicted Tidal Transport, ft² s⁻¹
30
20
10
0
-10
-20
Discharge, in 1000s of ft³ sec⁻¹
100
50
0
-50
-100

Figure D13

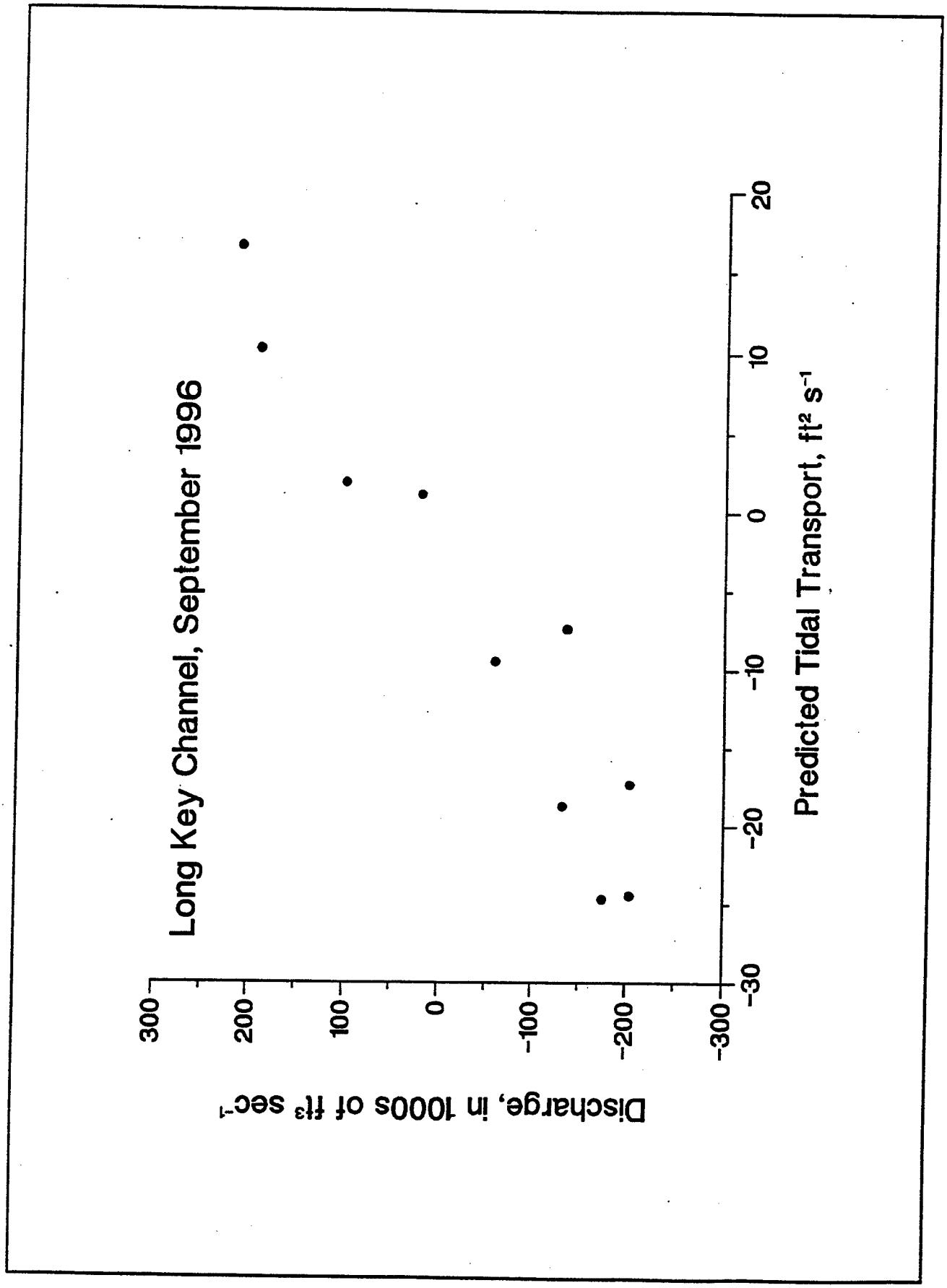
Long Key Channel, September 1996
Predicted Tidal Transport, ft² s⁻¹
Discharge, in 1000s of ft³ sec⁻¹
20
10
0
-10
-20
-30
300
200
100
0
-100
-200
-300

Figure D14

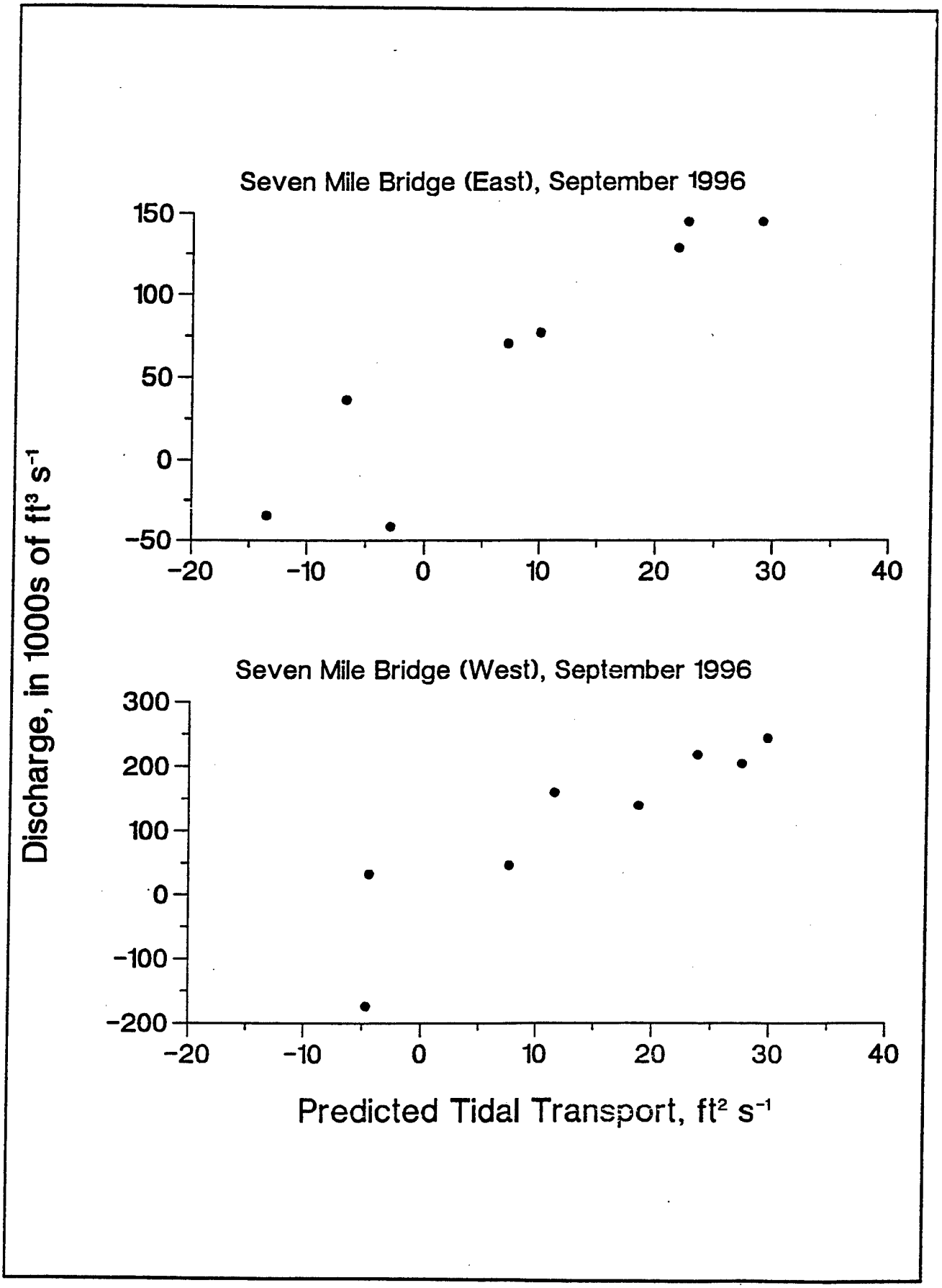
Seven Mile Bridge (East), September 1996
150
100
50
0
-50
-20
-10
0
10
20
30
40
Seven Mile Bridge (West), September 1996
300
200
100
0
-100
-200
-20
-10
0
10
20
30
40
Discharge, in 1000s of ft³ s⁻¹
Predicted Tidal Transport, ft² s⁻¹

Figure D15

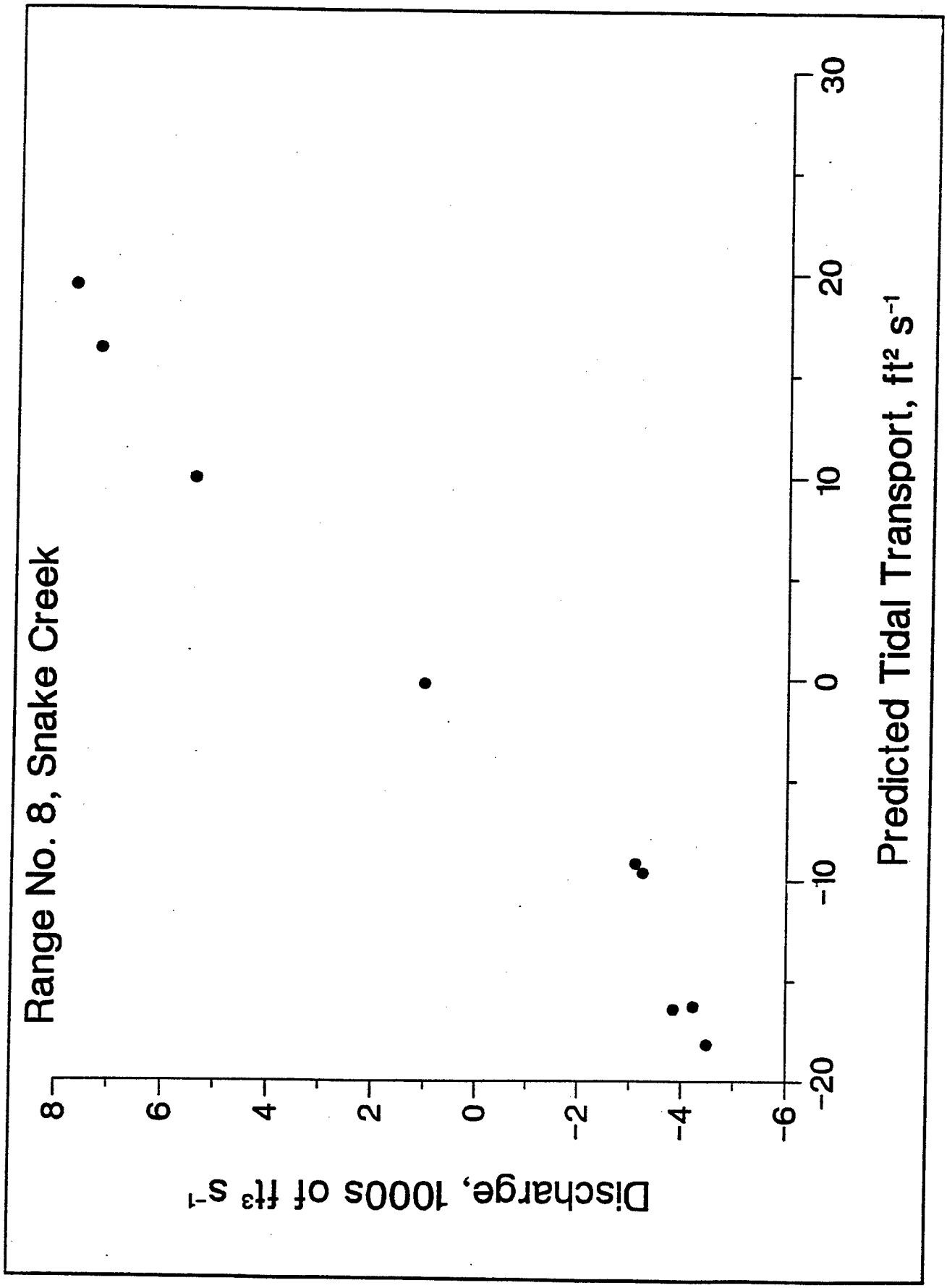
Range No. 8, Snake Creek
Discharge, 1000s of ft³ s⁻¹
8
6
4
2
0
-2
-4
-6
Predicted Tidal Transport, ft² s⁻¹
30
20
10
0
-10
-20

Figure D16

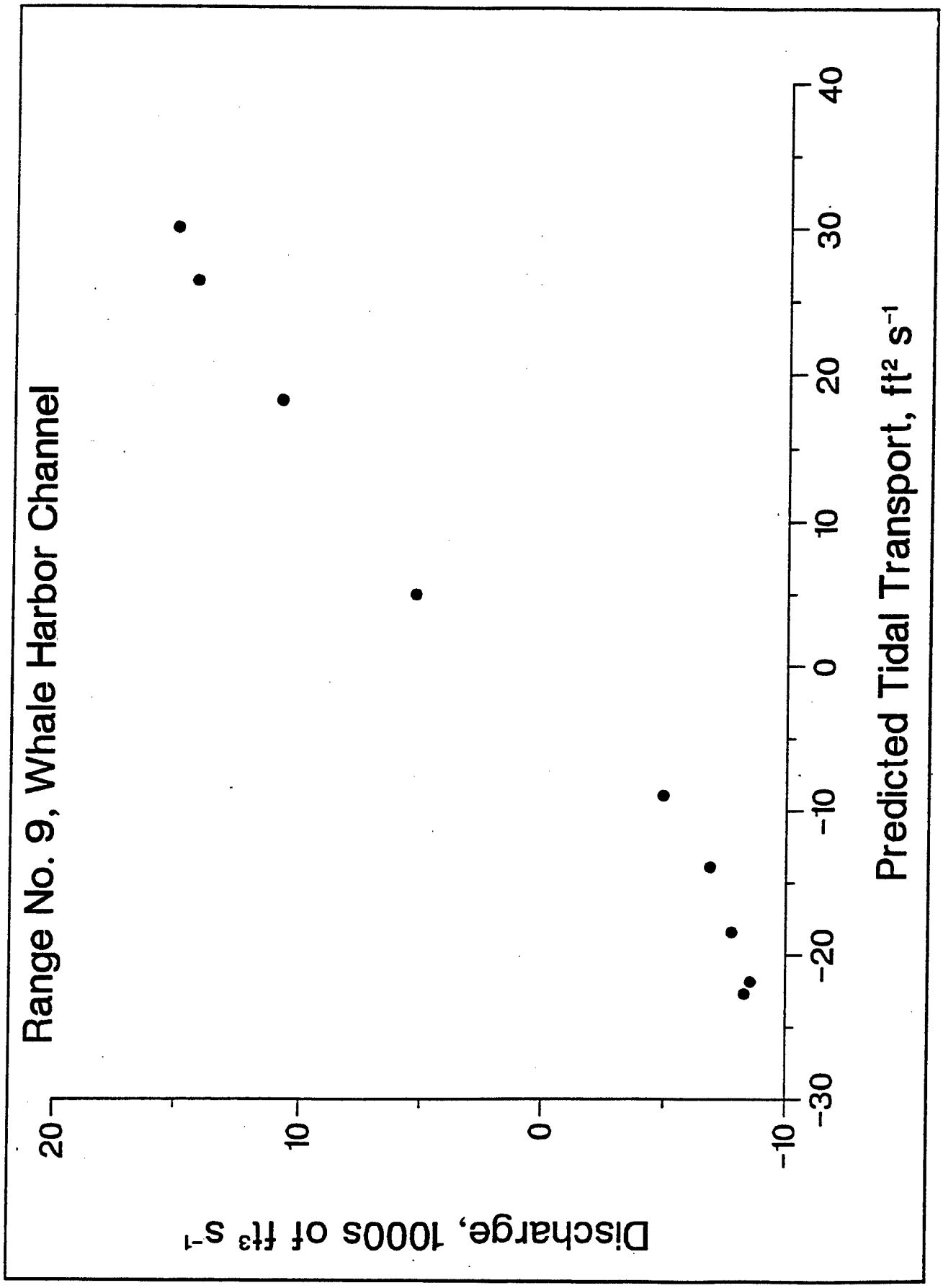
Range No. 9, Whale Harbor Channel
Predicted Tidal Transport, ft² s⁻¹
40
30
20
10
0
-10
-20
-30
Discharge, 1000s of ft³ s⁻¹
20
10
0
-10

Figure D17

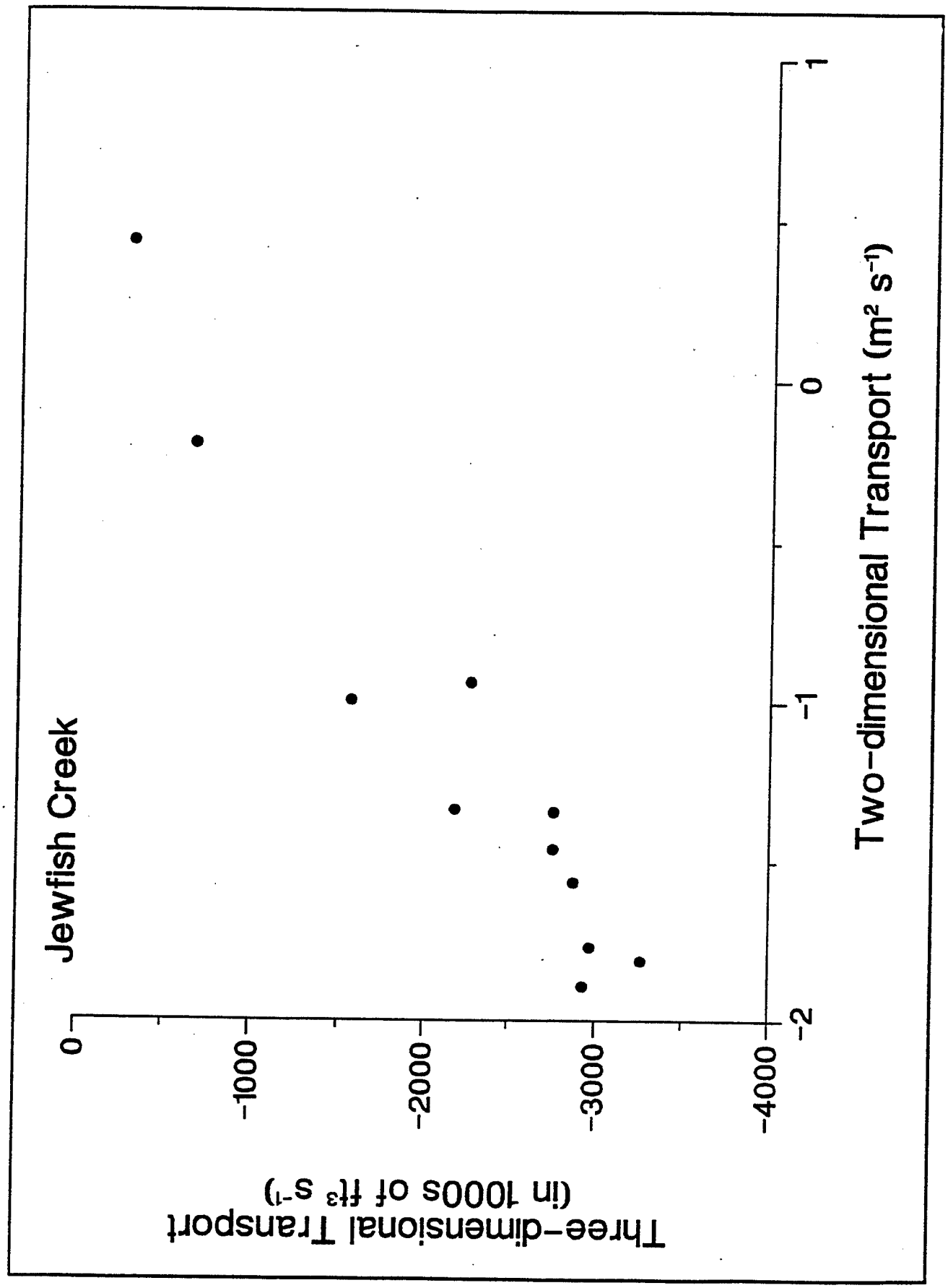
Jewfish Creek
Three-dimensional Transport
(in 1000s of ft³ s⁻¹)
0
-1000
-2000
-3000
-4000
Two-dimensional Transport (m² s⁻¹)
1
0
-1
-2

Figure D18

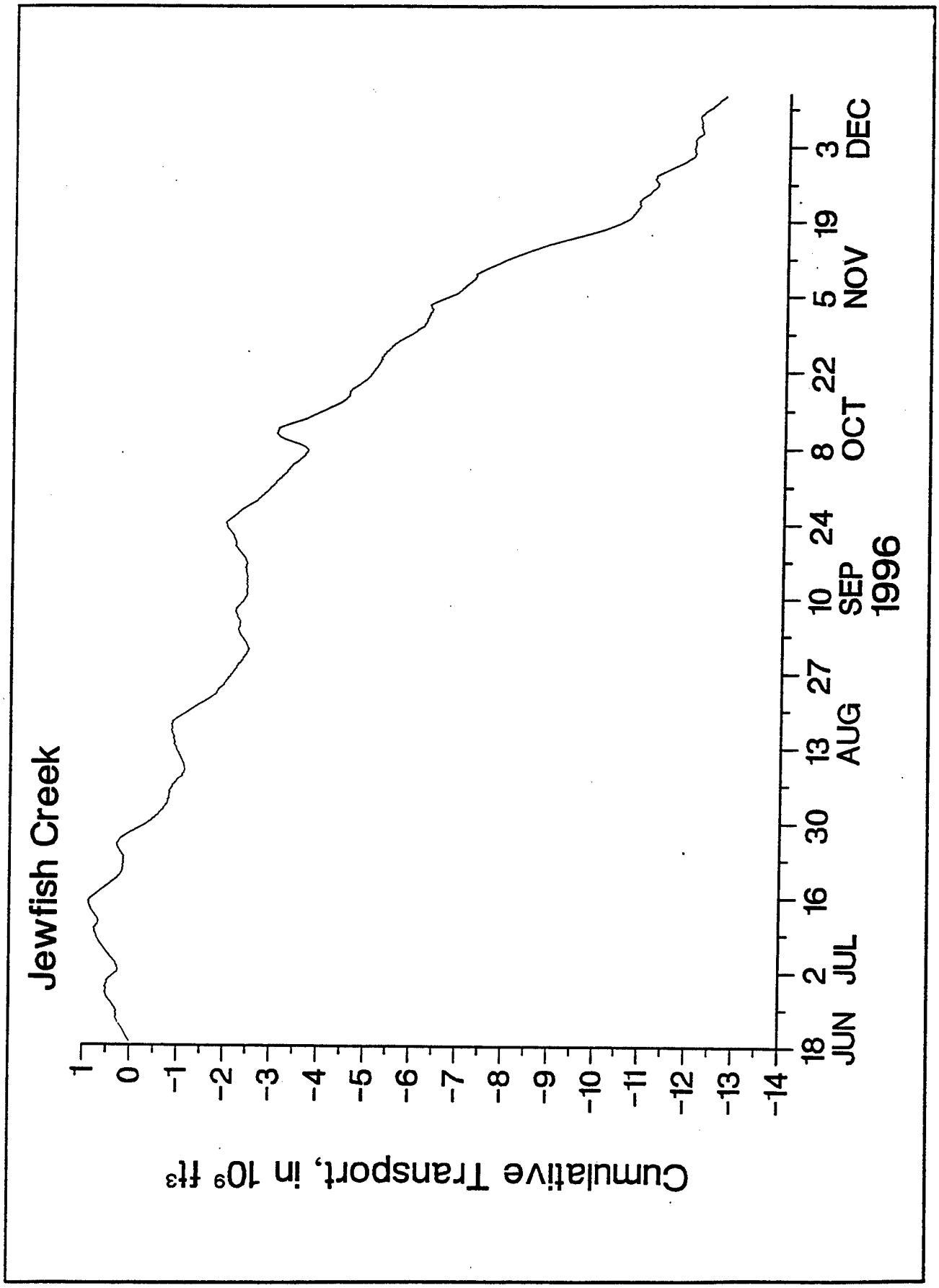
Jewfish Creek
Cumulative Transport, in 10^9 ft^3
1
0
-1
-2
-3
-4
-5
-6
-7
-8
-9
-10
-11
-12
-13
-14
18 JUN
2 JUL
16
30
13 AUG
27
10 SEP
24
8 OCT
22
5 NOV
19
3 DEC
1996

Figure D19

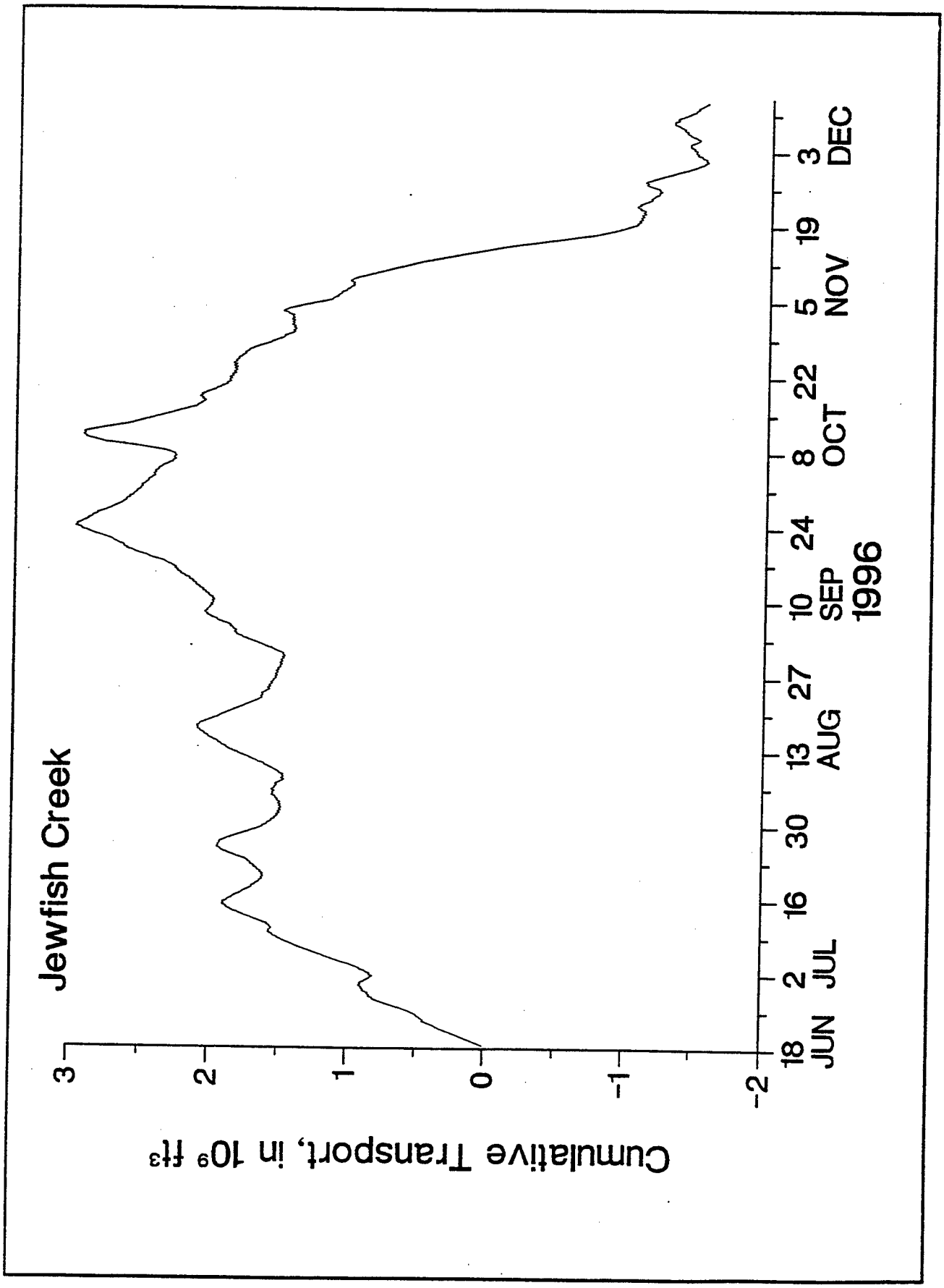
Jewfish Creek
Cumulative Transport, in 10^9 ft^3
3
2
1
0
-1
-2
18 JUN
2 JUL
16
30
13 AUG
27
10 SEP
24
8 OCT
22
5 NOV
19
3 DEC
1996

Figure D20

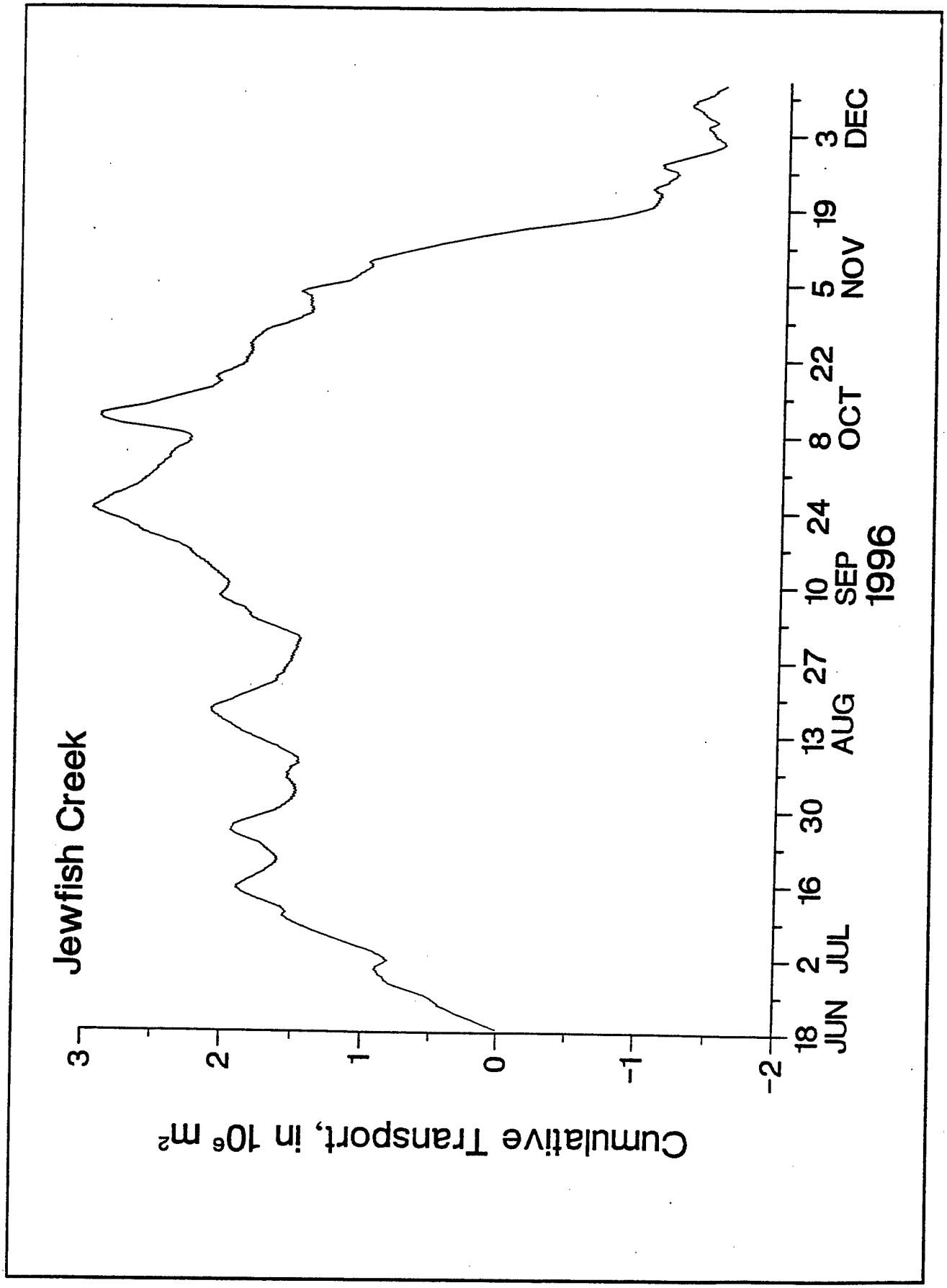
Jewfish Creek
Cumulative Transport, in 10⁶ m²
3
2
1
0
-1
-2
18 JUN
2 JUL
16
30
13 AUG
27
10 SEP
24
8 OCT
22
5 NOV
19
3 DEC
1996

Figure D21

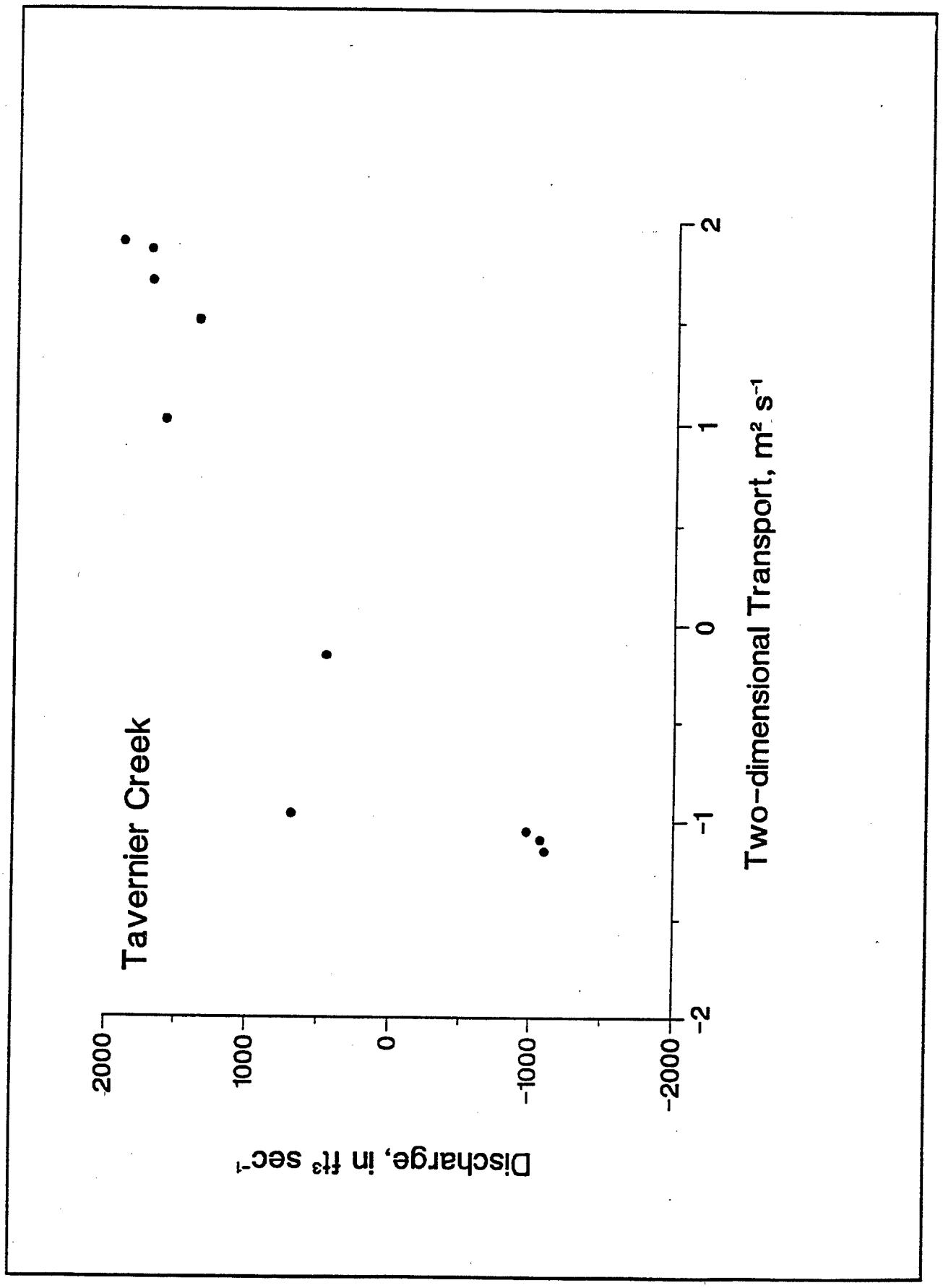
Tavernier Creek
Discharge, in ft³ sec⁻¹
2000
1000
0
-1000
-2000
Two-dimensional Transport, m² s⁻¹
2
1
0
-1
-2

Figure D22

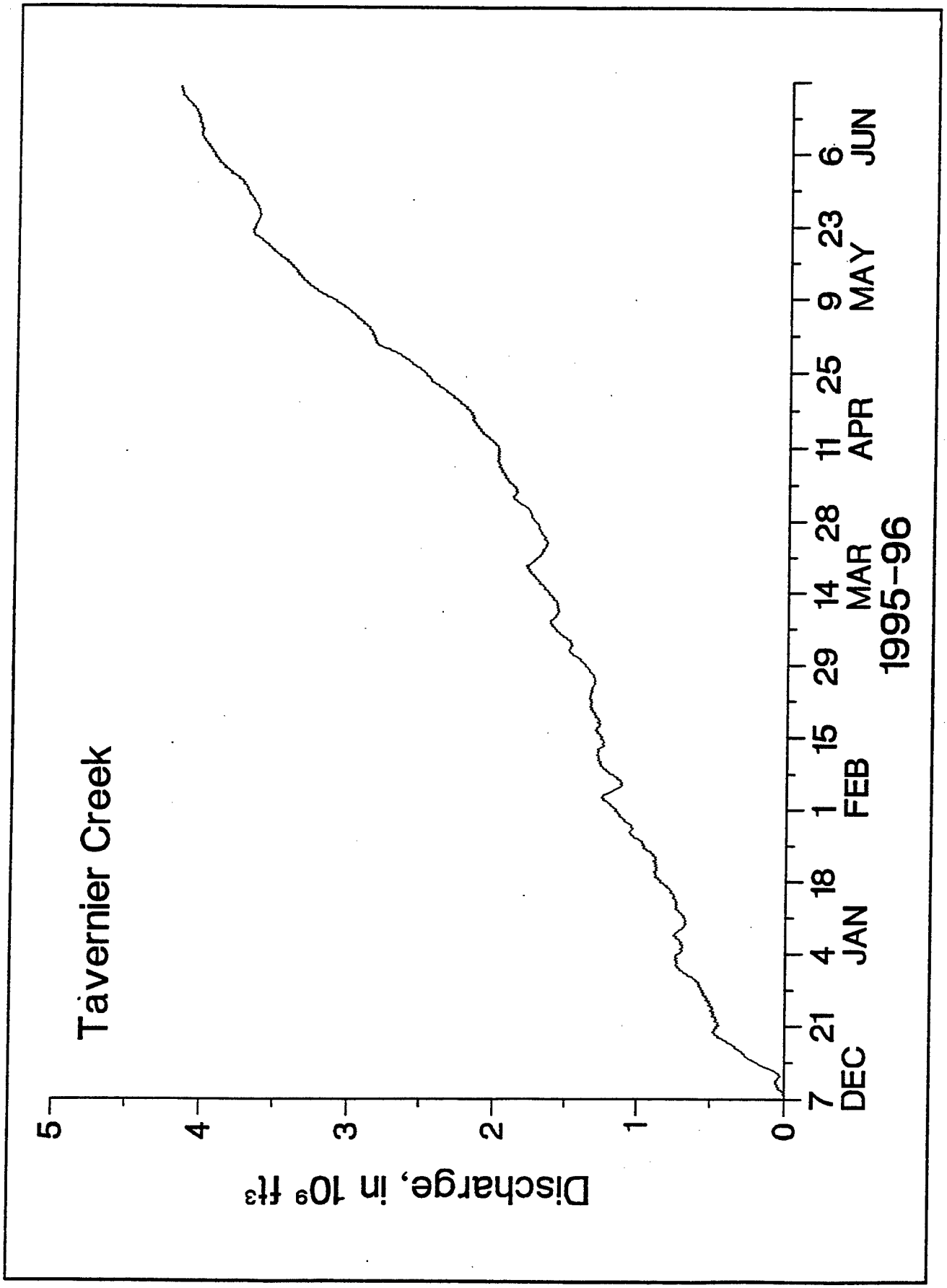
Tavernier Creek
Discharge, in 10⁹ ft³
0
1
2
3
4
5
7 DEC
21
4 JAN
18
1 FEB
15
29
14 MAR
28
11 APR
25
9 MAY
23
6 JUN
1995-96

Figure D23

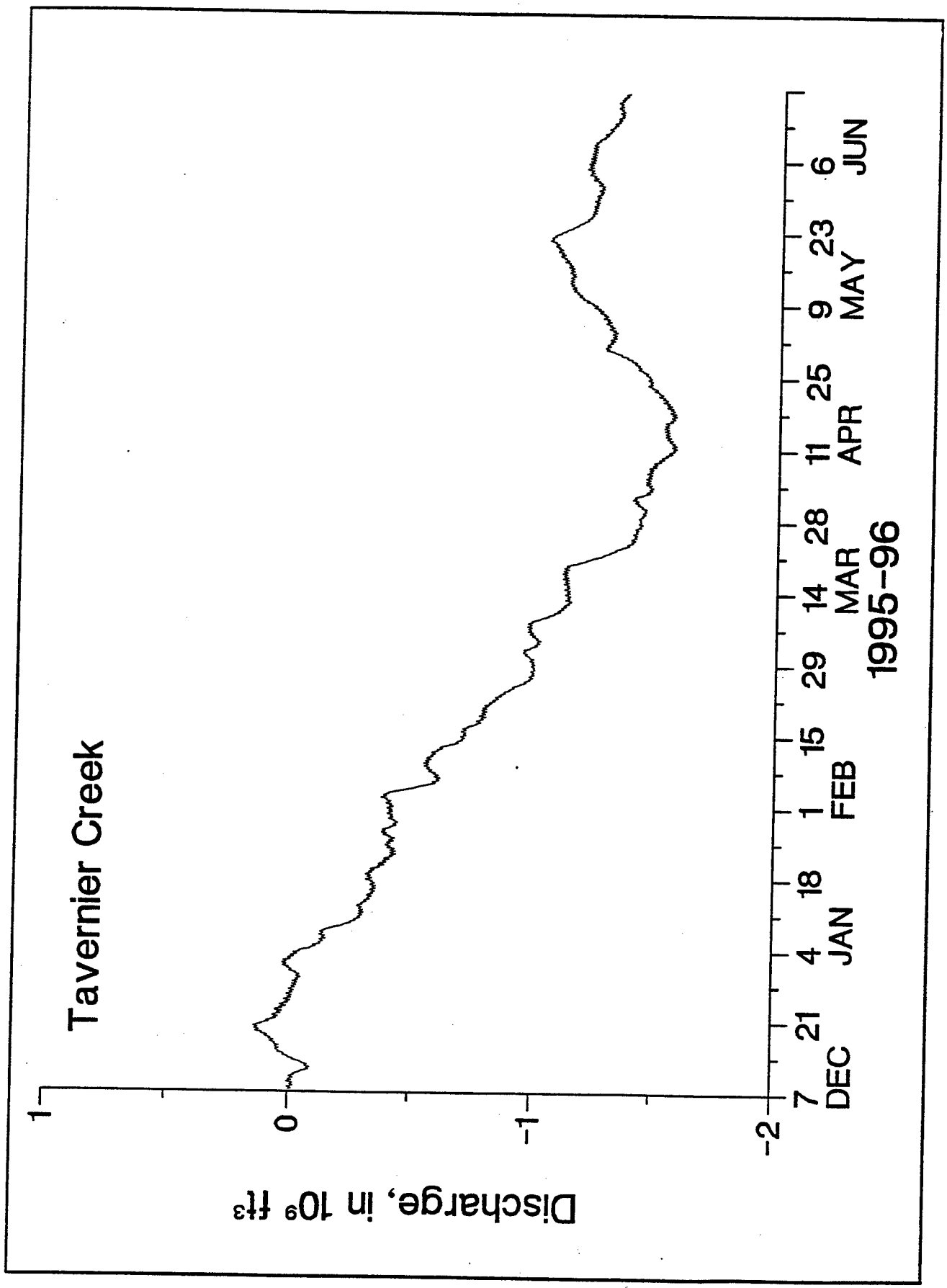
Tavernier Creek
Discharge, in 10^9 ft^3
1
0
-1
-2
7
21
4
18
1
15
29
14
28
11
25
9
23
6
DEC
JAN
FEB
MAR
APR
MAY
JUN
1995–96

Figure D24

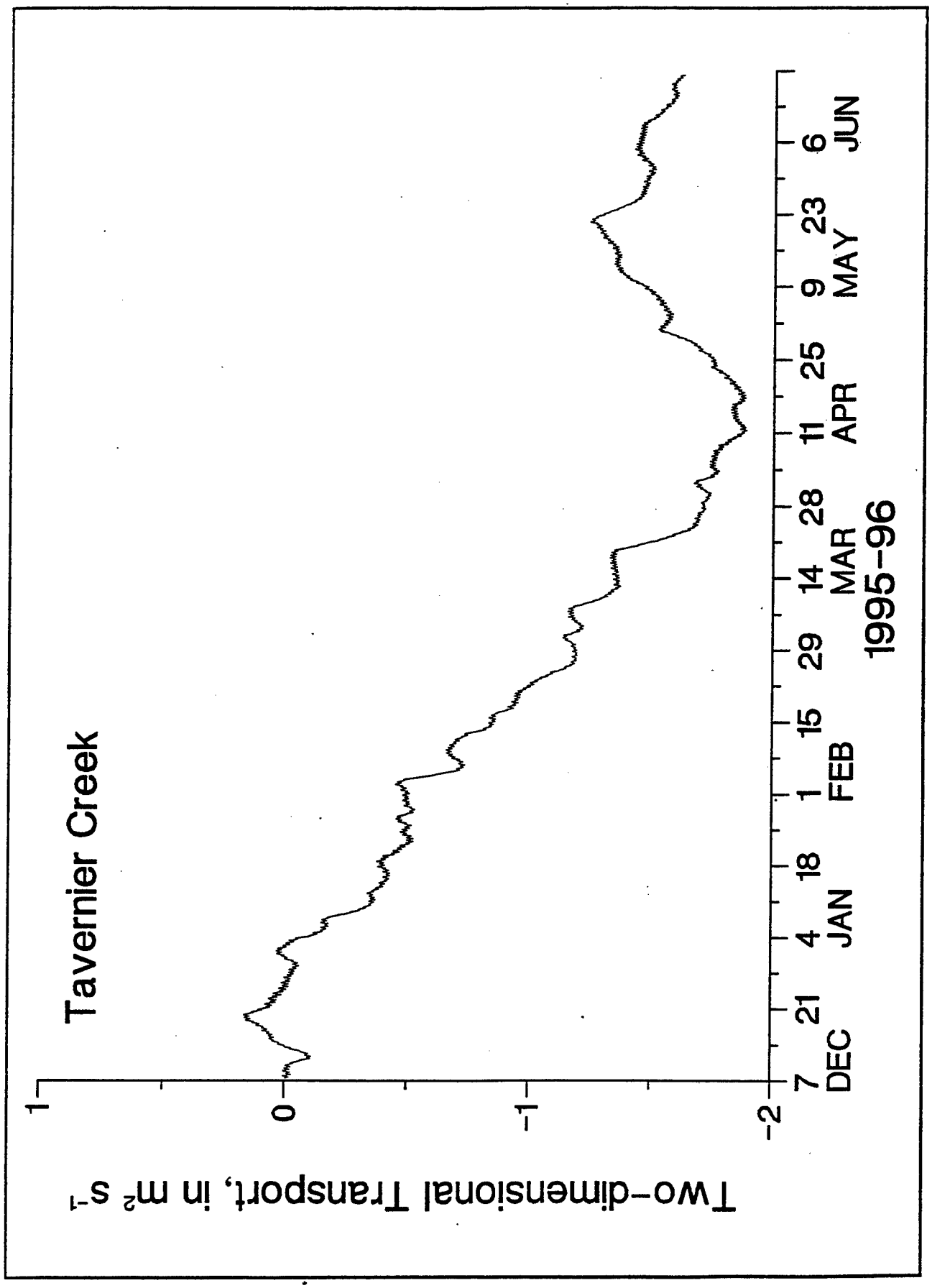
Tavernier Creek
Two-dimensional Transport, in m² s⁻¹
1
0
-1
-2
7 21 4 18 1 15 29 14 28 11 25 9 23 6
DEC JAN FEB MAR APR MAY JUN
1995-96

Figure D25

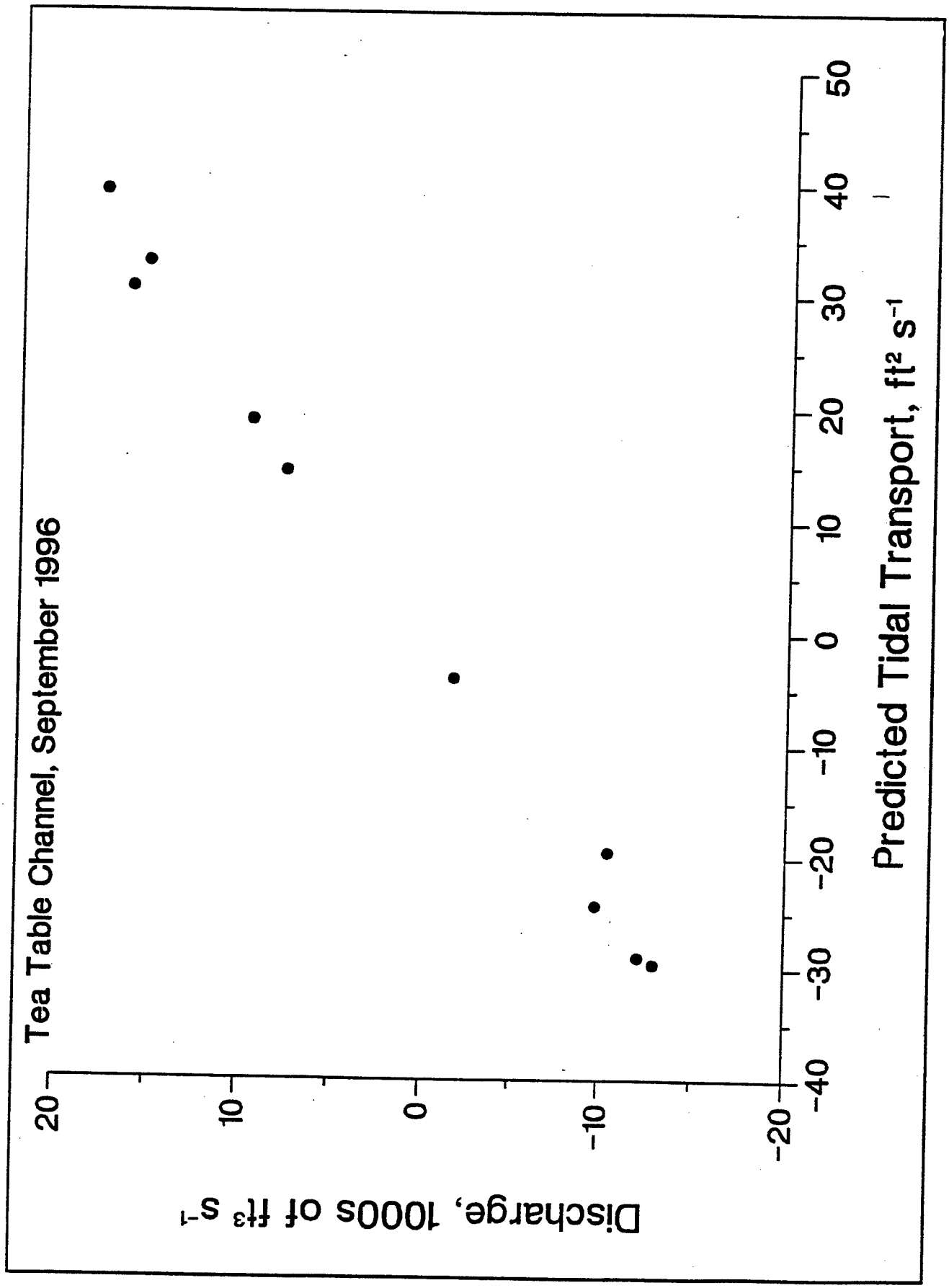
Tea Table Channel, September 1996
Discharge, 1000s of ft³ s⁻¹
20
10
0
-10
-20
Predicted Tidal Transport, ft² s⁻¹
50
40
30
20
10
0
-10
-20
-30
-40

Figure D26

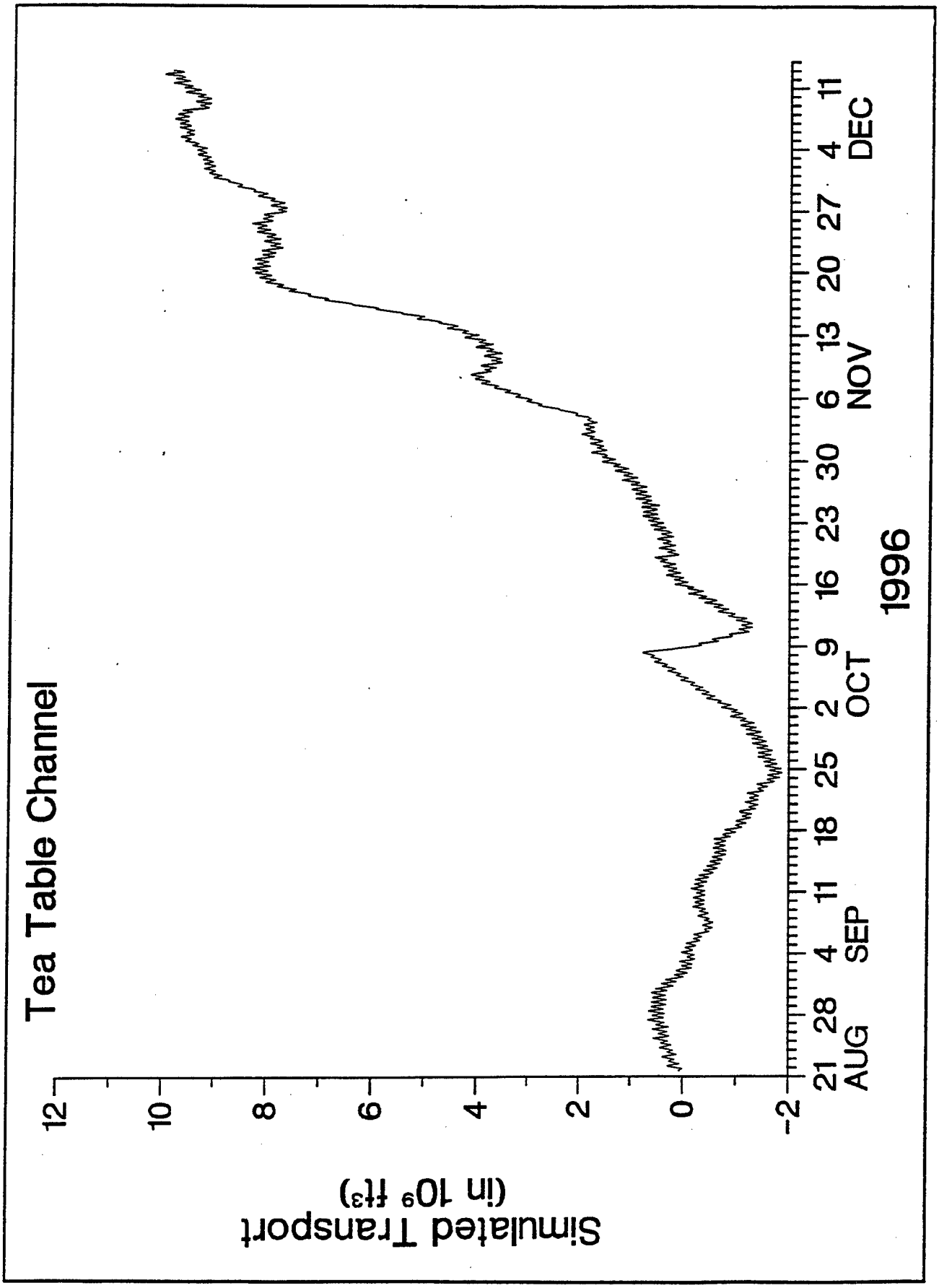
Tea Table Channel
Simulated Transport
(in 10⁹ ft³)
12
10
8
6
4
2
0
-2
21 28 4 11 18 25 2 9 16 23 30 6 13 20 27 4 11
AUG SEP OCT NOV DEC
1996

Figure D27

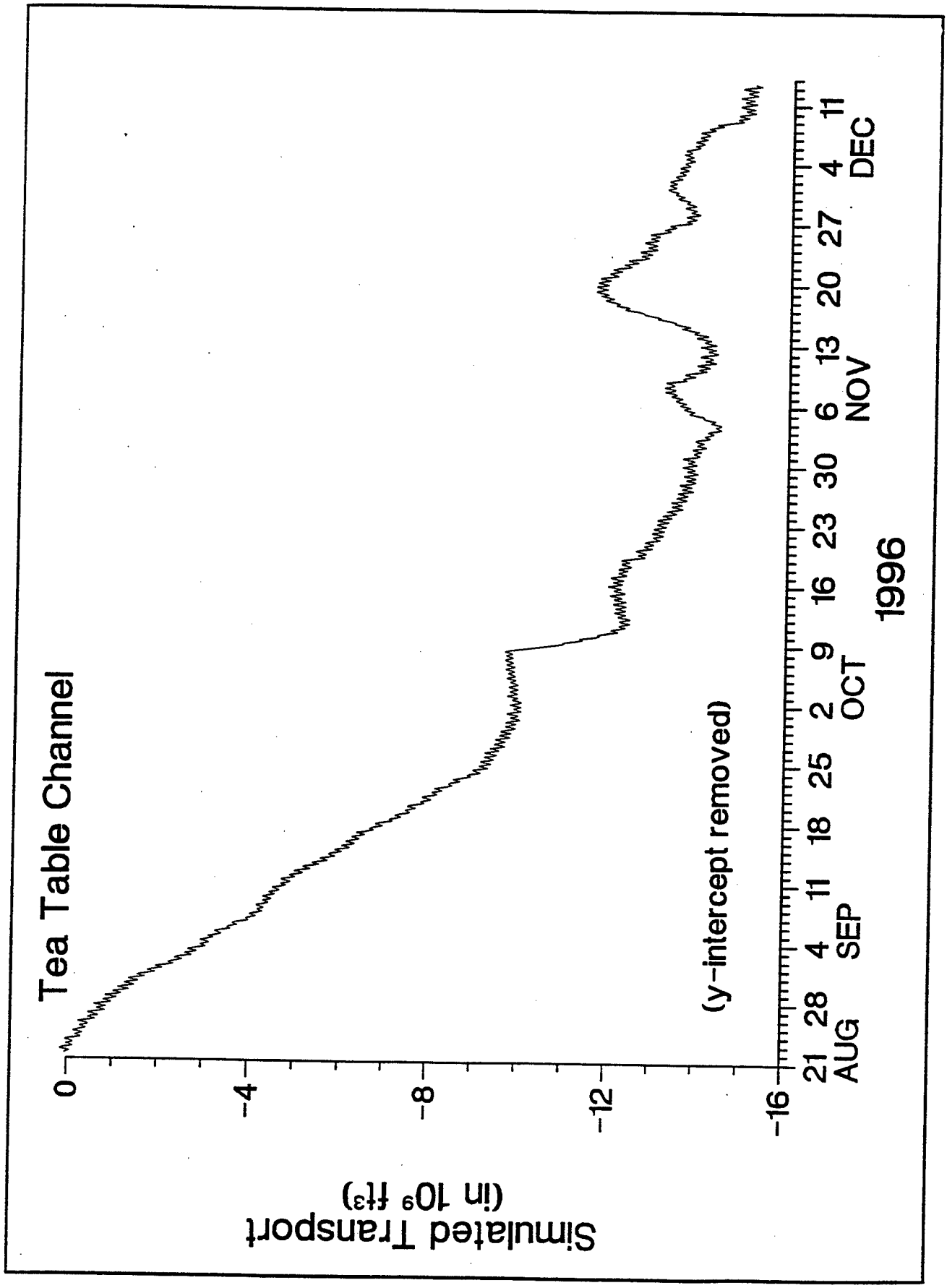
Tea Table Channel
Simulated Transport
(in 10⁹ ft³)
0
-4
-8
-12
-16
(y-intercept removed)
21 28 4 11 18 25 2 9 16 23 30 6 13 20 27 4 11
AUG SEP OCT NOV DEC
1996

Figure D28

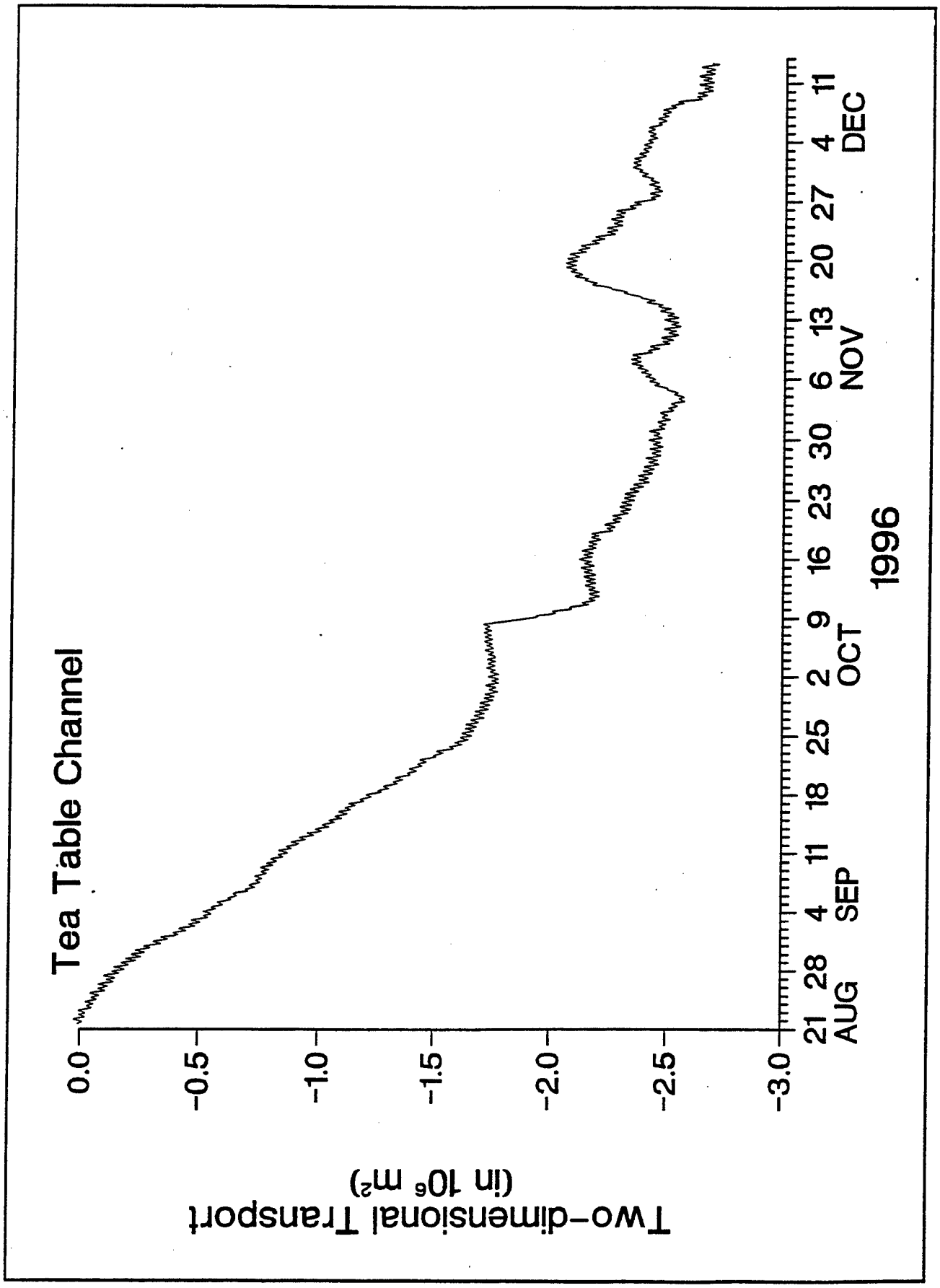
Tea Table Channel
Two-dimensional Transport
(in 10^6 m^2)
0.0
-0.5
-1.0
-1.5
-2.0
-2.5
-3.0
21 28 4 11 18 25 2 9 16 23 30 6 13 20 27 4 11
AUG SEP OCT NOV DEC
1996

Figure D29

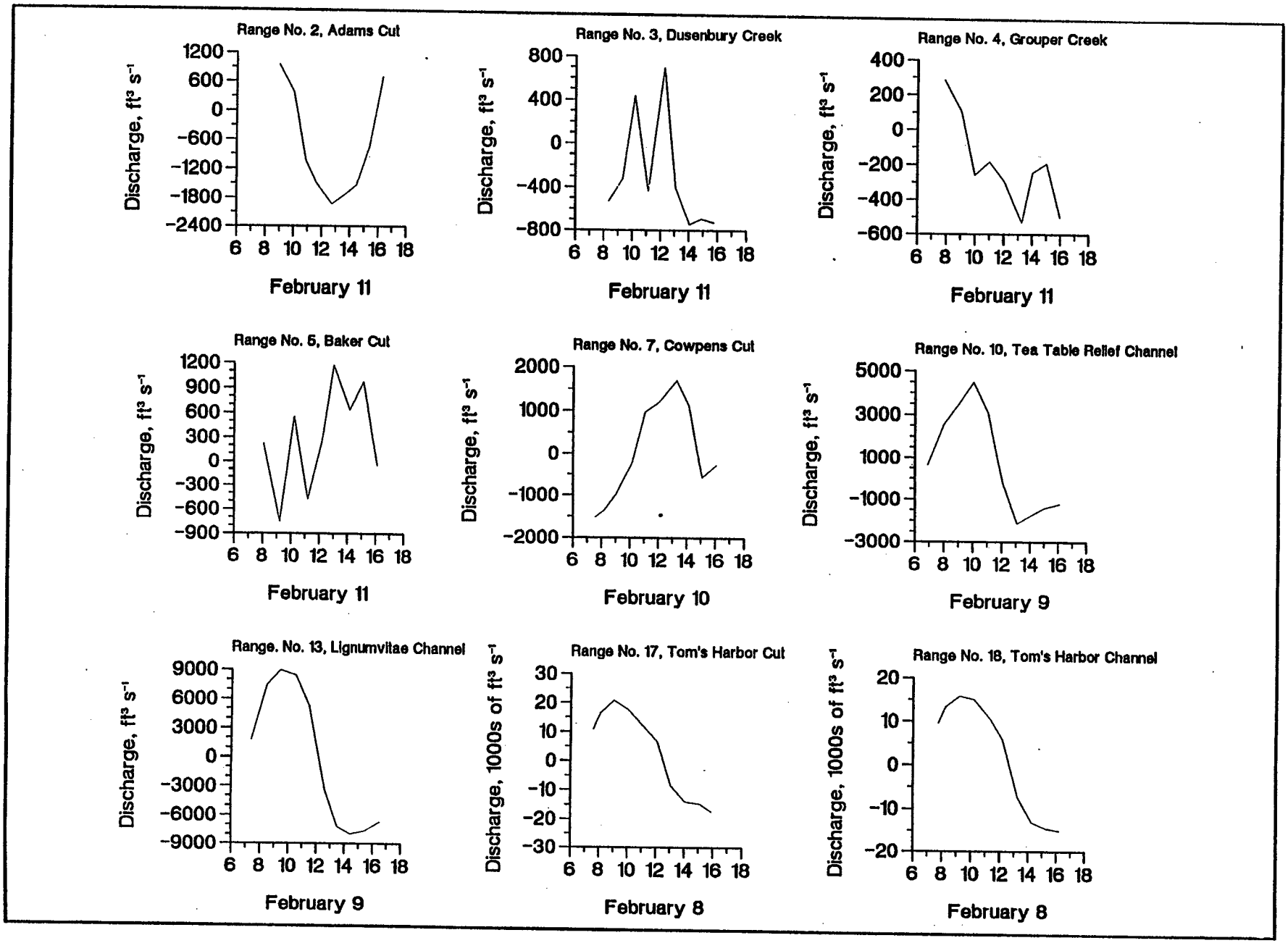
Range No. 2, Adams Cut
Discharge, ft³ s⁻¹
1200
600
0
-600
-1200
-1800
-2400
6 8 10 12 14 16 18
February 11
Range No. 3, Dusenbury Creek
Discharge, ft³ s⁻¹
800
400
0
-400
-800
6 8 10 12 14 16 18
February 11
Range No. 4, Grouper Creek
Discharge, ft³ s⁻¹
400
200
0
-200
-400
-600
6 8 10 12 14 16 18
February 11
Range No. 5, Baker Cut
Discharge, ft³ s⁻¹
1200
900
600
300
0
-300
-600
-900
6 8 10 12 14 16 18
February 11
Range No. 7, Cowpens Cut
Discharge, ft³ s⁻¹
2000
1000
0
-1000
-2000
6 8 10 12 14 16 18
February 10
Range No. 10, Tea Table Relief Channel
Discharge, ft³ s⁻¹
5000
3000
1000
-1000
-3000
6 8 10 12 14 16 18
February 9
Range. No. 13, Lignumvitae Channel
Discharge, ft³ s⁻¹
9000
6000
3000
0
-3000
-6000
-9000
6 8 10 12 14 16 18
February 9
Range No. 17, Tom's Harbor Cut
Discharge, 1000s of ft³ s⁻¹
30
20
10
0
-10
-20
-30
6 8 10 12 14 16 18
February 8
Range No. 18, Tom's Harbor Channel
Discharge, 1000s of ft³ s⁻¹
20
10
0
-10
-20
6 8 10 12 14 16 18
February 8

Figure D30

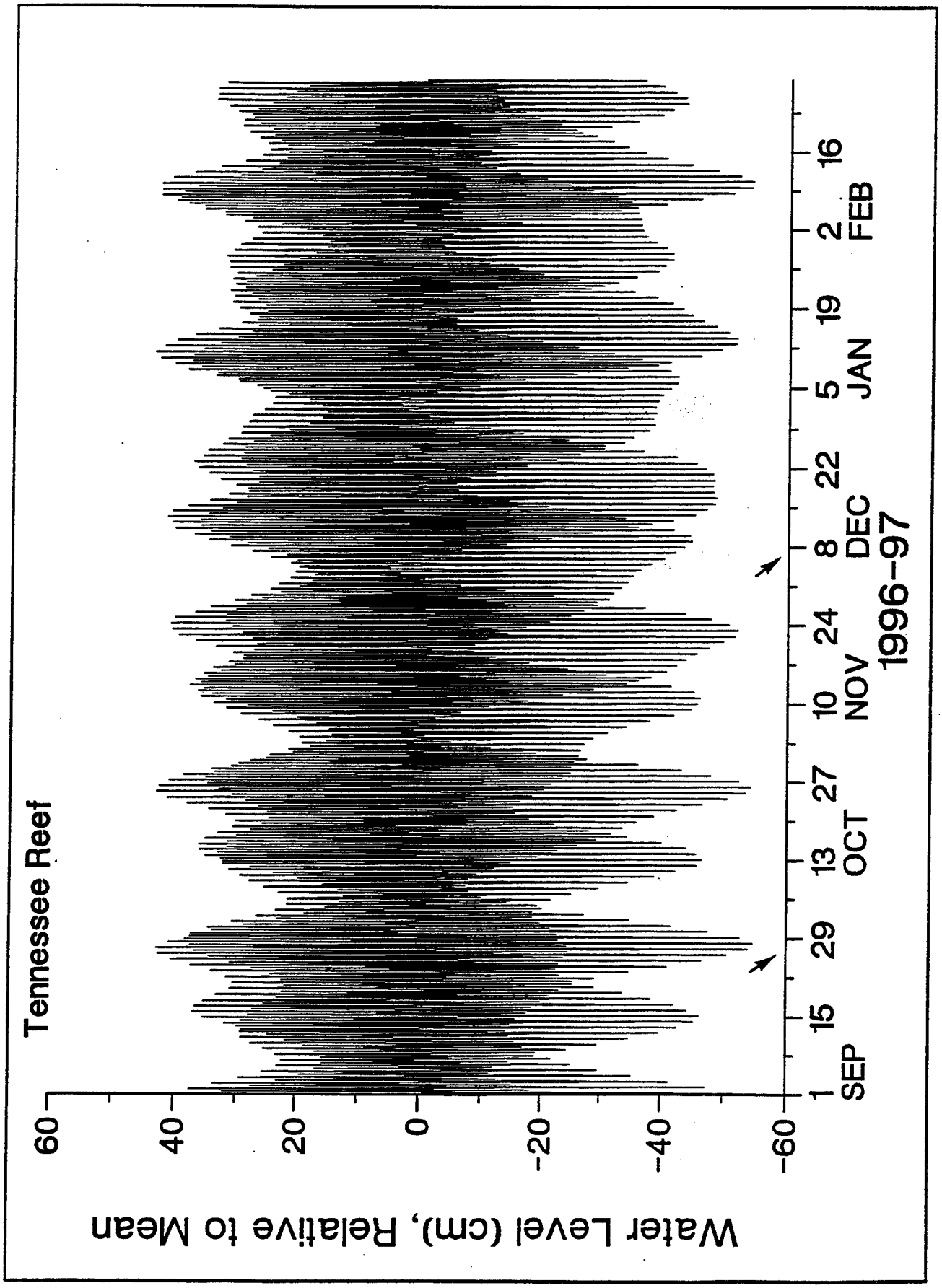
Tennessee Reef
Water Level (cm), Relative to Mean
60
40
20
0
-20
-40
-60
1
SEP
15
29
13
OCT
27
10
NOV
24
8
DEC
22
5
JAN
19
2
FEB
16
1996-97

Figure D31

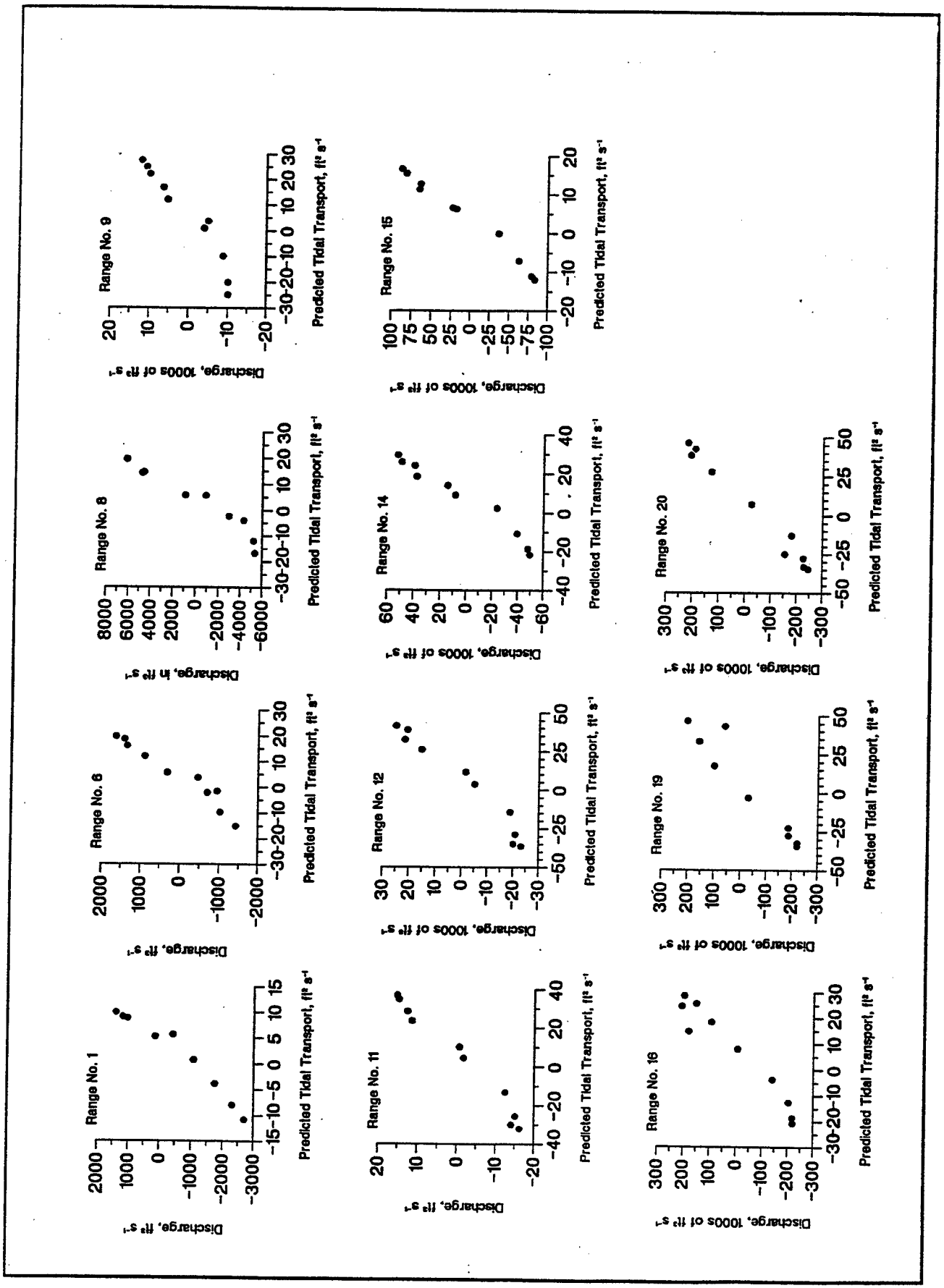
Range No. 1
Range No. 11
Range No. 16
Range No. 6
Range No. 12
Range No. 19
Range No. 8
Range No. 14
Range No. 20
Range No. 9
Range No. 15
Discharge, ft³ s⁻¹
Discharge, 1000s of ft³ s⁻¹
Predicted Tidal Transport, ft² s⁻¹

Figure D32

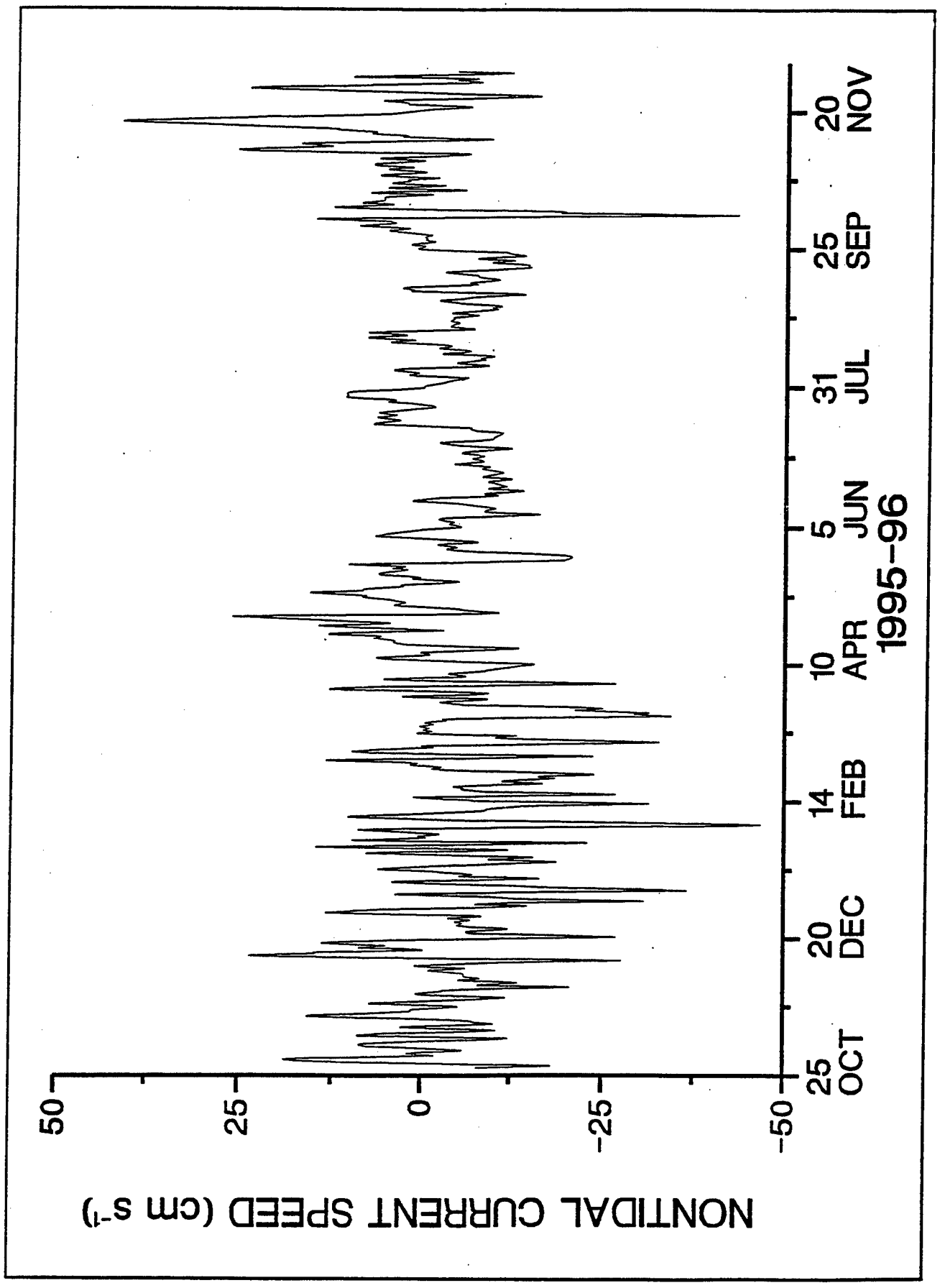
NONTIDAL CURRENT SPEED (cm s⁻¹)
50
25
0
-25
-50
25 OCT
20 DEC
14 FEB
10 APR
5 JUN
31 JUL
25 SEP
20 NOV
1995-96

Figure D33

REPORT DOCUMENTATION PAGE

Form Approved
OMB No. 0704-0188

Public reporting burden for this collection of information is estimated to average 1 hour per response, including the time for reviewing instructions, searching existing data sources, gathering and maintaining the data needed, and completing and reviewing the collection of information. Send comments regarding this burden estimate or any other aspect of this collection of information, including suggestions for reducing this burden, to Washington Headquarters Services, Directorate for Information Operations and Reports, 1215 Jefferson Davis Highway, Suite 1204, Arlington, VA 22202-4302, and to the Office of Management and Budget, Paperwork Reduction Project (0704-0188), Washington, DC 20503.

1. AGENCY USE ONLY *(Leave blank)*	2. REPORT DATE	3. REPORT TYPE AND DATES COVERED
	June 1999	Final report

4. TITLE AND SUBTITLE
Florida Bay Field Data Report

5.FUNDING NUMBERS

6. AUTHOR(S)
Thad C. Pratt, Ned P. Smith

7. PERFORMING ORGANIZATION NAME(S) AND ADDRESS(ES)
U.S. Army Engineer Waterways Experiment Station
3909 Halls Ferry Road, Vicksburg, MS 39180-6199;
Harbor Branch Oceanographic Institution, Inc.
5600 U.S. 1 North, Fort Pierce, FL 34946

8. PERFORMING ORGANIZATION REPORT NUMBER
Technical Report CHL-99-11

9. SPONSORING/MONITORING AGENCY NAME(S) AND ADDRESS(ES)
U.S. Army Engineer District, Jacksonville
P.O. Box 4970
Jacksonville, FL 32232-0019

10. SPONSORING/MONITORING AGENCY REPORT NUMBER

11. SUPPLEMENTARY NOTES
Available from National Technical Information Service, 5285 Port Royal Road, Springfield, VA 22161.

12a. DISTRIBUTION/AVAILABILITY STATEMENT
Approved for public release; distribution is unlimited.

12b. DISTRIBUTION CODE

13. ABSTRACT ***(Maximum 200 words)***

This report presents results of a field effort that included the long-term monitoring of velocity profiles and meteorological data and the short-term intensive data collection of current speed and direction, water-level fluctuations, conductivity, and temperature at several openings into Florida Bay. The field study was structured to incorporate existing information from previous studies wherever possible to provide better coverage and results. The data were returned to the U.S. Army Engineer Waterways Experiment Station for processing, analysis, and preparation into formats suitable for the numerical model and U.S. Army Engineer District, Jacksonville, needs. Further analysis and interpretation of portions of the data were provided by the Harbor Branch Oceanographic Institution, Fort Pierce, FL. The data were used in the development and verification of a two-dimensional numerical hydrodynamic model of the area. The purpose of the numerical model was to develop an understanding of the circulation patterns in Florida Bay and to determine the importance of winds, tides, and freshwater inflow on circulation patterns and salinity.

14. SUBJECT TERMS

Current velocities	Hydrodynamics	Tide data
Field data	Meteorological data	Water quality
Florida Bay	Salinity	Weather data

15. NUMBER OF PAGES
348

16. PRICE CODE

17. SECURITY CLASSIFICATION OF REPORT	18. SECURITY CLASSIFICATION OF THIS PAGE	19. SECURITY CLASSIFICATION OF ABSTRACT	20. LIMITATION OF ABSTRACT
UNCLASSIFIED	UNCLASSIFIED		